Michael J. Waring   *Editor*

Cancer II

Springer

28
Topics in Medicinal Chemistry

Aims and Scope

Drug research requires interdisciplinary team-work at the interface between chemistry, biology and medicine. Therefore, the new topic-related series Topics in Medicinal Chemistry will cover all relevant aspects of drug research, e.g. pathobiochemistry of diseases, identification and validation of (emerging) drug targets, structural biology, drugability of targets, drug design approaches, chemogenomics, synthetic chemistry including combinatorial methods, bioorganic chemistry, natural compounds, high-throughput screening, pharmacological in vitro and in vivo investigations, drug-receptor interactions on the molecular level, structure-activity relationships, drug absorption, distribution, metabolism, elimination, toxicology and pharmacogenomics.

In general, special volumes are edited by well known guest editors.

In references Topics in Medicinal Chemistry is abbreviated Top Med Chem and is cited as a journal.

More information about this series at http://www.springer.com/series/7355

Michael J. Waring

Editor

Cancer II

With contributions by

J. E. Campbell · C. Cano · K. W. Duncan · M. R. V. Finlay ·
N. S. Gray · I. R. Hardcastle · S. Harnor · P. A. Harris ·
J. M. Hatcher · P. W. Manley · O. Michielin · Z. Pan ·
J. Pickles · K. G. Pike · U. F. Röhrig · S. T. Staben ·
N. J. Stiefl · D. Toader · R. A. Ward · V. Zoete · Y. Zuo

Springer

Editor
Michael J. Waring
Northern Institute for Cancer Research, Chemistry,
Newcastle University
Newcastle upon Tyne, UK

Preface

Cancer as a Disease

Whilst cancer is considered a disease of the modern world, it is also recognised as being one of the oldest human diseases. The first known cancer case was discovered by the archaeologist Louis Leakey in a human skeleton dated back to 4,000 BC whose jawbone revealed evidence of lymphoma. The first written records of cancer incidence were made by the Egyptian polymath Imhotep in 2,500 BC in which he described a patient bearing a "bulging mass in the breast" and added ominously that it has no remedy. The disease was named "karkinos" around 2,000 years later by the physician Hippocrates in ancient Greece due to the appearance of a tumour he studied, which he believed to resemble a crab, giving rise to the name by which it is recognised today [1]. In spite of this, due to greater advances in the treatments of other diseases resulting in longer life expectancies as well as the effects of modern lifestyle on its incidence, we recognise cancer chiefly as a disease of the modern, developed world.

Today, cancer is a major global health problem and is the second leading cause of death in the United States. There were estimated to be 1.6 million new cases in the United States in 2016 and nearly 600,000 deaths arising from the disease [2]. The direct economic burden of cancer care in the United States is estimated to reach $172.8 billion by the year 2020 [3]. Most significantly, the human cost of cancer is almost universal and few people will not be personally affected by cancer at some stage of their lives. Hence, the treatment of cancer remains one of humanity's most worthy scientific challenges; it is also one of the most daunting.

Significant progress has been made in the last few decades in the treatment of cancer, and it is noteworthy that as of recently, more people now survive cancer diagnosis than die of it. This is, however, a distinctly irregular picture; certain types of cancer are treated very successfully, whereas others remain almost as intractable today as they have ever been. Progress thus far is due chiefly to the triumvirate of

surgery, radiotherapy and chemotherapy, coupled with early diagnosis. For the most part, if the disease is detected early, it is more likely to be localised and less advanced in terms of genetic transformation, and therefore, these treatments are likely to be more effective. In order to make further progress, treatments for advanced metastatic disease will be required, in particular for those cancers for which early diagnosis is challenging. In this setting, surgery and radiotherapy will be of limited effectiveness and systemic drug therapies are the most promising avenue of future research.

Drug Therapy for Cancer

The use of drug treatment for cancer (commonly referred to as chemotherapy) has been around for a long time. In the sixteenth century, surgeons attempted to treat tumours with sulfuric acid and apothecaries used poisons such as arsenic and lead. In the first half of the twentieth century, the first indications of successful treatments arose from the observations that mustard gas victims suffered from myelosuppression; derivatives of nitrogen mustards were developed as cancer treatments with some degree of initial success. Around the same time, it was shown that antifolates could be used to delay the progression of leukaemias. These discoveries paved the way to the development of an array of cytotoxic chemotherapeutic agents that, often used in combination with each other, remain a critical part of cancer treatment to this day.

Despite working through a variety of different mechanisms, simplistically, all cytotoxic chemotherapies act by disrupting the cell division process. Cancer is, most fundamentally, a disease of rapid, uncontrolled cell division, and its inhibition can lead to effective treatment with some degree of selective toxicity over less rapidly dividing, healthy cells. This indiscriminate approach nevertheless leads to common side effects associated with chemotherapy such as hair loss, nausea and vomiting and immunosuppression as rapidly dividing healthy cells in hair follicles, gastrointestinal tract and bone marrow are also targeted.

In the 1950s, the development of antihormonal therapies, pioneered by the discovery of tamoxifen to treat breast cancer, provided the first definitive evidence that targeting specific molecular targets within certain tumour cell types could also lead to effective therapy. Advances in the understanding of processes necessary for cancer cell survival and the underlying molecular biology of these processes have led to the identification of a myriad of potential targets for targeted therapy.

As a result so far of this pioneering research into cancer treatment, as of 2011, the median survival of a patient diagnosed with cancer in the United Kingdom was 10 years, compared to 1 year in 1971 [4]. This highlights the progress that has been made in discovering new treatments. It is, however, a rather mixed picture with some forms of the disease, such as testicular cancer and melanoma, being very effectively treated whilst others, such as stomach, brain, oesophageal and particularly pancreatic cancers, remain shockingly intransigent (Table 1).

Table 1 10 year survival rates (%age) in the United Kingdom by tumour type for 1971 and 2011
[4]

	1971	2011
Overall	**24**	**50**
Testis	69	98
Melanoma	46	90
Prostate	25	84
Hodgkin's disease	48	80
Breast	40	79
Uterus	56	77
Cervix	46	63
Non-Hodgkin lymphoma	22	63
Larynx	50	59
Colon	23	57
Rectum	20	56
Kidney	23	50
Bladder	32	50
Leukaemia	7	46
Other	35	42
Ovary	18	35
Multiple myeloma	6	33
Stomach	4	15
Brain	5	14
Oesophagus	4	12
Lung	3	5
Pancreas	1	1

The development of targeted therapies was introduced in the previous volume in this series [4]. This second volume seeks to update the important developments that have occurred over the subsequent decade. The volume is structured by mechanistic class with a focus on clinically successful approaches. The chapters all describe that biological context to the work but focus on the chemical innovations that have been crucial to making progress in the area. In all cases, the chapters are authored by researchers who are experts in the field and have contributed personally to the work described. Since the subject of the series is medicinal chemistry, the focus of the material is on small molecule drug approaches, although a number of new treatments are monoclonal antibody therapies and other biological approaches (see below).

Overview of Treatments Entering the Clinic in the Last Decade

In the decade since the publication of the previous volume (2007–2016), the United States Food and Drug Administration approved 70 new treatments with an oncology indication (Table 2) [5, 6]. Of these, 47 (67%) were small molecules, a further 17 were monoclonal antibodies and 2 were ADCs. Hence, despite a significant amount of investment into novel approaches to treatment, traditional small molecule approaches continue to form the mainstay of successful medicines. The most common indication for the new drugs were lung and melanoma (seven new treatments each) followed by breast, multiple myeloma and prostate (six new treatments). Of these, only lung cancer was identified in the analysis above as being the most poorly treated (10-year survival below 30%), and there were no new drug treatments for pancreatic, oesophageal, brain and stomach cancer, for which treatment outcomes were most poor.

The newly approved treatments targeted a diverse range of protein targets, with vascular endothelial growth factor (VEGF) and its receptors (VEGFR) being the most common targets (nine new therapies), albeit that these represent a mixture of antibody and small molecule approaches and target the ligand, the extracellular receptor and the intracellular kinase domain. Of the kinase inhibitors targeting VEGF, many were non-selective inhibitors and derive at least some of their efficacy from inhibition of other kinases. The next most frequently targeted proteins were epidermal growth factor receptor (EGFR), Her2/ERBB2 (four treatments) and anaplastic lymphoma kinase (ALK), histone deacetylases (HDAC) and RAF (three agents each). In total, almost half of the small molecule treatments were kinase inhibitors.

Table 2 FDA new oncology approvals from 2007 to 2016, their indications and mode of action

Drug name	Active ingredient	Year	Indication	Protein target	Class
Imfinzi	Durvalumab	2017	Urothelial	PD-L1	MAb
Rydapt	Midostaurin	2017	AML	VEGFR, Multikinase	Small molecule
Alunbrig	Brigatinib	2017	Lung	ALK, EGFR	Small molecule
Zejula	Niraparib	2017	Ovarian	PARP1, PARP2	Small molecule
Bavencio	Avelumab	2017	Merkel cell	PD-L1	MAb
Kisqali	Ribociclib	2017	Breast	CDK4, CDK6	Small molecule
Rubraca	Rucaparib	2016	Ovarian	PARP1	Small molecule
Lartruvo	Olaratumab	2016	Soft tissue sarcoma	PDGFRα	MAb
Tecentriq	Atezolizumab	2016	Urothelial	PD-L1	MAb

(continued)

Table 2 (continued)

Drug name	Active ingredient	Year	Indication	Protein target	Class
Venclexta	Venetoclax	2016	CLL	BCL2	Small molecule
Alecensa	Alectinib	2015	Lung	ALK	Small molecule
Empliciti	Elotuzumab	2015	Multiple myeloma	CD319	MAb
Portrazza	Necitumumab	2015	Lung	EGFR	MAb
Ninlaro	Ixazomib	2015	Multiple myeloma	Proteosome	Small molecule
Darzalex	Daratumumab	2015	Multiple myeloma	CD38	MAb
Tagrisso	Osimertinib	2015	Lung	EGFR	Small molecule
Cotellic	Cobimetinib	2015	Melanoma	MEK	Small molecule
Yondelis	Trabectedin	2015	Soft tissue sarcoma	FUS-CHOP	Small molecule
Lonsurf	Trifluridine and Tipiracil	2015	Colorectal	DNA synthesis, thymidine phosphorylase	Small molecule
Odomzo	Sonidegib	2015	Basal cell	SMO	Small molecule
Unituxin	Dinutuximab	2015	Neuroblastoma	GD2	MAb
Farydak	Panobinostat	2015	Multiple myeloma	HDAC	Small molecule
Lenvima	Lenvatinib	2015	Thyroid	VEGFR	Small molecule
Ibrance	Palbociclib	2015	Breast	CDK4, CDK6	Small molecule
Opdivo	Nivolumab	2014	Melanoma	PD-1	MAb
Lynparza	Olaparib	2014	Ovarian	PARP1	Small molecule
Blincyto	Blinatumomab	2014	ALL	CD19, CD3	MAb
Keytruda	Pembrolizumab	2014	Melanoma	PD-1	MAb
Zydelig	Idelalisib	2014	CLL, SLL, FL	PI3K	Small molecule
Beleodaq	Belinostat	2014	PTCL	HDAC	Small molecule
Zykadia	Ceritinib	2014	Lung	ALK	Small molecule
Sylvant	Siltuximab	2014	MCD	IL6	MAb
Cyramza	Ramucirumab	2014	Gastric	VEGFR	MAb
Imbruvica	Ibrutinib	2013	MCL	BTK	Small molecule
Gazyva	Obinutuzumab	2013	CLL	CD-20	MAb
Gilotrif	Afatinib	2013	Lung	EGFR	Small molecule

Table 2 (continued)

Drug name	Active ingredient	Year	Indication	Protein target	Class
Mekinist	Trametinib	2013	Melanoma	MEK	Small molecule
Tafinlar	Dabrafenib	2013	Melanoma	RAF	Small molecule
Xofigo	Radium Ra 223 dichloride	2013	Prostate	DNA	Radioisotope
Kadcyla	Ado-trastuzumab emtansine	2013	Breast	HER2	ADC
Pomalyst	Pomalidomide	2013	Multiple myeloma	Unknown	Small molecule
Iclusig	Ponatinib	2012	CML, ALL	BCR-ABL	Small molecule
Cometriq	Cabozantinib	2012	Thyroid	VEGFR, Multikinase	Small molecule
Synribo	Omacetaxine mepesuccinate	2012	CML	Ribosome	Small molecule
Stivarga	Regorafenib	2012	Colorectal	RAF	Small molecule
Bosulif	Bosutinib	2012	CML	VEGFR, Multikinase	Small molecule
Xtandi	Enzalutamide	2012	Prostate	AR	Small molecule
Zaltrap	Ziv-aflibercept	2012	Colorectal	VEGF	Antibody fusion protein
Kyprolis	Carfilzomib	2012	Multiple myeloma	Proteosome	Small molecule
Perjeta	Pertuzumab	2012	Breast	HER2	MAb
Erivedge	Vismodegib	2012	Basal cell	SMO	Small molecule
Inlyta	Axitinib	2012	Renal	VEGFR, Multikinase	Small molecule
Xalkori	Crizotinib	2011	Lung	ALK	Small molecule
Adcetris	Brentuximab vedotin	2011	Hodgkin's lymphoma, ALCL	CD30	ADC
Zelboraf	Vemurafenib	2011	Melanoma	RAF	Small molecule
Zytiga	Abiraterone acetate	2011	Prostate	CYP17A1	Small molecule
Caprelsa	Vandetanib	2011	Thyroid	VEGFR, Multikinase	Small molecule
Yervoy	Ipilimumab	2011	Melanoma	CTLA-4	MAb
Halaven	Eribulin mesylate	2010	Breast	Microtubules	Small molecule

Table 2 (continued)

Drug name	Active ingredient	Year	Indication	Protein target	Class
Herceptin	Trastuzumab	2010	Gastric	HER2	MAb
Jevtana	Cabazitaxel	2010	Prostate	Tubulin	Small molecule
Provenge	Sipuleucel-T	2010	Prostate	Immunostimulant	Cell based therapy
Afinitor	Everolimus	2009	Renal	TOR	Small molecule
Arzerra	Ofatumumab	2009	CLL	CD-20	MAb
Avastin	Bevacizumab	2009	Renal	VEGF	MAb
Folotyn	Pralatrexate injection	2009	PTCL	Antifolate	Small molecule
Istodax	Romidepsin	2009	CTCL	HDAC	Small molecule
Votrient	Pazopanib	2009	Renal	VEGFR, Multikinase	Small molecule
Degarelix	Degarelix for injection	2008	Prostate	GnRH	Synthetic peptide
Mozobil	Plerixafor injection	2008	Non-Hodgkin's lymphoma, multiple myeloma	CXCR4, CXCR7	Small molecule
Treanda	Bendamustine hydrochloride	2008	Non-Hodgkin's lymphoma, CLL	DNA	Small molecule
Hycamtin	Topotecan hydrochloride	2007	Lung	Topoisomerase	Small molecule
Ixempra	Ixabepilone	2007	Breast	Tubulin	Small molecule
Tasigna	Nilotinib hydrochloride monohydrate	2007	CML	BCR-ABL	Small molecule
Torisel	Temsirolimus	2007	Renal	TOR	Small molecule
Tykerb	Lapatinib	2007	Breast	ERBB2, EGFR	Small molecule

In this volume, the science leading to many of the above therapies is described. Developments of inhibitors of BCR ABL, EGFR, BTK, VEGFR, FGFR, PI3K and ALK are described specifically in dedicated chapters (Chapters "Progress in the Discovery of BCR-ABL Kinase Inhibitors for the Treatment of Leukemia", "Small Molecule Inhibitors of the Epidermal Growth Factor Receptor", "Small-Molecule Inhibitors of Bruton's Tyrosine Kinase", "Inhibitors of Vascular Endothelial Growth Factor Receptor", "Inhibitors of the Fibroblast Growth Factor Receptor", "Isoform Selective PI3K Inhibitors for Treating Cancer", and "Small Molecule Inhibitors of ALK", respectively). In Chapter "Modulation of the DNA-Damage Response by Inhibitors of the Phosphatidylinositol 3-Kinase Related Kinase (PIKK) Family", new inhibitors of kinases involved in DNA damage response are discussed, and emerging approaches to targeting epigenetic mechanisms are covered in Chapter "Epigenetic Modulators".

As highlighted above, a number of new treatments arising from the last decade are antibody-based therapies for which there is little medicinal chemistry input. Notable in this field is the great promise of immunooncology approaches as heralded by the arrival of PD-1 and PD-L1 antibodies to the market. This field is dominated by antibody approaches but it also presents opportunities for small molecule approaches, and developments in this field are discussed in Chapter "Inhibitors of the Kynurenine Pathway". However, the demarcation between categories of therapeutic is becoming less well defined as researchers explore more innovative approaches to the discovery of new treatments. Traditionally intractable small molecule targets such as protein–protein interactions (Chapter "Protein–Protein Interaction Inhibitors") are now being successfully targeted with traditional medicinal chemistry approaches. Creative medicinal chemistry is also manifest in non-traditional modalities such as antibody–drug conjugates which are now progressing to the market (Chapter "Antibody–Drug Conjugates").

Future Perspectives

It is clear that there has been great progress in the fight against cancer, and this volume highlights some of the critical contributions that medicinal chemistry has made to these endeavours. Nevertheless, it is also clear that the problem presented by the disease is huge and significant challenges remain. In subsequent chapters, it will be seen that tumours are able to develop resistance to targeted therapies as they are to traditional cytotoxic therapies, and making further improvements to patients' long-term survival will require identification and targeting of these resistance mechanisms. With these challenges come opportunities for chemists, and initial encouragement into targeting resistance mechanisms is provided by the development of next-generation BCR ABL and EGFR inhibitors (Chapters "Progress in the Discovery of BCR-ABL Kinase Inhibitors for the Treatment of Leukemia" and "Small Molecule Inhibitors of the Epidermal Growth Factor Receptor"). It might be reasonably expected that in the future, similar situations will arise for newer mechanisms.

References

1. Mukherjee S (2010) The emperor of all maladies: a biography of cancer. Scribner, New York
2. Siegel RL, Miller KD, Jemal A (2016) Cancer statistics, 2016. CA Cancer J Clin 66:7–30
3. Yabroff KR, Lund J, Kepka D, Mariotto A (2011) Economic burden of cancer in the United States: estimates, projections, and future research. Cancer Epidemiol Biomarkers Prev 20:2006–2014
4. Bradbury RH (2007) Cancer. Topics in medicinal chemistry. Springer, Berlin
5. www.fda.gov/Drugs
6. www.centerwatch.com

Contents

Progress in the Discovery of BCR-ABL Kinase Inhibitors for the Treatment of Leukemia

Paul W. Manley and Nikolaus J. Stiefl

Abstract Chemists first employed structure–activity relationships in designing busulphan, a chemotherapeutic for chronic myeloid leukemia (CML) in the 1950s. However, despite chemotherapy and later interferon immunotherapy, the median survival of patients remained less than 5 years. The elucidation that CML is driven by a tyrosine kinase mutation in haematopoietic stem cells enabled the discovery of imatinib, the first oncoprotein-targeted drug. Imatinib revolutionised CML therapy and set a new paradigm for the discovery of improved cancer drugs. Subsequently, medicinal chemists have capitalised upon X-ray co-crystal structures to rationally design superior ATP-competitive and allosteric ABL inhibitors. This progress has translated into clinical practice, such that chronic phase CML patients treated according to current guidelines have a normal life expectancy and many might in the future be able to discontinue treatment and maintain treatment-free remission. This review documents the history of CML drug discovery from arsenic through to asciminib, and progress towards a potential leukemia cure.

Keywords Abelson tyrosine kinase (BCR-ABL), Allosteric inhibitor, Chronic myeloid leukemia (CML), Kinase inhibitor design, Leukemia molecular response, Targeted cancer drug

Contents

P.W. Manley (✉) and N.J. Stiefl
Global Discovery Chemistry, Novartis Institutes for Biomedical Research, Basel, Switzerland
e-mail: paul.manley@novartis.com

1 Introduction

Historically the treatment of cancer relied on therapies which were intended to se-
lectively kill tumour cells by exploiting their abnormally fast proliferation rates.
However, with the exception of some types of pediatric leukemia and testicular can-
cer, the effect of such chemotherapeutic agents on disease progression and survival
rates in cancer patients has generally been quite small [1]. Following Health Author-
ity approval of imatinib (**11**; Sect. 3.1) as the first BCR-ABL1 kinase inhibitor for the
treatment for chronic myeloid leukemia (CML) in 2001, this drug set a new paradigm
for treatments that target the underlying genetic abnormalities of cancer. With such
drugs, CML has been transformed from a malignancy with a very poor prognosis into
what can now be almost regarded as a chronic disease (Fig. 1). This article documents
progress from the first treatments of CML until the present time.
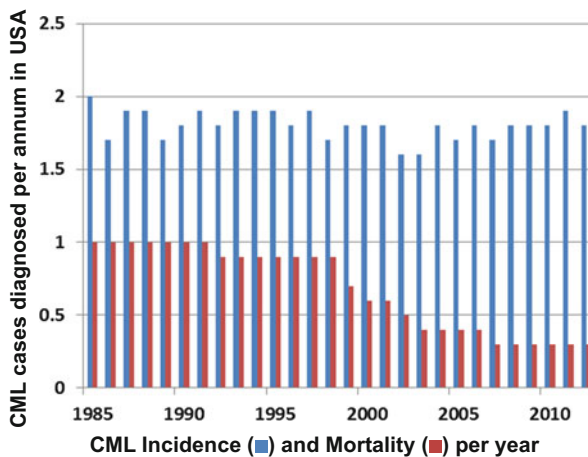
Fig. 1 Change in incidence and mortality of CML in the USA, based upon The Surveillance,
Epidemiology, and End Results (SEER) Program of the National Cancer Institute (http://seer.cancer.
gov/statfacts/html/cmyl.html). In 2000 CML mortality was 2,300, compared to 600 in 2006, with the
74% decrease largely attributable to imatinib. In 2006 the prevalence of CML was 24,800, with the
number of patients increasing to 36,800 in 2010, reflecting the control of the malignancy

2   Chronic Myeloid Leukemia, the Disease and Early Treatments

Leukemias have long been recognised as being diseases of the bone marrow [2] and are categorised according to cell lineage involvement into four major types: acute lymphoid leukemia (ALL), acute myeloid leukemia (AML), chronic lymphoid leukemia (CLL) and chronic myeloid leukemia (CML). CML is a rare disease which represents about 15% of adult leukemias, with an annual incidence in Europe and the USA of about 1–2 cases per 100,000 inhabitants and a median age at diagnosis of 57–60 years [3]. The first step towards understanding CML at the genomic level came in 1960, when Nowell and Hungerford identified the Philadelphia (Ph) chromosome as being a hallmark of the malignancy [4]. Following this, a sequence of studies over the next 25 years elucidated the molecular basis of the disease (reviewed in Hunter [5]). Thus it is now established that CML is a clonal malignancy, which originates in a pluripotent haematopoietic stem cell when unfaithful double-strand DNA break repair leads to a reciprocal t(9;22)(q34,q11) chromosome translocation, thereby forming the Ph-chromosome, which is a shortened version of 22, together with an elongated chromosome 9 [6, 7]. The Ph-chromosome, which is specific to and diagnostic of CML, carries a chimeric gene that comprises of a portion of *ABL1* from chromosome 9 joined to a portion of the *BCR* gene from chromosome 22. This *BCR-ABL1* fusion gene encodes the BCR-ABL1 protein, in which the normally tightly regulated ABL1 tyrosine kinase domain is constitutively activated. The ensuing protein phosphorylation results in the activation of multiple intracellular signalling pathways and is critical for the initiation, progression and maintenance of CML [8].

CML patients are usually diagnosed in a relatively asymptomatic chronic phase, with typical symptoms of splenomegaly and leukocytosis, in which the clonal expansion of mature Ph-positive myeloid cells leads to an elevated white blood cell count, typically >100,000 per μL compared to the normal range of 4,500–10,000 per μL. In the absence of effective treatment, chronic phase CML will invariably progress within 3–4 years to an accelerated phase (approximate duration 3–6 months), which is associated with further cytogenetic changes and where immature myeloid cells appear in the peripheral blood [9, 10]. Progression then proceeds to a brief, terminal blast crisis phase, where progenitor cells fail to differentiate and immature blast cells accumulate in the bone marrow, peripheral blood, CNS and other tissues. Death is generally from infarction, haemorrhage or infection, resulting from the absence of normal granulocytes and platelets.

Prior to the year 2000, the primary measure of assessing the effectiveness of CML treatments was survival, with the median survival of CML patients being approximately 5 years, but as therapies evolved to provide dramatically improved patient responses with greatly prolonged survival, the methods employed to monitor drug efficacy and furnish prognostic indicators have had to become much more sensitive (Fig. 2) [11, 12]. Upon diagnosis most chronic phase CML patients present with a leukemic burden of $\approx 10^{12}$ cells. The first meaningful level of response is a complete

| Tumor burden at diagnosis ≈10^{12} cells	Fold reduction in BCR-ABL	Log reduction in BCR-ABL
Complete Hematologic Response (CHR)	10	1
Complete Cytogenic Response (CCyR)	100	2
Major Molecular Response (MMR)	1,000	3
4-log Molecular Response (MR^4)	10,000	4
$MR^{4.5}$	32,000	4.5
MR^5	100,000	5
Towards Cure		
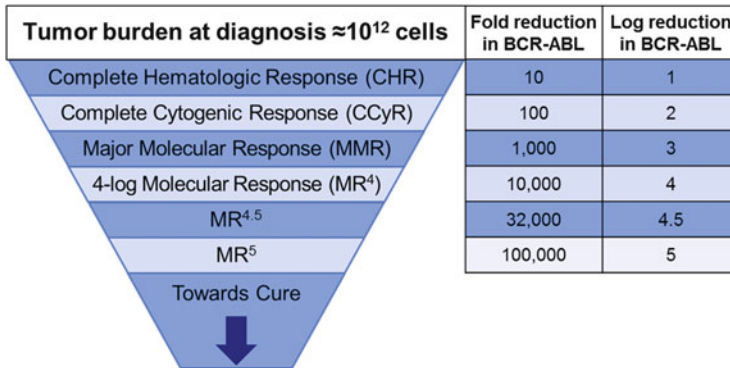
Fig. 2 Representation of the approximate relationships between the level of treatment response and leukemic cell burden, as quantified by polymerase chain reaction (PCR). Current PCR technology enables the detection of a single BCR-ABL1 expressing cell in up to a million white blood cells. Thus, residual disease levels below MR^5, which are still far from what could be considered as a cure, cannot currently be assessed

haematological response (CHR), the definition of which includes a white blood cell count of <10,000 cells per μL of peripheral blood and a non-palpable spleen, and this approximates to a ten-fold (1-log) reduction in tumour cells. The next level of response involves cytogenetic analysis, but even a complete cytogenic response (CCyR) where the Ph-chromosome is not detectable upon staining dividing cells (by assessing ≥20 metaphases) from bone marrow cultures, may only represent a 100-fold (2-log) reduction in disease burden. In order to monitor deeper responses, *BCR-ABL1* messenger RNA levels, analysed either in bone marrow or more conveniently in peripheral blood, are quantified using a reverse transcription polymerase chain reaction (RT-PCR) [13, 14]. The mRNA levels are calibrated in relation to a standardised baseline using reference samples with an established International Scale and the molecular responses graded either as Major Molecular Response (MMR), which represents a ≥3-log reduction in tumour burden, MR4 or MR4.5, representing ≥4- or ≥4.5-log reductions, respectively. A key aspect of molecular monitoring is that CML relapse is now known to be rare in patients who maintain a response level ≥ MMR and consensus recommendations support an MMR as an important endpoint for drug treatment. As methodologies improve, yet deeper responses are now becoming assessable, although the ability to quantify lower numbers of leukemic cells is very dependent on the assay and an undetectable read-out might reflect insufficient sensitivity of the method.

Following the first descriptions of leukemia by Donné (1844), Bennett (1845) and Virchow (1845) (reviewed in Kampen, Geary and Piller [15–17]), in 1865 David Lissauer (Kassel Landeskrankenhaus, Germany) reported the first clinical success when he treated a patient with arsenic trioxide dissolved in potassium bicarbonate (Fowler's solution) [18]. Arsenic then became an established treatment for leukemia until 1903, when Senn (Presbyterian Hospital, Chicago) reported a case study where splenic irradiation with X-rays afforded disease regression [19] and thereafter radiotherapy with either irradiation or intravenous administration of

$[^{32}P]$-Na_2HPO_4 was frequently employed until the mid-1950s and the dawn of the chemotherapy era [20–23].

1
(mustard gas)

2
(chlorambucil)

3
(GT-41; busulphan; Myleran®)

4
(hydroxycaramide; Hydrea®)
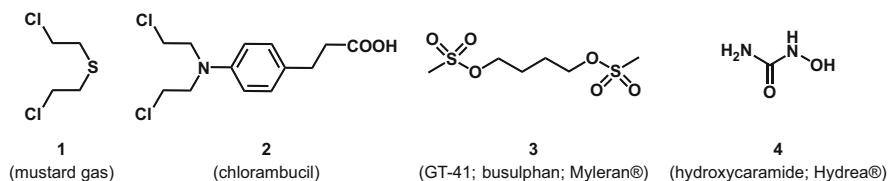
Improved symptomatic treatment came with the use of cytotoxic drugs. The observation that bone marrow and lymph nodes were markedly depleted in victims exposed to mustard gas (**1**) during World War I stimulated cancer research on alkylating agents [24]. This led to the identification of nitrogen mustards, such as chlorambucil (**2**), which is still used to treat CLL [25]. In endeavours to improve the therapeutic efficacy of nitrogen mustards, Haddow and Timmis (Chester Beatty Research Institute, London) found that sulphonic acid ester derivatives of diols could selectively decrease numbers of peripheral blood neutrophils while sparing lymphoid cells in a rat tumour growth model [26]. Moreover, they were able to develop some SAR regarding the length of the alkyl chain separating the esters, with four methylene groups being optimal. This early example of medicinal chemistry research prompted clinical studies leading to the introduction of busulphan (**3**; Myleran®, GlaxoSmithKline) as the first drug to treat CML in 1953 [22, 27]. A typical course of treatment comprised of daily oral administration (4 mg or 0.065 mg kg^{-1}) until leukocyte numbers normalised, with treatment resumed upon relapse, and this regimen was found to be superior to radiotherapy [28]. The mechanism of action of busulphan is now known to involve both intra- and inter-strand DNA cross-linking, as well as formation of DNA–protein linkages, which results in cell senescence [29, 30]. Although as an alkylating agent, busulphan is associated with substantial toxicities, it is still used in otherwise unresponsive CML patients, with dosing regimens carefully designed to minimise side-effects which include excessive weakness, bone marrow toxicity, myelosuppression, as well as pulmonary, hepatic and cardiac fibrosis.

The second drug to emerge was hydroxyurea (**4**), originally synthesised in 1869 by reacting $NH_2OH.H_2SO_4$ with KOCN [31], and almost a century later discovered to prolong the survival of mice bearing leukemia and solid tumours [32, 33]. Based upon these findings and its overall profile, clinical investigations were initiated in multiple malignancies and, in 1967 first approvals were granted for the use of hydroxyurea (Hydrea®; Bristol-Myers Squibb) in the treatment of head and neck cancer, as well as CML [34]. It is now known that hydroxyurea reversibly inhibits ribonucleotide reductase through a free-radical mechanism, thereby preventing reduction of ribonucleotides to the corresponding deoxynucleoside triphosphates. This then starves DNA polymerase to impede replication by preventing cells from progressing through S-phase and concurrently leads to double-strand DNA breaks [35, 36]. Because of its superior efficacy (median survival 58 months versus 45) and tolerability

[37], hydroxyurea superceded busulphan to become the mainstay of CML therapy, with side-effects mainly limited to myelosuppression, cutaneous toxicities and genotoxicity.

However, despite the ability of busulphan and hydroxyurea to achieve haematological responses and reduce the symptoms of CML, these drugs, either as monotherapies or in combination with other available cytotoxic agents, did not appreciably increase the life expectancy of patients [38]. The next advance came with alpha-interferon (IFN-α), which was generally accepted as the best first-line treatment for CML until 2001. The type-1 interferons, IFN-α and IFN-β, are glycoproteins which are secreted by many types of human cells to modulate antiviral, antibacterial and antiparasitic host-defense responses, and which also play important roles in inflammatory diseases, autoimmunity and cancer. The pleiotropic effects of these proteins are mediated by their binding to a common cell surface receptor (IFNAR) that comprises of two subunits, one of which interacts with Janus kinase 1 (JAK-1) and the other with the related tyrosine kinase, TYK-2 [39, 40]. Interferon-bound IFNAR activates the kinases, resulting in the phosphorylation and subsequent dimerisation of STAT (signal transducer and activators of transcription) family members. The dimerised STATs are then transported into the nucleus where they bind to the promoter region of numerous genes, the nature of which depends upon the cell-type and the stimulus, thereby stimulating transcription. Based upon preclinical studies which showed that IFN-α had significant antiproliferative activities against normal myeloid and CML progenitor cells, Talpaz and co-workers investigated the effects of human leukocyte-derived IFN-α in CML patients [41]. Whereas early clinical studies showed promise, inter-batch variability in the content and purity of IFN-α, together with its short half-life, led to large fluctuations in plasma levels, and compounded by a small therapeutic index this hampered sustained administration of the drug. However, the advent of genetically engineered recombinant protein (rIFN-α), comprising of 165 amino-acid residues with either Arg (Intron-A®, Schering) or Lys (Roferon-A®, Roche) at position 23, enabled the accurate control of drug delivery by once-daily subcutaneous injection. Thereafter, in chronic phase CML trials treatment with rIFN-α significantly improved 5-year survival rates to 50–59%, compared with 29–44% for patients randomised to receive either hydroxyurea or busulphan [42]. Furthermore, improved survival with rIFN-α was associated with the achievement of a cytogenetic response and, although the median time to CCyR was 9–18 months, this suggested the first response biomarker that might be prognostic for survival. However, toxicities with rIFN-α were more common than with busulphan or hydroxyurea, with 4–18% of patients discontinuing due to side-effects. Adding arabinosyl cytosine to rIFN-α reduced the time to cytogenic response, but led to increased toxicity and 5-year survival rates were not increased [43].

5
(PEG-IFNα-2b; PEG-Intron®)

6
(PEG-IFNα-2a; Pegasys®)
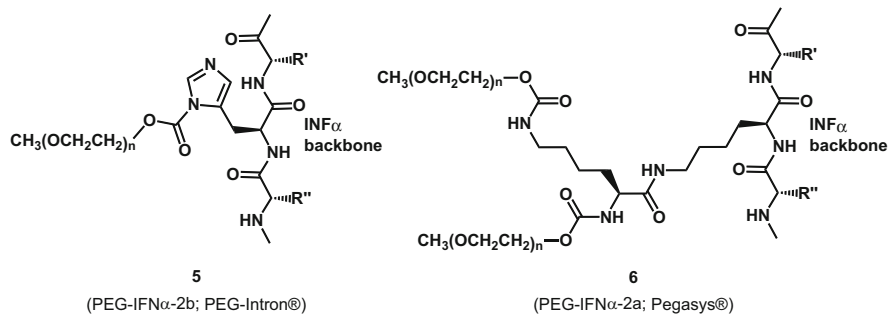
Covalently attaching one or more linear or branched poly(ethylene oxide) (PEG) side-chains (pegylation) of various molecular weights to therapeutic proteins is an established strategy to improve their pharmacological properties. In the case of INF-α two such products were developed for the treatment of CML: **5** (PEG-INF-α-2b; PEG-Intron®; Schering-Plough), prepared by attaching rINFα-2b to methoxy-PEG (a single, linear 12 kDa chain), is a mixture of predominantly (95%) mono-pegylated protein, comprising of 48% pegylated-His34 (shown by X-ray crystal-lography to be highly solvent exposed) and 13% pegylated-Cys1, together with smaller amounts of isomers pegylated on various other residues [44]. The second product, **6** (PEG-INFα-2a; Pegasys®; Roche), consists of a mixture of six monopegylated Lys regioisomers, prepared by coupling a Lys side-chain of rINFα-2a to a lysine carrying two 20 kDa PEG dendrons [45]. Both pegylated drugs have an extended half-life, allowing for once-weekly injection and both are efficacious in CML [40, 46]. Although they are important components of treatment regimens for hepatitis C patients [47], PEG-INF-α is now only used for the treatment of CML patients for whom more recent targeted therapies (see following section) are not appropriate.

3 Discovery and Development of Targeted Kinase Inhibitors for the Treatment of CML

The human kinome encodes 517–518 distinct kinases [48, 49], many of which play a central role in signal transduction pathways in all cells. These intracellular en-zymes catalyse the transfer of the terminal phosphate group from adenosine tri-phosphate (ATP) onto particular side-chain hydroxyl groups of serine, threonine or tyrosine amino-acid residues of their client proteins, thus enabling the phosphory-lated residues to provide docking sites for other proteins and thereby allow signal transmission. Because of their critical roles, the tight regulation of kinase activity is crucial and dysregulation by various mechanisms has been observed for many kinases in association with a number of human diseases. Thus gain- or loss-of-function mutations in kinases are frequently the cause of the dysregulated signal transduction in cells leading to the cancer phenotype, and by inhibiting the mutated

kinase in tumour cells, it is often possible to impede cell proliferation and restore apoptosis. Because the ATP-binding sites of kinases are drugable, these enzymes are particularly attractive targets for cancer therapy [1]. However, the sequence homology of the ATP-binding site is highly conserved across the kinome, so that adequate selectivity towards a particular target is often difficult to achieve.

The treatment landscape for CML changed substantially with the introduction of targeted therapies. These drugs have been designed and developed on the foundations of the enhanced understanding of the mechanisms driving CML at the molecular level and Sects. 3.1–3.5 describe the discovery of these agents.

3.1 Imatinib (STI-571; Gleevec®; Glivec®; Novartis Pharmaceuticals)

Although studies had pointed towards the tyrosine kinase activity of BCR-ABL1 as being a potential drug target for the treatment of CML, in the mid-1980s there was considerable scepticism regarding the drugability of protein kinases. This was based upon arguments that it would be demanding for ATP-competitive kinase inhibitors to compete with the millimolar concentrations of ATP in cells and difficult to achieve selectivity, as well as the likelihood of inducing unacceptable side-effects through the inhibition of the target in normal cells. However, with the conviction that protein kinases presented good drug targets for the treatment of cancer, researchers at Ciba-Geigy embarked upon several kinase inhibitor programmes, one of which was directed towards ABL1.
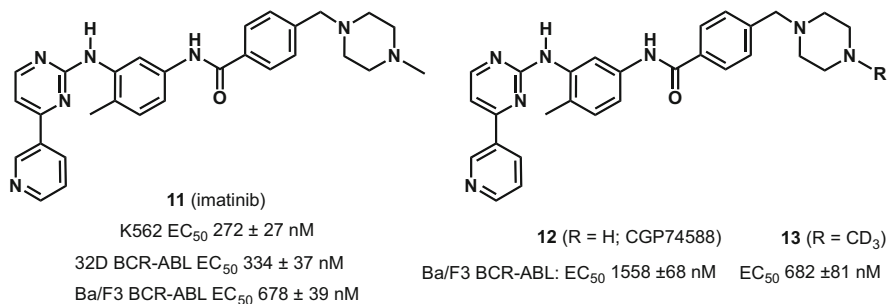
In order to extend their work on staurosporine-related inhibitors of the serine–threonine kinase, protein kinase C (PKC) [50], new chemical starting points were required. PKC inhibitors were known to inhibit histamine release from human basophils [51] and, as one approach to lead-finding (high-throughput screening being unavailable at that time), compounds reported to have anti-inflammatory properties as a result of unknown mechanisms were evaluated for their effects on PKC. A patent from American Cyanamid disclosed a series of 2-aminopyrimidines that inhibited histamine release from human leukocytes [52, 53] and as an example compound **7** was synthesised and found to be an ATP-competitive inhibitor of PKCα (K_i 3.2 μM) [54]. Compound **7** was also found to inhibit several other kinases (as assessed by phosphorylation of peptide substrates by recombinant kinase domains), with a rank order of potency (IC_{50} μM) of PKCα (1.0) > SRC (1.7) > ABL1 (2.6) > PKCδ (21) > EGFR, PKA (>100). To extend their studies on ABL1 kinase inhibitors [55], this new kinase inhibitor chemotype was optimised towards this target [56–58].

		R2				
	R1	H	H	CH$_3$	H	CH$_3$
	Compound	7	8	9 (CGP53716)	10	11
ABL1 IC$_{50}$ (μM)		2.63 ± 2.04	0.4 (n=1)	0.36 ± 0.14	0.1 (n=1)	0.08 ± 0.06
PKCa IC$_{50}$ (μM)		1.0 (n=1)	1.2 (n=1)	72 (n=1)	>10	>100
SRC IC$_{50}$ (μM)		1.70 ± 0.14	15.7 (n=1)	>100	7.8 (n=1)	>100

Two key SAR findings were that activity against SRC was reduced by replacing the imidazole with benzamide moieties (e.g. as in **8**), and that the introduction of an *ortho*-methyl group (e.g. **9**), which increased the torsion angle between the pyrimidine and toluene rings, abrogated activity against PKC, but maintained potency against ABL1. However, aryl amides such as **9** (logP$_{oct/water}$ 4.2; solubility 2 mg L^{-1} at pH 4, i.e. 5,200 μM) failed to demonstrate target inhibition in cellular assays, which was attributed to their high lipophilicity and poor aqueous solubility. In an attempt to improve solubility, the effect of incorporating polar groups, such as the ionisable *N*-methylpiperazine moiety, was investigated. Based upon the SAR for ABL1 inhibition, the *N*-methylpiperazine was attached to the *para*-position of the benzamide ring via a methylene-linker in order to avoid the introduction of a further aromatic amino group, in the belief that this would extend out of the protein into the aqueous phase and therefore not interfere with ligand binding.

This strategy afforded **11** (imatinib; logP$_{oct/water}$ 3.1; solubility >200 mg L^{-1} at pH 4), whose biochemical potency translated into inhibition of ABL1 tyrosine autophosphorylation in transfected murine PB-3c mast cells and full-length BCR-ABL1 kinase in transfected murine 32D haematopoietic cells, but had no effect on SRC tyrosine kinase activity in 32D SRC cells [59, 60]. Most encouragingly, the compound also showed similar antiproliferative activity in human BCR-ABL1 dependent K562 blast crisis CML cells as it had done in BCR-ABL1 transformed murine haematopoietic cell lines (PB-3c, 32D or Ba/F3). The effects in cells further translated into efficacy in a tumour model, where intraperitoneal administration of **11** dose-dependently inhibited the growth of BCR-ABL1 dependent xenografts in mice, but was inactive against SRC-driven tumours [60].

11 (imatinib)

K562 EC$_{50}$ 272 ± 27 nM

32D BCR-ABL EC$_{50}$ 334 ± 37 nM

Ba/F3 BCR-ABL EC$_{50}$ 678 ± 39 nM

12 (R = H; CGP74588)   **13** (R = CD$_3$)

Ba/F3 BCR-ABL: EC$_{50}$ 1558 ±68 nM   EC$_{50}$ 682 ±81 nM

Although initial development as an intravenous infusion failed, the development of an oral formulation was successful and Phase I clinical trials with the β-crystal form of the methanesulphonate salt of imatinib started in 1998, with once-daily oral dosing in CML patients who had failed IFNα therapy. For an anticancer drug the findings, which were first presented in 1999, were unprecedented [61, 62]. The drug was rapidly absorbed giving dose-proportional increases in exposure with a plasma half-life of 13–16 h, and 53 of 54 patients who received doses of ≥300 mg day^{-1} for a period of at least 4 weeks, achieved a CHR and, of these, 13% had a CCyR. Phase II studies, which commenced in 1999, substantiated the early results and following accelerated review, the drug (Gleevec®; Glivec®) was approved by the US Food and Drugs Administration (FDA) in 2001 for the treatment of CML refractory to treatment with IFNα. A Phase 3 open-label trial that compared imatinib to the previous standard of care IFNα plus cytarabine showed significantly greater CCyR response rate and improved survival [63] and confirmed the long-term safety and durability of response [64]. Imatinib then became standard of care for first-line treatment of CML and set a new paradigm for cancer therapies targeted towards the underlying genomic mutation driving a malignancy.

The next major breakthrough with imatinib, which has had a major impact on kinase inhibitor design [65, 66], was the elucidation of the structural basis for the inhibition of ABL1 kinase by imatinib. The highly conserved catalytic domains of protein kinases have a bilobal structure, connected through a segment known as the 'hinge-region'. The *N*-lobe, which contains a five-stranded beta sheet and an αC-helix binds ATP through its adenine, and the *C*-lobe, comprising of α-helices and an 'activation-segment' that positions the Mg involved in phosphate-transfer and binds substrate proteins [67]. Kuriyan and colleagues described X-ray structures of un-phosphorylated murine ABL1 bound to several inhibitors, which indicated that imatinib inhibited phosphorylation activity by stabilising an inactive conformation of the ABL1 kinase domain [68–70]. Thus, imatinib binds within the cleft between the *N*- and *C*-lobes of the protein, with the phosphate-binding, glycine-rich G-loop of the *N*-lobe folding down to form a cage around the pyridine, pyrimidine and phenylamine groups of the inhibitor (Fig. 3a). Most importantly, in this mode of binding, imatinib induces an inactive conformation of the activation segment (A-loop; coloured cyan in Fig. 3a). In this conformation the *N*-terminal segment containing
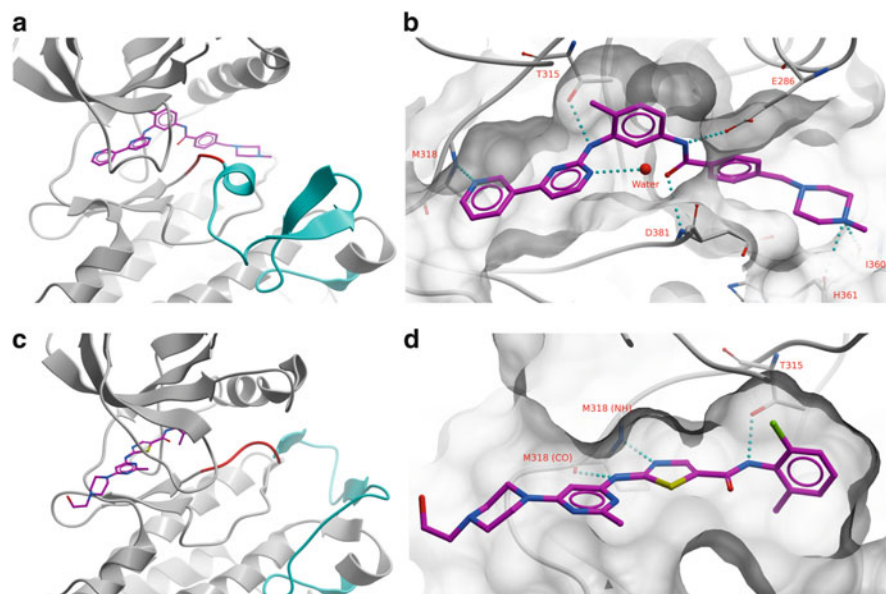
Fig. 3 Cartoon representations of the crystallographic binding modes of imatinib (Protein database, PDB entry: 2HYY) [71] and dasatinib (PDB entry: 2GQG) [72] to the catalytic domain of ABL1 kinase. Protein backbones are coloured in *grey*, with the DFG motifs highlighted in *red* and the activation loops in *cyan*; hydrogen bonds are indicated by *dotted lines* and water molecules are shown as *red spheres*. Figure 3a shows an overview of imatinib bound to an inactive conformation of ABL1 whereas Fig. 3c shows dasatinib bound to the active conformation. Key interactions made by imatinib and dasatinib with the protein are shown in Fig. 3a and d respectively. For imatinib, the 'back-pocket' is opened up by the DFG motif adopting an out-conformation, whereas for dasatinib the DFG-in conformation results in a closed 'back-pocket'

the conserved DFG motif (Asp381-Phe382-Gly383; coloured red), the aspartate residue of which normally has a role in positioning Mg and the phosphates of ATP, adopts a 'DFG-out' conformation, in which the phenylalanine flips out to form contacts with the inhibitor. The rest of the activation loop also assumes an inactive conformation where the segment of the loop containing Tyr393 imitates the substrate by binding in and blocking the substrate cleft of the enzyme. Thus, imatinib binds to and therefore stabilises an inactive conformation of ABL1, impeding the enzyme from adopting the catalytically active conformation necessary to bind ATP, which results in it being inhibited. Because the catalytically active conformations of protein kinases that are most conformationally very similar throughout the human kinome, binding an 'inactive' conformation probably contributes to the relatively high selectivity of imatinib towards its target kinase [73–75]. Following the discovery of this important binding mode, protein kinase inhibitors that bind to their targets in an 'imatinib-like' DFG-out conformation are typically classified as 'type-2' inhibitors, in contrast to 'type-1' inhibitors which bind to the DFG-in conformation in direct competition with ATP [65].

At the atomic level, imatinib interacts with ABL1 via a large number of van der Waals interactions which play a major part in driving the binding energy, and these are supplemented by an array of hydrogen bonds that define the geometry of the interactions (Fig. 3b). Imatinib participates in six direct hydrogen-bond interactions with the protein, involving the pyridyl-N and the backbone-NH of Met318 in the hinge-region, the pyrimidine-NH and the side-chain hydroxyl of Thr315, the amido-NH and side-chain carboxylate of Glu286, as well as the amido-C=O and backbone-NH of Asp381, and two involving the protonated *N*-methylpiperazine group with the backbone C=O of Ile360 and His361. In addition, a pyrimidine-N atom of imatinib makes a strong interaction with a water molecule, whose position is probably also favoured by stacking face-on to the methylphenyl group and additional hydrogen bonds to other well-defined water molecules. Thus, counter to the original design principle, the *N*-methylpiperazine is not solvent exposed, but makes key interactions with the protein, which presumably help to counteract the energy cost of desolvation upon binding.

Despite the success of imatinib therapy, those chronic phase CML patients not achieving a CCyR, or patients who were diagnosed in more advanced stages of the disease, often rapidly lost their initial responses to the drug and relapse [76, 77]. Examination of peripheral blood and bone marrow cells from patients showed that the emergence of imatinib-resistance and subsequent relapse resulted from reactivation of BCR-ABL1 signalling in the leukemic cells [78]. Furthermore, analysis of *BCR-ABL1* RNA from relapsed patients revealed a single cytosine to thymine substitution in the *ABL1* sequence, that encodes isoleucine in place of threonine at position 315 and that the tyrosine kinase activity of the Thr315Ile mutant form of BCR-ABL1 was not inhibited by imatinib. This insensitivity was readily explained on a molecular basis, since the binding of imatinib to ABL1 involves an H-bond to the side-chain of Thr315, and the isoleucine substitution abrogates this, and introduces a steric clash with its more bulky side-chain. Subsequently, more than 100 BCR-ABL1 mutations have been detected in imatinib-resistant patients [79]. These resistant mutations either impede binding by directly changing the surface between imatinib and the kinase domain, leading to steric clashes and/or the loss of hydrogen-bond interactions (e.g. Thr315Ile), or destabilise the imatinib-binding conformation, such that the active DFG-in conformation becomes thermodynamically preferred. An example of the latter case is the Glu255Val substitution, where loss of H-bond interactions between the side-chains of Glu255 and those of Tyr257 and Lys247 destabilise the DFG-out conformation [71, 73]. Such structural-based explanations of why most of the resistant mutations impeded binding provided compelling evidence that the crystallographically observed binding mode of imatinib is physiologically relevant, which is not always the case.
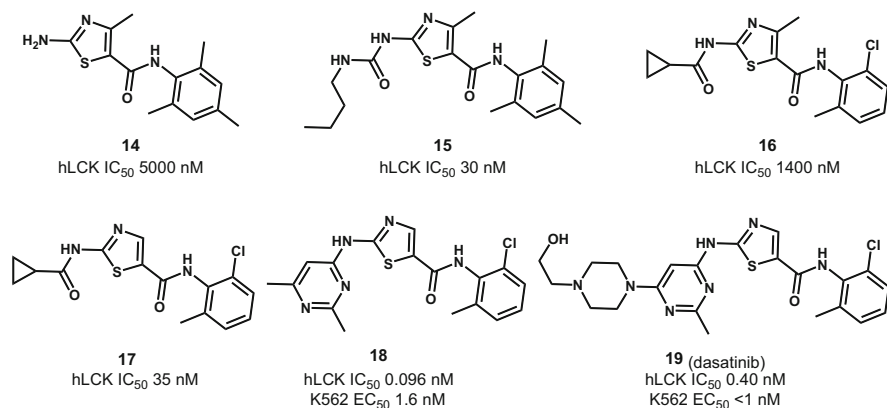
Although in most patients following oral administration, imatinib is well absorbed with high bioavailability, it is metabolically deactivated by *N*-demethylation to **12** [80, 81]. Thus among newly diagnosed CML patients, the quartile with the lowest imatinib exposure has been shown to achieve an inferior clinical response rate and had a mean steady-state trough level of **12** (153 ng mL^{-1}), which was 32% of that of imatinib (490 ng mL^{-1}) and ranged up to 84%. Patients with such inferior responses are more likely to develop resistance. However, an attempt to improve efficacy by hindering

metabolism, by employing the deuterium isotope effect as in compound **13**, did not appear to hinder 'demethylation' in preclinical pharmacokinetic studies.

In terms of target selectivity, in cellular assays imatinib inhibits the kinase activity of the discoidin domain receptors (DDR1 and DDR2), the stem cell factor receptor (KIT), the platelet-derived growth factor receptors (PDGFRα and PDGFRβ) and the colony stimulating factor receptor (CSF-1R) [82] and the activity against KIT, PDGFRβ and CSF-1R has translated into clinical use of the drug as standard of care in the treatment of gastrointestinal stromal tumours, chronic myelomonocytic leukaemia and pigmented villonodular synovitis, respectively.

3.2 *Dasatinib (BMS-354825; Sprycel*®*; Bristol-Myers Squibb)*

An awareness of the proof-of-concept and efficacy of imatinib in CML prompted a number of research groups to evaluate the activity of other kinase inhibitors against ABL1. At Bristol Myers Squibb such an approach led to the development of dasatinib, which originated from an immunology drug discovery programme, and was eventually approved for use in CML.

14
hLCK IC$_{50}$ 5000 nM

15
hLCK IC$_{50}$ 30 nM

16
hLCK IC$_{50}$ 1400 nM

17
hLCK IC$_{50}$ 35 nM

18
hLCK IC$_{50}$ 0.096 nM
K562 EC$_{50}$ 1.6 nM

19 (dasatinib)
hLCK IC$_{50}$ 0.40 nM
K562 EC$_{50}$ <1 nM

Initially, this programme was focused on discovering inhibitors of lymphocyte specific kinase (LCK). LCK is a member of the SRC-family of cytosolic kinases [83] and it plays a fundamental role in T-cell signalling. Inhibitors of LCK have been postulated to have potential as immunosuppressive agents in the treatment of autoimmune and anti-inflammatory diseases. High-throughput screening identified **14** as a lead compound that inhibited the recombinant human LCK catalysed trans-phosphorylation of enolase protein substrate with an IC$_{50}$ of 5 μM [84, 85]. During the course of lead optimisation, 2,6-disubstitution of the aniline was found to be optimal and a dramatic increase in potency was observed upon carbonylation of the

thiazole amino group, as with the urea **15**. Subsequently, whereas replacing the thiazole methyl substituent with either hydrogen or other groups generally attenuated activity, a surprising finding was that in the case of the cyclopropylamide derivative **16**, the desmethyl compound **17** was 40-fold more potent. A rationale for the potency of **16** was developed from docking studies with a model of LCK and suggested that the carbonyl group of the cyclopropylamide did not directly interact with the protein. This prompted the synthesis of constrained 'amide mimetics', such as the heterocyclic analogue **18**, which had substantially improved activity. Selectivity testing revealed that **18** potently inhibited all of the SRC-family kinases, as well as ABL1, with subnanomolar activity. With the realisation of the potential of this chemotype for oncology indications, the effects of **18** were evaluated for effects on a panel of human cancer cell lines, including blast crisis CML K562 cells, where it potently inhibited proliferation (EC_{50} 1.6 nM). Further optimisation of **18** by appending polar substituents on the pyrimidine ring, culminated in the discovery of dasatinib (BMS35425), **19** [86], as a broad spectrum kinase inhibitor that inhibits ABL1 and SRC-family kinases in biochemical assays with subnanomolar IC_{50} values [75]. Dasatinib possessed potent antiproliferative activity against K562, as well as human breast, colon and prostate cells lines, and had a favourable pharmacokinetic profile such that the in vitro activity translated into tumour regression following once-daily, oral administration of 5 mg kg^{-1} day^{-1} to nude mice bearing K562 xenografts [87].

The crystal structure of dasatinib in complex with unphosphorylated human ABL1 kinase has been determined at 2.4 Å resolution [72] and shows that it binds to an active conformation of ABL1 (Fig. 3c) with the 'DFG-in' motif (coloured red in the figure) and the A-loop (coloured cyan) folding away from the ATP-binding pocket. This type-1 binding mode has been confirmed by nuclear magnetic resonance studies, where the DFG-out, inactive conformation seen with imatinib could not be detected [88]. Dasatinib has a good topological fit within its binding site, with the 2-chloro-6-methylphenyl moiety being orthogonal to the thiazole and occupying a narrow hydrophobic cleft. The resulting van der Waals interactions are supplemented by three hydrogen bonds (Fig. 3d): The pyrimidine-NH and the thiazole-N interact with the backbone C=O and –NH of the hinge-region Met318, and the amine-NH forms an H-bond with the side-chain hydroxyl of Thr315. The hydroxyethylpiperazine group of dasatinib rests upon the solvent-exposed surface of the protein and does not appear to be engaged in any hydrogen bonds.

By binding strongly within the ATP-binding site, dasatinib efficiently competes with ATP. As a consequence, with a different binding mode to that of imatinib, dasatinib maintains cellular activity against 18 of 19 imatinib-resistant BCR-ABL1 mutations, although the T315I mutation remains refractory due to the loss of interaction T315 and steric clash with the bulky isobutyl chain the isoleucine [89, 90]. However, in binding the more highly conserved active conformation, dasatinib is less selective than imatinib and inhibits many additional protein kinases at physiologically relevant concentrations [74, 75].

On the basis of its preclinical efficacy, pharmacokinetic and safety profile, dasatinib was selected for development and proceeded into clinical trials. Following encouraging results from a phase I dose-escalation study in imatinib-resistant or -intolerant CML [91], phase II studies were performed in different patient populations with a dasatinib starting dose of 75 mg twice-daily (BID) (reviewed in Aguilera and Tsimberidou [92]). In chronic phase CML, 91% of patients achieved CHR and 49% achieved CCyR leading to mean progression free survival (PFS) at 15 months of 90% [93]. Furthermore, in accelerated phase disease the CHR and CCyR rates were 39% and 24%, respectively, providing for 76% PFS at 10 months [94], and although similar reductions in tumour burden were achieved in blast crisis, PFS in these patients was ≤6.7 months. On the basis of these preliminary results, dasatinib (Sprycel®) received its first approval from the FDA for the treatment of imatinib-resistant and -intolerant patients in all three phases of CML in 2006. Phase III dose-optimisation studies in chronic phase patients showed that dasatinib at 100 mg QD gave comparable responses to 70 mg BID, but with an improved safety profile and this led to the approval of the lower dose for use in this setting.
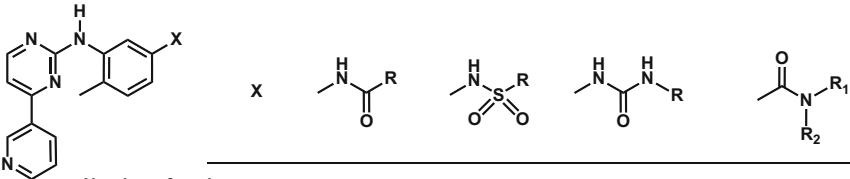
With efficacy and safety having been confirmed, clinical trials were initiated to compare dasatinib (100 mg QD) with imatinib (400 mg QD) in newly diagnosed chronic phase CML [95]. The 12-month data from the pivotal DASISION trial revealed that the CCyR rate was higher with dasatinib than with imatinib (77% vs 66%) and that the achievement of MMR was also higher (46% vs 28%). Based upon these findings and both drugs having a similar safety profile, dasatinib received approval from the FDA in 2010 for the treatment of newly diagnosed CML patients.
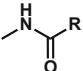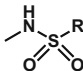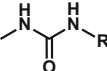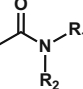
As in the case of imatinib, CML patients (particularly those with advanced disease) can develop resistance to dasatinib, usually through the emergence of clones carrying BCR-ABL1 mutations that impede the binding of the drug to the ABL1 kinase domain [72, 96]. These are most frequently single mutations (T315I, F317L/V/I/C and V299L), although multiple mutations have also been detected [97].

The dose-limiting toxicities with dasatinib are primarily myelosuppression and pleural effusion, with tolerability being generally good. An increased incidence of infections has been noted, which is probably related to SRC-family kinase inhibition [95, 96]. Consequently, the side-effects are managed by coadministration of other medications or, in the case of intolerance, by switching to an alternative BCR-ABL1 inhibitor. However, despite the tolerability of the drug at doses used in CML, the promising preclinical target profile and efficacy of dasatinib in murine tumour models have not translated into adequate clinical efficacy in malignancies other than Ph-positive leukemias.

3.3 Nilotinib (AMN107; Tasigna®; Novartis Pharmaceuticals)

Based upon the early clinical trial data for imatinib and knowing that doubling the standard 400 mg dose could result in improved responses [98], medicinal chemists at Novartis postulated that adequate exposure to a more potent BCR-ABL1 inhibitor might provide greater efficacy. Furthermore, by reducing the residual pool of CML cells in patients, it was thought that the emergence of resistance would be slowed. Consequently, using the knowledge gleaned from crystallographic studies on liganded-ABL1 complexes, a structure-guided strategy to reengineer the imatinib-chemotype was adopted [71]. This commenced with keeping the hinge-binding pyridylpyrimidine fragment fixed, and probing the pocket opened up in the DFG-out conformation with focused libraries employing various linker groups, X:
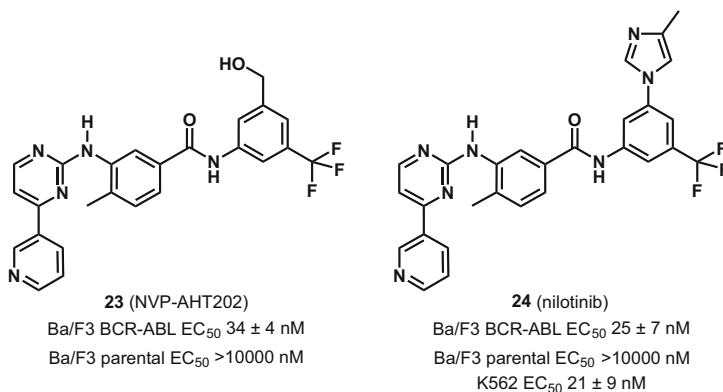

X	$\overset{H}{N}\overset{}{\underset{O}{C}}R$	$\overset{H}{N}\overset{}{\underset{O}{S}}\overset{R}{\underset{O}{}}$	$\overset{H}{N}\overset{}{\underset{O}{C}}\overset{H}{N}R$	$\overset{O}{C}\overset{R_1}{\underset{R_2}{N}}$
Number of analogues	135	20	61	80
Optimal substituent R	3-F$_3$CC$_6$H$_4$ (20)	None	3-Me$_2$NC$_6$H$_4$ (21)	3-F$_3$CC$_6$H$_4$ / H (22)
ABL IC$_{50}$ (nM)	85 ± 35	> 5000	47 ± 8	27 ± 10

Whereas the sulphonamides with their marked N-S-C-C torsion angles were devoid of activity, the relatively planar carboxamide and urea series each provided compounds with potent activities. The ureas (typified by compound 21) were optimised against PDGFR [99], but the most promising lead compounds for ABL1 (assessed by their effects on transphosphorylation of poly(AEKY) substrate) were from the anilide (X = NHCOR) and benzamide chemotypes (X = CONR$_1$R$_2$), bearing meta-trifluoromethyl substituted phenyl groups, 20 and 22, respectively.

Soon after this research commenced it was recognised that there was a poor correlation between different biochemical assay formats used to assess the effects of compounds on recombinant ABL1 kinase constructs, as well as little correlation between the biochemical assays and cellular effects [100]. Consequently, for further SAR studies a pragmatic approach was adopted employing BCR-ABL1 dependent cell proliferation assays, with the anti-proliferative data (EC$_{50}$) being corroborated with effects on BCR-ABL1 autophosphorylation using a capture enzyme-linked immunosorbent assay (ELISA) [101].

SAR studies to optimise the binding interactions of the lead series were supported by X-ray crystallography with emphasis on improving the topological fit to the pocket opened up in the DFG-out conformation of ABL1. This revealed that the trifluoromethylphenyl group could be further substituted, both to increase potency and selectivity

towards BCR-ABL1, as well as to optimise drug-like properties (e.g. lipophilicity, oral bioavailability, cytochrome P450 inhibition). An early discovery was **23**, the hydroxy-group of which participated in a water mediated H-bond with the side-chain of Asp381 in ABL1. However, despite having an excellent kinase inhibition profile, this compound had poor drug-like properties and alternative H-bond donor/acceptor substituents were investigated [71].

23 (NVP-AHT202)
Ba/F3 BCR-ABL EC_{50} 34 ± 4 nM
Ba/F3 parental EC_{50} >10000 nM

24 (nilotinib)
Ba/F3 BCR-ABL EC_{50} 25 ± 7 nM
Ba/F3 parental EC_{50} >10000 nM
K562 EC_{50} 21 ± 9 nM

These studies culminated in the discovery of nilotinib (**24**), which showed up to 30-fold greater potency than imatinib against BCR-ABL1, together with an improved selectivity profile (rank order of inhibition in cellular assays DDR-1/-2 > BCR-ABL1 > PDGFR > KIT > EPHB4 > CSF-1R, compared to that of imatinib of DDR-1/-2 > PDGFR > KIT > BCR-ABL1 > CSF-1R > > EPHB4) [82, 102]. Consistent with a good pharmacokinetic profile in rodents, whereas vehicle-treated mice developed a rapidly fatal CML-like disease following inoculation of 32D cells transfected to express BCR-ABL1 and luciferase, oral treatment with nilotinib dose-dependently reduced disease burden, as assessed by light emission, with tumour stasis observed at 45 mg kg^{-1} QD or 30 mg kg^{-1} BID [103, 104].

The crystal structure of nilotinib in complex with unphosphorylated human ABL1 kinase has been determined at 2.2 Å resolution [71, 98]. This shows that the drug binds in a similar manner to that of imatinib, with the P-loop folding down to form a cage around the pyridine, pyrimidine and phenylamine groups of the inhibitor, and the *N*-terminal part of the A-loop containing the conserved DFG motif adopting a 'DFG-out' conformation, in which the phenylalanine flips out to form contacts with the inhibitor (Fig. 4a). However, there are major differences in the molecular interactions through which the drugs bind (compare Fig. 3b). Nilotinib participates in four direct hydrogen-bond interactions with protein, involving the pyridyl-N and the backbone-NH of Met318, the anilino-NH and the side-chain hydroxyl of Thr315, the amido-NH and side-chain carboxylate of Glu286, as well as the amido-C=O and backbone-NH of Asp381. In addition, a pyrimidine-N atom of nilotinib makes a strong interaction with a water molecule, whose position is probably also favoured by stacking face-on to the
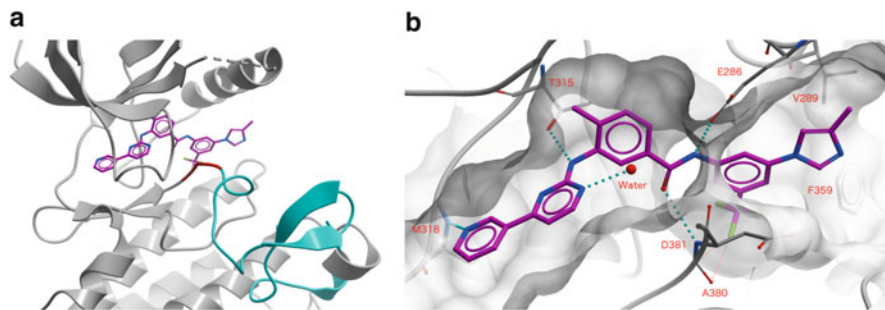
Fig. 4 Cartoon representations of the crystallographic binding mode of nilotinib (PDB entry: 3CS9) [102] to the catalytic domain of ABL1 kinase. The protein backbone is coloured in *grey*, with the DFG motif highlighted in *red* and the activation loop in *cyan*; hydrogen bonds are indicated by *dotted lines* and water molecules are shown as *red spheres*. Figure 4a shows an overview of nilotinib bound to an inactive conformation of ABL1 and Fig. 4b highlights key interactions to protein; this binding mode is similar to that of imatinib (Fig. 3a, b). In addition to the hydrogen bond to the A380 backbone NH, the CF_3 group makes an electrostatic interaction with the A380 backbone carbonyl

methylphenyl group and additional hydrogen bonds to other well-defined water molecules (Fig. 4b). There are also close contacts between carbon atoms of nilotinib and both the carbonyl group of Met318 and the carboxyl group of Glu286, indicating weak hydrogen-bond interactions [105]. In addition, nilotinib participates in an electrostatic interaction involving a fluorine of the trifluoromethyl group and the polarised carbon of the carbonyl group of Ala380 (Fig. 4b). This type of C-F to C=O interaction has been seen in other protein-ligand complexes [106], in which the carbonyl bond is perpendicular to the C-F bond (angle $F \ldots C - O = 90°$) and the distance between the F and C atoms is on average 3.1 Å. The average distance in the four molecules in the asymmetric unit of the nilotinib complex is 3.0 Å, and the atoms are also at 90°, indicating that this interaction between the electronegative F and the positively polarised C of the carbonyl group is contributing favourably to the binding of nilotinib. The imidazole group does not make any H-bonds interactions with the protein, but makes important van der Waals interactions with Glu286, Val289 and Phe359.

The strong binding of nilotinib to ABL1 is reflected in it having a slow kinetic off-rate [101, 107], reflecting prolonged target engagement, which is a common characteristic of type-2 kinase inhibitors due to the process of conformational selection [66]. Thus in binding to dephosphorylated ABL1, nilotinib showed a k_{off} rate of $8.2 \times 10^{-5} \ s^{-1}$ (corresponding to a residence time of 200 min) compared to values of 59×10^{-5} and $110 \times 10^{-5} \ s^{-1}$ obtained for imatinib and dasatinib, respectively (the latter fast off-rate is typical of type-1 kinase inhibitors). The slow binding kinetics of nilotinib and imatinib are therefore consistent with the enigmatic lack of correlation seen between biochemical assays in early studies, since the incubation times (<30 min) used were insufficient for equilibrium to be reached between the drugs and the protein.

Nilotinib inhibits 32/33 tested imatinib-resistant BCR-ABL1 mutants, with T315I remaining resistant [108]. This is consistent with nilotinib having an increased binding affinity to the inactive conformation of the ABL1 kinase domain through largely lipophilic interactions, and a less stringent requirement in the absolute shape and charge of the binding surface of the protein compared to imatinib, which relies upon highly directional H-bonding interactions to make it very sensitive to changes in the protein surface.

The preclinical profile of nilotinib, coupled with a satisfactory preclinical safety assessment, supported the clinical evaluation of the drug as the hydrochloride salt [109]. Because it lacks the basic *N*-methylpiperazine group, nilotinib is significantly less basic (pK_a1 5.6) and more lipophilic (logP 4.9) than imatinib (pK_a1 7.8; logP 3.1). Consequently, whereas imatinib is highly soluble in water nilotinib, as its hydrochloride salt is moderately soluble (0.29 mg mL^{-1}). This led to solubility-limited nilotinib absorption in patients, such that administration of 400 mg BID resulted in a 35% increase in AUC as compared to a once-daily dose of 800 mg [110]. However, 400 mg BID delivered nilotinib steady-state plasma trough levels of 1.95 μM, well above the EC_{50} concentrations required to inhibit the proliferation of most imatinib-resistant cells in vitro. Being well tolerated, this regimen was employed for Phase II studies in imatinib-resistant and -intolerant CML patients. The drug produced sustained cytogenetic and haematological responses, particularly in chronic- and accelerated-phase patients [111, 112] and, as a consequence, nilotinib (Tasigna®) gained FDA approval in 2007 for the treatment of patients with CML in chronic and accelerated phases following imatinib failure. With efficacy at well-tolerated doses having been established in imatinib-resistant CML, a randomised study (ENESTnd) was initiated to compare the efficacy of nilotinib (300 or 400 mg BID) with that of imatinib (400 mg QD) in patients with newly diagnosed CML. The ENESTnd study demonstrated that both doses of nilotinib produced significantly faster and greater reduction in the number of BCR-ABL1 expressing cells than did imatinib, as assessed by CCyR, MMR, MR4 and MR4.5 [113]. The results of this study supported the approval of nilotinib at 300 mg BID in newly diagnosed CML patients in 2010.

As with both imatinib and dasatinib, nilotinib treatment may have to be discontinued in CML patients due to resistance or intolerance. The primary mechanism resulting in nilotinib resistance is the presence of point mutations (most frequently T315I, Y253H, E255K/V and F359V/C), although multiple mutations can also contribute [97]. The structural differences between nilotinib and imatinib result in the two drugs having different safety and tolerability profiles, and this is particularly evident in the lack of cross-intolerance in patients who failed prior therapy with imatinib and have subsequently been treated with nilotinib [82].
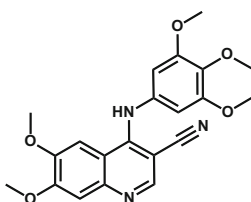
3.4 Bosutinib (SKI-606; Bosulif®; Pfizer)

Researchers at Wyeth-Ayerst first discovered bosutinib (**28**) as a potent inhibitor of the SRC-family kinases and, as for dasatinib, following repositioning this compound
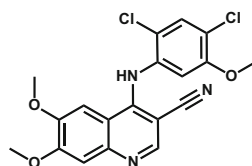
was eventually developed by Pfizer as a BCR-ABL1 inhibitor for the treatment of CML.
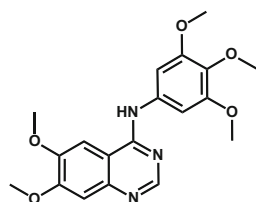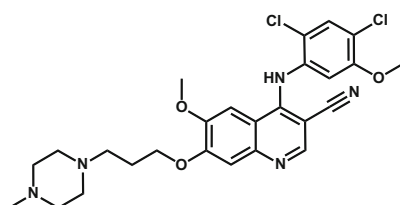

25 (RPR-108518A)
SRC IC$_{50}$ 280 nM

26
SRC IC$_{50}$ 35 nM
EGFR IC$_{50}$ 1500 nM

27
SRC IC$_{50}$ 4.3 nM

28 (bosutinib)
SRC IC$_{50}$ 1.2 nM
K562 EC$_{50}$ 20 nM

The gene product of the Rous avian sarcoma virus (*v-SRC*) was the first onco-gene to be discovered and, in the first report of such an enzyme, Hunter and Sefton found that it encoded a tyrosine kinase (SRC) [114]. Overexpression of SRC and increased SRC kinase activity has been shown to contribute to the growth and pro-gression of a number of human cancers, thereby suggesting that this enzyme could be a valuable target for anticancer therapy [83].

Following the publication that **25**, a member of the anilinoquinazoline class of endothelial growth factor receptor (EGFR) kinase inhibitors, possessed similar ac-tivity against both EGFR and the SRC-family kinase LCK [115], Boschelli and co-workers prepared the corresponding cyanoquinoline derivative **26** and found that it was substantially more potent against SRC-catalysed transphosphorylation of a CDC2 substrate peptide than **25** [116, 117]. As a strategy to improve potency and selectivity towards SRC, alternative aniline substitution patterns were investigated, which re-vealed a steep SAR and led to the identification of **27**, having a seven-fold increase in SRC potency [117, 118]. In order to improve efficacy against the proliferation of SRC-dependent rat fibroblasts, the effects of elaboration of the quinoline methoxy groups were investigated, resulting in the discovery of bosutinib **28**, which had an EC$_{50}$ of 100 nM in the cellular assay. In murine tumour models, bosutinib inhibited the growth of SRC-dependent xenografts following intraperitoneal administration (25–30 mg kg^{-1} BID) and was also active in an HC29 colon carcinoma model following oral

administration (50 mg kg^{-1} BID), despite showing only weak (EC$_{50}$ 5 μM) antiproliferative activity against HC29 cells.

Further profiling revealed that in addition to inhibiting the SRC-family kinases, bosutinib also potently inhibited ABL1 kinase activity and showed antiproliferative activity in CML cell lines, with ten-fold greater efficacy than imatinib in K562 cells [119]. Consistent with its in vitro profile, oral administration of bosutinib (100 mg kg^{-1}) to mice bearing K562 xenografts resulted in tumour regression and increased animal survival, which supported further preclinical development towards use in CML [120].

The co-crystal structure of bosutinib bound to ABL1 (Fig. 5a) shows that the protein adopts the active conformation, with the 'DFG-in' motif and the A-loop folding away from the ATP-binding pocket [121]. The quinoline-N of bosutinib makes an H-bond with the backbone amide-NH of the hinge-region residue Met318 and the cyano-group makes van der Waals contacts with the side-chain of the 'gate-keeper' Thr315 (Fig. 5b). The 2,4-dichloro-5-methoxyaniline moiety fills the proximal hydrophobic pocket available in the DFG-in conformation of the protein and the *N*-propoxy-*N*-methylpiperazine moiety extends through a hydrophobic channel out of the ATP-binding site, making further van der Waals contacts with residues of the hinge-region.

Like dasatinib and nilotinib, bosutinib maintains potency against most imatinib-resistant mutant forms of BCR-ABL1, although again the T315I mutation remains uninhibited, due to the additional bulk of the isoleucine leading to a steric clash with the methoxyphenyl moiety [120]. Like the other type-1 inhibitor dasatinib, bosutinib is a rather unselective tyrosine kinase inhibitor [122]. However, a distinguishing feature over dasatinib, imatinib and nilotinib is that bosutinib does not appreciably inhibit either KIT or the PDGFR receptor kinases at physiologically relevant concentrations.

Following encouraging Phase I data, bosutinib (starting dose 500 mg QD) was evaluated in several Phase II studies in patients with the different phases of CML who were resistant or intolerant to imatinib or prior TKI therapies. After attaining
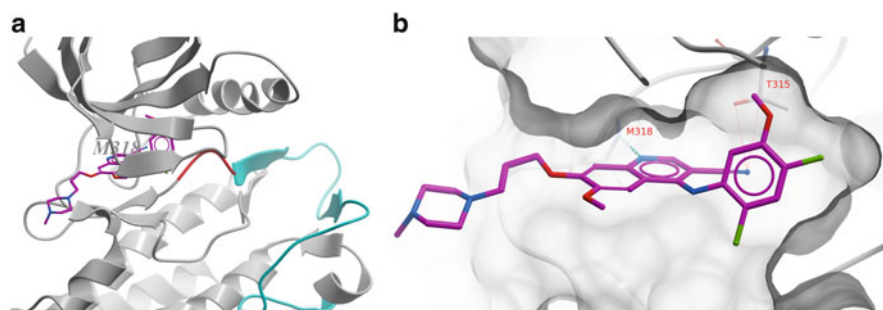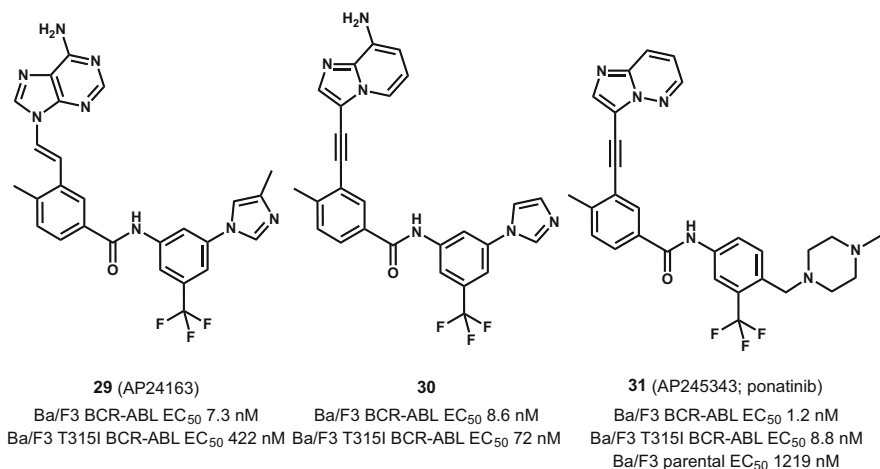

Fig. 5 Cartoon representations of the crystallographic binding mode of bosutinib (PDB entry: 3UE4) [121] to the catalytic domain of ABL1 kinase. The protein backbone is coloured in *grey*, with the DFG motif highlighted in *red* and the activation loop in *cyan*; hydrogen bonds are indicated by *dotted lines*. Figure 5a shows an overview of bosutinib bound to the active conformation of ABL1 and Fig. 5b highlights key interactions to protein; this type-1 binding mode is similar to that of dasatinib (Fig. 3c, d)

satisfactory results (reviewed in Vi Doan and Prescott [123]) bosutinib (Bosulif®) received FDA approval for the treatment of patients with chronic, accelerated, or blast phase Ph + CML with resistance or intolerance to prior therapy in 2012. However, in newly diagnosed CML bosutinib failed to induce a superior CCyR rate compared to imatinib and consequently this drug has not been registered for use as front-line therapy [124]. In comparison to imatinib, the safety profile of bosutinib is characterised by a higher rate of diarrhea, which might result from EGFR inhibition [122], but less frequent neutropenia and oedema, which might be the consequence of bosutinib sparing KIT and PDGFR signalling.

3.5 Ponatinib (AP24534; Iclusig®; Ariad Pharmaceuticals)

As an approach towards dual SRC/ABL1 inhibitors, researchers at Ariad Pharmaceuticals incorporated structural features of nilotinib into a 9-vinyl-6-aminopurine class of inhibitors to give **29**, which possessed modest antiproliferative activity in Ba/F3 cells transformed to express T315I BCR-ABL1 [125]. Modelling provided a clear rationale for the binding mode of **29**, with the vinyl-linker avoiding contact with the Ile315 side-chain of the mutant T315I kinase. Replacing the vinyl-linker with an acetylene and morphing the purine to the amino-imidazopyridine afforded **30**, which possessed greater in vitro potency, but had poor oral bioavailability in rats (5%) [126]. Further optimisation of the heterocycle and modification of the aniline to incorporate imatinib-like features (i.e. solubility and the potential to H-bond to Ile 360 and His 361) resulted in the discovery of ponatinib, **31**, which has more potent antiproliferative activity in both *wt*-BCR-ABL1 and T315I BCR-ABL1 transformed Ba/F3 cells. Following oral administration to rodents, ponatinib displayed improved rat bioavailability (17%) and prolonged plasma half-life; the compound also showed good blood–brain-barrier penetration in mice. Consistent with this profile, ponatinib was efficacious following once-daily oral administration in subcutaneous xenograft models. Markedly, in mice bearing T315I BCR-ABL1 Ba/F3 cell tumours, ponatinib dose-dependently inhibited tumour growth, with 50 mg kg^{-1} day^{-1} resulting in almost complete tumour regression and being well-tolerated for 19 days (body weight decrease <12%).

29 (AP24163)
Ba/F3 BCR-ABL EC$_{50}$ 7.3 nM
Ba/F3 T315I BCR-ABL EC$_{50}$ 422 nM

30
Ba/F3 BCR-ABL EC$_{50}$ 8.6 nM
Ba/F3 T315I BCR-ABL EC$_{50}$ 72 nM

31 (AP245343; ponatinib)
Ba/F3 BCR-ABL EC$_{50}$ 1.2 nM
Ba/F3 T315I BCR-ABL EC$_{50}$ 8.8 nM
Ba/F3 parental EC$_{50}$ 1219 nM

From the crystal structure of ponatinib bound to ABL1, it is clear that the compound binds to the DFG-out inactive conformation of the ABL1 kinase domain (Fig. 6a) [127]. Specifically, the imidazo[1,2b]pyridazine of ponatinib, like the pyridine of imatinib and nilotinib, occupies the adenine pocket of the enzyme, with the N-1 atom participating in an H-bond with the backbone-NH of Met318. Although there is no interaction with the hydroxyl group of Thr315, in the case of the Ile315 mutant, the acetylenic-linkage of ponatinib makes favourable van der Waals interactions with the isoleucine side-chain (Fig. 6b). Like imatinib, despite the different connectivities of the amide group in the two molecules, ponatinib also participates via its amide-NH in an H-bond interaction with the side-chain of Glu286 and via the amide-carbonyl in an
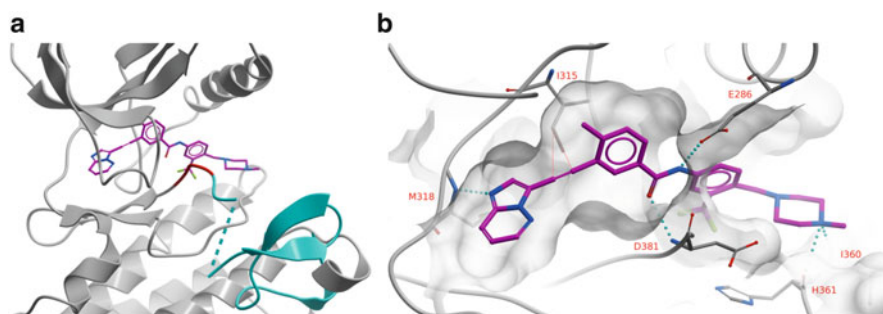

Fig. 6 Cartoon representations of the crystallographic binding mode of ponatinib (PDB entry: 3IK3) [127] to the catalytic domain of ABL1 kinase. The protein backbone is coloured in *grey*, with the DFG motif highlighted in *red* and the activation loop in *cyan*; hydrogen bonds are indicated by *dotted lines*. Figure 6a shows an overview of ponatinib bound to an inactive conformation of ABL1 and Fig. 6b highlights key interactions to protein; this binding mode is similar to that of imatinib (Fig. 3a, b) and nilotinib (Fig. 4), but the drug makes no interaction with the side-chain of T315

H-bond with the backbone-NH of Asp381 to stabilise the DFG-out conformation. Unlike nilotinib, no interaction is seen between the trifluoromethyl group and Ala380. Finally, like imatinib the methylpiperazine group participates in H-bond interactions with the backbone carbonyl groups of Ile360 and His361.

Consistent with this type-2 binding mode, ponatinib maintains potent activity across all common imatinib-resistant BCR-ABL1 mutations, with EC_{50} values in transformed Ba/F3 cells <40 nM [126]. However, in addition to being a potent inhibitor of the SRC-family kinases, it also strongly inhibits many other kinases, including the members of the FGFR, KIT, PDGFR and VEGFR families, although it does not effect the insulin receptor kinase, cyclin-dependent kinase 2 or the aurora kinases.

On the strength of an assessment of efficacy and safety in Phase I studies, where trough plasma concentrations surpassed 40 nM following doses ≥30 mg QD of po-natinib hydrochloride [128], patients harbouring T315I BCR-ABL1 or with resis-tance to two or more targeted BCR-ABL1 inhibitors were enrolled to receive an initial dose of 45 mg day^{-1} in the Phase 2 PACE trial. Ponatinib elicited robust clinical ac-tivity in this heavily pretreated patient population, with response rates meeting the primary trial objectives in all stages of the disease and regardless of mutation status [129]. The early findings from this study prompted the FDA to grant accelerated approval for ponatinib hydrochloride (Iclusig®) in 2012, although with warnings for arterial thrombosis and hepatotoxicity [130]. However in 2013, due to increasing rates of vas-cular thrombotic events, Ariad suspended sales of the drug and a clinical trial compar-ing ponatinib with imatinib was closed [131, 132]. Following risk-benefit reassessment, late in 2013, ponatinib was reintroduced for the treatment of Ph-positive leukemia patients for whom no other tyrosine kinase inhibitor is indicated or for those having the T315I mutation. Whereas it is difficult to attribute a single ponatinib target to its adverse event profile, one might speculate that the safety issues with this drug are the result of the disadvantageous inhibition of a combination of kinase targets.

3.6 Asciminib (ABL001; Novartis Pharmaceuticals)

32 (NVP-BBT594) **33** (GNF-7)
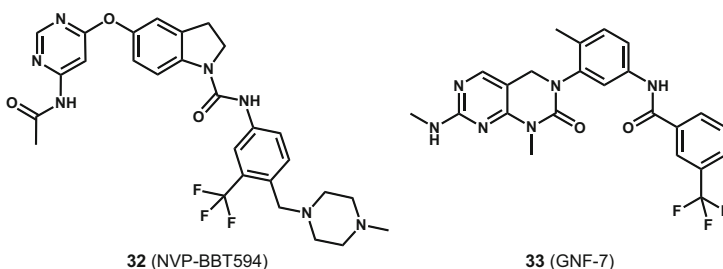
With a legacy of ATP-competitive BCR-ABL1 inhibitors, such as **32** and **33**, that potently inhibited the T315I mutation, but having insufficient selectivity and preclinical safety profiles that were unsatisfactory for their advancement into

clinical studies [133–136], Novartis scientists performed a phenotypic, differential cytotoxicity screen to find new lead structures [137, 138]. This approach afforded **34**, which inhibited the proliferation of BCR-ABL1 transformed murine 32D cells, but had no effect on the parental cell line. Medicinal chemistry optimisation then afforded **35**, which potently inhibited the proliferation of BCR-ABL1 dependent cells, but did not affect the viability of Ba/F3 cells transformed with other oncogenic kinases. It subsequently emerged that these compounds were allosteric inhibitors of the ABL1 kinase.

34 (GNF-1)   **35** (GNF-2)

36 (asciminib)
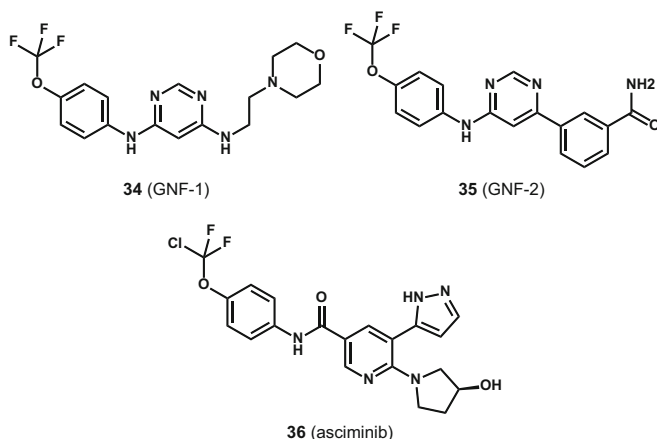
ABL1 is a ubiquitously expressed enzyme and its activity in cells is tightly regulated. One regulatory mechanism involves myristoylation of the Gly2 residue in the *N*-terminal cap (NCap) region (≈80 amino-acid residues) of the ABL1 SH3 domain, with the myristate group then interacting with a binding site within the SH1 catalytic domain leading to the assembly of a catalytically inactive conformation [70]. In CML, the breakpoint on chromosome 9 is such that the Ncap is not transposed to the Ph-chromosome, leading to the loss of myristate autoregulation in BCR-ABL1. Mechanism of action studies using solution NMR, X-ray crystallography, mutagenesis and hydrogen-exchange mass spectrometry confirmed that GNF-2 inhibits ABL1 kinase activity allosterically, by interacting with the myristate-binding site in the SH1 domain, to mimic the myristoylated Gly2-residue and stabilise the inactive conformation of the enzyme [138, 139]. However, optimisation studies on this chemotype did not result in substantial advances towards clinical candidates [140].

In an attempt to capitalise upon this mechanism of action, hit finding activities employing NMR, X-ray crystallography and molecular modelling were undertaken, which identified new lead compounds [141]. Lead optimisation culminated in the identification of asciminib, **36** [142]. Asciminib is a potent and specific inhibitor ABL1/BCR-ABL1, and maintains biochemical and cellular activity against the mutations that lead to clinical resistance of ATP-competitive inhibitors of the enzyme. In a mouse xenograft model (human KCL22 cells), oral administration of asciminib gave dose-dependent inhibition of tumour growth at well-tolerated doses. Furthermore,

combinations of asciminib in combination with the nilotinib prevent the emergence of drug resistance in vitro and in vivo. With this preclinical profile, asciminib was promoted into development and is currently under clinical evaluation in CML patients.

4 Conclusions and Perspectives

The introduction of imatinib in 2001 heralded the new era of cancer therapies targeted towards the underlying genomic mutation driving a particular malignancy [1]. Subsequently, through targeting the ABL1 tyrosine kinase activity of the BCR-ABL1 oncoprotein, medicinal chemistry research has been successful in providing a palette of first-, second- and third-line drugs for the treatment of CML. Although preclinical research activities have identified a number of additional compounds, such as the imatinib-analogue flumatinib (37), the nilotinib-analogue radotinib (38) and the sorafenib-analogue, rebastinib (39) [143–145], these are generally based upon established chemotypes and to date none of these agents have demonstrated appreciable advantages to the established drugs.
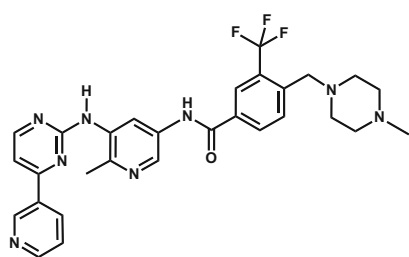
37 (flumatinib)
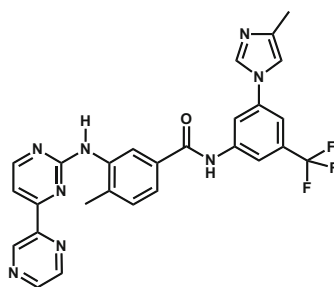
38 (radotinib)
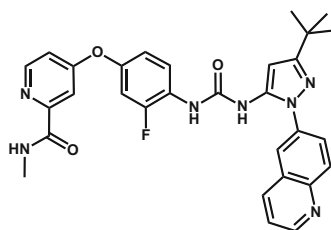
39 (rebastinib)

In terms of clinical practice, following an initial consultation with patients that reveals the potential diagnosis of leukemia, hydroxycarbamide (3) is often administered, pending a diagnosis of CML. Then following detection of either the Ph-chromosome or *BCR-ABL1* RNA, either imatinib (11), dasatinib (19) or nilotinib (24) are usually prescribed as front-line therapies, with the selection typically based upon

the patient's comorbidities that favour one drug over another. If the first-line choice is poorly tolerated or elicits a sub-optimal response, patients can switch therapy as appropriate and if this fails to resolve any issues, then bosutinib (**28**) and ponatinib (**31**) are available. For those patients diagnosed with chronic phase CML, such a strategy aims to prevent the malignancy from progressing to advanced/blast crisis phase and has had a marked impact on prognosis (Fig. 1), with most patients remaining in long-term remission and likely to die of non-CML related causes. The current recommendation is for CML patients to continue tyrosine kinase inhibitor therapy indefinitely, and therefore selecting the most efficacious drug whose adverse event profile that is least impacted by or has a minimal impact on the comorbidities of an individual patients is paramount [146, 147]. However, as discussed below, indefinite therapy might not be necessary for all CML patients.

Historically, the complete remission of CML was only achievable by depleting the patient's bone marrow of cells using high-dose chemotherapy in combination with either busulphan (**4**) or total body radiation, followed by reconstitution with stem cells derived from an appropriate healthy donor [148, 149]. Unfortunately, this procedure is associated with substantial rates of mortality and morbidity, primarily due to acute graft-versus-host disease which necessitates prophylactic immunosuppressant therapy (usually cyclosporin-A). Recently, in clinical trials with chronic phase patients who had deep (beyond MMR) molecular responses on imatinib that had been sustained for more than 2 years, following cessation of CML therapy approximately 40% of patients achieved prolonged treatment-free remission (TFR), and of those who did lose their molecular response, MMR was reattained upon recommencing imatinib [150]. Although prognostic factors for successful TFR have not been established for imatinib-treated patients and definitive studies with dasatinib and nilotinib have not yet yielded mature data, it appears that for at least some chronic phase CML patients, life-long chronic therapy might not be necessary, and that sustained deep responses for just a few years might be adequate to achieve TFR [151]. Additional clinical studies that are designed to ascertain whether combining ABL1 inhibitors with other modalities, such as drugs targeted towards cancer stem cells or agents stimulating the patients' immune systems, are ongoing and might improve the prospects of patients for successful TFR.

Monotherapy with ABL1 kinase inhibitors is clearly inadequate for patients with either accelerated or blast crisis CML. In such cases, there is some hope that chimeric antigen receptor (CAR) therapy might emerge in the future [152]. This immunotherapy approach involves the engineering of the antigen receptor on T-cells to specifically recognise and attack leukemic cells after being introduced into the patient. Other immunological approaches, such as combining ABL1 inhibitors with anti-PD1 antibodies (e.g. dasatinib plus nivolumab), are also under clinical evaluation.

In summary, following the introduction of the iconic drug imatinib, chronic phase CML has been transformed from a malignancy associated with a poor prognosis into a chronic disease, which might become curable in the foreseeable future. This remarkable success can be attributed to multi-disciplinary drug discovery teams being able to capitalise upon the genomic understanding of CML, by developing predictable preclinical models that enabled the medicinal chemists to follow robust structure–activity

data and tune pharmacokinetic properties of potent compounds to furnish developable drugs.

References

1. Manley PW, Holzer P, Möbitz H, Skaanderup PR, Stauffer F (2015) Progress into the era of genomically targeted cancer drugs: 50 years of anticancer medicinal chemistry. Med Chem Rev 50:185–203
2. Neumann E (1872) Ein neuer Fall von Leukamie mit Erkrankung des Knochenmarks. Archives Heilkunde 13:502–508
3. Höglund M, Sandin F, Simonsson B (2015) Epidemiology of chronic myeloid leukaemia: an update. Ann Hematol 94(Suppl 2):241–247
4. Nowell PC (2007) Discovery of the Philadelphia chromosome: a personal perspective. J Clin Invest 117:2033–2035
5. Hunter T (2007) Treatment for chronic myelogenous leukemia: the long road to imatinib. J Clin Invest 117:2036–2043
6. Rowley JD (1973) A new consistent chromosomal abnormality in chronic myelogenous leukaemia identified by quinacrine fluorescence and Giemsa staining. Nature 243:290–293
7. Byrne M, Wray J, Reinert B, Wu Y, Nickoloff J, Lee S-H, Hromas R, Williamson E (2014) Mechanisms of oncogenic chromosomal translocations. Ann N Y Acad Sci 1310:89–97
8. Faderl S, Talpaz M, Estrov Z, O'Brien S, Kurzrock R, Kantarjian HM (1999) The biology of chronic myeloid leukemia. New Engl J Med 341:164–172
9. Griffin JD (1986) Management of chronic myelogenous leukemia. Semin Hematol 23(3 Suppl 1):20–26
10. Radich JP, Dai H, Mao M, Oehler V, Schelter J, Druker B, Sawyers C, Shah N, Stock W, Willman CL, Friend S, Linsley PS (1986) Gene expression changes associated with progression and response in chronic myeloid leukemia. Proc Natl Acad Sci U S A 103:2794–2799
11. Baccarani M, Saglio G, Goldman J, Hochhaus A, Simonsson B, Appelbaum F, Apperley J, Cervantes F, Cortes J, Deininger M, Gratwohl A, Guilot F, Horowitz M, Hughes T, Kantarjian H, Larson R, Niederwieser D, Silver R, Hehlman R (2006) Evolving concepts in the management of chronic myeloid leukemia: recommendations from an expert panel on behalf of the European LeukemiaNet. Blood 108:1809–1820
12. Mahon F-X, Etienne G (2014) Deep molecular response in chronic myeloid leukemia: the new goal of therapy? Clin Cancer Res 20:310–322
13. Press RD (2010) Major molecular response in CML patients treated with tyrosine kinase inhibitors: the paradigm for monitoring targeted cancer therapy. Oncologist 15:744–749
14. Cross NCP, Hochhaus A, Müller MC (2015) Molecular monitoring of chronic myeloid leukemia: principles and interlaboratory standardization. Ann Hematol 94(Suppl 2):219–225
15. Kampen KR (2012) The discovery and early understanding of leukemia. Leuk Res 36:6–13
16. Geary CG (2000) The story of chronic myeloid leukaemia. Br J Haematol 110:2–11
17. Piller GJ (2001) Leukaemia – a brief historical review from ancient times to 1950. Br J Haematol 112:282–292
18. Lissauer D (1865) Zwei Fälle von Leucaemie. Berl Klin Wochenschr 2:403–404
19. Senn N (1903) Case of splenomedullary leukemia successfully treated by the use of Roentgen rays. Med Rec 64:281–282
20. Paulino AC, Reddy SP (1996) Splenic irradiation in the palliation of patients with lymphoproliferative and myeloproliferative disorders. Am J Hosp Palliat Care 13(6):32–35
21. Osgood EE, Seaman AJ, Tivey H (1955) Comparative survival times of x-ray treated versus P32 treated patients with chronic leukemias under the program of titrated, regularly spaced total-body irradiation. Radiology 64:373–381

22. Galton DAG (1956) Use of myleran and similar agents in chronic leukemias. Adv Cancer Res 4:73–112
23. Lawrence JH, Dobson RL, Low-Beer BVA, Brown BR (1948) Chronic myelogenous leukemia: a study of one hundred and twenty-nine cases treated with radioactive phosphorus. JAMA 136:672–677
24. Papac RJ (2001) Origins of cancer therapy. Yale J Biol Med 74:391–398
25. Avendano C, Menendez JC (2008) DNA alkylating agents. In: Medicinal chemistry of anti-cancer drugs. Elsevier, Amsterdam, pp 139–176
26. Haddow A, Timmis GM (1953) Myleran in chronic myeloid leukemia. Chemical constitution and biological action. Lancet:207–208
27. Galton DAG (1953) Myleran in chronic myeloid leukaemia: results of treatment. Lancet:208–213
28. Medical Research Council's Working Party for Therapeutic Trials in Leukaemia (1968) Chronic granulocytic leukaemia: comparison of radiotherapy and busulphan therapy. Br Med J 1(5586):201–208
29. Galaup A, Paci A (2013) Pharmacology of dimethane sulfonate alkylating agents: busulfan and treosulfan. Expert Opin Drug Metab Toxicol 9:333–347
30. Probin V, Wang Y, Zhou D (2007) Busulfan-induced senescence is dependent on ROS production upstream of the MAPK pathway. Free Radic Biol Med 42:1858–1865
31. Dresler WFC, Stein R (1869) Ueber den Hydroxylharnstoff. Justus Liebigs Ann Chem 150:242–252
32. Stearns B, Losee KL, Bernstein J (1963) Hydroxyurea: a new type of potential antitumor agent. J Med Chem 6:201
33. Kennedy BJ, Yarbro JW (1966) Metabolic and therapeutic effects of hydroxyurea in chronic myeloid leukemia. JAMA 195:1038–1043
34. Stevens MR (1999) Hydroxyurea: an overview. J Biol Regul Homeost Agents 13:172–175
35. Alvino GM, Collingwood D, Murphy JM, Delrow J, Brewer BJ, Raghuraman MK (2007) Replication in hydroxyurea: it's matter of time. Mol Cell Biol 27:6396–6406
36. Koc A, Wheeler LJ, Mathews CK, Merrill GF (2004) Hydroxyurea arrests DNA replication by a mechanism that preserves basal dNTP pools. J Biol Chem 279:223–230
37. Hehlmann R, Heimpel H, Hasford J, Kolb HJ, Pralle H, Hossfeld DK, Queisser W, Loffler H, Heinze B, Georgii A (1993) Randomized comparison of busulfan and hydroxyurea in chronic myelogenous leukemia: prolongation of survival by hydroxyurea. The German CML Study Group. Blood 82:398–407
38. Hehlmann R (1988) Cytostatic therapy of chronic myelogenous leukemia: review and perspectives. In: Huhn D, Hellriegel KP, Niederle N (eds) Chronic myelocytic leukemia and interferon. Springer, Berlin, pp 102–112
39. Gonzalez-Navajas JM, Lee J, David M, Raz E (2012) Immunomodulatory functions of type I interferons. Nat Rev Immunol 12:125–135
40. Talpaz M, Mercer J, Hehlmann R (2015) The interferon-alpha revival in CML. Ann Hematol 94(Suppl 2):S195–S207
41. Talpaz M, McCredie KB, Mavligit GM, Gutterman JU (1983) Leukocyte interferon-induced myeloid cytoreduction in chronic myelogenous leukemia. Blood 62:689–692
42. Silver RT, Woolf SH, Hehlmann R, Appelbaum FR, Anderson J, Bennett C, Goldman JM, Guilhot F, Kantarjian HM, Lichtin AE, Talpaz M, Tura S (1999) An evidence-based analysis of the effect of busulfan, hydroxyurea, interferon, and allogeneic bone marrow transplantation in treating the chronic phase of chronic myeloid leukemia: developed for the American Society of Hematology. Blood 94:1517–1536
43. Baccarani M, Rosti G, De Vivo A, Bonifazi F, Russo D, Martinelli G, Testoni N, Amabile M, Fiacchini M, Montefusco E et al (2002) A randomized study of interferon-α versus interferon-α and low-dose arabinosyl cytosine in chronic myeloid leukemia. Blood 99:1527–1535
44. Wang Y, Youngster S, Grace M, Bausch J, Bordens R, Wyss DF (2002) Structural and biological characterization of pegylated recombinant interferon alpha-2b and its therapeutic implications. Adv Drug Deliv Rev 54:547–570

45. Dhalluin C, Ross A, Leuthold L, Foser S, Gsell B, Mueller F, Senn H (2005) Structural and biophysical characterization of the 40 kDa PEG-interferon-α2a and its individual positional isomers. Bioconjug Chem 16:504–517

46. Lipton JH, Khoroshko N, Golenkov A, Abdulkadyrov K, Nair K, Raghunadharao D, Brummendorf T, Yoo K, Bergstrom B (2007) Phase II, randomized, multicenter, comparative study of peginterferon-α-2a (40 kD) (Pegasys) versus interferon α-2a (Roferon-A) in patients with treatment-naive, chronic-phase chronic myelogenous leukemia. Leuk Lymphoma 48:497–505

47. European Association for the Study of the Liver (2015) EASL recommendations on treatment of hepatitis C 2015. J Hepatol 63:199–236

48. Hanks SK (2003) Genomic analysis of the eukaryotic protein kinase superfamily: a perspective. Genome Biol 4:111

49. Manning G, Whyte DB, Martinez R, Hunter T, Sudarsanam S (2002) The protein kinase complement of the human genome. Science 298:1912–1934

50. Meyer T, Regenass U, Fabbro D, Alteri E, Rosel J, Muller M, Caravatti G, Matter A (1989) A derivative of staurosporine (CGP41251) shows selectivity for protein kinase C inhibition and in vitro anti-proliferative as well as in vivo anti-tumor activity. Int J Cancer 43:851–856

51. Morita Y, Takaishi T, Honda Z, Miyamoto T (1988) Role of protein kinase C in histamine release from human basophils. Allergy 43:100–104

52. Torley LW, Johnson BB, Dusza J (1987) Preparation of 4,5,6-substituted 2-pyrimidinamines as allergy inhibitors, antiasthmatics, and hypoglycemics. Eur Patent Appl 233461, 26 Aug 1987

53. Paul R, Hallett WA, Hanifin JW, Reich MF, Johnson BD, Lenhard RH, Dusza JP, Kerwar SS, Lin Y, Pickett WC, Seifert CM, Torley LW, Tarrant ME, Wrenn S (1993) Preparation of substituted N-phenyl-4-aryl-2-pyrimidinamines as mediator release inhibitors. J Med Chem 36:2716–2725

54. Zimmermann J, Caravatti G, Mett H, Meyer T, Mueller M, Lydon NB, Fabbro D (1996) Phenylamino-pyrimidine (PAP) derivatives: a new class of potent and selective inhibitors of protein kinase C (PKC). Arch Pharm 329:371–376

55. Geissler JF, Roesel JL, Meyer T, Trinks UP, Traxler P, Lydon NB (1992) Benzopyranones and benzothiopyranones: a class of tyrosine protein kinase inhibitors with selectivity for the v-abl kinase. Cancer Res 52:4492–4498

56. Zimmermann J (1993) Preparation of 2-anilinopyrimidines as antiatherosclerotics and neoplasm inhibitors. Eur Patent Appl 564409, 6 Oct 1993

57. Zimmermann J, Buchdunger E, Mett H, Meyer T, Lydon NB, Traxler P (1996) (Phenylamino)pyrimidine (PAP) derivatives: a new class of potent and highly selective PDGF-receptor autophosphorylation inhibitors. Bioorg Med Chem Lett 6:1221–1226

58. Zimmermann J, Buchdunger E, Mett H, Meyer T, Lydon NB (1997) Potent and selective inhibitors of the ABL-kinase: phenylaminopyrimidine (PAP) derivatives. Bioorg Med Chem Lett 7:187–192

59. Buchdunger E, Zimmermann J, Mett H, Meyer T, Muller M, Druker BJ, Lydon NB (1996) Inhibition of the Abl protein-tyrosine kinase in vitro and in vivo by a 2-phenylaminopyrimidine derivative. Cancer Res 56:100–104

60. Druker BJ, Tamura S, Buchdunger E, Ohno S, Segal GM, Fanning S, Zimmermann J, Lydon NB (1996) Effects of a selective inhibitor of the Abl tyrosine kinase on the growth of Bcr-Abl positive cells. Nat Med 2:561–566

61. Druker BJ, Talpaz M, Resta DJ, Peng B, Buchdunger E, Ford JM, Sawyers CL (1999) Clinical efficacy and safety of an ABL specific tyrosine kinase inhibitor as targeted therapy for chronic myelogenous leukemia. Blood 94:368a

62. Druker BJ, Talpaz M, Resta DJ, Peng B, Buchdunger E, Ford JM, Lydon NB, Kantarjian H, Capdeville R, Ohno-Jones S, Sawyers CL (2001) Efficacy and safety of a specific inhibitor of the BCR-ABL tyrosine kinase in chronic myeloid leukemia. N Engl J Med 344:1031–1037

63. Roy L, Guilhot J, Krahnke T, Guerci-Bresler A, Druker BJ, Larson RA, O'Brien S, So C, Massimini G, Guilhot F (2006) Survival advantage from imatinib compared with the combination

interferon plus cytarabine in chronic-phase chronic myelogenous leukemia: historical comparison between two phase 3 trials. Blood 108:1478–1484

64. Hochhaus A, O'Brien SG, Guilhot F, Druker BJ, Branford S, Foroni L, Goldman JM, Müller MC, Radich JP, Rudoltz M, Mone M, Gathmann I, Hughes TP, Larson RA (2009) Six-year follow-up of patients receiving imatinib for the first-line treatment of chronic myeloid leukemia. Leukemia 23:1054–1061

65. Liu Y, Gray NS (2006) Rational design of inhibitors that bind to inactive kinase conformations. Nat Chem Biol 2:358–364

66. Tong M, Seeliger MA (2014) Targeting conformational plasticity of protein kinases. ACS Chem Biol 10:190–200

67. Kornevc AP, Taylor SS (2015) Dynamics-driven allostery in protein kinases. Trends Biochem Sci 40:628–647

68. Schindler T, Bornmann W, Pellicena P, Miller WT, Clarkson B, Kuriyan J (2000) Structural mechanism for STI-571 inhibition of Abelson tyrosine kinase. Science 289(5486):1938–1942

69. Nagar B, Bornmann WG, Pellicena P, Schindler T, Veach DR, Miller WT, Clarkson B, Kuriyan J (2002) Crystal structures of the kinase domain of c-Abl in complex with the small molecule inhibitors PD173955 and imatinib (STI-571). Cancer Res 62:4236–4243

70. Nagar B, Hantschel O, Young MA, Scheffzek K, Veach D, Bornmann W, Clarkson B, Superti-Furga G, Kuriyan J (2003) Structural basis for the autoinhibition of c-Abl tyrosine kinase. Cell 112:859–871

71. Cowan-Jacob SW, Fendrich G, Floersheimer A, Furet P, Liebetanz J, Rummel G, Rheinberger P, Centeleghe M, Fabbro D, Manley PW (2007) Structural biology contributions to the discovery of drugs to treat chronic myelogenous leukemia. Acta Crystallogr 63:80–93

72. Tokarski JS, Newitt JA, Chang CYJ, Cheng JD, Wittekind M, Kiefer SE, Kish K, Lee FY, Borzillerri R, Lombardo LJ, Xie D, Zhang Y, Klei HE (2006) The structure of Dasatinib (BMS-354825) bound to activated ABL kinase domain elucidates its inhibitory activity against imatinib-resistant ABL mutants. Cancer Res 66:5790–5797

73. Cowan-Jacob SW, Guez V, Fendrich G, Griffin JD, Fabbro F, Furet P, Liebetanz J, Mestan J, Manley PW (2004) Imatinib (STI571) resistance in chronic myelogenous leukemia: molecular basis of the underlying mechanisms and potential strategies for treatment. Mini Rev Med Chem 4:285–299

74. Bantscheff M, Eberhard D, Abraham Y, Bastuck S, Boesche M, Hobson S, Mathieson T, Perrin J, Raida M, Rau M, Reader V, Sweetman G, Bauer A, Bouwmeester T, Hopf C, Kruse U, Neubauer G, Ramsden N, Rick J, Kuster B, Drewes G (2007) Quantitative chemical proteomics reveals mechanisms of action of clinical ABL kinase inhibitors. Nat Biotechnol 25:1035–1044

75. Karaman MW, Herrgard S, Treiber DK, Gallant P, Corey E, Atteridge CE, Campbell BT, Chan KW, Ciceri P, Davis MI, Edeen PT, Faraoni R, Floyd M, Hunt JP, Lockhart DJ, Milanov ZV, Morrison MJ, Pallares G, Patel HK, Pritchard S, Wodicka LM, Zarrinkar PP (2008) A quantitative analysis of kinase inhibitor selectivity. Nat Biotechnol 26:127–132

76. Druker BJ, Sawyers CL, Kantarjian H, Resta DJ, Reese SF, Ford JM, Capdeville R, Talpaz M (2001) Activity of a specific inhibitor of the BCR-ABL tyrosine kinase in the blast crisis of chronic myeloid leukemia and acute lymphoblastic leukemia with the Philadelphia chromosome. N Engl J Med 344:1038–1042

77. Hochhaus A, La Rosee P (2004) Imatinib therapy in chronic myelogenous leukemia: strategies to avoid and overcome resistance. Leukemia 18:1321–1331

78. Gorre ME, Mohammed M, Ellwood K, Hsu N, Paquette R, Rao PN, Sawyers CL (2001) Clinical resistance to STI-571 cancer therapy caused by BCR-ABL gene mutation or amplification. Science 293:876–880

79. Apperley JF (2007) Part I: mechanisms of resistance to imatinib in chronic myeloid leukemia. Lancet Oncol 8:1018–1029

80. Larson RA, Druker BJ, Guilhot F, O'Brien SG, Riviere GJ, Krahnke T, Gathmann I, Wang Y (2008) Imatinib pharmacokinetics and its correlation with response and safety in chronic-phase chronic myeloid leukemia: a subanalysis of the IRIS study. Blood 111(8):4022–4028

81. Manley PW, Blasco F, Mestan J, Aichholz A (2013) The kinetic deuterium isotope effect as applied to metabolic deactivation of imatinib to the des-methyl metabolite, CGP74588. Bioorg Med Chem 21:3231–3239

82. Manley PW, Stiefl N, Cowan-Jacob SW, Kaufman S, Mestan J, Wartmann M, Wiesmann M, Woodman R, Gallagher N (2010) Structural resemblances and comparisons of the relative pharmacological properties of imatinib and nilotinib. Bioorg Med Chem 18:6977–6986

83. Kim LC, Song L, Haura EB (2009) Src kinases as therapeutic targets for cancer. Nat Rev Clin Oncol 6:587–595

84. Das J, Barrish JC (2010) Dasatinib, a kinase inhibitor to treat chronic myelogenous leukemia. In: Analogue-based drug discovery II, pp 493–506

85. Das J, Chen P, Norris D, Padmanabha R, Lin J, Moquin RV, Shen Z, Cook LS, Doweyko AM, Pitt S, Pang S, Shen DR, Fang Q, de Fex HF, McIntyre KW, Shuster DJ, Gillooly KM, Behnia K, Schieven GL, Wityak J, Barrish JC (2006) 2-Aminothiazole as a novel kinase inhibitor template. Structure–activity relationship studies toward the discovery of N-(2-chloro-6-methylphenyl)-2-[[6-[4-(2-hydroxyethyl)-1-piperazinyl]-2-methyl-4-pyrimidinyl] amino]-1, 3-thiazole-5-carbox-amide (dasatinib, BMS-354825) as a potent pan-Src kinase inhibitor. J Med Chem 49:6819–6832

86. Das J, Padmanabha R, Chen P, Norris DJ, Doweyko AMP, Barrish JC, Wityak J (2000) Preparation of cyclic protein tyrosine kinase inhibitors. PCT Int Appl 2000062778, 26 Oct 2000

87. Lombardo LJ, Lee FY, Chen P, Norris D, Barrish JC, Behnia K, Castaneda S, Cornelius LAM, Das J, Doweyko AM, Fairchild C, Hunt JT, Inigo I, Johnston K, Kamath A, Kan D, Klei H, Marathe P, Pang S, Peterson R, Pitt S, Schieven GL, Schmidt RJ, Tokarski J, Wen ML, Wityak J, Borzilleri RM (2004) Discovery of N-(2-chloro-6-methyl-phenyl)-2-(6-(4-(2-hydroxyethyl)-piperazin-1-yl)-2-methylpyrimidin-4-ylamino)thiazole-5-carboxamide (BMS-354825), a dual Src/Abl kinase inhibitor with potent antitumor activity in preclinical assays. J Med Chem 47:6658–6661

88. Vajpai N, Strauss A, Fendrich G, Cowan-Jacob SW, Manley PW, Grzesiek S, Jahnke W (2008) Solution conformations and dynamics of ABL kinase inhibitor complexes determined by NMR substantiate the different binding modes of imatinib/nilotinib and dasatinib. J Biol Chem 283:18292–18302

89. Shah NP, Tran C, Lee FY, Chen P, Norris D, Sawyers CL (2004) Overriding imatinib resistance with a novel ABL kinase inhibitor. Science 305:399–401

90. O'Hare T, Walters DK, Stoffregen EP, Jia T, Manley PW, Mestan J, Cowan-Jacob SW, Lee FY, Heinrich MC, Deininger MWN, Brian J, Druker BJ (2005) In vitro activity of Bcr-Abl inhibitors AMN107 and BMS-354825 against clinically relevant imatinib-resistant Abl kinase domain mutants. Cancer Res 65:4500–4505

91. Talpaz M, Shah NP, Kantarjian H, Donato N, Nicoll J, Paquette R, Cortes J, O'Brien S, Nicaise C, Bleickardt E, Blackwood-Chirchir MA, Iyer V, Chen TT, Huang F, Decillis AP, Sawyers CL (2006) Dasatinib in imatinib-resistant Philadelphia chromosome-positive leukemias. N Engl J Med 354:2531–2541

92. Aguilera DG, Tsimberidou AM (2009) Dasatinib in chronic myeloid leukemia: a review. Ther Clin Risk Manag 5:281–289

93. Hochhaus A, Baccarani M, Deininger M, Apperley JF, Lipton JH, Goldberg SL, Corm S, Shah NP, Cervantes F, Silver RT, Niederwieser D, Stone RM, Dombret H, Larson RA, Roy L, Hughes T, Müller MC, Ezzeddine E, Countouriotis AM, Kantarjian HM (2008) Dasatinib induces durable cytogenetic responses in patients with chronic myelogenous leukemia in chronic phase with resistance or intolerance to imatinib. Leukemia 22:1200–1206

94. Guilhot F, Apperley J, Kim DW, Eduardo O, Bullorsky EO, Michele Baccarani M, Roboz GJ, Amadori S, de Souza CA, Lipton JH, Hochhaus A, Heim D, Larson RA, Branford S, Muller MC, Agarwal P, Gollerkeri A, Talpaz M (2007) Dasatinib induces significant hematologic and cytogenetic responses in patients with imatinib-resistant or -intolerant chronic myeloid leukemia in accelerated phase. Blood 109:4143–4150

95. Kantarjian HM, Shah NP, Cortes JE, Baccarani M, Agarwal MB, Soledad Undurraga M, Wang J, Kassack IJJ, Kim D-W, Ogura M, Pavlovsky C, Junghanss C, Milone JH, Nicolini

FE, Robak T, Van Droogenbroeck J, Vellenga E, Bradley-Garelik M, Zhu C, Hochhaus A (2012) Dasatinib or imatinib in newly diagnosed chronic-phase chronic myeloid leukemia: 2-year follow-up from a randomized phase 3 trial (DASISION). Blood 19:1123–1129

96. Shah NP, Guilot F, Cortes JE, Schiffer CA, Le Coutre P, Brummendorf TH, Kantarjian HM, Hochhaus A, Rousselot P, Mohamed H, Healey D, Cunningham M, Saglio G (2014) Long-term outcome with dasatinib after imatinib failure in chronic-phase chronic myeloid leukemia: follow-up of a phase 3 study. Blood 123:2317–2324

97. Parker WT, Ho M, Scott HS, Hughes TP, Branford S (2012) Poor response to second-line kinase inhibitors in chronic myeloid leukemia patients with multiple low-level mutations, ir-respective of their resistance profile. Blood 119:2234–2238

98. Talpaz M, Silver RT, Druker BJ, Goldman JM, Gambacorti-Passerini C, Guilhot F, Schiffer CA, Fischer T, Deininger MWN, Lennard AL, Hochhaus A, Ottmann OG, Gratwohl A, Baccarani M, Stone S, Tura S, Mahon F-X, Fernandes-Reese S, Gathmann I, Capdeville R, Kantarjian HM, Sawyers CL (2002) Imatinib induces durable hematologic and cytogenetic responses in patients with accelerated phase chronic myeloid leukemia: results of a phase 2 study. Blood 99:1928–1937

99. Manley PW, Breitenstein W, Brüggen J, Cowan-Jacob SW, Furet P, Mestan J, Meyer T (2004) Urea-derivatives of STI571 as inhibitors of Bcr-Abl and PDGFR kinases. Bioorg Med Chem Lett 14:5793–5797

100. Eck MJ, Manley PW (2009) The interplay of structural information and functional studies in kinase drug design: insights from BCR-Abl. Curr Opin Cell Biol 21:288–295

101. Manley PW, Drueckes P, Fendrich G, Furet P, Liebetanz J, Martiny-Baron G, Mestan J, Trappe J, Wartmann M, Fabbro D (2010) Extended kinase profile and properties of the protein kinase inhibitor nilotinib. Biochim Biophys Acta 1804:445–453

102. Weisberg E, Manley PW, Breitenstein W, Brueggen J, Cowan-Jacob SW, Ray A, Huntly B, Fabbro D, Fendrich G, Hall-Meyers E, Kung AL, Mestan J, Daley GQ, Callahan L, Catley L, Cavazza C, Mohammed A, Neuberg D, Wright RD, Gilliland DG, Griffin JD (2005) Characterization of AMN107, a selective inhibitor of native and mutant Bcr-Abl. Cancer Cell 7:129–141

103. Jensen MR, Brüggen J, DiLea C, Mestan J, Manley PW (2006) AMN107: efficacy of the selective Bcr-Abl tyrosine kinase inhibitor in a murine model of chronic myelogenous leukemia. In: Abstracts of the 97th annual meeting of the American Association for Cancer Research, Washington, DC, 1-5 April 2006. Proc Am Assoc Cancer Res 47:61–62. Abstr 780

104. Manley PW, Zimmermann J (2012) Drug research leading to imatinib and beyond to nilotinib. In: Peters J-U (ed) Polypharmacology in drug discovery. Wiley, Hoboken, NJ, pp 409–421

105. Pierce AC, Sandretto KL, Guy W, Bemis GW (2002) Kinase inhibitors and the case for CH... O hydrogen bonds in protein–ligand binding. Proteins 49:567–576

106. Olsen JA, Banner DW, Seiler P, Wagner B, Tschopp T, Obst-Sander U, Kansy M, Müller K, Diederich F (2004) Fluorine interactions at the thrombin active site: protein backbone fragments H-Cα-C=O comprise a favourable C-F environment and interactions of C-F with electrophiles. ChemBioChem 5:666–675

107. Manley PW, Cowan-Jacob SW, Fendrich G, Jahnke W, Fabbro D (2011) Nilotinib, in comparison to both dasatinib and imatinib, possesses a greatly prolonged residence time when bound to the BCR-ABL kinase SH1 domain. In: Abstracts of the 53rd annual meeting of the American Society of Hematology, San Diego, CA, 10-13 Dec 2011. Blood 118(21):727. Abstr 1694

108. Weisberg E, Manley PW, Mestan J, Cowan-Jacob S, Ray A, Griffin JD (2006) AMN107 (nilotinib): a novel and selective inhibitor of BCR-ABL. Br J Cancer 94:1765–1769

109. Kantarjian H, Giles F, Wunderle L, Bhalla K, O'Brien S, Wassmann B, Tanaka C, Manley P, Rae P, Mietlowski W, Bochinski K, Hochhaus A, Griffin JD, Hoelzer D, Albitar M, Dugan M, Cortes J, Alland L, Ottmann OG (2006) Nilotinib in imatinib-resistant CML and Philadelphia chromosome-positive ALL. N Engl J Med 354:2542–2551

110. Tanaka C, Yin OQP, Sethuraman V, Smith T, Wang X, Grouss K, Kantarjian H, Giles F, Ottmann OG, Galitz L, Schran H (2009) Clinical pharmacokinetics of the BCR–ABL tyrosine kinase inhibitor nilotinib. Clin Pharmacol Ther 87:197–203

111. Kantarjian HM, Giles F, Gattermann N, Bhalla K, Alimena G, Palandri F, Ossenkoppele GJ, Nicolini FE, O'Brien SG, Litzow M, Bhatia R, Cervantes F, Haque A, Shou Y, Resta DJ, Weitzman A, Hochhaus A, le Coutre P (2007) Nilotinib (formerly AMN107), a highly selective BCR-ABL tyrosine kinase inhibitor, is effective in patients with Philadelphia chromosome-positive chronic myelogenous leukemia in chronic phase following imatinib resistance and intolerance. Blood 110:3540–3546

112. Le Coutre P, Ottmann OG, Giles F, Kim DW, Cortes J, Gattermann N, Apperley JF, Larson RA, Abruzzese E, O'Brien SG, Kuliczkowski K, Hochhaus A, Mahon FX, Saglio G, Gobbi M, Kwong YL, Baccarani M, Hughes T, Martinelli G, Radich JP, Zheng M, Shou Y, Kantarjian H (2008) Nilotinib (formerly AMN107), a highly selective BCR-ABL tyrosine kinase inhibitor, is active in patients with imatinib-resistant or -intolerant accelerated-phase chronic myelogenous leukemia. Blood 111:1834–1839

113. Hochhaus A, Rosti G, Cross NCP, Steegmann JL, le Coutre P, Ossenkoppele G, Petrov L, Masszi T, Hellmann A, Griskevicius L, Wiktor-Jedrzejczak W, Rea D, Coriu D, Brümmendorf TH, Porkka K, Saglio G, Gastl G, Müller MC, Schuld P, Di Matteo P, Pellegrino A, Dezzani L, Mahon F-X, Baccarani M, Giles FJ (2015) Frontline nilotinib in patients with chronic myeloid leukemia in chronic phase: results from the European ENEST1st study. Leukemia 30:57–64

114. Hunter T, Sefton BM (1980) Transforming gene product of Rous sarcoma virus phosphory-lates tyrosine. Proc Natl Acad Sci U S A 77:1311–1315

115. Myers MR, Setzer NN, Spada AP, Zulli AL, Hsu CYJ, Zilberstein A, Johnson SE, Hook LE, Jacoski MV (1997) The preparation and SAR of 4-(anilino), 4-(phenoxy), and 4-(thiophenoxy)-quinazolines: inhibitors of p56lck and EGF-R tyrosine kinase activity. Bioorg Med Chem Lett 7:417–420

116. Wang YD, Miller K, Boschelli DH, Ye F, Wu B, Floyd MB, Powell DW, Wissner A, Weber JM, Boschelli F (2000) Inhibitors of Src tyrosine kinase: the preparation and structure-activity relationship of 4-anilino-3-cyanoquinolines and 4-anilinoquinazolines. Bioorg Med Chem Lett 10:2477–2480

117. Boschelli DH (2002) 4-Anilino-3-quinolinecarbonitriles: an emerging class of kinase inhib-itors. Curr Top Med Chem 2:1051–1063

118. Boschelli DH, Ye F, Wang YD, Dutia M, Johnson SL, Wu B, Miller K, Powell DW, Yaczko D, Young M, Tischler M, Arndt K, Discafani C, Etienne C, Gibbons J, Grod J, Lucas J, Weber JM, Boschelli F (2001) Optimization of 4-phenylamino-3-quinolinecarbonitriles as potent inhibitors of Src kinase activity. J Med Chem 44:3965–3977

119. Golas JM, Arndt K, Etienne C, Lucas J, Nardin D, Gibbons J, Frost P, Ye F, Boschelli DH, Boschelli F (2003) SKI-606, a 4-anilino-3-quinolinecarbonitrile dual inhibitor of Src and Abl kinases, is a potent antiproliferative agent against chronic myelogenous leukemia cells in culture and causes regression of K562 xenografts in nude mice. Cancer Res 63:375–381

120. Boschelli F, Arndt K, Gambacorti-Passerini C (2010) Bosutinib: a review of preclinical studies in chronic myelogenous leukaemia. Eur J Cancer 46:1781–1789

121. Levinson NM, Boxer SG (2012) Structural and spectroscopic analysis of the kinase inhibitor bosutinib and an isomer of bosutinib binding to the Abl tyrosine kinase domain. PLoS One 7 (4):e29828

122. Rix LLR, Rix U, Colinge J, Hantschel O, Bennett KL, Stranzl T, Müller A, Baumgartner C, Valent P, Augustin M, Till JH, Superti-Furga G (2009) Global target profile of the kinase inhibitor bosutinib in primary chronic myeloid leukemia cells. Leukemia 23:477–485

123. Vi Doan AW, Prescott H (2015) Bosutinib for the treatment of chronic myeloid leukemia. Am J Health Syst Pharm 72:439–447

124. Bruemmendorf TH, Cortes JE, Antonio de Souza C, Guilhot F, Duvillie L, Pavlov D, Gogat K, Countouriotis AM, Gambacorti-Passerini C (2015) Bosutinib versus imatinib in newly

diagnosed chronic-phase chronic myeloid leukaemia: results from the 24-month follow-up of the BELA trial. Br J Haematol 168:69–81

125. Huang WS, Zhu X, Wang Y, Azam M, Wen D, Sundaramoorthi R, Thomas RM, Liu S, Banda G, Lentini SP, Das S, Xu Q, Keats J, Wang F, Wardwell S, Ning Y, Snodgrass JT, Broudy MI, Russian K, Daley GD, Iuliucci J, Dalgarno DC, Clackson T, Sawyer TK, Shakespeare WC (2009) 9-(Arenethenyl)purines as dual Src/Abl kinase inhibitors targeting the inactive conformation: design, synthesis, and biological evaluation. J Med Chem 52:4743–4756

126. Huang W, Metcalf CA, Sundaramoorthi R, Wang Y, Zou D, Thomas RM, Zhu X, Cai L, Wen D, Liu S, Romero J, Qi J, Chen I, Banda G, Lentini SP, Das S, Xu Q, Keats J, Wang F, Wardwell S, Ning Y, Snodgrass JT, Broudy MI, Russian K, Zhou T, Commodore L, Narasimhan NI, Mohemmad QK, Iuliucci J, Rivera VM, Dalgarno DC, Sawyer TK, Clackson T, Shakespeare WC (2010) Discovery of 3-[2-(imidazo[1,2-b]pyridazin-3-yl)ethynyl]-4-methyl-N-[4-((4-methylpiperazin-1-yl)methyl)-3-(trifluoromethyl)phenyl]benzamide (AP24534), a potent, orally active pan-inhibitor of breakpoint cluster region-abelson (BCR-ABL) kinase including the T315I gatekeeper mutant. J Med Chem 53:4701–4719

127. O'Hare T, Shakespeare WC, Zhu X, Eide CA, Rivera VM, Wang F, Adrian LT, Zhou T, Huang W, Xu Q, Metcalf CA, Tyner JW, Loriaux MM, Corbin AS, Wardwell S, Ning Y, Keats JA, Wang Y, Sundaramoorthi R, Thomas M, Zhou D, Snodgrass J, Commodore L, Sawyer TK, Dalgarno DC, Deininger MWN, Druker BJ, Clackson T (2009) AP24534, a pan-BCR-ABL inhibitor for chronic myeloid leukemia, potently inhibits the T315I mutant and overcomes mutation-based resistance. Cancer Cell 16:401–412

128. Cortes JE, Kantarjian H, Shah NP, Bixby D, Mauro MJ, Flinn I, O'Hare T, Hu S, Narasimhan NI, Rivera VM, Clackson T, Turner CD, Haluska FG, Druker BJ, Deininger MW, Talpaz M (2012) Ponatinib in refractory Philadelphia chromosome-positive leukemias. N Engl J Med 367:2075–2088

129. Cortes JE, Kim DW, Pinilla-Ibarz J, Le Coutre P, Paquette R, Chuah C, Nicolini FE, Apperley JF, Khoury HJ, Talpaz M, DiPersio J, DeAngelo DJ, Abruzzese E, Rea D, Baccarani M, Müller MC, Gambacorti-Passerini C, Wong S, Lustgarten S, Rivera VM, Clackson T, Turner CD, Haluska FG, Guilhot F, Deininger MW, Hochhaus A, Hughes T, Goldman JM, Shah NP, Kantarjian H (2013) A phase 2 trial of ponatinib in Philadelphia chromosome-positive leukemias. N Engl J Med 369:1783–1796

130. Iclusig [package insert] (2012) ARIAD Pharmaceuticals, Cambridge, MA

131. Fava C, Morotti A, Dogliotti I, Saglio G, Rege-Cambrin G (2015) Update on emerging treatments for chronic myeloid leukemia. Expert Opin Emerg Drugs 20:183–196

132. Lipton JH, Chuah C, Guerci-Bresler A, Rosti G, Simpson D, Assouline S, Etienne G, Nicolini FE, Le Coutre P, Clark RE, Stenke L, Andorsky D, Oehler V, Lustgarten S, Rivera VM, Clackson T, Haluska FG, Baccarani M, Cortes JE, Guilhot F, Hochhaus A, Hughes T, Kantarjian HM, Shah NP, Talpaz M, Deininger MW (2016) Ponatinib versus imatinib for newly diagnosed chronic myeloid leukaemia: an international, randomised, open-label, phase 3 trial. Lancet Oncol 17:612–621

133. Manley PW, Bruggen J, Floersheimer A, Furet P, Jensen MR, Mestan J, Pissot C, Cowan-Jacob S (2008) Rational design of T315I BCR-Abl inhibitors for the treatment of chronic myelogenous leukemia (CML): BGG463. In: Abstracts of the fall meeting of the Swiss Chemical Society, Zurich, Switzerland, 11 Sept 2008. Chimia 62(7–8):579. Abstr 88

134. Andraos R, Qian Z, Bonenfant D, Rubert J, Vangrevelinghe E, Scheufler C, Marque F, Régnier CH, De Pover A, Ryckelynck H, Bhagwat N, Koppikar P, Goel A, Wyder L, Tavares G, Baffert F, Pissot-Soldermann C, Manley PW, Gaul C, Voshol H, Levine RL, Sellers WR, Hofmann F, Radimerski T (2012) Modulation of activation-loop phosphorylation by JAK inhibitors is binding mode dependent. Cancer Discov 2:512–523

135. Ren P, Wang X, Zhang G, Ding Q, You S, Zhang Q, Chopiuk G, Pamela A, Sim T, Gray NS (2005) Preparation of imidazolylpyrimidinamines as protein kinase inhibitors. PCT Int Appl WO 2005123719, 29 Dec 2005

136. Choi HG, Ren P, Adrian F, Sun F, Lee HS, Wang X, Ding Q, Zhang G, Xie Y, Zhang J, Liu Y, Tove T, Warmuth M, Manley PW, Mestan J, Gray NS, Sim T (2010) A type-II kinase inhibitor capable of inhibiting the T315I "gatekeeper" mutant of Bcr-Abl. J Med Chem 53:5439–5448

137. Adrian FJ, Ding Q, Sim T, Velentza A, Sloan C, Liu Y, Zhang G, Hur W, Ding S, Manley PW, Mestan J, Fabbro D, Gray NS (2006) Allosteric inhibitors of Bcr-Abl-dependent cell proliferation. Nat Chem Biol 2:95–102

138. Zhang J, Adrian FJ, Jahnke W, Cowan-Jacob SW, Li AG, Iacob RE, Sim T, Powers J, Dierks C, Sun F, Guo GR, Ding Q, Okram B, Choi Y, Wojciechowski A, Deng X, Liu L, Fendrich G, Strauss A, Vajpai N, Grzesiek S, Tuntland T, Liu Y, Bursulaya B, Azam M, Manley PW, Engen JR, Daley GQ, Warmuth M, Gray NS (2010) Targeting Bcr–Abl by combining allosteric with ATP-binding-site inhibitors. Nature 463:501–506

139. Choi Y, Seeliger MA, Panjarian SB, Kim H, Deng X, Sim T, Couch B, Koleske AJ, Smithgall TE, Gray NS (2009) N-Myristoylated c-Abl tyrosine kinase localizes to the endoplasmic reticulum upon binding to an allosteric inhibitor. J Biol Chem 284:29005–29014

140. Deng X, Okram B, Ding Q, Zhang J, Choi Y, Adrian FJ, Wojciechowski A, Zhang G, Che J, Bursulaya B, Cowan-Jacob SW, Rummel G, Sim T, Gray NS (2010) Expanding the diversity of allosteric Bcr-Abl inhibitors. J Med Chem 53:6934–6946

141. Jahnke W, Grotzfeld RM, Pelle X, Strauss A, Fendrich G, Cowan-Jacob SW, Cotesta S, Fabbro D, Furet P, Mestan J, Marzinzik AL (2010) Binding or bending: distinction of allosteric Abl kinase agonists from antagonists by an NMR-based conformational assay. J Am Chem Soc 132:7043–7048

142. Schoepfer J, Berellini G, Cai H, Caravatti G, Dodd S, Furet P, Gangal G, Grotzfeld RM, Quamrul HA, Hood T, Cowan-Jacob S, Jahnke W, Loo A, Manley PW, Pelle X, Salem B, Sharma S, Zhu W, Marzinzik A, Gabriel T, Keen N, Petruzzelli L, Vanasse G, Sellers WR, Wylie A (2015) Discovery and pharmacological properties of ABL001, a novel potent and specific BCR-ABL allosteric inhibitor. In: Abstracts of the 250th American Chemical Society national meeting, Boston, MA, 16-20 Aug 2015, MEDI-285

143. Xu G, Shen H, Tong T, Lu A, Gou S (2010) Synthesis, crystal structure, and spectral characterization of flumatinib mesylate. Synth Comm 40:2564–2570

144. Kim S, Menon H, Jootar S, Saikia T, Kwak J, Sohn S, Park JS, Jeong SH, Kim HJ, Kim Y, Oh SJ, Kim H, Zang DY, Chung JS, Shin HJ, Do YR, Kim J, Kim D, Choi CW, Park S, Park HL, Lee GL, Cho DJ, Shin JS, Kim D (2014) Efficacy and safety of radotinib in chronic phase chronic myeloid leukemia patients with resistance or intolerance to BCR-ABL1 tyrosine kinase inhibitors. Haematologica 99:1191–1196

145. Chan WW, Wise SC, Kaufman MD, Ahn Y, Ensinger CL, Haack T, Hood MM, Jones J, Lord JW, Lu W, Miller D, Patt WC, Smith BD, Petillo PA, Rutkoski TJ, Telikepalli H, Vogeti L, Yao T, Chun L, Clark R, Evangelista P, Gavrilescu LC, Lazarides K, Zaleskas VM, Stewart LJ, Van Etten RA, Flynn DL (2011) Conformational control inhibition of the BCR-ABL1 tyrosine kinase, including the gatekeeper T315I mutant, by the switch-control inhibitor DCC-2036. Cancer Cell 19:556–568

146. Gugliotta G, Castagnetti F, Fogli M, Cavo M, Baccarani M, Rosti G (2013) Impact of comorbidities on the treatment of chronic myeloid leukemia with tyrosine-kinase inhibitors. Expert Rev Hematol 6:563–574

147. Efficace F, Cannella L (2016) The value of quality of life assessment in chronic myeloid leukemia patients receiving tyrosine kinase inhibitors. Hematology Am Soc Hematol Educ Program 206:170–179

148. Pavlu J, Szydlo RM, Goldman JM, Apperley JF (2011) Three decades of transplantation for chronic myeloid leukemia: what have we learned? Blood 117:755–763

149. Yong ASM, Eolia Brissot E, Rubinstein S, Savani BN, Mohty M (2015) Transplant to treatment-free remission: the evolving view of 'cure' in chronic myeloid leukemia. Expert Rev Hematol 8:785–797

150. Mahon F-X (2015) Discontinuation of tyrosine kinase therapy in CML. Ann Hematol 94(Suppl 2):S187–S193
151. Hughes TP, Ross DM (2016) Moving treatment-free remission into mainstream clinical practice in CML. Blood 128:17–23
152. Vonka V, Petráčková M (2015) Immunology of chronic myeloid leukemia: current concepts and future goals. Expert Rev Clin Immunol 11:511–522

Small Molecule Inhibitors of the Epidermal Growth Factor Receptor

M. Raymond V. Finlay and Richard A. Ward

Abstract The epidermal growth factor receptor (EGFR) has emerged over the past two decades as a key target in therapeutic approaches to the treatment of non-small cell lung cancer (NSCLC). This chapter describes the evolution of the EGFR small molecule inhibitor field, from early exploratory work and growing insight into the role of EGFR activating mutations, through to the first approved therapies, gefitinib and erlotinib. Advances in understanding resistance to these initial therapies and the role of the T790M mutation are discussed, along with drug discovery efforts culminating in the discovery of a number of EGFR mutant selective inhibitors, including osimertinib (TAGRISSO™), the first approved treatment for patients with EGFR T790M mutation-positive metastatic NSCLC.

Keywords Irreversible inhibitor, Kinase, Mutant, Resistance, T790M

Contents

M.R.V. Finlay (✉) and R.A. Ward
IMED Oncology, AstraZeneca, Darwin Building, 310 Cambridge Science Park, Milton Road, Cambridge CB4 0WG, UK
e-mail: ray.finlay@astrazeneca.com

1 Introduction

Non-small cell lung cancer (NSCLC) remains a leading cause of human mortality in both the western and developing worlds [1]. Nevertheless, over the past two decades, considerable therapeutic progress has been made in the treatment of the disease by exploiting our growing understanding of the role of the epidermal growth factor receptor (EGFR) and its etiology in NSCLC.

1.1 The Epidermal Growth Factor Receptor (EGFR)

EGFR belongs to the erbB (*erythroblastosis oncogene B*) family of receptors [2, 3], which consists of four members (Fig. 1):

- ErbB-1, also known as epidermal growth factor receptor (EGFR) and HER1
- ErbB-2, also known as HER2 (human epidermal growth factor receptor 2) in humans
- ErbB-3, also known as HER3
- ErbB-4, also known as HER4
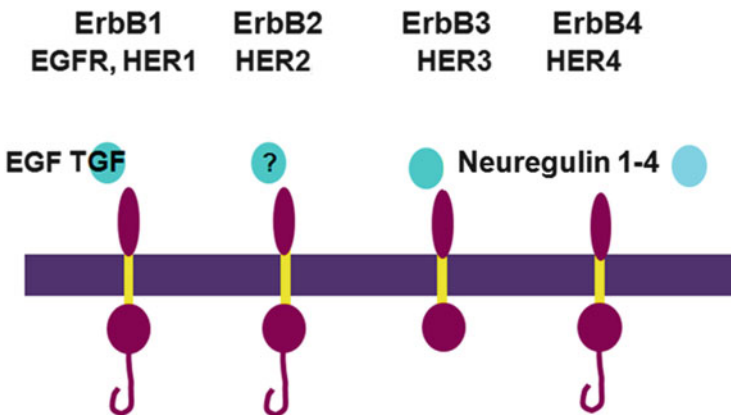
Fig. 1 ErbB family of receptors and their ligands. See text for further details

Table 1 ErbB family of receptors and their ligands

Receptor	Ligands
EGFR	EGF, TGF-α, HBEGF (heparin-binding EGF-like growth factor), AREG (amphiregulin), BTC (betacellulin), EREG (epiregulin), EPGN (epigen)
ErbB-2	No known ligand
ErbB-3	Neuregulins
ErbB-4	Neuregulins

Note that ErbB-2 has no ligand and ErbB-3 has a non-functional kinase domain, so both receptors act as subunits of other ErbBs

These transmembrane glycoproteins are composed of an extracellular ligand binding domain, a transmembrane domain and an intracellular portion, which possesses a tyrosine kinase domain. Upon ligand binding to the extracellular domain (by peptidic molecules such as epidermal growth factor (EGF) or transforming growth factor α (TGF-α), Table 1 and Fig. 1) receptor activation occurs. This process involves receptor homo-dimerisation or hetero-dimerisation with another family member. This leads to an autophosphorylation event whereby the tyrosine kinase domains of the dimer phosphorylate each other, initiating a cascade of further signaling in the cell, a process known as signal transduction. The end results of this signaling cascade can include cell proliferation and maturation, cell survival or apoptosis and in some instances angiogenesis and metastasis.

It should be noted that mutated EGF receptors with non-functional kinase domains are unable to elicit the same degree of signal transduction as the intact system, suggesting a possible role for inhibitors of the kinase domain of EGFR in prevention of EGFR mediated signal transduction.

2 The Rationale for EGFR Inhibitors

Clearly, the processes that follow activation of EGFR described above can be important in both tumour maintenance and progression, and intervention in these cascades by EGFR inhibition could offer therapeutic benefit. However, EGFR is expressed in both neoplastic and healthy tissue, where it has a function in maintaining skin and other internal epithelial cells, such as those of the gastrointestinal tract. A key observation though is that EGFR is highly expressed in a number of tumour types [2, 4] (including NSCLC) and these high expression levels have been correlated with poor prognosis and more rapid disease progression. This body of evidence implicating over-expression of the receptor as a tumour driver has prompted a variety of approaches to target tumours using EGFR inhibitors.

3   The Discovery of gefitinib and erlotinib

3.1   gefitinib

Early work in the field of EGFR kinase inhibitors was first disclosed by Ward et al. [5] at Zeneca Pharmaceuticals (now AstraZeneca). These workers investigated the catalytic mechanism of phosphorylation by the EGFR kinase domain in order to facilitate structure based searching for inhibitors and allow the identification of a more focused set of compounds for screening. Rate studies showed that EGFR forms a ternary complex with ATP and the peptidic substrate, and the detailed catalytic mechanism was then exploited to define a query used to interrogate a database of predicted 3D chemical structures. This involved searching for motifs that mimic that ATP γ-phosphate and the tyrosine phenol, key features of this complex catalytic system. This then enabled further 2D searching culminating in the discovery of 4-(3-chloroanilino)quinazoline (**1**, Fig. 2) as a potent inhibitor ($K_i = 16$ nM) of the isolated enzyme.

The compound showed competitive kinetics with respect to ATP, whereas it was non-competitive with respect to the peptidic substrate, implying that it behaves as a mimic of ATP. Also noteworthy was the observation that upon limited kinase selectivity testing, **1** did not inhibit PKC (Protein Kinase C), dispelling the initial preconceptions of the time that selective kinase inhibition in this manner would not be possible. The first patent to claim anilinoquinazolines as kinase inhibitors was then filed as a result of this work [6, 7]. Interestingly, researchers at Parke-Davis were also active in the area at the same time, with their initial findings following soon after (For a refreshingly candid account of this work and the impact of the Zeneca group's and others publications on it, see [8]).

A subsequent optimisation of **1** [9, 10] led to the observation [11, 12] that electron-donating substituents at the 6- and 7-positions of the quinazoline enhanced in vitro potency against EGFR, leading to compound **2** (Fig. 3) as a potent inhibitor of EGF-stimulated human tumour cell growth (IC_{50} 50 nM KB oral carcinoma cells).

However, although **2** showed efficacy in a relevant in vivo tumour xenograft disease model in nude mice (A431 cell line), it was rapidly metabolised with a half-life of approximately 1 h. Metabolite identification work (Fig. 3) revealed the presence of two major products, both resulting from oxidation. Methyl oxidation led to benzyl alcohol **3**, whereas oxidation at the *para*-position of the aniline moiety produced the corresponding phenol metabolite **4**. Reinstalling the chloro group in place of the methyl (as in **1**) and fluorination at the *para* position of the aniline delivered **5** (Fig. 4) which avoided the oxidation issues encountered by **2** and
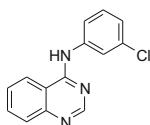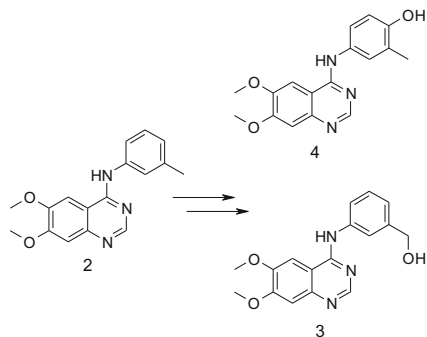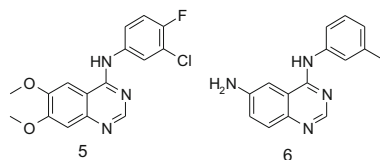

Fig. 2 Structure of 4-(3-chloroanilino)quinazoline (**1**)

**Fig. 3** Structure of **2** and in vivo **3** and **4** metabolites

Fig. 4 Structures of **5** and **6**

displayed a better in vivo profile with improved efficacy in disease models following oral dosing, accompanied by reduced plasma clearance and longer half life in mice (3 h). In addition, these beneficial properties were accompanied by only a slight reduction in target potency (EGFR-TK enzyme test, IC$_{50}$ 9 nM; EGF stimulated KB cell growth, IC$_{50}$ 80 nM). The authors also noted that whilst related compound **6** (Fig. 4) showed relatively lower potency than other analogues, it had much improved oral exposure in mice and superior in vivo efficacy, reflecting the importance of sustained inhibition of EGFR in achieving meaningful activity in this model when using a once-daily dosing regimen.

A key structural change in this regard appeared to be the substitution at the 6-position of the quinazoline and modification here formed an important part of the strategy for the remainder of the groups' efforts, employing **5** as the template for further work. The authors designs included modulation of the physicochemical properties of the template by incorporation of basic functionality into the ether side chain at the 6-position as this offered the possibility of retaining both the potency enhancing ethers at C6 and C7 and the substituted aniline at C4 which gave the optimal combination of metabolic stability and potency.

A selection of compounds prepared is shown below (Fig. 5). Using **5** as a start point, the authors prepared a series of analogues incorporating basic side chains with two or three carbon atoms between the 6-oxygen and the side-chain nitrogen atom.
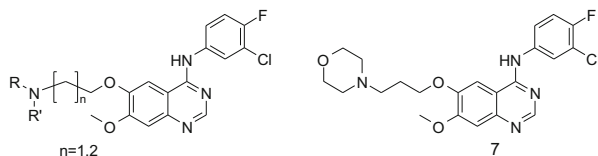
Fig. 5 Structures of optimisation targets and ZD1839 (gefitinib, Iressa[TM]) **7**. R, R′ = alkyl, cycloalkyl and heteroaromatic

From this work, compound **7** showed high potency in the EGF-stimulated cell proliferation test (GI_{50} = 80 nM in KB2 cells) and excellent oral exposure in mouse and resultant high in vivo disease model efficacy and was selected as clinical candidate ZD1839. As well as having good oral bioavailability, ZD1839 inhibited the growth of a broad range of human solid tumour xenografts in a dose-dependent manner with marked regressions seen in some tumours [10]. A431 xenograft tumour growth was particularly sensitive to ZD1839 treatment, with complete tumour growth inhibition observed in animals that received a once-daily oral dose of 200 mg/kg. Treatment for up to 4 months in nude mice was also well tolerated and interestingly, withdrawal of drug treatment did allow some tumours to resume growth. When ZD1839 was used to treat large, well-established A431 tumours, rapid tumour regression was observed, and this was maintained for the duration of treatment. The compound was also reported to be retained in cells and consequently in vivo showed some characteristics of an irreversible inhibitor [13]. ZD1839 was assigned the international nonproprietary name gefitinib and the brand name Iressa[TM], and demonstrated a long half-life in humans (approximately 48 h) compatible with once-daily oral dosing. Extensive Phase I clinical trials also showed biomarker evidence for inhibition of the EGFR signal transduction pathway and antitumour activity [14–16]. The maximum tolerated dose in patients was 800 mg, with dose limiting toxicities of diarrhea and skin rash being observed. Pharmacokinetic analysis of patient samples showed that doses of 150 mg/day and above led to plasma concentrations of >200 nM and drove responses in around a third of patients treated, with tumour responses not limited to NSCLC but ranging from ovarian and prostate to colorectal and head and neck.

3.2 erlotinib

Erlotinib hydrochloride (**8**, Fig. 6) was originally discovered as an EGFR kinase inhibitor by researchers working at Pfizer [17]. Subsequent development was to be conducted in collaboration with OSI (Oncogene Science Inc.), however the 2000 merger between Pfizer and Warner-Lambert meant that Pfizer were obliged to grant all development and marketing rights for the compound to OSI pharmaceuticals and was given the international nonproprietary name erlotinib. Under the brand name of
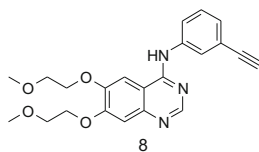
Fig. 6 Structure of OSI-774 (erlotinib, Tarceva[TM]) **8**

Tarceva[TM], the compound is currently marketed by OSI in collaboration with Roche/Genentech.

Although a good deal of data have been published around erlotinib [18, 19], to date the medicinal chemistry story does not appear to have been disclosed. Nevertheless, the SAR that was exploited in the discovery of gefitinib and related anilinoquinazoline EGFR inhibitors is visible in the erlotinib structure. A lipophilic substituent at the *meta* position of the aniline (in this case an alkyne), combined with C6, C7 ether substituents drives high potency. Interestingly, the symmetrical C6, C7 ether substitution pattern of erlotinib imparts good physicochemical properties relative to other substitution patterns, and higher blood levels in pre-clinical species than gefitinib. The compound is reported to be less potent than gefitinib in many in vivo models, but an oral dose of 50 mg/day provides sufficient exposure (plasma concentration >1.25 μM) for efficacy [20]. In the case of erlotinib, the maximum tolerated dose is 200 mg/day and, as for gefitinib, the dose limiting toxicities observed are diarrhea and skin rash [21]. The binding modes of gefitinib and erlotinib in the EGFR kinase domain are illustrated by the X-ray structures shown in Fig. 7. The quinazoline templates are oriented in a very similar fashion, with the quinazoline N1 accepting a hydrogen bond from the backbone NH of methionine 793 in the hinge region of the kinase. The hinge region (the segment that connects the amino- and carboxy-terminal lobes of the kinase domain, so called because it moves to enclose itself around ATP when it binds like a hinge) contains several conserved residues that provide the catalytic machinery and makes up an essential part of the ATP binding pocket. The aniline rings are also positioned in a similar way in the protein, with the lipophilic *meta*-group also occupying the same space. Finally, the ether linked groups in both examples are directed towards the solvent channel.

Iressa[TM] was first approved by the United States FDA on the 5th of May 2003 on the basis of Phase II data and under accelerated approval as "monotherapy for the treatment of patients with locally advanced or metastatic non-small cell lung cancer after failure of both platinum based and docetaxel chemotherapies" employing a 250 mg once-daily oral dose. However, this initial registration was based on objective response rates and subsequent studies did not show an increase in overall survival. The median survival in the "ISEL" trial for gefitinib patients was 6.3 months, versus 5.4 months for placebo, just short of statistical significance. Consequently, in June 2005, the product was withdrawn and only supplied to patients who had previously shown benefit from Iressa[TM] treatment. Tarceva[TM] received its first approval as a 100 mg dose of the hydrochloride salt from the FDA
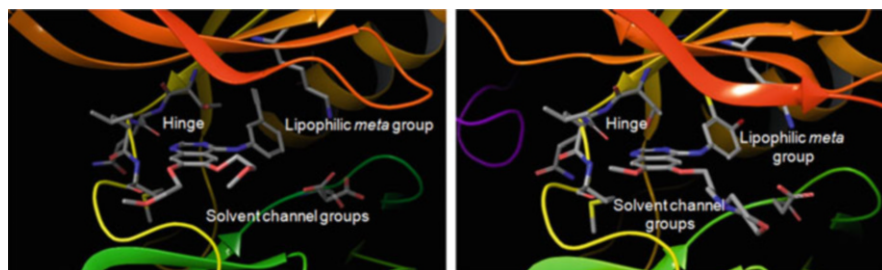
Fig. 7 X-ray structures of erlotinib (A, 1M17) and gefitinib (B, 2ITZ) bound to EGFR kinase domain

on the 19th of November 2004, and did demonstrate a slight but statistically significant increase in overall survival of 6.7 months versus 4.7 months in the placebo control group. Some consideration should be given to the possible reasons behind the contrasting outcomes of the pivotal studies for these two similar compounds. Certainly the patient populations studied were different, with gefitinib being dosed in a high proportion of Eastern European trial centres, with more heavy smokers and possibly more seriously ill patients. Gefitinib was also not studied at its maximum tolerated dose which may also have had an influence on the trial outcome. However, sub-population analysis of all trial data showed Asian, female, non-smokers (a segment that frequently carries EGFR sensitising mutations, vide infra) benefited significantly from Iressa[TM], and marketing approval was confirmed in Japan and the Far-East. After these initially disappointing clinical results with gefitinib and erlotinib in broad NSCLC patient populations, these compounds have subsequently shown clinical efficacy in NSCLC patients with activating mutations of EGFR.

4 Quinazoline-Based Irreversible EGFR Kinase Inhibitors

Over the past decade and a half, a number of groups have disclosed their efforts towards the identification of anilinoquinazoline-based irreversible EGFR kinase inhibitors that form a covalent bond with C797 in the ATP binding site of the kinase. Covalent inhibitors offer a number of advantages over their reversible counterparts, including extended pharmacodynamic activity (often lasting well beyond the detectable systemic presence of the inhibitor) as well as opportunities for exceptionally high target potency due to no-longer having to compete with high cellular ATP concentrations [8, 22, 23]. Nevertheless, the clear advantages with this approach do need to be weighed in the presence of potential risks, and in particular the possibility of idiosyncratic toxicology of compounds due to haptenisation. This can occur when the reactive warhead of the covalent inhibitor reacts with protein nucleophilic residues other than that which it was designed to target. The modified
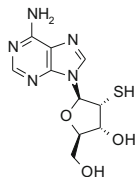
Fig. 8 Structure of 2′-thioadenosine **9**

protein can then be recognised by the immune system as being "non-native" and the accompanying immunological response can be severe. Consequently, it is important that the affinity of the ligand for the target protein (K_i) should be as high as possible, thus allowing the reactivity of the warhead (k_{inact}) to be relatively modest and less likely to indiscriminately react with available nucleophilic residues.

Whilst some early mechanistic studies in the area of covalent EGFR inhibitors were reported by Clark [24] and Woltjer [25], the first structure based design of an irreversible Erb family kinase domain inhibitor was reported by Singh et al. [26] who examined the nucleotide binding site of EGFR for possible positions for the attachment of a covalent inhibitor. C797 in the ATP binding site was postulated as a potential target due to its relative ease of access, and the residue's ability to form a covalent bond to an inhibitor was tested by incubation with 2′-thioadenosine (**9**, Fig. 8).

This agent was able to covalently inactivate EGFR and the inhibition was reversed by 1 mM dithiothreitol, implying that this inhibition is occurring through covalent modification of C797 by formation of a disulfide bond. Interestingly, kinetic data showed that inhibition occurred through formation of a non-covalent complex followed by slow formation of the disulfide bond. Selectivity was also achieved over FGF, PDGF or insulin receptor tyrosine kinases which were not inhibited by 2′-thioadenosine.

4.1 canertinib

Building on this work, joint studies by workers at Auckland University and Parke-Davis [27] employed an anilinoquinazoline as their template to examine covalent EGFR inhibitors. Rather than relying on disulfide bond formation, these workers instead studied an electrophilic acrylamide warhead on the template (Fig. 9). Guided by molecular modelling, the C6 position of the quinazoline template was viewed as being suitably close in space to C797 to allow covalent modification and this did prove to be the case in practice with the C7 analogue **12** reacting with C797 at a much slower rate than **10**. An X-ray structure of the simple quinazoline analogue **13** bound to the EGFR kinase domain (generated after this work by a different group) illustrates this point (Fig. 10). Additional work showed that the alkylation reaction occurs with a 1:1 stoichiometry. The compounds were also stable in solution and only undergo reaction when bound to the protein. A final
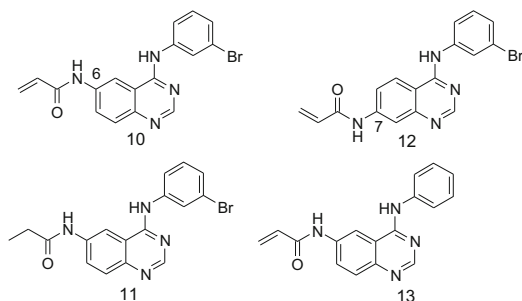
**Fig. 9** Early anilinoquinazoline based EGFR irreversible inhibitors and reversible comparator
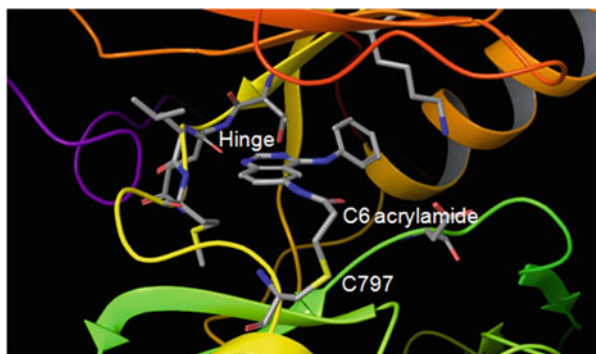
Fig. 10 X-ray structures of quinazoline **13** (2J5E) bound to EGFR kinase domain

outcome from this work was that a comparison between 6-acrylamido-4-anilinoquinazoline **10** and an equally potent but reversible analogue **11** showed that the irreversible inhibitor had far superior in vivo efficacy in a human epidermoid carcinoma xenograft model.

In a report of further efforts on these scaffolds by these groups [28], the cell potency of pairs of compounds bearing C6 or C7 acrylamides was examined (Table 2). As before, the C6 position delivered higher potency than C7 substitution, and this was particularly evident in a cellular autophosphorylation assay (compare **14** and **15**).

Modifications to the central core of the parent quinazoline motif were also investigated. Three new cores were prepared, and representative examples **16**, **17** and **18** are shown in Table 3. In the case of the examples bearing the acrylamide at the 7-position (e.g. **17**), aza substitution led to a loss of cell potency, reinforcing the view that this position is not optimal for acrylamide attachment, especially when considering that the heteroatom introduction should make the warhead more reactive.

The remainder of the examples studied in these new cores were all 6-substituted and in general tolerated the structural changes made. Of note though is the observation that the two heterocyclic analogues **16** and **18** were less potent than expected

Table 2 Comparison of EGFR potencies of C6 and C7 acrylamide isomers
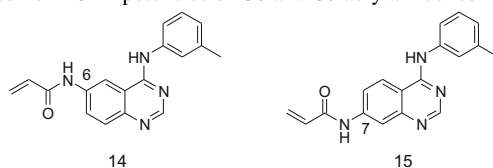
Compound	**14**	**15**
EGFR isolated enzyme IC$_{50app}$ (nM)	0.42	1.6
EGFR cell autophosphorylation (A431) IC$_{50app}$ (nM)	4.7	90

Table 3 Comparison of EGFR potencies of heterocyclic C6 and C7 acrylamide isomers
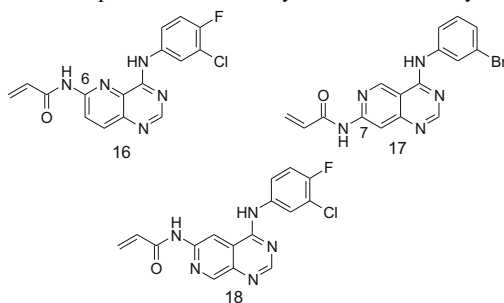
Compound	**16**	**17**	**18**
EGFR isolated enzyme IC$_{50app}$ (nM)	0.75	0.54	0.77
EGFR cell autophosphorylation (A431) IC$_{50app}$ (nM)	18	108	3.3
ErbB2 cell autophosphorylation (MDA-MB-453) IC$_{50app}$ (nM)	12		3.0

in the cell assay, and the authors speculate that this could be attributable to increased electrophilicity associated with the more electron deficient acrylamide leading to non-specific alkylation and consequently loss of active inhibitor. Alternatively the authors also suggest that the aniline may adopt a different conformation in the presence of the 5-aza atom. It was also observed that pyridopyrimidines were now equipotent against EGFR and ErbB2 in the cell based assays employed. Finally, the effect of different substitution patterns in the aniline ring of the anilinoquinazoline template was examined. These compounds largely recapitulated earlier observations described above that a lipophilic aniline *meta* substituent seemed most favourable for potency and that a metabolic blocking group at the *para*-position tended to reduce clearance and prolong in vivo half lives. Compounds with large, sterically demanding groups at the *para*-position were generally not beneficial for potency.

Six compounds from this work (including **18**) were all active in vivo when dosed either orally or via the IP route in A431 or H125 tumour xenograft models (both EGFR wild-type), but it was not possible to discern major efficacy differences between the compounds, although it did become clear that IP dosing caused greater

tolerability issues than the oral route. Although cytostatic activity was evident for these compounds, aqueous solubility was also reported to be challenging, and as a consequence the compounds were dosed as fine particulate emulsions. Solubility could be altered slightly by modification of the aniline substituent (in the order $3'$-Br $< 3'$-Cl $< 3'$-CF$_3 < 3'$-CH$_3$), but it was apparent that further improvement would be required before this chemotype could be progressed towards a clinical candidate.

Initial efforts to improve aqueous solubility were focussed on the introduction of cationic solubilising groups at the $4'$ position [29]. As has been described above, introduction of groups here previously led to a slight reduction in potency compared to the unelaborated systems, and so the authors elected to also incorporate a *meta* bromo substituent, known to enhance EGFR potency, compound **19**, Table 4.

Unfortunately, whilst these compounds did show improved solubility relative to parent, they suffered a large loss of potency against EGFR as well as no longer displaying a covalent mode of inhibition. A more fruitful avenue for exploration was the 7-position of the quinazoline. Previous work had shown that ether linkers at this position improved EGFR potency, and in addition modelling work and earlier SAR had established that solubilising side chains were tolerated at this location [11, 12]. Fixing the aniline *meta* group initially as a bromine and incorporating a variety of bases with differing pK$_a$s and two or three carbon chain linkers proved successful in delivering soluble, potent irreversible EGFR inhibitors. In contrast, an S-linked basic example was much less potent. The C7 methylpiperazinepropoxy and morpholinopropoxy ether derivatives were also combined with the 3-Me aniline head group, although these analogues did show reduced potency in the cell assay. Finally, two $4'$-F analogues (to reduce clearance and extend in vivo half life, vide supra) were combined with the morpholinylpropoxy sidechain and $3'$ Br and $3'$ Cl potency enhancing groups to provide compounds **20** and **21** (Table 5) with comparable potency to the non-solubilised or fluorinated versions, showing that the positive benefits of improved solubility and reduced clearance can be achieved without compromising potency.

As has been described above, the authors had previously examined the introduction of additional heteroatoms to the anilinoquinazoline core, and it was postulated that this might also benefit the solubility of this system by reducing

**Table 4** Structure of analogues **10** and **19**
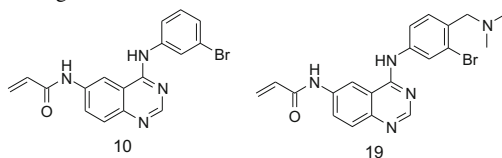
Compound	10	19
EGFR isolated enzyme IC$_{50app}$ (nM)	0.7	45
EGFR cell autophosphorylation (A431) IC$_{50app}$ (nM)	2.7	416

Table 5 Structure of analogues **20** and **21** (canertinib, CI-1033, PD-0183805, Parke-Davis/University of Auckland)
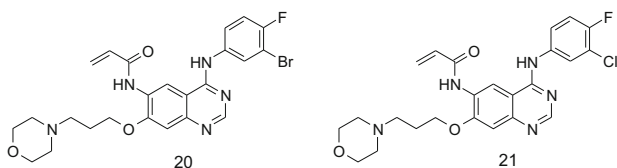
Compound	**20**	**21**
EGFR isolated enzyme IC$_{50app}$ (nM)	1.8	1.5
EGFR cell autophosphorylation (A431) IC$_{50app}$ (nM)	4.7	7.4

Table 6 Structure of analogues **22**, **23** and **24**
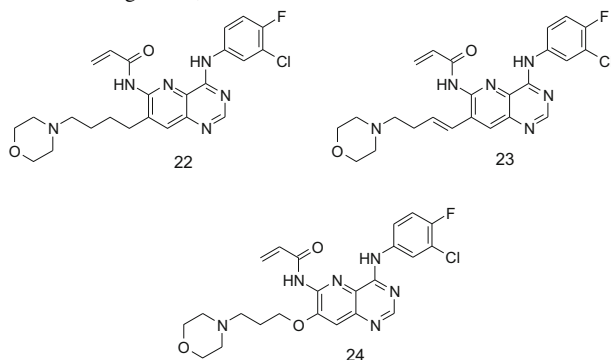
Compound	**22**	**23**	**24**
EGFR isolated enzyme IC$_{50app}$ (nM)	2.7	0.16	1.5
EGFR cell autophosphorylation (A431) IC$_{50app}$ (nM)	5,100	119	434
ErbB2 cell autophosphorylation (MDA-MB-453) IC$_{50app}$ (nM)	>5,000	12	189

lipophilicity. Consequently, a number of pyrido[3,2-*d*]-pyrimidines bearing cationic side chains at C7 were prepared (Table 6).

Analogue **22**, in which the basic sidechain was attached via a carbon as opposed to the more usual oxygen linker showed good activity in the EGFR biochemical assay but much reduced activity in the cellular autophosphorylation setting. In a similar vein, unsaturated analogue **23** again was a potent enzyme inhibitor but once more showed a large drop off when moving to the cell assay. The remaining examples prepared in this core were characterised by basic side chains appended to the pyrido[3,2-*d*]-pyrimidine core with the more usual ether linker. As described in their previous work, the authors once again noted that whilst these compounds were potent biochemical EGFR inhibitors, upon moving to the cell assay, their activities were, on the whole, disappointing. A number of studies were performed to further investigate this disconnect. By using mass spectrometry, it was shown that

22 formed a 1:1 adduct with the EGFR protein (some 1:2 protein:drug adduct was also observed). By using trypsin digestion of the drug-bound protein and analyses by LC-ESI tandem mass spectrometry (MS/MS) it was shown that C797 was the residue being alkylated. Examination of the permeability and efflux profile of **24** using a CACO2 assay demonstrated that the compounds were permeable with low efflux potential. Following examination of relative warhead stability using a gluta-thione conjugation assay, it was eventually concluded that, as initially proposed before in their earlier work, the introduction of the heteroatom renders the acryl-amide in **22** too reactive to and it is therefore not sufficiently long-lived in a cellular environment to bind appreciably to EGFR.

With a selection of potent inhibitors available, the in vivo efficacy of three compounds in a tumour xenograft model (A431 cell line) was then examined. Compound **21** (Table 5) was well tolerated and showed excellent activity at an oral dose of 5 mg/kg for 14 days. This compound (as the dihydrochloride salt) was subsequently selected as a clinical candidate for further investigation, receiving the identifier CI-1033 and subsequently being known as canertinib. The structural similarities between canertinib and gefitinib can be seen, both contain an identical anilinoquinazoline core with the only differences between the compounds being migration of the basic side chain from C6 to C7 and the incorporation of the acrylamide functionality at C6.

Initial Phase I clinical testing of canertinib was conducted in NSCLC patients, but was discontinued due to skin toxicity. Subsequent trials in metastatic breast cancer appeared more favourable, with the compound advancing as far as Phase II trials. However, its development has been discontinued due to the observation of thrombocytopenia.

4.2 pelitinib

Almost simultaneously with the studies that delivered canertinib, researchers at Wyeth–Ayerst had also been exploring a similar quinazoline-based approach to covalent EGFR inhibitors. Following their initial disclosures [30], this group subsequently described their work around the quinazoline acetylene derivative **25** [31], before finally settling on the clinical candidate EKB-569 (**26**, Fig. 11) now known as pelitinib [32]. During the course of this work, the group performed insightful studies on the relative reactivity of butynamide, crotonamide and methacrylamide cysteine targeting warheads. Of particular note was the obser-vation that incorporating a dialkylamino group onto the acrylamide β-position gave compounds with greater cysteine reactivity, postulated to be due to the basic group mediating intramolecular proton transfer during the Michael addition. The presence of the base also imparted generally improved physicochemical properties to the compounds due to lowered lipophilicity. As for canertinib, the architectural similarity with gefitinib is evident, although in this case, the hinge binding template is cyanoquinoline rather than quinazoline based. Despite entering the clinic and

Fig. 11 Structures of Wyeth-Ayerst quinazoline **25**, pelitinib (EKB-569, Wyeth-Ayerst) **26**, dacomitinib (PF-00299804, Pfizer) **27** and afatinib (Gilotrif™, Tovok™, BIBW-2992, Boerhinger Ingelheim), **28**
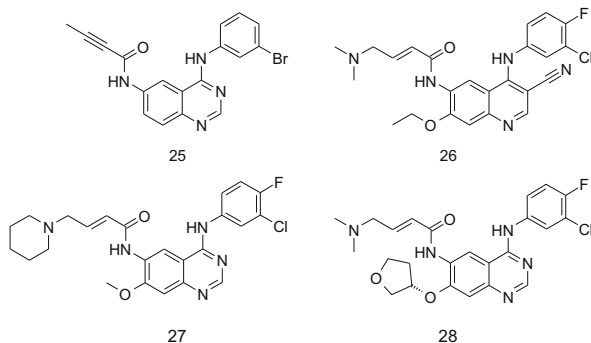
proceeding to phase II testing in both NSCLC and colorectal cancer, no further updates have been reported and the compound is believed to have been discontinued.

4.3 *dacomitinib*

The medicinal chemistry program leading to the discovery of dacomitinib (PF-00299804, **27**, Fig. 11) has not been disclosed. The compound is described as an oral, once-daily, pan-HER inhibitor. It is an irreversible inhibitor of HER-1 (EGFR), HER-2 and HER-4 tyrosine kinases, and is structurally related to canertinib (**21**) and pelitinib (**26**). The main differences between canertinib and dacomitinib are the migration of the base at C7 in the former to the acrylamide functionality at C6 of the latter, a feature also seen originally in pelitinib.

Nevertheless, it has been reported [33] that dacomitinib possesses greater oral bioavailability, longer half-life, larger volume of distribution and lower plasma clearance than canertinib. Clinical investigation of this agent is ongoing [34], although progress in its use in the treatment of recurrent and/or metastatic head and neck squamous cell cancer has not been updated for some time. Dacomitinib was also studied in the treatment of patients with locally advanced or metastatic NSCLC. Unfortunately, in January 2014 it was announced that in this setting, neither progression free survival relative to erlotinib nor overall survival compared with placebo was improved. A further trial comparing dacomitinib to gefitinib in treatment naïve advanced NSCLC patients remains ongoing at the time of writing. Most recently, in 2015, the compound received orphan drug status designation for the treatment of non-small cell lung cancer with EGFR, HER2, HER4, or DDR2 mutations.

4.4 afatinib

Afatinib (BIBW2992) (**28**, Fig. 11) is another anilinoquinazoline-based irreversible EGFR inhibitor and was discovered by researchers at Boerhinger Ingelheim [35].

   Again, little has been published around the medicinal chemistry program that led to the identification of this agent. It has been noted that the potent HER2 activity of afatinib, in addition to its EGFR potency, may offer additional indications relative to earlier inhibitors [36]. Afatinib and dacomitinib are structurally similar, with afatinib employing a dimethylamine rather than piperidine as the base appended to the acrylamide. In addition, afatinib also now contains a 3*S*-tetrahydrofuarn-3-yl-oxy group at C7. To date, afatinib is the only irreversible anilinoquinazoline-based EGFR inhibitor approved by the FDA and it was launched in the USA as Gilotrif^{TM} in July 2013. Currently it is approved for first-line treatment for patients with metastatic NSCLC who carry an activating EGFR mutation (see below) with a recommended daily dose of 40 mg. The drug was also launched for this indication in the UK and Japan in 2014. Afatinib is also in Phase III clinical trials for a variety of other tumour types including metastatic breast cancer, as well as recurrent and/or metastatic head and neck squamous cell carcinoma.

5 EGFR Mutant Selective Inhibitors

5.1 Sensitising/Activating Mutations

The clinical development of both gefitinib (**7**) and erlotinib (**8**) was complicated by a lack of knowledge of the genetic backgrounds of the patients recruited into the trials and an understanding of how that genetic profile might impact their response to treatment. Following Phase I trials, broad, non-selected NSCLC patient populations were targeted in subsequent studies and disappointing results were observed for these compounds, although, as described above, the erlotinib data was sufficient to allow approval. Subsequent analysis of the data revealed possible reasons for these outcomes. The intended target for these EGFR inhibitors was the wild-type form of the receptor, but retrospective examination of the tumours of those patients that responded to gefitinib and erlotinib showed an unexpected finding [37]. A common characteristic of the responding patients was the presence of mutations in the kinase domain of the receptor. The mutations identified (Fig. 12) were either the single point mutation of L858R or Exon19 deletion (deletion of the amino acid sequence 746–750 from the protein chain).

   These changes were found to render the receptor constitutively activated, independent of ligand stimulation [39]. In addition, further examination of these mutants also showed that they caused a reduced affinity of the kinase for ATP [40], thus rendering the receptors more susceptible to inhibition by an ATP competitive inhibitor (Table 7). Consequently, these mutations were termed activating, or sensitising, mutations of EGFR. Those patients carrying these mutations were
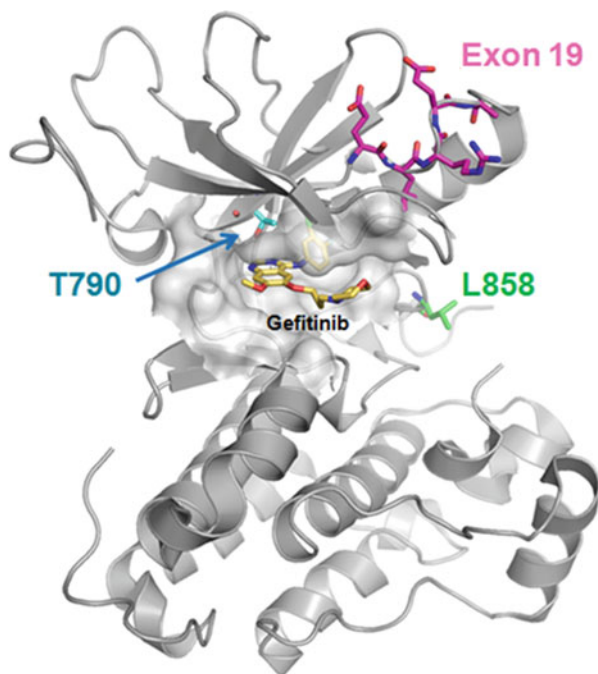
Fig. 12 Crystal structure of EGFR kinase domain, highlighting location of activating (Exon19 deletion and L858R) and resistance (T790M) mutations. Reprinted (adapted) with permission from Ward et al. [38]. Copyright (2013) American Chemical Society

Table 7 Cell data for gefitinib and erlotinib

Compound number	PC9 p-EGFR EC_{50} (µM)	LoVo p-EGFR EC_{50} (µM)	H1975 p-EGFR EC_{50} (µM)
7 (gefitinib)	0.007	0.059	3.1
8 (erlotinib)	0.006	0.084	6.1

PC9 cells (exon19 deletion EGFR), LoVo cells (wild-type EGFR), H1975 cells (L858R/T790M EGFR)

observed to be those who responded more favourably to gefitinib or erlotinib. As a result of the growing understanding of which patients would respond to gefitinib treatment, Iressa™ was approved for first-line treatment of patients with advanced EGFR mutation-positive NSCLC by the European Medicines Agency in June 2009 and subsequently by the FDA in July 2015. In addition, both erlotinib and afatinib have also been granted approval in this setting based on these findings. Further understanding has also emerged over the biological role of the wild-type form of the EGF receptor. As was noted above, EGFR has an important function in the maintenance of epithelial tissues such as the skin and the lining of the digestive tract, and its inhibition is believed to lead to the dose limiting toxicities of skin rash

and diarrhea [41] that are observed in the clinic with gefitinib, erlotinib and afatinib. Key to the successful utilisation of erlotinib and gefitinib in the clinic has been the fortuitous difference in ATP affinity between wild-type EGFR and the sensitising mutations. As the latter forms have lower affinity for ATP than wild-type (and consequently are easier to inhibit), then it is possible to have a degree of selectivity for the mutants over the wild type (see Table 7), allowing disease efficacy before the onset of toxicity, although this will still limit the achievable dose.

5.2 Resistance Mutations

Around 70% of patients carrying a sensitising mutation respond to treatment with EGFR inhibitors, but most patients develop resistance to these therapies after an average of 10–11 months. In around two thirds of these cases, resistance and subsequent disease progression is due to the acquisition of a second mutation in the EGFR kinase domain, in addition to the sensitising mutation [42]. This "double mutant" now possesses a methionine residue in place of the natural threonine at position 790 (the so-called gatekeeper residue as it controls ease of inhibitor access to the so-called back pocket, Fig. 12). As in the case of the sensitising mutation, the presence of the double mutant impacts several key aspects of the kinase function, and these can help rationalise why the double mutant leads to resistance. It has been shown that, in contrast to the sensitising mutations that reduce the ATP affinity of the kinase, the double mutant has a similar ATP to that of the wild-type and consequently diminishes the ability of an ATP competitive inhibitor to impede double mutant kinase function whilst maintaining a margin to wild-type (Table 7) [40, 43]. The change from a threonine to methionine gatekeeper also reduces the ability of anilinoquinazolines to bind to the T790M mutant form, due to the increased steric demands of the methionine residue, which is postulated to interact less favourably with the aniline portion. Given the above findings, it was hypothesised that irreversible EGFR inhibitors such as afatinib described above might offer a way to circumvent the high ATP affinity of the double mutant system, and in vitro this was shown to be the case [44]. However, the C797 residue that these inhibitors covalently bind to is conserved across not just the sensitising and T790M mutants but also in the wild-type form of the kinase. As such afatinib, canertinib and dacomitinib exhibit potency against the mutated receptor forms, but they also display potent wild-type inhibition to the extent that the toxicity from the latter prevents dosing these agents at a sufficient level to meaningfully inhibit the double mutant in a clinical setting. In light of the clinical challenges posed by the double mutant, a number of groups attempted to design "mutant selective" inhibitors that preferentially inhibit both sensitising and resistance mutations while sparing the wild-type form of the receptor. Such an agent would potentially lead to a therapy that would overcome the T790M resistance issue whilst also delivering a more benign tolerability profile due to reduced wild-type activity.

Researchers from the Dana-Farber Cancer Institute (DFCI) were the first group to disclose their efforts towards EGFR inhibitors with a T790M "mutant selective" profile [45]. This group prepared a library of common kinase inhibitor core scaffolds in which one of the sidechains was modified by incorporation of an acrylamide motif, placed in such a way as predicted by molecular modeling to interact covalently with C797 as described above. The library was then screened in cells expressing both the sensitising and resistance EGFR mutations. Three closely related pyrimidines (**29**, **30** and **31**, Fig. 13) identified from this work showed high potency against the L858R/T790M mutant EGFR cells (H1975) with selectivity over the wild-type expressing cell line HN11.

Further work also showed that the compounds formed a 1:1 adduct with the protein, and mass spectrometry analysis of a pepsin digest of the modified protein showed C797 as the site of modification. An X-ray crystal structure of compound **30** bound to EGFR T790M kinase domain explained several aspects of their potency and wild-type selectivity observations (Fig. 14).

Key findings were the interaction of the pyrimidine 5-chloro group with the methionine gatekeeper, with the authors postulating that this lipophilic interaction drove the observed double mutant potency and increased wild-type selectivity.
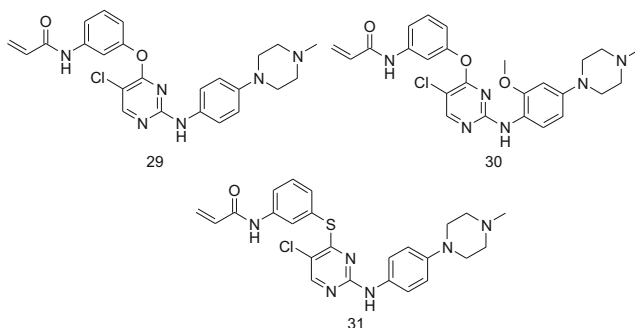
Fig. 13 Structures of Dana Farber EGFR hits (**29**), (**30**) and (**31**)
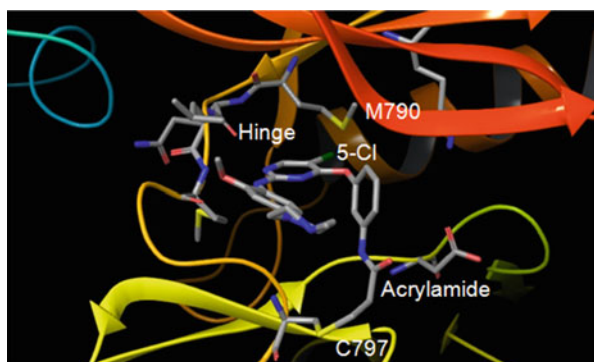
Fig. 14 X-ray structure of **30** (3IKA) bound to EGFR kinase domain

In addition the X-ray structure confirmed the formation of a covalent bond between C797 and the acrylamide group and the role of the anilinopyrimidine group in providing a hydrogen bond donor and acceptor motif with the kinase "hinge". **30** was then selected for in vivo profiling, largely based on its primary potency for the double mutant along with low wild-type EGFR potency and lack of activity against other cysteine containing kinases. Pharmacokinetic evaluation revealed an oral half-life of 2.5 h and a bioavailability of 24%. Mouse pharmacodynamic studies demonstrated significant knock down of both phospho-EGFR and downstream markers such as AKT and ERK1/2. Additionally, the compound showed good efficacy in anti-tumour studies against T790M xenografts, with tumour regressions being evident following 14 days oral dosing. Finally, in vitro the authors were able to demonstrate that treating cells harbouring sensitising mutations with **30** did not lead to the emergence of the T790M mutation, in contrast to gefitinib treatment. No further development **30** has been disclosed.

An initial disclosure from Celgene Avilomics Research (originally Avila Therapeutics) described the discovery of the covalent inhibitor **32** (Table 8) [46].

Table 8 Structures and selected cell data for Celgene compounds **32**, **33**, **34**, **35**, **36** and **37**
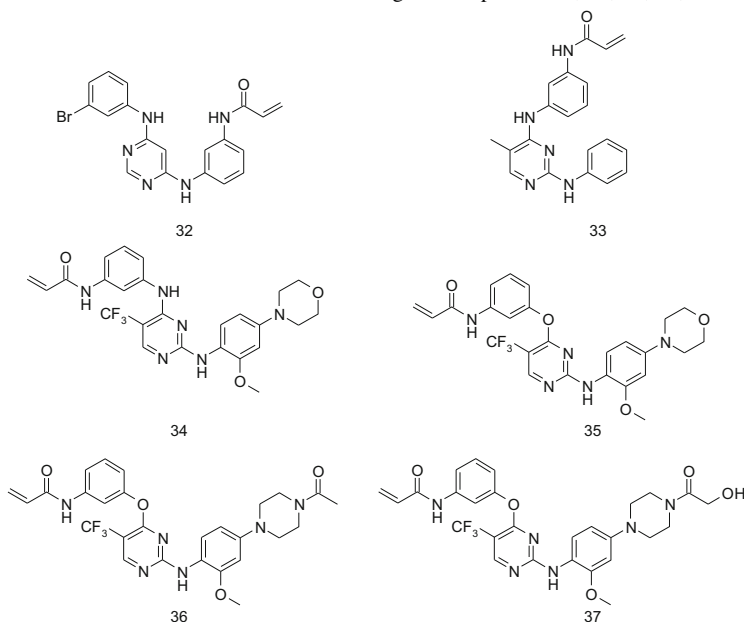
Compound number	A431 p-EGFR EC$_{50}$ (nM)	H1975 p-EGFR EC$_{50}$ (nM)	A431 proliferation GI$_{50}$ (nM)	H1975 proliferation GI$_{50}$ (nM)
34	3,304	48	1,305	130
35	2,529	35	1,416	132
36	>4,331	58	602	48
37	1,669	75	727	50

A431 cells (wild-type EGFR), H1975 cells (L858R/T790M EGFR)

Whilst **32** was shown to bind to C797 and displayed impressive activity against the sensitising and T790M double mutant in both cellular EGFR phosphorylation and proliferation assays, this was also accompanied by very high levels of wild-type activity. Modifying the pyrimidine substitution pattern and incorporation of a methyl group at the pyrimidine 5-position gave compound **33** (Table 8) [47], which showed modest selectivity for the double mutant over the wild-type kinase.

Encouraged by this finding, the group then went on to explore further lipophilic groups at this position to interact with the gatekeeper methionine, including halogens, CF_3, methyl ketone and cyclopropyl [48–51]. Additional SAR was also generated around the nature of the pyrimidine C4 linker group with an NH in combination with a 5-CF_3 group appearing optimal for potency. Broader kinome selectivity (in particular over BTK) was improved by the incorporation of a methoxy group at the 2-position of the aniline. In an attempt to reduce the lipophilicity of the lead compounds, a number of examples were prepared with a basic group appended to the acrylamide warhead, but cell potency tended to be negatively impacted by this change. The addition of a piperazine to the 4-position of the aniline did improve properties and the compounds' in vivo profiles, but wild-type selectivity was reduced and affinity for the hERG ion channel was increased to unacceptable levels. More productive was the move to a morpholine or acylated piperazine at the aniline 4-position, with the reduced pK_a afforded by these changes removing the hERG liability. This led to the identification of a shortlist of four compounds (**34**, **35**, **36**, **37**, Table 8).

The compounds were all shown to be potent inhibitors in cells of the T790M mutant (Table 8), with compound **37** being selected for further in-depth evaluation, largely based on its excellent wild-type selectivity.

When dosed orally at 100 mg/kg in an H1975 mouse tumour xenograft model, **37** (now known as CO-1686 or rociletinib) showed excellent tumour growth inhibition, with partial tumour regressions being evident after 24 days of dosing. In contrast, when dosed in an A431 (EGFR wild-type) tumour growth inhibition study, the compound showed only very modest activity. Rociletinib was licensed by Clovis Oncology Inc. and has shown clinical activity, with responses being evident in some NSCLC T790M positive patients who have progressed on previous EGFR TKI treatment. The compound was relatively well tolerated, with hyperglycaemia the major dose limiting toxicity observed. This is believed to be driven by the potent insulin receptor kinase inhibitory activity of the metabolite **38**, derived from in vivo deacylation of rociletinib [52]. Interestingly, responses in T790M negative patients have also been observed, although the reasons behind this are not entirely clear [53]. This may be arfetactual, arising from the heterogeneity of tumours, and that when a biopsy is taken it may sample a T790M negative region of the tumour, whereas the bulk may be T790M positive. Alternatively, the diagnostic test employed may in some cases lack the sensitivity to detect the presence of the T790M mutation and lead to a patient being incorrectly declared T790M negative. It has been reported that the insulin receptor/IGF1R pathway mediates resistance to EGFR inhibitors [54] and there has been some conjecture that the IGF1R kinase inhibitory activity of active metabolite **38** (Fig. 15) may contribute to activity in this segment. A rolling submission for approval of rociletinib as a second line treatment
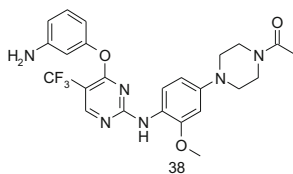
Fig. 15 Structure of rociletinib metabolite **38**, which carries potent insulin receptor activity

in NSCLC was made to the FDA in July 2015. However, in November 2015, Clovis announced that as their efficacy data matured, the number of patients with an unconfirmed response who converted to a confirmed response was lower than expected (the current confirmed response rate is 45 percent [53]. In many instances, progression due to brain metastases was noted. However, following an April 2016 FDA Oncologic Drugs Advisory Committee hearing that voted against the accelerated approval of rociletinib and recommended that a randomised Phase III study comparing the compound against single-agent chemotherapy be first completed, Clovis discontinued the development of rociletinib in May 2016.

AstraZeneca was responsible for the discovery of Iressa™ described above, and with a long-standing interest in the discovery of EGFR inhibitors, also commenced work to discover T790M inhibitors, starting with biochemical testing against the wild-type and T790M double mutant kinases [38]. The initial selection of compounds for testing fell into three classes: reversible anilinoquinazoline-based EGFR inhibitors, irreversible covalent anilinoquinazoline-based EGFR inhibitors and a selection of compounds from previous projects that had been targeting methionine gatekeeper kinases. The anilinoquinazoline-based compounds gave largely the expected inhibition profiles, with the reversibles showing greater activity against wild-type than double mutant, and the covalent compounds showing potent activity against both. However, in contrast to these findings, the methionine gatekeeper targeting examples showed good potency against the T790M mutant as well as selectivity over the wild-type kinase, presumably driven by the preference for the lipophilic pyrimidine 5-substituent of these compounds to interact with the methionine rather than threonine gatekeeper residue. An example of these initial selective hits was compound **39** (Table 9) which originated from AstraZeneca's IGF1R kinase inhibitor project [38].

While compounds such as **39** did show biochemical potency for the double mutant and selectivity over the wild-type kinase, when tested in a cellular phospho-EGFR assay, a large decrease relative to the isolated enzyme potency was observed (Table 9). This was perhaps not wholly unexpected, given the high affinity of the L858R/T790M double mutant for ATP described above.

In an attempt to circumvent this problem, the team elected to explore covalent targeting of cysteine 797 in an analogous fashion to that described above for afatinib and related compounds. Using a simplified template, which lacked the piperazine group of **39**, different potential positions for covalently targeting C797 using an acrylamide motif were explored. This ultimately led to the identification of

Table 9 Biochemical and cell data for AstraZeneca compounds **39** and **40**
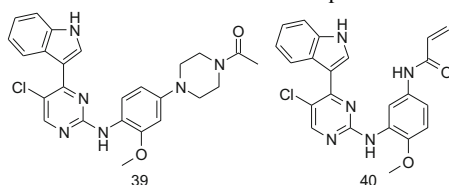
Compound number	L858R/T790M enzyme IC$_{50}$ (μM)	H1975 p-EGFR EC$_{50}$ (μM)	LoVo p-EGFR EC$_{50}$ (μM)
39	0.009	0.77	0.77
40	0.006	0.022	0.55

H1975 cells (L858R/T790M EGFR), LoVo cells (wild-type EGFR)
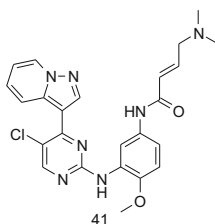
Fig. 16 Structure of compound **41**

inhibitor compound **40** (Table 9), which now showed good potency in the phospho-EGFR cell assay and a selectivity margin to wild-type activity.

Variation of the substituent at the pyrimidine 5-position was then undertaken. This was considered an important position to understand further, as it was speculated that groups here would be oriented towards the kinase gatekeeper residue. In general, double mutant potency was increased by lipophilic groups such as halogens, whereas the sensitising mutant potency remained largely unchanged by these alterations. Efforts were then directed towards reducing the relatively high lipophilicity of the compounds. This was ultimately achieved not only by incorporation of a pendant base on the acrylamide (as had been done with afatinib), but also by alteration of the heterocycle attached at the pyrimidine 4-position. Replacement of the indole moiety with a pyrazolo[1,5-a]pyridine group led to compound **41** (Fig. 16), which had reduced LogD$_{7.4}$ and improved physicochemical properties.

Although **41** was not viewed as having clinical candidate quality (due to low aqueous solubility, hERG affinity and IGF1R potency, Table 10), when dosed orally in mouse xenograft studies at 60 mg/kg for 7 days, it produced significant tumour growth inhibition in both the H1975 (double mutant) and PC9 (sensitising mutant) models. Significantly lower tumour growth inhibition was noted in the A431 (wild-type) model, consistent with the in vitro cell profile. Interestingly, when dosed in the same models at a clinically relevant dose of 6.25 mg/kg for 7 days,

Table 10 Data for AstraZeneca probe compound **41**

	PC9 p-EGFR EC$_{50}$ (µM)	H1975 p-EGFR EC$_{50}$ (µM)	LoVo p-EGFR EC$_{50}$ (µM)	hERG IC$_{50}$ (µM)	Solubility (pH = 7.4)	LogD$_{7.4}$	% tumour growth inhibition (DM/SM/WT)	IGF1R enzyme IC$_{50}$ (µM)
41	0.4	0.096	23	4.2	1.6	3.6	105/141/46	0.004

PC9 cells (exon19 deletion EGFR), H1975 cells (L858R/T790M EGFR), LoVo cells (wild-type EGFR). % tumour growth inhibition is from a PO dose QD for 7 days at 60 mg/kg
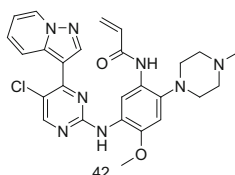
Fig. 17 Structure of compound **42**

Table 11 Data for AstraZeneca compound **43**

	PC9 p-EGFR EC$_{50}$ (µM)	H1975 p-EGFR EC$_{50}$ (µM)	LoVo p-EGFR EC$_{50}$ (µM)	hERG IC$_{50}$ (µM)	LogD$_{7.4}$	IGF1R enzyme IC$_{50}$ (µM)
42	0.14	0.019	23	7.1	3.6	0.002

PC9 cells (exon19 deletion EGFR), H1975 cells (L858R/T790M EGFR), LoVo cells (wild-type EGFR)

gefitinib showed good activity in the sensitising (142% tumour growth inhibition) and wild-type models (79% tumour growth inhibition) but was inactive in the double mutant model, even when dosed as high as 100 mg/kg/day.

Encouraged by this initial data, the team devised and prepared a series of further analogues based on compound **41**. Whilst higher levels of T790M potency were achievable in this template, the structural changes that delivered these improvements always caused increased lipophilicity and compromised physicochemical properties, and it was concluded that these compounds did not have the potential to deliver a cell potent inhibitor with a sufficiently low LogD$_{7.4}$ value to deliver acceptable ADMET properties. A way to increase potency without increasing lipophilicity needed to be found. It was apparent from the SAR of reversible analogues that incorporation of a base in the aniline 4-position led to improved biochemical potency with no accompanying increase in LogD. These SAR findings were incorporated into a covalent scaffold, resulting in compound **42** (Fig. 17), which displayed a highly attractive profile (Table 11).

Compound **42** was observed to have the same LogD$_{7.4}$ as **41** (Table 11), but showed approximately a fourfold increase in double mutant cell potency,

i.e. increased lipophilicity ligand efficiency (LLE, calculated as the cellular pIC_{50} minus $LogD_{7.4}$) and further analogues of **42** were targeted for synthesis, with a focus on further modification and exploration of the basic side chain group.

Three distinct sub-series were designed [55] based on the scaffold of **42**, piperazinyl amides, open chain diamines and cyclic diamine piperazine replacements of varying ring size (Fig. 18).

Whilst the piperazinyl amides such as **43** were attractive compounds, they were overshadowed by the surprising findings from the other two subseries. The examples where the piperazine ring had been contracted (**44** and **46**) or opened up (**45**) delivered double mutant cell potent (<1 nM in the case of **45**), wild-type selective inhibitors with good LLE (Table 12). The compounds also had good pharmacokinetic profiles in mouse, and they showed excellent acute biomarker modulation when dosed orally at 10 mg/kg in mice carrying H1975 or PC9 tumour xenografts.
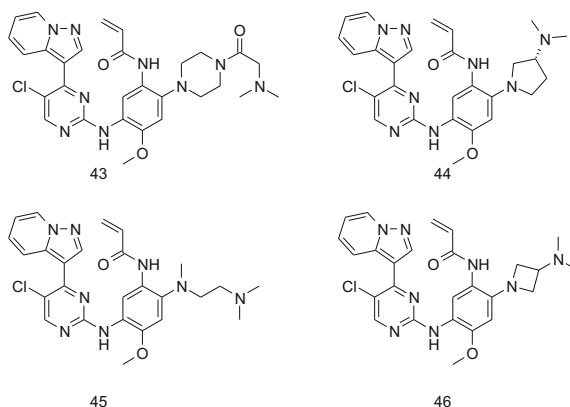
Fig. 18 Structures of compounds **43**, **44**, **45** and **46**

Table 12 Data for AstraZeneca compound **43**, **44**, **45** and **46**

	PC9 p-EGFR EC_{50} (μM)	H1975 p-EGFR EC_{50} (μM)	LoVo p-EGFR EC_{50} (μM)	$LogD_{7.4}$	Solubility (μM, pH = 7.4)	% tumour growth inhibition (DM/SM/WT)	hERG IC_{50} (μM)	IGF1R enzyme IC50 (μM)
43	0.074	0.016	10.1	2.6	290	–	18	0.002
44	0.016	0.002	0.357	3.1	28	134/227/27	5.6	0.007
45	0.002	0.0006	0.145	2.8	400	130/243/35	6.7	0.006
46	0.02	0.004	0.938	3.3	43	113/169/16	4.0	0.026

PC9 cells (exon19 deletion EGFR), H1975 cells (L858R/T790M EGFR), LoVo cells (wild-type EGFR). % tumour growth inhibition is from a PO dose QD for 7 days at 10 mg/kg

In addition, when tested in the three previously described in vivo tumour models, the compounds all had excellent efficacy at 10 mg/kg in 7 day studies, with mutant tumour regressions evident, accompanied by very little wild-type activity. The compounds still carried IGF1R activity, reflecting their origins, and hERG affinity was generally less than 10 μM. Nevertheless, rat and dog PK testing delivered attractive profiles, with dose to man predictions suggesting these compounds might be of candidate quality and consequently **44**, **45** and **46** were shortlisted as possible clinical candidates.

Given the positive benefits delivered by migration of the base from the acrylamide to the aniline series, in the pyrazolo[1,5-a]pyridine series, the same change was investigated in the original indole series. Consequently, a small library of compounds varying the basic side chain, the pyrimidine 5-position and methylation of the indole head group was explored. A selection of compounds from this work is shown below (Fig. 19).

It was apparent that the ethylene diamine sidechain was the more potent motif and the other groups investigated will not be discussed further. Analysis of matched molecular pairs [55] produced some useful SAR observations. Whilst a lipophilic group at the pyrimidine 5-position drove higher wild-type selectivity and increased IGF1R potency, the impact of its presence or absence on potency was much more pronounced in the latter kinase. In addition, indole methylation was also observed to both increase selectivity over the wild-type kinase and reduce IGF1R potency. These findings offered an opportunity to reduce the IGF1R activity. In the indole series, replacing the 5-chloro group with hydrogen would be predicted to show less IGF1R potency, but also reduced selectivity over wild-type EGFR as well as lower double mutant potency. However, application of the indole SAR described above could suggest a 5-H substituted compound with a suitable overall profile: good potency could be achieved by employing the indole head group combined with the ethylene diamine sidechain and wild-type selectivity could be recovered by employing the methylated indole 4-substituent. The compounds in Table 13 are illustrative of this SAR, with compound **49** displaying a favourable hERG and IGF1R profile, as well as good mutant potency and wild-type kinase selectivity. On
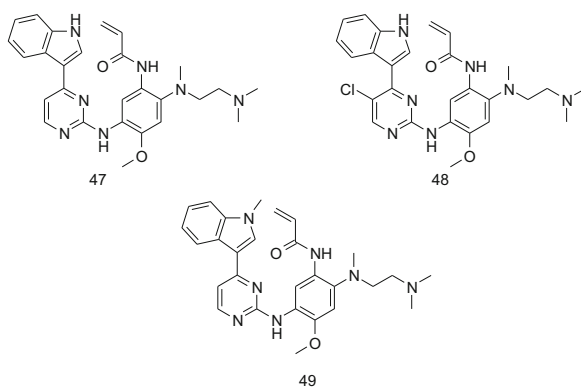
Fig. 19 Structures of compounds **47**, **48** and **49** (osimertinib, AZD9291)

Table 13 Data for AstraZeneca compounds **47**, **48** and **49**

	PC9 p-EGFR EC_{50} (μM)	H1975 p-EGFR EC_{50} (μM)	LoVo p-EGFR EC_{50} (μM)	Mouse PO AUC/Cmax (μM h/μM)	hERG IC_{50} (μM)	IGF1R enzyme IC_{50} (μM)	% tumour growth inhibition (DM/SM/WT)
47	0.002	0.002	0.032	0.2/0.05	17	0.026	–
48	0.0002	0.0006	0.011	3.3/1.2	15	0.007	–
49	0.014	0.016	0.541	1.4/0.38	16	2.9	134/242/79

PC9 cells (exon19 deletion EGFR), H1975 cells (L858R/T790M EGFR), LoVo cells (wild-type EGFR). % tumour growth inhibition is from a PO dose QD for 7 days at 5 mg/kg

the basis of this profile, this compound was advanced into the previously described in vivo efficacy studies, and gratifyingly, it displayed excellent mutant tumour growth inhibition at 10 mg/kg, but also at the lower oral dose of 5mpk and indeed lower. With this excellent profile, **49** was also shortlisted for development.

The AstraZeneca researchers were aware that inhibition of IGF1R kinase tends to lead to concomitant inhibition of the insulin receptor, itself possessing a methionine gatekeeper kinase domain. Consequently, the team designed a rat toxicological study to examine this further. Rats received a single oral dose of each compound at 200 mg/kg and significant compound exposure was achieved in all four cases. Insulin and glucose levels were then monitored. Compounds **44** and **45** were caused an almost immediate increase in blood glucose levels, whilst **46** and **49** were largely similar to control. When examining the data for insulin, a more sensitive biomarker, **44** and **45** elevated insulin levels to a marked extent almost immediately. Compound **46** was found to have a lower impact on insulin levels, while **49** was indistinguishable from control. These in vivo data showed the same relative trend as the in vitro IGF1R potencies of the four compounds. At this point, it was decided that **44** and **45** should not be taken further forward and the compounds were discontinued from further study. Cardiovascular safety assessment of **46** and **49** revealed that **46**, when dosed in the guinea pig monophasic action potential study, caused marked QT prolongation. In contrast, even at very high doses **49** was devoid of this effect and as a consequence was selected as clinical candidate AZD9291 (international nonproprietary name osimertinib) [54]. More chronic in vivo tumour growth inhibition studies have been performed with osimertinib in addition to the relatively brief initial studies that were described above [56]. In the PC9 in vivo model (activating mutation, Exon 19 deletion), osimertinib at an oral dose of 5 mg/kg/day exhibited superior efficacy to gefitinib with tumours being essentially non-palpable by day 40 of the experiment (Fig. 20).

In addition, in a study employing the H1975 cell line (L858R/T790M), a dose of 5 mg/kg/day showed substantial regression for a 200 day period [56]. Also, a dose of 25 mg/kg/day orally rendered tumours essentially non-palpable by day 20 and as before this activity was maintained up to the cessation of dosing at day 200. Smaller oral doses of osimertinib (1 mg/kg/day) showed initial activity, which was lost at day 50, but could be restored by an increase of dose to 25 mg/kg/day, again
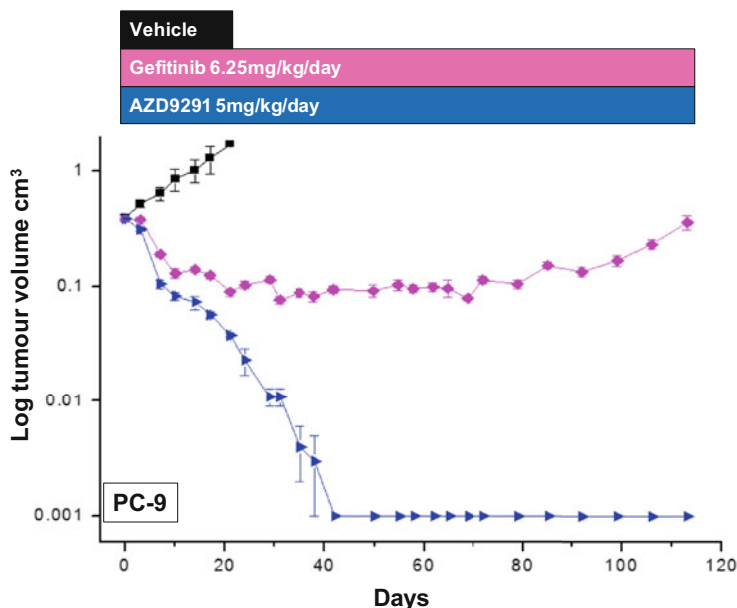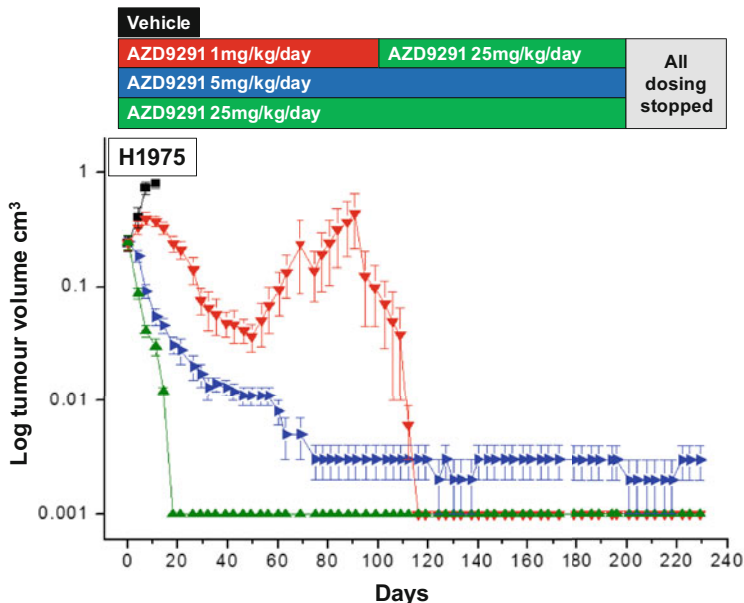
Fig. 20 Mouse in vivo tumour growth inhibition comparison of gefitinib and osimertinib employing PC-9 xenografts. Adapted by permission from the American Association for Cancer Research: Cross et al. [56]

resulting in very significant tumour regression for 200 days. These data are summarised in Fig. 21.

The compound was first dosed to NSCLC patients in March 2013. The initial dose selected for testing was 20 mg and, unusually for a phase I "first into human" study, clinical activity was seen in the very first dose cohort tested [56], enabling rapid acceleration of the clinical program. No maximum tolerated dose was defined during phase I, so the phase II dose was selected based on efficacy and safety data reviewed across the 20–240 mg dose range, with a once-daily 80 mg dose being selected for registration studies. Interestingly, clinical activity with osimertinib has also been anecdotally reported in NSCLC patients presenting with brain metastases and more detailed studies here are ongoing in the clinic [57]. On the 13th of November 2015, osimertinib was granted accelerated approval by the United States FDA "for the treatment of patients with metastatic epidermal growth factor receptor (EGFR) T790M mutation-positive non-small cell lung cancer (NSCLC), as detected by an FDA-approved test, who have progressed on or after EGFR tyrosine kinase inhibitor (TKI) therapy". This approval was based on data from the pre-planned analysis of two clinical trials at the 80 mg QD dose, and osimertinib is now marketed as TAGRISSO^{TM}. A recent disclosure showed an objective response rate (ORR) of 66.1% in T790M positive patients (Fig. 22) [58]. Further disclosures from this analysis demonstrated a median progression free survival (PFS) of 9.7 months (maturity 39%). On the 3rd of February 2016, the European Medicines

Fig. 21 Mouse in vivo tumour growth inhibition comparison of doses of osimertinib employing H1975 xenografts. Adapted by permission from the American Association for Cancer Research: Cross et al. [56]
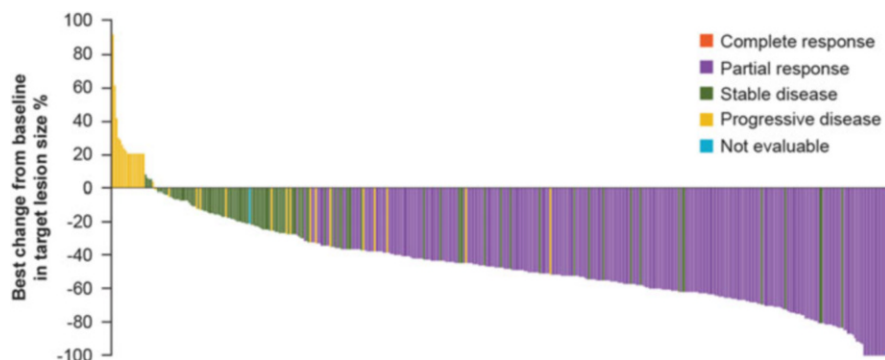
Fig. 22 Osimertinib in pre-treated patients with T790M positive advanced non-small cell lung cancer (NSCLC): pooled analysis. By blinded independent central review. Evaluable for response analysis set ($n = 398$). Mean best percentage change in target lesion size -45%, standard deviation 28.0 (median best percentage change -47.6%; range: -100% to $+90.8\%$). Adapted from a presentation by Goss [58]

Agency also granted conditional marketing authorisation for TAGRISSO™ for the treatment of adult patients with locally advanced or metastatic T790M mutation-positive non-small cell lung cancer. Regulatory approval in Japan was also granted in March 2016.

Additional clinical investigation with osimertinib continues, both in combination with other targeted therapies and as a first line treatment (vide infra).

A number of other mutant selective EGFR inhibitors have recently been disclosed in the literature, and some are now advancing through clinical trials. Data and structures of these compounds (where disclosed) are captured below (Fig. 23), but it is beyond the scope of this chapter to discuss these in any detail. Olmutinib (Olita^{TM}, HM61713, BI1482694, Fig. 23) is now approved in South Korea for patients with EGFR T790M mutation-positive lung cancer, although based on a re-evaluation of available clinical data and recent treatment advances made in EGFRm NSCLC, Boehringer Ingelheim has announced that it has returned development and commercial rights of olmutinib to Hanmi. Taiho Pharma is known to be developing TAS-121 as an oral mutant EGFR selective inhibitor and is currently in Phase 1 clinical trials, but no structure has yet been disclosed. In addition, numerous additional pre-clinical T790M inhibitors have been described in the literature (For example, see: [59–61]).
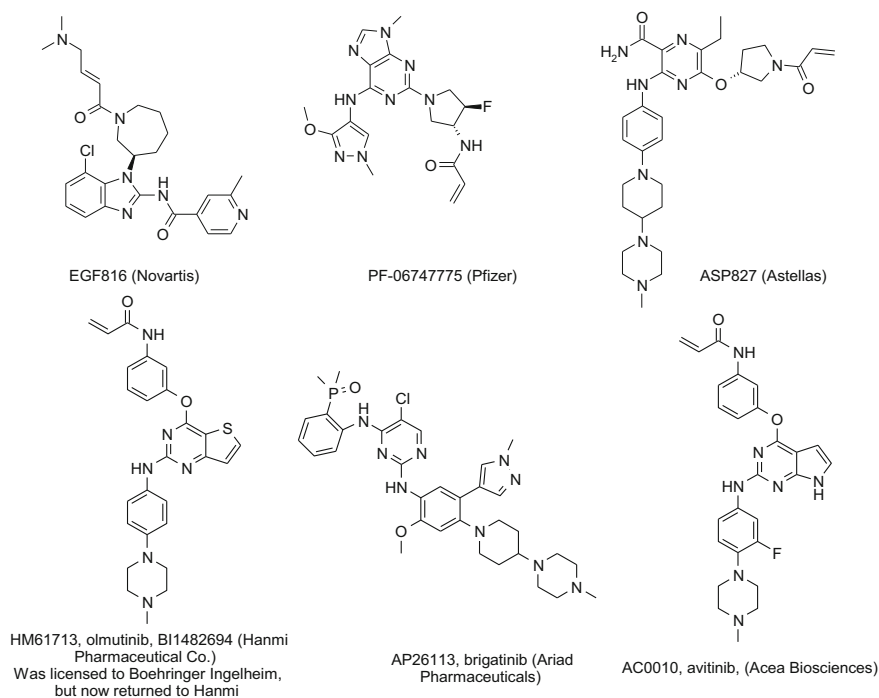
Fig. 23 Structures of Novartis, Pfizer, Astellas, Hanmi, Ariad and Acea clinical mutant selective EGFR inhibitors

6 Future Perspectives

The progress in identifying and developing EGFR inhibitors over the past three decades has been remarkable and has resulted in clear and meaningful benefit to NSCLC patients. Also noteworthy is the growth in knowledge and understanding of the area, moving from broadly targeted use of inhibitors with mixed results, to more clearly understanding the significance of sensitising mutations and the role of the wild-type receptor in driving toxicity. The emergence of the EGFR T790M resistance mutation prompted a flurry of discovery activity and patients are now starting to see the benefits of these endeavours. It is likely that resistance in the clinic will again emerge to these treatments as tumour cells continue to evolve mechanisms to evade their effects, and indeed in the case of osimertinib, a C797S "triple mutant" (removing the possibility of covalent bond formation to osimertinib) has been observed in some patients who have progressed on this treatment [62]. In the case of rociletinib, clinical resistance has been observed in a variety of forms including re-emergence of the T790 wild-type protein, and EGFR amplification [63]. However, with much greater understanding now at their disposal, clinicians and pre-clinical scientists are able to more quickly explore ways to circumvent the next resistance mechanism. Further research has shown that in addition to EGFR mutations, other signalling pathways (MET [64] and see also Cross et al. [56], MEK [65]) can also be upregulated in response to EGFR inhibitor treatment and the combination of an EGFR inhibitor with a compound to inhibit these pathways may have clinical potential. In the past such combinations were challenging due to the toxicity burden imposed by the two combined agents. However, the wild-type margin and improved tolerability of agents such as osimertinib and olmutinib now makes these combination opportunities more attractive, and such studies are currently ongoing in the clinic [66, 67]. Whilst compounds such as rociletinib and osimertinib have been extensively studied as second line treatments in patients who have progressed following gefitinib or erlotinib therapy, in the case of osimertinib, use as a first line treatment in TKI naïve patients has also recently shown very encouraging clinical activity. In 60 patients who received osimertinib once daily at either 80 or 160 mg, the median progression-free survival (PFS) was 19.3 months, and the confirmed objective response rate (ORR) was 77% [68]. Further data for osimertinib in this setting is awaited. The EGFR inhibitor landscape continues to evolve and challenge the research community, but it is likely that the target will continue to provide both scientific challenges and patient benefit for a considerable time to come.

References

1. Stewart BW, Wild CP (eds) (2014) World cancer report 2014. International Agency for Research on Cancer, Lyon
2. Normanno N, De Luca A, Bianco C, Strizzi L, Mancino M, Maiello MR, Carotenuto A, De Feo G, Caponigro F, Salomon DS (2006) Gene 366:2–16
3. Schneider MR, Wolf E (2009) J Cell Physiol 218:460–466
4. Baselga J (2002) Oncologist 7(Suppl 4):2–8
5. Ward WHJ, Cook PN, Slater AM, Davies DH, Holdgate GA, Green LR (1994) Biochem Pharmacol 48:659–666
6. Barker AJ, Davies DH, Imperial Chemical Industries PLC (1992) Preparation of 4-anilinoquinazolines as neoplasm inhibitors. EP 520722 A1 19921230
7. Barker AJ, Zeneca Ltd. (1993) Quinazoline tyrosine kinase-inhibiting anticancer agents. CA 2086968 A1 19930721
8. Bridges AJ (2001) Chem Rev 101:2541–2571
9. Barker AJ, Gibson KH, Grundy W, Godfrey AA, Barlow JJ, Helay MP, Woodburn JR, Ashton SE, Curry BJ, Scarlett L, Henthorn L, Richards L (2001) Bioorg Med Chem Lett 11:1911–1914
10. Wakeling AE, Guy SP, Woodburn JR, Ashton SE, Curry BJ, Barker AJ, Gibson KH (2002) Cancer Res 62:5749–5754
11. Rewcastle GW, Denny WA, Bridges AJ, Zhou H, Cody DR, McMichael A, Fry DW (1995) J Med Chem 38:3482–3487
12. Denny WA, Rewcastle GW, Bridges AJ, Fry DW, Kraker AJ (1996) Clin Exp Pharmacol Physiol 23:424–427
13. Woodburn JR, Barker AJ, Gibson KH, Ashton SE, Wakeling AE, Curry BJ, Scarlett L, Henthorn LR (1997) In: Proceedings of the 88th annual meet, AACR 1997, vol 38, Abstract 4251
14. Basalga J, LoRusso P, Herbst R, Rischin D, Ranson M, Maddox A-M, Feyereislova A, Averbuch S (1999) In: Proceedings of the AACR-NCIEORTC international conference 1999, Abstract 29
15. Kris M, Ranson M, Ferry D, Hammond L, Averbuch S, Ochs J, Rowinsky E (1999) In: Proceedings of the AACR-NCI-EORTC international conference 1999, Abstract 99
16. Baselga J, Averbuch SD (2000) Drugs 60:33
17. Arnold LD, Schnur RC. WO1996030347
18. Moyer JD, Barbacci EG, Iwata KK, Arnold L, Boman B, Cunningham A, DiOrio C, Doty J, Morin MJ, Moyer MP, Neveu M, Pollack VA, Pustilnik LR, Reynolds MM, Sloan D, Theleman A, Miller P (1997) Cancer Res 57:4838
19. Pollack VA, Savage DM, Baker DA, Tsaparikos KE, Sloan DE, Moyer JD, Barbacci EG, Pustilnik LR, Smolarek TA, Davis JA, Vaidya MP, Arnold LD, Doty JL, Iwata KK, Morin MJ (1999) J Pharmacol Exp Ther 291:739
20. Siu LL, Hidalgo M, Nemunaitis J, Rizzo J, Moczygemba J, Eckhardt SG, Tolcher A, Smith L, Hammond L, Blackburn A, Tensfeldt T, Silberman S, Von Hoff DD, Rowinsky EK (1999) In: Proceedings of the 35th annual meet, ASCO 1999, vol 18, 388a Abstract 1498
21. Karp DD, Silberman SL, Tensfeldt T, Csudae R, Wirth F, Gaynes L, Posner M, Bubley G, Koon H, Bergman M, Pandya S, Schnipper LE (1999) In: Proceedings of the 35th annual meet, ASCO 1999, vol 18, 388a Abstract 1499.
22. Barf T, Kaptein AJ (2012) Med Chem 55:6243–6262
23. Liu Q, Sabnis Y, Zhao Z, Zhang T, Buhrlage SJ, Jones LH, Gray NS (2013) Chem Biol 20:146–159
24. Clark S, Konstantopoulos N (1993) Biochem J 292:217–223
25. Woltjer RL, Staros JV (1997) Biochemistry 36:9911–9916
26. Singh J, Dobrusin EM, Fry DW, Haske T, Whitty A, McNamara DJJ (1997) Med Chem 40:1130–1135

27. Fry DW, Bridges AJ, Denny WA, Doherty A, Gries KD, Hicks JL, Hook KE, Keller PR, Leopold WR, Loo JA, McNamara DJ, Nelson JM, Sherwood V, Smaill JB, Trumpp-Kallmeyer S, Dobrusin EM (1998) Proc Natl Acad Sci U S A 95:12022–12027

28. Smaill JB, Palmer BD, Rewcastle GW, Denny WA, McNamara DJ, Dobrusin EM, Bridges AJ, Zhou H, Showalter HDH, Winters RT, Leopold WR, Fry DW, Nelson JM, Slintak V, Elliot WL, Roberts BJ, Vincent PW, Patmore SJ (1999) J Med Chem 42:1803–1815

29. Smaill JB, Rewcastle GW, Loo JA, Greis KD, Chan H, Reyner EL, Lipka E, Hollis Showalter HD, Vincent PW, Elliott WL, Denny WA (2000) J Med Chem 43:1380–1397

30. Wissner A, Johnson BD, Floyd MB, Kitchen DB (1998) US Pat. 5,760,041

31. Discafani CM, Carroll ML, Floyd MB, Hollander IJ, Husain Z, Johnson BD, Kitchen D, May MK, Malo MS, Minnick AA, Nilakantan R, Shen R, Wang YF, Wissner A, Greenberger LM (1999) Biochem Pharmacol 57:917

32. Wissner A, Overbeek E, Reich MF, Floyd MB, Johnson BD, Mamuya N, Rosfjord EC, Discafani C, Davis R, Shi X, Rabindran SK, Gruber BC, Ye F, Hallett WA, Nilakantan R, Shen R, Wang YF, Greenberger LM, Tsou HRJ (2003) Med Chem 46:49–63

33. Engelman JA, Zejnullahu K, Gale C-M, Lifshits E, Gonzales AJ, Shimamura T, Zhao F, Vincent PW, Naumov GN, Bradner JE, Althaus IW, Ghandi L, Shapiro GI, Nelson JM, Heymach JV, Meyerson M, Wong K-K, Janne PA (2007) Cancer Res 67:11924–11932

34. Brzezniak C, Carter CA, Giaccone G (2013) Expert Opin Pharmacother 14:247–253

35. Li D, Ambrogio L, Shimamura T, Kubo S, Takahashi M, Chirieac LR, Padera RF, Shapiro GI, Baum A, Himmelsbach F, Rettig WJ, Meyerson M, Solca F, Greulich H, Wong K-K (2008) Oncogene 27:4702–4711

36. Lin NU, Winer EP, Wheatley D, Carey LA, Houston S, Mendelson D, Munster P, Frakes L, Kelly S, Garcia AA, Cleator S, Uttenreuther-Fischer M, Jones H, Wind S, Vinisko R, Hickish T (2012) Breast Cancer Res Treat 133:1057–1065

37. Sharma SV, Bell DW, Settleman J, Haber DA (2007) Nat Rev Cancer 7:169–181

38. Ward RA, Anderton MJ, Ashton S, Bethel PA, Box M, Butterworth S, Colclough N, Chorley CG, Chuaqui C, Cross DA, Dakin LA, Debreczeni JE, Eberlein C, Finlay MRV, Hill GB, Grist M, Klinowska TC, Lane C, Martin S, Orme JP, Smith P, Wang F, Waring MJ (2013) J Med Chem 56:7025–7048

39. Pines G, Köstler WJ, Yarden Y (2010) FEBS Lett 584:2699–2706

40. Yun C, Mengwasser KE, Toms AV, Woo MS, Greulich H, Wong K, Meyerson M, Eck MJ (2008) Proc Natl Acad Sci U S A 105:2070–2075

41. Johnston JB, Navaratnam S, Pitz MW, Maniate JM, Wiechec E, Baust H, Gingerich J, Skliris GP, Murphy LC, Los M (2006) Curr Med Chem 13:3483–3492

42. Kobayashi S, Boggon TJ, Dayaram T, Jaenne PA, Kocher O, Meyerson M, Johnson BE, Eck MJ, Tenen DG, Halmos B (2005) N Engl J Med 352:786–792

43. Yun C, Woo MS, Greulich H, Meyerson M, Eck MJ, Wong K (2008) 236th national meeting of the American Chemical Society, Philadelphia, PA, Aug 17–21, 2008. American Chemical Society, Washington; COMP 373

44. Sos ML, Rode HB, Heynck S, Peifer M, Fischer F, Klüter S, Pawar VG, Reuter C, Heuckmann JM, Weiss J, Ruddigkeit L, Rabiller M, Koker M, Simard JR, Getlik M, Yuza Y, Chen T-H, Greulich H, Thomas RK, Rauh D (2010) Cancer Res 70:868–874

45. Zhou W, Ercan D, Chen L, Yun C, Li D, Capelletti M, Cortot AB, Chirieac L, Iacob RE, Padera R, Engen JR, Wong K, Eck MJ, Gray NS, Janne PA (2009) Nature 462:1070–1074

46. Singh J, Evans E, Hagel M, Labinski M, Dubrovskiy A, Nacht M, Petter RC, Prasad A, Sheets M, St Martin T, Sjin RTT, Westlin W, Zhu Z (2012) Med Chem Commun 3:780

47. Kluge AF, Petter RC, Tester RW, Qiao L, Niu D, Westlin WF, Singh J, Mazdiyasni H. WO2009158571

48. Baevsky MF, Lee K, Niu D, Petter RC, Singh J. WO2012061299

49. Sjin RTT, Lee K, Walter AO, Dubrovskiy A, Sheets M, St. Martin T, Labenski T, Zhu Z, Tester R, Karp R, Medikonda A, Chaturvedi P, Ren Y, Haringsma H, Etter J, Raponi M, Simmons AD, Harding TC, Niu D, Nacht M, Westlin WF, Petter RC, Allen A, Singh J (2014) Mol Cancer Ther 13:1468–1479

50. Walter AO, Sjin RTT, Haringsma HJ, Ohashi K, Sun J, Lee K, Dubrovskiy A, Labenski M, Zhu Z, Wang Z, Sheets M, St Martin T, Karp R, van Kalken D, Chaturvedi P, Niu D, Nacht M, Petter RC, Westlin W, Lin K, Jaw-Tsai S, Raponi M, Van Dyke T, Etter J, Weaver Z, Pao W, Singh J, Simmons AD, Harding TC, Allen A (2013) Cancer Discov 3:1404–1415

51. Niu D (2008) 250th national meeting of the American Chemical Society, Boston, MA, Aug 16–20, 2015. American Chemical Society, Washington; MEDI 337

52. Soria JC (2014) In: 26th EORTC-NCI-AACR symposium on molecular targets and therapeutics, Barcelona, 18–21 Nov 2014

53. Sequist LV, Soria J-C, Camidge DR (2016) N Engl J Med 374:2296–2297

54. Lee Y, Wang Y, James M, Jeong JH, You M (2015) Mol Carcinog. doi:10.1002/mc.22342

55. Finlay MRV, Anderton M, Ashton S, Ballard P, Bethel PA, Box MR, Bradbury RH, Brown SJ, Butterworth S, Campbell A, Chorley C, Colclough N, Cross DAE, Currie GS, Grist M, Hassall L, Hill GB, James D, James M, Kemmitt P, Klinowska T, Lamont G, Lamont SG, Martin N, McFarland HL, Mellor MJ, Orme JP, Perkins D, Perkins P, Richmond G, Smith P, Ward RA, Waring MJ, Whittaker D, Wells S, Wrigley GL (2014) J Med Chem 57:8249–8267

56. Cross DAE, Ashton SE, Ghiorghiu S, Eberlein C, Nebhan CA, Spitzler PJ, Orme JP, Finlay MRV, Ward RA, Mellor MJ, Hughes G, Rahi A, Jacobs VN, Brewer MR, Ichihara E, Sun J, Jin H, Ballard P, Al-Kadhimi K, Rowlinson R, Klinowska T, Richmond GHP, Cantarini M, Kim D-W, Ranson MR, Pao W (2014) AZD9291, an irreversible EGFR TKI, overcomes T790M-mediated resistance to EGFR inhibitors in lung cancer. Cancer Discov 4:1046–1061

57. Kim D-W, Ahn M-J, Lee DH, Cho BC, Lee JS, Ye X, Yang P, Jiang H, Yang JC-H (2015) In: AACR-NCI-EORTC international conference on molecular targets and cancer therapeutics, Boston, 5–9 Nov 2015

58. Goss GD, Yang JCH, Ahn M, Tsai CM, Bazhenova L, Sequist LV, Ramalingam SS, Shepherd FA, Ghiorghiu S, Cantarini M, Mann H, Mitsudomi T, Jänne PA (2015) AZD9291 in pre-treated patients with T790M positive advanced non-small cell lung cancer (NSCLC): pooled analysis from two phase II studies [abstract no. 3113 plus poster]. In: European Cancer Congress, 2015

59. Heald R, Bowman KK, Bryan MC, Burdick D, Chan B, Chan E, Chen Y, Clausen S, Dominguez-Fernandez B, Eigenbrot C, Elliott R, Hanan EJ, Jackson P, Knight J, La H, Lainchbury M, Malek S, Mann S, Merchant M, Mortara K, Purkey H, Schaefer G, Schmidt S, Seward E, Sideris S, Shao L, Wang S, Yeap K, Yen I, Yu C, Heffron TP (2015) J Med Chem 58:8877–8895

60. Wurz RP, Pettus LH, Ashton K, Brown J, Chen JJ, Herberich B, Hong F-T, Hu-Harrington E, Nguyen T, St. Jean Jr DJ, Tadesse S, Bauer D, Kubryk M, Zhan J, Cooke K, Mitchell P, Andrrws KL, Hsieh F, Hickman D, Kalyanaraman N, Wu T, Reid DL, Lobenhofer EK, Andrews DA, Everds N, Guzman R, Parsons AT, Hedley SJ, Tedrow J, Thiel OR, Potter M, Radinsky R, Beltran PJ, Tasker AS (2015) ACS Med Chem Lett 6:987–992

61. Chan S, Han K, Qu R, Tong L, Li Y, Zhang Z, Cheng H, Lu X, Patterson A, Smaill J, Ren X, Ding J, Xie H, Ding K (2015) Bioorg Med Chem Lett 25:4277–4281

62. Thress KS, Paweletz CP, Felip E, Cho BC, Stetson D, Dougherty B, Lai Z, Markovets A, Vivancos A, Kuang Y, Ercan D, Matthews SE, Cantarini M, Barrett JC, Janne PA, Oxnard GR (2015) Nat Med 21:560–562

63. Piotrowska Z, Niederst MJ, Karlovich CA, Wakelee HA, Neal JW, Mino-Kenudson M, Fulton L, Hata AN, Lockerman EL, Kalsy A, Digumarthy S, Muzikansky A, Raponi M, Garcia AR, Mulvey HE, Parks MK, DiCecca RH, Dias-Santagata D, Iafftae AJ, Shaw AT, Allen AR, Engelman JA, Sequist LV (2015) Cancer Discov 5:713–722

64. Planchard D, Loriot Y, Andre F, Gobert A, Lacroix L, Soria JC (2015) Ann Oncol 26:2073–2078

65. Eberlein CA, Stetson D, Markovets AA, Al-Kadhimi KJ, Lai Z, Fisher PR, Meador CB, Spitzler P, Ichihara E, Ross SJ, Ahdesmaki MJ, Ahmed A, Ratcliffe LE, Obrien EL, Barnes CH, Brown H, Smith PD, Dry JR, Beran G, Thress KS, Dougherty B, Pao W, Cross DA (2015) Cancer Res 75:2489–2500

66. Oxnard GR, Ramalingam SS, Ahn M-J, Kim S-W, Yu HA, Saka H, Horn L, Goto K, Ohe Y, Cantarini M, Frewer P, Lahn M, Yang JC-H (2015) J Clin Oncol 33. Suppl; abstract 2509
67. Simmons AD, Haringsma HJ, Nguyen M, Robillard L, Allen A, Harding TC (2015) In: 16th world conference on lung cancer, Denver CO, 6–9 Sept 2015, Abstract 3010
68. Ramalingam SS, Yang JC-H, Lee CK, Kurata T, Kim D-W, John T, Nogami N, Ohe Y, Janne PA (2016) J Thorac Oncol 11(Suppl):S152

Small-Molecule Inhibitors of Bruton's Tyrosine Kinase

Yingying Zuo and Zhengying Pan

Abstract Bruton's tyrosine kinase has emerged as a promising drug target for multiple diseases, particularly hematopoietic malignancies. As a result of intensive efforts, many inhibitors have been developed to target BTK. Among them, considerable progress has been made in covalent inhibitors. In this chapter, example compounds will be discussed to highlight our current understanding of the functional and structural features of BTK inhibitors.

Keywords B-cell malignancies, BTK, Inhibitors, Signaling pathway, Tec family kinase

Contents

Y. Zuo and Z. Pan (✉)
School of Chemical Biology and Biotechnology, Shenzhen Graduate School, Peking University, Shenzhen, China
e-mail: panzy@pkusz.edu.cn

Abbreviations

BCR	B-cell receptor
BTK	Bruton's tyrosine kinase
CLL	Chronic lymphocytic leukemia
CR	Complete response
DAG	Diacylglycerol
DLBCL	B-cell-like diffuse large B-cell lymphoma
FDA	Food and Drug Administration
IP3	Inositol triphosphate
ITAMs	Immunoreceptor tyrosine kinase activation motifs
LPS	Bacterial lipopolysaccharide
MCL	Mantle cell lymphoma
MM	Multiple myeloma
ORR	Overall response rate
OS	Overall survival
PFS	Progressive-free survival rate
PH	Pleckstrin homology
PID	Primary immunologic deficiency
SH	Src homology
Syk	Spleen tyrosine kinase
TH	TEC homology
TLR	Toll-like receptor
WM	Waldenström's macroglobulinemia
XID	X-linked immunodeficiency
XLA	X-linked agammaglobulinemia

1 Introduction

Bruton's tyrosine kinase is a member of the Tec tyrosine kinase family (BTK, BMX, ITK, TEC, and TXK), which is the second largest family of cytoplasmic non-receptor tyrosine kinases in humans [1, 2]. It is expressed in most hematopoietic cells, primarily B-cells, as well as monocytes/macrophages [3], platelets [4], neutrophils [5], but not T cells and normal plasma cells [6, 7], The discovery of BTK can be traced back to the 1950s, when an American pediatrician, Ogden Bruton, reported the first case of inherited agammaglobulinemia in young boys with immunodeficiency who were vulnerable to pathogen infection [8]. He and Charles Janeway subsequently found that this primary immunologic deficiency (PID), later termed X-linked agammaglobulinemia (XLA) or Bruton's agammaglobulinemia, was caused by a lack of the serum globulin fraction [9]. However, its molecular basis was not determined until 1993, 41 years later, when the *btk* gene and XLA-associated mutations were first identified and cloned [1, 10–12]. As a result, interest in BTK was renewed.

The *btk* gene is located in the X chromosome, and its XLA-associated mutations are recessive [13]. Affected males show the fatal XLA-positive phenotype, which is characterized by an almost complete absence of peripheral mature B-cells and circulating antibodies because of a severe defect in B-cell development [13]. In contrast, females harboring a defective *btk* allele suffer from a selective disadvantage. In mice, *btk* mutations also result in X-linked immunodeficiency (XID) with reduced B-cell population [14]. BTK has been universally acknowledged for its vital role in B-cell receptor (BCR), chemokine receptor, and Toll-like receptor (TLR) signaling pathways associated with B-cell development, proliferation, maturation, adhesion, and migration [15].

2 Bruton's Tyrosine Kinase: Structure and Functions

BTK comprises several domains from the N-terminus to the C-terminus: the pleckstrin homology (PH), proline-rich TEC homology (TH), Src homology (SH) 2 and SH3, as well as the kinase (SH1) domains [16]. Of these, the PH and TH domains are unique to the Tec family [17, 18]. However, all of these domains can interact with many of the proteins that regulate intracellular activities (Fig. 1) [15, 16]. For example, the PH domain binding to PIP3, a second messenger generated by PI3K, is critical for BTK's recruitment to the cell membrane and activation [19–21]. The TH domain has a highly conserved zinc finger motif, which is also known as the BTK motif, which is associated with zinc ion binding and coordination to BTK [17, 22–24]. The SH3 domain contains the autophosphorylation site Y223, which is required for the full activation of BTK, and SH2 domain has a BLNK (SLP-65) binding site for the recruitment of BTK [25, 26]. In addition, inositol-5′-phosphatase-1 (SHIP1) binds to the SH2 domain and mediates a negative feedback loop in which PIP3 is dephosphorylated and BTK membrane recruitment is thus inhibited [15]. The kinase domain contains the primary phosphorylation site Y551 and an ATP-binding site, which is responsible for BTK activation and trans-phosphorylation [25] (Fig. 1).

BTK activity is stimulated by a wide variety of surface receptor molecules, including antigen, chemokine, and growth factor receptors, and can transmit and amplify these signals to downstream signaling pathways, thereby regulating cell survival, proliferation, homing, and communication with the microenvironment. Among the pathways that involve BTK, BCR, chemokine, and Toll-like receptor (TLR) signaling have been studied most thoroughly [56–58] (Fig. 2).

BCR signaling plays a critical role in B-cell development and maturation and contributes to the peripheral circulating mature B-cells and antibodies, facilitating the adaptive immune response [59, 60]. The BCR complex is composed of a membrane immunoglobulin that is non-covalently associated with a heterodimer composed of Igα and Igβ, which is also called CD79a/b. In normal B-cells, upon BCR engagement by antigens, the Igα/β cluster becomes phosphorylated at the cytoplasmic tails of their immunoreceptor tyrosine kinase activation motifs (ITAMs) by an Src family kinase, probably LYN, which creates docking sites for SYK [61]. LYN also can phosphorylate
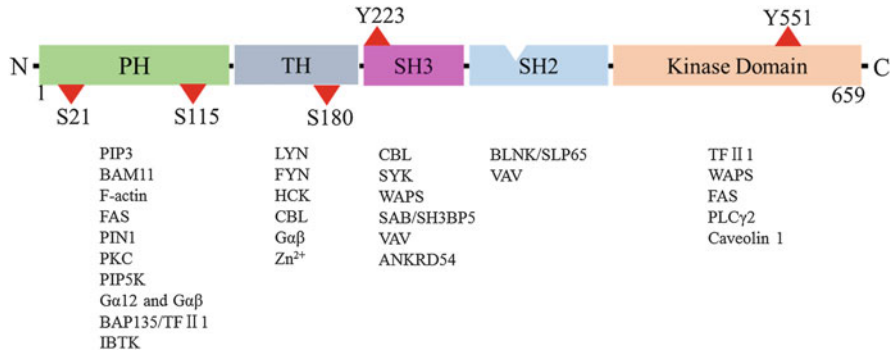
Fig. 1 Scheme of BTK's structure and interaction partners [22, 27–55]
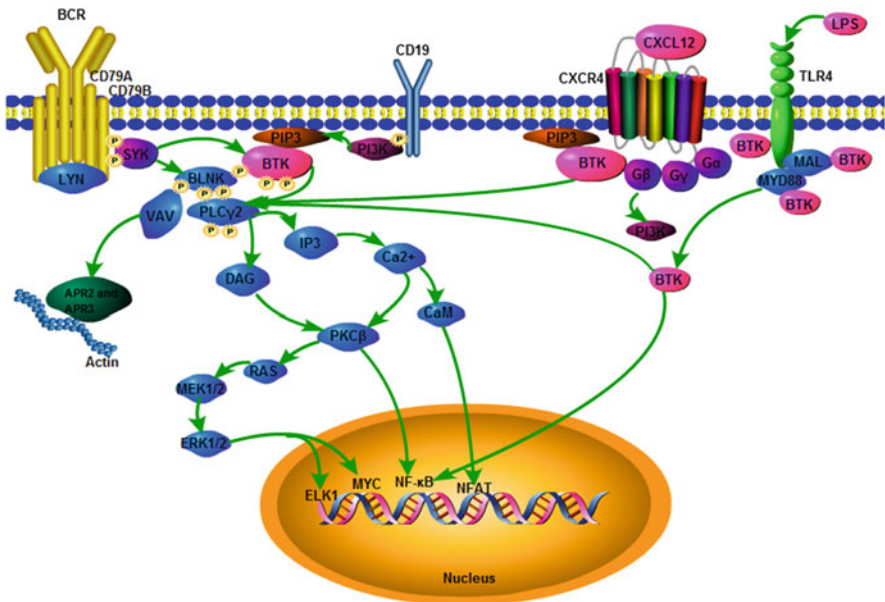
Fig. 2 Involvement of BTK in BCR signaling, chemokine signaling, and TLR signaling pathways

BTK and CD19, a transmembrane protein, activating PI3K and the subsequent PIP3-mediated BTK recruitment to the cytoplasmic side of the cell membrane, where BTK is activated by an Src family kinase [62, 63]. BTK achieves full activation through trans-phosphorylation at Y551 within the activation loop of the kinase domain and the accompanying autophosphorylation at Y223, which is located in the SH3 domain [19, 20]. Simultaneously, the SYK binds to the ITAM and becomes activated. Activated SYK recruits and phosphorylates the B-cell linker scaffold protein (BLNK, an adapter

protein), generating docking sites for the SH2 domain of BTK and its direct substrate PLCγ2 and promoting the downstream propagation of the signals [64, 65]. BTK primarily phosphorylates PLCγ2 at positions Y753 and Y759, which is responsible for its lipase activity [66]. Activated PLCγ2 creates two second messengers: inositol triphosphate (IP3) and diacylglycerol (DAG). IP3 is involved in Ca^{2+} mobilization, which induces NFAT signaling and cytoskeleton rearrangements, whereas DAG can activate RAS/MAPK signaling, PKC/NFκB signaling, and RAP1 signaling, which are associated with integrin activation [24, 67–70]. All of these kinases, messengers, and signaling pathways regulate B-cell proliferation, differentiation, survival, and adhesion. Furthermore, activated BTK also can recruit PIP5K and stimulate a positive-feedback loop in the production of PIP2, which serves as a substrate for PI3K and PLCγ2 [32].

BTK is also involved in chemokine receptor pathways, and the CXCR4 and CXCR5 pathways have been well established [71]. CXC-chemokine ligand 12 (CXCL12), which is highly expressed in stromal cells in the bone marrow and germinal centers, can bind to CXCR4, and thus, its linked heterotrimeric G protein subunits bind directly to the PH and TH domains of BTK and result in its translocation to the cell membrane [41, 42], where it is phosphorylated and activated by SRC kinases. A series of downstream signaling pathways that are essential for B-cell adhesion, migration, and homing are subsequently activated [56, 72–74].

Bacterial lipopolysaccharide (LPS) binding to Toll-like receptor (TLR) can initiate TLR signaling pathways [58]. Once activated, MYD88 is recruited; and then BTK interacts directly with the cytoplasmic tails of most TLRs, as well as MYD88 and TLR-collected MAL [3, 75–77]. TLR signaling induces the downstream transcriptional factor NFκB, which upregulates B-cell proliferation and the production and secretion of antibodies and pre-inflammatory cytokines.

3 BTK Signaling in B-Cell Malignancies and Autoimmune Diseases

Considering the molecular basis of the immunodeficiency disease – XLA in humans and xid in mice – BTK functional integrity is particularly critical for B-lymphocyte survival. Tonic, chronic, or antigen-driven BTK-dependent signaling pathways, including BCR signaling, chemokine signaling, and TLR signaling, are involved in the pathogenesis of most types of B-cell malignancies and autoimmune diseases [56, 72, 78]. BTK is considered to be a promising drug target because of its specificity for B-cells and its safety in the case of low selectivity against normal B-cells. BTK plays a critical role in the development of multiple cancers and disease maintenance.

Chronic lymphocytic leukemia (CLL) is the most common type of leukemia in adults and is characterized by swelling of the lymph nodes, spleen, and liver and eventual anemia and infections. CLL B-cells reside in different compartments, specifically lymphoid tissues and blood, and have different levels of IgM presentation on their

surfaces; however, all have much lower IgM expression levels than normal cells [79]. CLL's activation is partially dependent on internalized chronic BCR signaling and continuous antigen binding [79, 80]. Additionally, CLL B-cells grow in an uncontrolled manner and accumulate in the bone marrow, blood, and lymphoid tissues, where antigens, chemokines, TLR-ligand binding, and T cell co-stimulation can provide vital signals relating to proliferation, survival, and migration [81]. Accumulated CLL B-cells can crowd out healthy blood cells, increasing the leukocyte concentration in blood, which is used for diagnosis. In CLL, BTK is critical for BCR and NFκB signaling, supporting both cell migration to proliferative centers in lymph nodes and proliferation [56, 72]. Chronic active CLL signaling primarily depends on continued antigen binding [80] and/or BTK overexpression and hyper-activation [82]. CLL patients are treated with ibrutinib, a BTK inhibitor, which disrupts CXCL-mediated adhesion and migration, causes a rapid and sustained decrease in lymphadenopathy, and results in transient lymphocytosis [56, 83]. However, CLL cells are not directly killed by BTK inhibition but instead die because of their "forced" mobilization from the lymphoid tissues to the peripheral circulating system, which results in the loss of their nursing microenvironments [81].

Mantle cell lymphoma (MCL) is a type of non-Hodgkin's lymphoma (NHL) that is caused by constitutive phosphorylation and activation of BCR-related kinases, such as Lyn, SYK, and PKCβ [84, 85], as well as kinase overexpression [86–88] and internalized activation [74]. BCR or TLR signaling pathways are crucial for MCL cell survival and proliferation. Similar to CLL, ibrutinib-treated patients exhibit reduced lymph nodes and transient lymphocytosis because of disrupted chemokine signaling [74].

B-cell-like diffuse large B-cell lymphoma (DLBCL) is partially caused by mutations in the BCR signaling pathway, such as Igα/β mutations [78], which activate a series of downstream antigen-independent pathways. NF-κB signaling, which depends on BCR or TLR signaling, is critical for DLBCL cell survival and proliferation [89–93]. Thus, removing the critical activities of one or more kinases can induce death in tumor cells.

The pathogenesis of Waldenström's macroglobulinemia (WM) and multiple myeloma (MM) also relates to BTK-involved signaling pathways. A key mechanism in WM is the constitutively active form of MYD88 involved in TLR signaling [94], which promotes hyperactivated NF-κB signaling. Ibrutinib can induce WM cell apoptosis and migration [95]. In contrast, MM cells do not express the BCR complex on their surfaces, and their survival and proliferation rely on osteoclastic activity and bone remodeling [96, 97]. As shown in mice, BTK is vital for osteoclast formation [98, 99]. Ibrutinib can disturb MM cell growth and survival and CXCL12-induced adhesion and migration [100].

In addition to BTK's critical roles in B-cell malignancies, it also plays a central role in autoimmune diseases, interfering with TLR signaling and contributing to the activation of NF-κB and the regulation of pro- and anti-inflammatory chemokine production [101]. The overexpression of BTK can result in autoantibody production and SLE-like autoimmunity [102]. In preclinical studies, treating mouse models with BTK inhibitors was shown to relieve the symptoms [103–106]. However,

clinical trials relating to treating autoimmunity diseases with BTK inhibitors remain in their early stages, and additional studies are required.

4 BTK Kinase Inhibitors: Structural Biology Insights, Discovery, and Development

Identifying novel mediators that are crucial for the growth and death of cancer cells or that regulate the secretion of chemokines and cytokines has facilitated the development of anti-cancer and anti-inflammatory agents. For example, monoclonal antibodies have been shown to exhibit periodic effects in several types of lymphoma. Indeed, CD20 and CD19 antibodies have moved rapidly through clinical trials and have become key components in treatment regimens for B-cell lymphoma and autoimmune diseases [107–110]. Given the development of monoclonal antibodies, small-molecule BTK inhibitors have attracted substantial interest in the pharmaceutical industry and academia for the treatment of BTK-involved B-cell-related diseases.

The PH domain of BTK has been targeted by small molecules blocking the binding pocket of IP3 and disturbing BTK recruitment to the cell membrane [111]. However, most efforts have focused on the kinase domain.

The kinase domains of human kinases share a high degree of similarity. Additionally, their ATP-binding pockets have very similar 3D structures, although their primary amino acid sequences are diverse. The kinase domain consists of two lobes: the N-terminus lobe, which comprises five β-strands and one helix, and the C-terminus lobe, which is dominated by α-helixes. The ATP-binding site is a hydrophobic pocket located between these two lobes, which are linked by a flexible hinge region. ATP or inhibitors can interact with this hinge region through 1 to 3 hydrogen bonds. Since the so-called gatekeeper residue is a threonine in BTK, it is open to access to the hydrophobic pocket located behind it. A flexible activation loop that begins with a conserved Asp-Phe-Gly (DFG) sequence partially controls activation of the kinases and access to the active site. In the so-called DFG-out inactive conformation, an aspartate residue (D) rotates out of the ATP-binding pocket, which is accompanied by a rotation of the phenylalanine residue, revealing an important additional hydrophobic binding pocket (DFG pocket) [112] (Fig. 3).

Considering the high similarity of the 3D structures of the kinase domains, designing selective BTK inhibitors is challenging. Two approaches have been exploited to achieve high selectivity. One targets the specific non-catalytic cysteine 481 located at the rim of the ATP-binding pocket. Only ten other kinases have a cysteine at the equivalent position [113–115]. The other targets the binding pockets of inactive BTK conformations, which differ from those of other kinases or kinase families [116]. In addition, the gatekeeper also acts as a filter for selective BTK inhibitors [117]. Over the last decade, small-molecule BTK inhibitors have been developed as promising treatment agents for hematological malignancies and
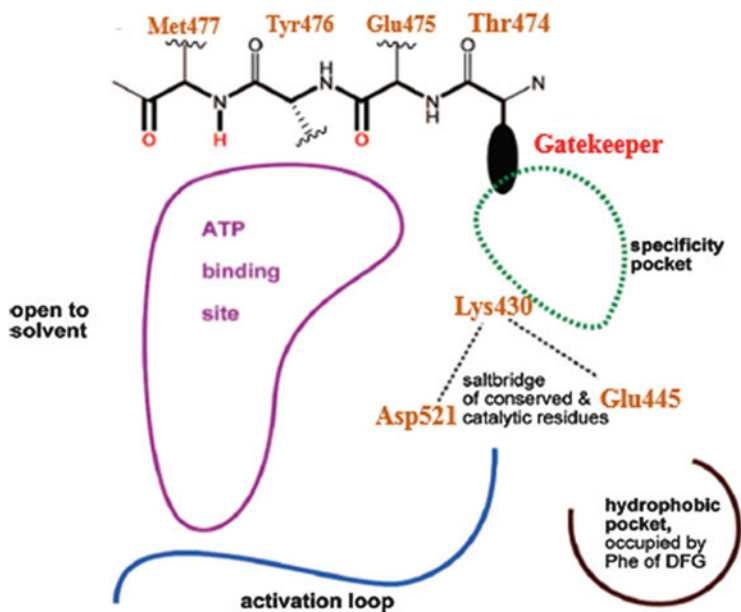
Fig. 3 A 2D representation of the kinase ATP-binding site of BTK (modified based on Fig. 2 in Ref. [112])

autoimmune diseases. A number of compounds have undergone rapid progress in preclinical development and clinical trials, and some of them are highlighted here.

4.1 Ibrutinib and Its Structurally Related Analogs

4.1.1 Ibrutinib

Ibrutinib (Imbruvica®, Pharmacyclics Inc.) is orally administered and is the most advanced BTK inhibitor. It was first designed and synthesized by researchers from Celera Genomics [113]. They initially identified CRA/PCI-29732 (Fig. 4a) through structure–activity relationship (SAR) studies. CRA/PCI-29732 is an ATP-competitive inhibitor with 8.2 nM potency against BTK and shows high inhibitory activity against Tec and Src family kinases. Bioinformatics analysis and the alignment of BTK and LCK sequences revealed a specific Cys residue (C481) at the rim of the hinge region of the ATP-binding pocket; only ten other kinases in the entire kinome have a homologous cysteine at this location, which suggests that an electrophilic group may covalently bind to the thiol group of this cysteine to provide additional potency and selectivity. Thus, a series of small molecules were synthesized, including CRA/PCI-32765 (ibrutinib, $IC_{50} = 0.5$ nM) (Fig. 4b), which irreversibly inhibits BTK through a covalent interaction
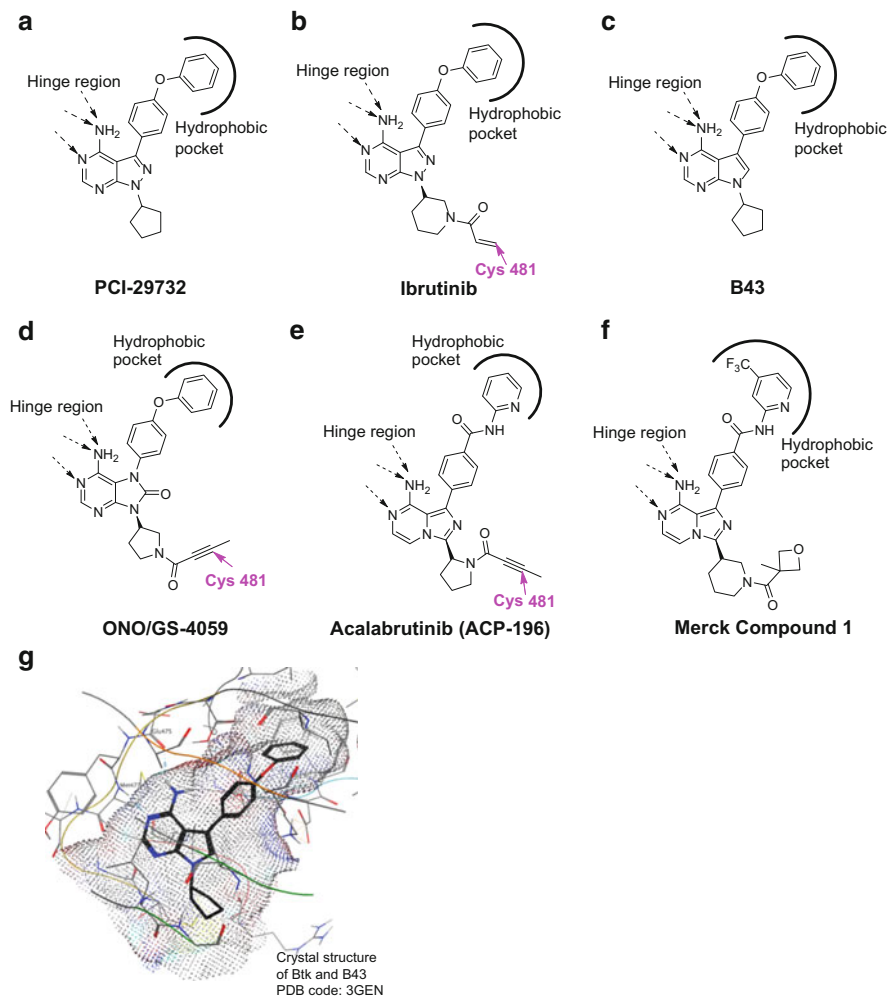
Fig. 4 Binding modes of BTK covalent small-molecule kinase inhibitors

between its reactive group and the targeted Cys481. As shown in Table 1, Michael acceptors were well tolerated, and some compounds exhibited sub-nanomolar IC_{50} values. Among them, the acrylamide compound appeared to be the best one. However, the selectivity of these molecules against kinases possessing structurally homologous cysteine, such as EGFR, is still not optimal [113].

A co-structure of BTK with ibrutinib remains to be determined, but one of BTK with a close analog of ibrutinib, B43, (Fig. 4c) has been solved and can facilitate understanding the general binding mode of BTK and ibrutinib [118]. B43 binds to the ATP-binding pocket of an active BTK with a DFG-in conformation. The 4-amino pyrrolopyrimidine mimics the adenine ring of the ATP, forming two hydrogen bond interactions with the

Table 1 Compounds with various types of Michael acceptors are potent BTK inhibitors [113]
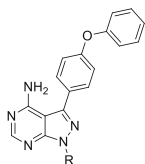
R	BTK IC$_{50}$ (nM)
	0.72
	<0.5
	1.4
	20
	2.5
	0.58
	0.72

hinge region and one with the gatekeeper, threonine (Thr), which guides the phenoxyphenyl group to extend into a backward hydrophobic pocket that is mainly composed of the N-lobe residues. The phenoxyphenyl group forms π-stacking interactions with the residues in this pocket. Moreover, the size of the gatekeeper's side chain serves as a filter, contributing to the inhibitor's selectivity. The cyclopentyl group points to the C481 at the C-terminus of the hinge region. In ibrutinib, the corresponding *N*-acryloylpiperidine also extends toward this cysteine and, presumably, this facilitates the reaction between the Michael acceptor and the nearby cysteine [119] (Fig. 4c, g).

As a covalent irreversible inhibitor, ibrutinib exhibits decoupled pharmacokinetic and pharmacodynamic properties. It is cleared rapidly from the blood by CYP450 (CYP3A4 and CYP2D6) mainly in the liver, but the inhibition of the BTK activity is not lost until protein re-synthesis occurs. Ibrutinib blocks the BCR signaling pathway by inhibiting the autophosphorylation of the Y223 of BTK, which resides in the SH2 domain, and the phosphorylation of PLCγ2 and ERK [103]. It can promote cell apoptosis, inhibit proliferation, and prevent homing, adhesion, and communication with the microenvironment. In vivo studies have shown that ibrutinib is well tolerated and efficacious when orally administered in

murine autoimmune models of RA and SLE and endogenous canine B-cell lymphoma [103]. Ibrutinib has shown clear promise as a potential treatment for rheumatoid arthritis (RA) and lupus. Additionally, other studies have demonstrated its efficacy in the treatment of multiple B-cell cancers [120], including MCL [88], CLL [82], DLBCL [78], MM [100], and WM [95]. This drug has rapidly progressed into clinical studies for cancer therapy.

In the first dose-escalating phase 1 study, ibrutinib showed antitumor activity in multiple B-cell malignancies. A total of 56 patients with relapsed or refractory (R/R) CLL/SLL and other B-cell NHLs, such as MCL, FL, MZL, DLBCL, and WM, were enrolled and treated with one of two regiments: four escalating doses (1.25, 2.5, 5, and 12.5 mg/kg daily) for 28 days followed by 7 days off or 8.3 mg/kg given continuously. The overall response in 50 enrolled patients was 60%, with 16% exhibiting complete response. The median progression-free survival (PFS) was 13.6 months, and most adverse events (AEs) were grades 1 and 2 in severity. BTK was fully inhibited at doses of 2.5 mg/kg and above [121], as revealed by a competition assay using a fluorescence probe (CRA/PCI-33380) of peripheral blood mononuclear cells (PBMC) collected from patients. CRA/PCI-33380 competes with ibrutinib for free BTK. When BTK is unoccupied by inhibitors, it becomes labeled by CRA/PCI-33380, resulting in a fluorescent BTK band after SDS-PAGE and fluorescence gel scanning [103]. Less-intense bands reflect greater inhibitor occupancy.

A phase 1b/2 multicenter study was conducted to assess the safety, efficacy, pharmacokinetics, and pharmacodynamics of ibrutinib in 85 patients with R/R CLL or SLL. These patients received ibrutinib 420 mg (51/85) or 840 mg (34/85) orally once daily and the two doses resulted in same overall response rate (ORR): 71%. After 26 months, the median progression-free survival (PFS) rate was 75%, and the overall survival rate was 83%. Because these two dosing arms exhibited no differences, 420 mg was chosen for the subsequent studies [83, 122]. Treating R/R CLL or SLL patients with ibrutinib caused some of their lymphocyte counts to rise rapidly, possibly because of the migration of CLL cells from the lymph nodes or bone marrow into the blood. This lymphocytosis reflects a positive response to the treatment and can typically be resolved by continuing or ending treatment [123–126]. More importantly, lymphocytosis does not indicate a greater tendency for patients to develop ibrutinib resistance [127].

In an open-label phase 2 study, 111 patients with R/R MCL who had previously received a median of three prior therapies (43% received bortezomib treatment) were enrolled. In this study, ibrutinib was orally administered at 560 mg once daily to assess its efficacy and safety. The ORR for all patients was 68%, with 21% exhibiting complete response (CR). The estimated median PFS was 13.9 months, and the overall survival (OS) rate was 58% at 18 months [128].

Based on the exciting clinical trial results described above, ibrutinib received accelerated approval on November 13, 2013, by the US Food and Drug Administration (FDA) for the treatment of previously treated MCL and subsequently for R/R CLL on February 12, 2014 [129]. Ibrutinib is the first approved drug that directly targets BTK. Further expansion to patients with 17p deletions in CLL and

WM were approved on July 28, 2014 and January 29, 2015, respectively. Additionally, ibrutinib has also been approved by the European Commission and the United Kingdom for R/R MCL and CLL. Clinical trials of ibrutinib for B-cell cancers and of combination therapies involving immunotherapy and chemotherapy are ongoing [130, 131].

In addition to B-cell lymphoma, ibrutinib has also been investigated for the treatment of ErbB2-positive breast cancer [132] and EGFR-mutant non-small cell lung cancer [133], indicating that ibrutinib also has efficacy in solid cancers, which may result from the additional activity of ibrutinib against EGFR and ErbB kinases.

Based on results from the early stages of CLL and MCL treatment, ibrutinib is well tolerated. The most common adverse effects were all grades 1 and 2 and can typically be resolved without interrupting treatment. The most common grade 3 and 4 adverse effects are neutropenia, thrombocytopenia, and infections, which subsequently improved and were not treatment related [120, 129, 134]. Bleeding is a grade 3 adverse effect and was previously thought to result from the inhibition of BTK and other kinases in platelets [4, 135, 136]. However, recent studies revealed that bleeding likely occurs because ibrutinib treatment affects collagen, von Willebrand factor-dependent functions, and platelet aggregation [137, 138].

The potential mechanisms of primary and acquired resistance to ibrutinib remain poorly understood, but mutations in the ibrutinib-binding site (C481S) of BTK that disrupt the covalent interaction between ibrutinib and BTK and gain-of-function mutations in PLCγ2, R665W, and L845R contribute to the resistance [137]. The identification of other potential resistance mechanisms is urgently needed.

4.1.2 ONO/GS-4059

ONO/GS-4059 (Fig. 4d), an analog of ibrutinib scaffold, is a highly selective and an irreversible Btk inhibitor with a 6-5-membered fused heterocyclic ring as the core structure making important hydrogen bond interactions with the hinge region; the phenoxyphenyl group was extended into the backward hydrophobic pocket; and the 2-butylacetylene amide group makes covalent interactions with the C481 of Btk [139]. In vitro, ONO/GS-4059 inhibited Btk with an IC_{50} of 2.2 nM [140]. It can also induce apoptosis in activated B-cell type of DLBCL cell lines at low nanomolar concentrations [141]. In addition, ONO/GS-4059 has showed significant inhibition of tumor growth in a TMD-8 xenograft model [142]. In a multicenter phase 1 dose-escalation study, ONO/GS-4059 was evaluated in 90 patients with relapsed/refractory B-cell malignancies, including 28 CLL patients, 16 MCL patients, 35 DLBCL patients, and 11 other NHL patients. They were given nine different dose-escalation cohorts ranging from 20 to 600 mg once daily with twice daily regimens of 240 and 300 mg. No maximal tolerated dose (MTD) was reached in the CLL cohort, while in the non-Hodgkin's lymphoma cohort, four patients developed a dose-limiting toxicity with an MTD of 480 mg once daily. The ORRs of CLL (80 weeks treatment), MCL (40 weeks treatment), and non-GCB-DLBCL (12 weeks treatment) were 96% (24/25), 92% (11/12), and 35% (11/31), respectively. ONO/GS-4059 was very well tolerated

with 75% of adverse events (AEs) being grades 1 and 2. Only one CLL patient suffered a grade 3 treatment-related bleeding event, but no any other severe AEs were observed [143]. Currently, the study of ONO/GS-4059's long-term safety and efficacy, and its combination use with other target anti-cancer therapies are still active [144].

4.1.3 Acalabrutinib (ACP-196)

Acalabrutinib (Fig. 4e) is also an analog of ibrutinib with a 6-5-membered fused heterocyclic ring as the core structure that mimics the adenine ring of the ATP and makes several hydrogen bonds with the hinge region. Additional interactions may include hydrophobic interactions with the backward hydrophobic pocket and covalent interactions with the target C481 [145]. Compared with ibrutinib, ACP-196 is believed to be a more selective, irreversible BTK inhibitor with improved safety and efficacy. ACP-196 demonstrated higher selectivity for Btk against other nine kinases sharing a cysteine residue in the same position as Btk [146]. Importantly, ACP-196 showed higher IC_{50} (>1 μM) or virtually no inhibition on kinases activity of EGFR, ITK, TEC, BLK, etc. In addition, ACP-196 has almost no inhibition of platelet activity [146, 147]. In preclinical studies, ACP-196 has been evaluated in several animal models of NHL, which showed that it can significantly reduce tumor cell proliferation by inhibiting BCR signaling pathway by both decreasing the phosphorylation of PLCγ2 and autophosphorylation of Btk, and reduction in expression of BCR activation markers CD86 and CD69 [148–150]. In an uncontrolled, multicenter phase 1-2 study, acalabrutinib was orally administered to 61 patients with relapsed CLL to assess its safety, efficacy, pharmacokinetics, and pharmacodynamics. The patients were given 100–400 mg once daily in the phase 1 study, whereas they received 100 mg twice daily in the phase 2 study. No dose-limiting toxic effects were observed during the dose-escalation study. At a median of 14.5 months, the ORR was 95%; 85% exhibited a partial response, and 10% showed a partial response with lymphocytosis. The adverse effects were grades 1 and 2 [147]. Currently, acalabrutinib is involved in multiple clinical trials, including one investigating its expansion to the treatment of multiple B-cell malignancies and combination with other agents [151].

4.1.4 Merck Compound 1

In 2015, scientists at Merck reported a series of compounds sharing many acalabrutinib's structural features without reactive groups. By using an aminopyridine moiety into the back pocket area, its interactions with Ser-538, Asp-539, and the hydrophobic pocket delivered a series of BTK inhibitors with improved selectivity (Fig. 4f) [152].

Spebrutinib(CC-292/AVL-292)
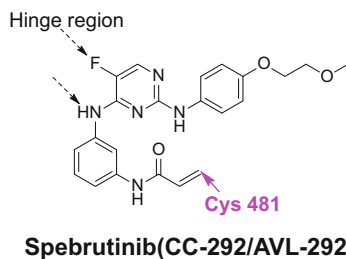
Fig. 5 Structures and binding modes of BTK covalent inhibitor: Spebrutinib(CC-292/AVL-292)

4.2 Spebrutinib (CC-292/AVL-292)

Spebrutinib (Fig. 5) is a covalent, orally bioavailable BTK inhibitor with an IC_{50} below 0.5 nM. It blocks BCR signaling in the Ramos human Burkitt's lymphoma cell line by covalent modification of the C481 of BTK and selectively inhibits the autophosphorylation of BTK and the trans-phosphorylation of its downstream substrates, including PLCγ2 and ERK [138]. However, it exhibits high selectivity against kinases containing the homologous cysteine residue, such as Jak3 and Tec [153]. Spebrutinib has demonstrated biological activity in xenografts of MM and established CIA mouse models [138, 154, 155]. Clinical trials have been conducted with Spebrutinib. In a double-blind, single-ascending-dose phase 1a study, Spebrutinib was orally administered to healthy adult volunteers to assess its safety and pharmacokinetics. Single oral doses of 0.5–7 mg/kg were well tolerated, and 1–2 mg/kg achieved BTK occupancy of 80% or more, which was sustained for several hours after its plasma levels had decreased to undetectable levels [138]. A phase 1b study was conducted in patients with B-cell disorders. Taking R/R CLL as an example, 34% of subjects achieved partial response [156]. Currently, several clinical studies of Spebrutinib as a single agent or in combination with other agents are ongoing.

4.3 CGI/GDC Compounds

4.3.1 CGI-560

CGI-560 (Fig. 6a), which is based on an imidazo[1,2-a]pyrazine scaffold, is a selective (>10-fold relative to an initial panel of 16 kinases) but modestly potent ATP-competitive inhibitor of BTK with an IC_{50} of 400 nM [104]. The 8-amino group and N-1 of the bicycle were suggested to form several hydrogen bonds with the hinge region of the BTK kinase domain. The *para* position of the 8-aniline ring showed a promiscuous site that was tolerant to diverse substitutions, which was later proven to be exposed to the solvent [104]. The optimization of CGI-560 led to the discovery of another potent and selective BTK inhibitor, CGI-1746 [104, 157].
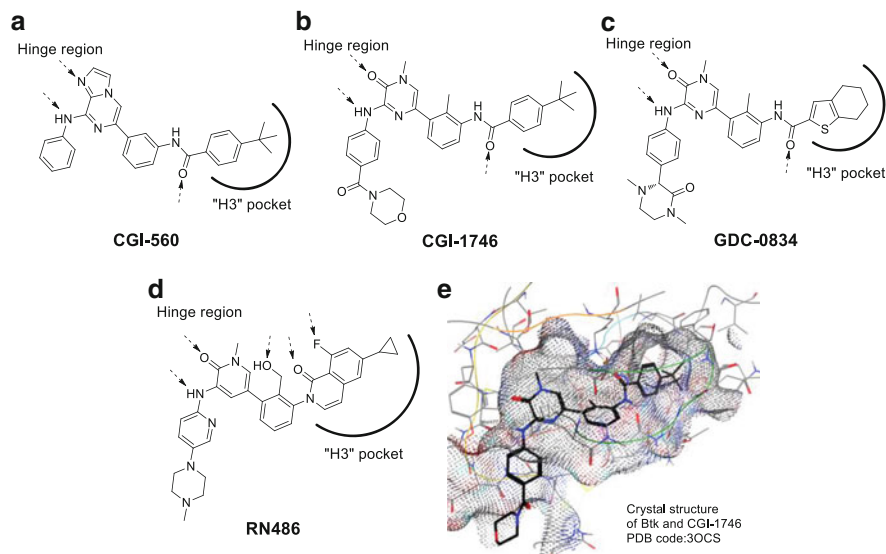
Fig. 6 Structures and binding modes of some reversible BTK inhibitors

4.3.2 CGI-1746

Replacing imidazo[1,2-a]pyrazine with bioisosteric pyrazinone followed by comprehensive SAR studies identified CGI-1746 (Fig. 6b) as a potent and selective ATP-competitive BTK inhibitor with a potency of 1.9 nM when the ATP concentration is equal to its experimental K_m value [104]. CGI-1746 binds to an inactive BTK conformation with its activation loop buried in the ATP-binding pocket, which blocks its trans-phosphorylation. The 3-amino group and N-4 of CGI-1746 are central to maintaining the hydrogen bonds with the hinge M477 corresponding to those of the 8-amino and N-1 in CGI-560. The *t*-butylphenyl amide that extends into a binding-induced pocket (the H3 hydrophobic pocket, created by residues of the G-loop and activation loop, such as L542, V546, S543, and Y551) is a critical pharmacophore for potency and selectivity. The 4-(morpholine-4-carbonyl)phenyl group is exposed to the solvent region [158] (Fig. 6b, e).

CGI-1746 effectively inhibits the trans- and autophosphorylation of BTK. Cellular assays revealed that this species can block BCR mediated B-cell proliferation and reduce chemokine production in macrophages. Additionally, in experimental mouse models, CGI-1746 showed anti-arthritic activity by suppressing chemokine and autoantibody secretion [104]. However, CGI-1746 was not subjected to further investigations because of its poor pharmacokinetic properties in rats [clearance (CL) = 87 ml/min/kg; oral bioavailability (F) <5%] [158].

4.3.3 GDC-0834

The optimization of CGI-1746 resulted in GDC-0834 (Fig. 6c), which exhibited improved clearance and appreciable oral bioavailability in rats (CL = 6.0 ml/min/kg; F = 29%) [158]. GDC-0834 is a reversible BTK inhibitor that exhibits the same activity and selectivity profile as CGI-1746 and has shown nanomolar activity in enzyme studies and excellent biochemical selectivity against a panel of 331 kinases [158]. Similar to CGI-1746, GDC-0834 binds to the ATP-binding pocket of BTK, inducing a conformational change in BTK that results in an inactive conformation of the kinase domain and reveals the specific H3 hydrophobic pocket. The tetrahydrobenzothiophene moiety extending to the H3 pocket is the structural basis of this species' potency and selectivity. Furthermore, the pyrazinone moiety forms two hydrogen bonds with the hinge M477, whereas the dimethyl-3-oxopiperazin-2-yl group is exposed to the solvent region [158].

GDC-0834 has been developed as a treatment agent for RA. It can suppress BCR- and CD40-mediated B-cell proliferation and activation and inflammatory cytokine production by inhibiting the auto- and trans-phosphorylation of BTK and blocking the downstream signaling pathways [159]. In collagen-induced arthritis (CIA) rat models, GDC-0834 administered at 30–100 mg/kg effectively blocked the phosphorylation of BTK in a dose-dependent manner and reduced the ankle swelling and morphological pathology [159]. GDC-0834 is metabolized via a non-CYP-mediated pathway, which is uncommon in other species (mouse, rat, and dog); thus, it was difficult to make accurate human clearance predictions for GDC-0834 [158]. A phase 1 study was conducted to investigate its pharmacokinetic properties in healthy volunteers orally administered GDC-0834 (35 mg or 105 mg). GDC-0834 was rapidly metabolized by the liver to an inactive metabolite via aldehyde oxidase and/or carboxyesterase-mediated amide cleavage [160]. No further clinical trials are being performed.

4.3.4 RN486

Comprehensive structure-based drug design identified RN486 (Fig. 6d) [161], an analog of CGI/GDC. RN486 is a potent, reversible BTK inhibitor with a K_d of 0.3 nM according to purified BTK enzyme assays and an IC_{50} of 17 nM based on human whole blood (HWB) assays [161]. In human cell-based assays, this compound displays functional activities in multiple cell types, including B-cells, monocytes, and mast cells, regulating their activation, proliferation, and degranulation, respectively. RN486 also shows robust anti-inflammatory and bone-protective effects in mouse CIA and rat adjuvant-induced arthritis (AIA) models [162]. Additionally, it can effectively abrogate type I and type III hypersensitivity responses in rodent models [162] and suppress the morphological pathology in SLE-prone NZB/W mouse models [163].
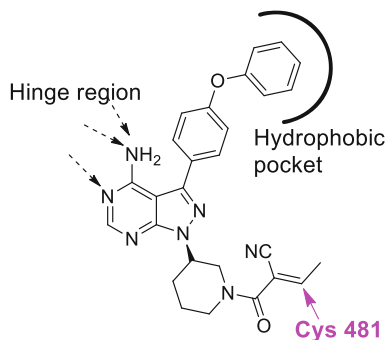
Compound 1 in Ref. [164]

Fig. 7 Structure and binding mode of a covalent reversible BTK inhibitor

4.4 Covalent Reversible Inhibitors

The potential toxicity of covalent inhibitors has been a source of concern. For example, adducts of small molecules and proteins could become antigens and trigger immune shock. Various techniques to modulate the residence times between inhibitors and protein targets have been developed by varying the reactive groups. Inverted cyanoacrylamide can react with the thiol group of cysteine reversibly under physiological conditions because the adduct is prone to elimination, and the reverse Michael addition reaction occurs, releasing the initial inhibitor (Fig. 7) [164]. The Taunton group at UCSF and scientists at Principia developed a series of BTK inhibitors using this strategy, and one of them (PRN-1008) has been involved in clinical trials for the treatment of autoimmune diseases [165].

4.5 Other Scaffold-Based BTK Inhibitors

4.5.1 PLS-123

In 2014, we reported a series of covalent BTK inhibitors based on a 2,5-diaminopyrimidine core structure derived from a reversible LCK inhibitor. Comprehensive bioinformatics and SAR studies revealed a potent, selective, irreversible BTK inhibitor, PLS-123 (Fig. 8a), with an IC$_{50}$ below 5 nM [166]. A modeling study suggested that PLS-123 binds to the ATP-binding pocket of BTK and adopts a DFG-out inactive conformation, forming several hydrogen bonds with Met477 in the hinge region, the gatekeeper residue Thr474, Glu445, and Ser538. More importantly, it covalently modifies the C481, contributing to both potency and selectivity [166].
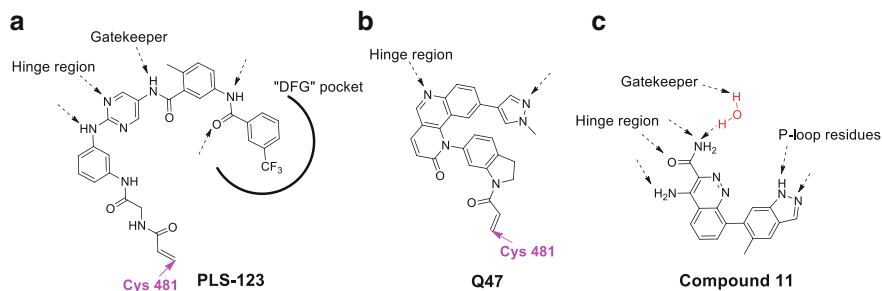
Fig. 8 Structures and binding modes of other scaffold-based BTK inhibitors

Unlike ibrutinib, PLS-123 shows a dual-action mode of inhibition, affecting both the upstream-regulated activation and downstream catalytic activity of BTK. Its selectivity profile differs from that of ibrutinib because of its additional interactions with the DFG pocket [167]. PLS-123 suppresses the proliferation of multiple B-cell lymphoma cell lines and dose-dependently attenuates lymphoma cell migration and adhesion. In a xenograft CB17/SCID mice model, the intravenous (iv) administration of PLS-123 significantly reduced the tumor size while only minimally affecting the animals' weights [167]. PLS-123, which is a covalent inhibitor, also displays a PK/PD decoupling phenomenon, and thus, its rapid distribution and elimination in vivo ($t_{1/2} = 0.6$ h; CL=11.49 ml/min/kg; $V_{ss} = 0.13$ l/kg) may reduce the possibility of off-target toxicity and adverse effects [166]. Currently, further investigations focusing on this series of compounds are ongoing.

4.5.2 QL47

QL47 (Fig. 8b) [168] is another potent covalent BTK inhibitor. It inhibits BTK kinase activity with an IC_{50} of 7 nM and blocks the BCR signaling pathway by inhibiting the autophosphorylation of BTK and the phosphorylation of the downstream substrate PLCγ2. QL47 shows potent inhibition activity affecting the proliferation of multiple B-cell lymphoma cancer cell lines. Additionally, it can induce G1 cycle arrest, promoting BTK protein degradation.

Compound 11 (Fig. 8c) [169] is a new scaffold-based reversible BTK inhibitor that forms three hydrogen bonds with the hinge region and a water-mediated hydrogen bond with the gatekeeper Thr474 side chain. In addition, the indazole is buried in the P-loop and creates hydrogen bonds with Gly414 and Phe413 in the backbone of the P-loop. In a CIA mouse model, compound 11 effectively reduced paw swelling in a dose-dependent manner. Further studies are ongoing.

In addition, HM-71224 [170] and BGB-3111 [171], which were developed at Hanmi and BeiGene, respectively, have also advanced into phase I clinical trials.

5 Conclusions and Perspectives

Less than 20 years after its discovery in 1996, BTK has emerged as a clinically validated drug target for the treatment of multiple hematopoietic malignancies. Inhibitors played an important role in elucidating BTK's functions in the treatment of these diseases, with abundant biological and pathological studies published during or after positive clinical trial results were reported. Covalent inhibitors were particularly critical. Ibrutinib was the first of a large number of molecules that exhibit significant benefits for patients. However, three main future research directions must be explored. One is to extend BTK inhibitors for the treatment of autoimmune diseases, which is strongly supported by numerous preclinical studies. Another is to develop combination therapies involving BTK inhibitors for oncology. The last one is to discover novel agents against mutated forms of BTK that are resistant to current inhibitors. Given the growing medicinal chemistry knowledge of the target, these goals should be attainable and would bring further clinical benefits to patients.

References

1. Vetrie D, Vorechovsky I, Sideras P, Holland J, Davies A, Flinter F, Hammarstrom L, Kinnon C, Levinsky R, Bobrow M, Smith CIE, Bentley DR (1993) The gene involved in X-linked agammaglobulinemia is a member of the SRC family of protein-tyrosine kinases. Nature 361:226–233
2. Vargas L, Hamasy A, Nore B, Smith C (2013) Inhibitors of BTK and ITK: state of the new drugs for cancer, autoimmunity and inflammatory diseases. Scand J Immunol 78:130–139
3. Liu X, Zhan Z, Li D, Xu L, Ma F, Zhang P, Yao H, Cao X (2011) Intracellular MHC class II molecules promote TLR-triggered innate immune responses by maintaining activation of the kinase Btk. Nat Immunol 12:416–424
4. Quek LS, Bolen J, Watson SP (1998) A role for Bruton's tyrosine kinase (Btk) in platelet activation by collagen. Curr Biol 8:1137–1140
5. Honda F, Kano H, Kanegane H, Nonoyama S, Kim ES, Lee SK, Takagi M, Mizutani S, Morio T (2012) The kinase Btk negatively regulates the production of reactive oxygen species and stimulation-induced apoptosis in human neutrophils. Nat Immunol 13:369–378
6. Genevier HC, Hinshelwood S, Gaspar HB, Rigley KP, Brown D, Saeland S, Rousset F, Levinsky RJ, Callard RE, Kinnon C, Lovering RC (1994) Expression of brutons tyrosine kinase protein within the B-cell lineage. Eur J Immunol 24:3100–3105
7. Smith CIE, Baskin B, Humiregreiff P, Zhou JN, Olsson PG, Maniar HS, Kjellen P, Lambris JD, Christensson B, Hammarstrom L, Bentley D, Vetrie D, Islam KB, Vorechovsky I, Sideras P (1994) Expression of brutons agammaglobulinemia tyrosine kinase gene, Btk, is selectively down-regulated in T-lymphocytes and plasma-cells. J Immunol 152:557–565
8. Bruton OC (1952) Agammaglobulinemia. Pediatrics 9:722–728
9. Bruton OC, Apt L, Gitlin D, Janeway CA (1952) Absence of serum gamma-globulins. AMA Am J Dis Child 84:632–636
10. Khan WN (2012) Colonel Bruton's kinase defined the molecular basis of X-linked agammaglobulinemia, the first primary immunodeficiency. J Immunol 188:2933–2935
11. Smith CIE, Notarangelo LD (1997) Molecular basis for X-linked immunodeficiencies. Adv Genet 35:57–115

12. Tsukada S, Saffran DC, Rawlings DJ, Parolini O, Allen RC, Klisak I, Sparkes RS, Kubagawa H, Mohandas T, Quan S, Belmont JW, Cooper MD, Conley ME, Witte ON (1993) Deficient expression of a B-cell cytoplasmic tyrosine kinase in human X-linked agammaglobulinemia. Cell 72:279–290

13. Conley ME, Parolini O, Rohrer J, Campana D (1994) X-linked agammaglobulinemia – new approaches to old questions based on the identification of the defective gene. Immunol Rev 138:5–21

14. Rawlings DJ, Saffran DC, Tsukada S, Largaespada DA, Grimaldi JC, Cohen L, Mohr RN, Bazan JF, Howard M, Copeland NG, Jenkins NA, Witte ON (1993) Mutation of unique region of brutons tyrosine kinase in immunodeficient XID mice. Science 261:358–361

15. Hendriks RW, Yuvaraj S, Kil LP (2014) Targeting Bruton's tyrosine kinase in B cell malignancies. Nat Rev Cancer 14:219–232

16. Mohamed AJ, Yu L, Backesjo C-M, Vargas L, Faryal R, Aints A, Christensson B, Berglof A, Vihinen M, Nore BF, Smith CIE (2009) Bruton's tyrosine kinase (Btk): function, regulation, and transformation with special emphasis on the PH domain. Immunol Rev 228:58–73

17. Hyvonen M, Saraste M (1997) Structure of the PH domain and Btk motif from Bruton's tyrosine kinase: molecular explanations for X-linked agammaglobulinaemia. EMBO J 16:3396–3404

18. Bradshaw JM (2010) The Src, Syk, and Tec family kinases: distinct types of molecular switches. Cell Signal 22:1175–1184

19. Park H, Wahl MI, Afar DEH, Turck CW, Rawlings DJ, Tam C, Scharenberg AM, Kinet JP, Witte ON (1996) Regulation of Btk function by a major autophosphorylation site within the SH3 domain. Immunity 4:515–525

20. Rawlings DJ, Scharenberg AM, Park H, Wahl MI, Lin SQ, Kato RM, Fluckiger AC, Witte ON, Kinet JP (1996) Activation of Btk by a phosphorylation mechanism initiated by SRC family kinases. Science 271:822–825

21. Saito K, Scharenberg AM, Kinet JP (2001) Interaction between the Btk PH domain and phosphatidylinositol-3,4,5-trisphosphate directly regulates Btk. J Biol Chem 276:16201–16206

22. Vihinen M, Nore BF, Mattsson PT, Backesjo CM, Nars M, Koutaniemi S, Watanabe C, Lester T, Jones A, Ochs HD, Smith CIE (1997) Missense mutations affecting a conserved cysteine pair in the TH domain of Btk. FEBS Lett 413:205–210

23. Smith CIE, Islam KB, Vorechovsky I, Olerup O, Wallin E, Rabbani H, Baskin B, Hammarstrom L (1994) X-linked agammaglobulinemia and other immunoglobulin deficiencies. Immunol Rev 138:159–183

24. Vihinen M, Nilsson L, Smith CIE (1994) TEC homology (TH) adjacent to the PH domain. FEBS Lett 350:263–265

25. Mohamed AJ, Nore BF, Christensson B, Smith CIE (1999) Signalling of Bruton's tyrosine kinase, Btk. Scand J Immunol 49:113–118

26. Ponader S, Burger JA (2014) Bruton's tyrosine kinase: from X-linked agammaglobulinemia toward targeted therapy for B-cell malignancies. J Clin Oncol 32:1830–1839

27. Nore BF, Vargas L, Mohamed AJ, Branden LJ, Backesjo CM, Islam TC, Mattsson PT, Hultenby K, Christensson B, Smith CIE (2000) Redistribution of Bruton's tyrosine kinase by activation of phosphatidylinositol 3-kinase and Rho-family GTPases. Eur J Immunol 30:145–154

28. Fruman DA, Snapper SB, Yballe CM, Davidson L, Yu JY, Alt FW, Cantley LC (1999) Impaired B cell development and proliferation in absence of phosphoinositide 3-kinase p85 alpha. Science 283:393–397

29. Suzuki H, Matsuda S, Terauchi Y, Fujiwara M, Ohteki T, Asano T, Behrens TW, Kouro T, Takatsu K, Kadowaki T, Koyasu S (2003) PI3K and Btk differentially regulate B cell antigen receptor-mediated signal transduction. Nat Immunol 4:280–286

30. Yang WY, Desiderio S (1997) BAP-135, a target for Bruton's tyrosine kinase in response to B cell receptor engagement. Proc Natl Acad Sci U S A 94:604–609

31. Kikuchi Y, Hirano M, Seto M, Takatsu K (2000) Identification and characterization of a molecule, BAM11, that associates with the pleckstrin homology domain of mouse Btk. Int Immunol 12:1397–1408

32. Yao LB, Janmey P, Frigeri LG, Han W, Fujita J, Kawakami Y, Apgar JR, Kawakami T (1999) Pleckstrin homology domains interact with filamentous actin. J Biol Chem 274:19752–19761

33. Vassilev A, Ozer Z, Navara C, Mahajan S, Uckun FM (1999) Bruton's tyrosine kinase as an inhibitor of the Fas/CD95 death-inducing signaling complex. J Biol Chem 274:1646–1656

34. Tumang JR, Negm RS, Solt LA, Schneider TJ, Colarusso TP, Hastings WD, Woodland RT, Rothstein TL (2002) BCR engagement induces Fas resistance in primary B cells in the absence of functional Bruton's tyrosine kinase. J Immunol 168:2712–2719

35. Yu L, Mohamed AJ, Vargas L, Berglof A, Finn G, Lu KP, Smith CI (2006) Regulation of Bruton tyrosine kinase by the peptidylprolyl isomerase Pin1. J Biol Chem 281:18201–18207

36. Yao L, Kawakami Y, Kawakami T (1994) The pleckstrin homology domain of bruton tyrosine kinase interacts with protein-kinase-C. Proc Natl Acad Sci U S A 91:9175–9179

37. Kang SW, Wahl MI, Chu J, Kitaura J, Kawakami Y, Kato RM, Tabuchi R, Tarakhovsky A, Kawakami T, Turck CW, Witte ON, Rawlings DJ (2001) PKC beta modulates antigen receptor signaling via regulation of Btk membrane localization. EMBO J 20:5692–5702

38. Johannes FJ, Hausser A, Storz P, Truckenmuller L, Link G, Kawakami T, Pfizenmaier K (1999) Bruton's tyrosine kinase (Btk) associates with protein kinase C mu. FEBS Lett 461:68–72

39. Crosby D, Poole AW (2002) Interaction of Bruton's tyrosine kinase and protein kinase C theta in platelets – cross-talk between tyrosine and serine/threonine kinases. J Biol Chem 277:9958–9965

40. Saito K, Tolias KF, Saci A, Koon HB, Humphries LA, Scharenberg A, Rawlings DJ, Kinet JP, Carpenter CL (2003) Btk regulates Ptdlns-4,5-P-2 synthesis: importance for calcium signaling and PI3K activity. Immunity 19:669–678

41. Jiang Y, Ma W, Wan Y, Kozasa T, Hattori S, Huang XY (1998) The G protein G alpha 12 stimulates Bruton's tyrosine kinase and a rasGAP through a conserved PH/BM domain. Nature 395:808–813

42. Tsukada S, Simon MI, Witte ON, Katz A (1994) Binding of beta-gamma-subunits of heterotrimeric G-proteins to the PH domain of bruton tyrosine kinase. Proc Natl Acad Sci U S A 91:11256–11260

43. Liu WM, Quinto I, Chen XN, Palmieri C, Rabin RL, Schwartz OM, Nelson DL, Scala G (2001) Direct inhibition of Brurton's tyrosine kinase by IBtk, a Btk-binding protein. Nat Immunol 2:939–946

44. Alexandropoulos K, Cheng GH, Baltimore D (1995) Proline-rich sequences that bind to Src homology-3 domains with individual specificities. Proc Natl Acad Sci U S A 92:3110–3114

45. Patel HV, Tzeng SR, Liao CY, Chen SH, Cheng JW (1997) SH3 domain of Bruton's tyrosine kinase can bind to proline-rich peptides of TH domain of the kinase and p120(cbl). Proteins 29:545–552

46. Ma YC, Huang XY (1998) Identification of the binding site for Gq alpha on its effector Bruton's tyrosine kinase. Proc Natl Acad Sci U S A 95:12197–12201

47. Morrogh LM, Hinshelwood S, Costello P, Cory GOC, Kinnon C (1999) The SH3 domain of Bruton's tyrosine kinase displays altered ligand binding properties when auto-phosphorylated in vitro. Eur J Immunol 29:2269–2279

48. Guinamard R, Aspenstrom P, Fougereau M, Chavrier P, Guillemot JC (1998) Tyrosine phosphorylation of the Wiskott-Aldrich syndrome protein by Lyn and Btk is regulated by CDC42. FEBS Lett 434:431–436

49. Matsushita M, Yamadori T, Kato S, Takemoto Y, Inazawa J, Baba Y, Hashimoto S, Sekine S, Arai S, Kunikata T, Kurimoto M, Kishimoto T, Tsukada S (1998) Identification and characterization of a novel SH3-domain binding protein, Sab, which preferentially associates with Bruton's tyrosine kinase (Btk). Biochem Biophys Res Commun 245:337–343

50. Yamadori T, Baba Y, Matsushita M, Hashimoto S, Kurosaki M, Kurosaki T, Kishimoto T, Tsukada S (1999) Bruton's tyrosine kinase activity is negatively regulated by Sab, the Btk-SH3 domain-binding protein. Proc Natl Acad Sci U S A 96:6341–6346

51. Hashimoto S, Iwamatsu A, Ishiai M, Okawa K, Yamadori T, Matsushita M, Baba Y, Kishimoto T, Kurosaki T, Tsukada S (1999) Identification of the SH2 domain binding protein of Bruton's tyrosine kinase as BLNK – functional significance of Btk-SH2 domain in B-cell antigen receptor-coupled calcium signaling. Blood 94:2357–2364

52. Egloff AM, Desiderio S (2001) Identification of phosphorylation sites for Bruton's tyrosine kinase within the transcriptional regulator BAP/TFII-I. J Biol Chem 276:27806–27815

53. Vargas L, Nore BF, Berglof A, Heinonen JE, Mattsson PT, Smith CIE, Mohamed AJ (2002) Functional interaction of caveolin-1 with Bruton's tyrosine kinase and Bmx. J Biol Chem 277:9351–9357

54. Guinamard R, Fougereau M, Seckinger P (1997) The SH3 domain of Bruton's tyrosine kinase interacts with Vav, Sam68 and EWS. Scand J Immunol 45:587–595

55. Rodriguez R, Matsuda M, Perisic O, Bravo J, Paul A, Jones NP, Light Y, Swann K, Williams RL, Katan M (2001) Tyrosine residues in phospholipase C gamma 2 essential for the enzyme function in B-cell signaling. J Biol Chem 276:47982–47992

56. Ponader S, Chen S-S, Buggy JJ, Balakrishnan K, Gandhi V, Wierda WG, Keating MJ, O'Brien S, Chiorazzi N, Burger JA (2012) The Bruton tyrosine kinase inhibitor PCI-32765 thwarts chronic lymphocytic leukemia cell survival and tissue homing in vitro and in vivo. Blood 119:1182–1189

57. Burger JA, Montserrat E (2013) Coming full circle: 70 years of chronic lymphocytic leukemia cell redistribution, from glucocorticoids to inhibitors of B-cell receptor signaling. Blood 121:1501–1509

58. Khan WN, Alt FW, Gerstein RM, Malynn BA, Larsson I, Rathbun G, Davidson L, Muller S, Kantor AB, Herzenberg LA, Rosen FS, Sideras P (1995) Defective B-cell development and function in Btk-deficient mice. Immunity 3:283–299

59. Aoki Y, Isselbacher KJ, Pillai S (1994) Bruton tyrosine kinase is tyrosine-phosphorylated and activated in pre-B lymphocytes and receptor-ligated b-cells. Proc Natl Acad Sci U S A 91:10606–10609

60. Deweers M, Brouns GS, Hinshelwood S, Kinnon C, Schuurman RKB, Hendriks RW, Borst J (1994) B-cell antigen receptor stimulation activates the human Brutons tyrosine kinase, which is deficient in X-linked agammaglobulinemia. J Biol Chem 269:23857–23860

61. Rolli V, Gallwitz M, Wossning T, Flemming A, Schamel WWA, Zurn C, Reth M (2002) Amplification of B cell antigen receptor signaling by a Syk/ITAM positive feedback loop. Mol Cell 10:1057–1069

62. O'Rourke LM, Tooze R, Turner M, Sandoval DM, Carter RH, Tybulewicz VLJ, Fearon DT (1998) CD19 as a membrane-anchored adaptor protein of B lymphocytes: costimulation of lipid and protein kinases by recruitment of Vav. Immunity 8:635–645

63. Inabe K, Ishiai M, Scharenberg AM, Freshney N, Downward J, Kurosaki T (2002) Vav3 modulates B cell receptor responses by regulating phosphoinositide 3-kinase activation. J Exp Med 195:189–200

64. Fu C, Turck CW, Kurosaki T, Chan AC (1998) BLNK: a central linker protein in B cell activation. Immunity 9:93–103

65. Oellerich T, Bremes V, Neumann K, Bohnenberger H, Dittmann K, Hsiao H-H, Engelke M, Schnyder T, Batista FD, Urlaub H, Wienands J (2011) The B-cell antigen receptor signals through a preformed transducer module of SLP65 and CIN85. EMBO J 30:3620–3634

66. Kim YJ, Sekiya F, Poulin B, Bae YS, Rhee SG (2004) Mechanism of B-cell receptor-induced phosphorylation and activation of phospholipase C-gamma 2. Mol Cell Biol 24:9986–9999

67. Spaargaren M, Beuling EA, Rurup ML, Meijer HP, Klok MD, Middendorp S, Hendriks RW, Pals ST (2003) The B cell antigen receptor controls integrin activity through Btk and PLC gamma 2. J Exp Med 198:1539–1550

68. Kuehn HS, Radinger M, Brown JM, Ali K, Vanhaesebroeck B, Beaven MA, Metcalfe DD, Gilfillan AM (2010) Btk-dependent Rac activation and actin rearrangement following Fc epsilon RI aggregation promotes enhanced chemotactic responses of mast cells. J Cell Sci 123:2576–2585

69. Su W, Wynne J, Pinheiro EM, Strazza M, Mor A, Montenont E, Berger J, Paul DS, Bergmeier W, Gertler FB, Philips MR (2015) Rap1 and its effector RIAM are required for lymphocyte trafficking. Blood 126:2695–2703

70. McLeod SJ, Ingham RJ, Bos JL, Kurosaki T, Gold MR (1998) Activation of the Rap1 GTPase by the B cell antigen receptor. J Biol Chem 273:29218–29223

71. de Gorter DJJ, Beuling EA, Kersseboom R, Middendorp S, van Gils JM, Hendriks RW, Pals ST, Spaargaren M (2007) Bruton's tyrosine kinase and phospholipase C gamma 2 mediate chemokine-controlled B cell migration and homing. Immunity 26:93–104

72. de Rooij MFM, Kuil A, Geest CR, Eldering E, Chang BY, Buggy JJ, Pals ST, Spaargaren M (2012) The clinically active BTK inhibitor PCI-32765 targets B-cell receptor- and chemokine-controlled adhesion and migration in chronic lymphocytic leukemia. Blood 119:2590–2594

73. Chang BY, Magadala P, Francesco M, Balasubramanian S, Elias L, Buggy JJ (2013) Mobilization of follicular lymphoma cells into peripheral blood following BTK inhibition by ibrutinib. Cancer Res 73:3519

74. Chang BY, Francesco M, De Rooij MFM, Magadala P, Steggerda SM, Huang MM, Kuil A, Herman SEM, Chang S, Pals ST, Wilson W, Wiestner A, Spaargaren M, Buggy JJ, Elias L (2013) Egress of CD19(+)CD5(+) cells into peripheral blood following treatment with the Bruton tyrosine kinase inhibitor ibrutinib in mantle cell lymphoma patients. Blood 122:2412–2424

75. Jefferies CA, Doyle S, Brunner C, Dunne A, Brint E, Wietek C, Walch E, Wirth T, O'Neill LAJ (2003) Bruton's tyrosine kinase is a toll/interleukin-1 receptor domain-binding protein that participates in nuclear factor kappa B activation by toll-like receptor 4. J Biol Chem 278:26258–26264

76. Lee K-G, Xu S, Kang Z-H, Huo J, Huang M, Liu D, Takeuchi O, Akira S, Lam K-P (2012) Bruton's tyrosine kinase phosphorylates Toll-like receptor 3 to initiate antiviral response. Proc Natl Acad Sci U S A 109:5791–5796

77. Marron TU, Martinez-Gallo M, Yu JE, Cunningham-Rundles C (2012) Toll-like receptor 4-, 7-, and 8-activated myeloid cells from patients with X-linked agammaglobulinemia produce enhanced inflammatory cytokines. J Allergy Clin Immunol 129:184–184

78. Davis RE, Ngo VN, Lenz G, Tolar P, Young RM, Romesser PB, Kohlhammer H, Lamy L, Zhao H, Yang Y, Xu W, Shaffer AL, Wright G, Xiao W, Powell J, Jiang J-K, Thomas CJ, Rosenwald A, Ott G, Muller-Hermelink HK, Gascoyne RD, Connors JM, Johnson NA, Rimsza LM, Campo E, Jaffe ES, Wilson WH, Delabie J, Smeland EB, Fisher RI, Braziel RM, Tubbs RR, Cook JR, Weisenburger DD, Chan WC, Pierce SK, Staudt LM (2010) Chronic active B-cell-receptor signalling in diffuse large B-cell lymphoma. Nature 463:88–88

79. Muzio M, Apollonio B, Scielzo C, Frenquelli M, Vandoni I, Boussiotis V, Caligaris-Cappio F, Ghia P (2008) Constitutive activation of distinct BCR-signaling pathways in a subset of CLL patients: a molecular signature of anergy. Blood 112:188–195

80. Mockridge CI, Potter KN, Wheatley I, Neville LA, Packham G, Stevenson FK (2007) Reversible anergy of sIgM-mediated signaling in the two subsets of CLL defined by V-H-gene mutational status. Blood 109:4424–4431

81. Herishanu Y, Perez-Galan P, Liu D, Biancotto A, Pittaluga S, Vire B, Gibellini F, Njuguna N, Lee E, Stennett L, Raghavachari N, Liu P, McCoy JP, Raffeld M, Stetler-Stevenson M, Yuan C, Sherry R, Arthur DC, Maric I, White T, Marti GE, Munson P, Wilson WH, Wiestner A (2011) The lymph node microenvironment promotes B-cell receptor signaling, NF-kappa B activation, and tumor proliferation in chronic lymphocytic leukemia. Blood 117:563–574

82. Herman SEM, Gordon AL, Hertlein E, Ramanunni A, Zhang X, Jaglowski S, Flynn J, Jones J, Blum KA, Buggy JJ, Hamdy A, Johnson AJ, Byrd JC (2011) Bruton tyrosine kinase represents a promising therapeutic target for treatment of chronic lymphocytic leukemia and is effectively targeted by PCI-32765. Blood 117:6287–6296

83. Byrd JC, Furman RR, Coutre SE, Flinn IW, Burger JA, Blum KA, Grant B, Sharman JP, Coleman M, Wierda WG, Jones JA, Zhao WQ, Heerema NA, Johnson AJ, Sukbuntherng J, Chang BY, Clow F, Hedrick E, Buggy JJ, James DF, O'Brien S (2013) Targeting BTK with ibrutinib in relapsed chronic lymphocytic leukemia. New Engl J Med 369:32–42

84. Boyd RS, Jukes-Jones R, Walewska R, Brown D, Dyer MJS, Cain K (2009) Protein profiling of plasma membranes defines aberrant signaling pathways in mantle cell lymphoma. Mol Cell Proteomics 8:1501–1515

85. Pighi C, Gu T-L, Dalai I, Barbi S, Parolini C, Bertolaso A, Pedron S, Parisi A, Ren J, Cecconi D, Chilosi M, Menestrina F, Zamo A (2011) Phospho-proteomic analysis of mantle cell lymphoma cells suggests a pro-survival role of B-cell receptor signaling. Cell Oncol 34:141–153

86. Rinaldi A, Kwee I, Taborelli M, Largo C, Uccella S, Martin V, Poretti G, Gaidano G, Calabrese G, Martinelli G, Baldini L, Pruneri G, Capella C, Zucca E, Cotter FE, Cigudosa JC, Catapano CV, Tibiletti MG, Bertoni F (2006) Genomic and expression profiling identifies the B-cell associated tyrosine kinase Syk as a possible therapeutic target in mantle cell lymphoma. Br J Haematol 132:303–316

87. Jares P, Colomer D, Campo E (2012) Molecular pathogenesis of mantle cell lymphoma. J Clin Invest 122:3416–3423

88. Cinar M, Hamedani FS, Mo Z, Cinar B, Amin HM, Alkan S (2013) Bruton tyrosine kinase is commonly expressed in mantle cell lymphoma and its attenuation by Ibrutinib induces apoptosis of mantle cell lymphoma cells. Mod Pathol 26:325A

89. Alizadeh AA, Eisen MB, Davis RE, Ma C, Lossos IS, Rosenwald A, Boldrick JG, Sabet H, Tran T, Yu X, Powell JI, Yang LM, Marti GE, Moore T, Hudson J, Lu LS, Lewis DB, Tibshirani R, Sherlock G, Chan WC, Greiner TC, Weisenburger DD, Armitage JO, Warnke R, Levy R, Wilson W, Grever MR, Byrd JC, Botstein D, Brown PO, Staudt LM (2000) Distinct types of diffuse large B-cell lymphoma identified by gene expression profiling. Nature 403:503–511

90. Davis RE, Brown KD, Siebenlist U, Staudt LM (2001) Constitutive nuclear factor kappa B activity is required for survival of activated B cell-like diffuse large B cell lymphoma cells. J Exp Med 194:1861–1874

91. Ngo VN, Davis RE, Lamy L, Yu X, Zhao H, Lenz G, Lam LT, Dave S, Yang LM, Powell J, Staudt LM (2006) A loss-of-function RNA interference screen for molecular targets in cancer. Nature 441:106–110

92. Lenz G, Davis RE, Ngo VN, Lam L, George TC, Wright GW, Dave SS, Zhao H, Xu W, Rosenwald A, Ott G, Muller-Hermelink HK, Gascoyne RD, Connors JM, Rimsza LM, Campo E, Jaffe ES, Delabie J, Smeland EB, Fisher RI, Chan WC, Staudt LM (2008) Oncogenic CARD11 mutations in human diffuse large B cell lymphoma. Science 319:1676–1679

93. Compagno M, Lim WK, Grunn A, Nandula SV, Brahmachary M, Shen Q, Bertoni F, Ponzoni M, Scandurra M, Califano A, Bhagat G, Chadburn A, Dalla-Favera R, Pasqualucci L (2009) Mutations of multiple genes cause deregulation of NF-kappa B in diffuse large B-cell lymphoma. Nature 459:717–717

94. Treon SP, Xu L, Yang G, Zhou Y, Liu X, Cao Y, Sheehy P, Manning RJ, Patterson CJ, Tripsas C, Arcaini L, Pinkus GS, Rodig SJ, Sohani AR, Harris NL, Laramie JM, Skifter DA, Lincoln SE, Hunter ZR (2012) MYD88 L265P somatic mutation in Waldenstrom's macroglobulinemia. New Engl J Med 367:826–833

95. Yang G, Zhou Y, Liu X, Xu L, Cao Y, Manning RJ, Patterson CJ, Buhrlage SJ, Gray N, Tai Y-T, Anderson KC, Hunter ZR, Treon SP (2013) A mutation in MYD88 (L265P) supports the survival of lymphoplasmacytic cells by activation of Bruton tyrosine kinase in Waldenstrom macroglobulinemia. Blood 122:1222–1232

96. Raje N, Roodman GD (2011) Advances in the biology and treatment of bone disease in multiple myeloma. Clin Cancer Res 17:1278–1286
97. Kuehl WM, Bergsagel PL (2012) Molecular pathogenesis of multiple myeloma and its premalignant precursor. J Clin Invest 122:3456–3463
98. Shinohara M, Koga T, Okamoto K, Sakaguchi S, Arai K, Yasuda H, Takai T, Kodama T, Morio T, Geha RS, Kitamura D, Kurosaki T, Ellmeier W, Takayanagi H (2008) Tyrosine kinases Btk and Tec regulate osteoclast differentiation by linking RANK and ITAM signals. Cell 132:794–806
99. Lee SH, Kim T, Jeong D, Kim N, Choi Y (2008) The Tec family tyrosine kinase Btk regulates RANKL-induced osteoclast maturation. J Biol Chem 283:11526–11534
100. Tai Y-T, Chang BY, Kong S-Y, Fulciniti M, Yang G, Calle Y, Hu Y, Lin J, Zhao J-J, Cagnetta A, Cea M, Sellitto MA, Zhong MY, Wang Q, Acharya C, Carrasco DR, Buggy JJ, Elias L, Treon SP, Matsui W, Richardson P, Munshi NC, Anderson KC (2012) Bruton tyrosine kinase inhibition is a novel therapeutic strategy targeting tumor in the bone marrow microenvironment in multiple myeloma. Blood 120:1877–1887
101. Hasan M, Lopez-Herrera G, Blomberg KEM, Lindvall JM, Berglof A, Smith CIE, Vargas L (2008) Defective Toll-like receptor 9-mediated cytokine production in B cells from Bruton's tyrosine kinase-deficient mice. Immunology 123:239–249
102. Kil LP, de Bruijn MJW, van Nimwegen M, Corneth OBJ, van Hamburg JP, Dingjan GM, Thaiss F, Rimmelzwaan GF, Elewaut D, Delsing D, van Loo PF, Hendriks RW (2012) Btk levels set the threshold for B-cell activation and negative selection of autoreactive B cells in mice. Blood 119:3744–3756
103. Honigberg LA, Smith AM, Sirisawad M, Verner E, Loury D, Chang B, Li S, Pan Z, Thamm DH, Miller RA, Buggy JJ (2010) The Bruton tyrosine kinase inhibitor PCI-32765 blocks B-cell activation and is efficacious in models of autoimmune disease and B-cell malignancy. Proc Natl Acad Sci U S A 107:13075–13080
104. Di Paolo JA, Huang T, Balazs M, Barbosa J, Barck KH, Bravo BJ, Carano RAD, Darrow J, Davies DR, DeForge LE, Diehl L, Ferrando R, Gallion SL, Giannetti AM, Gribling P, Hurez V, Hymowitz SG, Jones R, Kropf JE, Lee WP, Maciejewski PM, Mitchell SA, Rong H, Staker BL, Whitney JA, Yeh S, Young WB, Yu C, Zhang J, Reif K, Currie KS (2011) Specific Btk inhibition suppresses B cell- and myeloid cell-mediated arthritis. Nat Chem Biol 7:41–50
105. Chang BY, Huang MM, Francesco M, Chen J, Sokolove J, Magadala P, Robinson WH, Buggy JJ (2011) The Bruton tyrosine kinase inhibitor PCI-32765 ameliorates autoimmune arthritis by inhibition of multiple effector cells. Arthritis Res Ther 13:R115
106. Hutcheson J, Vanarsa K, Bashmakov A, Grewal S, Sajitharan D, Chang BY, Buggy JJ, Zhou XJ, Du Y, Satterthwaite AB, Mohan C (2012) Modulating proximal cell signaling by targeting Btk ameliorates humoral autoimmunity and end-organ disease in murine lupus. Arthritis Res Ther 14:R243
107. McLaughlin P, Grillo-Lopez AJ, Link BK, Levy R, Czuczman MS, Williams ME, Heyman MR, Bence-Bruckler I, White CA, Cabanillas F, Jain V, Ho AD, Lister J, Wey K, Shen D, Dallaire BK (1998) Rituximab chimeric Anti-CD20 monoclonal antibody therapy for relapsed indolent lymphoma: half of patients respond to a four-dose treatment program. J Clin Oncol 16:2825–2833
108. Colombat P, Salles G, Brousse N, Eftekhari P, Soubeyran P, Delwail V, Deconinck E, Haioun C, Foussard C, Sebban C, Stamatoullas A, Milpied N, Boue F, Taillan B, Lederlin P, Najman A, Thieblemont C, Montestruc F, Mathieu-Boue A, Benzohra A, Solal-Celigny P (2001) Rituximab (anti-CD20 monoclonal antibody) as single first-line therapy for patients with follicular lymphoma with a low tumor burden: clinical and molecular evaluation. Blood 97:101–106
109. Cang S, Mukhi N, Wang K, Liu D (2012) Novel CD20 monoclonal antibodies for lymphoma therapy. J Hematol Oncol 5:64

110. Wang K, Wei G, Liu D (2012) CD19: a biomarker for B cell development, lymphoma diagnosis and therapy. Exp Hematol Oncol 1:36
111. Yoon Y (2014) Small chemicals with inhibitory effects on PtdIns(3,4,5) P-3 binding of Btk PH domain. Bioorg Med Chem Lett 24:2334–2339
112. Arup KG, Torsten H, Douglas AP, Joseph MS, John PM (2008) Knowledge based prediction of ligand binding modes and rational inhibitor design for kinase drug discovery. J Med Chem 51:5149–5171
113. Pan Z, Scheerens H, Li SJ, Schultz BE, Sprengeler PA, Burrill LC, Mendonca RV, Sweeney MD, Scott KC, Grothaus PG, Jeffery DA, Spoerke JM, Honigberg LA, Young PR, Dalrymple SA, Palmer JT (2007) Discovery of selective irreversible inhibitors for Bruton's tyrosine kinase. Chem Med Chem 2:58–61
114. Barf T, Kaptein A (2012) Irreversible protein kinase inhibitors: balancing the benefits and risks. J Med Chem 55:6243–6262
115. Liu Q, Sabnis Y, Zhao Z, Zhang T, Buhrlage SJ, Jones LH, Gray NS (2013) Developing irreversible inhibitors of the protein kinase cysteinome. Chem Biol 20:146–159
116. Cowan-Jacob SW, Moebitz H, Fabbro D (2009) Structural biology contributions to tyrosine kinase drug discovery. Curr Opin Cell Biol 21:280–287
117. Lou Y, Owens TD, Kuglstatter A, Kondru RK, Goldstein DM (2012) Bruton's tyrosine kinase inhibitors: approaches to potent and selective inhibition, preclinical and clinical evaluation for inflammatory diseases and B cell malignancies. J Med Chem 55:4539–4550
118. Marcotte DJ, Liu YT, Arduini RM, Hession CA, Miatkowski K, Wildes CP, Cullen PF, Hong V, Hopkins BT, Mertsching E, Jenkins TJ, Romanowski MJ, Baker DP, Silvian LF (2010) Structures of human Bruton's tyrosine kinase in active and inactive conformations suggest a mechanism of activation for TEC family kinases. Protein Sci 19:429–439
119. Wu P, Nielsen TE, Clausen MH (2015) FDA-approved small-molecule kinase inhibitors. Trends Pharmacol Sci 36:422–439
120. Burger J, Buggy J (2013) Bruton tyrosine kinase inhibitor ibrutinib (PCI-32765) Leuk. Lymphoma 54:2385–2391
121. Advani R, Buggy J, Sharman J, Smith S, Boyd T, Grant B, Kolibaba K, Furman R, Rodriguez S, Chang B, Sukbuntherng J, Izumi R, Hamdy A, Hedrick E, Fowler N (2013) Bruton tyrosine kinase inhibitor ibrutinib (PCI-32765) Has significant activity in patients with relapsed/refractory B-cell malignancies. J Clin Oncol 31:88
122. Byrd JC, Brown JR, O'Brien S, Barrientos JC, Kay NE, Reddy NM, Coutre S, Tam CS, Mulligan SP, Jaeger U, Devereux S, Barr PM, Furman RR, Kipps TJ, Cymbalista F, Pocock C, Thornton P, Caligaris-Cappio F, Robak T, Delgado J, Schuster SJ, Montillo M, Schuh A, de Vos S, Gill D, Bloor A, Dearden C, Moreno C, Jones JJ, Chu AD, Fardis M, McGreivy J, Clow F, James DF, Hillmen P, Investigators R (2014) Ibrutinib versus Ofatumumab in previously treated chronic lymphoid leukemia. New Engl J Med 371:213–223
123. Spaargaren M, de Rooij MF, Kater AP, Eldering E (2014) BTK inhibitors in chronic lymphocytic leukemia: a glimpse to the future. Oncogene 34:2426–2436
124. Wodarz D, Garg N, Komarova NL, Benjamini O, Keating MJ, Wierda WG, Kantarjian H, James D, O'Brien S, Burger JA (2014) Kinetics of CLL cells in tissues and blood during therapy with the BTK inhibitor ibrutinib. Blood 123:4132–4135
125. Mustafa RZ, Herman SEM, Jones J, Gyamfi J, Farooqui M, Wiestner A (2013) Ibrutinib inhibits B-cell adhesion and causes an efflux of chronic lymphocytic leukemia cells from the tissue microenvironment into the blood leading to a transient treatment-induced lymphocytosis. Blood 122:671
126. Rossi D, Gaidano G (2014) Lymphocytosis and ibrutinib treatment of CLL. Blood 123:1772–1774
127. Woyach JA, Smucker K, Smith LL, Lozanski A, Zhong YM, Ruppert AS, Lucas D, Williams K, Zhao WQ, Rassenti L, Ghia E, Kipps TJ, Mantel R, Jones J, Flynn J, Maddocks K, O'Brien S, Furman RR, James DF, Clow F, Lozanski G, Johnson AJ, Byrd JC (2014) Prolonged lymphocytosis during ibrutinib therapy is associated with distinct

molecular characteristics and does not indicate a suboptimal response to therapy. Blood 123:1810–1817

128. Wang ML, Rule S, Martin P, Goy A, Auer R, Kahl BS, Jurczak W, Advani RH, Romaguera JE, Williams ME, Barrientos JC, Chmielowska E, Radford J, Stilgenbauer S, Dreyling M, Jedrzejczak WW, Johnson P, Spurgeon SE, Li L, Zhang L, Newberry K, Ou ZS, Cheng N, Fang BL, McGreivy J, Clow F, Buggy JJ, Chang BY, Beaupre DM, Kunkel LA, Blum KA (2013) Targeting BTK with ibrutinib in relapsed or refractory mantle-cell lymphoma. New Engl J Med 369:507–516

129. Lee CS, Rattu MA and Kim SS (2014) A review of a novel, Bruton's tyrosine kinase inhibitor, ibrutinib. J Oncol Pharm Pract 22:92–104

130. Kohrt HE, Sagiv-Barfi I, Rafiq S, Herman SEM, Butchar JP, Cheney C, Zhang XL, Buggy JJ, Muthusamy N, Levy R, Johnson AJ, Byrd JC (2014) Ibrutinib antagonizes rituximab-dependent NK cell-mediated cytotoxicity. Blood 123:1957–1960

131. Younes A, Flinn I, Berdeja J, Friedberg JW, Casulo C, Thieblemont C, Morschhauser F, Westin JR, Seetharam S, Hellemans P, Smit H, de Vries R, Dauphinee E, Badamo-Dotzis J, Fourneau N, Oki Y (2013) Combining ibrutinib with rituximab, cyclophosphamide, doxorubicin, vincristine, and prednisone (R-CHOP): updated results from a phase 1b study in treatment-naive patients with CD20-positive B-cell non-Hodgkin's lymphoma (NHL). Blood 122:852

132. Grabinski N, Ewald F (2014) Ibrutinib (Imbruvica TM) potently inhibits ErbB receptor phosphorylation and cell viability of ErbB2-positive breast cancer cells. Invest New Drugs 32:1096–1104

133. Gao W, Wang M, Wang L, Lu H, Wu S, Dai B, Ou Z, Zhang L, Heymach J, Gold K, Minna J, Roth J, Hofstetter W, Swisher S, Fang B (2014) Selective antitumor activity of ibrutinib in EGFR-mutant non-small cell lung cancer cells. J Natl Cancer Inst 106:dju204

134. Davids MS, Brown JR (2014) Ibrutinib: a first in class covalent inhibitor of Bruton's tyrosine kinase. Future Oncol 10:957–967

135. Liu J, Fitzgerald ME, Berndt MC, Jackson CW, Gartner TK (2006) Bruton tyrosine kinase is essential for botrocetin/VWF-induced signaling and GPIb-dependent thrombus formation in vivo. Blood 108:2596–2603

136. Farooqui M, Lozier JN, Valdez J, Saba N, Wells A, Soto S, Liu DL, Aue G, Wiestner A (2012) Ibrutinib (PCI 32765) rapidly improves platelet counts in chronic lymphocytic leukemia/small lymphocytic lymphoma (CLL/SLL) patients and Has minimal effects on platelet aggregation. Blood 120:1789

137. Woyach JA, Furman RR, Liu TM, Ozer HG, Zapatka M, Ruppert AS, Xue L, Li DHH, Steggerda SM, Versele M, Dave SS, Zhang J, Yilmaz AS, Jaglowski SM, Blum KA, Lozanski A, Lozanski G, James DF, Barrientos JC, Lichter P, Stilgenbauer S, Buggy JJ, Chang BY, Johnson AJ, Byrd JC (2014) Resistance mechanisms for the Bruton's tyrosine kinase inhibitor ibrutinib. New Engl J Med 370:2286–2294

138. Evans EK, Tester R, Aslanian S, Karp R, Sheets M, Labenski MT, Witowski SR, Lounsbury H, Chaturvedi P, Mazdiyasni H, Zhu Z, Nacht M, Freed MI, Petter RC, Dubrovskiy A, Singh J, Westlin WF (2013) Inhibition of Btk with CC-292 provides early pharmacodynamic assessment of activity in mice and humans. J Pharmacol Exp Ther 346:219–228

139. Yamamoto S, Yoshizawa T Inventors, Ono Pharmaceutical Co., Ltd., Assignee. Purinone derivative. United States Patent US 8,940,725. Accessed 27 Jan 2015

140. Yasuhiro T, Yoshizawa T, Daub H, Weber C, Narita M and Kawabata K (2012) ONO-WG-307, a novel, potent and selective inhibitor of Bruton's tyrosine kinase (Btk), results in sustained inhibition of the ERK, AKT and PKD signaling pathways. Cancer Res 72. doi: 10.1158/1538-7445.am2012-2021

141. Kozaki R, Hutchinson C, Sandrine J, Dyer MJS (2014) Kinome reprogramming in DLBCL by the Btk-specific inhibitor ONO-4059 highlights synergistic combinations for clinical application. Haematologica 99:137–138

142. Kozaki R, Yoshizawa T, Tohda S, Yasuhiro T, Hotta S, Ariza Y, Ueda Y, Narita M, Kawabata K (2011) Development of a Bruton's tyrosine kinase (Btk) inhibitor, ONO-WG-307: efficacy in ABC-DLBCL xenograft model potential treatment for B-Cell malignancies. Blood 118:1593–1593

143. Walter HS, Rule SA, Dyer MJS, Karlin L, Jones C, Cazin B, Quittet P, Shah N, Hutchinson CV, Honda H, Duffy K, Birkett J, Jamieson V, Courtenay-Luck N, Yoshizawa T, Sharpe J, Ohno T, Abe S, Nishimura A, Cartron G, Morschhauser F, Fegan C, Salles G (2016) A phase 1 clinical trial of the selective BTK inhibitor ONO/GS-4059 in relapsed and refractory mature B-cell malignancies. Blood 127:411–419. doi:10.1182/blood-2015-08-664086

144. https://clinicaltrials.gov/ct2/results?term=ONO%2FGS-4059&Search=Search

145. Barf TA, Jans CGJM, Man DAPA, Oubrie AA, Raaijmakers HCA, Rewinkel JBM, Sterrenburg J-G and JCHM W (2013) PCT Int Appl WO Patent WO 2013010868

146. Covey T, Barf T, Gulrajani M, Krantz F, van Lith B, Bibikova E, van de Kar B, de Zwart E, Hamdy A, Izumi R and Kaptein A (2015) ACP-196: a novel covalent Bruton's tyrosine kinase (Btk) inhibitor with improved selectivity and in vivo target coverage in chronic lymphocytic leukemia (CLL) patients. Cancer Res 75. doi: 10.1158/1538-7445.am2015-2596

147. Byrd JC, Harrington B, O'Brien S, Jones JA, Schuh A, Devereux S, Chaves J, Wierda WG, Awan FT, Brown JR, Hillmen P, Stephens DM, Ghia P, Barrientos JC, Pagel JM, Woyach J, Johnson D, Huang J, Wang X, Kaptein A, Lannutti BJ, Covey T, Fardis M, McGreivy J, Hamdy A, Rothbaum W, Izumi R, Diacovo TG, Johnson AJ, Furman RR (2016) Acalabrutinib (ACP-196) in relapsed chronic lymphocytic leukemia. N Engl J Med 374:323–332

148. Niemann CU, Montraveta A, Herman SEM, Ingallinera T, Barf T, Colomer D and Wiestner A (2014) The novel Bruton's tyrosine kinase inhibitor ACP-196 shows in vivo efficacy against human chronic lymphocytic leukemia cells xenografted to the NSG mouse model. Cancer Res 74. doi: 10.1158/1538-7445.am2014-2624

149. Herman SEM, Montraveta A, Niemann CU, Mora-Jensen H, Gulrajani M, Krantz F, Harrington BK, Covey T, Lannutti BJ, Izumi R, Ulrich RG, Byrd JC, Wiestner A, Johnson AJ, Woyach JA (2015) The Bruton tyrosine kinase (BTK) inhibitor ACP-196 demonstrates clinical activity in two mouse models of chronic lymphocytic leukemia. Blood 126:23

150. Herman SEM, Sun X, McAuley EM, Hsieh MM, Pittaluga S, Raffeld M, Liu D, Keyvanfar K, Chapman CM, Chen J, Buggy JJ, Aue G, Tisdale JF, Perez-Galan P, Wiestner A (2013) Modeling tumor-host interactions of chronic lymphocytic leukemia in xenografted mice to study tumor biology and evaluate targeted therapy. Leukemia 27:2311–2321. doi:10.1038/leu.2013.131

151. https://www.clinicaltrials.gov/ct2/results?term=ACP-196&Search=Search

152. Liu J, Guiadeen D, Krikorian A, Gao X, Wang J, Boga SB, Alhassan A-B, Yu Y, Vaccaro H, Liu S, Yang C, Wu H, Cooper A, de Man J, Kaptein A, Maloney K, Hornak V, Gao Y-D, Fischmann TO, Raaijmakers H, Vu-Pham D, Presland J, Mansueto M, Xu Z, Leccese E, Zhang-Hoover J, Knemeyer I, Garlisi CG, Bays N, Stivers P, Brandish PE, Hicks A, Kim R, Kozlowski JA (2016) Discovery of 8-amino-imidazo[1,5-a]pyrazines as reversible BTK inhibitors for the treatment of rheumatoid arthritis. ACS Med Chem Lett 7:198–203

153. Juswinder S, Russell C, Deqiang N, Lixin Q, Arthur K, Roy L, Shomir G, Zhendong Z (2011) United States patent US20110117073

154. Evans E, Tester R, Aslanian S, Chaturvedi P, Mazdiyasni H, Ponader S, Tesar B, Sheets M, Nacht M, Stiede K, Witowski S, Lounsbury H, Petter R, Brown JR, Burger JA, Singh J, Westlin WF (2011) Clinical development of AVL-292; a potent, selective covalent Btk inhibitor for the treatment of B cell malignancies. Blood 118:1487–1487

155. Eda H, Santo L, Cirstea DD, Yee AJ, Scullen TA, Nemani N, Mishima Y, Arastu-Kapur S, Evans E, Singh J, Kirk CJ, Westlin WF, Raje NS (2013) A novel Bruton's tyrosine kinase inhibitor CC-292 in combination with the proteasome inhibitor carfilzomib impacts multiple myeloma bone microenviroment with resultant anti-myeloma activity. Blood 122:682

156. Brown JR, Harb WA, Hill BT, Gabrilove J, Sharman JP, Schreeder MT, Barr PM, Foran JM, Miller TP, Burger JA, Kelly KR, Mahadevan D, Ma S, Barnett E, Marine J, Nava-Parada P,

Azaryan A, Mei J, Kipps TJ (2013) Phase 1 study of single agent CC-292, a highly selective Bruton's tyrosine kinase (BTK) inhibitor, in relapsed/refractory chronic lyrnphocytic leukemia (CLL). Blood 122:1630

157. Brittelli DR, Currie KS, Darrow JW, Kropf JE, Lee SH, Gallion SL Mitchell SA (2006) PCT Int Appl WO Patent WO2006099075

158. Young W, Barbosa J, Blomgren P, Bremer M, Crawford J, Dambach D, Gallion S, Hymowitz S, Kropf J, Lee S, Liu L, Lubach J, Macaluso J, Maciejewski P, Maurer B, Mitchell S, Ortwine D, Di Paolo J, Reif K, Scheerens H, Schmitt A, Sowell C, Wang X, Wong H, Xiong J, Xu Z, Zhao Z, Currie K (2015) Potent and selective Bruton's tyrosine kinase inhibitors: discovery of GDC-0834. Bioorg Med Chem Lett 25:1333–1337

159. Liu L, Di Paolo J, Barbosa J, Rong H, Reif K, Wong H (2011) Antiarthritis effect of a novel Bruton's tyrosine kinase (BTK) inhibitor in rat collagen-induced arthritis and mechanism-based pharmacokinetic/pharmacodynamic modeling: relationships between inhibition of BTK phosphorylation and efficacy. J Pharmacol Exp Ther 338:154–163

160. Liu L, Halladay JS, Shin Y, Wong S, Coraggio M, La H, Baumgardner M, Le H, Gopaul S, Boggs J, Kuebler P, Davis JC Jr, Liao XC, Lubach JW, Deese A, Sowell CG, Currie KS, Young WB, Khojasteh SC, Hop CE, Wong H (2011) Significant species difference in amide hydrolysis of GDC-0834, a novel potent and selective Bruton's tyrosine kinase inhibitor. Drug Metab Dispos 39:1840–1849

161. Lou Y, Han X, Kuglstatter A, Kondru R, Sweeney Z, Soth M, McIntosh J, Litman R, Suh J, Kocer B, Davis D, Park J, Frauchiger S, Dewdney N, Zecic H, Taygerly J, Sarma K, Hong J, Hill R, Gabriel T, Goldstein D, Owens T (2015) Structure-based drug design of RN486, a potent and selective Bruton's tyrosine kinase (BTK) inhibitor, for the treatment of rheumatoid arthritis. J Med Chem 58:512–516

162. Xu D, Kim Y, Postelnek J, Minh Diem V, Hu D-Q, Liao C, Bradshaw M, Hsu J, Zhang J, Pashine A, Srinivasan D, Woods J, Levin A, O'Mahony A, Owens TD, Lou Y, Hill RJ, Narula S, DeMartino J, Fine JS (2012) RN486, a selective Bruton's tyrosine kinase inhibitor, abrogates immune hypersensitivity responses and arthritis in rodents. J Pharmacol Exp Ther 341:90–103

163. Mina-Osorio P, LaStant J, Keirstead N, Whittard T, Ayala J, Stefanova S, Garrido R, Dimaano N, Hilton H, Giron M, Lau K-Y, Hang J, Postelnek J, Kim Y, Min S, Patel A, Woods J, Ramanujam M, DeMartino J, Narula S, Xu D (2013) Suppression of glomerulone-phritis in lupus-prone NZB x NZW mice by RN486, a selective inhibitor of Bruton's tyrosine kinase. Arthritis Rheum 65:2380–2391

164. Bradshaw JM, McFarland JM, Paavilainen VO, Bisconte A, Tam D, Phan VT, Romanov S, Finkle D, Shu J, Patel V, Ton T, Li X, Loughhead DG, Nunn PA, Karr DE, Gerritsen ME, Funk JO, Owens TD, Verner E, Brameld KA, Hill RJ, Goldstein DM, Taunton J (2015) Prolonged and tunable residence time using reversible covalent kinase inhibitors. Nat Chem Biol 11:525–531

165. Hill RJ, Smith P, Krishnarajah J, Bradshaw JM, Masjedizadeh M, Bisconte A, Karr D, Owens TD, Brameld K, Funk JO, Goldstein DM, Nunn PA, Gourlay SG (2015) Discovery of PRN1008, a novel, reversible covalent BTK inhibitor in clinical development for rheumatoid arthritis [abstract]. Arthritis Rheumatol 67(suppl 10):1671

166. Li XT, Zuo YY, Tang GH, Wang Y, Zhou YQ, Wang XY, Guo TL, Xia MY, Ding N, Pan ZY (2014) Discovery of a series of 2,5-diaminopyrimidine covalent irreversible inhibitors of Bruton's tyrosine kinase with in vivo antitumor activity. J Med Chem 57:5112–5128

167. Ding N, Li X, Shi Y, Ping L, Wu L, Fu K, Feng L, Zheng X, Song Y, Pan Z, Zhu J (2015) Irreversible dual inhibitory mode: the novel Btk inhibitor PLS-123 demonstrates promising anti-tumor activity in human B-cell lymphoma. Oncotarget 6:15122–15136

168. Wu H, Wang WC, Liu FY, Weisberg EL, Tian B, Chen YF, Li BH, Wang AL, Wang BL, Zhao Z, McMillin DW, Hu C, Li H, Wang JH, Liang YK, Buhrlage SJ, Liang JT, Liu J, Yang G, Brown JR, Treon SP, Mitsiades CS, Griffin JD, Liu QS, Gray NS (2014) Discovery of a potent, covalent BTK inhibitor for B-cell lymphoma. ACS Chem Biol 9:1086–1091

169. Smith CR, Dougan DR, Komandla M, Kanouni T, Knight B, Lawson JD, Sabat M, Taylor ER, Vu P, Wyrick C (2015) Fragment-based discovery of a small molecule inhibitor of Bruton's tyrosine kinase. J Med Chem 58:5437–5444
170. https://clinicaltrials.gov/ct2/show/NCT01765478. Accessed 16 June 2016
171. Tam C, Grigg AP, Opat S, Ku M, Gilbertson M, Anderson MA, Seymour JF, Ritchie DS, Dicorleto C, Dimovski B, Hedrick E, Yang J, Wang L, Luo L, Xue L and Roberts AW (2015) The BTK inhibitor, Bgb-3111, is safe, tolerable, and highly active in patients with relapsed/refractory B-cell malignancies: initial report of a phase 1 first-in-human trial. Blood 126:23

Inhibitors of Vascular Endothelial Growth Factor Receptor

Philip A. Harris

Abstract Angiogenesis-targeting agents, predominantly inhibitors of vascular endothelial growth factor and its receptors, have become a mainstay in oncology practice over the last decade. The approved drugs, which include two antibodies and seven small molecule inhibitors, represent strong validation for the field of anti-angiogenesis in the treatment of cancer. In addition to ongoing clinical studies assessing new indications for these agents, novel inhibitors are undergoing clinical evaluations and combination therapies of anti-angiogenic drugs with other targeted approaches are being investigated. This chapter will review the development of the currently marketed drugs targeting VEGFR, as well as the new inhibitors currently being assessed in the clinic.

Keywords Anti-angiogenesis, Development review, VEGFR inhibitors

Contents

P.A. Harris (✉)
GlaxoSmithKline Inc., Collegeville, PA, USA
e-mail: philip.a.harris@gsk.com

1 Introduction

Angiogenesis-targeting agents have become a mainstay of oncology practice over the last decade. The first agent was bevacizumab (Avastin®), a monoclonal antibody to Vascular Endothelial Growth Factor (VEGF), which was approved initially by the FDA in 2004 for the treatment of colorectal cancer and expanding to include approvals in certain types of lung, kidney, brain, ovarian, and cervical cancers [1]. This was followed in the following decade by small molecule inhibitors of the VEGF-receptor (VEGFR) pathway: sorafanib (Nexavar®), sunitinib (Sutent®), pazopanib (Votrient®), axitinib (Inlyta®) regorafenib (Stivarga®), nintedanib (Ofev®/Vargatef®), and lenvatinib (Lenvima®), and the VEGFR-2 antibody ramucirumab [1]. Taken together these drugs treat multiple oncology indications and represent strong validation for the field of anti-angiogenesis in the treatment of cancer that had begun with the pioneering work of Judah Folkman in 1971 [2]. The approved VEGFR inhibitors are being studied in the clinic for new indications, novel inhibitors are undergoing clinical assessment, and combination therapies of anti-angiogenic drugs with other targeted approaches are being investigated. This chapter will review the history and development of the currently marketed drugs targeting VEGFR, as well as the new inhibitors currently being assessed in the clinic.

2 Mechanism of Action

The growth of solid tumors depends on the supply of nutrients and oxygen from newly formed capillaries sprouting from existing blood vessels, a process known as angiogenesis [2]. Tumors induce angiogenesis by secretion of a number of endogenous proteins, notably VEGF, which binds to one of three transmembrane tyrosine kinase receptors, VEGFR-1,2,3, on nearby endothelial cells [3]. The VEGFRs have an extracellular portion consisting of seven immunoglobulin-like domains, a single transmembrane spanning region and an intracellular portion containing a split tyrosine-kinase domain [4]. In response to ligand binding, the VEGFRs undergo

dimerization as both homo- and hetero-dimers, facilitating the trans autophosphorylation of intracellular tyrosine kinases and subsequent activation of downstream signaling pathways that elicit various angiogenic responses (Fig. 1).

VEGFs produced by cells are 34–46-kDa homodimeric glycoproteins that act as potent mitogens that stimulate the growth of new blood vessels [3]. The mammalian VEGF gene family consists of five groups, VEGF-A, VEGF-B, VEGF-C, VEGF-D, and PLGF (placenta growth factor), along with two structurally related proteins, VEGF-E from parapoxvirus and VEGF-F from snake venom. The VEGFRs have three main subtypes: VEGFR-1 (also known as Flt-1), VEGFR-2 (also known as KDR/Flk-1), and VEGFR-3 (also known as Flt-4). The VEGF ligands have distinctive binding specificities for the three transmembrane tyrosine kinase receptors as shown in Fig. 2 [5]. VEGF-A and VEGF-E bind to VEGFR-2, which is located on the surface of vascular endothelial cells, and is the major mediator of the mitogenic, angiogenic, and permeability enhancing effects of VEGF. VEGF-A, VEGF-B, and PLGF bind to VEGFR-1 expressed on hematopoietic stem cells, macrophages, and monocytes as well as on the vascular endothelium. The function of VEGFR-1 is less well defined, being required for recruitment of hematopoietic
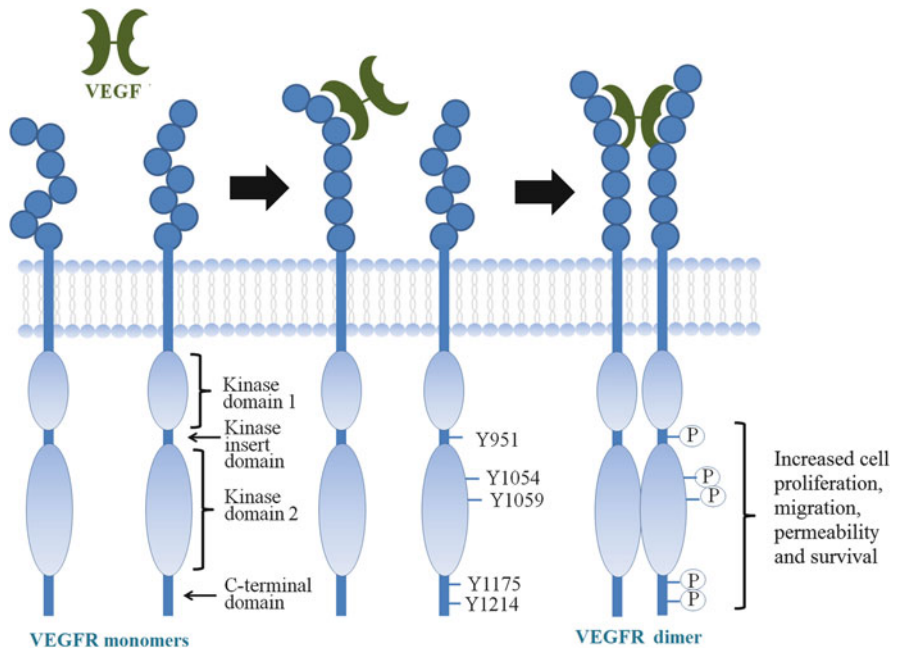
Fig. 1 The binding mode of the ligand VEGF and receptor VEGFR-2 located on endothelial cells. In the first step, VEGF binds to domains 2 and 3 of the 7 immunoglobulin homology domains in the extracellular domain of VEGFR-2 monomer. Binding of VEGF induces the dimerization of VEGFR-2, leading to trans autophosphorylation of tyrosine sites in the intracellular kinase domain region. These provide docking sites for adaptor proteins, which initiate pro-angiogenic signal transduction cascades, resulting in the increased cellular proliferation, migration, permeability, and survival of the endothelial cells
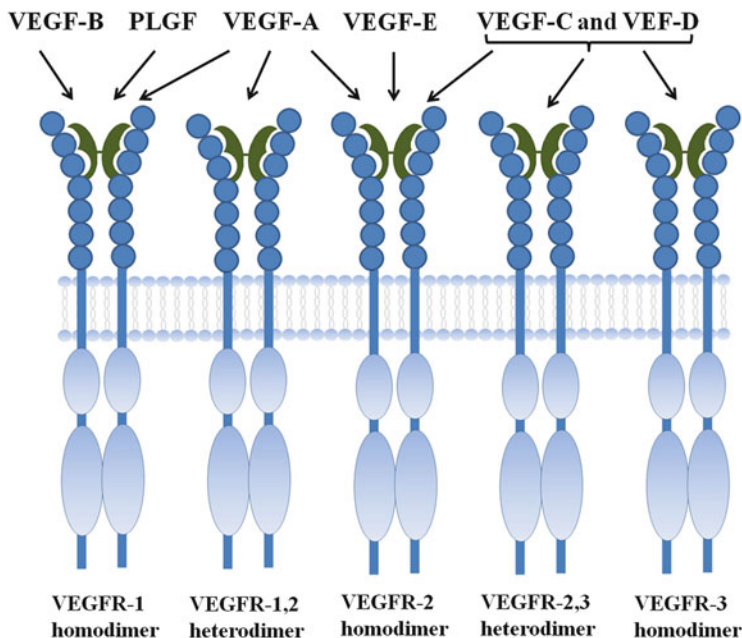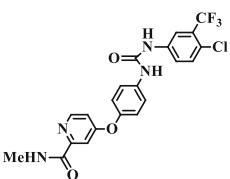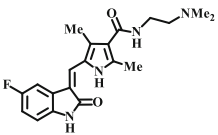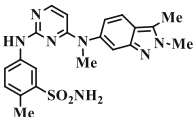
Fig. 2 Activation of the VEGFR homo- and hetero-dimer receptors by VEGF ligands

precursors, but also playing a negative regulatory role in embryonic angiogenesis by acting as a decoy receptor to VEGFR-2. VEGF-C and VEGF-D bind to VEGFR-3, which is largely located at the lymphatic endothelium.

3 First Generation Marketed Anti-Angiogenesis Inhibitors in Oncology

The clinical use of anti-angiogenesis agents in oncology began with the approval of the VEGF monoclonal antibody bevacizumab in 2004 by the FDA for the treatment of colorectal cancer, followed by additional approvals in certain types of lung, kidney, brain, ovarian, and cervical cancers [1]. This first generation of anti-angiogenesis agent was followed in the following 5 years by the small molecule inhibitors of VEGFR, sorafanib, sunitinib, and pazopanib, as shown in Table 1. All three were initially approved for kidney cancer, with sunitinib receiving simultaneous approval for gastrointestinal stromal tumors, and each have subsequently received approval for additional indications; sorafanib for liver and thyroid cancers, sunitinib for pancreatic tumors, and pazopanib for soft tissue sarcomas. It should also be noted that bevacizumab was also initially approved for breast cancer, but

Table 1 First generation marketed VEGFR-2 inhibitors

Drug	Structure	FDA approved indications[a]
Bevacizumab (Avastin®) Genentech/ Roche	Recombinant humanized monoclonal VEGF antibody	Metastatic colorectal cancer (2004) Advanced nonsquamous non-small cell lung cancer (2006) Metastatic renal cell carcinoma (2009) Recurrent glioblastoma (2009) Platinum-resistant ovarian cancer (2014) Advanced cervical cancer (2014)
Sorafenib (Nexavar®) Onyx/Bayer		Advanced renal cell carcinoma (2005) Hepatocellular carcinoma (2007) Radioiodine-refractory advanced thyroid carcinoma (2013)
Sunitinib (Sutent®) Sugen/Pfizer		Renal cell carcinoma (2006) Imatinib-resistant gastrointestinal stromal tumors (2006) Neuroendocrine pancreatic tumors (2011)
Pazopanib (Votrient®) GSK/Novartis		Advanced/metastatic renal cell carcinoma (2009) Soft tissue sarcoma (2012)

[a]Source: www.fda.gov

that approval was withdrawn by the FDA when later studies showed lack of evidence of safety and efficacy for that use [1].

4 Bevacizumab (Avastin®)

As a VEGF antibody, bevacizumab strictly falls outside the scope of this chapter, but its importance as the first approved anti-angiogenesis agent and its widespread clinical use merits a brief description of its discovery and clinical development, to set the stage for the discussion on VEGFR inhibitors. The path to bevacizumab began with the discovery by Ferrara et al. at Genentech in 1989 of the VEGF growth factor isolated from medium conditioned by bovine pituitary follicular cells [6, 7]. By the early 1990s, they were able to demonstrate that a murine anti-human monoclonal antibody (MAb) to VEGF was able to potently suppress angiogenesis and growth in a variety of human tumor cells lines transplanted in nude mice, with no direct effect on tumor cells. In 1997 the same group reported that a recombinant humanized anti-VEGF MAb was able to inhibit VEGF-induced

proliferation of endothelial cells in vitro and tumor growth in vivo with potency and efficacy very similar to those of murine VEGF. This humanized anti-VEGF monoclonal antibody binds selectively to VEGF-A isoforms, with a $K_d \sim 0.5$ nM, but does not neutralize the other members of the VEGF gene family. The human portion (accounting for 93%) contains the antibody framework and the murine portion (accounting for 7%) contains the regions that bind VEGF-A with high affinity.

Phase I clinical trials were initiated in 1997 in patients at dose levels from 0.1 to 10 mg/kg [8]. Bevacizumab showed a linear pharmacokinetic profile administered intravenously over 90 min on days 0, 28, 35, and 42 and a terminal half life of 21 days. One patient with renal cell cancer (RCC) achieved a minor response and nearly half (48%) of the remaining patients achieved disease stabilization. A phase Ib trial then assessed bevacizumab at 3 mg/kg weekly for 8 weeks in combination with a number of standard cytotoxics [9]. This showed that the antibody was relatively non-toxic and when combined with chemotherapy did not significantly exacerbate the toxicological profile. Subsequently five parallel phase II trials were initiated, three of bevacizumab alone in prostate, metastatic breast, and RCC, and two in combination with standard therapy in non-small cell lung cancer (NSCLC) and metastatic colorectal (mCRC) cancers [7]. The most encouraging results were observed when used in patients with RCC, NSCLC, and mCRC cancers [10]. In renal cancer, patients received bevacizumab 3 mg/kg or 10 mg/kg or placebo administered every 2 weeks. The percentage of patients being progression-free was 64% in the high dose group, compared to 34% and 20% in the low dose and placebo groups, respectively. Toxicity included increased blood pressure and asymptomatic proteinuria. In the NSCLC phase II trial, patients received carboplatin and paclitaxel, plus or minus bevacizumab, at 7.5 or 15 mg/kg every 3 weeks. The trial indicated no significant increase in toxicity for bevacizumab compared to chemotherapy alone, and the 15 mg/kg dose showed an increase in time to progression (7.4 versus 4.2 months) and a modest increase in survival (17.7 versus 14.9 months). In the first phase II trial in mCRC, patients received 5-fluorouracil/leucovorin plus bevacizumab (5 or 10 mg/kg) or placebo, every 2 weeks. Interestingly, the objective response rate was superior for the lower bevacizumab dose (40%), compared to the higher dose (24%), or placebo (17%). A second phase II trial in CRC then commenced dosing bevacizumab 10 mg/kg infusion every 2 weeks in combination with 5-fluorouracil/leucovorin/irinotecan (IFL). Overall the complete response rate, partial response rate, and stabilization rate were 5.4%, 38%, and 36% respectively, giving an overall disease control rate of 79% [10].

In phase III trials, in patients with mCRC, a median overall survival (OS) increase of 20.3 months was demonstrated with bevacizumab plus IFL, compared to 15.6 months with IFL alone [11]. In NSCLC, an OS of 12.3 months was observed with paclitaxel/carboplatin (PC) plus bevacizumab, compared to 10.3 months with PC alone [12]. In renal cancer, bevacizumab plus interferon alfa (IFN-α) improved median progression-free survival (PFS) by 89%: 10.2 months with bevacizumab plus IFN-α, compared to 5.4 months with IFN-α alone [13]. Median OS with bevacizumab

plus IFN-α was 23 months, a non-significant increase compared to 21 months with IFN-α. In cervical cancer, OS increased to 16.8 months with bevacizumab plus chemotherapy, compared to 12.9 months with chemotherapy alone [14]. In platinum-resistant ovarian cancer, median PFS increased to 6.8 months with bevacizumab plus chemotherapy, compared to 3.4 months with chemotherapy alone [15]. In glioblastoma, bevacizumab showed an improvement in the objective response rate of 26% with a median duration response of 4.2 months compared to placebo; there are no data demonstrating an improvement in disease-related symptoms or increased survival [16]. A recently completed phase III trial in patients with malignant pleural mesothelioma, a rare cancer often diagnosed in people who have been exposed to asbestos, showed that adding bevacizumab to the standard treatment, pemetrexed and cisplatin, resulted in longer survival with acceptable toxicity [17].

5   Sorafenib (Nexavar®)

Sorafenib (**5**) is a tyrosine kinase inhibitor which was initially codeveloped by Bayer and Onyx as an inhibitor of c-RAF in the proliferative RAF/MEK/ERK MAP kinase pathway, but ultimately reached clinical success targeting VEGFR and platelet-derived growth factor receptor (PDGFRβ) [18]. It was the first small molecule approved by the FDA for the treatment of renal cell carcinoma in 2005, with a subsequent approval 2 years later for hepatocellular carcinoma (HCC), the most common form of liver cancer [1]. Clinical trials of sorafenib against melanoma, based primarily on its inhibition of the RAF kinase pathway, were unsuccessful [19].

The initial hit discovery took place in 1995 starting from the phenyl-urea thiophene ester **1** which was identified from a high-throughput screen against the c-RAF/MEK/ERK kinase cascade (see Fig. 3) [18]. The medicinal chemistry was optimization based around improving the c-RAF activity. This hit had moderate activity against c-RAF (IC$_{50}$ 17 μM) and a tenfold improvement was observed by 4-methyl substitution on the phenyl ring yielding **2**. A library of bis-aryl urea analogs of the lead compound was then constructed to further explore the structure–activity relationship (SAR) of the series which identified the 3-amino-isoxazole **3** with c-RAF kinase inhibition IC$_{50}$ of 1.1 μM. A fivefold increase in c-RAF activity was achieved by replacing its distal ring with a 4-pyridine **4**, which also decreased lipophilicity, improved the aqueous solubility, and imparted significant inhibitory activity against human colon carcinoma HCT116 cell proliferation. Compound **4** possessed oral bioavailability and inhibited the growth of HCT116 xenografts in vivo, thereby providing proof of principle for this new kinase inhibitor class. Further SAR studies were then undertaken including evaluation of aromatic replacements of the isoxazole moiety, which identified the para-choro-meta-trifuroromethylphenyl ring as optimal for potency. Incorporation of a carboxamide functionality adjacent to the pyridyl ring further increased potency, with small groups such as methyl showing the best activity. These modifications led to the

Kinase	IC$_{50}$ μM
VEGFR2	0.090
PDGFRβ	0.057
RET	0.006
c-RAF	0.006
b-RAF	0.025
b-RAF^{V600E}	0.038
Flt-3	0.033
p38	0.038
c-Kit	0.068
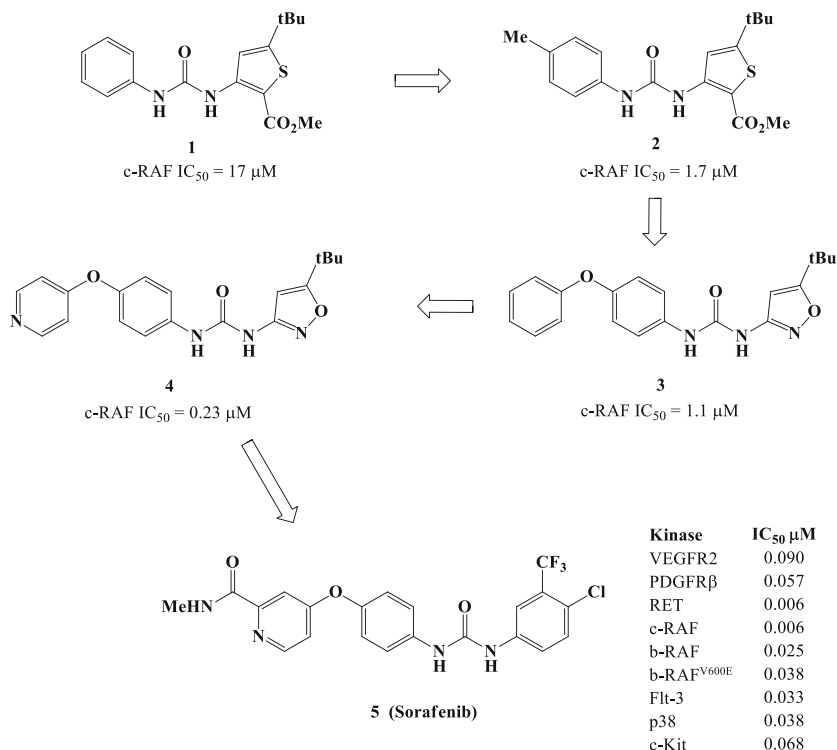
Fig. 3 Key steps leading to the discovery of sorafenib (**5**)

identification of sorafenib (**5**) with c-RAF kinase inhibition IC$_{50}$ of 0.006 μM. Further profiling revealed that sofarenib potently inhibits b-RAF, as well as VEGFR-2 (IC$_{50}$ = 0.09 μM), PDGFRβ (IC$_{50}$ = 0.057 μM), RET kinase (IC$_{50}$ = 0.006 μM), and a number of other kinases.

   Crystallography detailing the structure of various VEGFR-2 and inhibitor complexes has allowed for a detailed understanding of their binding modes and contributed greatly to drug design. Initial attempts to crystallize the catalytic kinase domain of VEGFR-2 containing the highly charged kinase-insert domain (KID) (see Fig. 1) failed to produce crystals after exhaustive screening. Crystallization was achieved using a construct in which the central 50 residues of the KID were deleted, leaving a loop of 20 residues to mimic the length of the analogous loop in the structure of FGFR-1 kinase. This truncated phosphorylated construct crystallized much more readily, producing a structure of the apo catalytic domain [20]. This construct was then used to obtain co-crystal structures of unphosphorylated kinase complexed with inhibitors. In the co-crystal structure of sorafenib bound to VEGFR-2, the nitrogen of the 4-pyridyl group of sorafenib accepts a hydrogen bond from the backbone NH of Cys919 in the hinge, whereas the methylamide NH donates a hydrogen bond to the carbonyl of Cys919, as shown in Fig. 4 [21]. It is interesting to note that the pyridyl moiety was introduced late in the lead optimization stage,
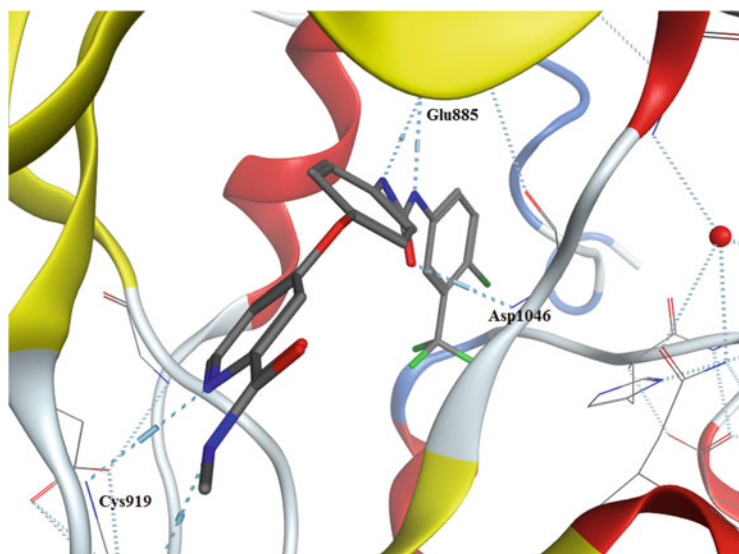
Fig. 4 Sorafenib (**5**) binding in the ATP pocket of VEGFR-2 kinase domain

meaning that the initial hit and early leads (**1–3**) did not possess the hinge binding motif. The inhibitor binds to the DFG-out or type II inactive conformation of the kinase, characterized by an almost 180° rotation of the conserved Asp-Phe-Gly (DFG) motif at the start of the activation loop in the ATP-binding cleft, relative to the active form, and a shift in the αC-helix. This creates a hydrophobic pocket (DFG-out pocket) that is occupied by the aryl-urea portion of sorafenib, with the lipophilic trifluoromethyl group of sorafenib occupying an additional small hydrophobic pocket. The urea group makes a pair of hydrogen bonding interactions, firstly with the backbone of Asp1046 from the DFG on the activation loop, and secondly a bidentate interaction with the acid side chain of Glu885 located in the middle of the αC helix, respectively.

In a phase I clinical trial of sorafenib in patients with advanced refractory solid tumors, the maximum-tolerated dose was 400 mg twice daily, with dose-limiting toxicities of diarrhea, fatigue, and grade 3 skin toxicity observed at higher doses [22]. Of the 45 patients assessed for efficacy, 1 hepatocellular carcinoma patient had a partial response, 25 patients had stable disease, with 8 lasting over 6 months and 5 for over 12 months.

Sorafenib was evaluated in a phase II trial patients with metastatic renal cell carcinoma (mRCC) [23]. The PFS was 24 versus 6 weeks in favor of sorafenib. The high rate of mRCC patients who were progression-free after 12 weeks of dosing led to its approval for this indication by the FDA. In a subsequent phase III study, the OS of patients receiving sorafenib was comparable with that of patients receiving placebo (17.8 versus 15.2 months); however, when crossover placebo survival data were censored, the difference became significant (17.8 versus 14.3 months,

respectively) [24]. These results established the efficacy and safety of sorafenib in advanced mRCC.

In preclinical experiments, sorafenib had anti-proliferative activity in liver-cancer cell lines and it reduced tumor angiogenesis and increased tumor cell apoptosis in a mouse xenograft model of human hepatocellular carcinoma (HCC) [25]. It is known that the RAS/RAF/MEK/ERK pathway plays a role in HCC and that such tumors are highly vascularized and VEGF augments HCC development and metastasis. This provided a good rationale for investigating sorafenib for this indication. In a randomized phase III study the median OS increased from 7.9 months in the placebo group to 10.7 months in the sorafenib group [26]. On the basis of these findings, sorafenib was approved for the treatment of advanced HCC.

Sorafenib increased PFS for patients with radioactive iodine–refractory advanced thyroid cancer in a phase III trial, which supported the approval of sorafenib in this indication in 2013 [27]. Median PFS was 10.8 months in the sorafenib group, versus 5.8 months for placebo. PFS was improved with sorafenib in all clinical and genetic biomarker subgroups, irrespective of mutation status. RET kinase, BRAF V600E mutations, RAS mutations, and increased expression of VEGF and its receptors VEGFR have all been implicated in the pathogenesis and poor outcome of thyroid carcinoma; so it is likely the multi-kinase profile of sorafenib is contributing to its efficacy with this group.

6   Sunitinib (Sutent®)

The development of Sunitinib (**10**) began in 1994 at Sugen with a high-throughput screen of PDGFR kinase, which identified the indolin-2-ones **6** and **7** shown in Fig. 5, with moderate potency against PDGFR and additional potency against VEFGR-2 [28]. Cellular efficacy was observed in VEGF-induced human umbilical vein endothelial cell (v-HUVEC) signaling, compared to that induced by bFGF (b-HUVEC). Expansion of the SAR of this series led to the discovery of **8** (SU5416). SU5416 had no direct cytotoxic effects on tumor cell lines in vitro, but inhibited tumor vascular density and vascular leakage, suggestive of an anti-angiogenesis mechanism for its antitumor activity. In 1997, SU5416 became the first small molecule anti-angiogenic agent to enter the clinic, dosed by IV admin-istration. However, despite evidence of clinical anti-angiogenesis activity, limita-tions in its pharmacokinetics and solubility profile restricted its further development. The addition of the propionic acid functionality attached to the dimethylpyrrole, as represented by **9**, both served to increase the activity against PDGFR and improve the aqueous solubility and orally bioavailability of the series. The combination of both PDGFR and VEGFR activity for **9** translated to increased efficacy in mouse models of tumor xenografts compared to SU5416, and it was evaluated in the clinic as an oral drug in 1999. To further improve the develop-ability profile, additional optimization at the dimethylpyrrole led to the
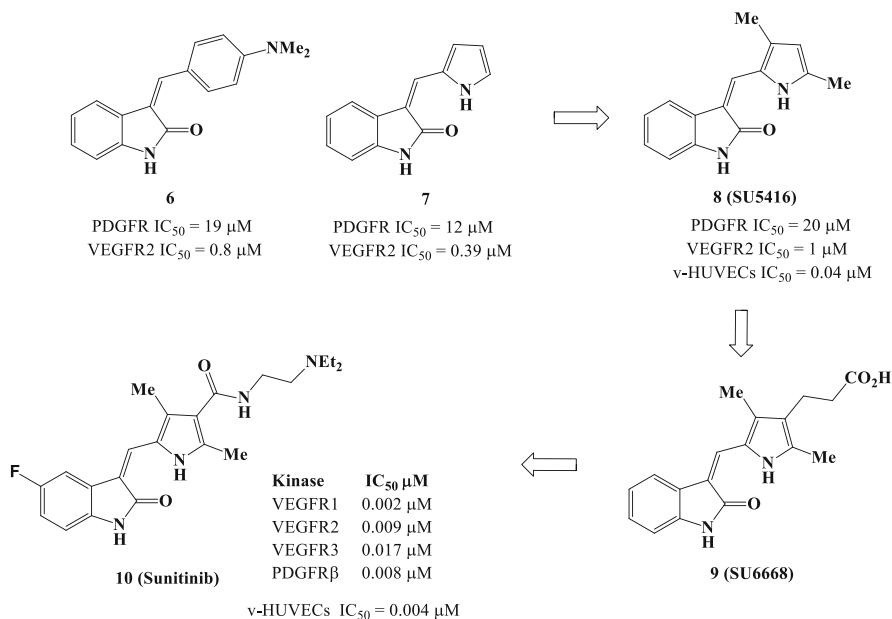
Fig. 5 Key steps leading to the discovery of sunitinib (**10**)

identification of sunitinib (**10**). This contained the optimal profile in terms of potency, solubility, protein binding, pharmacokinetic properties, and antitumor efficacy.

Compared with the binding of the type II inhibitor sorafenib deep into the pocket, sunitinib binds towards the front of the ATP site as shown in Fig. 6, leaving the interior unfilled [21]. The indole NH makes a hydrogen bond donation to the backbone carbonyl of Glu917 at the hinge of the kinase, whereas the carbonyl oxygen of the indole accepts a hydrogen bond from the NH backbone of Cys919. The dimethylamine function attached to the pyrrole ring is orientated out towards the solvent exposed region.

Sunitinib had good potency against VEGFR-1-3 and PDGFRβ (see Fig. 5) as well as the structurally related tyrosine kinases c-Kit, RET, and CSF1R [28]. It inhibited cellular proliferation of v-HUVECs (IC$_{50}$ = 0.004 μM) and serum stimulated endothelial tube formation of human microvascular endothelial cells (IC$_{50}$ = 0.055 μM). Sunitinib demonstrated marked tumor regression in mouse tumor xenograft models (e.g., HT29 colon carcinoma, A431 epidermoid carcinoma) with no direct cytotoxic effects observed against these tumor cell lines in vitro, supportive of the anti-angiogenic mechanism. Evaluation at different doses in these xenograft studies for tumor inhibition/regression, as well as inhibition of PDGFRβ and VEGFR-2 phosphorylation in tumor lysates, demonstrated that a minimal effective plasma concentration of 50 ng/mL was required to achieve full efficacy.
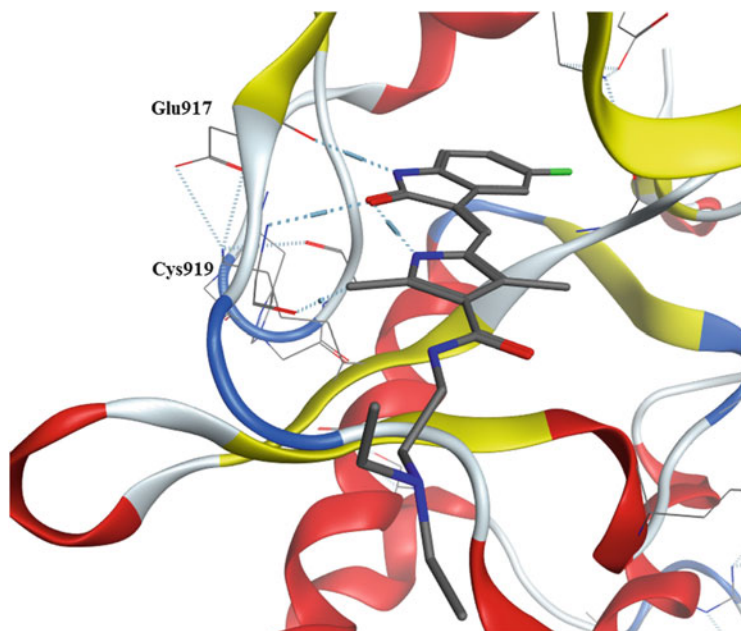
Fig. 6 Sunitinib (**10**) binding in the ATP pocket of VEGFR-2 kinase domain

In the clinical setting, a phase I trial of patients with advanced solid tumors identified 50 mg/day (administered on a 4 weeks on and 2 weeks off schedule) as the recommended dose [29]. This achieved a median peak plasma concentration (C_{max}) at steady state of 100–125 ng/mL (approximately 0.01 μM unbound), achieving adequate target plasma concentration to support further studies. In phase I studies assessing sunitinib as a single agent, from 117 patients there were a total of 16 confirmed objective partial responses, including 4 in metastatic renal cell carcinomas (mRCC), 4 in gastrointestinal stromal tumors (GIST), and 2 in tumors of neuroendocrine origin [30]. The GIST activity can be attributed to the inhibition of c-Kit by sunitinib, since GIST tumors frequently contain activating gene mutations in c-Kit. Sunitinib was shown to inhibit mutated variants of KIT (e.g., T670I, V654A) that are associated with imatinib resistance and tumor progression. Subsequent phase III clinical trials were carried with patients with mRCC, imatinib-refractory GIST, and neuroendocrine tumors. In mRCC patients, the PFS was significantly longer in the sunitinib group compared to interferon alpha therapy (11 versus 5 months) [31]. In patients with advanced GIST who failed on imatinib, the median time to tumor progression was 27.3 weeks with sunitinib, compared to 6.4 weeks for placebo [32]. In patients with pancreatic neuroendocrine tumors, PFS was increased to 11.4 months for sunitinib treatment, as compared with 5.5 months for placebo [33]. This led to the approval of sunitinib indicated for patients with advanced RCC and imatinib-resistant/intolerant GIST cancers in 2006, and subsequently neuroendocrine pancreatic tumors in 2011.

7 Pazopanib (Votrient®)

Pazopanib (**17**) was developed by GlaxoSmithKline and approved by the FDA for the treatment of renal cell carcinoma in 2009, with a subsequent approval 3 years later for soft tissue sarcoma [1]. The initial hit discovery took place in the late 1990s starting from two distinct screening hits: the moderately potent dianilino-2,4-pyrimidine **11** (VEGFR-2 IC_{50} = 0.4 μM), and the more potent 4-anilino-6,7-dimethoxyquinazoline **12** (VEGFR-2 IC_{50} = 0.006 μM), shown in Fig. 7 [34]. Combination of the key structural features of these generated *N*-(3-bromoanilino)-*N'*-(4-methyl-3-hydroxyanilino)-2,4-pyrimidine (**13**) (VEGFR-2 IC_{50} = 0.006 μM), with a cellular potency inhibiting v-HUVEC cells of IC_{50} = 0.54 μM. The pharmacokinetic profile of **13** and similar analogs was poor, presumably due to rapid phase II glucuronidation or sulfation reactions of the phenol functionality. Replacing the phenol with a 3-methylindazole heterocycle yielded the indazolylpyrimidine **14**, which possessed both good potency against VEGFR-2 (IC_{50} = 0.006 μM) and v-HUVECs (IC_{50} = 0.18 μM), combined with significantly improved pharmacokinetics, with a clearance of 16 mL/min/kg and an oral bioavailability of 85% at a dose of 10 mg/kg in the rat.
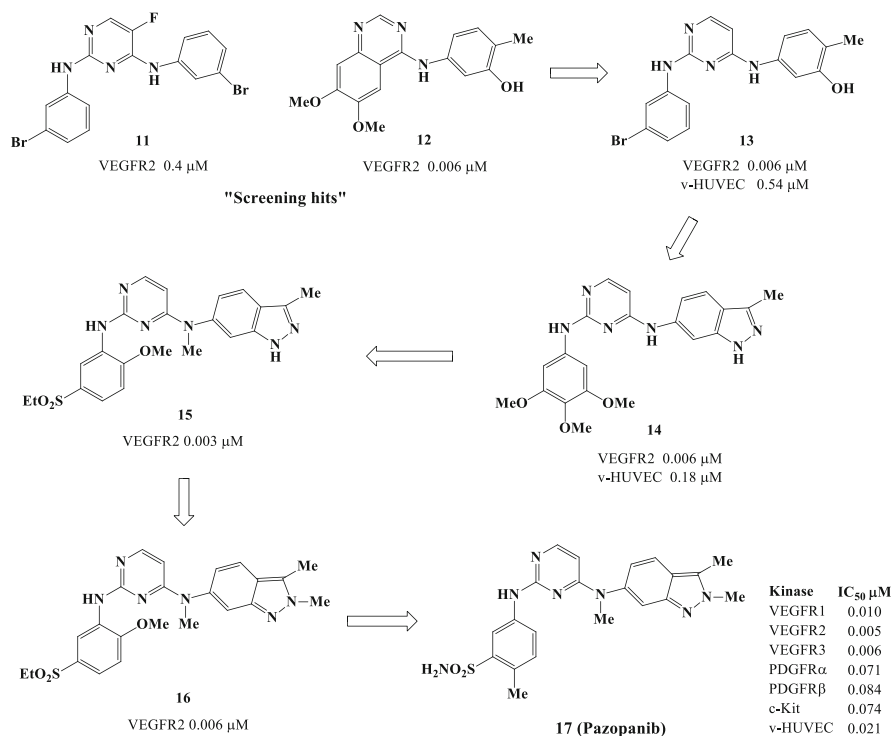
Fig. 7 Key steps leading to the discovery of pazopanib (**17**)

Inhibitor **14** was assessed in an in vivo efficacy study using HT29 human colon tumor xenografts in nude mice, and doses of 30 or 100 mg/kg over 23 days resulted in a 53 and 91% reduction in tumor size, respectively [34]. The *N*-methylated pyrimidine **15** showed an improved pharmacokinetic profile in the rat with lower clearance (10 mL/min/kg) and higher oral bioavailability (65%). At this stage, pyrimidines containing the 3-methylindazole heterocycle and methylated at the C-4 amino nitrogen possessed both good in vitro and cross-species pharmacokinetic profiles. However, significant inhibition ($IC_{50} < 10$ μM) was observed against a number of cytochrome P450 (CYP) isozymes, in particular 2C9. This presumably results from binding of the indazole nitrogens to the heme iron of the CYP enzyme. This activity was diminished by methylation of the indazole 2-nitrogen leading to 2,3-dimethylindazole becoming the preferred heterocycle, as represented by **16**. A final optimization of the aniline ring led to the identification of pazopanib (**17**) with the optimal combination of in vitro potency and pharmacokinetic developability profiles.

Pazopanib is an ATP-competitive inhibitor of VEGFR-2 with a K_i of 24 nM in an in vitro assay. In cellular assays, pazopanib inhibited proliferation of v-HUVECs with an IC_{50} of 0.021 nM, with a 35-fold selectivity over b-HUVEC proliferation [34]. It also inhibited VEGF-induced phosphorylation of VEGFR-2 in HUVEC cells with an IC_{50} of ~8 nM. A greater than 1400-fold selectivity was observed against a variety of tumor cells and greater than 48-fold against fibroblasts as compared with v-HUVEC proliferation. Pazopanib possessed good pharmacokinetics in rat, dog, and monkey with low clearance, low volume of distribution, and good oral bioavailability.

The pazopanib co-crystal structure in VEGFR-2 shows that it binds in the ATP pocket (Fig. 8) [21]. The pyrimidine N-1 and the C-2 anilino N-H make hydrogen acceptor and donor interactions with the peptide backbone of Cys919 at the hinge. The 2,3-dimethylindazole head group pushes into the back pocket of the ATP site, whilst the NH of the sulfonamide makes a hydrogen bond interaction with Lys920.

As a measure of its ability to inhibit angiogenesis in vivo, pazopanib was examined in the mouse matrigel plug assay [35]. In this assay a gel plug of extracellular matrix containing b-FGF is implanted subcutaneously to stimulate vascularization inside the plug. Following once-daily oral administration of pazopanib for 5 days, the plug was removed and angiogenesis, as determination by the hemoglobin content, was inhibited in a dose-dependent manner, at doses from 10 to 100 mg/kg. Pazopanib was also examined in a second animal model of angiogenesis, the mouse corneal micropocket assay, in which ocular angiogenesis is induced by implantation of slow release pellets of VEGF into the mouse cornea. Treatment of mice with 100 mg/kg of pazopanib twice daily for 5 days resulted in significant inhibition in the degree of vascularization. The anti-angiogenic activity of pazopanib was demonstrated in mice bearing established human xenografts using HT29 (colon carcinoma), A375P (melanoma), and HN5 (head and neck carcinoma) tumors, showing a clear dose response following daily doses from 10 to 100 mg/kg over 3 weeks.
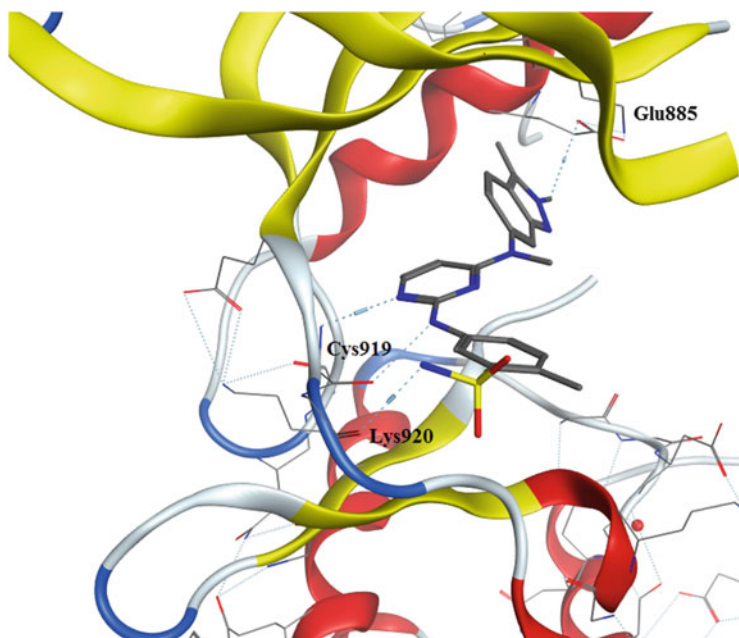
Fig. 8 Pazopanib (**17**) binding in the ATP pocket of VEGFR-2 kinase domain

To establish a pharmocokinetic-pharmodynamic (PK-PD) correlation, the effect of pazopanib on VEGF-induced VEGFR-2 phosphorylation in vivo was evaluated in mouse lungs, which were chosen due to their high endothelial cell content [35]. A single oral dose of 30 mg/kg pazopanib inhibited phosphorylation for more than 8 h, corresponding to >40 µM plasma concentration. At 16 and 24 h, the plasma concentration dropped below 40 µM and the inhibition of VEGFR-2 phosphorylation was minimal, indicating that a ≥ 40 µM steady state concentration of pazopanib is required for optimal in vivo activity.
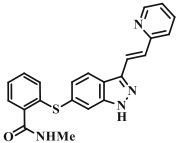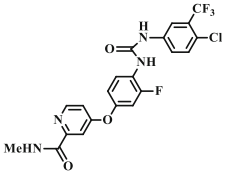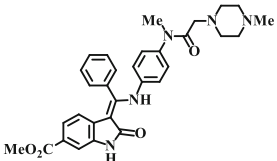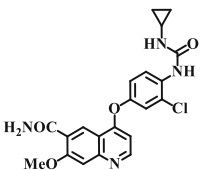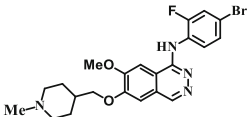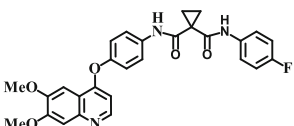
A phase I study evaluating safety and tolerability led to a recommended dose of 800 mg daily [36] with the most common adverse events being nausea, diarrhea, anorexia, hypertension, fatigue, hair depigmentation, and vomiting. A phase II study evaluating patients with advanced renal cell carcinoma (RCC) showed a 35% response to treatment, with stable disease achieved in 45% of patients [37]. Responses were durable with median duration of 68 weeks and an estimated median PFS of 11.9 months. In a phase III trial patients with advanced and/or metastatic RCC, PFS was significantly prolonged with pazopanib compared with placebo in the overall study population (9.2 versus 4.2 months) [38]. In the treatment-naive subpopulation a median PFS of 11.1 versus 2.8 months was observed, compared to the cytokine-pretreated subpopulation median PFS of 7.4 versus 4.2 months. The objective response rate was 30% with pazopanib compared with 3% for placebo, and the median duration of response was longer than 1 year. This led to the approval of pazopanib indicated for patients with RCC in 2009.

A phase II study was conducted in patients with advanced and/or metastatic soft tissue sarcoma (STS) who had relapsed following standard therapies [39]. The progression free rate for patients after 12 weeks was 44% with leiomyosarcoma, 49% with synovial sarcomas, and 39% in other STS types, but no activity observed in adipocytic STS. In a subsequent phase III study, patients were randomly assigned to receive pazopanib or placebo, and the median PFS was 4.6 months for pazopanib compared with 1.6 months for placebo [40]. Overall survival was 12.5 months with pazopanib, versus 10.7 months with placebo. This led to the additional approval of pazopanib for patients with soft tissue sarcomas in 2012.

8 Second Generation Marketed Anti-Angiogenesis Inhibitors in Oncology

With the approval of the VEGF monoclonal antibody bevacizumab in 2004, followed by the three small molecule kinase inhibitors, sorafenib, sunitinib, and pazopanib, and their adoption in clinical practice, the clinical path for subsequent VEGFR inhibitors became more challenging. The next generation of VEGFR inhibitors (Table 2) would need to demonstrate either superior efficacy over these in their respective indications or show efficacy in indications not covered by these approved drugs. For example, axitinib was approved in 2012 after showing extended PFS when compared to sorafenib in patients with advanced kidney cancer, but only as a second line treatment [1]. Regorafenib was approved in the same year for mCRC cancer, the first small molecule VEFGR-2 inhibitor for this indication, and the following year for advanced gastrointestinal stromal tumors, but only for patients resistant to imatinib and sunitinib [1]. Nintedanib is only FDA approved for a non-oncology indication (idiopathic pulmonary fibrosis), but has been approved in Europe in 2015 for combination therapy in NSCLC (retrieved from http://www.ema.europa.eu/ema). Lenvatinib was approved in 2015 for the treatment of radioactive iodine refractory differentiated thyroid cancers, 2 years after the approval for sorafenib for the same indication [1]. Vandetanib and cabozantinib have both been approved for late-stage (metastatic) medullary thyroid cancer [1]. Although both are multi-kinase inhibitors, including VEGFR-2, their mechanism of action is thought to be primarily inhibition of RET kinase, since both hereditary germline and somatic mutations in the RET proto-oncogene are known to cause medullary thyroid carcinomas. From this perspective their development falls out of the scope of this chapter. Ramucirumab is a VEGFR-2 antibody recently approved as second line treatment for advanced gastric cancer, metastatic NSCLC, and metastatic renal cell carcinoma [1].

Table 2 Second generation approved small molecule VEGFR inhibitors

Drug	Structure	FDA approved indications[a]
Axitinib (Inlyta®) Pfizer		Second-line treatment for advanced renal cell carcinoma (2012)
Regorafenib (Stivarga®) Bayer		Metastatic colorectal cancer (2012) Advanced gastrointestinal stromal tumors resistant to imatinib and sunitinib (2013)
Nintedanib (Ofev®/ Vargatef®) Boehriger Ingelheim		Idiopathic pulmonary fibrosis (2014) Combination therapy non-small-cell lung cancer (2015)[b]
Lenvatinib (Lenvima®) Eisai		Radioactive iodine refractory differentiated thyroid cancer (2015)
Vandetanib (Caprelsa®) AstraZeneca		Late-stage (metastatic) medullary thyroid cancer (2011)[c]
Cabozantinib (Cometriq®)		Medullary thyroid cancer (2012)[c]
Ramucirumab (Cyramza®) Eli Lilly/Imclone	Recombinant humanized monoclonal VEGFR-2 antibody	Second-line treatment for advanced gastric cancer (2014) Second-line treatment for metastatic non-small cell lung cancer (2014) Second-line treatment for metastatic renal cell carcinoma (2015)

[a]Source: www.fda.gov
[b]European Union approval
[c]Primary mechanism of action: RET kinase inhibition

9   Axitinib (Inlyta®)

Axitinib (**23**) was developed at Pfizer using a structure-based drug design approach, relying on solved co-crystal structures to guide ligand design, combined with a focus on optimizing binding efficiencies [41]. Screening identified the pyrazole **18** with moderate potency against VEFGR-2, which was selected over other hits for optimization based on superior ligand efficiency (Fig. 9). The initial goals were to improve potency, increase permeability, and remove the metabolic labile aryl hydroxy and methoxy groups. Two strategies were employed, first to truncate the molecule to determine the key features that exhibited high efficiency, and second to introduce conformational constraints to lock the molecule into the preferred bound conformation. Together this led to the identification of indazole **19** which became the core pharmacophore. Adding back the styrene functionality led to the full-length indazole possessing excellent potency and ligand efficiency, but poor kinase selectivity and low oral exposure in mouse. The co-crystal structures of indazole **20** revealed that it binds to the active DFG-in conformation, providing a rationale for the broad kinase activity observed. By contrast, other hits which bound the DFG-out conformation demonstrated a superior kinase selectivity profile, leading the team to design DFG-out features into this indazole series. Attachment of a phenyl thiol functionality at the 6-position of the indazole ring, as represented by **21**, achieved the targeting of the DFG-out conformation, whilst also removing the metabolic aryl hydroxy and methoxy liabilities. Adding back the styrene function-ality gave **22** with significant improved potency. Although **22** is less potent than **20**, it possesses similar overall ligand efficiency and a superior kinase selectivity. Addition of a *N*-methylcarboxamide at the ortho position of the phenyl thiol, adding critical hydrogen-bond interactions in the DFG-out conformation, and replacement of the terminal phenyl with ortho-pyridine, led to axitinib (**23**) with pico-molar potency and lowered lipophilicity.

The solved structure of axitinib bound to VEGFR-2 shown in Fig. 10 provides insight into how the indazole series induced the DFG-out conformation with excellent efficiency [21]. The indazole core makes two hydrogen bond interactions to the hinge, the NH donating to the backbone carbonyl of Glu917 and the nitrogen accepting from the NH backbone of Cys919. The styryl group fills the narrow tunnel as it extends out toward the solvent front. Compared with the other inhibitors, the axitinib phenyl thiol head group is positioned slightly higher and deeper into the back pocket. The carboxamide forms one direct H-bond to the NH backbone of Asp1046 and a second direct H-bond to the carboxylate side chain of Glu885. The head group substantially complements the full length of the channel, contributing to high affinity with both polar charge stabilization and hydrophobic interactions.

Axitinib demonstrated antitumor activity in a range of human tumor models in mice, including colon, lung, breast, pancreas, kidney, brain, melanoma, and hema-topoietic malignancy. In the first study of axitinib in patients with advanced cancer, axitinib dosed 5 mg orally twice daily, showed evidence of clinical activity, with

18

VEGFR2 K_i 5.1 μM
vHUVEC IC$_{50}$ 2.1 μM

19

VEGFR2 K_i 2.3 μM

20

VEGFR2 K_i 0.0003 μM
vHUVEC IC$_{50}$ 0.018 μM

23 (Axitinib)

VEGFR2 K_i 0.000028 μM
vHUVEC IC$_{50}$ 0.0002 μM

22

VEGFR2 K_i 0.017 μM
vHUVEC IC$_{50}$ 0.28 μM

21

VEGFR2 K_i 6.6 μM
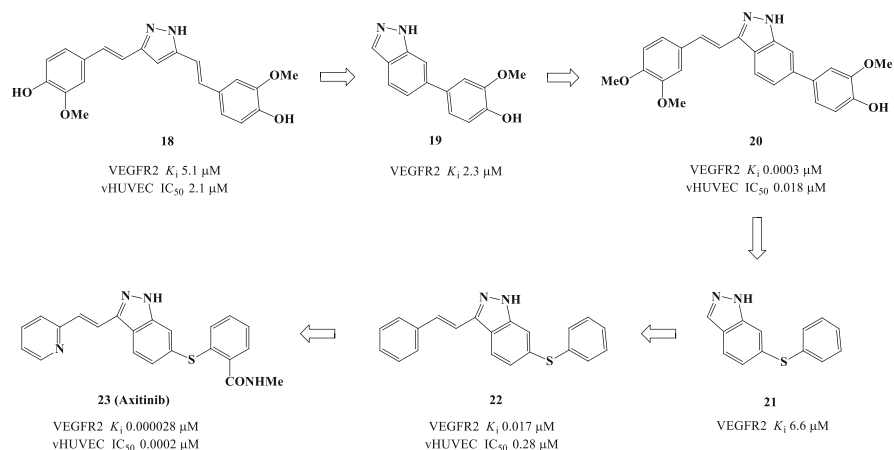
Fig. 9 Key steps leading to the discovery of axitinib (**23**)
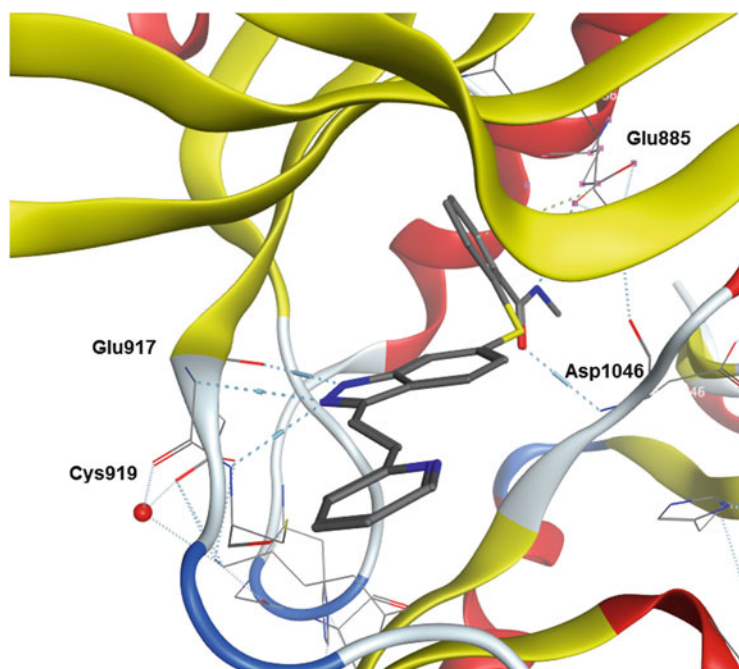
Fig. 10 Axitinib (**23**) binding in the ATP pocket of VEGFR-2 kinase domain

sustained tumor response seen in patients with RCC as well as adenoid cystic cancer [42]. Hypertension, a common side effect in VEGFR-2 targeted therapies, was the most frequently reported adverse effect. A phase II study showed activity in

patients with metastatic renal cell carcinoma (mRCC) refractory to sorafenib (including subgroups refractory to both sunitinib and sorafenib, or to cytokines and sorafenib) [43]. A phase III study of 723 patients with advanced RCC randomized to receive either axitinib or sorafenib as second-line treatment showed a PFS of 8.3 months for axitinib compared to 5.7 months for sorafenib [44]. Overall survival, a secondary endpoint for the study, did not differ between the two groups. Based on this axitinib was approved for the second-line treatment of patients with advanced RCC in 2012.

A phase II clinical trial showed good response in combination chemotherapy with gemcitabine for advanced pancreatic cancer [45]. However a phase III trial comparing axitinib plus gemcitabine with gemcitabine alone for this patient population found no evidence of improvement in the primary endpoint of survival with the combination [46].

Additional phase II studies in patients with refractory thyroid cancer, NSCLC, and metastatic melanoma have been carried out with evidence of efficacy. At the time of writing, trials were recruiting for patients with melanoma and neurofibromatosis type 2, whilst trials for liver cancer, soft tissue sarcomas, and nasopharyngeal carcinomas were active.

10 Regorafenib (Stivarga®)

Regorafenib (24) is a follow-up to sorafenib codeveloped by Bayer and Onyx [47]. It is structurally very similar to sorafenib, differing by only addition of a fluorine atom ortho to the urea at the central phenyl group (Fig. 11). Biochemically this leads to a ~20-fold increase in potency for regorafenib against VEFGR-2 compared to sorafenib.

5 (Sorafenib)

Kinase	IC$_{50}$ μM
VEGFR2	0.090
PDGFRβ	0.057
Flt-3	0.033
p38	0.038
c-Kit	0.068
RET	0.006
C-RAF	0.006
B-RAF	0.025
B-RAF^{V600E}	0.038

24 (Regorafenib)

Kinase	IC$_{50}$ μM
VEGFR1	0.013
VEGFR2	0.004
VEGFR3	0.046
PDGFRβ	0.022
FGFR-1	0.202
c-Kit	0.007
RET	0.015
C-RAF	0.0025
B-RAF	0.028
B-RAF^{V600E}	0.019
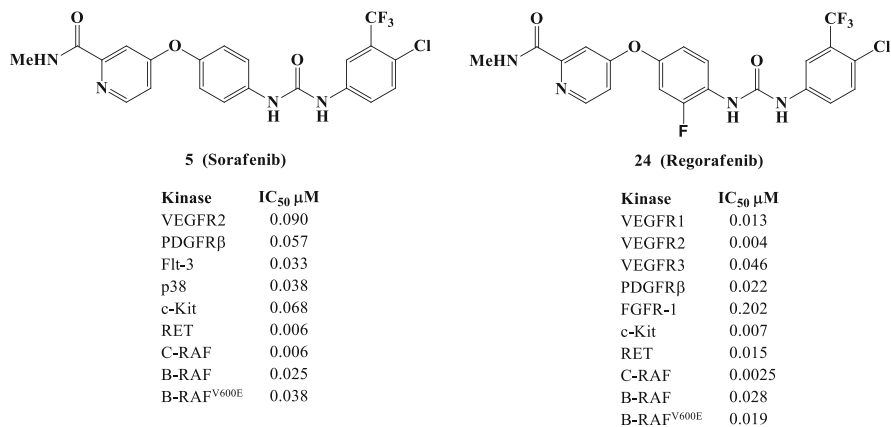
Fig. 11 Comparison of regorafenib (24) with sorafenib (5)

Regorafenib demonstrated inhibition of tumor cell proliferation in various cell lines, with most notable activity in Kit and RET-mutated cell lines, including GIST 882 and thyroid TT cancer cells, with IC_{50} values of 45 and 34 nM, respectively [47]. Dose-dependent antitumor activity has been documented in colorectal (COLO 205), breast (MDA-MB-231), and renal cell (786-0) cancer xenograft models in mice.

Regorafenib was assessed as a single-agent in a phase I study in patients with a variety of tumors who had received multiple prior treatments [48]. Grade 3–4 adverse events did occur with hand-foot skin reaction, hypertension, diarrhea, rash, and fatigue being most frequently noted and the final recommended dose was 160 mg daily for 21 days in a 28-day cycle.

The approval for regorafenib in metastatic colorectal cancer was based on the results of a phase III trial of patients with who had previously received standard chemotherapies, including fluoropyrimidine, oxaliplatin, irinotecan, bevacizumab, and, if they were KRAS exon 2 wild-type, the anti-EGFR therapies panitumumab or cetuximab [49]. Regorafenib improved prolongation in OS in patients from 5 to 6.4 months compared to the placebo group. The trial also demonstrated an improvement in PFS from 1.7 to 2.0 months.

Regorafenib was subsequently approved for patients with advanced GIST that cannot be surgically removed and no longer respond to imatinib and sunitinib. The approval was based on the results of a phase III trial of patients with metastatic or unresectable GIST who experienced disease progression on, or were intolerant to, imatinib and sunitinib [50]. The primary endpoint was PFS, which increased from 0.9 to 4.8 months for patients who received regorafenib compared to placebo. Overall survival was not significantly different between the two groups, although 85% of patients in the placebo group ultimately crossed over to the regorafenib group.

A phase II study evaluating regorafenib in patients with advanced hepatocellular carcinoma who had progressed on sorafenib therapy demonstrated efficacy and a manageable safety profile [51]. A follow-up phase III trial was ongoing at the time of writing, and its results will determine if regorafenib can be approved for this type of liver cancer.

11 Nintedanib (Ofev®/Vargatef®)

Nintedanib (**27**) was developed starting from cross-screening of compounds prepared for a CDK4 program at Boehriger Ingelheim, which identified the 6-amido-substituted indolinone **25** (Fig. 12) as a sub-micromolar inhibitor of VEGFR-2 [52]. Interestingly, **25** itself had no CDK4 activity and showed a favorable kinase selectivity profile. Replacing the central aryl group with smaller alkyl substituents was detrimental to the chemical stability, probably because the phenyl group adopts a strain-free conformation perpendicular to the rest of the molecule (as shown Fig. 13 for the nintedanib co-crystal structure in VEGFR-2). The central aryl
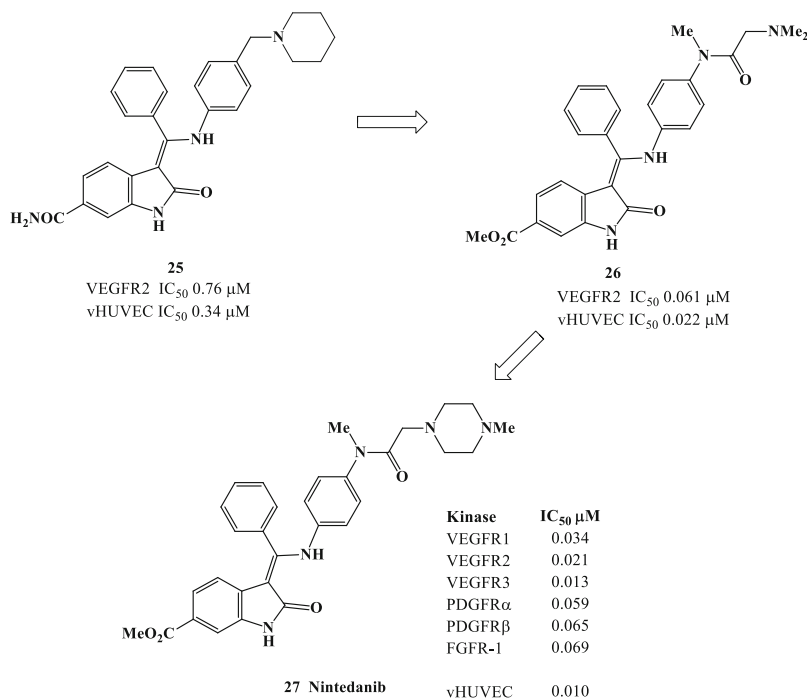
Fig. 12 Key steps leading to the discovery of nintedanib (**27**)

group also improved aqueous solubility, likely because it disrupts the overall flat shape and reduces aromatic-aromatic stacking in the crystalline state. Substitution at the 6-position of the oxindole core had a significant impact on potency and the overall kinase selectivity profile. 6-Chloro-substitution was favorable, but led to poorer selectivity profiles. The 6-methyl ester substituted oxindoles, such as **26**, gave good potency and kinase selectivity and surprisingly demonstrated acceptable oral exposures in rodents. At the other end of the molecule, the basic amine functionality substituted para to the anilino moiety gave a flat SAR profile since it is orientated towards the solvent front of the kinase pocket, but it was a useful handle to fine-tune cell selectivity and solubility. After evaluation in xenograft experiments, nintedanib (**27**) was chosen to progress into preclinical development in 2001.

Nintedanib binds to the ATP-binding site in the hinge region with the oxindole forming two hydrogen bonds to the backbone nitrogen of Cys919 and the backbone carbonyl oxygen of Glu917, as shown in Fig. 13 [53]. This oxindole binding mode resembles closely that of sunitinib (see Fig. 6). The methyl piperidine is directed towards the solvent region with the 4-nitrogen atom forming a bidentate ionic interaction with the carboxylate oxygens of Glu850. The carbonyl of the methyl ester at the 6-position of the oxindole forms a hydrogen bond with Lys868.
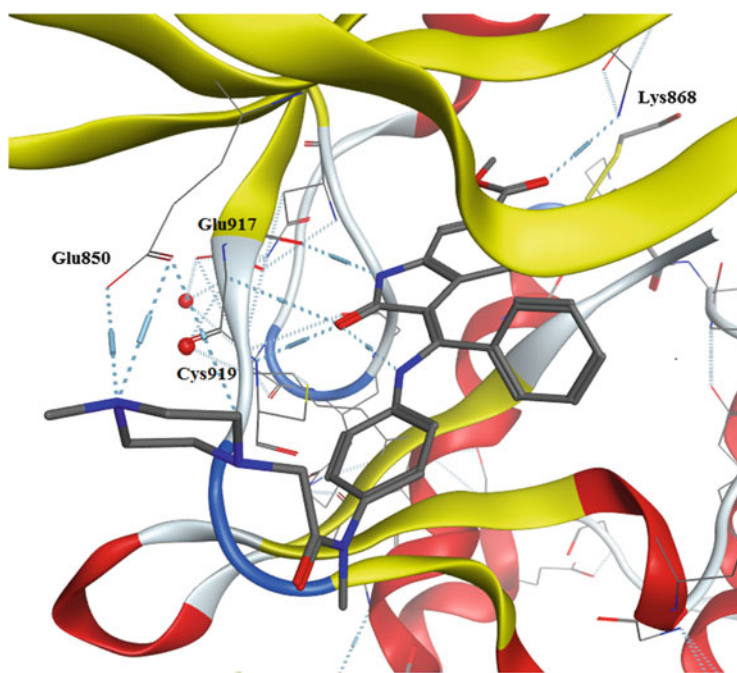
Fig. 13 Nintedanib (**27**) binding in the ATP pocket of VEGFR-2 kinase domain

Nintedanib gave significant plasma levels after oral administration in various species but is rapidly cleared from plasma by ester hydrolysis at later points in time [53]. Part of the in vivo efficacy may be attributed to a sustained duration of VEGFR-2 inhibition, lasting up to 32 h after compound exposure. The mechanistic reason for this prolonged inhibition is not yet understood. It is possible that such prolonged receptor blockade in combination with a fast clearance in vivo may lead to efficacy combined with a clean safety profile. Nintedanib demonstrated significant antitumor activity in xenograft models such as NSCLC (Calu-6 cells), human renal cell carcinoma (RCC) (Caki-1), colorectal (HT-29), ovarian (SKOV-3), and prostate carcinoma (PAC-120). In H460 cell NSCLC xenografts, nintedanib also demonstrated synergistic effects in combination with the cytotoxic drugs docetaxel or pemetrexed.

A phase I study evaluated nintedanib combined with docetaxel in patients with advanced NSCLC. The maximum tolerated dose of nintedanib was between 150 and 200 mg twice daily in combination with docetaxel [52]. The dose-limiting toxicity was grade 3 hepatic enzyme elevations in both alanine and aspartate aminotransferase, and drug-related adverse events included neutropenia, leukopenia, fatigue, alopecia, and decreased appetite. Among evaluable patients, 26% had a partial response and 47% had stable disease. In a phase III study as second-line therapy in patients with NSCLC, patients received nintedanib 200 mg twice daily plus docetaxel 75 mg/m^2 daily, or docetaxel plus placebo [52]. Nintedanib, when

added to docetaxel, extended OS from 10.3 to 12.6 months for patients with adeno-carcinoma, with 25.7% of patients surviving for 2 years or more with nintedanib plus docetaxel, compared to 19.1% for patients on placebo plus docetaxel. Nintedanib demonstrated a manageable adverse event profile and did not significantly increase discontinuation rates compared to docetaxel alone. Based on this study the EU granted approval for nintedanib for use as second-line therapy in combination with docetaxel in patients with NSCLC of adenocarcinoma tumor histology in 2015.

At the time of writing, Nintedanib is being investigated in a phase III study in patients with ovarian cancer and in phase II studies for mesothelioma and kidney cancers. It has recently completed phase III studies in advanced NSCLC and phase II trials in refractory colorectal and liver cancers.

12 Lenvatinib (Lenvima®)

Developed by Eisai, lenvatinib (**28**) potently inhibits VEGFR-1,2,3, FGFR-1, and RET tyrosine kinases and has recently been approved for patients with radioiodine-refractory differentiated thyroid cancers [54]. The efficacy against thyroid cancers is likely based on a combination of both VEGFR anti-angiogenic and RET antitumorigenic pathway inhibition. Lenvatinib inhibits RET kinase and VEGFR-2 kinase with K_i values of 1.5 and 0.74 nM, respectively (Fig. 14). Lenvatinib inhibited proliferation and phosphorylation of RET as well that of downstream ERK1/2 in medullary thyroid carcinoma cell lines, which expressed RET kinase in a dose-dependent manner. Significant antitumor activity was observed in mouse xenografts from these cell lines at doses of 10–100 mg/kg without affecting

Fig. 14 Kinase profile of lenvatinib (**28**)

28 (Lenvatinib)
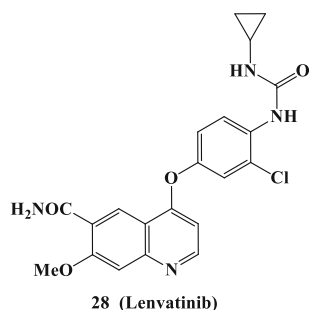
Kinase	$IC_{50}\,\mu M$	Kinase	$K_i\,\mu M$
VEGFR1	0.022	VEGFR2	0.00074
VEGFR2	0.004	RET	0.0014
VEGFR3	0.005		
PDGFRα	0.051		
PDGFRβ	0.039		
c-Kit	0.100		
FGFR1	0.046		

microvessel density, suggesting that activity was caused primarily by RET kinase inhibition. However, lenvatinib did also significantly inhibit in vivo growth of SW579 tumors in nude mice, a cell line which does not express RET kinase, accompanied by decreased microvessel density within the tumors, indicative of anti-angiogenic activity.

A co-crystal structure revealed that the quinoline nitrogen of lenvatinib accepts a hydrogen bond from the hinge Cys919 as shown in Fig. 15 [55]. As observed with sorafenib, the urea makes two hydrogen bonding interactions, first with the backbone of Asp1046 from the DFG on the activation loop and second a bidentate interaction with the acid side chain of Glu885 located in the middle of the αC-helix. Interestingly, lenvatinib, in contrast to sorafenib, binds to the active DFG-in conformation. This is likely due to the much smaller cyclopropane urea substituent of lenvatinib located in the back of the pocket, compared to the 4-chloro-3-(trifluoromethyl) phenyl group of sorafenib. The polar carboxamide substituent at the 6-position of the quinoline ring is located towards the solvent front and forms a number of water mediated hydrogen bond interactions to Asn923.

A phase I study of lenvatinib in Japanese patients with advanced solid tumors established an optimal daily dose of 24 mg [56]. In a phase II trial of lenvatinib in advanced radioiodine-refractory differentiated thyroid cancer (RR-DTC), patients who received lenvatinib 24 mg daily in 28-day cycles until disease progression had an objective response rate (ORR) of 50%, with only partial responses reported. The
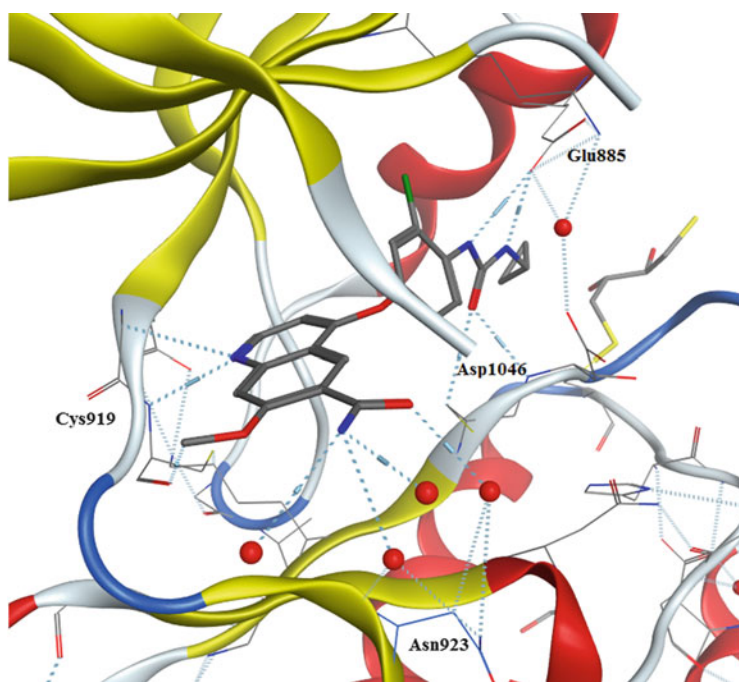
Fig. 15 Lenvatinib (**28**) binding in the ATP pocket of VEGFR-2 kinase domain

median time to response was 3.6 months, the median response duration was 12.7 months, and the median PFS was 12.6 months. The ORR for patients who had received previous VEGF therapy was 59%. Adverse events, regardless of their relation to treatment, occurred in 72% of patients and most frequently included weight loss, hypertension, proteinuria, and diarrhea.

In a randomized phase III study involving patients with RR-DTC given the same dose, lenvatinib treated subjects lived a median of 18.3 months without their disease progressing, compared to 3.6 months for subjects who received placebo [57]. Additionally, 65% of subjects treated with lenvatinib saw a reduction in tumor size, compared to 2% of subjects who received a placebo. The median OS was not reached in either group. Treatment-related adverse effects of all grades occurred in more than 40% of patients in the lenvatinib group, including hypertension, diarrhea, fatigue, decreased appetite and weight, and nausea. In the lenvatinib group, 6 of 20 deaths that occurred during the treatment period were considered to be drug-related. Based on this, lenvatinib was approved for patients with RR-DTC in 2015.

At the time of writing, Lenvatinib was also under phase III clinical investigation for hepatocellular carcinoma and phase II studies for NSCLC, biliary tract, and RCC cancers. Two phase II studies for melanoma and endometrial cancers have completed.

13 Third Generation Anti-Angiogenesis Inhibitors in Oncology Under Development

The third generation of VEGFR inhibitors under clinical development faces a prohibitively crowded field with multiple anti-angiogenesis drugs now approved and indicated for a wide range of tumor types. The clinical trials for these investigational drugs aimed at demonstrating superior efficacy over the approved VEGFR drugs have largely failed. Their focus would now appear to be on exploring new indications for VEGFR inhibitors, such as ovarian, gastric, and mesothelioma cancers, as well as NSCLC cancers driven by specific gene amplifications (Table 3).

14 Cediranib

Cediranib (**29**) is a potent inhibitor against VEGFR-1-3, c-Kit, and PDGFR kinases which is currently under investigation by AstraZeneca for ovarian cancer (Fig. 16) [58].

Cediranib had been investigated by AstraZeneca in a number of advanced clinical trials, but the company had abandoned its development in 2011 after these trials were not successful [59]. For example, in a phase III trial for patients with mCRC cancer who had progressed following first-line therapy, addition of

Table 3 Clinical activity of small molecule VEGFR inhibitors under development

Drug	Structure	Clinical trials[a]
Cediranib (Recentin) AstraZenneca		Ovarian, fallopian tube, peritoneal cancer, or recurrent triple-negative breast cancer Alveolar soft part sarcoma Malignant pleural mesothelioma
Tivozanib (AV-951) Kirin Brewery/ AVEO		Metastatic or inoperable liver cancer
Dovitinib (TKI258) Novartis		Gastric cancer with FGFR-2 amplification Relapsed glioblastoma
Apatinib (YN968D1) HengRui Medicine/ LSK BioPartners/ Bukwang		Metastatic esophageal cancer RET fusion positive advanced NSCLC Gastric cancer Advanced NSCLC with wild-type EGFR Hepatocellular carcinoma

[a]Source: ClinicalTrials.gov

Fig. 16 Kinase profile of cediranib (**29**)
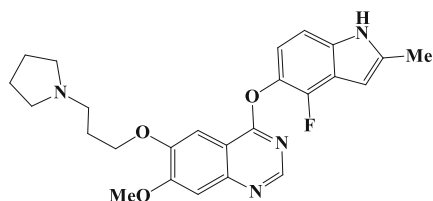
29 (Cediranib)

Kinase	IC$_{50}$ μM
VEGFR1,2,3	0.005, <0.001, 0.003
c-Kit	0.002
PDGFRβ	0.005

cediranib (20 or 30 mg daily) or bevacizumab to the combination chemotherapy oxaliplatin/leucovorin/5-fluorouracil showed no differences in PFS [60]. A demonstration of improvement over bevacizumab was required to move forward with registration. In a phase III trial comparing cediranib with carboplatin/paclitaxel

chemotherapy in NSCLC patients, cediranib (20 mg daily) did increase the response rates (52% versus 34%), albeit with an increase in toxicity (grade 3 hypertension, diarrhea, and anorexia), but showed no increase in either PFS or OS [60]. In a phase II trial with first line treatment-naive renal cell carcinoma patients, cediranib demonstrated comparable anti-tumor activity, but no benefit over the approved VEGFR inhibitors sunitinib and pazopanib. In a phase III trial comparing cediranib with the alkylating agent lomustine for patients with recurrent glioblastoma, there was no significant difference in PFS or OS for either cediranib alone (30 mg daily) or cediranib/lomustine (20 mg daily) compared with lomustine alone [60].

However, recent investigator-initiated studies in gynecological cancers have revived interest in cediranib. In a trial sponsored by Cancer Research UK, cediranib combined with platinum-based chemotherapy improved PFS and OS in patients with relapsed ovarian cancer [59]. It was reported that cediranib (20 mg daily) had extended PFS by 3.2 months and OS by 2.7 months in combination with chemotherapy and in maintenance treatment, compared with chemotherapy alone. This is the first VEGFR inhibitor to demonstrate an OS benefit in recurrent ovarian cancer.

Investigators at the National Cancer Institute reported phase II results showing that cediranib combined with olaparib nearly doubled PFS in women with platinum-sensitive recurrent ovarian cancer or ovarian cancer associated with BRCA mutations [59]. Women taking the drug combination had PFS lasting 17.7 months, compared with 9 months among those given olaparib alone. However, these findings were tempered by grade 3 and 4 toxicities being higher with the drug combination, with reports of fatigue, diarrhea, and hypertension, in addition to more serious side effects, including myelodysplastic syndrome, weight loss, and one case of vaginal fistula.

AstraZeneca is now reportedly looking to move forward for regulatory approval for cediranib specifically in ovarian cancer [59]. Patients whose tumors are sensitive to platinum-based chemotherapy may offer an opportunity for cediranib, especially since bevacizumab's approval is limited to platinum-resistant patients. At the time of writing, additional investigator-initiated trials were also underway in sarcoma and mesothelioma (Table 3).

15 Tivozanib

Tivozanib (30) is a very potent VEGFR inhibitor that is being codeveloped by Kirin Brewery and AVEO Pharmaceuticals with sub-nanomolar IC_{50} values against all three isoforms, as shown in Fig. 17 [61]. The drug has a very long half-life of more than 4 days (112 h) in humans. The exceptional potency and long half-life led to low doses of 1, 1.5, and 2 mg/day being explored for clinical use. Based on these studies, a maximum tolerated dose of 1.5 mg/day, 4 weeks on and 2 weeks off, was determined. At this dose, the adverse events observed were similar to other oral VEGFR inhibitors including hypertension, dysphonia, diarrhea, and abnormal liver functions.
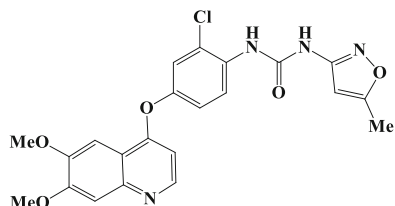
30 (Tivozanib)

Kinase	IC_{50} μM
VEGFR1,2,3	0.00021, 0.00016, 0.00024
c-Kit	0.00163
PDGFRβ	0.00172

A phase III trial compared tivozanib with sorafenib in patients with metastatic renal cell carcinoma (mRCC) who were either untreated or had received cytokines [62]. The study met its primary end point of improving PFS for tivozanib compared to sorafenib (11.9 versus 9.1 months), but showed a lowered OS (28.8 versus 29.3 months). Crossover of patients from sorafenib to tivozanib may have confounded the survival comparison. Because of the survival findings, the FDA rejected approval in May 2013 and requested additional clinical studies, casting uncertainty over its future development for mRCC.

A phase II trial in patients with stage IV mCRC cancer compared addition of tivozanib or bevacizumab to the combination chemotherapy oxaliplatin/leucovorin/5-fluorouracil [62]. An interim analysis showed comparable efficacy, but without the necessary demonstration of superiority over bevacizumab the trial was discontinued. However, one of the potential biomarkers explored in this study was neuropilin-1 (NRP-1), a signaling protein known to bind to VEGF-A in serum. NRP-1 was found to be a potential prognostic marker for angiogenesis inhibitor activity and could be predictive of tivozanib activity relative to bevacizumab [63]. One current proposal for further development of tivozanib is a subsequent trial targeting mCRC patients with low baseline expression of NRP-1. At the time of writing, an additional investigator-initiated trial was also currently underway in liver cancers (Table 3).

16 Dovitinib

Developed by Novartis, dovitinib (**31**) is a potent inhibitor against the VEGFR and FGFR isoforms, plus PDGFR (Fig. 18) [64]. The potent activity against FGFR in combination with VEGFR was the main rationale to evaluate dovitinib in patients who had relapsed with one of the more VEGFR selective first-generation VEGFR inhibitors.

Fig. 18 Kinase profile of dovitinib (**31**)
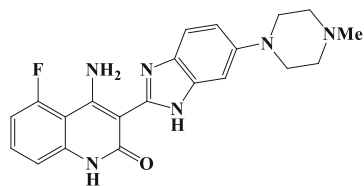
31 (Dovitinib)

Kinase	IC$_{50}$ μM
VEGFR1-3	0.008–0.013
PDGFRβ	0.012
FGFR1	0.008
FGFR2	0.040
FGFR3	0.009

In phase I studies, dovitinib showed accumulation at doses over 400 mg/day; thus a well-tolerated intermittent dosing schedule of 500 mg on a 5 days on, 2 days off schedule was adopted [64]. Antitumor activity was observed in pretreated patients with metastatic RCC. Two patients (13%) achieved a partial response, and the PFS and OS were 8.1 and 13.3 months, respectively. Pharmacodynamic analysis of plasma biomarkers and tumor biopsies showed both VEGFR inhibition (via increased PLGF levels and decreased sVEGFR-2 levels) and FGFR inhibition (via induction of FGF23, a biomarker of FGFR-1 inhibition), thus demonstrating clinical inhibition of both pathways. However, a phase III trial comparing dovitinib with sorafenib in patients with metastatic RCC, who had received one prior VEGF/VEGFR-targeted agent and one prior mTOR inhibitor, did not demonstrate superior efficacy [64]. Similar PFS (3.7 and 3.6 months) and OS (11.1 and 11.0 months) values were found for dovitinib and sorafenib, respectively. A phase II trial evaluated the efficacy of dovitinib in patients with metastatic GIST, after the failure of at least imatinib and sunitinib, showed only modest antitumor activity, with one patient (3%) showing a partial response. Dovitinib was being actively studied at the time of writing in patients with gastric cancer and relapsed glioblastoma, as shown in Table 3. More specific patient selection for tumors where FGFR amplification is observed may be the key to observe superior efficacy compared to the current standard of care treatments with this drug.

17 Apatinib

Apatinib (**32**) is a VEGFR-2 inhibitor being codeveloped by Jiangsu Hengrui Medicine (China), LSK BioPartners (USA), and Bukwang Pharmaceutical Company (Korea) (see Fig. 19) [65]. A phase I study in patients with advanced solid malignancies showed encouraging antitumor activity, with several patients achieving complete or partial responses, and a manageable toxicity profile leading to a maximum tolerated

Fig. 19 Kinase profile of apatinib (**32**)
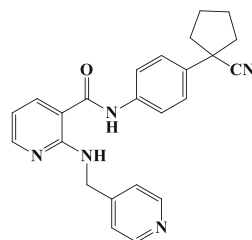
32 (Apatinib)

Kinase	IC$_{50}$ μM
VEGFR2	0.001
Ret	0.013
c-Kit	0.429
PDGFRα	>1
FGFR1	>10

dose of 850 mg daily. A phase II/III study with apatinib (850 mg daily or 425 mg twice daily) was evaluated in patients with metastatic gastric cancer who had failed two lines of chemotherapy [65]. Progression-free survival was increased from 1.4 months for placebo to 3.67 and 3.2 months for single and twice daily dosed apatinib, respectively. The OS times were increased from 2.5 months for placebo to 4.83 and 4.27 months for single and twice daily dosed apatinib, respectively. Apatinib was approved by the Chinese FDA in December 2014 for patients with late-stage gastric cancer.

At the time of writing, Apatinib was being studied in patients with esophageal, gastric, and liver cancers. Additional trials are also underway with advanced NSCLC patients with either RET fusion positive or wild-type EGFR tumors (Table 3).

18 Inhibitors No Longer Under Development

Despite the success of the field, a number of VEGFR-2 inhibitors have progressed to late stage clinical trials and have not met their primary endpoints and appear to be discontinued. Motesanib was being developed by Amgen and Takeda. It was evaluated in a phase III trial in combination with paclitaxel and carboplatin chemotherapy for NSCLC, but demonstrated no benefit on OS [66]. No further development of motesanib appears to have taken place.

Brivanib was being developed by Bristol-Myer Squibb (BMS), but recently failed in three randomized controlled phase III trials: a first-line trial in hepatocellular carcinoma (HCC) against sorafenib [67]; a second-line trial in HCC patients who were intolerant or failed with sorafenib [68]; and a combination trial (brivanib plus cetuximab vs cetuximab alone) in patients with metastatic, chemotherapy-refractory, wild-type KRAS colorectal carcinoma [69]. No further development of brivanib has since been reported by BMS.

Linifanib was developed by Abbott and was studied in patients with liver cancer in comparison to sorafenib. Linifanib and sorafenib had similar OS profiles with these patients, but linifanib did not meet predefined superiority and non-inferiority criteria and was discontinued [70].

Vatalanib, developed by Novartis, was studied in two separate phase III trials as combination with fluorouracil, leucovorin, and oxaliplatin for mCRC cancer, but had only a marginal effect on PFS and no detectable effect on OS [71]. No further development of vatalanib is currently reported by Novartis.

19 Conclusions

In a little over a decade following their introduction, the field of VEGF/VEGFR antiangiogenic agents appears to have reached maturity, with two antibodies and seven small molecule inhibitors of VEGFR are now approved for clinical use. The range of cancer indications they currently target includes liver, kidney, lung, ovarian, cervical, thyroid, pancreas, brain, soft tissue sarcoma, gastric, and GIST. New drugs being studied in the clinic appear to focus on lung, ovarian, gastric, and mesothelioma cancers. Novel combination therapies may provide additional opportunities to improve the clinical benefits of anti-angiogenesis drugs. Perhaps the most promising is the combination of antiangiogenic agents with the rapidly emerging field of immunomodulation. For example, multiple active clinical trials with the recently approved PD-1 inhibitors nivolumab (Opdivo®) and pembrolizumab (Keytruda®) with the approved drugs described in this chapter are listed in ClinicalTrials.gov. Identifying the most suitable agents, stand-alone or combination therapies, as well as the optimal dosage and schedules will continue to evolve as these drugs increasingly become standards of care in cancer therapy.

References

1. FDA approved drug products. https://www.accessdata.fda.gov/scripts/cder/drugsatfda/
2. Folkman J (2007) Nat Rev Drug Discov 6:273
3. Holmes K, Roberts OL, Thomas AM, Cross MJ (2007) Cell Signal 19:2003
4. Stuttfeld E, Ballmer-Hofer K (2009) IUBMB Life 61:915
5. Olsson AK, Dimberg A, Kreuger J, Claesson-Welsh L (2006) Nat Rev Mol Cell Biol 7:359
6. Ferrara N (2011) Int J Dev Biol 55:383
7. Ferrara N, Hillan KJ, Gerber H-P, Novotny W (2004) Nat Rev Drug Discov 3:391
8. Gordon MS, Margolin K, Talpaz M, Sledge Jr GW, Holmgren E, Benjamin R, Stalter S, Shak S, Adelman D (2001) J Clin Oncol 19:843
9. Lu JF, Bruno R, Eppler S, Novotny W, Lum B, Gaudreault J (2008) Cancer Chemother Pharmacol 62:779
10. Keating GM (2014) Drugs 74:1891
11. Hurwitz HI, Fehrenbacher L, Hainsworth JD, Heim W, Berlin J, Holmgren E, Hambleton J, Novotny WF, Kabbinavar F (2005) J Clin Oncol 23:3502

12. Sandler A, Gray R, Perry MC, Brahmer J, Schiller JH, Dowlati A, Lilenbaum R, Johnson DH (2006) N Engl J Med 355:2542
13. Escudier B, Bellmunt J, Négrier S, Bajetta E, Melichar B, Bracarda S, Ravaud A, Golding S, Jethwa S, Sneller V (2010) J Clin Oncol 28:2144
14. Tewari KS, Sill MW, Long 3rd HJ, Penson RT, Huang H, Ramondetta LM, Landrum LM, Oaknin A, Reid TJ, Leitao MM, Michael HE, Monk BJ (2014) N Engl J Med 370:734
15. Pujade-Lauraine E, Hilpert F, Weber B, Reuss A, Poveda A, Kristensen G, Sorio R, Vergote I, Witteveen P, Bamias A, Pereira D, Wimberger P, Oaknin A, Mirza MR, Follana P, Bollag D, Ray-Coquard I (2014) J Clin Oncol 32:1302
16. Gilbert MR, Dignam JJ, Armstrong TS, Wefel JS, Blumenthal DT, Vogelbaum MA, Colman H, Chakravarti A, Pugh S, Won M, Jeraj R, Brown PD, Jaeckle KA, Schiff D, Stieber VW, Brachman DG, Werner-Wasik M, Tremont-Lukats IW, Sulman EP, Aldape KD, Curran Jr WJ, Mehta MP (2014) N Engl J Med 370:699
17. Zalcman G, Mazières J, Margery J, Greillier L, Audigier-Valette C, Moro-Sibilot D, Molinier O, Corre R, Monnet I, Gounant V, Janicot H, Gervais R, Locher C, Milleron B, Tran Q, Lebitasy MP, Morin F, Creveuil C, Parienti J-J, Scherpereel A (2015) J Clin Oncol 33 (Suppl); abstr 7500
18. Wilhelm S, Carter C, Lynch M, Lowinger T, Dumas J, Smith RA, Schwartz B, Simantov R, Kelley S (2006) Nat Rev Drug Discov 5:835
19. Mangana J, Levesque MP, Karpova MB, Dummer R (2012) Exp Opin Invest Drugs 21:557
20. McTigue MA, Wickersham JA, Pinko C, Showalter RE, Parast CV, Tempczyk-Russell A, Gehring MR, Mroczkowski B, Kan CC, Villafranca JE, Appelt K (1999) Structure 7:319
21. McTigue M, Murray BW, Chen JH, Deng YL, Solowiej J, Kania RS (2012) Proc Natl Acad Sci U S A 109:18281
22. Strumberg D, Richly H, Hilger RA, Schleucher N, Korfee S, Tewes M, Faghih M, Brendel E, Voliotis D, Haase CG, Schwartz B, Awada A, Voigtmann R, Scheulen ME, Seeber S (2005) J Clin Oncol 23:965
23. Ratain MJ, Eisen T, Stadler WM, Flaherty KT, Kaye SB, Rosner GL, Gore M, Desai AA, Patnaik A, Xiong HQ, Rowinsky E, Abbruzzese JL, Xia C, Simantov R, Schwartz B, O'Dwyer PJ (2006) J Clin Oncol 24:2505
24. Escudier B, Eisen T, Stadler WM, Szczylik C, Oudard S, Staehler M, Negrier S, Chevreau C, Desai AA, Rolland F, Demkow T, Hutson TE, Gore M, Anderson S, Hofilena G, Shan M, Pena C, Lathia C, Bukowski RM (2009) J Clin Oncol 27:3312
25. Liu L, Cao Y, Chen C, Zhang X, McNabola A, Wilkie D, Wilhelm S, Lynch M, Carter C (2006) Cancer Res 66:11851
26. Llovet JM, Ricci S, Mazzaferro V, Hilgard P, Gane E, Blanc JF, de Oliveira AC, Santoro A, Raoul JL, Forner A, Schwartz M, Porta C, Zeuzem S, Bolondi L, Greten TF, Galle PR, Seitz JF, Borbath I, Häussinger D, Giannaris T, Shan M, Moscovici M, Voliotis D, Bruix J (2008) N Engl J Med 359:378
27. Brose MS, Nutting CM, Jarzab B, Elisei R, Siena S, Bastholt L, de la Fouchardiere C, Pacini F, Paschke R, Shong YK, Sherman SI, Smit JW, Chung J, Kappeler C, Peña C, Molnár I, Schlumberger MJ (2014) Lancet 384:319
28. Sun CL, Christensen JG, McMahon G (2009) Discovery and development of sunitinib (SU11248): a multitarget tyrosine kinase inhibitor of tumor growth, survival, and angiogenesis. In: Li R, Stafford JA (eds) Kinase inhibitor drugs. Wiley, Hoboken, p. 1
29. Britten CD, Kabbinavar F, Hecht JR, Bello CL, Li J, Baum C, Slamon D (2008) Cancer Chemother Pharmacol 61:515
30. Faivre S, Delbaldo C, Vera K, Robert C, Lozahic S, Lassau N, Bello C, Deprimo S, Brega N, Massimini G, Armand JP, Scigalla P, Raymond E (2006) J Clin Oncol 24:25
31. Motzer RJ, Hutson TE, Tomczak P, Michaelson MD, Bukowski RM, Rixe O, Oudard S, Negrier S, Szczylik C, Kim ST, Chen I, Bycott PW, Baum CM, Figlin RA (2007) N Engl J Med 356:115

32. Demetri GD, van Oosterom AT, Garrett CR, Blackstein ME, Shah MH, Verweij J, McArthur G, Judson IR, Heinrich MC, Morgan JA, Desai J, Fletcher CD, George S, Bello CL, Huang X, Baum CM, Casali PG (2006) Lancet 368:1329

33. Raymond E, Dahan L, Raoul JL, Bang YJ, Borbath I, Lombard-Bohas C, Valle J, Metrakos P, Smith D, Vinik A, Chen JS, Hörsch D, Hammel P, Wiedenmann B, Van Cutsem E, Patyna S, Lu DR, Blanckmeister C, Chao R, Ruszniewski P (2011) N Engl J Med 364:501

34. Harris PA, Stafford JA (2009) Discovery of pazopanib, a pan vascular endothelial growth factor kinase inhibitor. In: Li R, Stafford JA (eds) Kinase inhibitor drugs. Wiley, Hoboken, p. 57

35. Kumar R, Knick VB, Rudolph SK, Johnson JH, Crosby RM, Crouthamel MC, Hopper TM, Miller CG, Harrington LE, Onori JA, Mullin RJ, Gilmer TM, Truesdale AT, Epperly AH, Boloor A, Stafford JA, Luttrell DK, Cheung M (2007) Mol Cancer Ther 6:2012

36. Hurwitz H, Dowlati A, Savage S, Fernando N, Lasalvia S, Whitehead B, Suttle B, Collins D, Ho P, Pandite L (2005) J Clin Oncol 23:3012

37. Hutson TE, Davis ID, Machiels JH, de Souza PL, Baker K, Bordogna W, Westlund R, Crofts T, Pandite L, Figlin RA (2008) J Clin Oncol 26:5046

38. Sternberg CN, Davis ID, Mardiak J, Szczylik C, Lee E, Wagstaff J, Barrios CH, Salman P, Gladkov OA, Kavina A, Zarbá JJ, Chen M, McCann L, Pandite L, Roychowdhury DF, Hawkins RE (2010) J Clin Oncol 28:1061

39. Sleijfer S, Papai Z, Le Cesne A, Scurr M, Ray-Coquard I, Collin F, Pandite L, Marreaud S, De Brauwer A, Blay J (2007) J Clin Oncol 25:10031

40. van der Graaf WT, Blay JY, Chawla SP, Kim DW, Bui-Nguyen B, Casali PG, Schöffski P, Aglietta M, Staddon AP, Beppu Y, Le Cesne A, Gelderblom H, Judson IR, Araki N, Ouali M, Marreaud S, Hodge R, Dewji MR, Coens C, Demetri GD, Fletcher CD, Dei Tos AP, Hohenberger P (2012) Lancet 379:1879

41. Kania RS (2009) Structure-based design and characterization of axitinib. In: Li R, Stafford JA (eds) Kinase inhibitor drugs. Wiley, Hoboken, p. 167

42. Rugo HS, Herbst RS, Liu G, Park JW, Kies MS, Steinfeldt HM, Pithavala YK, Reich SD, Freddo JL, Wilding G (2005) J Clin Oncol 23:5474

43. Rini BI, Wilding G, Hudes G, Stadler WM, Kim S, Tarazi J, Rosbrook B, Trask PC, Wood L, Dutcher JP (2009) J Clin Oncol 27:4462

44. Motzer RJ, Escudier B, Tomczak P, Hutson TE, Michaelson MD, Negrier S, Oudard S, Gore ME, Tarazi J, Hariharan S, Chen C, Rosbrook B, Kim S, Rini BI (2013) Lancet Oncol 14:552

45. Spano J, Chodkiewicz C, Maurel J, Wong RP, Wasan HS, Pithavala YK, Bycott PW, Liau K, Kim S, Rixe O (2007) J Clin Oncol 25:4551

46. Kindler HL, Ioka T, Richel DJ, Bennouna J, Létourneau R, Okusaka T, Funakoshi A, Furuse J, Park YS, Ohkawa S, Springett GM, Wasan HS, Trask PC, Bycott P, Ricart AD, Kim S, Van Cutsem E (2011) Lancet Oncol 12:256

47. Davis SL, Eckhardt SG, Messersmith WA, Jimeno A (2013) Drugs Today 49:105

48. Mross K, Frost A, Steinbild S, Hedbom S, Büchert M, Fasol U, Unger C, Krätzschmar J, Heinig R, Boix O, Christensen O (2012) Clin Cancer Res 18:2658

49. Grothey A, Sobrero AF, Siena S, Falcone A, Ychou M, Lenz H-J, Yoshino T, Cihon F, Wagner A, Van Cutsem E (2012) J Clin Oncol 30(Suppl 4); abstr LBA385

50. Demetri GD, Reichardt P, Kang Y-K, Blay J-Y, Joensuu H, Maki RG, Rutkowski P, Hohenberger P, Gelderblom H, Leahy MG, von Mehren M, Schoffski P, Blackstein ME, Le Cesne A, Badalamenti G, Xu J-M, Nishida T, Laurent D, Kuss I, Casali PG (2012) J Clin Oncol 30(Suppl); abstr LBA10008

51. Bruix J, Tak WY, Gasbarrini A, Santoro A, Colombo M, Lim HY, Mazzaferro V, Wiest R, Reig M, Wagner A, Bolondi L (2013) Eur J Cancer 49:3412

52. Roth GJ, Binder R, Colbatzky F, Dallinger C, Schlenker-Herceg R, Hilberg F, Wollin SL, Kaiser R (2015) J Med Chem 58:1053

53. Hilberg F, Roth GJ, Krssak M, Kautschitsch S, Sommergruber W, Tontsch-Grunt U, Garin-Chesa P, Bader G, Zoephel A, Quant J, Heckel A, Rettig WJ (2008) Cancer Res 68:4774

54. Matsui J, Yamamoto Y, Funahashi Y, Tsuruoka A, Watanabe T, Wakabayashi T, Uenaka T, Asada M (2008) Int J Cancer 122:664
55. Okamoto K, Ikemori-Kawada M, Jestel A, von König K, Funahashi Y, Matsushima T, Tsuruoka A, Inoue A, Matsui J (2014) ACS Med Chem Lett 6:89
56. Nakamichi S, Nokihara H, Yamamoto N, Yamada Y, Honda K, Tamura Y, Wakui H, Sasaki T, Yusa W, Fujino K, Tamura T (2015) Cancer Chemother Pharmacol 76:1153
57. Schlumberger M, Tahara M, Wirth LJ, Robinson B, Brose MS, Elisei R, Habra MA, Newbold K, Shah MH, Hoff AO, Gianoukakis AG, Kiyota N, Taylor MH, Kim SB, Krzyzanowska MK, Dutcus CE, de las Heras B, Zhu J, Sherman SI (2015) N Engl J Med 372:621
58. Sorbera LA, Serradell N, Rosa E, Bolós J, Bayés M (2007) Drugs Future 32:577
59. Schmidt C (2015) J Natl Cancer Inst 107:3
60. Sahade M, Caparelli F, Hoff PM (2012) Future Oncol 8:775
61. Haberkorn BC, Eskens FA (2013) Future Oncol 9:13
62. Jamil MO, Hathaway A, Mehta A (2015) Curr Oncol Rep 17:24
63. Benson A, Krivoshik A, Van Sant C, Needle M (2015) Ann Oncol 26(Suppl 4):108
64. Porta C, Giglione P, Liguigli W, Paglino C (2015) Future Oncol 11:39
65. Tian S, Quan H, Xie C, Guo H, Lü F, Xu Y, Li J, Lou L (2011) Cancer Sci 102:1374
66. Scagliotti GV, Vynnychenko I, Park K, Ichinose Y, Kubota K, Blackhall F, Pirker R, Galiulin R, Ciuleanu TE, Sydorenko O, Dediu M, Papai-Szekely Z, Banaclocha NM, McCoy S, Yao B, Hei YJ, Galimi F, Spigel DR (2012) J Clin Oncol 30:2829
67. Johnson PJ, Qin S, Park JW, Poon RT, Raoul JL, Philip PA, Hsu CH, Hu TH, Heo J, Xu J, Lu L, Chao Y, Boucher E, Han KH, Paik SW, Robles-Aviña J, Kudo M, Yan L, Sobhonslidsuk A, Komov D, Decaens T, Tak WY, Jeng LB, Liu D, Ezzeddine R, Walters I, Cheng AL (2013) J Clin Oncol 31:3517
68. Llovet JM, Decaens T, Raoul JL, Boucher E, Kudo M, Chang C, Kang YK, Assenat E, Lim HY, Boige V, Mathurin P, Fartoux L, Lin DY, Bruix J, Poon RT, Sherman M, Blanc JF, Finn RS, Tak WY, Chao Y, Ezzeddine R, Liu D, Walters I, Park JW (2013) J Clin Oncol 31:3509
69. Siu LL, Shapiro JD, Jonker DJ, Karapetis CS, Zalcberg JR, Simes J, Couture F, Moore MJ, Price TJ, Siddiqui J, Nott LM, Charpentier D, Liauw W, Sawyer MB, Jefford M, Magoski NM, Haydon A, Walters I, Ringash J, Tu D, O'Callaghan CJ (2013) J Clin Oncol 31:2477
70. Cainap C, Qin S, Huang WT, Chung IJ, Pan H, Cheng Y, Kudo M, Kang YK, Chen PJ, Toh HC, Gorbunova V, Eskens FA, Qian J, McKee MD, Ricker JL, Carlson DM, El-Nowiem S (2015) J Clin Oncol 33:172
71. Sobrero AF, Bruzzi P (2011) J Clin Oncol 29:1938

Inhibitors of the Fibroblast Growth Factor Receptor

Kurt G. Pike

Abstract Signaling through the fibroblast growth factor receptor (FGFR) tyrosine kinase is crucial to a number of key pharmacological processes; however, dysregulation of this signaling is observed with a number of different cancers suggesting that inhibition of FGFR may provide an important therapeutic agent in the treatment of cancers. This chapter provides an overview of the development of FGFR inhibitors beginning with the identification of nonselective FGFR inhibitors, then describing the medicinal chemistry optimization resulting in the delivery of a number of highly selective FGFR inhibitors, some of which are currently being assessed in clinical trials. The development of isoform selective FGFR inhibitors as well as covalent inhibitors and inhibitors of the inactive form of FGFR are also described.

Keywords Fibroblast growth factor receptor, Receptor tyrosine kinase, Selective kinase inhibitor

Contents

K.G. Pike (✉)
Oncology Innovative Medicines, AstraZeneca, Darwin Building, 310 Cambridge Science Park, Milton Road, Cambridge CB4 0WG, UK
e-mail: kurt.pike@astrazeneca.com

1   Introduction

The development of human cancers, in which normal cells are transformed into highly malignant cells, is usually a multistage process that may extend over decades [1]. The transformation process involves cells accumulating a number of genetic changes which result in a specific set of properties commonly referred to as the hallmarks of cancer (including sustained proliferative signaling, evasion of growth suppressors, active invasion and metastasis, replicative immortality, induction of angiogenesis, and resistance to cell death) [2, 3]. The genetic alterations acquired by the cell can result in overactivation of growth-promoting oncogenes or the inactivation of growth-inhibitory suppressor genes. Receptor tyrosine kinases, such as epidermal growth factor receptor (EGFR, "Inhibitors of Vascular Endothelial Growth Factor Receptor"), fibroblast growth factor receptor (FGFR), platelet-derived growth factor receptor (PDGFR), and vascular endothelial growth factor receptor (VEGFR, "Inhibitors of Vascular Endothelial Growth Factor Receptor"), represent an important family of genes which have been found to be altered in human cancer.

1.1   Fibroblast Growth Factor Receptor (FGFR)

FGFR is a receptor tyrosine kinase (RTK), which consists of an extracellular ligand-binding domain, a single *trans*membrane helix and an intracellular tyrosine kinase domain. The binding of fibroblast growth factors (FGFs) to FGFR induces receptor dimerization, which in turn results in a conformational shift in the structure of the receptor and activation of the tyrosine kinase domain. Subsequent downstream signaling occurs mostly through FGFR substrate 2 (FRS2) and phospholipase Cγ (PLCγ), leading to upregulation of the Ras-dependent mitogen-activated protein kinase (MAPK) and Ras-independent phosphoinositide 3-kinase (PI3K)–Akt-signaling pathways. These signals are critical to a number of physiological processes, such as the regulation of organ development, skeletal development, cell proliferation, cell migration, and angiogenesis. There are 18 known FGF ligands, the hormone-like FGFs (FGF19, 21, and 23) and the canonical FGFs (FGF1–10, 16–18, and 20), and

Fig. 1 Schematic of
FGF/FGFR binding
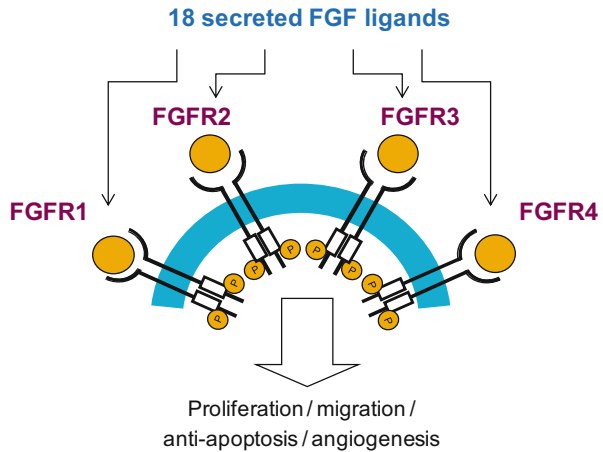
five isoforms of the FGFR receptor, of which only FGFR1–4 possess the intracellular
tyrosine kinase domain (Fig. 1). The specificity of the FGF/FGFR interaction is
dependent on the ligand-binding capacities of the four receptor isoforms as well as
the tissue-specific expression of both ligands and receptors [4–6].

1.2 The Role of FGFR in Cancer

FGFRs are known to be overexpressed in many types of human cancer cells, and
our understanding of the mechanisms by which FGFR signaling is dysregulated and
drives cancer has increased significantly in recent years. FGFRs are among the most
commonly mutated kinase genes observed in human cancers. Mutations in FGFR
that confer constitutive activation have been seen in many cancers including
non-muscle invasive and high-grade bladder cancer (FGFR3 activation), endo-
metrial cancer (FGFR2 activation), and rhabdomyosarcoma (FGFR4 activation).
Amplification of FGFR genes will often result in FGFR overexpression, which can
also allow ligand-independent signaling to occur. FGFR amplification has been
observed in cancers including estrogen receptor-positive breast cancer (FGFR1
amplification), squamous non-small cell lung cancer (FGFR1 amplification), and
gastric cancer (FGFR2 amplification). FGFR translocations have been identified in
hematologic malignancies, which result in a protein fusing to the intracellular
tyrosine kinase domain of an FGFR. This fusion results in the permanent dimer-
ization, and therefore activation, of the protein as well as the removal of mecha-
nisms of feedback inhibition. Such translocations have been observed to result in
FGFR3 overexpression and continuous signaling. In addition to aberrations within
the receptor proteins, overexpression of the FGF ligands has also been shown to
play a role in cancer development; FGF5 overexpression has been observed in a
number of lung, esophagus, melanoma, and colon and prostate tumor cell lines, and
overexpression/upregulation of FGF2, 8, 17, 18, and 19 has been observed in
hepatocellular carcinomas (HCC).

Brivanib alaninate

Nintedanib

Lucitanib

Ponatinib
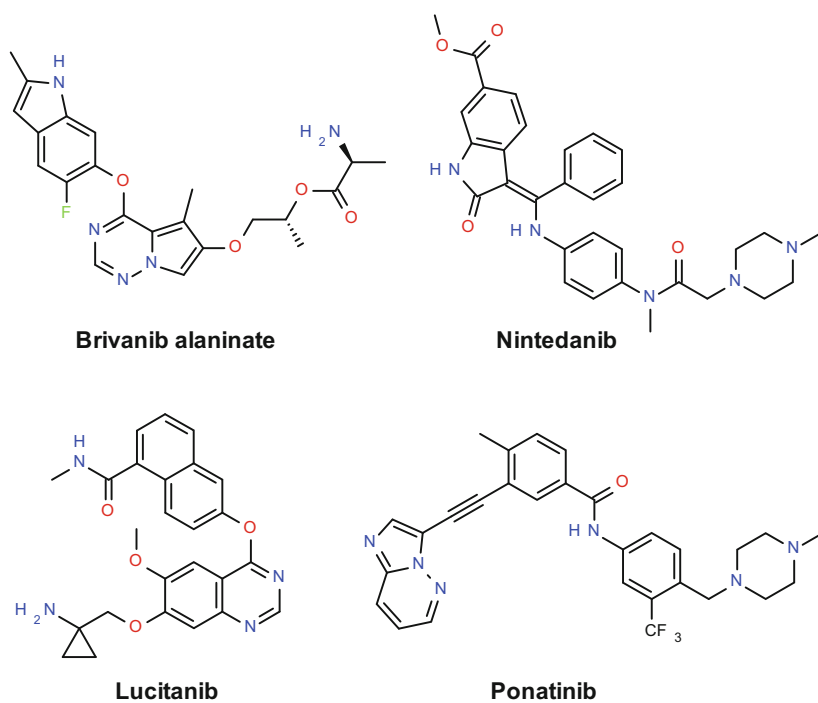
Drug Name	Company	Kinase target	Clinical development (indication)
Brivanib	Bristol-Myers Squibb	VEGFR, FGFR	Phase III (CRC, HCC, liver)
Nintedanib	Boehringer Ingelheim	VEGFR, PDGFR, FGFR	Phase III (NSCLC, ovarian)
Lucitanib	Eisai	VEGFR, FGFR1, CSF-1R	Phase I (solid tumors)
Ponatinib	Ariad Pharmaceutical	PDGFR, VEGFR, FGFR, BCR-ABL	Phase II (AML, CML)

Fig. 2 Structures and targets of selected first generation FGFR inhibitors

2 The Development of Nonselective FGFR Inhibitors

The strong association of dysregulated FGF/FGFR signaling with human cancer has instigated considerable research efforts aimed at the identification of inhibitors of the tyrosine kinase domain of FGFR. The FGFR inhibitors developed to date can be classified in two distinct groups, a first generation of multi-targeted RTK inhibitors and a second generation of FGFR-selective inhibitors. The first generation inhibitors include compounds such as brivanib (BMS-540215), nintedanib (BIBF1120), lucitanib (E-3810), and ponatinib (AP24534) (Fig. 2). While these compounds are inhibitors of FGFR, they also show potent inhibition of a range of other kinases, most notably VEGFR ("Inhibitors of Vascular Endothelial Growth Factor Receptor") and PDGFR [4, 6]. Overall, emerging data from the clinical studies suggest that these nonselective FGFR inhibitors may indeed have utility in the treatment of cancer patients, and despite their polypharmacology, some studies have reported bioactivity against FGFR at the doses employed. However, the main toxicology profile of these agents remains related to pharmacology of VEGFR inhibition [5]. These observations highlight the potential benefit in developing selective FGFR inhibitors with improved therapeutic margins thus enabling more complete target engagement in vivo, in addition to displaying differentiated toxicity profiles.

3 The Development of Selective FGFR Inhibitors

3.1 Pyrido[2,3-d]pyrimidine-Based Inhibitors of FGFR

The identification of compounds designed to specifically target FGFR was first reported by Connolly et al. from the laboratories of Parke–Davis [7]. The authors utilized high-throughput screening techniques to identify inhibitors of PDGFR and FGFR. This approach resulted in the identification of the pyrido[2,3-d]pyrimidine hit **1**, which showed potent inhibition of FGFR ($IC_{50} = 0.13$ μM) in a biochemical assay and was observed to act in an ATP-competitive manner suggesting the compound binds at the ATP-binding site. Additional screening showed hit **1** to have broad kinase activity (PDGFR $IC_{50} = 1.11$ μM, EGFR $IC_{50} = 0.45$ μM, and c-Src $IC_{50} = 0.22$ μM) leading the authors to speculate that this scaffold might provide a useful start point for the optimization of a variety of novel, targeted kinase inhibitors. The physicochemical properties of hit **1**, however, resulted in poor exposure following both oral and intraperitoneal (i.p.) dosing; the very poor aqueous solubility, coupled with the inability to form soluble salts with strong acids, precluded intravenous (i.v.) administration. Thus, hit **1** was deemed not suitable for in vivo characterization. The efforts to identify potent, selective, and orally available kinase inhibitors were described by Hamby et al. and are summarized below [8] (Fig. 3).

Fig. 3 Structure of hit **1**
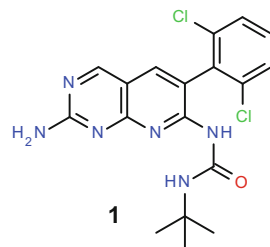
To understand the underlying structure-activity relationship (SAR), the authors began a systematic examination of different positions on the pyrido[2,3-d] pyrimidine scaffold, with particular attention focused on the 6-, 7-, and 2-positions. In the 6-position it was found that phenyl rings possessing small *ortho*-substituents displayed increased kinase activity against a range of tyrosine kinases (comparing hit **1** with compound **2**). A crystal structure of hit **1** shows the C6-aryl ring adopts an orthogonal relationship to the pyrido[2,3-d]pyrimidine core, presumably driven by the presence of the *ortho*-chlorine atoms. Further optimization of the phenyl substituent revealed that *meta*-, but not *para*-substitution, could infer high levels of selectivity for FGFR over the other tyrosine kinases tested. In particular, the 3,5-dimethoxyphenyl containing compound **3** was identified as a potent inhibitor of FGFR with excellent selectivity over closely related kinases (Fig. 4).

Compounds such as **4** and **5** highlight the opportunity to modulate the kinase inhibitory activity, while simultaneously improving the aqueous solubility of the molecules, through the incorporation of aminoalkyl groups in the 2-position of the pyridopyrimidine ring. Furthermore, compounds **4** and **5** display significantly improved oral bioavailability, presumably driven by the increased aqueous solubility. Examination of the 7-position revealed the importance of the urea NH for kinase inhibitory activity and identified a range of tolerated urea substituents, such as compound **6**; however, large substituents were generally associated with a loss in potency. A combination of the systematically optimized substituents resulted in the discovery of PD173074 (**7**), a potent and selective inhibitor of FGFR (Fig. 5).

PD173074 (**7**) was shown to inhibit the autophosphorylation of FGFR1 in NIH 3T3 cells with an IC_{50} of 0.001–0.005 μM, whereas the autophosphorylation of VEGFR2 in the same cell line was inhibited with significantly reduced potency ($IC_{50} = 0.1$–0.2 μM). PD173074 (7) inhibited the bFGF-stimulated HUVEC growth ($IC_{50} = 0.007$ μM) but was less active against VEGF-stimulated HUVEC growth ($IC_{50} = 0.194$ μM). The bioavailable nature of **7** allowed for the in vivo characterization of the compound, and it was shown to inhibit bFGF-induced angiogenesis in an in vivo mouse cornea model but was significantly less effective at blocking VEGF-induced angiogenesis in the same model [9].

Researchers at the Kaplan Comprehensive Cancer Center and Skirball Institute of Biomolecular Medicine, in collaboration with researchers at Parke–Davis, successfully crystallized **7** bound into the ATP-binding site of FGFR1 and utilized the X-ray crystal structure to rationalize the observed SAR (Fig. 6) [10]. The pyrido
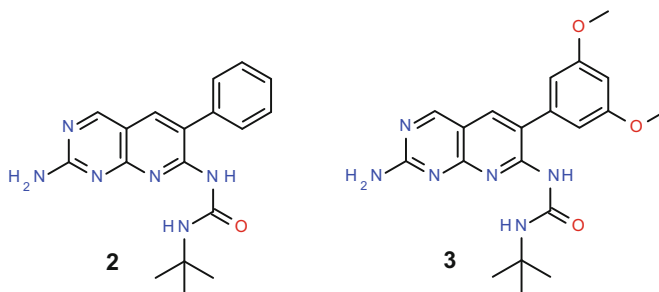
Compound	1	2	3
FGFR IC$_{50}$ (μM)	0.13	3.71	0.06
PDGFR IC$_{50}$ (μM)	1.11	4.67	>50
EGFR IC$_{50}$ (μM)	0.45	5.53	>50
c-Src IC$_{50}$ (μM)	0.22	>50	>50

Fig. 4 SAR of C6-phenyl substitution

[2,3-d]pyrimidine core was found to occupy the same position as the adenosine ring of ATP and forms two hydrogen-bonding interactions with the hinge region of the kinase: between the pyrimidine N3 and the amide nitrogen of Ala564 and between the NH of the 2-amino substituent and the carbonyl oxygen of Ala564. The C6-phenyl ring accesses a hydrophobic back pocket in the binding site with one of the *meta*-methoxy substituents forming a hydrogen bond to the amide nitrogen of Asp641 at the beginning of the activation loop. The C6-phenyl ring is perpendicular to the plane of the pyrido[2,3-d]pyrimidine core and displays exceptional complimentarily to the shape of the pocket. Interestingly, the back pocket in FGFR1 is lined by two valine residues (Val559 and Val561), whereas, in many kinases this pocket is lined by larger residues. The authors speculate that the highly optimized 3,5-dimethoxyphenyl ring would be unlikely to fit well into the back pocket of a kinase with larger residues in this region, and as such this may well explain the high selectivity of the molecule. However, it should be noted that both VEGFR1 and VEGFR2 also contain valine at the corresponding positions which may therefore explain the moderate activity of **7** at VEGFR2. The urea substituent in the 7-position forms an internal hydrogen bond to the N8 nitrogen of the core and is also involved in a water-mediated interaction with the side chains of Asp641 and Lys514. The importance of this internal hydrogen bond is likely to explain the importance of the urea NH for kinase binding. The electron density for the amino-alkyl substituent in the 2-position is poorly defined suggesting that considerable flexibility exists in this region. This is consistent with the observation that the

Fig. 5 SAR of C2- and C7-substitution
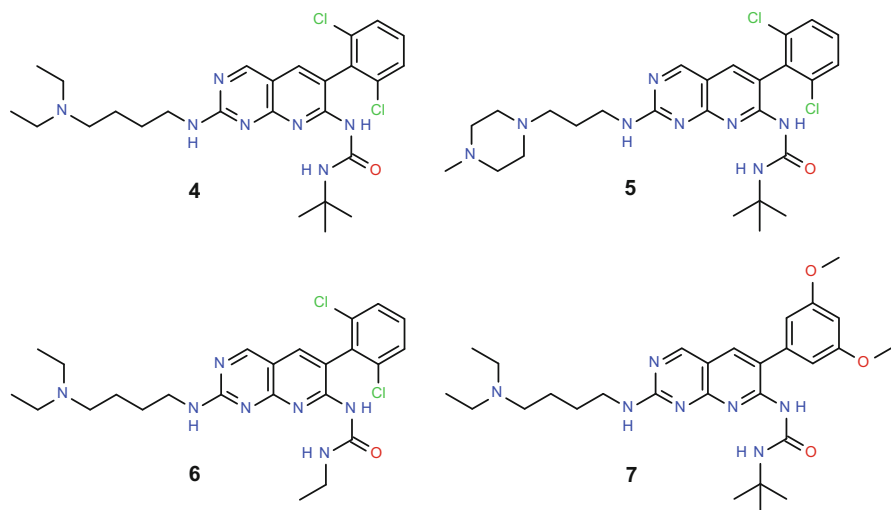
Compound	4	5	6	7
FGFR IC$_{50}$ (μM)	0.048	0.051	0.033	0.026
PDGFR IC$_{50}$ (μM)	0.31	0.47	0.19	15.5
EGFR IC$_{50}$ (μM)	0.24	0.15	1.26	>40
c-Src IC$_{50}$ (μM)	0.044	0.031	0.023	20.3

2-aminoalkyl substituent has a greater impact on the physicochemical properties of the molecule than on its biological activity. The SAR identified by the researchers at Parke–Davis during the identification of **7**, together with the structural information regarding the binding mode and specific interactions with FGFR, has informed the subsequent work of many groups also looking to identify selective inhibitors of FGFR.

Continued exploration of the scaffold revealed the ability to replace the pyrido [2,3-d]pyrimidine N1 nitrogen with a CH, **8**; an observation that is also consistent with the anticipated binding mode and highlighting the limited contribution of this nitrogen to the overall binding affinity of the scaffold [11]. Interestingly, this modification appears to increase in VEGFR potency. More detailed exploration of the 2-aminoalkyl group confirms that the basic center is not a requirement for biological activity with neutral analogue **9** displaying a similar potency and selectivity profile, although solubility is reduced dramatically. As anticipated from the

Fig. 6 Structure of **7** bound to FGFR1 (PDB accession code 2FGI) with hydrogen bonds highlighted in *magenta*
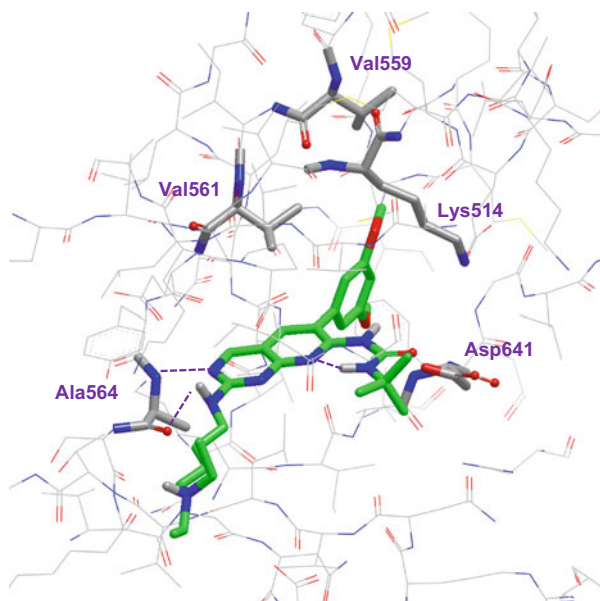
binding mode, removal of the 2-amino NH results in a significant loss of potency (Fig. 7).

In parallel with the optimization of hit **1**, the researchers at Parke–Davis also optimized a related pyrido[2,3-d]pyrimidin-7-one hit **10** with the expectation of identifying kinase inhibitors with differing profiles with respect to inhibitory activity, metabolism, and pharmacokinetic properties [12]. Optimization of this scaffold resulted in the discovery of PD166285 (**11**), a potent inhibitor of a range of tyrosine kinases (including FGFR, PDGFR, EGFR, and c-Src) which displays excellent physicochemical properties [13].

3.2 Indolin-2-One-Based FGFR Inhibitors

The discovery of a series of indolin-2-one compounds possessing a broad kinase inhibition profile (including PDGFRβ, VEGFR2, EGRF, HER-2, and IGF-1R) was reported by Sun et al. from the laboratories of Sugen [14]. The initial SAR was developed against a broad spectrum of kinase inhibition and highlighted the important role the configuration at the C3-position of the indolin-2-one scaffold plays on both the potency and selectivity profile of the molecule. In particular, it was observed that compounds with a 3-[(pyrrolyl)methylidene]indolin-2-one scaffold, such as **12**, exist predominantly in the Z-configuration and that these compounds exhibit selectivity for VEGFR2 and PDGFRβ (IC$_{50}$ values 0.039, 12 μM, respectively) over EGFR, HER-2, and IGF-1R (all >100 μM). Elaboration of the

Fig. 7 SAR of 1,6-naphthyridine core and pyrido[2,3-d]pyrimidin-7-one core
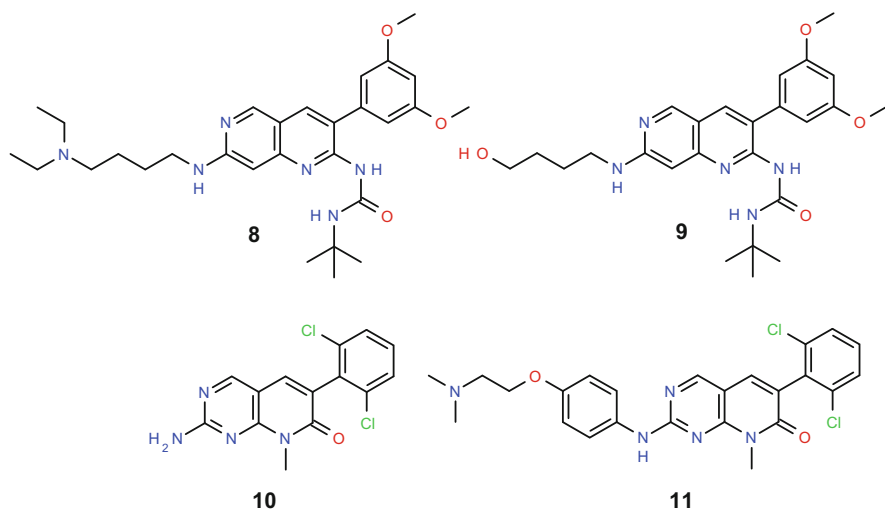
Compound	8	9	10	11
FGFR IC$_{50}$ (μM)	0.060	0.052	1.3	0.043
PDGFR IC$_{50}$ (μM)	18.0	23.0	4.9	0.079
VEGFR IC$_{50}$ (μM)	0.015	0.008	-	-
EGFR IC$_{50}$ (μM)	-	-	5.6	0.044
c-Src IC$_{50}$ (μM)	16.0	>50	0.26	0.009

pyrrolyl motif resulted in the identification of SU5402 (**13**), a relatively selective inhibitor of VEGFR2 (IC$_{50}$ = 0.02 μM) and FGFR1 (IC$_{50}$ = 0.03 μM) (Fig. 8).

A crystal structure of SU5402 (**13**) bound to FGFR1 revealed the indolin-2-one moiety to occupy the region of the binding site normally occupied by the adenosine ring of ATP (albeit that the orientation of the bicyclic ring systems differs dramatically) and that a bidentate hydrogen-bonding interaction with the kinase hinge region is formed from both the indoline NH and the oxygen of the indoline carbonyl group (Fig. 9). An intramolecular hydrogen bond was observed between the pyrrole NH and the indoline carbonyl oxygen, thus helping favor the optimal Z-configuration. The structure highlights the presence of water molecules near the C5 position of the indolin-2-one ring, perhaps suggestive that hydrophilic substitution may be tolerated at this position. The structure also shows the propionic acid

Fig. 8 The structure of indolin-2-ones **12** and **13**

12

13
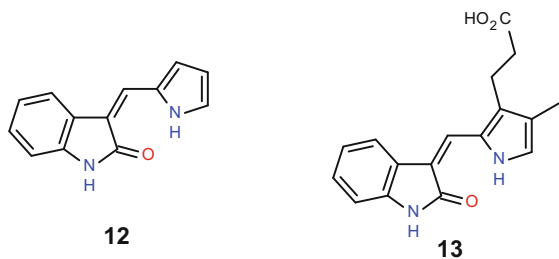
Fig. 9 Structure of **13** bound to FGFR1 (PDB accession code 1FGI) with hydrogen bonds highlighted in *magenta*
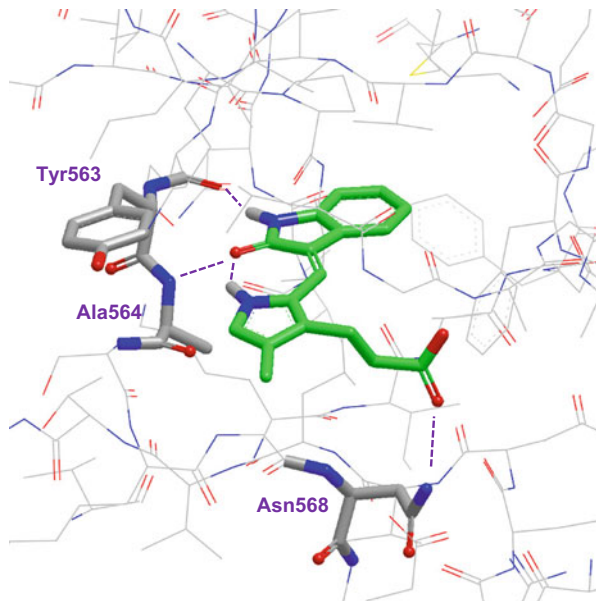
chain to reach into the ribose binding pocket where it makes an interaction with Asn568 [15].

A comparison of the structure with the published structural data for PD173074 (**7**) bound to FGFR1 suggested to the authors the possibility to build out from the 6-position of the indolin-2-one ring to access the hydrophobic back pocket of the binding site. These insights resulted in the examination of phenyl substitution in the 6-position of the indolin-2-one ring [16]. Initial investigations resulted in an unexpected loss of potency, such as **14**; however, parallel SAR studies conducted on a structurally related start point, exemplified by the PDGFRβ selective compound SU6668 (**15**), did suggest that the back pocket could be accessed from this position of the indolin-2-one ring and that improved FGFR1 and VEGFR2 potency could be attained, for example compound **16**. Computational modeling suggests that the propionic acid motif in **15** forms an interaction with a lysine residue rather than the asparagine residue observed for **13** and the authors speculate that the

6-phenyl substituent causes a slight movement of the indolin-2-one ring in the binding site resulting in the weakening of the propionic acid/asparagine interaction for one series and strengthening the propionic acid/lysine interaction in the other. As suggested from the crystal structure, hydrophilic substituents were found to be tolerated in the C5 position, exemplified by **17**, and were found to generally enhance FGFR activity compared to VEGFR2 and PDGFRβ activity (Fig. 10).

Interestingly, throughout the reported SAR investigation, the authors note an apparent disconnect between biochemical potency and cell potency. They postulate that poor cell permeability, related to the physicochemical properties of some of the molecules described, contributes to this observed disconnect.

Further optimization of this scaffold was reported by Kammasud et al. from Mahidol University in Thailand, collaborating with researchers from the Khon Kaen University in Thailand, the University of Tayama in Japan, and the Institut Curie in Orsay, France [17]. This optimization utilized computational docking studies in an attempt to identify more efficient binders. Libraries of virtual compounds were docked into a template constructed from the published crystal structure of PD173074 (**7**) and ranked based on the calculated docking energies. This
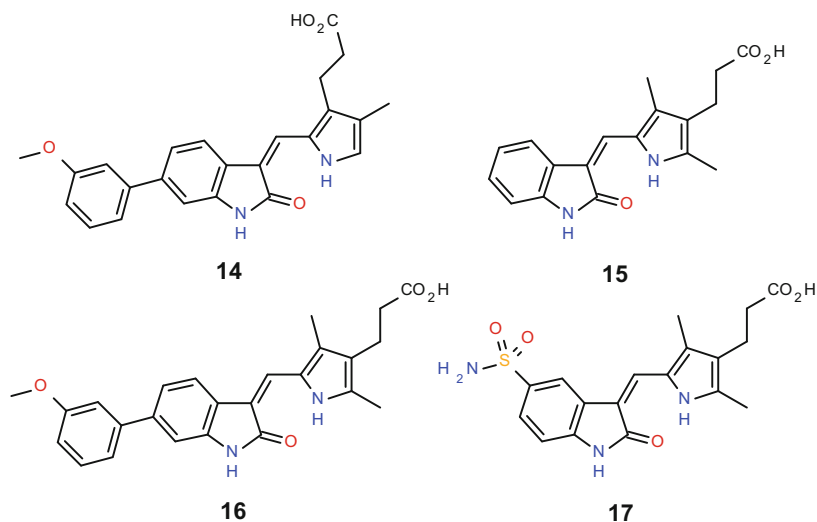
Compound	14	15	16	17
FGFR1 IC$_{50}$ (μM)	1.2	3.04	1.40	0.28
VEGFR2 IC$_{50}$ (μM)	28.3	2.43	0.30	1.26
PDGFRβ IC$_{50}$ (μM)	0.45	0.06	0.10	1.53

Fig. 10 SAR of indolin-2-one compounds
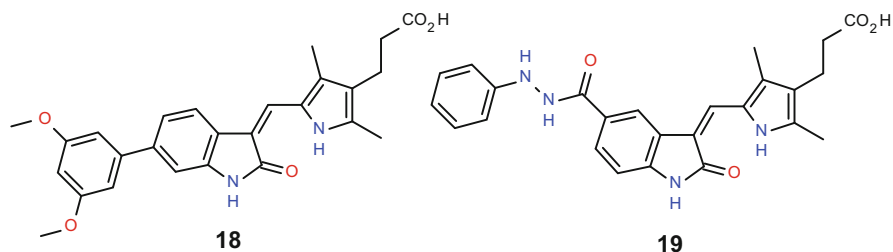
Fig. 11 Structure of NP603 (**18**) and NP506 (**19**)

approach identified NP603 (**18**) as a potential compound of interest, which was subsequently synthesized and found to bind to FGFR1 with moderate potency in a biochemical assay (IC$_{50}$ = 0.52 μM). Compound **18** showed slightly reduced activity against VEGFR2 and PDGFRβ in biochemical assays (IC$_{50}$'s = 0.93 and 0.78 μM, respectively) and was inactive against EGFR (IC$_{50}$ >100 μM). Unfortunately, the relatively modest activity of **18** in an antiproliferative HUVEC cell model (IC$_{50}$ = 18.2 μM), and in an FGF-2-stimulated HUVEC tube-forming assay, precluded the more detailed profiling of this compound. Interestingly, the authors postulate that a 3,5-dicyanophenyl group in the 6-position of the indolin-2-one ring might confer additional potency due to the extended delocalization of the π-electrons; however, despite the promising docking score, no data are reported for this compound (Fig. 11).

Computational modeling was also used to prioritize the SAR investigations into substitution of the 5-position of the indolin-2-one core. As a result of this in silico approach, NP506 (**19**) was synthesized and shown to possess good activity against FGFR1, VEGFR2, and PDGFRβ in biochemical assays (IC$_{50}$'s = 0.10 μM, 0.07 μM, and 0.04 μM, respectively) but was less active against EGFR (IC$_{50}$ = 3.48 μM) [18]. The proposed binding mode for **19** locates the phenylhydrazine moiety more deeply in to the hydrophobic back pocket compared to the 3,5-dimethoxyphenyl moiety of **18** and forms a π–π interaction with Phe642. However, despite the improved biochemical potency of **19**, little difference is observed between the potency of this compound in a cellular antiproliferation assay compared with **18** (IC$_{50}$ = 18.2 and 27.4 μM, respectively). The authors postulate that the physicochemical properties of **19** may result in poor cellular permeability. Compound **19** also appears to show activity against the PI3K/AKT-signaling pathway perhaps indicating that the compound is less selective than **18**.

3.3 Benzimidazol-2-Ylhydroquinolin-2-One-Based FGFR Inhibitors

Renhowe et al. have described work performed within Novartis that resulted in the discovery of a benzimidazol-2-ylhydroquinolin-2-one scaffold [19]. The commercially available compound **20** was identified as a potent inhibitor of VEGFR2, FGFR1, and PDGFR following a high-throughput screening approach (IC$_{50}$'s = 0.24, 0.090 and 0.020 μM, respectively). However, the poor physicochemical properties of the molecule, in particular the low aqueous solubility, precluded in vivo characterization for this compound and hence optimization of this scaffold was initiated (Fig. 12).

Initial SAR studies revealed the important role of the hydroquinolin-2-one NH and the benzimidazole NH on binding, with methylation of either one, or of both (**21**), of these groups resulting in a significant decrease in biochemical activity. The authors rationalize this observation based on molecular modeling studies, which suggest the involvement of both NH groups, along with the hydroquinolin-2-one carbonyl oxygen, in a tridentate donor-acceptor-donor interaction with the hinge region of the kinases. The research also highlighted the requirement for a hydrogen bond donor motif in the C4-position of the hydroquinolin-2-one ring (comparing **20** and **23** with compound **22**). The authors postulate that the presence of a hydrogen bond donor in this position allows the formation of an intramolecular hydrogen bond with the benzimidazole motif thereby maintaining a coplanar arrangement of the rings while simultaneously favoring the benzimidazole tautomeric form required for the tridentate interaction with the kinase hinge. Basic functionality could be appended to this position and was unexpectedly found to modulate the kinase selectivity profile of the molecules in addition to the anticipated impact on physicochemical properties. In particular, large basic substituents, such as the aminoquinuclidine in **24**, resulted in compounds with significantly increased activity against PDGFR compared to VEGFR and FGFR. Such compounds also showed considerable activity against other kinases, including CHK-1 and GSK-3. However, given the desire to identify selective inhibitors of tyrosine kinases, the authors conclude that the 4-amino substituent was optimal for the program (Fig. 13).

Modulation of the physicochemical properties without undue impact on the kinase selectivity profile was achieved by modifying the periphery of the molecule.

20
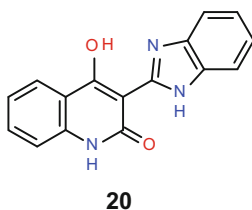
Fig. 12 Structure of screening hit **20**

Fig. 13 SAR of the hydroquinolin-2-one scaffold
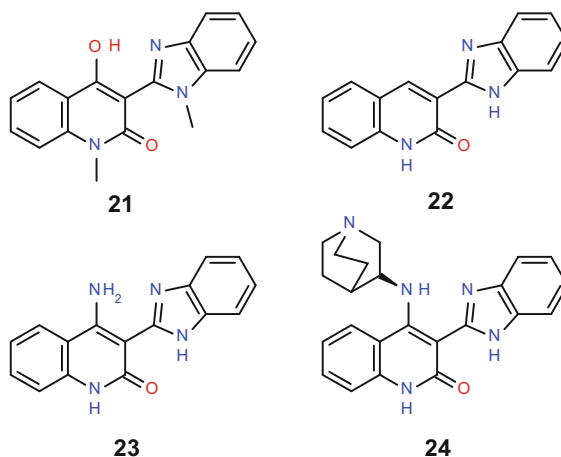
Compound	21	22	23	24
FGFR1 IC$_{50}$ (μM)	>25	0.39	0.030	0.19
PDGFRβ IC$_{50}$ (μM)	>25	0.070	0.010	0.0002
VEGFR2 IC$_{50}$ (μM)	>25	1.7	0.058	0.17

A wide range of solubilizing groups could be incorporated on the benzimidazole ring with substitution in the 5-position of this ring appearing optimal, exemplified by **25** and **26**. The observation that both acidic and basic functionality was tolerated in this position with little impact on kinase selectivity (data not shown) led the authors to postulate that substitution at this position allows access to a region of the protein which is exposed to solvent. Activity in cellular systems appears improved for compounds in which the basic substituent has a pK_a in the range of 7–9, and the *N*-methylpiperazine motif in particular is reported to possess a good balance of potency and physicochemical properties. Final optimization of the scaffold focused on substituents on the phenyl ring of the hydroquinolin-2-one core. Small electron-donating groups were tolerated in the 5-,6-, and 7-positions of the hydroquinolin-2-one ring, such as **27** and **28**, but larger substituents could be accommodated in the 5-position of the hydroquinolin-2-one ring only. Substitution of any type was not tolerated in the 8-position of the hydroquinolin-2-one ring, presumably due to the substituent interfering with the kinase hinge interaction. Although substitution on this ring generally resulted in compounds with increased activity for PDGFR over FGFR and VEGFR, such as **28**, the authors identified that compound **27** possessed a more balanced profile and thus selected this compound for further profiling.

Compound **27** has subsequently been referred to as TKI-258, CHIR-258, and eventually as dovitinib (Fig. 14).

In addition to being a potent inhibitor of FGFR1, PDGFRβ, and VEGFR2 in biochemical assays, dovitinib (**27**) also inhibits VEGFR1 and 3, FGFR3, c-Kit, CSF1R, and Flt3 with IC$_{50}$'s ranging between 0.001 and 0.036 μM. It potently inhibits the phosphorylation of FGFR1, VEGFR2, and PDGFRβ in cells (EC$_{50}$'s = 0.166 μM, 0.046 μM, and 0.051 μM, respectively) [20]. Dovitinib (**27**) shows increased aqueous solubility and attractive pharmacokinetic properties with good oral bioavailability (>70% in mice and rat), moderate to high clearance, and a large volume of distribution resulting in a terminal half-life of approximately 3 h. Dovitinib (**27**) shows potent inhibition of bFGF-driven angiogenesis in a mouse Matrigel model of neovascularization and tumor regression in both KM12L4a and HCT116 xenograft models at doses >60 mg/kg. The observed efficacy is associated with a significant reduction of phosphorylated PDGFRβ and a reduction of phosphorylation of the downstream protein ERK in the tumor cells. Based on the preclinical data, dovitinib (**27**) has
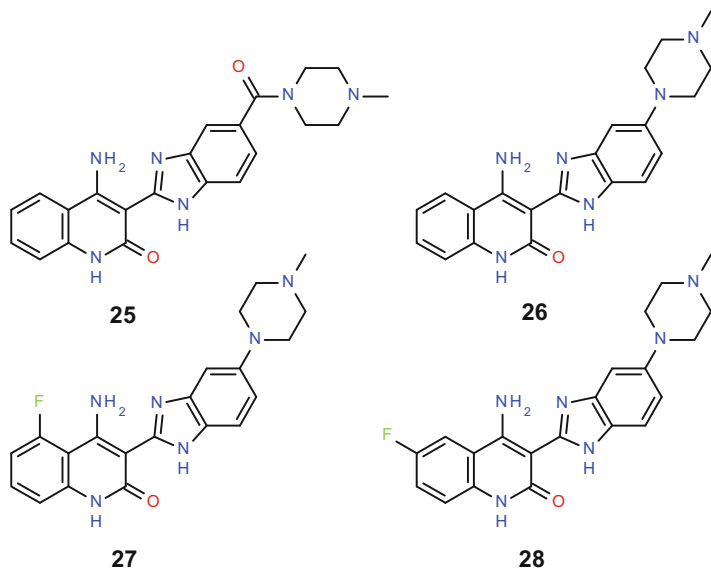
Compound	25	26	27	28
FGFR1 IC$_{50}$ (μM)	0.010	0.009	0.011	0.040
PDGFRβ IC$_{50}$ (μM)	0.0009	0.002	0.005	0.001
VEGFR2 IC$_{50}$ (μM)	0.026	0.042	0.065	0.078

Fig. 14 SAR of the hydroquinolin-2-one scaffold

been described as a multi-targeted growth factor receptor kinase inhibitor and has been studied in a number of clinical studies, including a phase I/II study in patients with advanced melanoma; a phase II study in patients with previously treated, metastatic, HER2-negative breast cancer; and a phase II study in combination with fulvestrant in postmenopausal, HER2-negative/HR-positive advanced breast cancer patients.

3.4 Pyrimidinyl Ureas as FGFR Inhibitors

In parallel with the development of dovitinib (**27**), Guagnano et al. describe complementary work within the Novartis laboratories designed to identify an inhibitor of FGFR with increased selectivity over VEGFR and PDGFR [21]. The authors postulate that the identification of such a compound would not only aid the understanding of the role of FGFR in cancer but may also provide a superior therapeutic agent with a potentially more favorable toxicity profile compared to more promiscuous drugs. The approach adopted by the authors built on a strategy successfully employed within Novartis for the identification of a range of novel kinase inhibitors and relies on the use of stable "pseudo" ring systems (formed by intramolecular hydrogen-bonding interactions) to replace the cyclic structures of known kinase inhibitors. The authors utilized ab initio calculations on a model system to support the hypothesis that a pyrimidine-urea motif would preferentially adopt a pseudo cyclic conformation (**B**) in which the pyrimidine and the methyl substituents adopt a *cis* relationship over an open *trans* conformation (**A**) (Fig. 15) [22]. A search of the Cambridge Structural Database identified seven examples of crystal structures where this motif is present and in all cases the structural data supported the presence of the *cis* conformation **B**.

The pyrido[2,3-d]pyrimidin-7-one scaffold, developed within Parke–Davis during the optimization of PD166285 (**11**), was selected as an appropriate start point resulting in the synthesis and evaluation of pyrimidinyl urea **29**. Compound **29** showed activity against a broad range of kinases, including FGFR1 (IC$_{50}$ = 0.57 μM); interestingly, the activity was limited to kinases with small gatekeeper residues. Modeling of **29** based on the known binding mode of the pyrido[2,3-d]pyrimidin-7-one scaffold in c-Abl suggests the 2,6-dichlorophenyl motif binds to the hydrophobic back pocket with a high degree of complimentarily and that a steric clash would be apparent in this region should the kinase have a large gatekeeper residue. The reported SAR and structure of **7** bound to FGFR1 led the authors to postulate that
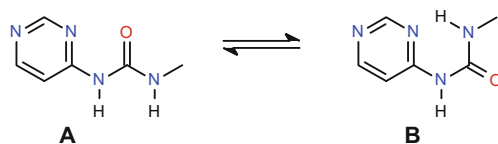
Fig. 15 Possible conformations for pyrimidinyl urea motif
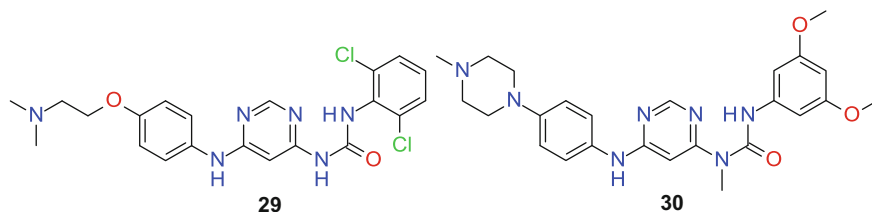
Fig. 16 Structure of pyrimidinyl ureas **29** and **30**

improved FGFR potency and selectivity might be achieved through the incorporation of a 3,5-dimethoxyphenyl motif into the pyrimidinyl urea scaffold and resulted in the identification of compound **30** (Fig. 16).

Compound **30** was a moderately potent inhibitor of FGFR3 in both a biochemical assay using constitutively active FGFR3-K650E kinase ($IC_{50} = 0.505$ μM) and a cell assay using an FGFR3-dependent BaF3 cell line ($IC_{50} = 1.5$ μM). A homology model of FGFR3 was also constructed to aid compound design. The authors appreciated the requirement for the 3,5-dimethoxyphenyl ring to adopt an orthogonal orientation with respect to the pyrimidine ring to best compliment the hydrophobic back pocket and so focused on molecular conformational. Ab initio calculations predict that **7** is likely to have a torsional angle of 127° between the 3,5-dimethoxyphenyl ring and the pyrido[2,3-d]pyrimidine ring when in a relaxed conformation in water and that an energy penalty of 0.5 kcal/mol would be required to access the perpendicular conformation observed in the binding mode (tortional angle of ~90°). In contrast, the 3,5-dimethoxyphenyl ring in compound **30** is predicted to be coplanar with the pyrimidinyl urea motif in the relaxed conformation (torsional angle of 180°) with an energy penalty of 1.5 kcal/mol required to access the postulated binding conformation. This energy difference arises from the higher deconjugation energy penalty for compound **30** compared to **7**, and the hypothesis is consistent with the observed reduction in potency. The introduction of *ortho*-substituents to the 3,5-dimethoxyphenyl ring was anticipated to reduce the deconjugation energy, and compound **31**, bearing *diortho*-substitution, was predicted to have a torsional angle of 109° in the relaxed conformation with an energy penalty of only 0.1 kcal/mol to access the postulated binding conformation. Compound **31** does indeed show significantly increased potency in both biochemical and cell assays. Modeling of **31** in the FGFR3 homology model suggests a tridentate interaction with the kinase hinge between the anilino NH, the adjacent pyrimidine nitrogen, and the pyrimidine C(2)-H as well as the potential for a water-mediated interaction between the urea carbonyl and the side chain of Lys508 (Lys514 in FGFR1). The optimized fit of the tetra-substituted phenyl ring was predicted to result in productive interactions between the methoxy substituent and Asp635 (Asp641 in FGFR1) as well as favorable hydrophobic interactions between the two chlorine atoms and the Val555 and Ala634 residues (Val561 and Ala640 in FGFR1). Interestingly, the latter residue is replaced by a larger cysteine in

VEGFR2, and the authors speculate that as a result of increased steric congestion an energy penalty might be incurred when the compound binds to VEGFR2.

The methyl group on the urea nitrogen can be replaced with either hydrogen or an ethyl substituent with little impact on potency, suggesting that there is minimal interaction between this substituent and the protein. The anilino substituent was postulated to occupy the solvent channel of the kinase and, as such, was anticipated to provide a handle to modulate the physicochemical and pharmacokinetic properties of the molecule. A range of anilino substituents could be tolerated, resulting in potent compounds such as **32** and **33**. Evaluation of compounds in a panel of cytochrome P450 (CYP450) drug-metabolizing enzymes highlighted the potential for many compounds from this scaffold to act as inhibitors. CYP450 inhibitors can alter the metabolism and exposure of coadministered compounds, which may in turn result in toxicity. Interestingly, compound **31** did not show inhibitory activity against any of the CYP450 enzymes tested (IC$_{50}$ >10 μM) and was hence selected for further profiling and given the corporate identifier BGJ-398. A crystal structure of BGJ-398 (**31**) bound to FGFR1 was obtained and found to validate the putative interactions suggested by the homology model of FGFR3 (Figs. 17 and 18).

More thorough testing revealed that **31** was an exceptionally potent inhibitor of FGFR1–3 (IC$_{50}$ ~0.001 μM) but was a significantly less potent inhibitor of FGFR4 (IC$_{50}$ = 0.060 μM) and VEGFR2 (IC$_{50}$ = 0.18 μM). Compound **31** was largely
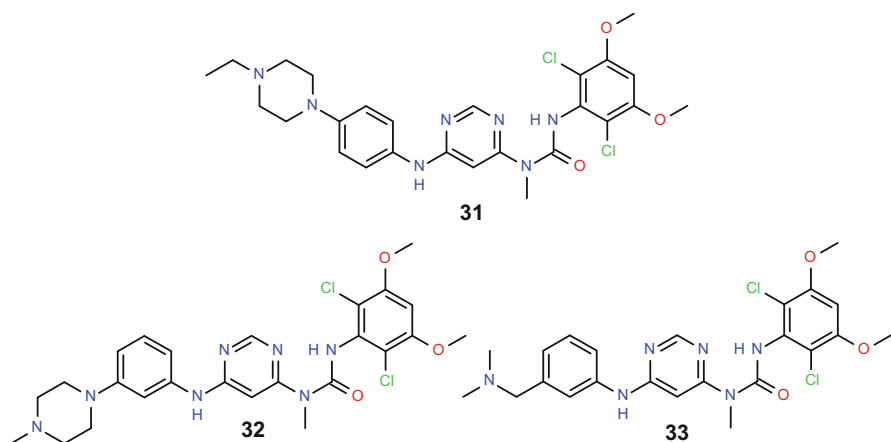
Compound	31	32	33
FGFR3-K650E IC$_{50}$ (μM)	0.005	0.009	0.019
BaF3-TEL-FGFR3 IC$_{50}$ (μM)	0.002	0.002	0.011

Fig. 17 SAR of pyrimidinyl ureas
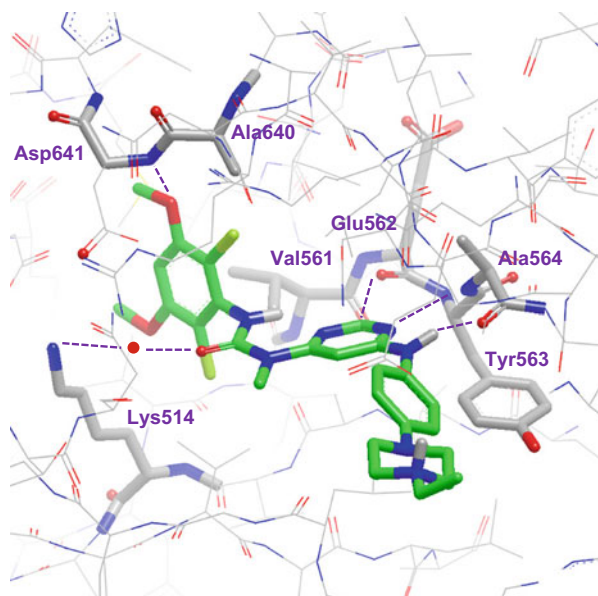
Fig. 18 Structure of **31** bound to FGFR1 (PDB accession code 3TT0) with hydrogen bonds highlighted in *magenta*

inactive when tested against a panel of 76 kinases with only KIT and LYN showing IC_{50} values below 1 μM. When tested against a panel of 31, BaF3 cell line **31** was highly potent in the FGFR1–3 lines (IC_{50} ~0.001 μM) but was approximately 400 times less active against VEGFR2 lines and inactive against most other lines. The compound displays high clearance and high volume of distribution in mouse and rat with moderate to good bioavailability and some evidence of increased exposure in tumor tissue compared to plasma. Efficacy was observed in orthotopic mouse xenograft models and subcutaneous rat xenograft models, and this was associated with in vivo knockdown of pFRS2 and pMAPK. It also inhibited bFGF-stimulated angiogenesis in a murine agar chamber model but had no effect on VEGF-stimulated angiogenesis, further demonstrating the selectivity for FGFR over VEGFR. Compound **31** was evaluated in a phase I study in patients with advanced solid tumors and is currently undergoing evaluation phase II trials in patients with solid tumors, glioblastoma multiforme, and melanoma.

3.5 *Pyrazolylaminopyrimidines and Pyrazolylbenzamides as FGFR Inhibitors*

Leach et al. have reported the early work undertaken with the laboratories of AstraZeneca toward the identification of selective FGFR inhibitors [23]. A

pyrazolylaminopyrimidine scaffold, exemplified by **34**, was identified from routine kinase selectivity screening as displaying increased potency against FGFR1 and VEGFR2 compared to IGF-1R, the biological target against which the scaffold had originally been optimized. A crystal structure of compound **34** bound into FGFR1 was obtained, and the authors note the high degree of similarity of the observed protein structure with those reported by other groups (Fig. 19). The equipotent nature of **34** against both FGFR1 and VEGFR2 suggested that binding sites of the two proteins are likely to be highly similar. The authors constructed a "map" of the binding site using the sequence alignment of the two proteins and used this map to identify the position of sequence differences between the two proteins within the binding site. They then postulate that by designing molecules which occupy these areas, it may be possible to exploit these differences to achieve selectivity. In particular, this highlights the Ala640 residue in FGFR1, which is replaced by Cys1043 in VEGFR2, and they note that the side chain of the residue lies in a constricted indentation at the base of the ATP pocket. The authors refer to this region as the "pit" and suggest that inhibitors that are able to effectively target this region may show selectivity for FGFR over VEGFR. When bound into FGFR1 compound **34** appears to make a tridentate donor-acceptor-donor interaction between the three nitrogens in the aminopyrazolyl motif and the kinase hinge. Two conformations are observed for the aminoethylpyridine motif illustrating the flexible nature of the aminoethyl linker, and while one of the observed conformations does position the pyridyl ring in the vicinity of the "pit," the authors speculate that the compound is sufficiently flexible to adapt to the VEGFR binding site, thus explaining the apparent lack of selectivity.

Fig. 19 Structure of **34** bound to FGFR1 (PDB accession code 4F63) with hydrogen bonds highlighted in *magenta*
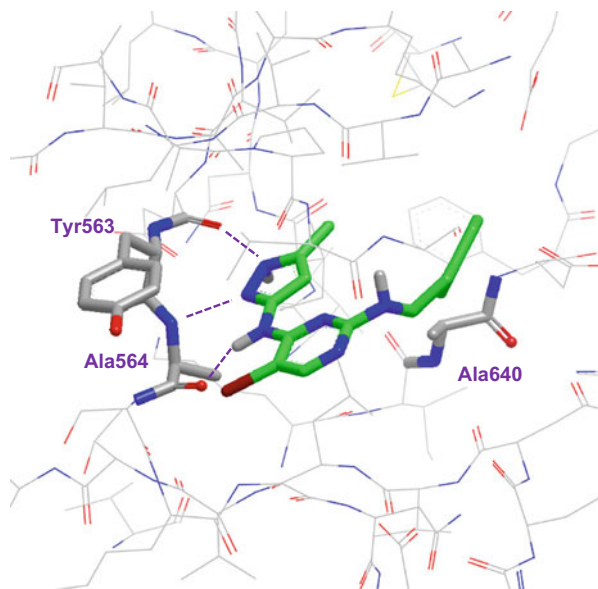
Compounds with more rigid linkers in this region of the molecule, such as **35**, do show a preference for binding to FGFR suggesting that the "pit" region can indeed be targeted to achieve selectivity. The crystal structure of a more soluble analogue of **35** bound into FGFR1 was obtained which showed the methyl of the isoxazole to be directed at Ala640 further supporting the hypothesis (Fig. 20).

Exploration of different regions of the molecule quickly established that the bromine could be removed with little impact on potency, **36**. This change is associated with a reduction in logP of approximately one unit, thereby demonstrating improved binding efficiency as measured by lipophilicity ligand efficiency (LLE). Comparison of the structures of both **34** and PD173074 (**7**) bound to FGFR1 suggested an opportunity to target the hydrophobic back pocket of the ATP-binding site by building from the 5-position of the pyrazole ring. The incorporation of a 3,5-dimethyoxyphenyl ring, known to have high complementarity to the back pocket in other scaffolds, linked to the pyrazole with a two-carbon spacer, resulted in compound **37** which shows a dramatic improvement in FGFR1 potency while retaining good selectivity over VEGFR2. However, despite the promising profile of **37**, the lipophilic nature of the compound resulted in poor aqueous
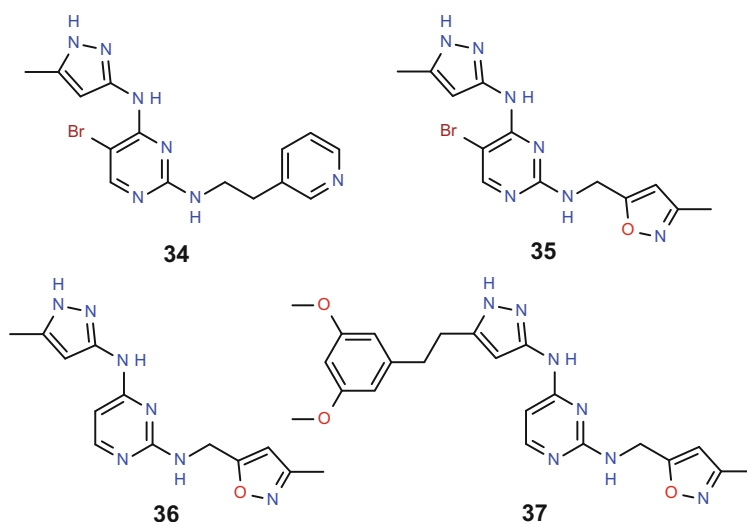
Compound	34	35	36	37
FGFR1 IC$_{50}$ (μM)	0.54	0.069	0.079	0.0018
VEGFR2 IC$_{50}$ (μM)	0.59	0.68	1.0	0.126
IGF-1R IC$_{50}$ (μM)	6.0	7.8	12.6	12.6

Fig. 20 SAR of pyrazolylaminopyrimidines

solubility (0.6 μM) and was felt to preclude the in vivo characterization of the compound.

The continued optimization of the scaffold within AstraZeneca has been described by Thomas et al. [24]. The requirement to identify compounds with reduced lipophilicity was appreciated, and the researchers looked to introduce a broad range of structural changes to the scaffold while maintaining the aminopyrazole hinge binder motif. These studies resulted in the identification of the pyrazolylbenzamide scaffold, exemplified by **38**. Compound **38** showed promising activity against FGFR1 in a biochemical assay and inhibited the phosphorylation of FGFR in Cos-1 cells transfected with FGFR1. Once again significant improvements in potency and selectivity were observed by successfully targeting the hydrophobic back pocket, for example, compound **39**. Attempts to further optimize this region of the molecule were largely unsuccessful, thereby suggesting that the identified substituent was achieving an optimal interaction with the hydrophobic back pocket (Fig. 21).

A crystal structure of compound **39** bound in to FGFR1 showed the *N*-methylpiperazinyl unit to be situated in the solvent channel of the kinase and thus
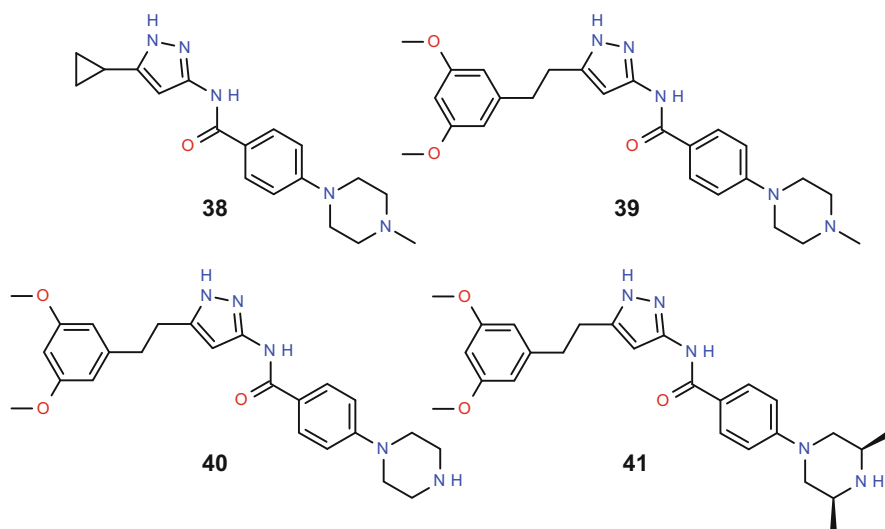
Compound	38	39	40	41
FGFR1 IC$_{50}$ (μM)	0.066	0.0007	0.0009	0.0002
Cos-1 pFGFR1 IC$_{50}$ (μM)	0.61	0.019	0.017	0.013

Fig. 21 SAR of pyrazolylbenzamide scaffold

might provide an opportunity to modulate physicochemical and pharmacokinetic properties. More detailed profiling of **39** revealed high clearance of the compound in rat hepatocyte incubations (Cl_{int} = 60 µL/min/10^6 cells) and in rat in vivo pharmacokinetic studies (Cl = 46 mL/min/kg). Metabolite identification studies highlighted significant N-demethylation and N-oxidation of the N-methylpiperazinyl functionality. The high clearance of the compound, driven by metabolism of the N-methylpiperazinyl motif, limited the oral bioavailability of the compound. The strategies adopted to lower clearance included the removal of the N-methyl on the piperazine ring as well as reducing the potential of the piperazine to undergo both N-oxidation and N-dealkylation by increasing the pK_a, thereby increasing the fraction of the basic center existing in a protonated form. Removal of the N-methyl group, **40**, was well tolerated and did result in a reduction of clearance in both in vitro rat hepatocyte incubations (Cl_{int} = 12 µL/min/10^6 cells) and in rat in vivo pharmacokinetic studies (Cl = 23 mL/min/kg); however, oral bioavailability in rat was low (3%) presumably due to compromised permeability. The optimization goal was therefore to balance reduced clearance with acceptable permeability. The introduction of methyl groups to sterically "mask" the hydrogen bond donor, while concurrently increasing lipophilicity, resulted in the discovery of compound **41**, subsequently given the corporate identifier AZD4547, which retains excellent potency against FGFR1 in biochemical and cell assays while displaying low clearance in in vitro rat hepatocyte incubations (Cl_{int} = 11 µL/min/10^6 cells) and in rat in vivo pharmacokinetic studies (Cl = 16 mL/min/kg) and good oral bioavailability in rat (54%). Gavine et al. report on the detailed pharmacological profiling of AZD4547 (**41**) and show the compound to be an extremely potent inhibitor of FGFR1–3 in biochemical assays (IC_{50}'s = 0.0002 µM, 0.0025 µM and 0.0018 µM, respectively) but less active against FGFR4 (IC_{50} = 0.165 µM). A similar profile was observed when looking at the inhibition of phosphorylation of FGFR in Cos-1 cells transfected with FGFR1–4 (IC_{50}'s = 0.013 µM, 0.002 µM, 0.040 µM and 0.142 µM, respectively). AZD4547 (**41**) showed reduced activity for the inhibition of phosphorylation of VEGFR2 in HUVEC cells (IC_{50} = 0.258 µM) and showed excellent selectivity when tested against a broad panel of kinases. AZD4547 (**41**) has potent in vitro antiproliferative effects on tumor cell lines with dysregulated FGFR expression, such as the FGFR3 driven KMS11 cell line, but was inactive in over 100 additional tumor cell lines. This result is believed to indicate that the antiproliferative effects observed are driven by FGFR inhibition rather than any nonspecific cytotoxicity. AZD4547 (**41**) showed dose proportional antitumor efficacy in KMS11 xenograft models with concurrent pharmacodynamic modulation of FGFR phosphorylation. AZD4547 (**41**) did not induce any significant changes in blood pressure in conscious telemetered rats at in vivo exposure levels equivalent to those observed to give efficacy in mouse xenograft models. This observation supports the suggestion that at these efficacious doses there is no significant in vivo activity against VEGFR2 [25]. At the time of writing, AZD4547 (**41**) was being evaluated in phase II clinical trials in patients with solid tumors.

3.6 Indazoles as FGFR Inhibitors

Zhoa et al. have reported the discovery of a potent and selective inhibitor of FGFR from the laboratories of Eli-Lilly and Company, LY2874455 (**42**). Compound **42** is based on a novel indazole scaffold [26]. While the detailed SAR investigations which result in the discovery of **42** have yet to be released, a binding mode of the compound in a homology model of FGFR3 has been proposed based on crystal structures of close analogues bound to an FGFR3 construct. The proposed binding mode appears to show the indazole motif forming a key bidentate interaction with the kinase hinge region, while the 5-(1-(3,5-dichloropyridin-4-yl)ethoxy) substituent appears to head toward the region of the ATP-binding site previously described as the "pit" and makes an interaction between the pyridinyl nitrogen and the protein. The 2-vinylpyrazolyl motif appears to be positioned in the solvent channel and therefore may have provided the researchers with an opportunity to modulate physicochemical and pharmacokinetic properties. In the binding mode presented, the molecule does not appear to exploit the hydrophobic back pocket which has been a common feature in many of the previously reported selective FGFR inhibitors (Fig. 22).

LY2874455 (**42**) is reported to inhibit all four isoforms of FGFR to a similar degree in a biochemical assay (IC_{50}'s = 0.0028 μM, 0.0026 μM, 0.0064 μM, and 0.006 μM, for FGFR 1–4, respectively), in contrast to many of the selective FGFR inhibitors reported that show a preference for FGFR1–3. However, **42** is also a potent inhibitor of VEGFR2 in biochemical assays (IC_{50} = 0.007 μM). The authors state that the lack of high quality antibodies against pFGFRs has hampered their attempts to measure the impact of **42** on the phosphorylation of the individual FGFR isoforms in cellular systems. However, the compound was shown to inhibit the FGF2- and FGF9-stimulated phosphorylation of ERK in HUVEC and RT-112 cells (average IC_{50} between 0.3 and 0.8 nM) as well as showing potent antiproliferative effects in the FGFR3 driven KMS11 and OPM-2 cell lines (IC_{50}'s = 0.57 and 1.0 nM, respectively). LY2874455 (**42**) inhibits both FGF2- and VEGF-induced tube-forming activities in an assay (IC_{50}'s = 0.0006 and 0.0036 μM, respectively). A similar preference (six- to ninefold) for **42** to inhibit FGF-induced signaling in vivo over VEGF-induced signaling was observed in an

Fig. 22 Structure of LY2874455

42
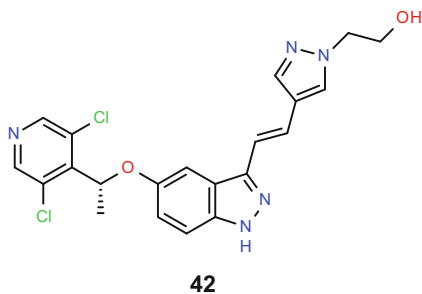
IVTI assay to measure VEGFR-2 phosphorylation in the heart tissues of mice, suggesting a potential margin between FGFR-mediated effects and VEGFR-mediated effects exists in vivo. Compound **42** was reported to cause a significant regression of tumor growth in RT-112, SNU-16, and OPM-2 tumor xenograft models at doses of 3 mg/kg bid. At the time of writing, **42** had now completed a phase I clinical trial in patients with advanced cancer.

3.7 Imidazopyridine-Based Inhibitors of FGFR

Astex Therapeutics has also developed a series of selective FGFR inhibitors. Squires et al. have reported the use of fragment screening, using a combination of nuclear magnetic resonance spectroscopy, thermal denaturation, and X-ray crystallography, to identify low-molecular-weight hits with good binding affinity [27]. This approach resulted in the identification of compound **43**, which shows relatively low potency against FGFR3 in a biochemical assay (IC$_{50}$ = 120 μM). However, when the size of **43** is taken into account using a parameter such as ligand efficiency, the compound can be seen to bind to FGFR3 with an encouraging efficiency of 0.38 kcal/heavy atom. The crystal structure of **43** bound to FGFR1 highlighted a single hydrogen-bonding interaction between the imidazopyridine N1 and the backbone NH of Ala564 in the hinge region of the kinase. The binding mode of **43** also suggested the opportunity to replace the 3-chloro substituent with an aromatic ring thereby allowing the possibility of interactions with the side chain of Asp641 as well as with Ala640. The binding mode also suggested that 7-substitution would be more optimal than 6-substitution. The authors appreciated that interaction with Ala640 may result in improved selectivity, especially against VEGFR2, which possesses a larger residue in this position (Fig. 23).
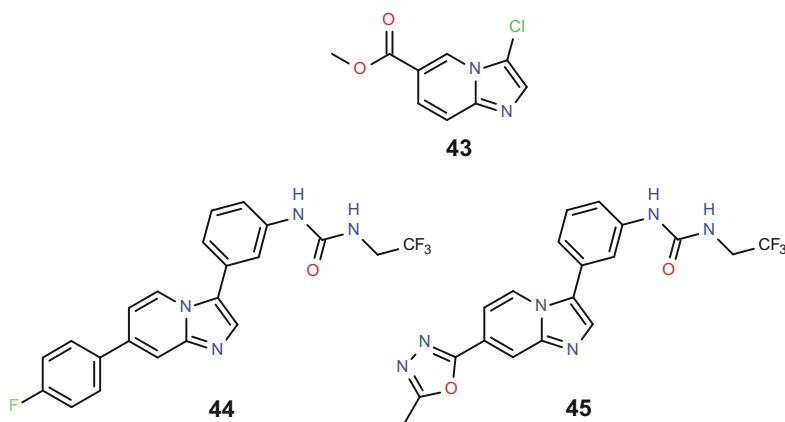
Fig. 23 Structure of imidazopyridine FGFR inhibitors

Although detailed SAR investigations for this scaffold have yet to be published, the structure-based design resulted in the identification of urea-containing compounds, such as **44**, which showed good potency against FGFR1–4 (IC_{50}'s = 0.013 μM, 0.033 μM, 0.003 μM, and 0.034 μM, respectively) and moderate selectivity over VEGFR1-3 (IC_{50}'s = 0.013 μM, 0.100 μM, and 0.068 μM, respectively). A crystal structure of **44** bound into FGFR1 highlighted good surface complementarity of the 7-aryl substituent with the protein and also indicated that the urea group forms an interaction between the two urea NHs and the carboxylate of Asp641. The urea carbonyl also appears to be involved in a water-mediated interaction with the side chain of Arg627. Interestingly, the authors note that the positioning of Arg627 is shifted with respect to its position in other FGFR1 structures. The importance of the urea group on both FGFR potency and selectivity is stated to be apparent from the detailed SAR (data not disclosed), and the authors speculate that the unusual positioning of Arg627 may contribute to the selectivity observed. Further optimization of the scaffold, playing particular attention to the reduction of lipophilicity, resulted in the identification of compound **45**. Compound **45** shows good potency against FGFR1–4 (IC_{50}'s = 0.078 μM, 0.066 μM, 0.015 μM, and 0.094 μM, respectively) and selectivity over VEGFR1-3 (IC_{50}'s = 0.44 μM, 0.38 μM, and 0.32 μM, respectively). Compounds **44** and **45** both show antiproliferative effects in BaF3 cell lines engineered to express constitutively active forms of FGFR1, 3, and 4 and were also shown to inhibit the phosphorylation of FGFR3 in KMS11 cells. Compounds **44** and **45** both exhibit high bioavailability in mice (79% and 100%, respectively) and are efficacious in FGFR-dependent tumor xenograft models but show no efficacy in FGFR-independent models.

3.8 Quinoxaline- and Naphthyridine-Based Inhibitors of FGFR

Scientists at Astex Therapeutics, in conjunction with scientists at Janssen Pharmaceutica, utilized fragment screening approaches to design novel, highly potent compounds, which were subsequently screened in vivo using a BaF3-FGFR3 xenograft model. This in vivo screening approach resulted in the identification of the pyrazolyl quinoxaline compound JNJ-42756493 (**46**) [28], which is a potent inhibitor of all 4 FGFR isoforms in biochemical assays (FGFR1, 2, and 4 IC_{50}'s all <0.001 μM, FGFR3 IC_{50} = 0.001 μM) with reduced activity against PDGFRβ and VEGFR2 (IC_{50}'s = 0.0036 μM and 0.0059 μM, respectively) and good selectivity when tested against a commercial panel of 450 different kinases. JNJ-42756493 (**46**) has potent inhibitory activity in a range of cell models harboring activating FGFR alterations, including Kato III, SNU-16, RT-112, and KMS-11 models (IC_{50}'s = 0.06 nM, 0.37 nM, 1.1 nM, and 0.0276 μM, respectively) and is active in a range of standard and patient-derived xenograft models. Compound **46** induced prolonged target inhibition in in vitro washout experiments, and it has been

postulated that the basic nature of the compound results in the retention of the compound in the more acidic environment of the cellular lysosomes. This effect may also result in the cellular accumulation of the compound and might account for the differential tissue distribution observed following oral administration to rats. Although there has currently been no publication outlining the medicinal chemistry optimization of **46**, a crystal structure of the compound bound to FGFR1 shows the 3,5-dimethoxyphenyl moiety to bind in the selectivity pocket, and the nitrogen in the 4-position of the quinoxaline ring makes an interaction with the hinge region of the kinase. The pyrazolyl moiety in the 2-position of the quinoxaline ring appears to head out to a solvent-exposed region, and the alkyl amine chain makes an interaction with an aspartic acid residue in the selectivity pit region of the molecule. Compound **46** has been investigated in a phase I clinical trial in patients with advanced solid tumors where it is reported to have been safe, with manageable side effects, at dose levels that elicit antitumor activity (Fig. 24).

Later disclosures from the group highlight the discovery of potent inhibitors of FGFR based on similar compounds with a pyrazolyl naphthyridine scaffold, such as **47** [29, 30]. In contrast to **46**, **47** does not appear to be retained in the lysosomes, and there is no evidence of cellular accumulation. Compound **47** is reported to show a more even distribution of compound between plasma and lung tissue when compared to **46**. Patent literature from this group also highlights the potential to cyclize the aminoalkyl chain onto the 3,5-dimethoxyphenyl moiety to give compounds such as **48**, although potency against FGFR appears reduced [31].
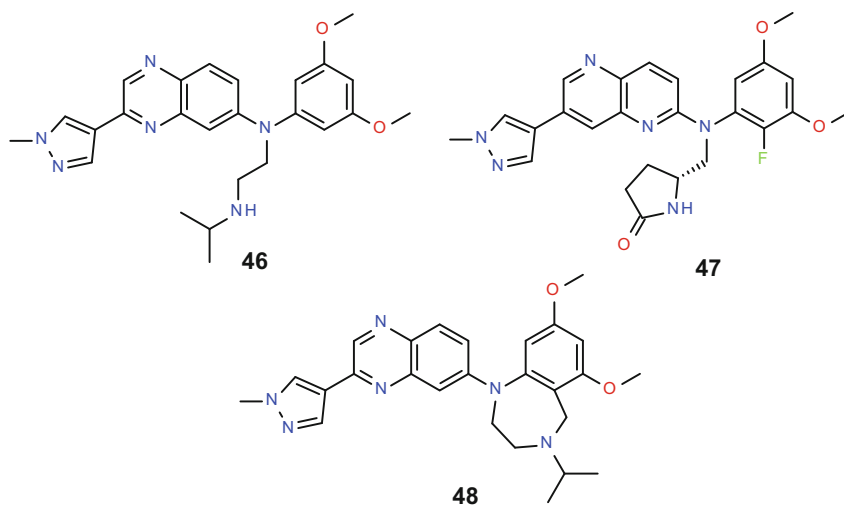
Fig. 24 Structure of quinoxaline and naphthyridine FGFR inhibitors

3.9 Aminopyrazolyl Inhibitors of FGFR

The development of selective FGFR1–3 inhibitors based on a novel aminopyrazolyl scaffold has been described by scientists at Debiopharm International in conjunction with scientists at Chugai [32, 33]. A high-throughput screening campaign resulted in the identification of **49**, a moderately potent inhibitor of FGFR with similar potency against closely related kinases such as VEGFR2 and Src. A crystal structure of **49** bound into FGFR1 highlighted an interaction between both the carbonyl and the amino substituent with the hinge region of the kinase. The structure also highlighted the potential to target additional π–π interactions between the inhibitor and Tyr566 and also the potential to access the back pocket to improve FGFR selectivity. Replacement of the methylphenyl ring with an azaindole group resulted in the discovery of **50**, which shows a significant increase in kinase activity although a similar selectivity profile. Interestingly, these compounds appear to inhibit FGFR1–3 to a greater extent than FGFR4, which has also been observed with previously reported FGFR inhibitors. In addition to additional π–π interactions with Tyr566, this azaindole moiety also participates in an additional hydrogen bond interaction with the kinase hinge. While seeking improvements in kinase selectivity, the authors also appreciated the need to improve the solubility (20 μg/mL in simulated intestinal fluid) and metabolic stability ($Cl_{int} = 15$ μL/min/mg in human microsome incubations) of **50** in order to find a compound suitable for clinical development. A variety of basic functionality is reported to be tolerated when attached to the 5- or 6-positions of the azaindole ring, and while improvements were seen in both kinase activity and solubility, these improvements were offset by increased turnover in human microsome incubations. The importance of the phenolic functionality was also highlighted with its removal resulting in a significant reduction in potency resulting in the authors examining known phenol isosteres such as benzimidazole. Replacement of the phenol ring with a benzimidazole ring was tolerated, and, in particular, replacement with a methylbenzimidazole moiety gave improved FGFR activity and a significant improvement in selectivity, for example, **51**. The authors suggest that the high levels of selectivity observed for **51** are derived from an interaction with Met535 which is unique among the previously reported FGFR inhibitors. In addition to selectivity over closely related kinases, compound **51** displays high levels of selectivity when assessed in a commercially available panel of 442 kinases and was subsequently given the corporate identifier of CH5183284 (also referred to as Debio 1347). The solubility of CH518284 (**51**) in FaSSIF remains modest (19 μg/mL), but the compound shows significantly improved stability in human microsomal incubations ($Cl_{int} = 0.16$ μL/min/mg) and shows good oral exposure in both rat and monkey following oral administration. Further improvements in both potency and solubility were obtained following the addition of a weakly basic morpholine unit to give compound **52**; however, despite the stability of the compound in human microsomal incubations ($Cl_{int} = 0.87$ μL/min/mg), the compound shows significantly lower exposure in rat and monkey studies (Fig. 25).

Fig. 25 Structure of aminopyrazolyl FGFR inhibitors
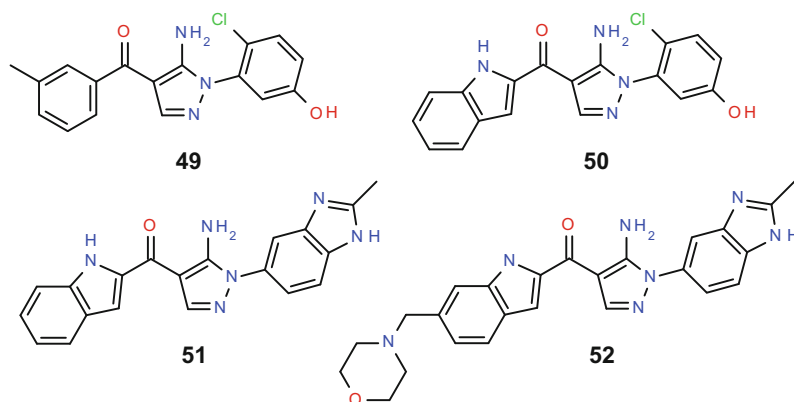
Compound	49	50	51	52
FGFR1 IC$_{50}$ (μM)	1.9	0.13	0.0093	0.0015
FGFR2 IC$_{50}$ (μM)	0.94	0.03	0.0076	0.0036
FGFR3 IC$_{50}$ (μM)	7.4	0.025	0.022	0.0035
FGFR4 IC$_{50}$ (μM)	4.1	0.20	0.29	0.013
VEGFR2 IC$_{50}$ (μM)	2.9	0.028	2.1	0.12

Western blot analysis shows that CH518284 (**51**) can potently inhibit the phosphorylation of FGFR1–3 in cells but that it has significantly reduced activity against FGFR4, VEGFR2, and PDGFRβ. Compound **51** shows strong antiproliferative activity against a range of cancer cell lines harboring genetic alterations in FGFR and activity in a range of xenograft models which also harbor genetic alterations in FGFR. At doses similar to those shown to be efficacious in certain xenograft models, **51** shows little impact on the in vivo diastolic blood pressure in rats and has no effect in an in vitro VEGF-induced tube-forming assay at concentrations of 1 μM. The authors also report that **51** shows activity in both in vitro and in vivo models of a relevant FGFR2 gatekeeper mutant (V564F), and they speculate that this may differentiate the compound from other FGFR inhibitors reported. At the time of writing, CH518284 (**51**) was undergoing phase I clinical evaluation in selected patients harboring genetic alterations in FGFR.

3.10 Selected Other FGFR Kinase Inhibitors

A wide variety of additional ATP-competitive inhibitors of FGFR have been reported but with only limited details on the structure and medicinal chemistry discovery disclosed. A brief description of the available data for a selection of compounds which have recently entered clinical investigation is reported below.

Scientists at Bayer have recently disclosed BAY 1163877, a potent and selective inhibitor of FGFR1–3 kinase activity with oral exposure [34, 35]. BAY1163877 is reported to potently inhibit the activity of FGFR1–3 in biochemical assays (IC$_{50}$'s = 0.011 μM, <0.001 μM, and 0.0185 μM, respectively) while showing good levels of selectivity when tested against a panel of 222 kinases. BAY 1163877 is reported to inhibit the proliferation of various cancer cell lines in vitro and to show in vivo efficacy in a range of xenograft models presenting at least one FGFR alteration. In the PDX HN9897 model, shown to over express FGFR3, efficacy was observed at doses of 35 and 50 mg/kg bid. BAY 1163877 is reported to be in phase 1 clinical trials, and while no structure has yet been disclosed for this molecule, a number of patents have recently been published disclosing a series of pyrrolo[2,1-f] [1,2,4]triazin-4-amine-based inhibitors of FGFR, exemplified by **53**, **54**, and **55** [36–38]. It is therefore possible that BAY 1163877 may be contained within these publications. Comparison of these published structures with those of known FGFR inhibitors would suggest that the triazine-amine portion of the molecule is likely to be involved in the key interaction with the kinase hinge, while the substitution pattern on the benzothiophene moiety is similar to that observed with many substituents often located in the back pocket (Fig. 26).

The discovery of the amidopyridyl compound E7090 (**56**) has recently been disclosed by scientists from the laboratories of Eisai [39]. Compound **56** is a potent and selective inhibitor of FGFR1–3 currently in early clinical studies. It is active against FGFR1–3 in biochemical assays (IC$_{50}$'s = 0.0007 μM, 0.0005 μM, and 0.0012 μM, respectively) but shows reduced activity against both FGFR4 and VEGFR2 (IC$_{50}$'s = 0.12 μM and 0.016 μM, respectively). While the medicinal

Fig. 26 Examples of pyrrolo[2,1-f] [1,2,4]triazin-4-amine-based FGFR inhibitors described in WO 2013124316, WO2013087578, and WO 2013087647

chemistry which resulted in the discovery of **56** has yet to be disclosed, comparison with other kinase inhibitors suggests that the pyridyl amide motif is likely to bind to the kinase hinge, while the hydroxyethyl piperidine moiety is likely to be positioned in the solvent channel. Interestingly, **56** is one of the few selective FGFR inhibitors reported which does not utilize a 3,5-disubstituted aryl motif to bind into the back pocket. Compound **56** appears to be broadly selective for FGFR1–3 when tested in a panel of 93 kinases. Compound **56** inhibits the proliferation of various cancer cell lines harboring alterations to FGFR, for example, SNU-16 and KMS-11 (IC_{50}'s = 0.003 μM and 0.008 μM, respectively), while having lower activity in VEGFR-stimulated HUVEC cells (IC_{50} = 0.19 μM). E7090 (**56**) is active in a range of xenograft models, including SNU-16 where the activity is associated with inhibition of phosphorylation of FGFR2 and elevation of plasma FGF23 levels, and has shown improved survival times in a 4T1 lung metastasis model in mice (Fig. 27).

Scientists at Incyte Corporation Inc. have recently reported the discovery of a selective inhibitor of FGFR1–3. The inhibitor, INCB54828, is a potent inhibitor of FGFR1–3 in biochemical assays (IC_{50}'s = 0.0004 μM, 0.0005 μM, and 0.001 μM, respectively) but with reduced activity against both FGFR4 and VEGFR2 (IC_{50}'s = 0.030 μM and 0.071 μM, respectively) [40]. INCB54828 was shown to be a selective inhibitor of FGFR when tested against a panel of 161 kinases and inhibited the phosphorylation of FGFR in KATO-III cells with an IC_{50} of 0.0003 μM. INCB54828 selectively inhibited the growth of cancer cell lines in which FGFR was activated, such as KATO-III and RT-112 (GI_{50}'s = 0.003 μM and 0.007 μM, respectively), and has shown efficacy in KATO-III and RT-112 xenograft models at doses of 0.3 and 1 mg/kg qd. INCB54828 is currently undergoing a clinical phase I study. While the unique structure of INCB54828 has yet to be disclosed, a generalized scaffold has been presented (**57**). Recent patent publications from Incyte have disclosed a number of closely related FGFR inhibitors (exemplified by **58**) [41, 42]. Comparison of these structures with those of known FGFR inhibitors suggests that the azaindole/azabenzimidazole core of INCB54828 is likely to be involved in a bidentate interaction with the kinase hinge, while the
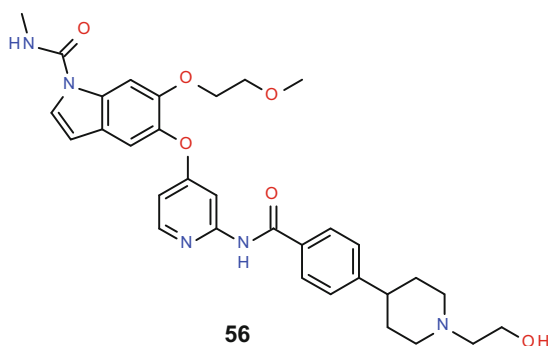
Fig. 27 Structure of E7090
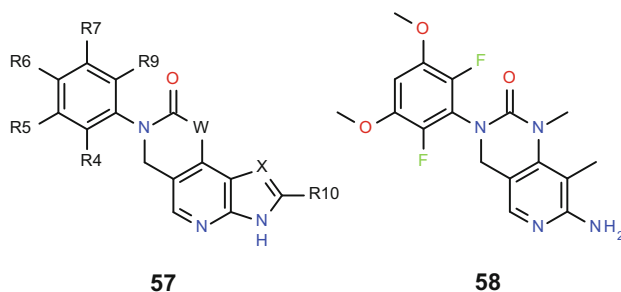
Fig. 28 Generalized structure of INCB54828 (**57**) and representative compound from WO 2014172644 (**58**)

3,5-dimethoxy substituents exemplified in the patents suggest that this pendant phenyl ring is likely to occupy the back pocket. The R^{10} substituent is likely to be positioned such that it could access the solvent channel and may therefore provide an opportunity to modulate the physicochemical and pharmacokinetic properties of the molecule in addition to the binding affinity (Fig. 28).

4 Irreversible Inhibitors of FGFR

A different approach to the identification of selective FGFR inhibitors has been described by Gray et al. from the Dana-Farber Cancer Institute, Harvard Medical School, working in collaboration with researchers at the Scripps Research Institute and the Massachusetts General Hospital Cancer Center. The approach described involved the design of compounds to inhibit FGFR in an irreversible manner [43]. Irreversible inhibitors developed to date usually possess electrophilic functionality, often α,β-unsaturated carbonyls such as acrylamides, to react with nucleophilic thiol groups on cysteine residues in a binding site. Irreversible inhibitors can exploit both the inherent selectivity resulting from non-covalent binding interactions, in addition to the requirement for a protein to possess a suitably located cysteine residue, to achieve high levels of selectivity. The authors identified a suitable cysteine present at the rim of the *P*-loop in FGFR1 (Cys486), which is conserved across all four FGFR isoforms and thus looked to develop irreversible inhibitors targeting this residue. In addition to increased selectivity, it was also appreciated that the kinetics of irreversible binding may, in part, overcome issues with suboptimal pharmacokinetics, such as rapid clearance, which may have limited the efficacy of other FGFR inhibitors described.

Careful inspection of the published crystal structure of PD173074 (**7**) bound to FGFR1 identified the Cys486 residue to be located was approximately 10 Å from the pyridine nitrogen of **7**. The authors selected a related pyrimido[4,5]pyrimidine scaffold and introduced a phenyl ring bearing a *meta*-acrylamide group to the pyridine nitrogen to give compound **59**. Compound **59** binds to FGFR1 but shows

a 300-fold reduction in antiproliferative activity compared to **7** in assays using BaF3 cells transfected with FGFR1. The authors postulate that electrophilic functionality in **59** was not optimally positioned to form a covalent bond with the cysteine and instigated the investigation of alternate linking groups. The inclusion of a methylene group between the nitrogen and the phenyl ring resulted in compound **60** which shows improved potency. Computational modeling suggests that the β-carbon of the acrylamide unit in **60** is positioned 2.9 Å from Cys486, a distance considered suitable for covalent bond formation. The authors were able to utilize previously disclosed SAR studies from other scaffold to rapidly design FIIN-1 (**61**), which contains a 2,6-dichloro-3,5-dimethoxyphenyl ring anticipated to better fill the hydrophobic back pocket of the binding site. FIIN-1 (**61**) showed potent antiproliferative activity in BaF3 cells transfected with either FGFR1 or FGFR3. The reduced compound, FRIN-1 (**62**), which is unable to form a covalent bond with Cys486, was observed to be significantly less potent in these assays thus suggesting a functional importance for the acrylamide unit (Fig. 29).
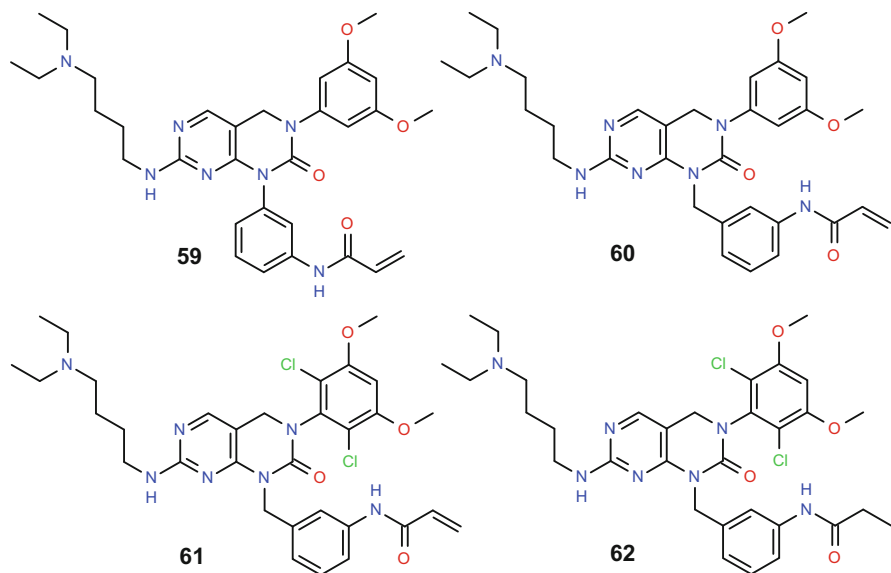
Compound	**59**	**60**	**61**	**62**
BaF3-FGFR1 IC$_{50}$ (μM)	1.5	0.40	0.014	0.34
BaF3-FGFR3 IC$_{50}$ (μM)	-	-	0.010	1.04

Fig. 29 SAR of irreversible inhibitors of FGFR

The selectivity of FIIN-1 (**61**) was investigated against a panel of 402 different kinase-binding assays using the Ambit KinomeScan technology at a concentration of 10 μM, and dissociation constants (K_D's) were determined for those kinases which were displaced to greater than 90% of the DMSO control. Compound **61** was seen to bind strongly to FGFR1–3 (K_D's = 0.0028 μM, 0.0069 μM and 0.0054 μM, respectively) but was significantly less potent against FGFR4 (K_D = 0.12 μM). Only two other kinases were found to have K_D values below 0.1 μM; these were Blk (0.065 μM) and Flt1 (0.032 μM). FIIN-1 (**61**) is reported to exhibit good selectivity over kinases such as c-Src, TNK1, and YES which have cysteine residues located in the same region of the binding site. Together these results indicate that **61** is a potent and selective inhibitor of FGFR1–3. Interestingly, similar biochemical potency was observed for FRIN-1 (**62**) against FGFR1–4 (K_D = 0.0031 μM, 0.0056 μM, 0.0054 μM, and 0.28 μM, respectively) suggesting that the majority of the binding energy arises from non-covalent interactions within the binding site. Washout experiments in MCF10A cells demonstrate that **61** gives sustained inhibition of phosphorylation of both FGFR1 and ERK1/2 following washout of the drug, consistent with the proposed mechanism of irreversible inhibition. In contrast, similar experiments with either **7** or **62** demonstrate that inhibitory activity is almost completely eradicated by the washout procedure suggesting these agents act in a reversible manner. Further evidence supporting the covalent binding of **61** was developed by synthesizing biotinylated versions of both FIIN-1 (**61**) and FRIN-1 (**62**). These biotinylated analogues maintained cellular potency and FIIN-1-biotin, but not FRIN-1-biotin was found to covalently label FGFR1. Furthermore, FIIN-1-biotin was shown to covalently label wild-type FGFR1 but not an FGFR1C486S construct supporting the initial hypothesis that Cys486 is the site of covalent modification.

5   Isoform-Selective FGFR Inhibitors

Although significant progress has been made in identifying FGFR inhibitors devoid of broad spectrum kinase activity and with promising selectivity over closely related growth factor receptor tyrosine kinases, such as VEGFR2, identifying compounds which display selectivity between the individual isoforms of FGFR remains a challenge. Given the high degree of homology between the ATP-binding sites of the four FGFR isoforms, it is perhaps not surprising that the inhibitors discussed so far have shown a pan-FGFR profile; although it is worth noting that a number of the more selective pan-FGFR inhibitors developed to date actually show a preference for FGFR1–3 over FGFR4. It has been widely postulated that the ability to selectivity inhibit a single isoform of FGFR may result in compounds with improved therapeutic margins. In particular, there is evidence that inhibition of FGFR1 is associated with mineralization in preclinical models and may cause dose-limiting effects in the clinic [44].

5.1 FGFR4-Selective Inhibitors

The preferential inhibition of FGFR1–3, displayed by many compounds including BGJ-398 (**31**), AZD4547 (**41**), and FIIN-1 (**61**), has been appreciated by a number of groups who suggest such compounds may be unsuited to treat FGFR4-mediated disease as a result of the concomitant FGFR1–3-mediated pharmacology. FGFR4 is overexpressed in several cancers including colon, liver, breast, and prostate, although the role of FGFR4 in cancer is yet to be fully elucidated [45]. FGFR4 has also been implicated in rhabdomyosarcoma (RMS) in which mutations have been identified in 7–8% of RMS tumors, and high expression of FGFR4 is associated with poor prognosis [46]. More recently evidence has emerged demonstrating a key role for FGFR4 in hepatocellular cancer (HCC). FGF19 has unique specificity for FGFR4, and hence the FGFR4 receptor is considered the principal controller of FGF19 signaling. For FGF19 to bind to FGFR4, an additional transmembrane protein β-Klotho is required. High expression levels of both FGFR4 and β-Klotho are seen in the liver thereby strengthening the evidence that the FGFR4–FGF19 signaling axis is a key driver in HCC. Recent results have shown that in preclinical models of HCC, an FGFR4-neutralizing antibody inhibits tumor formation and development in FGF19 transgenic mice, thus suggesting the potential for FGFR4 inhibition to have therapeutic utility [47].

Pike et al. have described the work undertaken within the laboratories of AstraZeneca to identify selective small molecule inhibitors of FGFR4 [48]. When screening approaches failed to identify FGFR4-selective chemical equity within the existing AstraZeneca compound collection, the researchers looked to adopt a strategy of structure-guided drug design. Detailed inspection of the ATP-binding sites in the different FGFR isoforms highlighted a number of subtle differences in the residues lining the solvent channel of FGFR4 compared with FGFR1–3. A more significant difference was observed in the hinge region of the kinase where a bulky tyrosine residue in FGFR1–3 (Tyr563 in FGFR1) is replaced with a smaller cysteine residue in FGFR4 (Cys552 in FGFR4). The authors hypothesized that compounds that protrude into these regions may display differential binding to the individual isoforms thereby delivering compounds with selectivity for FGFR4. Interestingly, only five other kinases in the kinome contain a cysteine in this position suggesting that an FGFR4-selective inhibitor may also show excellent selectivity against a broad spectrum of kinases. For the optimization of such compounds, the authors selected an imidazopyridine scaffold which was known to bind to FGFR from in-house kinase selectivity screening. A crystal structure of compound **63** bound into FGFR1 highlights a key interaction between the imidazopyridine N1 and Ala564 in the kinase hinge region. In addition, hydrogen-bonding interactions are seen between Asp641 and both the terminal amide group and aminopyrazine NH. The aminoamide aryl substituent is positioned in a hydrophobic pocket under the *P*-loop, and the orientation is controlled by the chirality of the terminal substituents. Importantly, while compound **63** shows no inherent selectivity for FGFR4, in fact it shows a preferential inhibition of FGFR1

in biochemical assays and preferential inhibition of phosphorylation of FGFR in Cos-1 cells transfected with either FGFR1 or FGFR4; the imidazopyridine scaffold was appreciated to contain suitable vectors for substitution to target the identified differences in both the solvent channel and the hinge region of the protein.

While substitution on the 6-position of the imidazopyridine ring could indeed access the solvent channel and result in increased kinase potency, no evidence of FGFR4 selectivity was observed (data not shown). Substitution at the 7-position of the imidazopyridine ring was envisaged to position substituents in close proximity to the kinase hinge with the potential to exploit the presence of the less bulky cysteine residue in FGFR4. However, despite the potential extra space in the hinge region of FGFR4, it was appreciated that additional steric bulk in this region might adversely affect the interaction between the imidazopyridine N1 and the kinase hinge thus resulting in an erosion of kinase activity (Fig. 30).

The introduction of small substituents such as fluoro, **64**, or cyano, **65**, was observed to reduce potency against FGFR4, albeit the impact was moderate. Interestingly, FGFR1 potency was eroded to a much greater extent, supporting the hypothesis that FGFR1 is less able to accommodate steric bulk in this region. As
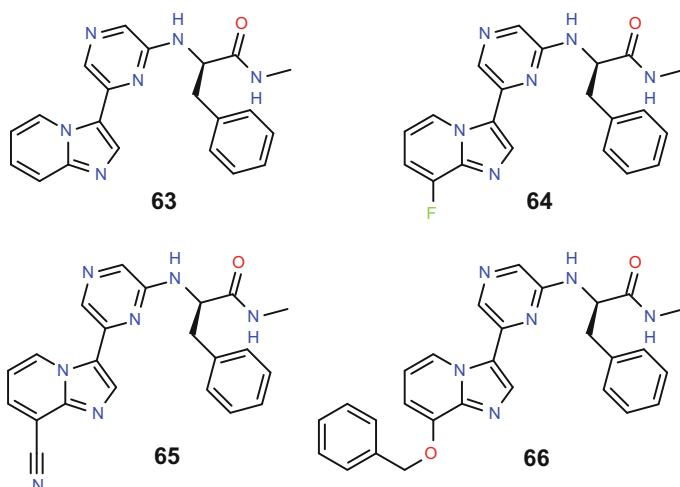
Compound	63	64	65	66
FGFR1 IC$_{50}$ (μM)	0.025	0.059	1.33	3.88
FGFR4 IC$_{50}$ (μM)	0.048	0.162	0.24	0.050
Cos-1 pFGFR1 IC$_{50}$ (μM)	0.028	0.361	5.76	>4.7
Cos-1 pFGFR4 IC$_{50}$ (μM)	0.124	0.268	0.496	0.064

Fig. 30 SAR of 7-substituted imidazopyridines

a result, low levels of FGFR4 selectivity were apparent. The incorporation of the large 7-benzyloxy substituent resulted in almost complete eradication of FGFR1 activity, while FGFR4 potency was maintained, **66**. Compound **66**, therefore, represents a potent and selective inhibitor of FGFR4 and validates the original hypothesis. The authors report that computational simulations suggest that the incorporation of a large substituent in the 7-position of the imidazopyridine core results in a reorganization the hinge residue side chains. The energy penalty for this is calculated to be lower in the case of FGFR4 due to the presence of the smaller cysteine residue. However, the authors also note that the high lipophilicity and low aqueous solubility of compounds such as **66** will limit the ability to characterize compounds in vivo. Reducing the bulk of the aminoamide substituent, **67**, does result in improved physicochemical properties but is accompanied by a reduction in FGFR4 activity. A wide range of substituents was investigated in the 7-position of the imidazopyridine core resulting in the identification of AZ9709 (**68**). Compound **68** is a potent inhibitor of FGFR4 with excellent levels of selectivity over FGFR1 in both biochemical and cell assays. The broad kinase selectivity of **68** was assessed against a commercially available panel of 76 different kinases binding assays. None of the kinases tested were inhibited by greater than 50% when treated with **68** at 1 μM suggesting that the compound has excellent general kinase selectivity. Compound **68** showed potent antiproliferative effects against Huh-7 cells which are known to overexpress FGF19 and possess functional FGFR4 ($GI_{50} = 0.116$ μM). The pharmacokinetic profile of **68** in mouse was considered suitable for in vivo assessment of target engagement, and it, **68**, showed a dose-dependent inhibition of phosphorylation FRS2 which was maintained for up to 8 h following a single dose of either 150 or 300 mg/kg in mice bearing Huh-7 tumors. This result supports the assertion that **68** can effectively inhibit FGFR4 in vivo. A crystal structure of **68** bound to both FGFR1 and a construct of FGFR1 mutated to resemble the binding site of FGFR4 (FGFR1Y563C) confirms that the 7-triazole substituent is positioned in contact with the kinase hinge as predicted and that Tyr563 present in the FGFR1 is required to move 2.8 Å compared to where it is located in the majority of other FGFR1-inhibitor complexes with available structural information. Such a reorganization is not apparent in the structure of **68** bound to the FGFRY563C construct. The reorganization of the tyrosine residue is consistent with the initial hypothesis explaining the observed FGFR4 selectivity (Fig. 31).

The presence of an FGFR4-specific cysteine residue in the ATP-binding site also allows the possibility of gaining FGFR4 selectivity through the use of an irreversible inhibitor. Pike et al. also describe the synthesis of compound **69** which contains electrophilic functionality directed toward the kinase hinge. Compound **69** shows selectivity for FGFR4 over FGFR1, and the irreversible nature of the inhibition is supported by the observation of covalent adducts between FGFR4 and **69** upon incubation of compound with protein.

The potential to achieve selectivity for FGFR4 over FGFR1–3 through the covalent modification of Cys552 has also been appreciated by Hagel et al. who have reported the discovery of BLU9931 (**70**) from the laboratories of Blueprint Medicines [49]. The authors drew inspiration from the structure of the known

Fig. 31 SAR of FGFR4 selective imidazopyridines
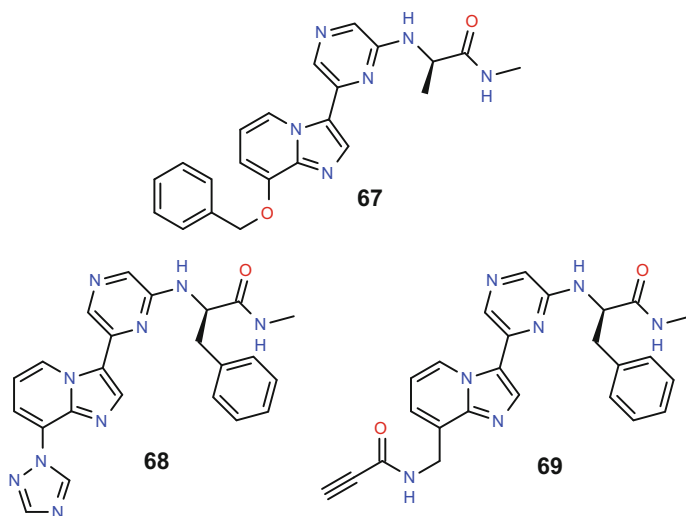
Compound	67	68	69
FGFR1 IC$_{50}$ (μM)	28.0	5.17	0.688
FGFR4 IC$_{50}$ (μM)	1.33	0.050	0.009
Cos-1 pFGFR1 IC$_{50}$ (μM)	>10	>10	>8.6
Cos-1 pFGFR4 IC$_{50}$ (μM)	2.67	0.053	0.070

inhibitor PD173074 (**7**) bound into FGFR1 and used this knowledge to design a series of anilinoquinazoline compounds targeting Cys552. Although detailed SAR for this scaffold has yet to be disclosed, it is clear that a 2,6-dichloro-3,5-dimethoxyphenyl substituent was introduced to the C6 position of the quinazoline core in an attempt to efficiently occupy the hydrophobic back pocket. Exploration of the 2-anilino moiety revealed that covalent modification of Cys552 was possible when an electrophilic acrylamide motif was positioned adjacent to the aniline nitrogen. However, the level of selectivity achieved for FGFR4 with initial compounds was disappointing suggesting the positioning of the electrophile was suboptimal. The incorporation of a methyl group in the remaining *ortho*-position of the anilino ring was anticipated to increase the rotation of the ring out of the plane of the quinazoline core thereby achieving a more optimal geometry for the formation of the covalent bond and resulted in the discovery of **70**. The rotation of this anilino ring is also believed to induce a steric clash with the more bulky tyrosine residue in FGFR1–3 thereby increasing FGFR4 selectivity. BLU9931

(**70**) shows good potency and selectivity for FGFR4 in biochemical assays (FGFR1–4 IC_{50}'s 0.591 μM, 0.493 μM, 0.150 μM, and 0.003 μM, respectively). The authors report that reduction of BLU9931 (**70**) results in an analogue possessing significantly lower activity against FGFR4 ($IC_{50} = 0.938$ μM) thus supporting the importance of the covalent bond formation on the inhibitory activity. Further evidence of the irreversible inhibition mechanism is provided by the observation of a covalent adduct between **70** and recombinant FGFR4 protein following incubation. A crystal structure of **70** bound to FGFR4 indicates the anticipated binding mode in which the anilinoquinazoline core forms a bidentate hydrogen-bonding interaction with the hinge region, while the 2,6-dichloro-3,5-dimethoxyphenyl residue occupies the hydrophobic back pocket. The aniline phenyl ring is rotated through approximately 60° compared to the plane of the quinazoline ring orientating the acrylamide toward the sulfur of the Cys552 residue (Fig. 32).

Testing of BLU9931 (**70**) against a broad panel of 456 wild type and disease-relevant mutant kinases at 3 μM resulted in only two kinases showing inhibition of greater than 90% of DMSO control (FGFR4 = 99.7%, CSF1R = 90.1%) thereby highlighting the exceptional kinase selectivity of the molecule. Compound **70** showed potent antiproliferative effects in HCC cell lines known to overexpress FGF19 and contain functional FGFR4 (such as Hep3B $EC_{50} = 0.07$ μM, Huh-7 $EC_{50} = 0.11$ μM, JHH-7 $EC_{50} = 0.02$ μM). Compound **70** displays a moderate bioavailability of 18% and a half-life of 2.3 h in mouse and showed tumor regression in mice bearing Hep3B tumors following administration of 100 mg/kg twice a day for 21 days. Furthermore, two of the animals from this treatment group showed no regrowth of tumor 30 days after cessation of treatment suggesting that selective inhibition of FGFR4 can give durable efficacy in FGFR4–FGF19-driven HCC tumors.

Information issued by Novartis regarding the current equity within its pipeline reports the development of a compound, FGF401, which binds to and inhibits the activity of FGFR4. They report that FGF401 is at least 1,000-fold more potent against FGFR4 than it is against other kinases, including FGFR1–3. They report that the compound inhibits the proliferation of HCC cell lines and shows blockage of both FGFR4 signaling and tumor growth in animal models of human HCC. At the time of writing, a phase I clinical trial to evaluate FGF401 in patients with HCC

Fig. 32 Structure of BLU9931

70
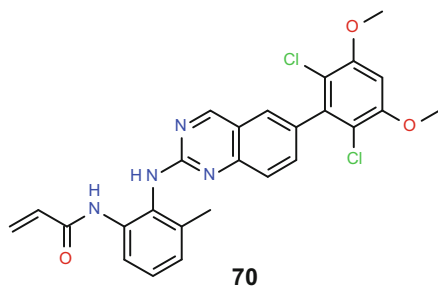
or solid malignancies characterized by positive FGFR4 and β-Klotho was recruiting, but no specific biological data or structural data concerning the compound or close analogues had been disclosed.

5.2 FGFR3-Selective Inhibitors

More recently Winski et al. have reported the identification of novel inhibitors developed in the laboratories of Array BioPharma, in collaboration with researchers from LOXO Oncology, Stamford, which display nanomolar inhibition of FGFR3 but relatively spare FGFR1 [50]. The authors report that these inhibitors have minimal activity against a panel of over 200 kinases. Although no structures have yet been disclosed for these inhibitors, they are reported to give high oral exposure in rodents and demonstrate tumor regression in the FGFR3-driven RT-122/84 subcutaneous xenograft models, when dosed for 14 days at either 30 or 45 mg/kg/day. The authors report only minimal hyperphosphatemia at these doses suggesting in vivo selectivity for FGFR3 over FGFR1 and supporting the hypothesis that isoform-selective FGFR inhibitors may provide treatments with improved efficacy and tolerability when compared to the pan-FGFR inhibitors currently undergoing clinical trials.

6 Inhibitors of Inactive Forms of FGFR

Targeting the inactive form of a kinase has long been considered an attractive concept due to the hypothesis that the inactive form would be more likely to adopt a distinct conformation, thereby presenting an opportunity to identify inhibitors of greater selectivity. The most widely reported approach to targeting an inactive form of a kinase focuses on the identification of so-called type II inhibitors. Such inhibitors characteristically induce a DFG-out conformation in which the Phe side chain of the activation loop (the *F* of the DFG) is flipped out to leave a hydrophobic pocket which is subsequently occupied by the inhibitor. Norman et al. at AstraZeneca have reported detailed crystallographic studies into the binding of the nonselective inhibitor ponatinib ("Inhibitors of Vascular Endothelial Growth Factor Receptor") in both FGFR1 and FGFR4 [51]. These studies reveal that ponatinib acts as a type II inhibitor of FGFR and induces a DFG-out conformation. Previous to this disclosure, all reported crystal structures of FGFR-inhibitor complexes have shown the FGFR protein in the DFG-in conformation. The authors speculate that the ability to induce a DFG-out conformation of FGFR might open new avenues for the design of novel type II inhibitors of FGFR with differing selectivity profiles and the potential for different inhibition kinetics.

Researchers at ArQule have also been interested in developing kinase inhibitors to target inactive forms of the kinase, and Eathiraj et al. have described the
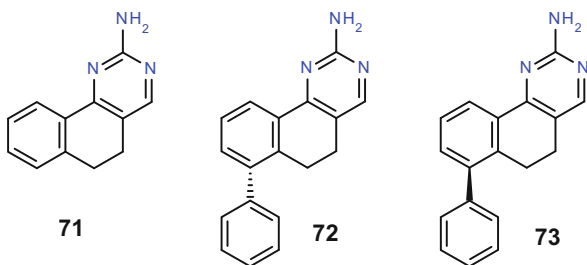
discovery of the FGFR inhibitor ARQ069 (**73**) [52]. The authors examined the
ATP-binding sites from multiple structures of kinases in inactive forms and were
able to identify a hydrophobic pocket which is not present in active kinase structures
and is distinct from the pockets described with type II inhibitors. To identify scaffolds
with the potential to bind to this pocket, compound databases were screened in silico
against a homology model of FGFR2. Docking studies and receptor pharmacophore
fitting resulted in the identification of the 5,6-dihydrobenzo[h]quinazolin-2-amine
compound ARQ523 (**71**) which was shown to bind to FGFR2 and inhibit its auto-
phosphorylation with an IC_{50} value of 18 µM. Optimization of this scaffold was
guided by in silico models and resulted in the identification of the enantiomeric pair of
ARQ068 (**72**) and ARQ069 (**73**) (Fig. 33).

ARQ069 (**73**) was found to inhibit the inactive (unphosphorylated) forms of both
FGFR1 and FGFR2 in biochemical assays (IC_{50}'s = 0.84 µM and 1.23 µM, respec-
tively), whereas **72** did not. Neither compound showed significant activity against the
phosphorylated (active) forms of FGFR1 or FGFR2. The inhibition of FGFR1 and
FGFR2 by **73** was found to be independent of ATP concentration. In KATO-III cells,
which are known to overexpress FGFR2, **73** inhibited the phosphorylation of FGFR
with an IC_{50} value of 9.7 µM. Consistent with the observed lack of biochemical
activity, **72** was inactive in this assay. A crystal structure of **73** in the autoinhibited
form of FGFR1 shows that the aminopyrimidine group forms a bidentate interaction
with the hinge region, while the 5,6-dihydrobenzo[h]quinazolin-2-amine core is
sandwiched in a hydrophobic cleft. The phenyl substituent of **73** is positioned ortho-
gonal to the 5,6-dihydrobenzo[h]quinazolin-2-amine core occupying the main pocket
and making hydrophobic interactions with the gatekeeper residue (Val561). The
authors suggest that the ability to target kinases in the autoinhibited conformation
may provide a new generation of kinase inhibitors that exhibit a high degree of
selectivity across the kinome.

7   Future Perspectives

The increasing evidence for dysregulated FGF/FGFR signaling to play a key role in
the development of human cancers means the appetite for efficacious and well-
tolerated FGFR inhibitors remains strong. The nonselective FGFR inhibitors

represent the most advanced clinical agents and have shown activity in patients; however, the multi-kinase inhibition profile of these compounds (in particular VEGFR inhibition) does result in a toxicity profile which will limit their utility. The more recent emergence of selective FGFR inhibitors has allowed for a more targeted approach to FGFR inhibition but has also revealed a different toxicology profile, namely, hyperphosphatemia and tissue mineralization, which are thought to represent on-target class effects. While it may be possible to manage these effects in the clinic through the modification of diet or with additional drugs, it is not surprising that recent attention has turned toward making isoform-selective FGFR inhibitors. While it is too early to say with any certainty whether such compounds will show clinical utility, it is anticipated that such compounds would possess a more favorable toxicity profile. As with many targeted therapies, the most likely role for FGFR inhibitors is likely to be in combination with chemotherapy, radiotherapy, or other molecularly targeted agents. This means that to achieve a "best in class" profile for an FGFR inhibitor, the right balance between clinical effectiveness and patient toxicity will need to be attained. Given the important role FGF/FGFR signaling plays in normal human biology and the multitude of different aberrations identified in cancer cells, the successful treatment of patients will require a personalized medicine approach based on the genetic aberrations presented, to select those patients who will gain the maximum clinical benefit from FGFR inhibition. In addition, technology designed to give tissue-specific exposure of drugs may also help increase the therapeutic margin for FGFR inhibitors.

As the use of FGFR inhibitor in the clinic increases, it would seem likely that resistance mechanisms will start to emerge as has been observed following the inhibition of other RTKs, such as EGFR. Mutations in the ATP-binding site, such as gatekeeper mutations similar to those observed to cause resistance to first generation EGFR inhibitors, may decrease the effectiveness of current FGFR inhibitors therefore requiring the development of new inhibitors. Irreversible inhibition of FGFR, or the targeting of inactive forms of the protein, may provide opportunities to overcome resistance mutations. In addition to the small molecule inhibitors of FGFR discussed above, research is also underway to develop antibody approaches to target both FGF ligands and the ligand-binding domains of FGFR. Such approaches might also provide effective inhibition of single FGFR isoforms although it is currently unclear whether the long duration of action often associated with antibody therapies would be a benefit or concern in the context of FGFR inhibition.

References

1. Wesche J, Haglund K, Haugsten EM (2011) Fibroblast growth factors and their receptors in cancer. J Biochem 437:199–213
2. Hanahan D, Weinberg RA (2000) The hallmarks of cancer. Cell 100:57–70

3. Hanahan D, Weinberg RA (2011) The hallmarks of cancer: the next generation. Cell 144: 464–674

4. Dieci MV, Arnedos M, Andre F, Soria JC (2013) Fibroblast growth factor receptor inhibitors as a cancer treatment: from a biologic rationale to a medical perspective. Cancer Discov 3(3): 264–279

5. Brooks AN, Kilgour E, Smith PD (2012) Molecular pathways: fibroblast growth factor signaling: a new therapeutic opportunity in cancer. Clin Cancer Res 18:1855–1862

6. Liang G, Chen G, Wei X, Zhao Y, Li X (2013) Small molecule inhibition of fibroblast growth factor receptors in cancer. Cytokine Growth Factor Rev 24:467–475

7. Connolly CJC, Hamby JM, Schroeder MC, Barvian M, Panek RL, Amar A, Shen C, Kraker AJ, Fry DW, Klohs WD, Doherty AM (1997) Discovery and structure-activity studies of a novel series of pyrido[2,3-d]pyrimidine tyrosine kinase inhibitors. Bioorg Med Chem Lett 7(18): 2415–2420

8. Hamby JM, Connolly CJC, Schroeder MC, Winters RT, Showalter HDH, Panek RL, Major TC, Olsewski B, Ryan MJ, Dahring T, Lu GH, Keiser J, Amar A, Shen C, Kraker AJ, Slintak V, Nelson JM, Fry DW, Bradford L, Hallak H, Doherty AM (1997) Structure-activity relationships for a novel series of pyrido[2,3-d]pyrimidine tyrosine kinase inhibitors. J Med Chem 40: 2296–2303

9. Dimitroff CJ, Klohs W, Sharma A, Pera P, Driscoll D, Veith J, Steinkampf R, Schroeder M, Klutchko S, Sumlin A, Henderson B, Dougherty TJ, Bernaki RJ (1999) Anti-angiogenic activity of selected receptor tyrosine kinase inhibitors, PD166285 and PD173074: implications for combination treatment with photodynamic therapy. Investig New Drugs 17:121–135

10. Mohammadi M, Froum S, Hamby JM, Schroeder MC, Panek RL, Lu GH, Eliseenkova AV, Green D, Schlessinger J, Hubbard SR (1998) Crystal structure of an angiogenesis inhibitor bound to the FGF receptor tyrosine kinase domain. EMBO 17(20):5896–5904

11. Thompson AM, Delaney AM, Hamby JM, Schroeder MC, Spoon TA, Crean SM, Showalter HDH, Denny WA (2005) Synthesis and structure-activity relationships of soluble 7-substituted 3-(3,5-dimethoxyphenyl)-1,6-naphthyridin-2-amines and related ureas as dual inhibitors of the fibroblast growth factor receptor-1 and vascular endothelial growth factor receptor-2 tyrosine kinases. J Med Chem 48:4628–4653

12. Klutchko SR, Hamby JM, Boschelli DH, Wu Z, Kraker AJ, Amar AM, Hartl BG, Shen C, Klohs WD, Steinkampf RW, Driscoll DL, Nelson JM, Ellliott WL, Roberts BJ, Stoner CL, Vincent PW, Dykes DJ, Panek RL, Lu GH, Major TC, Dahring TK, Hallak H, Bradford LA, Showalter HDH, Doherty AM (1998) 2-Substituted aminopyrido[2,3-d]pyrimidin-7(8H)-ones. Structure-activity relationships against selected tyrosine kinases and in vitro and in vivo anticancer activity. J Med Chem 41:3276–3292

13. Panek RL, Lu GH, Klutchko SR, Batley BL, Dahring TK, Hamby JM, Hallek H, Doherty AM, Keiser JA (1997) In vitro pharmacological characterization of PD166285, a new nanomolar potent and broadly active protein tyrosine kinase inhibitor. J Pharmacol Exp Ther 283(3): 1433–1444

14. Sun L, Tran N, Tang F, App H, Hirth P, McMahon G, Tang C (1998) Synthesis and biological evaluation of 3-substituted indolin-2-ones: a novel class of tyrosine kinase inhibitors that exhibit selectivity toward particular receptor tyrosine kinases. J Med Chem 41:2588–2603

15. Mohammadi M, McMahon G, Sun L, Tang C, Hirth P, Yeh BK, Hubbard SR, Schlessinger J (1997) Structures of the tyrosine kinase domain of fibroblast growth factor receptor in complex with inhibitors. Science 276:955–960

16. Sun L, Tran N, Liang C, Tang F, Rice A, Schreck R, Waltz K, Shawver LK, McMahon G, Tang C (1999) Design, Synthesis, and evaluations of substituted 3-[(3- or 4-carboxyethylpyrrol-2-yl) methylidenyl]indolin-2-ones as inhibitors of VEGF, FGF, and PDGF receptor tyrosine kinases. J Med Chem 42:5120–5130

17. Kammasud N, Boonyarat C, Tsunoda S, Sakurai H, Saiki I, Grierson DS, Vajragupta O (2007) Novel inhibitor for fibroblast growth factor receptor tyrosine kinase. Bioorg Med Chem Lett 17:4812–4818

18. Kammasud N, Boonyarat C, Sanphanya K, Utsintong M, Tsunoda S, Sakurai H, Saiki I, Andre I, Grierson DS, Vajragupta O (2009) 5-Substituted pyrido[2,3-d]pyrimidine, an inhibitor against three receptor tyrosine kinases. Bioorg Med Chem Lett 19:745–750

19. Renhowe PA, Pecchi S, Shafer CM, Machajewski TD, Jazan EM, Taylor C, Antionios-McCrea W, McBride CM, Frazier K, Wiesmann M, Lapointe GR, Feucht PH, Warne RL, Heise CC, Menezes D, Aardalen K, Ye H, He M, Le V, Vora J, Jansen JM, Wernette-Hammond ME, Harris AL (2009) Design, structure-activity relationships and in vivo characterisation of 4-amino-3-benzimidazol-2-ylhydroquinolin-2-ones: a novel class of receptor tyrosine kinase inhibitors. J Med Chem 52:278–292

20. Lee SH, Lopes de Menezes D, Vora J, Harris A, Ye H, Nordahl L, Garrett E, Samara E, Aukerman SL, Gelb AB, Heise C (2005) In vivo target modulation and biological activity of CHIR-258, a multitargeted growth factor receptor kinase inhibitor, in colon cancer models. Clin Cancer Res 11(10):3633–3641

21. Guagnano V, Furet P, Spanka C, Bordas V, Le Douget M, Stamm C, Brueggen J, Jensen MR, Schnell C, Schmid H, Wartmann M, Berghausen J, Drueckes P, Zimmerlin A, Brussiere D, Murray J, Porta DG (2011). J Med Chem 54:7066–7083

22. Furet P, Caravatti G, Guagnano V, Lang M, Meyer T, Schoepfer J (2008) Entry into a new class of protein kinase inhibitors by pseudo ring design. Bioorg Med Chem Lett 18:897–900

23. Norman RA, Schott A-K, Andrews DA, Breed J, Foote KM, Garner AP, Ogg D, Orme JP, Pink JH, Roberts K, Rudge DA, Thomas AP, Leach AG (2012) Protein-ligand crystal structures can guide the design of selective inhibitors of the FGFR tyrosine kinase. J Med Chem 55:5003–5012

24. Thomas A, Theoclitou M-E, Buttar D, Ruston L, Wrigley G, Dennis M, Rudge D, Coleman T, Smith R, Gavine P, Klinowska T, Mooney L, Brooks N (2012) The discovery of AZD4547: an orally bioavailable, potent and selective N-(pyrazolyl)benzamide FGFR1-3 inhibitor. Poster #3912 103rd AACR annual meeting

25. Gavine PR, Mooney L, Thomas AP, Al-Kadhimi K, Beck S, Coleman T, Baker D, Mellor MJ, Brooks AN, Klinowska T (2012) AZD4547: an orally bioavailable, potent, and selective inhibitor of the fibroblast growth factor receptor tyrosine kinase family. Cancer Res 72:2045

26. Zhao G, Li W-Y, Chen D, Henry JR, Li H-Y, Chen Z, Zia-Ebrahimi M, Bloem L, Zhai Y, Huss K, Peng S-B, McCann DJ (2011) A novel, selective inhibitor of fibroblast growth factor receptors that shows a potent broad spectrum of antitumor activity in several tumor xenograft models. Mol Cancer Ther 10:2200–2210

27. Squires M, Ward G, Saxty G, Berdini V, Cleasby A, King P, Angibaud P, Perera T, Fazal L, Ross D, Jones CG, Madin A, Benning RK, Vickerstaffe E, O'Brien A, Frederickson M, Reader M, Hamlett C, Batey MA, Rich S, Carr M, Miller D, Feltell R, Thiru A, Bethell S, Devine LA, Graham BL, Pike A, Cosme J, Lewis EJ, Freyne E, Lyons J, Irving J, Murray C, Newell DR, Thompson NT (2011) Potent, selective inhibitors of fibroblast growth factor receptor define fibroblast growth factor dependence in preclinical cancer models. Mol Cancer Ther 10(9):1542–1552

28. Perera TPS, Jovcheval E, Vialard J, Verhulst T, Esser N, King P, Wroblowski B, Platero S, Querolle O, Mevellec L, Freyne E, Gilissen R, Murray C, Woodhead S, Fazal L, Saxty G, Newell D, Ward G, Squires M, Thompson N, Angibaud P (2014) JNJ-42756493 is an inhibitor of FGFR-1, 2, 3, and 4 with nanomolar affinity for targeted therapy. Poster #1738 AACR annual meeting

29. Angibaud PR et al (2015) Identification of naphthyridines as potent inhibitors of fibroblast growth factor receptor kinase family. Poster #3641 AACR annual meeting

30. Angibaud PR, Obringer M, Marin JJJ, Jeanty M. Preparation of naphthyridine derivatives useful in the treatment of cancer. WO 2013061077

31. Vermeulen W, Hostyn SA, Cuyckens FAC, Jones RM, Broggini DFD. Preparation of quinoxaline derivatives useful as FGFR kinase modulators. WO 2015144803

32. Nakanishi Y, Akiyama N, Tsukaguchi T, Tachibana-Kondo Y, Fujii T, Sakata K, Sase H, Isobe T, Sato Y, Morikami K, Shindoh H, Mio T, Ebiike H, Taka N, Aoki Y, Ishii N (2014)

FGFR genetic alterations as a potential predictor of the sensitivity to CH5183284? Debio 1347, a novel selective FGFR inhibitor. Poster #2729 AACR annual meeting

33. Ebiike H, Taka N, Nakanishi Y, Akiyama N, Sawamura F, Morikami K, Matsushita M, Ohmori M, Takami K, Hyohdoh I, Kohchi M, Hayase T, Nishii H, Ishii N, Matsuoka H (2014) Design and preclinical profile of CH5183284/Debio 1347, a novel orally available and selective FGFR inhibitor acting on a gatekeeper mutant of FGFR2. Poster #2533 AACR annual meeting

34. Heroult M, Ellinghaus P, Sieg C, Brohm D, Gruenewald S, Collin M-P, Boemer U, Lobell M, Huebsch W, Ocker M, Ince S, Hagebarth A, Jautelat R, Hess-Stumpp H, Brands M, Ziegelbauer K (2014) BAY 1163877. Poster #1739 AACR annual meeting

35. Heroult M, Ocker M, Kneip C, von Ashen O, Kopitz C, Zopf D, Hagebarth A, Ziegelbauer K, Ince S, Ellinghaus P (2015) Anti-tumor efficacy of the selective pan-FGFR inhibitor BAY 1163877 in preclinical squamous-cell carcinoma models of different origin. Poster #772 AACR annual meeting

36. Lobell M, Huebsch W, Schirok H, Heroult M, Brohm D, Collin M-P, Gruenewald S, Lustig K, Boemer U, Voehringer V, Lindner N. Preparation of substituted benzothienyl-pyrrolotriazines and uses thereof. WO 2013124316

37. Brohm D, Heroult M, Collin M-P, Huebsch W, Lobell M, Lustig K, Gruenewald S, Boemer U, Voehringer V. Preparation of disubstituted benzothienyl-pyrrolotriazines and their use as FGFR kinase inhibitors. WO 2013087578

38. Collin M-P, Brohm D, Heroult M, Lobell M, Huebsch W, Lustig K, Gruenewald S, Boemer U, Voehringer V, Lindner N Preparation of substituted benzothienylpyrrolotriazines as selective fibroblast growth factor receptor kinase inhibitors for treatment of cancer. WO 2013087647

39. Miyano SW, Yamamoto Y, Kodama K, Funaska S Nagao S, Sugi NH, Kuramochi H, Ishikawa K, Okamoto K, Minoshima Y, Nakagawa T, Nakatani Y, Karoji Y, Ohashi I, Yamane Y, Tanaka K, Okada T, Matsushima T, Matsui J, Iwata M, Tsuroka A, Uenaka T (2015) E7090: a potent and selective FGFR inhibitor with activity in multiple FGFR-driven cancer models with distinct mechanisms of activation. Poster #770 AACR annual meeting

40. Lui PCC, Wu L, Koblish H, Bowman K, Zhang Y, Klabe R, Leffet L, DiMatteo D, Rupar M, Gallagher K, Hansbury M, Zhang C, He C, Collier P, Covington M, Wynn R, Yeleswaram S, Vaddi K, Burn T, Yao W, Huber R, Scherle P, Hollis G (2015) Preclinical characterization of the selective FGFR inhibitor INCB54828. Poster #771 AACR Annual meeting

41. Sun L, Lu L, Yao W, Zhuo J, Wu L, Xu M, Qian D-Q, Zhang F, He C. Preparation of bicyclic heterocycles as FGFR inhibitors in the treatment of cancer. WO 2014172644

42. Wu L, Zhang C, He C, Sun Y, Lu L, Qian D-Q, Xu M, Zhuo J, Yao W. Preparation of substituted tricyclic compounds as FGFR inhibitors for treatment of cancer and other diseases. US 20130338134

43. Zhuo W, Hur W, McDermott U, Dutt A, Xian W, Ficarro SB, Zhang J, Sharma SV, Brugge J, Meyerson M, Settleman J, Gray NS (2010) A structure-guided approach to creating covalent FGFR inhibitors. Chem Biol 17:285–295

44. Packer ML, Pollock PM (2015) Paralog-specific kinase inhibition of FGFR4: adding to the arsenal of anti-FGFR agents. Cancer Discov 5(4):355–357

45. Wesche J, Haglund K, Haugsten EM (2011) Fibroblast growth factors and their receptors in cancer. Biochem J 437(2):199–213

46. Taylor VI JG, Cheuk AT, Tsang PS, Chung J-Y, Song YK, Desai K, Yu Y, Chen Q-R, Shah K, Youngblood V, Fang J, Kim SY, Yeung C, Helman LJ, Mendoza A, Ngo V, Staudt LM, Wei JS, Khanna C, Catchpoole D, Qualman SJ, Hewitt SM, Merlino G, Chanock SJ, Khan J (2009) Identification of FGFR4-activating mutations in human rhabdomyosarcomas that promote metastasis in xenotransplanted models. J Clin Investig 119(11):3395–3407

47. French DM, Lin BC, Wang M, Adams C, Shek T, Hotzel K, Bolon B, Ferrando R, Blackmore B, Schroeder K, Rodriguez LA, Hristopoulos M, Venook R, Ashkenazi A, Desnoyers LR (2012) Targeting FGFR4 inhibits hepatocellular carcinoma in preclinical mouse models. PLoS One 7(5):e36713

48. Pike KG, Buttar D, Tucker J, Ford S, Glossop S, Culshaw J, Gill K, Perkins D, Eden J, Hayter B, Mooney L, Brooks N, Ruston L, Smith R, Jones C (2014) Identifying selective inhibitors of FGFR4 kinase. Oral presentation given at EFMC-ISMC 2014, XXIII international symposium on medicinal chemistry
49. Hagel M, Miduturu C, Sheets M, Rubin N, Weng W, Stransky N, Bifluco N, Kim JL, Hodous B, Brooijmans N, Shutes A, Winter C, Langauer C, Kohl NE, Guzi T (2015) First selective small molecule inhibitor of FGFR4 for the treatment of hepatocellular carcinomas with an activated FGFR4 signaling pathway. Cancer Discov 5(4):424–437
50. Winski S, Nanda N, Brown E, Tang T, Brandhuber B, Hamor R, Tuch B, Ebata K, Low J, Sullivan F, Smith D, Vigers G, Strough M, Rieger R, Blake J, Moreno D, Chantry D, Rothenberg SM, Andrews S (2015) Identification of first-in-class, highly potent FGFR kinase inhibitors that spare FGFR1. Abstract #C196 AACR-NCI-EORTC international conference
51. Tucker JA, Klein T, Breed J, Breeze AL, Overman R, Philips C, Norman RA (2014) Structural insights into FGFR kinase isoform selectivity: diverse binding modes of AZD4547 and ponatinib in complex with FGFR1 and FGFR4. Structure 22:1764–1774
52. Eathiraj S, Palma R, Hirschi M, Volckova E, Nakuci E, Castro J, Chen C-R, Chan TCK, France DS, Ashwell MA (2011) A novel mode of protein kinase inhibition exploiting hydrophobic motifs of autoinhibited kinases. J Biol Chem 286(23):20677–20687

Modulation of the DNA-Damage Response by Inhibitors of the Phosphatidylinositol 3-Kinase Related Kinase (PIKK) Family

Suzannah Harnor, James Pickles, and Celine Cano

Abstract The ability of cancer cells to repair DNA damage is an important determinant of their susceptibility to DNA-damaging anticancer therapies, and inhibition of DNA-repair processes can thus lead to the potential therapeutic endpoints of radio- and chemo-sensitisation. As such, a number of agents that target DNA-repair enzymes are currently the subject of clinical trials. The phosphatidylinositol 3-kinase related kinase (PIKK) family of enzymes, which includes DNA-dependent protein kinase (DNA-PK), ataxia-telangiectasia mutated (ATM), ataxia-telangiectasia mutated related (ATR), mammalian target of rapamycin (mTOR) and hSMG1, are thought to act as nucleic acid surveillance proteins. DNA-PK and ATM, the normal function of which is lost in ataxia-telangiectasia, both play an important role in the detection and repair of DNA double-strand breaks (DSBs). DNA-PK is an essential component of the non-homologous end-joining (NHEJ) pathway of DNA DSB repair, whilst ATM signals to cell cycle and DNA-repair components by phosphorylating multiple downstream targets, including p53, checkpoint kinase 2 (CHK2), NBS1 and BRCA1. Crucially, loss of DNA-PK or ATM activity results in an increased sensitivity to ionising radiation and certain chemotherapeutic agents that elicit DNA DSBs. These kinases therefore represent attractive targets for the development of radio- and chemo-sensitising agents.

Keywords Chemopotentiation, DNA damage, Inhibitor, Kinase, Radio-potentiation

S. Harnor, J. Pickles, and C. Cano (✉)

Northern Institute for Cancer Research, School of Chemistry, Newcastle University, Newcastle upon Tyne NE1 7RU, UK

e-mail: celine.cano@newcastle.ac.uk

Contents

1   DNA Damage

DNA within cells is constantly exposed to damage, which requires repair in order for the integrity of DNA to be maintained. Damage to DNA can lead to harmful mutations, which affect normal cellular processes and can cause cancer if left unrepaired. DNA is intrinsically susceptible to modification by reactive species and estimates suggest that there are in the region of 10^{16}–10^{18} repair events which take place in a human on a daily basis [1].

Fortunately, cells have evolved efficient processes for the repair of DNA damage, collectively known as the DNA-damage response (DDR) (Fig. 1) [2]. Examples of endogenous damaging agents are ROS from cellular metabolism and endogenous methylating agents, whereas damage can be induced from external sources such as ultraviolet (UV) light and xenobiotics and in response to established cancer treatment such as DNA-damaging chemotherapy and ionising radiation [3, 4].

1.1   DNA Inter- and Intra-strand Crosslinks

Well-characterised forms of DNA damage include inter- and intra-strand crosslinks. A covalent bond is formed between two bases on opposite strands of DNA in the case of an inter-strand crosslink and within the same strand with intra-strand crosslinks [5]. Inter-strand crosslinks are extremely toxic to the cell as they prevent the separation of the different strands, an important part of both DNA replication and transcription [5]. Intra-strand crosslinks are less toxic given that they can be bypassed by certain enzymes. The nitrogen mustards are known to elicit this type of damage [6].
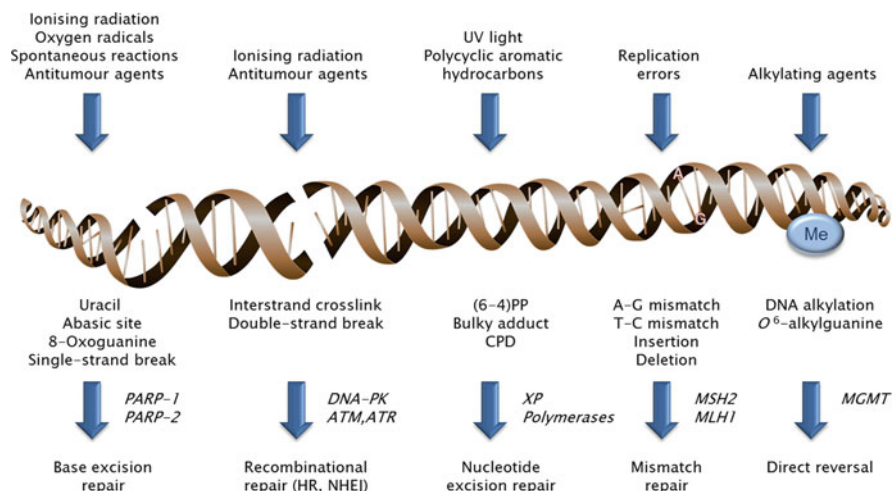
Fig. 1 DNA damage and response. Adapted from Hoeijmakers [2]

1.2   DNA Backbone Damage

Deoxyribose moieties within the DNA backbone are particularly susceptible to attack by ROS generated intracellularly [6]. Hydroxyl radicals, for example, can abstract a hydrogen atom from the sugar to give a radical species which, after degradation, can result in a break to the DNA backbone. The structural units **1**, **2** and **3** are all formed in this manner [7]. These single-strand breaks (SSBs) can be repaired by base excision repair (BER) but when numerous SSBs occur in close proximity to one another, a DNA double-strand break (DSB) can be formed [6, 8]. Ionising radiation is capable of inducing DNA DSBs and these lesions are the most cytotoxic to the cell.
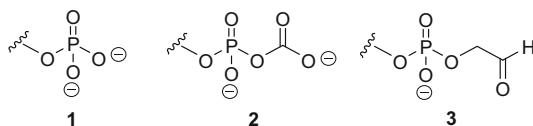
1.3   DNA Base Damage

Abasic sites can be produced when the glycosidic bond in DNA is hydrolysed (Scheme 1), which is a very common occurrence. It has been estimated that this process can occur 10,000 times per cell per day [9]. Loss of a base is harmful to the

Scheme 1 Mechanism by which abasic sites are formed on DNA [9]

Scheme 2 Deamination of cytosine (**8**) to yield uracil (**9**)

cell for two reasons. Firstly, this can lead to mutations when the DNA is replicated and, secondly, SSBs can also occur if they are left untreated [6, 10].

Deamination is another process which may impair the DNA sequence and this occurs on amino groups of bases, most commonly on cytosine (**8**). Compound **8** can undergo nucleophilic attack by water and, following liberation of ammonia, uracil (**9**) is produced (Scheme 2), resulting in a change in the genetic code.

External agents such as UV radiation can cause damage to DNA bases as Fig. 9 shows. UV light leads to the formation of photoadducts such as the cyclobutane dimer (**10**) [6]. Xenobiotics such as polycyclic hydrocarbons can, upon metabolic activation, react with DNA, leading to the formation of bulky adducts such as **11**. Due to the steric bulk added by such modifications, they interfere with the secondary structure of DNA and this can affect cellular processes such as transcription [6].

10   11

2   The DNA-Damage Response

The wide diversity of DNA-lesion types necessitates multiple, largely distinct DNA-repair mechanisms.

2.1   Base Excision Repair

BER, discovered by Lindhal, is a DDR process employed when, for example, oxygen radicals and alkylating agents act on genetic material (Fig. 1) [11]. The BER pathway relies on proteins recognising the damage [11]. The downstream effect of this impairment is often mutations, which is clearly disadvantageous. Interestingly, this error free repair mechanism can occur via one of the two mechanisms, short-patch repair (in which a single nucleotide is replaced) or long-patch repair (where at least two nucleotides are replaced) [11, 12]. However, it is poorly understood as to what determines which of these options is undertaken. Short-patch repair does, nevertheless, constitute the main pathway [2]. Essentially, a damaged base is replaced in order to prevent potentially dangerous mutations [11].

2.2   Nucleotide Excision Repair

Nucleotide excision repair (NER) acts on the products of damage induced in DNA by UV light or with any covalent adducts (Fig. 1) and occurs during G1 phase of the cell cycle [13, 14]. Altogether, a broad range of damage is repaired via this mechanism and it can be subdivided into three subcategories: global genome repair (GGR), transcription-coupled repair (TCR) and transcription domain-associated repair (DAR) [14]. TCR, as the name suggests, is coupled to transcription, DAR

works on both strands of active genes and GGR is any other NER that occurs [14]. Unlike BER, NER does not rely on having specific enzymes each recognising a different lesion; instead, inaccuracies in the structure of genetic material are enough to trigger a response [14]. Following identification of the damage, the site of impairment is removed, leaving a break which DNA polymerases act upon to liberate the repaired DNA [14].

2.3   Mismatch Repair

DNA has to be duplicated many times in order to pass vital genetic information on from one generation to the next, a process which is not without error. Fortunately, there is a repair mechanism that can recognise faults in the daughter strand post-replication [15]. Mismatch repair (MMR) maintains genetic integrity by correcting insertions, deletions and discrepancies in base pairings [2, 13]. Figure 2 shows the key phases involved in MMR. In Stage I (upper strand), hMSH2/6 recognises non-complimentary bases whereas hMSH2/3 recognises insertion/deletion errors (Stage II, lower strand). Following recognition, other essential proteins, for example, mutator S (MutS), are recruited, exonucleases excise the errors and, finally, resynthesis can occur (Stage III) [2].

2.4   Double-Strand Break Repair

Although less prevalent than other DNA lesions, the DSB is considered to be the most cytotoxic and difficult to repair and there is evidence to suggest that a single DSB may prove lethal to a cell [16]. Two principal mechanisms are responsible for the repair of DSBs, namely the error free homologous recombination (HR) process, and non-homologous end joining (NHEJ), which is an error-prone ligation mechanism (Fig. 3). Whereas HR repair is, by necessity, restricted to S and G2, NHEJ may operate at any phase of the mitotic cell cycle, although this repair process occurs predominantly in G1 and G0 [1, 18]. Importantly, initiation of the DDR as a consequence of DSB detection has far reaching implications within a cell, resulting in the activation of a complex signalling network, which modulates cell cycle progression, gene expression and protein synthesis [1, 19]. Members of an atypical class of protein kinases termed the phosphatidylinositol (PI) 3-kinase related kinase (PIKK) family are major players in the detection, signalling and repair of DNA DSBs.

The process of HR is initiated, following DSB detection, by the Rad50/Mre11/NBS1 (MRN) complex (Fig. 3a). This complex performs a nucleolytic resection to expose single-stranded $3'$ overhangs of double-stranded DNA, which facilitates binding of a RAD51 nucleoprotein filament [20]. This nucleoprotein filament has the capability to exchange the single strand of DNA with the identical sequence in a

Fig. 2 The process by which DNA is repaired by mismatch repair (MMR) [2]. In Stage I, heterodimers of hMSH2/6 focus on mismatches and single-base loops, whereas in Stage II, hMSH2/3 dimers recognise insertion/deletion loops. In Stages II and III, a number of proteins, including exonuclease 1, are associated in the excision of the new strand past the mismatch and resynthesis steps
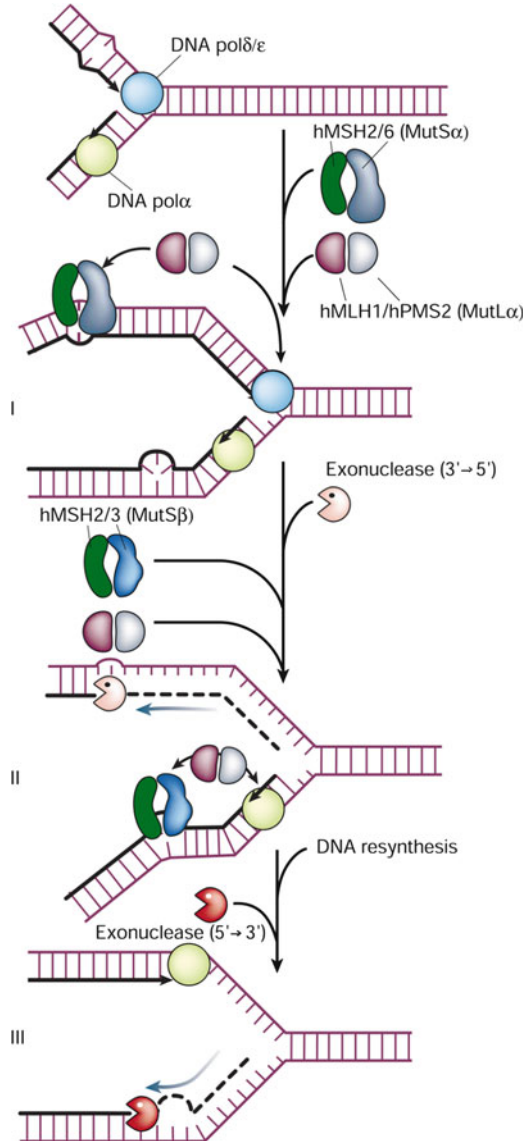
double-stranded DNA counterpart. The intact double-stranded copy is then used as a template to repair the DSB by the action of DNA ligases [21]. The DNA strand invasion results in the formation of Holliday junctions. These are mobile junctions between four strands of DNA that are repaired by resolvase enzymes thus completing the overall repair process [22].

NHEJ can operate at any stage of the cell cycle as it does not require a DNA template for the restoration process but it predominantly acts at G1 and G0 (Fig. 3b). NHEJ functions by directly ligating the end of DNA DSBs
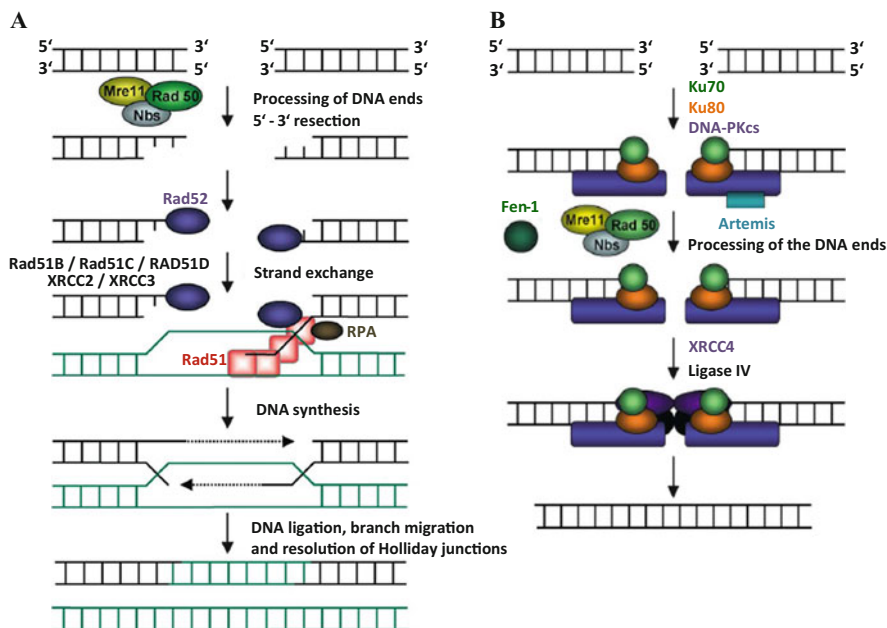
Fig. 3 Recombinational repair processes [17]. (**a**) Mechanism of homologous recombination (HR). Nucleolytic resection of DSB in direction $5' \rightarrow 3'$ by the MRE11–Rad50–NBS1 complex forms a $3'$ single-stranded DNA fragment. Rad 52 binds, and interacts with Rad51 to elicit a DNA strand exchange with undamaged, homologous DNA molecule. The resulting structure is resolved after DNA synthesis, ligation and branch migration. (**b**) Mechanism of non-homologous end joining (NHEJ). Ku70–Ku80 complex binds to damaged DNA, and then the Ku heterodimer binds to catalytic subunit of the DNA-dependent protein kinase (DNA-PKcs) to form the DNA-PK holoenzyme. The X-Ray repair cross complementing 4 (XRCC4)-ligase IV is activated by DNA-PK, which links the broken DNA ends

[23, 24]. NHEJ is a rapid process, compared to HR, but can sometimes result in a loss/gain of nucleotides [2].

3 The Phosphatidylinositol 3-Kinase Related Kinase Family

The phosphatidylinositol 3-kinase related kinase (PIKK) family is a group of six atypical serine/threonine protein kinases (Fig. 4). They are so named due to their similarities with the phosphoinositide 3-kinase (PI3K) family which are a series of lipid kinases possessing a variety of biological activities.

Comprising the PIKK family are DNA-PK, ataxia-telangiectasia mutated (ATM), ataxia-telangiectasia mutated related kinase (ATR), mammalian target of rapamycin (mTOR), transformation/transcription domain-associated protein
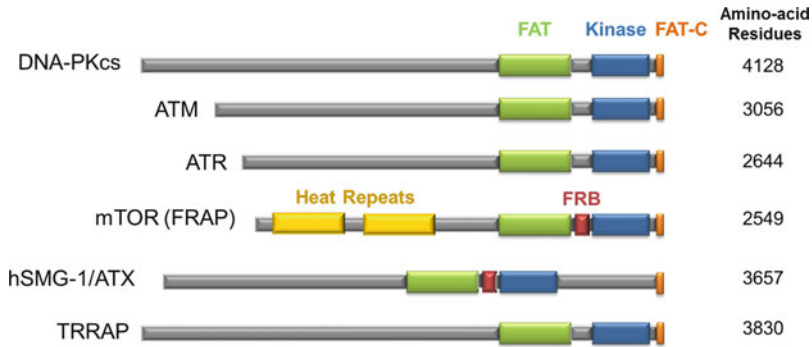
Fig. 4 The phosphatidylinositol 3-kinase related kinase (PIKK) family of atypical protein kinases. Adapted from Ref. [25]

(TRRAP) and suppressor of morphogenesis in genitalia 1 (SMG-1). ATM, ATR and DNA-PK are all involved in DNA repair and are discussed further later. mTOR is involved in organismal growth and homeostasis whilst SMG-1 is involved in nonsense-mediated RNA decay [26, 27].

The PIKK proteins consist of a PI3K domain and, also, FRAP–ATM–TRAPP (FAT) and FAT carboxy-terminal (FATC) regions surrounding the catalytic region, with FAT being located on the *N*-terminal side. Although some of the functions of these domains remain unclear, it has been reported that the FAT domain of ATM contains a serine residue which is key for the activation of the kinase [25].

3.1 DNA-Dependent Protein Kinase

3.1.1 Structural Features of DNA-Dependent Protein Kinase

The DNA-PK catalytic subunit is the largest of the PIKK family members, consisting of a polypeptide of 4,128 amino acids. Owing to the large size of the peptide, crystal structure determination has proven challenging. However, in January 2010 Sibonda et al. published the first known crystal structure of DNA-PKcs in complex with C-terminal fragments of Ku80 (the 80 kDa protein subunit of the Ku complex, also known as ATP-dependent DNA helicase II), albeit at a resolution of 6.6 Å [4]. Whilst this resolution cannot provide useful information on the structure of the ATP-binding domain, it gives a general overview of the structural features of the protein (Fig. 5).

The major role of the Ku70/Ku80 heterodimer within the NHEJ pathway is recognition and binding of DNA ends to facilitate correct alignment for subsequent processing and ligation. The proteins themselves are known to consist of three distinct functional regions. An amino terminal Willebrand A-domain (vWA) is thought to be a protein–protein interacting domain which may play a key role in
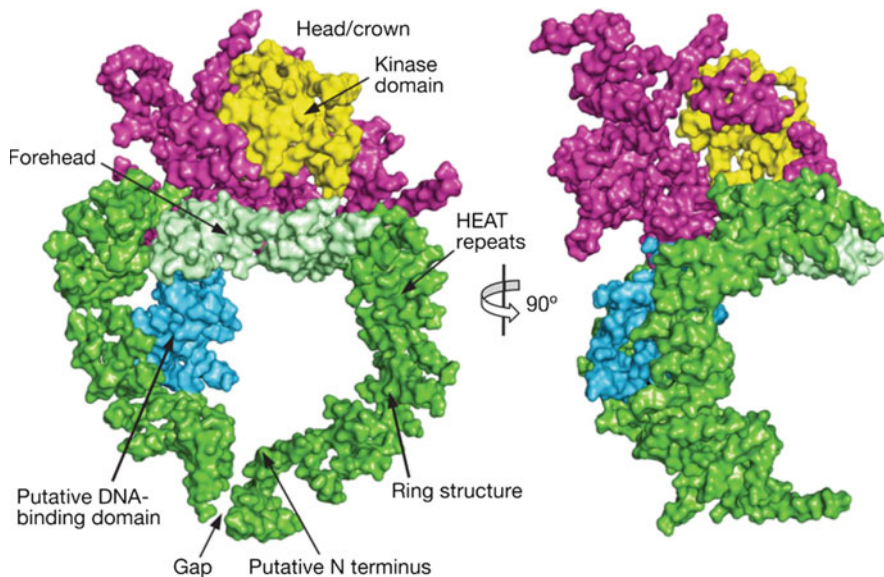
Fig. 5 Crystal structure of DNA-dependent protein kinase (DNA-PKcs). *Yellow*: kinase domain, *green*: ring structure, *light green*: forehead region that is part of the ring structure, *blue*: putative DNA-binding domain, and *magenta*: C-terminal region carrying the FRAP–ATM–TRAPP (FAT) and FAT carboxy-terminal (FATC) domains [4]
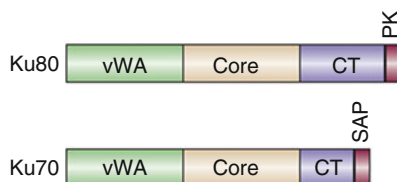
Fig. 6 Depiction of the Ku70 and Ku80 protein domains [28]

heterodimerisation. A central core domain is then linked to a carboxy-terminal region, which in Ku80 is elongated and contains the regions to which the DNA-PKcs binds (Fig. 6) [28].

3.1.2 DNA-Dependent Protein Kinase and the Non-homologous End-Joining DNA-Repair Pathway

As previously mentioned, the major pathway for DSB repair in non-replicating mammalian cells is NHEJ, and DNA-PK plays a key role in this process (Fig. 3). The Ku70/Ku80 heterodimer is responsible for binding to the broken DNA ends [29]. Ku binds to both of the broken strands and forms a bridging complex to lock the damaged ends in place [30]. The catalytic subunit of the DNA-PKcs is recruited

to the site of damage to form a 'synaptic complex'. Formation of the holoenzyme greatly enhances the serine/threonine protein kinase activity of DNA-PKcs resulting in autophosphorylation of multiple sites on the protein. A small cluster of seven phosphorylation sites between residues 2,609 and 2,647 are thought to be key for a change in the tertiary structure of the DNA-PK complex, which makes the DNA termini accessible for further processing [31]. DNA docks in the DNA-binding site within DNA-PKcs, which is in the *N*-terminal domain [29]. Should Ku be absent, then another process can anneal DNA DSBs via alternative NHEJ that involves poly(ADP-ribose) polymerase 1 (PARP1) and XRCC1 [32].

Once the DNA is bound, processing enzymes, such as Artemis and DNA polymerases, locate to the site of damage. Artemis is a nuclease that is phosphorylated by DNA-PKcs following formation of the DNA-PK holoenzyme. It is responsible for the cleavage of non-complementary bases from the DNA termini [33]. Whilst the exact types of lesions requiring Artemis-mediated repair have not been identified, it is thought that 15–20% of DSBs resulting from the action of ionising radiation remain unrepaired in cells deficient in the Artemis protein [34].

The complexity of the DSBs formed by ionising radiation dictates that, whilst some may require DNA base removal, a number will conversely require base insertion. This role is fulfilled by a number of DNA polymerases, most notably DNA polymerase μ and λ, both of which are recruited to the break site through their interaction with Ku [35]. It has been demonstrated that cells deficient in either DNA polymerase μ or λ are not highly sensitised to ionising radiation, suggesting that these processing factors are only required in a small subset of strand breaks [34].

Current literature reports implicate a number of different processing factors in the NHEJ pathway including PNF, APLF and the WRN complex. The increasing number implicated would seem to suggest that the specific enzymes recruited for end processing may be relatively flexible, depending upon the nature of the break [35].

Upon completion of end processing, the remainder of the pathway is directed towards end ligation. This is performed following the recruitment of a DNA ligase IV/XRCC4 complex to the break site. XRCC4 has no known enzymatic activity but instead acts as a scaffolding protein for the interaction of DNA ligase IV with Ku, and thus the DSB. Binding of XRCC4 to DNA ligase IV promotes its enzymatic activity, which subsequently instigates the ligation and repair of the break site [36].

3.1.3 DNA-Dependent Protein Kinase Small-Molecule Inhibitors

Following the discovery that DNA-PK inhibition can potentiate in vitro cytotoxicity of ionising radiation and a number of anticancer drugs, a number of small molecules with DNA-PK inhibitory activity have been developed. To date, the most successful approach to DNA-PK inhibition has been with small molecule targeting the ATP-binding site of the kinase.

Wortmannin

The first example within this specific group of compounds is wortmannin (**12**), a steroidal derivative reported as a potent PI3K inhibitor in 1994 [37].
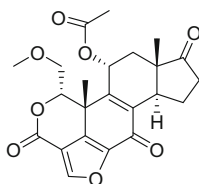
12

Wortmannin is a natural fungal metabolite, derived from *Penicillium wortmannii K* and first observed to have antifungal and anti-inflammatory properties. This sterol-like compound is a potent and selective inhibitor of PI3K family kinases without activity against other intracellular signalling enzyme targets, inhibiting PI3K activity with an IC_{50} of 4.2 nM [37]. Kinetic analysis of the PI3K inhibition by wortmannin indicated a non-competitive irreversible inhibition, which was further verified by Williams. et al. with co-crystallographic studies of the resulting covalent complex in the ATP-binding pocket of PI3Kγ [38, 39]. Further studies demonstrated that wortmannin also inhibits DNA-PK (IC_{50} = 16 nM) by a non-competitive mechanism, forming covalent adducts with DNA-PKcs lysine 802 in the region of the molecule harbouring its kinase domain [40]. Although the activity of this sterol-like structure and its mode of interaction make it very attractive, the relative structural complexity of wortmannin, together with its irreversible inhibition and poor selectively, limits its potential as a drug molecule.

Chromen-4-Ones and Surrogates: LY2094002 and Derivatives

The chromen-4-one structure LY294002 (**13**) was reported by Lilly pharmaceuticals in 1994 as an inhibitor of PI3K [41]. It was identified through a screen of compounds derived from quercetin (**14**) with the objective of developing PI3K-specific inhibitors.

Table 1 Reported inhibitory activity of LY294002 (**13**) against different PIKK family members

	DNA-PK	PI3K (p110$_\alpha$)	ATM	ATR	mTOR
IC$_{50}$ (μM)	1.5 ± 0.2[a]	2.3 ± 0.8[a] (1.4)[b]	>100[a]	>100[a]	2.5 ± 0.2[a]

[a]Values from Ref. [42]
[b]Literature value from Ref. [41]

13; X = O
15; X = S
16; X = CH$_2$

14
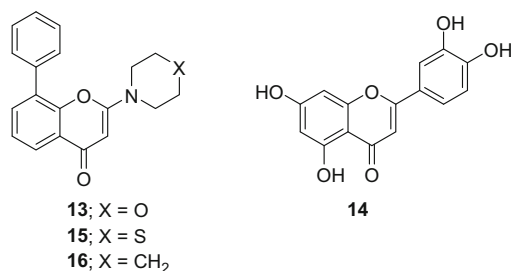
Subsequent evaluation of **13** as a DNA-PK inhibitor showed that the compound exhibited similar DNA-PK inhibitory activity to that against PI3K, highlighting the non-selective profile of the compound (Table 1) [41, 42].

Research conducted at the Northern Institute for Cancer Research at Newcastle University and KuDOS Pharmaceuticals (now part of AstraZeneca) revealed the importance of the oxygen of the morpholine substituent of **13**, and whilst replacement by thiomorpholine (**15**) dramatically reduced potency, the piperidine derivative **16** proved essentially devoid of DNA-PK inhibitory activity. The key role of the morpholine substituent of **13** was later confirmed by X-ray crystallography when the structure of **13** in complex with human PI3Kγ revealed that the morpholine oxygen makes a hydrogen bond interaction with the backbone amide group of Val-882 within the ATP-binding domain of the kinase (Fig. 7) [39].

Although **13** suffered from rapid metabolic clearance (1 h), in vivo toxicity and lack of specificity, the compound helped the design of derivatives with improved potency against DNA-PK, selectivity and better physico-chemical properties.

The first generation of analogues were benzopyranone and pyrimidoisoquinolinone derivatives. Incorporation of a fused ring on the chromenone gave a fivefold improvement in potency against DNA-PK (**17**; DNA-PK IC$_{50}$ = 0.23 μM) (Table 2). Introduction of a methyl group on the morpholine ring gave no improvement in activity against DNA-PK (**18**; DNA-PK IC$_{50}$ = 0.19 μM). However, additional methyl groups, at the 2- or 6-position of morpholine, or replacement of the morpholine ring (e.g. piperidine, and piperazine) resulted in a loss of activity [42, 43]. Encouragingly, all early derivatives showed better selectivity for DNA-PK over other PIKK family members than the parent compound, e.g. **17** is 60-fold more potent against DNA-PK than PI3K (p110α) (Table 2).
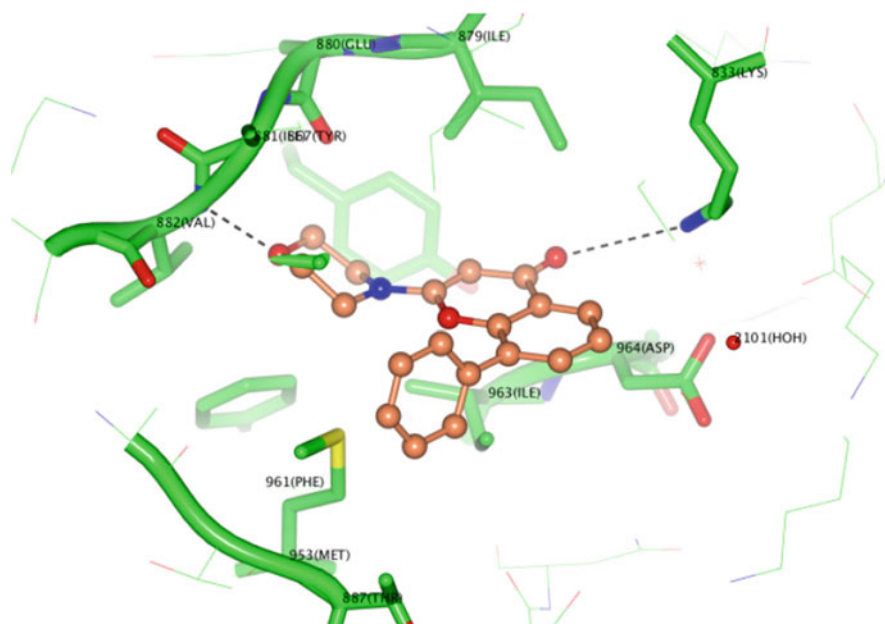
Fig. 7 Crystal structure of LY294002 (**13**) in complex with the ATP-binding domain of PI3Kγ [39]

Table 2 Inhibitory activity (IC$_{50}$ μM) against different PIKK family members [42]

	DNA-PK	PI3K (p110α)	ATM	ATR	mTOR
17	0.23	13	>100	>100	6.2
18	0.19	2.4	>100	>100	4.8
19	0.28	>100	>100	>100	5.3
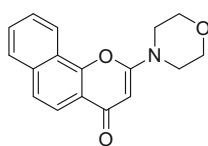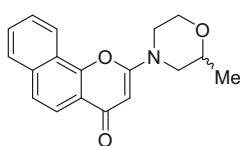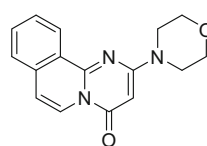
Replacement of the chromen-4-one scaffold by the isosteric pyrimidoisoquinolinone structure gave equipotent compounds (**19**; IC$_{50}$ = 0.28 μM) [44]. Several studies have demonstrated that **17** acts in vitro as a radiosensitiser [45], and as a chemo-potentiator of topoisomerase II poisons in human leukaemia cell lines [46].

A simplification of the chromenone core was attempted with the synthesis of a series of substituted monocyclic pyran-2-one, pyran-4-one, thiopyran-4-one and pyridin-4-one derivatives [47]. The pyran-4-one system and substitution at the pyranone 3- or 5-positions gave a loss of activity. However, library work on

6-substituted-2-morpholino-pyran-4-one and 6-substituted-2-morpholinothio-pyran-4-one led to the identification of **20** (DNA-PK; IC$_{50}$ = 0.18 μM) and **21** (DNA-PK IC$_{50}$ = 0.19 μM), both tenfold more potent against DNA-PK than the parent **13** [47, 48].
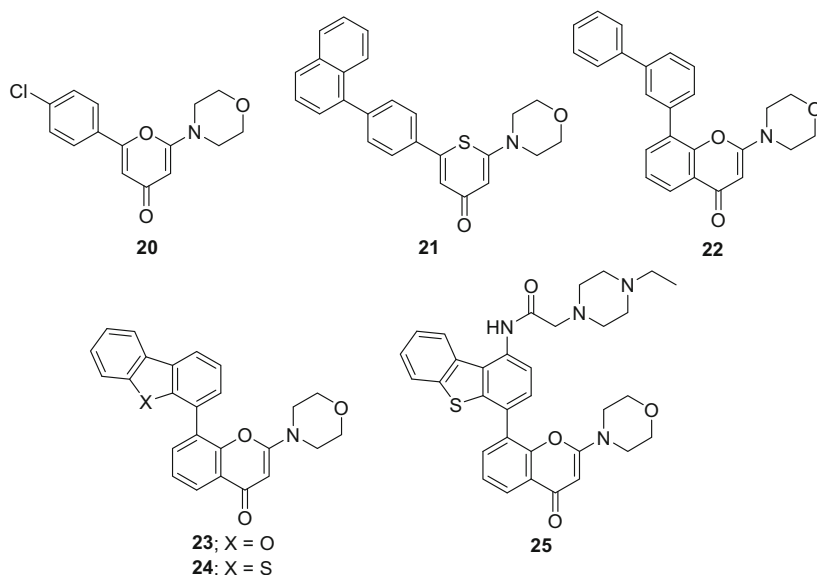
A library of 6-, 7- and 8-substituted chromenones were synthesised using a multi-parallel approach [49]. Interestingly, compound **22** (DNA-PK IC$_{50}$ = 0.11 μM) showed a tenfold increase in potency compared to **13**, whereas the dibenzofuranyl derivative (**23**) (DNA-PK IC$_{50}$ = 0.04 μM) displayed impressive potency against DNA-PK. The incorporation of a dibenzothiophenyl group led to NU7441 (**24**), a compound with a 100-fold increase in potency compared with the parent phenyl derivative **13** (DNA-PK IC$_{50}$ = 0.02 μM), along with excellent selectivity over the other PIKK family members (Table 3).

Compound **24** has been reported to sensitise tumour cells to ionising radiations (Fig. 8a) and increase the effect of etoposide (Fig. 8b) in vitro, indicating a good cellular permeability with a low inherent growth inhibitory activity [43, 50]. The compound has also been reported to cause doxorubicin-induced DNA DSBs (measured by γ-H2AX foci) to persist and also slightly decrease homologous recombination activity (assessed by Rad51 foci) [51].

An homology model of the ATP-binding site of DNA-PK, derived from the crystal structure of PI3Kγ, was used to guide further inhibitor design [39]. The newly synthesised compounds all possessed polar substituents at the dibenzothiophene 1-position, with an aim to improve physico-chemical properties [52]. Several exhibited high potency against DNA-PK and potentiated the

Table 3 NU7441 (**24**) inhibitory activity against different kinases of the PIKK family

	DNA-PK	PI3K	PI4K$_\beta$	ATM	ATR	mTOR
IC$_{50}$ (μM)	0.012	5	40	>100	>100	1.7
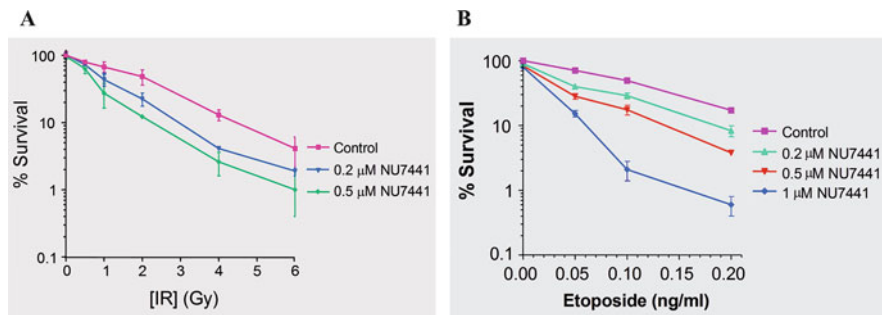
Fig. 8 (**a**) Radiosensitisation of HeLa cells by NU7441 (**24**). (**b**) Enhancement of etoposide cytotoxicity by NU7441 (**24**) in HeLa cells [43, 50]

cytotoxicity of ionising radiation (IR) in vitro tenfold or more (e.g. **25**; DNA-PK IC$_{50}$ = 5.0 ± 1 nM, IR dose modification ratio = 13). Furthermore, **25** was shown to potentiate not only IR in vitro but also DNA-inducing cytotoxic anticancer agents, both in vitro and in vivo. Counter-screening against other members of the PIKK family unexpectedly revealed that some of the compounds were potent mixed DNA-PK and PI3K inhibitors [52, 53]. The promising biological activity of **25** was accompanied by better drug-like properties compared to NU7441 (**24**), and acceptable plasma protein binding, combined with weak activity against hERG and a panel of CYP450 enzymes [52].

In efforts to optimise the biological and pharmaceutical properties of **24**, and to expand structure–activity relationships (SARs), the core chromenone scaffold and the dibenzothiophen-4-yl moiety have been systematically modified [54, 55]. As **22** is approximately tenfold more potent than the parent 8-phenylchromenone (**13**), this strongly indicated that the 3-phenyl substituent of **22** made additional binding interactions within the ATP-binding domain of DNA-PK. By probing this presumed binding interaction further, replacement of the 3-phenyl group of **22** by an isosteric thiophen-2-yl substituent (**26**) improved DNA-PK inhibitory activity approximately tenfold (DNA-PK; IC$_{50}$ = 18 nM) [54]. Subsequent homology modelling studies suggested that the heteroaryl substituent may occupy a putative hydrophobic pocket that could be further exploited, with further SAR resulting in the discovery of *O*-alkoxyphenylchromen-4-one (**27**) (DNA-PK; IC$_{50}$ = 8 nM) [54, 55].

Resolvable atropisomeric derivatives of **13** have also been described. Introduction of a methyl substituent, as a representative example, at the dibenzothiophene 3-position (**28**) (DNA-PK; IC$_{50}$ = 1.7 μM) or at the chromenone 7-position (**29**) (DNA-PK; IC$_{50}$ = 0.005 μM) of NU7441, generated stable pairs of atropisomers

Table 4 Inhibition of DNA-PK (IC$_{50}$ μM) by 3-substituted dibenzothiophen-4-yl derivatives and 7-substituted chromen-4-one derivatives

	R^1	R^2	DNA-PK inhibition
24	H	H	0.03
28	Me	H	1.7
28-(−)	Me	H	1.2
28-(+)	Me	H	100
29	H	Me	0.005
29-(−)	H	Me	0.002
29-(+)	H	Me	7

due to restricted rotation between the chromen-4-one and dibenzothiophene rings [56, 57]. Substitution at the dibenzothiophene 3-position (**28**) resulted in an approximately 60-fold reduction in potency of the racemic compound against DNA-PK compared with the parent compound (**24**). Interestingly, **29** showed a sixfold improvement in potency compared with the parent compound (Table 4).

Following resolution by chiral high-performance liquid chromatography (HPLC), biological evaluation against DNA-PK of each pair of atropisomers showed that DNA-PK inhibitory activity resided exclusively in the (−)-atropisomer ('eutomer') enantiomer, with the antipodal (+)-atropisomer ('distomer') proving inactive at 100 μM [57, 58].

26   **27**   **28**; R^1 = Me, R^2 = H
29; R^1 = H, R^2 = Me
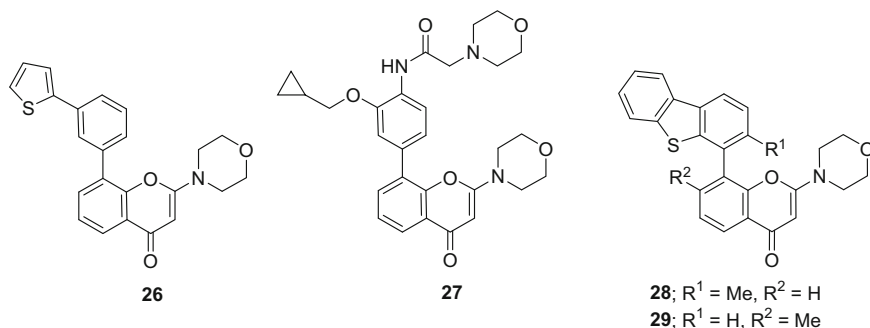
Pyridone OK-1035

3-Cyano-5-(4-pyridyl)-6-hydrazonomethyl-2-pyridone, OK-1035 (**30**), was reported to inhibit DNA-PK activity with an IC$_{50}$ of 8 μM and excellent selectivity (Table 5), appearing at first to be a good candidate for optimisation. However, this proved not to be the case and subsequent structural modifications provided only compounds with inferior potency against DNA-PK [59].

Table 5 Inhibition of DNA-PK and various protein kinases by OK-1035 (**30**)

	DNA-PK	PKA	PKC	CDK2	CKI	CKII	MAPK	EGFRK
IC$_{50}$ (µM)	8	390	>500	>500	>500	420	>500	>500
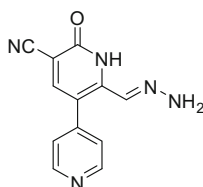
30

Phenol Related IC Series

Reported by the ICOS Corporation and Array BioPharma as part of a new series of DNA-PK inhibitors, 2-hydroxy-4-morpholin-4-yl-benzaldehyde (IC60211, IC$_{50}$ = 400 nM) (**31**) is a representative example of DNA-PK inhibitors possessing a morpholine motif. Optimisation of **31** led to the identification of a number of selective inhibitors (**32–36**; Table 6), all of which maintain the arylmorpholine substructure [60].
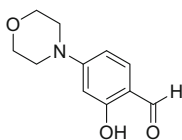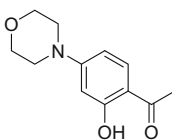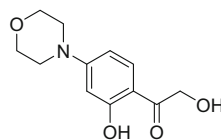
31   **32**   **33**
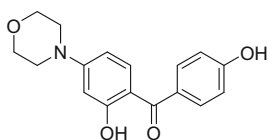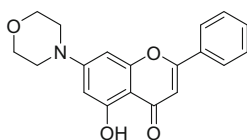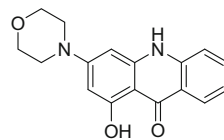
34   **35**   **36**

Compounds **32–34** have been reported to inhibit DNA DSB repair in cells not only as single agents but also in combination with chemotherapy and radiotherapy [61]. In vivo efficacy has also been demonstrated in combination studies using ionising radiation [62]. The small-molecule DNA-PK inhibitor **36** was found to synergise with 7-ethyl-10-hydroxy-camptothecin (SN38), to enhance killing of colon cancer cells in vitro. Compound **36** is relatively non-toxic, with an IC$_{50}$ of 29 µM in both HCT-116 and HT-29 cell lines. Significant reductions in the IC$_{50}$

Table 6 Inhibitory activity (IC$_{50}$ nM) of representative DNA-PK inhibitors against various PI3Ks [60]

	DNA-PK	p110$_\alpha$	p110$_\beta$	p110$_\delta$	p110$_\gamma$
31	400	10,000	2,800	5,100	37,000
32	120	1,400	135	880	1,000
33	44	890	42	490	180
34	35	2,700	400	1,800	5,000
35	34	3,800	1,700	2,800	7,900

values of SN38 were detected at 5 and 10 μM of inhibitor [51]. Additionally, **36** can synergistically sensitise three genetically diverse breast cancer cell lines to doxorubicin and cisplatin [63]. Improved cytotoxicity and significant synergy were observed with the topoisomerase II inhibitor, doxorubicin or cisplatin in the presence of non-toxic concentrations of **36**. Furthermore, **36** was shown to decrease doxorubicin-induced DNA-PKcs autophosphorylation on Ser2056 and increase doxorubicin-induced DNA fragmentation [64].

SU11752

In an effort to develop a specific DNA-PK inhibitor, Sugen undertook a screening campaign of 3-substituted indolin-2-ones and successfully identified the ATP-competitive DNA-PK inhibitor SU11752 (**37**). Interestingly, the compound showed good potency against DNA-PK (IC$_{50}$ = 0.13 ± 0.028 μM) combined with selectivity over PI3K (p110γ; IC$_{50}$ = 1.10 μM) [40, 65]. The compound was also reported as a poor inhibitor of ATM kinase activity in cells [65].

37
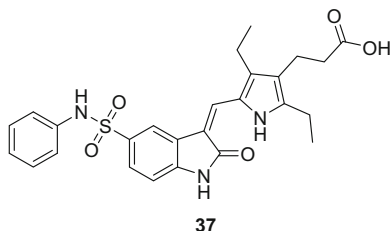
Vertex

In a patent published by Vertex Pharmaceuticals, 251 of the compounds described had a K_i of less than 0.1 μM for the inhibition of DNA-PK [66]. More recently, it has been disclosed that VX-984 (**38**) is a DNA-PK inhibitor currently undergoing a phase I clinical study, in combination with pegylated liposomal doxorubicin in patients with advanced solid tumours or lymphomas.

38
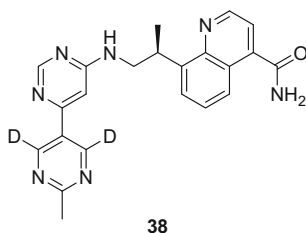
Compound **38** is reported to have an IC_{50} of 88 ± 64 nM for inhibition of DNA-PKcs autophosphorylation (Ser2056) in A549 lung cancer cells, with good selectivity versus other PI3K family members [67].

3.2   Ataxia-Telangiectasia Mutated Kinase

3.2.1   Structural Features of Ataxia-Telangiectasia Mutated Kinase

The ATM gene codes for a 350 kDa protein, consisting of 3,056 amino acids. Characteristic for ATM are five domains: from the N-terminus to C-terminus these are the HEAT repeat domain, the FAT domain, the kinase domain (KD), the PIKK-regulatory domain (PRD) and the FAT-C-terminal (FATC) domain. The FAT domain interacts with the kinase domain of ATM to stabilise the C-terminal region. The KD effects kinase activity, whilst the PRD and the FATC domain regulate it. Although no structure for ATM has been solved, the overall shape of ATM is envisaged to be very similar to DNA-PKcs, comprised of a head and a long arm, which wraps around double-stranded DNA after a conformational change. The entire N-terminal domain, together with the FAT domain, is predicted to adopt an α-helical structure. This α-helical structure is believed to form a tertiary structure, which has a curved, tubular shape. FATC is the C-terminal domain with a length of about 30 amino acids. It is highly conserved and consists of an α-helix followed by a sharp turn, which is stabilised by a disulfide bond [68].

### 3.2.2   Ataxia-Telangiectasia Mutated Kinase and the Repair Pathway

ATM is one of the best known PIKK members. The absence of this protein is characteristic of a neurodegenerative disorder termed ataxia-telangiectasia, which involves a high sensitivity to ionising radiation, neurodegeneration and immuno-deficiency [69]. ATM has the main function of regulating the G1/S and G2/M cell cycle checkpoints in response to DSBs, preventing progression of the cell cycle when DNA is damaged. The cascade mechanism involves activation of tumour suppressor protein p53 via phosphorylation [70], which stimulates the transcription

of p21 protein and interacts with CDK2/Cyclin E halting progression of the cycle from G1 to S phase and allowing DNA repair [71]. Another pathway of interaction between ATM and p53 involves activation of CHK2 protein kinase by ATM [72]. CHK2 obstructs the p53-MDM2 interaction by phosphorylation of p53, leading to arrest of the cell cycle. In addition, ATM also directly phosphorylates MDM2 (Ser395), altering its interaction with p53. These pathways act via ATM to halt cell cycle progression in response to DNA damage [73]. Thus, the main role of ATM is the detection of DNA damage, being itself an important component of the NHEJ pathway [74].

3.2.3   Ataxia-Telangiectasia Mutated Kinase Inhibitors

Although ATM has attracted considerable interest as a therapeutic target, very few useful inhibitors with potent activity have been reported. Many of the known inhibitors of ATM, including wortmannin (**12**) (IC_{50} = 150 nM) and caffeine (**39**) (IC_{50} = 200 μM), lack specificity, hence inhibiting a wide range of PIKKs [75].
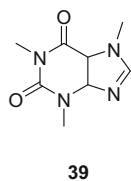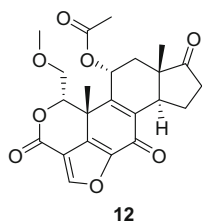
KU-55933, KU-60019 and KU-59403

Important inhibitors were developed by screening of combinatorial libraries around the structure of LY294002 (**13**). The KuDOS Pharmaceuticals-Newcastle group identified weak ATM-inhibitory activity within a pyran-4-one series (exemplified by **40**), which prompted further chemical library generation based on this scaffold [47]. Replacing the 4-methoxyphenyl group of **40** resulted in the identification of **41**, a highly selective inhibitor of ATM. Compound **41** has an IC_{50} of 13 nM and K_i of 2.2 nM, with marked sensitisation of cancer cells to IR and topoisomerase II inhibitors in vitro [47, 76].
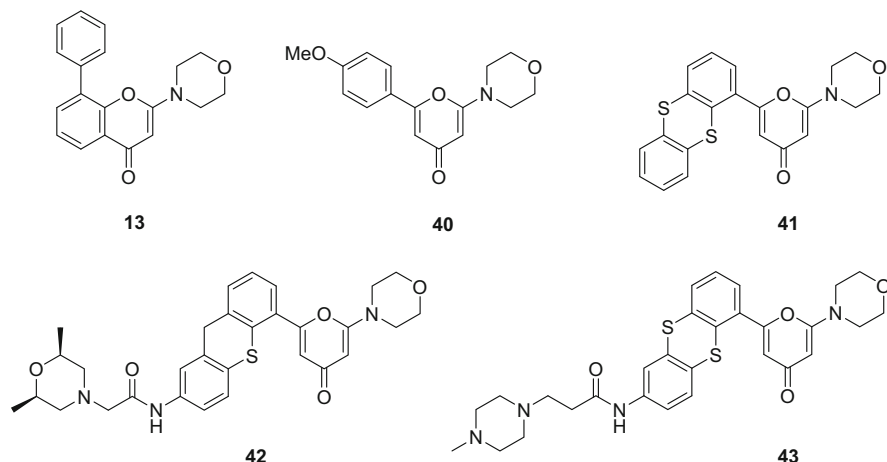
Modification of the thianthrene substituent of **41** was investigated, but minor structural changes were commonly detrimental to activity. An improved water-soluble analogue **42**, included a 2,6-dimethylmorpholin-4-yl group at position 2 on thioxanthene, leading to potent ATM-inhibitory activity (IC_{50} = 6.3 nM), a twofold improvement in ATM inhibition over **41**. Combining potency, cellular activity (enhancement ratios of 2.1–2.9 at 0.6 μM) and pharmacokinetics, **42** was proven to be highly selective with limited toxicity towards healthy cells. It was shown to inhibit the DDR and reduce AKT phosphorylation and prosurvival signalling. Inhibition of migration and invasion was also reported, along with effective radiosensitisation of human glioma cells [76, 77]. A further analogue KU-59403 (**43**) showed improved potency over **41** (Table 7), as well as improved solubility and bioavailability, allowing for in vivo studies and advanced preclinical evaluation. Compound **41** is without intrinsic cytotoxicity but is a potent enhancer of topoisomerase I and II poison cytotoxicity in vitro and was shown to increase the efficacy of topoisomerase I and II poisons in vivo without intrinsic toxicity despite normal tissue exposure [78].

CP466722

Identified by Pfizer from a targeted library screening campaign, CP466722 (**44**) is a highly selective and rapidly reversible ATM inhibitor that does not inhibit other PIKK family members or PI3K in a cellular setting [79].

Table 7 Inhibition of ATM and related kinase activity by LY294002 (**13**), KU55933 (**41**) and KU59403 (**43**) [78]

	Enzyme IC$_{50}$, µmol/L					
	ATM	DNA-PK	PI3K	ATR	PI4K	mTOR
13	>100	1.5	2	100	ND	3
41	0.013	2.5	1.7	>10	>10	9.3
43	0.003	9.1	10	>100	>10	14

44
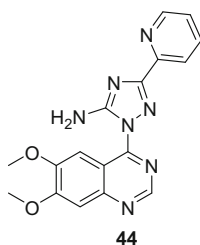
It has been shown in clonogenic survival assays to be sufficient to sensitise cells to IR and suggests that therapeutic radiosensitisation may only require ATM inhibition for short periods of time. Transient exposure of tumour cells to **44** inhibits ATM adequately to enhance the cell's sensitivity to irradiation. After compound washout, the inhibition was rapidly and completely reversed, suggesting that a treatment with a minimal dose of **44** for brief periods may achieve a maximum therapeutic effect [79].

3-Quinoline Carboxamides

A novel series of 3-quinoline carboxamides was recently identified at AstraZeneca through a direct screening approach [80]. Initial screening hit **45** was a submicromolar inhibitor of ATM (IC$_{50}$ = 0.008 µM), displaying promising selectivity over other PIKKs and PI3K isoforms (>tenfold against DNA-PK and >400-fold against mTOR). Compound **46** exhibited a tenfold improvement in potency (IC$_{50}$ = 0.073 µM) over **45**, along with increased selectivity over ATR.
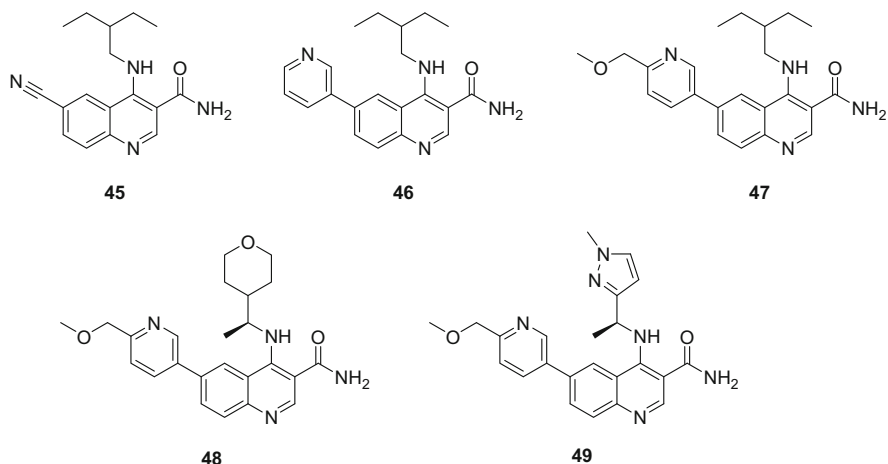
Subsequent investigation at the C4 position did not provide any significant improvement but rather gave vital insight into the how the nature of substituents could influence pharmacokinetic profiles and selectivity. Investigation at C6 was carried out in parallel, whereby it was discovered that p-substituted analogue **47** exhibited improved potency ($IC_{50} = 0.045$ μM) and kinase selectivity. Extensive SAR at each position on the quinoline core allowed the rapid discovery of optimum combinations and resulted in the finding of **48** ($IC_{50} = 0.046$ μM) and **49** ($IC_{50} = 0.033$ μM) as potent and highly selective ATM inhibitors, with overall absorption, distribution, metabolism and excretion (ADME) properties suitable for oral dosing. In combination with the DSB-inducing agent irinotecan, significant tumour volume reductions were observed in an SW620 colorectal cancer xenograft model [80].

3.3 Ataxia-Telangiectasia and Rad3-Related Kinase

3.3.1 Structural Features of Ataxia-Telangiectasia and Rad3-Related Kinase

ATR (human AT and Rad3 related) is a large kinase comprising 2,644 amino acids, with a molecular weight of 300 kDa. ATR-interacting protein (ATRIP) is the 85 kDa binding partner of ATR, which binds to the N-terminus to promote localisation to sites of replication stress [81]. There are no recognised differences in the phenotypes that result from the loss of ATR or ATRIP, which suggests that ATRIP should be considered a subunit of ATR holoenzyme [82].

Fig. 9 Cascade pathways initiated by ataxia-telangiectasia mutated (ATM) and ataxia-telangiectasia and Rad3-related (ATR) kinase
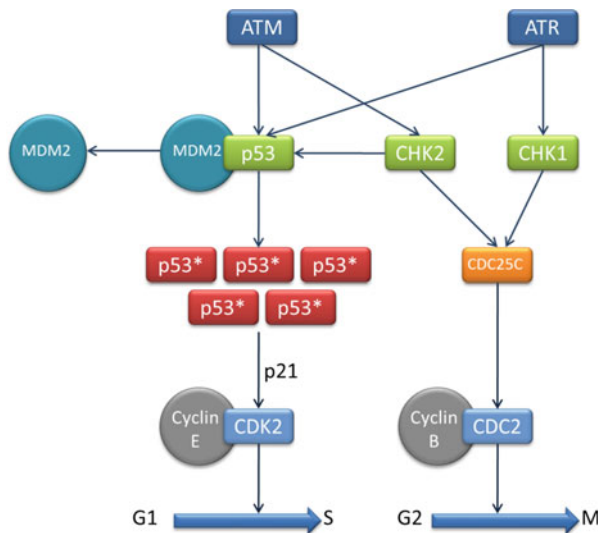
3.3.2 Ataxia-Telangiectasia and Rad3-Related Kinase and the Repair Pathway

ATR is a member of the PIKK family closer in size and function to ATM, and sharing around 60% of the kinase domain. This similarity is reflected by a degree of overlapping function between the two kinases (Fig. 9) [73]. ATR has shown ability to phosphorylate p53 on Ser15 in vitro [83] and in vivo [84] similar to ATM. However, ATR phosphorylation responds mainly to DNA damage induced by UV radiation and has a faster response to DNA damage. It is believed that ATR is responsible for maintaining the phosphorylated state of the targets p53, murine double minute 2 (MDM2) and CHK2 [84]. ATR is also involved in a pathway initiated by phosphorylation of checkpoint kinase 1 (CHK1) kinase (Ser345) [85].

3.3.3 Ataxia-Telangiectasia and Rad3-Related Kinase Small-Molecule Inhibitors

Research on inhibitors of ATR (ATRis) has been on-going for more than a decade, with the first small-molecule inhibitors identified in the late 1990s. Despite this, novel patented data has only been disclosed from 2009 onwards, with the first report on ATR-selective small-molecule inhibitors published in 2009 [86]. In 2006, Knight et al. conducted a study in which a chemically diverse set of PI3K inhibitors in preclinical development were screened against several lipid kinases. Compounds **50–55** were identified as moderate ATRis in an enzymatic assay (ATR IC_{50} 0.85–21 μM), but with no selectivity over DNA-PK or ATM [87]. In the same study, LY294002 (**13**), originally developed as a PI3K inhibitor [41], but later

recognised as a pan-inhibitor of the PIKK family [88, 89], was determined to be inactive (ATR IC$_{50}$ = >100 µM) [87].
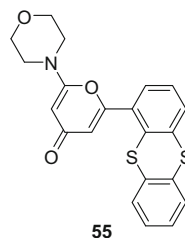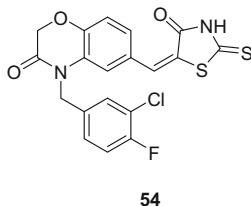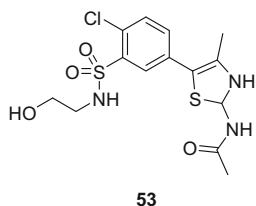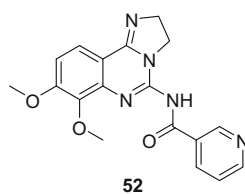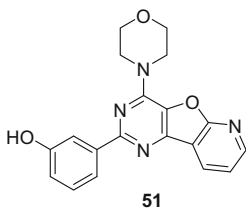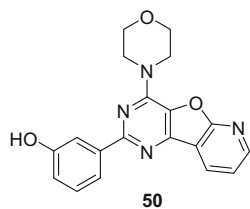
Wortmannin and Caffeine

The fungal metabolite wortmannin (12) is an irreversible pan-inhibitor of the PIKK family but has relatively weak ATR activity (ATR IC$_{50}$ = 1.8 µM, ATM IC$_{50}$ = 150 nM and DNA-PK IC$_{50}$ = 16 nM). It has been proposed that the radiosensitising effect is perhaps due to the inhibition of DNA-PK kinase activity rather than ATR inhibition [90].

Similarly, caffeine (39) has been recognised as a weak pan-PIKK inhibitor (ATR IC$_{50}$ = 1.1 mM, ATM IC$_{50}$ = 0.2 mM and DNA-PK IC$_{50}$ = 10 mM), with the radiosensitising effect attributed to both ATR and ATM kinases [91].

Schisandrin B
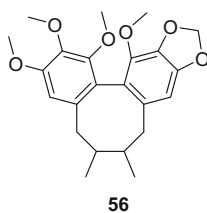
In 2007, Nishida et al. filed a patent which revealed the dibenzocyclooctadiene lignans schisandrins and gomisins as the first ATR-selective small-molecule inhibitors [92]. One of the compounds of interest, Schisandrin B (**56**), is a naturally occurring dibenzocyclooctadiene lignin found in *Schisandra chinensis*, a medicinal herb. It was demonstrated that Schisandrin B was able to abolish UV-induced intra-S-phase and G2/M cell cycle checkpoints and increase the cytotoxicity of UV radiation in human lung cancer cells (A549 adenocarcinoma). Furthermore, Schisandrin B was found to inhibit p53 and CHK1 ATR-dependent phosphorylation but did not prevent ATR-activating association to the ATRIP. It is selective for ATR kinase activity in vitro ($IC_{50} = 7.25$ µM), but due to the weak inhibitory potency against ATR, high drug concentrations (30 µM for cellular assays) were necessary [86].

Torin 2

Torin 2 (**57**) was described in 2013 as a potent ATP-competitive inhibitor of ATM and ATR (ATM $IC_{50} = <0.01$ µM, ATR $IC_{50} = <0.01$ µM) [93].

57
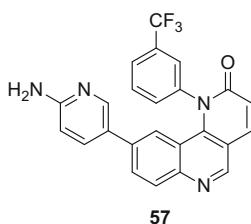
Torin 2 inhibited the cellular activity of the ATR kinase, as assessed by phosphorylation status of CHK1[S317] following exposure of HCT116 colon cancer cells to UV-induced DNA damage [94, 95].

ETP-46464

Researchers at the Spanish National Cancer Research Centre screened a collection of 623 PI3K inhibitors, aiming to find hits against the PI3KK family, specifically ATR [96]. Following a high-throughput microscopy screen, ETP-46464 (**58**), was identified as an encouraging hit, which potently inhibited ATR in vitro ($IC_{50} = 14$ nM) and showed some selectivity over ATM. ETP-46464 suffers from poor pharmacological properties in mice, halting development.
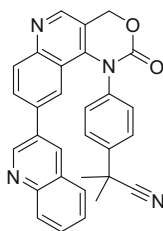
58

NU6027

In 2001, a more potent ATR inhibitor, NU6027 (**59**) ($IC_{50} = 0.1$ µM), was reported to sensitise several breast and ovarian cancer cell lines to IR and several chemotherapeutic agents [97].
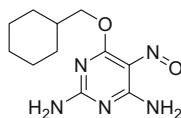
59

As **59** was originally developed as a CDK2 inhibitor ($IC_{50} = 2.2$ µM), it was found to be a non-selective inhibitor. Compound **59** was synergistic with the PARP inhibitor rucaparib, in MCF7 cells and synthetically lethal in XRCC1-defective EM9 cells, confirming that impaired DNA SSB repair is synthetically lethal with ATR inhibition.

NVP-BEZ235

In 2011, Toledo et al. reported the results of a cell-based compound library screening approach for the identification of potent ATR inhibitors [94]. One of the compounds identified to possess significant inhibitory against ATR kinase was NVP-BEZ235 (**60**) (ATR, ATM, DNA-PK $IC_{50} < 21$ nM), a drug originally revealed by Novartis [98] as a highly potent PI3K/mTOR inhibitor.

60
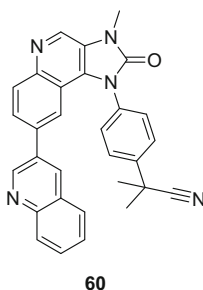
NVP-BEZ235 inhibited ionising radiation-induced ATM, CHK1, CHK2 and DNA-PK phosphorylation and affected ionising radiation-induced γH2AX formation. NVP-BEZ235 was, at the time of writing, undergoing clinical trials for solid tumours.

WYC02 and WYC0209

WYC02 (**61**) is a flavonoid isolated and identified from the whole plant extract of *Thelypteris torresiana*, a fern species native to Taiwan.

61   **62**
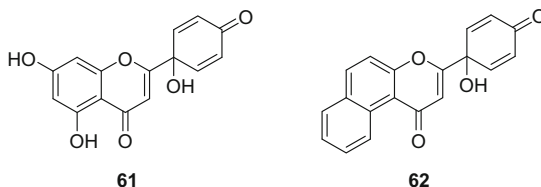
The natural compound **61** and its more potent synthetic analogue WYC0209 (**62**) have been shown to inhibit ATR-mediated CHK1 phosphorylation, impair the G2/M checkpoint and improve cancer sensitivity to cisplatin [99]. Further studies showed that **62** inhibits ATR kinase activity at least four times greater than **61** [100].

AZD6738

Another ATR inhibitor with excellent drug metabolism and pharmacokinetic (DMPK) properties currently in clinical development is the AstraZeneca inhibitor AZD6738 (**63**). Initial hit (**64**) was identified as a potent ATRi from a screening campaign (cellular IC_{50} = 1.1 nM), with high selectivity against other PIKK and PI3K kinases.
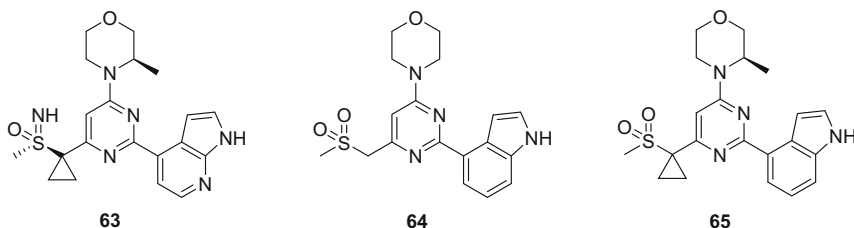
Optimisation from the superior screening hit **64** within tight SAR space enabled the discovery of **65**, a potent and selective ATR inhibitor which has been shown to possess substantial in vivo single agent activity in MRE11A-deficient cancer cells at well-tolerated doses [101, 102]. Compound **65** had poor aqueous solubility but displayed high Caco-2 permeability and good stability in rat hepatocytes, leading to satisfactory bioavailability in a rat PK study. In contrast to **65**, **63** incorporates a structural change, whereby a sulfoximine replaced the methyl sulfone as a rational attempt to improve solubility. As a result, **63** has notably improved solubility, bioavailability, pharmacokinetics and pharmacodynamics and is suitable for oral dosing [103]. It acts to inhibit phosphorylation of the ATR downstream target CHK1, whilst increasing phosphorylation of the DNA DSB marker γH2AX in vitro. It significantly increases antitumour activity of IR or carboplatin in vivo [103, 104]. A phase I clinical trial to assess the safety of AZD6738 alone and in combination with radiotherapy in patients with solid tumours was underway at the time of writing.

VE-821

A high-throughput screening campaign led to the discovery of the first series of both potent and selective ATR kinase inhibitors by Vertex Pharmaceuticals. The compounds generally featured a central 2-aminopyrazine core. Compounds that lacked the 2-amino group resulted in higher enzymatic ATR K_i values [105].
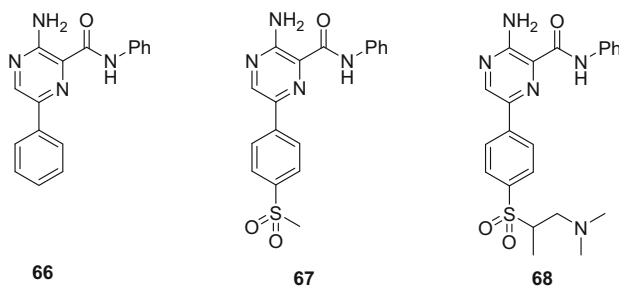
Pyrazine derivative (**66**) was a promising ATP-competitive hit (ATR; $IC_{50} = 0.62$ μM), with excellent selectivity over DNA-PK and ATM [106]. The suboptimal potency and cellular activity was addressed by further SAR, guided by homology modelling of the ATP-binding domain of ATR. The pyrazine N1 serves as the hydrogen bond acceptor group for the interaction with the backbone NH of Val2378, and the adjacent 2-amino group donates a hydrogen bond to the carbonyl of Glu2380 [107].

The introduction of a 4-sulfonyl group (**67**) ($IC_{50} = 26$ nM) increased the potency and selectivity, attributed to a favourable interaction between the sulfone oxygen and the NH of the ATR-specific residue Gly2385. Compound **67** was shown to be a potent ATP-competitive inhibitor of ATR ($K_i = 13$ nM) with good selectivity over a panel of the related PIKKs, ATM, DNA-PKcs and mTOR [106]. It inhibited phosphorylation of the ATR downstream target CHK1 at Ser345 and showed strong synergy with genotoxic agents from multiple classes in the colorectal cancer cell line HCT116. The observed chemo-sensitisation was most pronounced with DNA cross-linking agents such as cisplatin and carboplatin and was further enhanced by knockdown of p53 expression, in ATM-deficient cells or in combination with the specific ATM inhibitor KU-55933 (**41**) (see Sect. 3.2.3). Significantly, the cytotoxicity of **67** in normal cells appeared minimal, causing only a reversible growth arrest without significant induction of cell death [106].

Further optimisation of **67** led to compound **68**, which was selected for in-depth biological evaluation. Compound **68** combines potent ATP-competitive ATR-inhibitory activity ($K_i = 6$ nM) and excellent cellular activity. It also possesses good physico-chemical properties, including aqueous solubility, cell permeability and minimal efflux.

VE-822/VX-970

VE-822 (**69**) is an analogue of **67**, which possesses increased potency and selectivity against ATR. It also benefits from increased solubility and good pharmacokinetic properties.

69
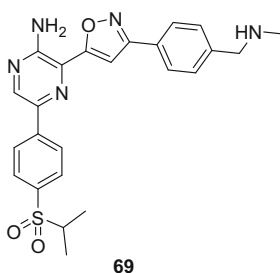
It was shown to potently radiosensitise pancreatic cancer cell lines in vitro. Additionally, treatment with **69** profoundly radiosensitised xenograft models of human pancreatic cancer and further increased the growth delay induced by IR combined with gemcitabine. Crucially, **69** was well tolerated in mice and did not enhance toxicity in normal cells and tissues [108]. The compound is now known as VX-970 and was the first selective ATR inhibitor to enter clinical trial development. In 2014, Vertex Pharmaceuticals published a study in which it was shown to markedly sensitise a panel of non-small cell lung cancer cell lines, but not normal cells, to multiple DNA-damaging drugs, namely cisplatin, oxaliplatin, gemcitabine and etoposide [109]. The data suggested that VX-970 may have the potential to increase the efficacy of DNA-damaging therapy in patients with lung cancer. The safety, tolerability and pharmacokinetics were, at the time of writing, being assessed in a phase I clinical trial. The strategy was to evaluate VX-970 in early stage trials in selected tumour types and patient subtypes that are expected to be responsive to ATR inhibition based on biomarker data. It is expected to be evaluated as monotherapy and in combination with other cancer therapies, including PARP inhibitors and other targeted agents, chemotherapy and radiotherapy.

References

1. Jackson SP, Bartek J (2009) The DNA-damage response in human biology and disease. Nature 461:1071–1078
2. Hoeijmakers JHJ (2001) Genome maintenance mechanisms for preventing cancer. Nature 411(6835):366–374
3. De Bont R, van Larebeke N (2004) Endogenous DNA damage in humans: a review of quantitative data. Mutagenesis 19(3):169–185
4. Sibanda BLD, Chirgadze DY, Blundell TL (2010) Crystal structure of DNA-PKcs reveals a large open-ring cradle comprised of HEAT repeats. Nature 463(1277):118–121
5. Deans AJ, West SC (2011) DNA interstrand crosslink repair and cancer. Nat Rev Cancer 11 (7):467–480
6. Schärer OD (2003) Chemistry and biology of DNA repair. Angew Chem Int Ed 42 (26):2946–2974
7. Pogozelski WK, Tullius TD (1998) Oxidative strand scission of nucleic acids: routes initiated by hydrogen abstraction from the sugar moiety. Chem Rev 98(3):1089–1108
8. Pâques F, Haber JE (1999) Multiple pathways of recombination induced by double-strand breaks in Saccharomyces cerevisiae. Microbiol Mol Biol Rev 63(2):349–404
9. Nakamura J, Walker VE, Upton PB, Chiang S-Y, Kow YW, Swenberg JA (1998) Highly sensitive apurinic/apyrimidinic site assay can detect spontaneous and chemically induced depurination under physiological conditions. Cancer Res 58(2):222–225
10. Loeb LA, Preston BD (1986) Mutagenesis by apurinic/apyrimidinic sites. Annu Rev Genet 20 (1):201–230
11. Robertson AB, Klungland A, Rognes T, Leiros I (2009) DNA repair in mammalian cells. Cell Mol Life Sci 66(6):981–993
12. Odell ID, Wallace SS, Pederson DS (2013) Rules of engagement for base excision repair in chromatin. J Cell Physiol 228(2):258–266
13. Furgason JM, Bahassi EM (2013) Targeting DNA repair mechanisms in cancer. Pharmacol Ther 137(3):298–308

14. Nouspikel T (2009) Nucleotide excision repair: variations on versatility. Cell Mol Life Sci 66 (6):994–1009
15. Iyer RR, Pluciennik A, Burdett V, Modrich PL (2005) DNA mismatch repair: functions and mechanisms. Chem Rev 106(2):302–323
16. Khanna KK, Jackson SP (2001) DNA-double-strand breaks: signalling, repair and the cancer connection. Nat Genet 27:247–254
17. Christmann M, Tomicic MT, Roos WP, Kaina B (2003) Mechanisms of human DNA repair: an update. Toxicology 193:3–34
18. Collis SP, DeWeese TL, Jeggo PA, Parker AR (2005) The life and death of DNA-PK. Oncogene 24:949–961
19. Shiloh Y (2006) The ATM-mediated DNA-damage response: taking shape. Trends Biochem Sci 31:402–410
20. Petrini JH (2000) The Mre11 complex and ATM: collaborating to navigate S phase. Curr Opin Cell Biol 12:293–296
21. Sancar A, Lindsey-Boltz LA, Unsal-Kacmaz K, Linn S (2004) Molecular mechanisms of mammalian DNA repair and the DNA damage checkpoints. Annu Rev Biochem 73:39–85
22. West SC (2003) Molecular views of recombination proteins and their control. Nat Rev Mol Cell Biol 4:435–445
23. Finlay MRV, Griffin RJ (2012) Modulation of DNA repair by pharmacological inhibitors of the PIKK protein kinase family. Bioorg Med Chem Lett 22(17):5352–5359
24. Ma C-C, Li H, Wan R-Z, Liu Z-P (2014) Developments of DNA-dependent protein kinase inhibitors as anticancer agents. Mini-Rev Med Chem 14:884–895
25. Shiloh Y (2003) ATM and related protein kinases: safeguarding genome integrity. Nat Rev Cancer 3(3):155–168
26. Grimson A, O'Connor S, Newman CL, Anderson P (2004) SMG-1 is a phosphatidylinositol kinase-related protein kinase required for nonsense-mediated mRNA decay in Caenorhabditis elegans. Mol Cell Biol 24(17):7483–7490
27. Laplante M, Sabatini DM (2012) mTOR signaling in growth control and disease. Cell 149 (2):274–293
28. Downs JA, Jackson SP (2004) A means to a DNA end: the many roles of Ku. Nat Rev Mol Cell Biol 5:367–378
29. Neal JA, Meek K (2011) Choosing the right path: does DNA-PK help make the decision? Mutat Res-Fund Mol M 711(1–2):73–86
30. Walker JR, Corpina RA, Goldberg J (2001) Structure of the Ku heterodimer bound to DNA and its implications for double-strand break repair. Nature 412:607–614
31. Hammel M, Yu Y, Mahaney BL, Cai B, Ye R, Phipps BM, Rambo RP, Hura GL, Pelikan M, So S, Abolfath RM, Chen DJ, Lees-Miller SP, Tainer JA (2010) Ku and DNA-dependent protein kinase dynamic conformations and assembly regulate DNA binding and the initial non-homologous end joining complex. J Biol Chem 285:1414–1423
32. Fang B (2014) Development of synthetic lethality anticancer therapeutics. J Med Chem 57 (19):7859–7873
33. Ma Y, Pannicke U, Schwarz K, Lieber MR (2002) Hairpin opening and overhang processing by an Artemis/DNA-dependent protein kinase complex in nonhomologous end joining and V (D)J recombination. Cell 108:781–794
34. Mahaney BL, Meek K, Lees-Miller SP (2009) Repair of ionizing radiation-induced DNA double-strand breaks by non-homologous end-joining. Biochem J 417:639–650
35. Pospiech H, Rytkinen AK, Syvaoja JE (2001) The role of DNA polymerase activity in human non-homologous end joining. Nucleic Acids Res 29:3277–3288
36. Dahm K (2008) Role and regulation of human XRCC4-like factor/Cernunnos. J Cell Biochem 104:1534–1540
37. Powis G, Bonjouklian R, Breggren MM, Gallegos A, Abraham R, Ashendel C, Zalkow L, Matter WF, Dodge J, Grindey G, Vlahos CJ (1994) Wortmannin, a potent and selective inhibitor of phosphatidylinositol-3-kinase. Cancer Res 54:2419–2423

38. Wymann MP, Bulgarelli-Leva G, Zvelebil MJ, Pirola L, Vanhaesebroeck B, Waterfield MD, Panayotou G (1996) Wortmannin inactivates phosphoinositide 3-kinase by covalent modification of Lys-802, a residue involve in the phosphate transfer reaction. Mol Cell Biol 16:1722–1733
39. Walker EH, Pacold ME, Perisic O, Stephens L, Hawkins PT, Wymann MP, Williams RL (2000) Structural determinants of phosphoinositide 3-kinase inhibition by wortmannin, LY294002, quercetin, myricetin and staurosporine. Mol Cell 6:909–919
40. Izzard RA, Jackson SP, Smith GCM (1999) Competitive and noncompetitive inhibition of the DNA-dependent protein kinase. Cancer Res 59:2581–2586
41. Vlahos CJ, Matter WF, Hui KY, Brown RFA (1994) Specific inhibitor of phosphatidylinositol 3-kinase, 2-(4-morpholinyl)-8-phenyl-4H-1-benzopyran-4-one (LY294002). J Biol Chem 269:5241–5248
42. Griffin RJ, Fontana G, Golding BT, Guiard S, Hardcastle IR, Leahy JJJ, Martin N, Richardson C, Rigoreau L, Stockley M, Smith GCM (2005) Selective benzopyranone and pyrimido[2,1-a]isoquinolin-4-one inhibitors of DNA-dependent protein kinase: synthesis, structure-activity studies, and radiosensitization of a human tumor cell line in vitro. J Med Chem 48:569–585
43. Hardcastle IR, Cockcroft X, Curtin NJ, Desage-El Murr M, Leahy JJJ, Stockley M, Golding BT, Rigoreau L, Richardson C, Smith GCM, Griffin RJ (2005) Discovery of potent chromen-4-one inhibitors of the DNA-dependent protein kinase (DNA-PK) using a small-molecule library approach. J Med Chem 48:7829–7846
44. Cano C, Barbeau RO, Bailey C, Cockcroft X, Curtin N, Duggan H, Frigerio M, Golding BT, Hardcastle IR, Hummersone MG, Knights C, Menear KA, Newell DR, Richardson C, Smith GCM, Spittle B, Griffin RJ (2010) DNA-dependent protein kinase (DNA-PK) inhibitors; synthesis and biological activity of quinolin-4-one and pyridopyrimidin-4-one surrogates for the chromen-4-one chemotype. J Med Chem 53:8498–8507
45. Veuger SJ, Curtin NJ, Richardson CJ, Smith GCM, Durkacz BW (2003) Radiosensitization and DNA repair inhibition by the combined use of novel inhibitors of DNA-dependent protein kinase and poly(ADP-ribose) polymerase-1. Cancer Res 63:6008–6015
46. Willmore E, de Caux S, Sunter NJ, Tilby MJ, Jackson GH, Austin CA, Durkacz BW (2004) A novel DNA-dependent protein kinase inhibitor, NU7026, potentiates the cytotoxicity of topoisomerase II poisons used in the treatment of leukemia. Blood 103:4659–4665
47. Hollick JJ, Rigoreau JM, Cano-Soumillac C, Cockcroft X, Curtin N, Frigerio M, Golding BT, Guiard S, Hardcastle IR, Hickson I, Hummersone MG, Menear KA, Martin N, Matthews I, Newell DR, Ord R, Richardson C, Smith GCM, Griffin RJ (2007) Pyranone, thiopyranone and pyridone inhibitors of phosphatidylinositol 3-kinase related kinases (PIKKs). Structure-activity relationships for DNA-dependent protein kinase (DNA-PK) inhibition, and identification of the first potent and selective inhibitor of the ataxia telangiectasia mutated (ATM) kinase. J Med Chem 50:1958–1972
48. Hollick JJ, Golding BT, Hardcastle IR, Martin N, Richardson C, Rigoreau L, Smith GCM, Griffin RJ (2003) 2,6-Disubstituted pyran-4-one and thiopyran-4-one inhibitors of DNA-dependent protein kinase (DNA-PK). Bioorg Med Chem Lett 13:3083–3086
49. Leahy JJJ, Golding BT, Griffin RJ, Hardcastle IR, Richardson C, Rigoreau L, Smith GCM (2004) Identification of a highly potent and selective DNA-dependent protein kinase (DNA-PK) inhibitor (NU7441) by screening of chromenone libraries. Bioorg Med Chem Lett 14:6083–6087
50. Zhao Y, Thomas HD, Batey M, Cowell I, Richardson C, Griffin R, Calvert AH, Newell DR, Smith GCM, Curtin N (2006) Preclinical evaluation of a potent novel DNA-dependent protein kinase inhibitor NU7441. Cancer Res 66:5354–5362
51. Tavecchio M, Munck JM, Cano C, Newell DR, Curtin NJ (2012) Further characterisation of the cellular activity of the DNA-PK inhibitor, NU7441, reveals potential cross-talk with homologous recombination. Cancer Chemother Pharmacol 69:155–164

52. Cano C, Saravanan K, Bailey C, Bardos J, Curtin NJ, Frigerio M, Golding BT, Hardcastle IR, Hummersone MG, Menear KA, Newell DR, Richardson CJ, Shea K, Smith GCM, Thommes P, Ting A, Griffin RJ (2013) 1-Substituted (dibenzo[*b*,*d*]thiophen-4-yl)-2-morpholino-4*H*-chromen-4-ones endowed with dual DNA-PK PI3-K inhibitory activity. J Med Chem 56:6386–6401

53. Munck JM, Batey MA, Zhao Y, Jenkins H, Richardson CJ, Cano C, Tavecchio M, Barbeau J, Bardos J, Griffin RJ, Menear K, Thommes P, Martin NMB, Newell DR, Smith GCM, Curtin NJ (2012) Chemosensitisation of cancer cells by KU-0060648; a dual inhibitor of DNA-PK and PI-3K. Mol Cancer Ther 11:1789–1798

54. Desage-El Murr M, Cano C, Golding BT, Hardcastle IR, Hummersone MG, Menear KA, Frigerio M, Curtin NJ, Richardson C, Smith GCM, Griffin RJ (2008) 8-Biarylchromen-4-one inhibitors of the DNA-dependent protein kinase (DNA-PK). Bioorg Med Chem Lett 18:4885–4890

55. Clapham K, Bardos J, Finlay R, Golding BT, Hardcastle IR, Menear KA, Newell DR, Turner P, Young G, Griffin RJ, Cano C (2011) DNA-dependent protein kinase (DNA-PK) inhibitors: structure-activity relationships for *O*-alkoxyphenylchromen-4-one probes of the ATP-binding domain. Bioorg Med Chem Lett 21:966–970

56. Cano C, Golding BT, Haggerty K, Hardcastle IR, Peacock M, Griffin RJ (2010) Atropisomeric 8-arylchromen-4-ones exhibit enantioselective inhibition of the DNA-dependent protein kinase (DNA-PK). Org Biomol Chem 8:1922–1928

57. Clapham KM, Rennison T, Jones G, Craven F, Bardos J, Golding BT, Griffin RJ, Haggerty K, Hardcastle IR, Thommes P, Cano C (2012) Potent enantioselective inhibition of DNA-dependent protein kinase (DNA-PK) by atropisomeric chromenone derivatives. Org Biomol Chem 10:6747–6757

58. Mould E, Berry P, Jamieson D, Hill C, Cano C, Tan N, Elliott S, Durkacz B, Newell D, Willmore E (2014) Identification of dual DNA-PK MDR1 inhibitors for the potentiation of cytotoxic drug activity. Biochem Pharmacol 88:58–65

59. Take Y, Kumano M, Hamano Y, Fukatsu H, Teraoka H, Nishimura S, Okuyama A (1995) OK-1035, a selective inhibitor of DNA-dependent protein kinase. Biochem Biophys Res Commun 215:41–47

60. Knight ZA, Chiang GG, Alaimo RJ, Kenski DM, Ho CB, Coan K, Abraham RT, Shokat KM (2004) Isoform-specific phosphoinositide-3-kinase inhibitors from an arylmorpholine scaffold. Bioorg Med Chem 12:4749–4759

61. Kashishian A, Douangpanya H, Clark D, Schlachter ST, Eary CT, Schiro JG, Huang H, Burgess LE, Kesicki EA, Halbrook J (2003) DNA-dependent protein kinase inhibitors as drug candidates for the treatment of cancer. Mol Cancer Ther 2:1257–1264

62. Shinohara ET, Geng L, Tan J, Chen H, Shir Y, Edwards E, Halbrook J, Kesicki EA, Kashishian A, Hallahan DE (2005) DNA-dependent protein kinase is a molecular target for the development of noncytotoxic rediation-sensitizing drugs. Cancer Res 65:4987–4992

63. Davidson D, Coulombe Y, Martinez-Marignac VL, Amrein L, Grenier J, Hodkinson K, Masson J, Aloyz R, Panasci L (2012) Irinotecan and DNA-PKcs inhibitors synergize in killing of colon cancer cells. Invest New Drugs 30:1248–1256

64. Davidson D, Grenier J, Martinez-Marignac VL, Amrein L, Shawi M, Tokars M, Aloyz R, Panasci L (2012) Effects of the novel DNA dependent protein kinase inhibitor, IC486241, on the DNA damage response to doxorubicin and cisplatin in breast cancer cells. Invest New Drugs 30:1736–1742

65. Hassan I, Martensson S, Moshinsky D, Rice A, Tang C, Howlett A, McMahon G, Hammarsten O (2004) SU11752 inhibits the DNA-dependent protein kinase and DNA double-strand break repair resulting in ionizing radiation sensitization. Oncogene 23:873–882

66. Maxwell JP, Charifson PS, Tang Q, Ronkin SM, Jackson KL, Pierce AC, Lauffer DJ, Li P, Giroux S (2014) DNA-PK inhibitors. US Patent 2014/0275059 A1, 18 Sept 2014

67. Boucher D, Hoover R, Wang Y, Gu Y, Newsome D, Ford P, Moody C, Damagnez V, Arimoto R, Hillier S, Wood M, Markland W, Eustace B, Cottrell K, Penney M, Furey B, Tanner K, Maxwell J, Charifson P (2016) Potent radiation enhancement with VX-984, a selective DNA-PKcs inhibitor for the treatment of NSCLC. Proc Amer Assoc Cancer Res, Abstract 3716

68. Lempiäinen H, Halazonetis TD (2009) Emerging common themes in regulation of PIKKs and PI3Ks. EMBO J 28:3067–3073

69. Lavin MF, Khanna KK (1999) ATM: the protein encoded by the gene mutated in the radiosensitive syndrome ataxia-telangiectasia. Int J Radiat Biol 75:1201–1214

70. Dumaz N, Meek DW (1999) Serine 15 phosphorylation stimulates p53 transactivation but does not directly influence interaction with HDM2. EMBO J 18:7002–7010

71. Harper JW, Adami GR, Wei N, Keyomarsi K, Elledge SJ (1993) The p21 Cdk-interacting protein Cip1 is a potent inhibitor of G_1 cyclin-dependent kinases. Cell 75:805–816

72. Unger T, Juven-Gershon T, Moallem E, Berger M, Sionov RV, Lozano G, Oren M, Haupt Y (1999) Critical role for Ser20 of human p53 in the negative regulation of p53 by MDM2. EMBO J 18:1805–1814

73. Shiloh Y (2001) ATM and ATR: networking cellular responses to DNA damage. Curr Opin Genet Dev 11:71–77

74. Suzuki K, Kodama S, Watanabe M (1999) Recruitment of ATM protein to double strand DNA irradiated with ionizing radiation. J Biol Chem 274:25571–25575

75. Ding J, Miao Z-H, Meng L-H, Geng M-Y (2006) Emerging cancer therapeutic opportunities target DNA-repair systems. Trends Pharmacol Sci 27:338–344

76. Hickson I, Zhao Y, Richardson CJ, Green SJ, Martin NMB, Orr AI, Reaper PM, Jackson SP, Curtin NJ, Smith GC (2004) Identification and characterization of a novel and specific inhibitor of the ataxia-telangiectasia mutated kinase ATM. Cancer Res 64:9152–9159

77. Andrs M, Korabecny J, Jun D, Hodny Z, Bartek J, Kuca K (2014) Phosphatidylinositol 3-kinase (PI3K) and phosphatidylinositol 3-kinase-related kinase (PIKK) inhibitors: importance of the morpholine ring. J Med Chem 58:41–71

78. Golding SE, Rosenburg E, Valerie N, Hussaini I, Frigerio M, Cockroft XF, Chong WY, Hummersone M, Rigoreau L, Menear KA, O'Connor MJ, Povirk LF, van Meter T, Valerie K (2009) Improved ATM kinase inhibitor KU-60019 radiosensitizes glioma cells, compromises insulin, AKT and ERK prosurvival signaling, and inhibits migration and invasion. Mol Cancer Ther 8:2894–2902

79. Batey MA, Zhao Y, Kyle S, Richardson C, Slade A, Martin NM, Lau A, Newell DR, Curtin NJ (2013) Preclinical evaluation of a novel ATM inhibitor, KU59403, in vitro and in vivo in p53 functional and dysfunctional models of human cancer. Mol Cancer Ther 12:959–967

80. Degorce SL, Barlaam B, Cadogan E, Dishington A, Ducray R, Glossop SC, Hassall LA, Lach F, Lau A, McGuire TM, Nowak T, Ouvry G, Pike KG, Thomason AG (2016) Discovery of novel 3-quinoline carboxamides as potent, selective, and orally bioavailable inhibitors of ataxia telangiectasia mutated (ATM) kinase. J Med Chem 59:6281–6292

81. Chen X, Zhao R, Glick GG, Cortez D (2007) Function of the ATR N-terminal domain revealed by an ATM/ATR chimera. Exp Cell Res 313:1667–1674

82. Cimprich K, Cortez D (2008) ATR: an essential regulator of genome integrity. Nat Rev Mol Cell Biol 9:616–627

83. Lakin ND, Hann BC, Jackson SP (1999) The ataxia-telangiectasia related protein ATR mediates DNA-dependent phosphorylation of p53. Oncogene 18:3989–3995

84. Tibbetts RS, Brumbaugh KM, Williams JM, Sarkaria JN, Cliby WA, Shieh SY, Taya Y, Prives C, Abraham RT (1999) A role for ATR in the DNA damage-induced phosphorylation of p53. Genes Dev 13:152–157

85. Liu Q, Guntuku S, Cui X-S, Matsuoka S, Cortez D, Tami K, Luo G, Carattini-Rivera S, DeMayo F, Bradley A, Donehower LA, Elledge SJ (2000) Chk1 is an essential kinase that is regulated by ATR and required for the G_2/M DNA damage checkpoint. Genes Dev 14:1448–1459

86. Nishida H, Tatewaki N, Nakajima Y, Magara T, Ko KM, Hamamori Y, Konishi T (2009) Inhibition of ATR protein kinase activity by schisandrin B in DNA damage response. Nucleic Acids Res 37:5678–5689

87. Knight ZA, Gonzalez B, Feldman ME, Zunder ER, Goldenberg DD, Williams O, Loewith R, Stokoe D, Balla A, Toth B, Balla T, Weiss WA, Williams RL, Shokat KM (2006) A pharmacological map of the PI3-K family defines a role for p110alpha in insulin signalling. Cell 125:733–747

88. Rosenzweig KE, Youmell MB, Palayoor ST, Price BD (1997) Radiosensitization of human tumor cells by the phosphatidylinositol-3-kinase inhibitors wortmannin and LY294002 correlates with inhibition of DNA-dependent protein kinase and prolonged G2-M delay. Clin Cancer Res 3:1149–1156

89. Lee CM, Fuhrman CB, Planelles V, Peltier MR, Gaffney DK, Soisson AP, Dodson MK, Tolley HD, Green CL, Zempolich KA (2006) Phosphatidylinositol 3-kinase inhibition by LY294002 radiosensitizes human cervical cancer cell lines. Clin Cancer Res 12:250–256

90. Sarkaria JN, Tibbetts RS, Busby EC, Kennedy AP, Hill DE, Abraham RT (1998) Inhibition of phosphoinositide 3-kinase related kinases by the radiosensitizing agent wortmannin. Cancer Res 58:4375–4382

91. Sarkaria JN, Busby EC, Tibbetts RS, Roos P, Taya Y, Karnitz LM, Abraham RT (1999) Inhibition of ATM and ATR kinase activities by the radiosensitizing agent, caffeine. Cancer Res 59:4375–4382

92. Nishida H, Hamamori Y, Konishi T (2007) ATR Inhibitor. Patent WO2007046426A1, Niigata Tlo Corp., Japan

93. Liu Q, Xu C, Kirubakaran S, Zhang X, Hur W, Liu Y, Kwiatkowski NP, Wang J, Westover KD, Gao P, Ercan D, Niepel M, Thoreen CC, Kang SA, Patricelli MP, Wang Y, Tupper T, Altabef A, Kawamura H, Held KD, Chou DM, Elledge SJ, Janne PA, Wong K-K, Sabatini DM, Gray NS (2013) Characterization of Torin2, an ATP-competitive inhibitor of mTOR, ATM, and ATR. Cancer Res 73:2574–2586

94. Toledo LI, Murga M, Zur R, Soria R, Rodriguez A, Martinez S, Oyarzabal J, Pastor J, Bischoff JR, Fernandez-Capetillo O (2011) A cell-based screen identifies ATR inhibitors with synthetic lethal properties for cancer-associated mutations. Nat Struct Mol Biol 18:721–727

95. Liu Q, Wang J, Kang SA, Thoreen CC, Ahmed T, Sabatini DM, Gray NS (2011) Discovery of 9-(6-aminopyridin-3-yl)-1-(3-(trifluoromethyl)phenyl)benzo[*h*][1,6]naphthyridin-2(1*H*)-one (Torin2) as a potent, selective, and orally available mammalian target of rapamycin (mTOR) inhibitor for treatment of cancer. J Med Chem 54:1473–1480

96. Toledo LI, Murga M, Gutierrez-Martinez P, Soria R, Fernandez-Capetillo O (2008) ATR signaling can drive cells into senescence in the absence of DNA breaks. Genes Dev 22:297–302

97. Peasland A, Wang L-Z, Rowling E, Kyle S, Chen T, Hopkins A, Cliby WA, Sarkaria J, Beale G, Edmondson RJ, Curtin NJ (2011) Identification and evaluation of a potent novel ATR inhibitor, NU6027, in breast and ovarian cancer cell lines. Br J Cancer 105:372–381

98. Maira S-M, Stauffer F, Brueggen J, Furet P, Schnell C, Fritsch C, Brachmann S, Chène P, De Pover A, Schoemaker K, Fabbro D, Gabriel D, Simonen M, Murphy L, Finan P, Sellers W, García-Echeverría C (2008) Identification and characterization of NVP-BEZ235, a new orally available dual phosphatidylinositol 3-kinase/mammalian target of rapamycin inhibitor with potent in vivo antitumor activity. Mol Cancer Ther 7:1851–1863

99. Wang H-C, Lee AY, Chou WC, Wu CC, Tseng CN, Liu KY, Lin WL, Chang FR, Chuang DW, Hunyadi A, Wu YC (2012) Inhibition of ATR-dependent signaling by protoapigenone and its derivative sensitizes cancer cells to interstrand cross-link-generating agents *in vitro* and *in vivo*. Mol Cancer Ther 11:1443–1453

100. Wang H-C, Lee AY-L, Wu C-C, Wu Y-C (2014) Discovery of ATR kinase inhibitors from natural products. Proceedings of the 105th Annual Meeting of the AACR; 2014 Apr 5-9 San Diego, CA. Cancer Res 74(19 Suppl):Abstract nr 1637

101. Jacq X, Smith L, Brown E, Hughes A, Odedra R, Heathcote D, Barnes J, Powell S, Maguire S, Pearson V, Boros J, Caie P, Thommes PA, Nissink W, Foote K, Jewsbury PJ, Guichard S (2012) AZ20, a novel potent and selective inhibitor of ATR kinase with in vivo antitumour activity. Proceedings of the 103rd Annual Meeting of the AACR; 2012 Mar 31-Apr 4 Chicago. Cancer Res 72(8 Suppl):Abstract nr 1823

102. Foote KM, Blades K, Cronin A, Fillery S, Guichard SS, Hassall L, Hickson I, Jacq X, Jewsbury PJ, McGuire TM, Nissink JW, Odedra R, Page K, Perkins P, Suleman A, Tam K, Thommes P, Broadhurst R, Wood C (2013) Discovery of 4-{4-[(3R)-3-methylmorpholin-4-yl]-6-[1-(methylsulfonyl)cyclopropyl]pyrimidin-2-yl}-1H-indole (AZ20): a potent and selective inhibitor of ATR protein kinase with monotherapy in vivo antitumor activity. J Med Chem 56:2125–2138

103. Jones CD, Blades K, Foote KM, Guichard SM, Jewsbury PJ, McGuire T, Nissink JW, Odedra R, Tam K, Thommes P, Turner P, Wilkinson G, Wood C, Yates JW (2013) Discovery of AZD6738, a potent and selective inhibitor with the potential to test the clinical efficacy of ATR kinase inhibition in cancer patients. Proceedings of the 104th Annual Meeting of the AACR; 2013 Apr 6-Apr 10 Washington DC. Cancer Res 73(8 Suppl):Abstract nr 2348

104. Guichard SM, Brown E, Odedra R, Hughes A, Heathcote D, Barnes J, Lau A, Powell S, Jones CD, Nissink W, Foote KM, Jewsbury PJ, Pass M (2013) The pre-clinical in vitro and in vivo activity of AZD6738: a potent and selective inhibitor of ATR kinase. Proceedings of the 104th Annual Meeting of the AACR; 2013 Apr 6-Apr 10 Washington DC. Cancer Res 73(8 Suppl): Abstract nr 3343

105. Charrier J-D, Durrant SJ, Knegtel RMA, Virani AN, Reaper PM (2011) Compounds useful as inhibitors of ATR kinase. Patent WO2011143425A2, Vertex Pharmaceuticals Inc., USA

106. Reaper PM, Griffiths MR, Long JM, Charrier J-D, MacCormick S, Charlton PA, Golec JMC, Pollard JR (2011) Selective killing of ATM- or p53-deficient cancer cells through inhibition of ATR. Nat Chem Biol 7:428–430

107. Charrier J-D, Durrant SJ, Golec JMC, Kay DP, Knegtel RMA, MacCormick S, Mortimore M, O'Donnell ME, Pinder JL, Reaper PM, Rutherford AP, Wang PSH, Young SC, Pollard JR (2011) Discovery of potent and selective inhibitors of ataxia telangiectasia mutated and Rad3 related (ATR) protein kinase as potential anticancer agents. J Med Chem 54:2320–2330

108. Fokas E, Prevo R, Pollard JR, Reaper PM, Charlton PA, Cornelissen B, Vallis KA, Hammond EM, Olcina MM, Gillies McKenna W, Muschel RJ, Brunner TB (2012) Targeting ATR in vivo using the novel inhibitor VE-822 results in selective sensitization of pancreatic tumors to radiation. Cell Death Dis 3:e441

109. Hall AB, Newsome D, Wang Y, Boucher DM, Eustace B, Gu Y, Hare B, Johnson MA, Milton S, Murphy CE, Takemoto D, Tolman C, Wood M, Charlton P, Charrier JD, Furey B, Golec J, Reaper PM, Pollard JR (2014) Potentiation of tumor responses to DNA damaging therapy by the selective ATR inhibitor VX-970. Oncotarget 5:5674–5685

Epigenetic Modulators

Kenneth W. Duncan and John E. Campbell

Abstract Epigenetic drug discovery has expanded significantly beyond histone deacetylases (HDAC) in the past decade. This review covers significant new advances in the field across three more targets classes: bromodomains (BRD), arginine/lysine methyltransferases (RMT/KMT), and lysine demethylases (KDM). In each target section, a broad overview from a medicinal chemistry perspective is presented covering high-quality chemical biology tools being used to further expand the innate role of each target in cancer biology and in some examples facilitating preclinical target validation. In each target space, the review will also cover candidates currently in clinical investigation.

Keywords Bromodomain, Cancer, Demethylase, Epigenetics, Methyltransferase

Contents

K.W. Duncan (✉) and J.E. Campbell
Molecular Discovery, Epizyme, Inc., Cambridge, MA, USA
e-mail: kduncan@epizyme.com

Abbreviations

Ac	Acetyl
ALL	Acute lymphoblastic leukemia
ApoA1	Apolipoprotein A1
ASN	Aspartame
ATAD2	ATPase family AAA domain-containing protein 2
ATP	Adenosine triphosphate
BAP1	BRCA1-associated protein-1
BAZ	Bromodomain adjacent to zinc finger domain protein
BET	Bromodomain and extra-terminal motif
BRD	Bromodomain
BRET	Bioluminescence resonance energy transfer
BTK	Bruton's tyrosine kinase
CHD	Chromodomain
CREBBP	CREB-binding protein
DNA	Deoxyribonucleic acid
DNMT	DNA methyltransferase
DOT1L	Disruptor of telomeric silencing 1-like
E2F	E2 factor
EBV	Epstein-Barr virus
EHMT	Euchromatin histone methyltransferase
EZH2	Enhancer of zeste 2 polycomb repressive complex 2 subunit
HAT	Histone acetyltransferase
HDAC	Histone deacetylase
HMT	Histone methyltransferase
JAK	Janus kinase
JMJD	JmjC domain-containing protein
KAT	Lysine acetyltransferase
KDM	Lysine demethylase
KMT	Lysine methyltransferase
LOF	Loss of function
LSD1	Lysine-specific histone demethylase 1
MBT	Malignant brain tumor
MEKK	MAP kinases kinase kinase
MEP50	Methylsome
MLL	Mixed lineage leukemia
mRNA	Messenger ribonucleic acid
NHL	Non-Hodgkin lymphoma
NUT	Nuclear protein of testis

2OG	2-Oxoglutarate
PARP1	Poly(ADP-ribose) polymerase 1
PDB	Protein Data Bank
PHD	Plant homeodomain
PMT	Protein methyltransferase
PRC2	Polycomb repressive complex
PRMT	Protein arginine methyltransferase
RMT	Arginine methyltransferase
RNA pol	RNA polymerase
SAH	S-Adenosyl-L-homocysteine
SAM	S-Adenosyl methionine
SCLC	Small cell lung cancer
SET	Su(var)3-9 and "enhancer of zeste" proteins
SETDB1	SET domain bifurcated 1
SFG	Sinefungin
SGC	Structural genomics consortium
SMARCA	SWI/SNF-related matrix-associated actin-dependent regulator chromatin
SMYD	SET and MYND domain-containing protein
STAT	Signal transducer and activator of transcription
SUV39H1	Suppressor of variegation 3-9 homolog 1
SWI/SNF	SWItch/sucrose non-fermentable
TCGA	The Cancer Genome Atlas
TGFb	Transforming growth factor beta
TLR	Toll-like receptor
TRIM24	Tripartite motif-containing 24
TWIST	Twist-related protein
WHO	World Health Organization

1   Introduction

To accommodate approximately 2 M of DNA into the nucleus of each cell, DNA is coiled around a core of histone proteins with the resulting tightly packaged chromatin units creating the well-known structure of the chromosome. The fully condensed chromatin state, known as heterochromatin, sterically limits access of gene promoter regions to transcription factors, polymerases, and other components for gene transcription. A less compacted state, known as euchromatin, is required before transcriptional machinery can access promoter genes and commence transcription (Fig. 1).

Epigenetic mechanisms are the processes that modulate chromatin structure, gating access to gene promoter regions for transcriptional machinery whether activating or repressive. These physicochemical mechanisms driving chromatin remodeling can be described under one of three broad categories, namely, (Type A) covalent modification of chromosomal DNA, (Type B) posttranslational

Fig. 1 Transcriptional activities of euchromatin and heterochromatin
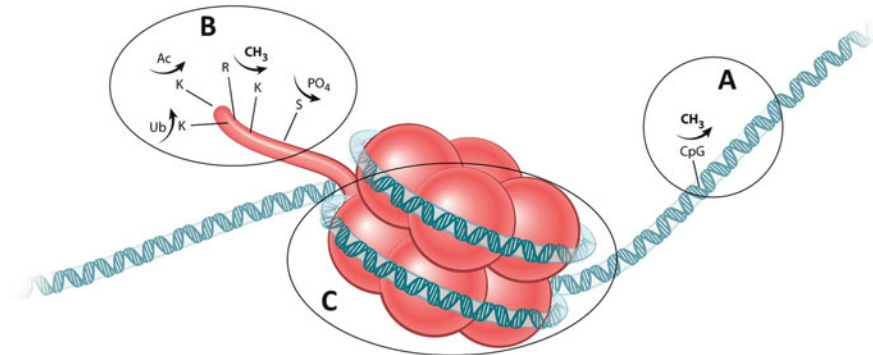
Fig. 2 Posttranslational epigenetic modifications of chromatin histone proteins and DNA

covalent modifications to histone tails, and (Type C) ATP hydrolysis-mediated alteration of DNA-histone interactions (Fig. 2).

A plethora of proteins interact with epigenetic "marks" (i.e., covalent modifications) to chromosomal DNA, histones, or other protein targets. These proteins contain domains capable of performing protein recognition based on these site-specific markings (readers) or are responsible for the addition (writers) or removal (erasers) of these marks (Fig. 3).

1.1 Readers

Histone acetyl and methyl marks are read by proteins containing one or more specialized reader domains with most of the methyl-reading domains belonging to the highly conserved "Royal" superfamily of homologs originally identified in plant or *Drosophila* chromatin-remodeling proteins [1]. The regulatory reader domain family members with relevant homologs in man include Tudor, malignant brain tumor (MBT), chromodomain (CHD), bromodomain (BRD), and plant homeodomain (PHD), among others. Tudor domain-containing proteins interact with di- and trimethylated lysine and are also known to be able to interact with methylated arginine. The MBT domain-containing proteins specifically bind mono- and dimethylated lysines. Methylation marks localized to the H3 histone subunit tail region can also be read by chromodomains, whereas bromodomains recognize only N-Ac residues on these same histone tails. PHD domains, in contrast, can recognize lysine acetylation and all three methylation states. At the time of writing this chapter, only one member of the methyl-reading MBT domain (L3MBTL3) has
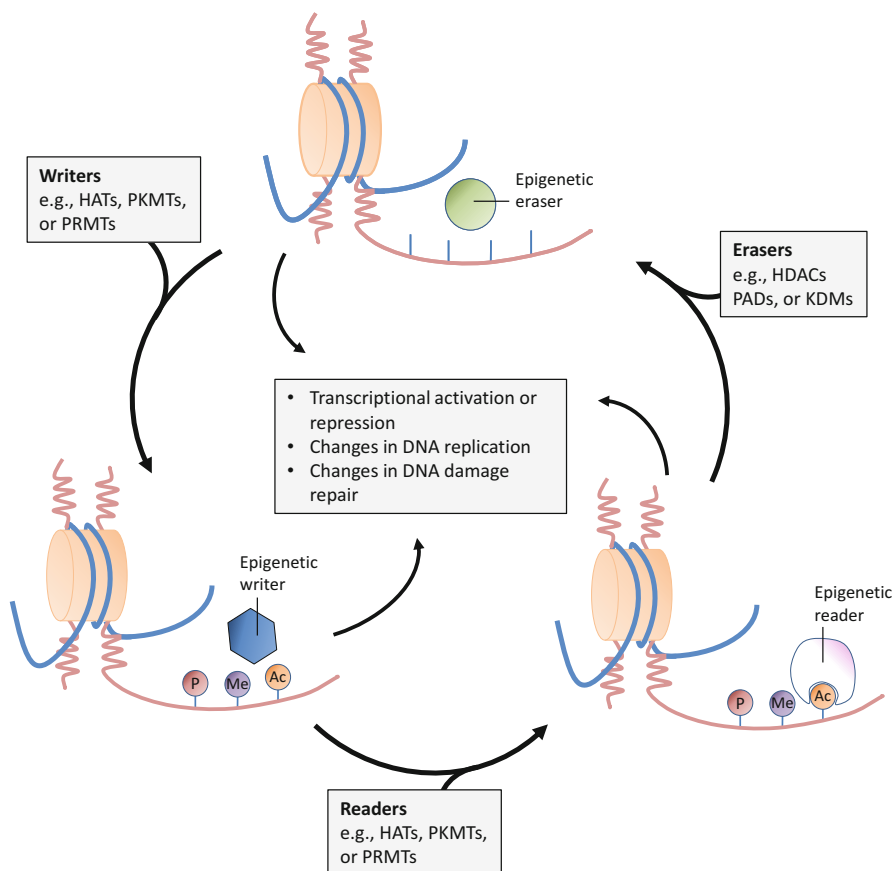
Fig. 3 The three different types of epigenetic modifiers that are responsible for installing, removing, and recognizing posttranslational modifications are known as writers, erasers, and readers

a validated inhibitor [2–4], while several bromodomain inhibitors have transitioned into clinical trials. Accordingly, this chapter will highlight the significant progress in development in targeting acetyl reader domains with a focus on BRD inhibitors.

1.2 Writers

Covalent modification of histone residues, commonly via methylation and acetylation, is a dynamic process that is utilized as a kind of code that, once recognized by reader domains, is translated into a relaxing or tightening of the chromatin complex to regulate transcription. Addition of up to two methyl groups to the ω-N atoms of arginine residues can be performed by a family of enzymes known as the arginine methyltransferases (RMTs). Similarly, lysine residues on histones can undergo ε-N-methylation up to three times by lysine methyltransferases (KMTs). Lysine residues

can also undergo covalent modification by one of the 18-member family of histone acetyltransferase (HAT or KATs) enzymes which mediate the mono-transfer of an acetate moiety to lysine residues from acetyl-CoA on histones and other proteins. At the time of writing this chapter, the HAT enzyme family has not been studied extensively; however, some putative inhibitors have been described in the literature [5–7]. Again, reflecting significant advances in the field over the past 10 years, our focus in this chapter will be on the protein methyltransferases for which clinical candidates have now been realized.

1.3 Erasers

Histone deacetylases (HDACs) were the first class of epigenetic erasers to be discovered and targeted for the treatment of human disease including cancer. As presented in the first volume of this title, HDAC enzymes are responsible for the removal of acetyl marks, and the blockade of this mechanism has led to the successful creation of pan-HDAC inhibitor drugs and more, recently, selective HDAC inhibitors that are currently in clinical trials.

Despite the discovery of deacetylase enzymes, lysine methylation was initially thought to be a static process, until the Zhang group demonstrated, for the first time, that lysine methylation was indeed reversible [8, 9]. Since the initial demethylase report, however, eight classes of lysine demethylases (KDMs) have now been reported even though their biological roles are still being defined. Interestingly however, despite a number of conflicting reports around the nonheme iron(II) and 2-oxoglutarate (2OG)-dependent oxygenase JMJD6 [10, 11], there appears to be no known enzyme capable of demethylation of modified arginine residues. However, arginine residues can be converted to citrulline by the arginine deiminase family of enzymes [12]. This chapter will provide a summary of the development of KDM inhibitors currently in early discovery and early stage clinical trials.

1.4 Current Status

Epigenetic drug discovery has changed much in the past 10 years. Since the first approval of azacitidine in 2004, drugs targeting epigenetic mechanisms have altered the clinical landscape for oncology patients. Hypomethylating agents, such as azacitidine and in 2006 decitabine, both act through limiting DNA methyltransferase (DNMT) activity as pseudo-substrates and are generally viewed as examples of the Type A chromatin modulators described above (Fig. 1).

The first example of a drug targeting a Type B epigenetic target, vorinostat, was approved in late 2006 acting as a pan-active histone deacetylase (HDAC) inhibitor [13]. A number of promising HDAC inhibitors were discussed in volume 1 of this title [14] and will not be discussed further in this chapter. Although a number of additional FDA approvals have followed for pan-active HDAC inhibitors (Table 1), no enzyme selective or subclass selective HDAC inhibitors (e.g., type I, type IIa, etc.) have successfully completed clinical trials to date. Drug discovery efforts have continued from a number of groups, leading to high-quality, class-specific inhibitors to facilitate further understanding of the underlying biology of these HDAC targets, developing new clinical hypotheses in oncology and beyond. This drug discovery effort has continued across a spectrum of epigenetic targets with a number currently being investigated in the clinic (Table 1).

In this chapter, we will cover the most recent epigenetic targets to progress into evaluation in a clinical setting, focusing on the rapid progress made on targets that utilize methyl- and acetyl-based epigenetic marks on histones and other proteins. This chapter will also review some additional epigenetic targets which have high-quality tool compounds available to test new therapeutic hypotheses and may provide a future path for novel, targeted therapies in oncology.

2 Readers: Bromodomains

2.1 Target Introduction

First described in the 1990s as part of the brahma gene from *Drosophila melanogaster* [15], the bromodomains are a set of evolutionarily conserved protein interaction modules capable of binding to, and thus recognizing, ε-*N*-acetylation of lysine residues. A total of 61 bromodomains are encoded within the human proteome and can be found in a diverse set of 46 nuclear and cytoplasmic proteins [16]. These proteins can contain one or more acetyl readers in addition to other domains which may contribute to a range of chromatin functions, including writing of acetyl [17, 18] or methyl groups [19, 20], demethylation [21], or larger chromatin remodeling roles as part of a larger complex [22, 23]. Further phylogenic analysis of these 61 domains has led to the definition of eight structural classes (Fig. 4).

A number of bromodomains have been linked to cancer indications [24] through aberrant expression levels, mutations, or genetic rearrangements of bromodomain-containing proteins, either in the form of wild-type domain rearrangements or translocations. The most studied of these in cancer drug discovery can be found on branch II of the phylogenic tree containing the bromodomain and extra C-terminal (BET) subfamily consisting of multiple isoforms of BRD2, BRD3, BRD4, and BRDT. BET proteins contain conserved tandem N-terminal bromodomains (BD1 and BD2), which allow for interaction with acetylated histones and various nuclear proteins. As functional readers of acetylated chromatin, these proteins mediate

Table 1 Clinical status of epigenetic focused therapies targeting enzymes which modulate acetylation or methylation status

Drug name	Target class/enzyme	Status	Indication
Belinostat	HDAC/pan-HDAC	Approved	Peripheral T-cell lymphoma
Panobinostat	HDAC/pan-HDAC	Approved	Multiple myeloma
Romidepsin	HDAC/Zn-dependent HDACS	Approved	Cutaneous T-cell lymphoma
Vorinostat	HDAC/pan-HDAC	Approved	Cutaneous T-cell lymphoma
Pracinostat	HDAC/class I, II, IV	Approved	AML, T-cell lymphoma
Entinostat	HDAC/class I, III	Phase II/III	Multiple cancers
Givinostat	HDAC/class I, II	Phase II	
Mocetinostat	HDAC/ pan-HDAC	Phase II	Lymphoma, leukemia
Quisinostat	HDAC/pan-HDAC	Phase II	Leukemia, MLL, lymphoma, solid malignancies
Resminostat	HDAC	Phase II	HCC
Tacedinaline	HDAC/HDAC1, HDAC2	Phase II	Multiple myeloma
Valproic acid	HDAC/pan-HDAC	Phase II	Multiple cancers
ACY-1215	HDAC/HDAC6	Phase I/II	Multiple myeloma
AR-42	HDAC/pan-HDAC	Phase I/II	MLL, lymphoma, leukemia
CUDC-907	HDAC/class I, IIB	Phase I	Lymphoma, multiple myeloma, solid tumors
Abexinostat	HDAC/pan-HDAC	Phase I	B-cell lymphoma
MK-8628/ OTX015	Bromodomain/BET	Phase I/II	Glioblastoma
INCB054329	Bromodomain	Phase I/II	Advanced malignancies
ABBV-075	Bromodomain	Phase I	Advanced cancers
BAY-1238097	Bromodomain/BET	Phase I	Neoplasms
BMS-986158	Bromodomain/BET	Phase I	Solid tumors
CPI-0610	Bromodomain/BET	Phase I	Lymphoma
TEN-010	Bromodomain/BET	Phase I	AML and solid tumors
Tazemetostat	HMT/EZH2	Phase II	Lymphoma, INI-deficient tumors, synovial sarcoma
CPI-1205	HMT/EZH2	Phase I	B-cell lymphoma
GSK2816126	HMT/EZH2	Phase I	B-cell lymphoma, follicular lymphoma
Pinometostat	HMT/DOT1L	Phase I	Leukemia
ORY-1001	KDM/KDM1A	Phase I/II	AML
Tranylcypromine	KDM/KDM1A	Phase I/II	AML
GSK2879552	KDM/KDM1A	Phase I	AML

interactions of BD1 and BD2, allowing for discrete localization of BET proteins at various acetylated chromosomal locations, thus permitting these BET proteins to recruit regulatory complexes and influence gene expression.
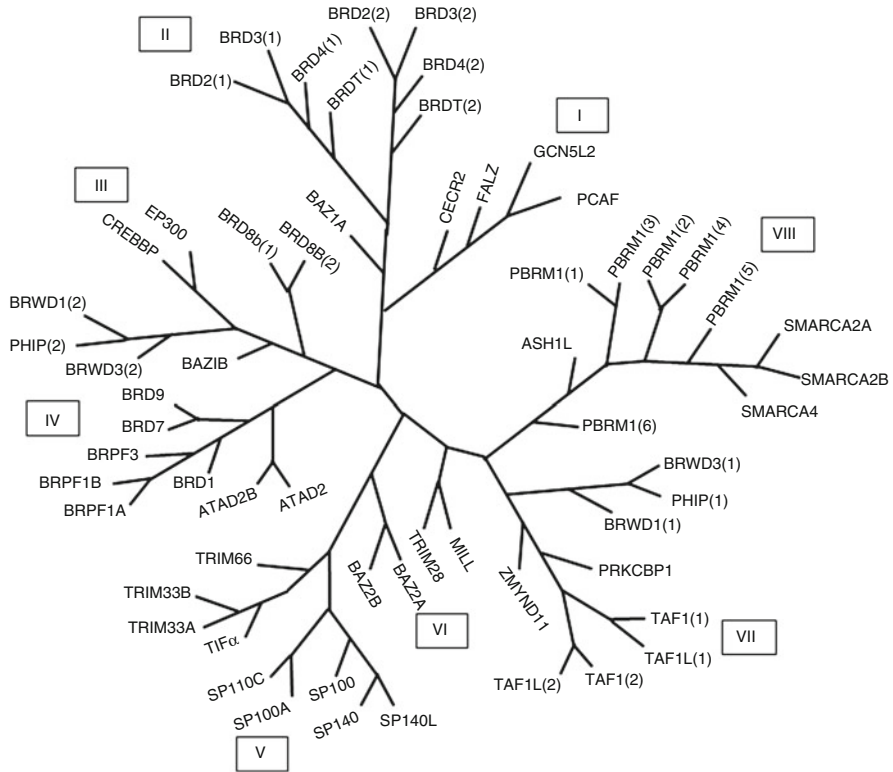
Fig. 4 Phylogenetic tree containing bromodomains

CREBBP (CREB-binding protein) with related protein EP300 have both acetyl-transferase (HAT) and bromodomain (BET) regions. CREBBP/EP300-mediated acetylation creates binding sites for the acetyl-lysine-specific CREBBP/EP300 bromodomain, which has been postulated to be required for accurate substrate targeting, the results of which is a positive feedback loop and corresponding maintenance of CREBBP/EP300 enzymatic activity [25]. Chromosomal transloca-tions of CREBBP/EP300 have been described in myeloid and acute lymphoid leukemia and may also contribute to tumorigenesis of NUP-HoxA9 and MOZ-TIF2 fusion proteins by activation of transcription [26, 27]. It is currently unclear which function is ideal as an anticancer target; however, inhibitors of both the HAT and BRD domains have been published recently [6, 28, 29].

Overexpression of bromodomain ATAD2 (ATPase family AAA domain-containing protein 2) occurs in some 70% of breast tumors and correlates with poor survival and a propensity for relapse [30] as is required recruitment of specific

E2F transcription factors and for chromatin assembly of the host cell factor 1-MLL histone methyltransferase complex. Mutations in ATAD2 can effectively disable this to promote cancer cell proliferation [31]. Closely related protein ATAD2B has recently been shown to be highly expressed in glioblastoma and oligodendroglioma, as well as in breast carcinoma [32].

Tripartite motif 24 protein (TRIM24) overexpression has been associated with poor overall survival of breast cancer patients [33], and high expression is reported in samples of numerous other cancer types such as hepatocellular carcinoma, glioblastoma, gastric cancer, non-small cell lung cancer, and head and neck squamous cancer [34–38]. Through additional mechanisms still being unearthed, TRIM24 may regulate levels of cancer-relevant proteins on the transcriptional and protein levels [39].

This section will however focus upon the BET bromodomains implicated in cancer highlighting the compounds currently in early clinical assessment. We will also review some examples of the breadth and depth of inhibitor chemotypes identified across the bromodomain family, with which additional chemical biology studies may enable validation in a wider range of cancer indications. An exhaustive review of bromodomain inhibitor chemical matter was written by Filippakopoulos and Knapp in 2014 [16].

2.2 Structural Biology

Crystallographic data have been collected on a number of bromodomains and first described in detail by Mutjaba et al. [40]. Although a large degree of sequence variation exists in the bromodomain modules, they shared a conserved tertiary structure. This feature consists of a left-handed bundle of four α-helices (αZ, αA, αB, and αC) connected by a diverse loop region which surround a central acetylated lysine binding site. For the BET subclass of bromodomains, two of these modules are contained within each protein. The large hydrophobic component of this *N*-acetyl-binding site has made it an attractive target for drug discovery efforts.

A 2012 study assessed the potential druggability of bromodomains using available structural information in the PDB using the software package SiteMap to analyze the size and solvent accessibility of each hydrophobic pocket, resulting in a set of predictions on overall druggability [41]. During the analysis, the authors attempted to rank the potential druggability of the bromodomain family in relation to other known target types. The BET (type I) subclass is predicted to be one of the most amenable to identifying small-molecule inhibitors. A number of type II bromodomains also fell into this category. The higher scoring predictions were driven, in part by the presence and positioning of key residues which define the size and access of the hydrophobic region, leading to a larger and exposed surface area.

Many of the other bromodomains showed lower predicted druggability scores suggesting lower hit rates from potential screening campaigns. Although classed as difficult to drug, the authors do describe these scores as consistently higher than many "featureless" protein-protein interaction sites. In contrast, the highest scoring results were deemed to be as druggable as kinases, such as aurora kinase, or Hsp90. Since this paper, an increasing number of small-molecule inhibitor chemotypes have been described for bromodomains with examples published covering many areas of the bromodomain phylogenic tree, including examples classified by the Vidler paper as difficult (e.g., BAZ2B).

2.2.1 BET Bromodomain Inhibitors

BET Bromodomain Target Introduction

BET inhibitors have been demonstrated to play oncogenic roles by mechanisms impacting proliferation, cell cycle, and apoptosis in a number of hematological and solid tumor models. More specifically, BET inhibitors are able to downregulate MYC expression in a range of preclinical models of myeloma and myeloid leukemia through multiple mechanisms [42, 43]. BRD2, BRD3, and BRD4 are implicated in the maintenance of aberrant chromatin states in a range of hematological cancers including leukemia, lymphomas, and myelomas. Of the BET family members, the function of BRD4 has been most thoroughly studied. BRD4 regulates RNA pol II-mediated elongation and transcription by directly interacting with mediator complex and pTEFb (positive transcription elongation factor complex) [21, 44, 45]. Additionally, recent literature has shown direct BRD4 interactions with transcription factors, including NF-κB, ERα, p53, TWIST, and GATA-1, across a range of cancer types [46–48]. Thus, bromodomains such as BRD4 serve as a node between disease-relevant transcription factors and the transcriptional machinery. In the context of oncology, BRD4 mediates combinatorial interactions among acetylated histones, transcription factors, nuclear proteins, and the transcriptional machinery, allowing translation of the epigenetic code into RNA synthesis. Amplifications of c-MYC are found in approximately 30% of prostate cancers, and MYC overexpression is proposed to play a role in prostate cancer initiation [49]. BET inhibitors have also been shown to be effective against NUT midline carcinoma (NMC), a particularly rare epithelial tumor driven by fusions of the NUT protein with either BRD3 or BRD4 genes [50].

BET bromodomain inhibitors have also been implicated in a number of non-oncology indications, due to their ability to selectively regulate specific inflammatory cytokines, including interleukins 1β, 6, 17, 21, and 23 [51, 52].

BET Tool Compounds
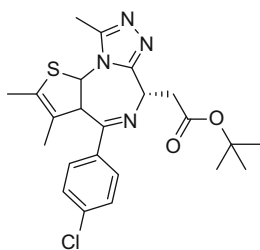
1
JQ-1
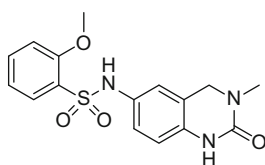
2
PFI-1
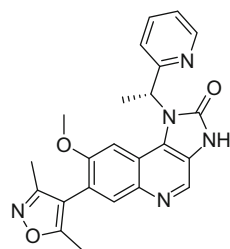
3
I-BET151
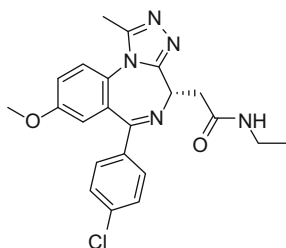
4
GSK525762
(I-BET762)
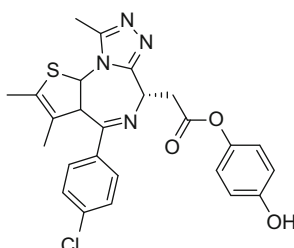
5
MK08628
(OTX-015)
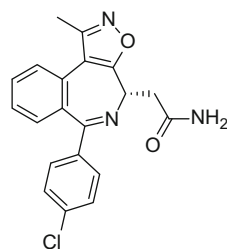
6
CPI-0610

A 2009 patent application from Mitsubishi Tanabe Pharma Corporation [53] first described the thienotriazolodiazepine scaffold as inhibitors of BRD enzymes. Multiple variations on this tricyclic scaffold chemotype were published by other groups in the following years. In late 2010, Filippakopoulos, Knapp, and Bradner et al. discussed the identification and characterization of JQ-1 (**1**), as a pan inhibitor of the BET domain proteins, and provided evidence of both in vitro and in vivo activity against NUT midline carcinoma [54]. Compound **1** binds in the *N*-acetyl-lysine binding cleft between the hydrophobic ZA and BC loops. Mimicking the natural *N*-acetyl substrate, the triazole ring of **1** interacts via hydrogen bonding with the conserved asparagine residue (Asn120 in BRD4, Asn429 in BRD2). The group demonstrated the cellular activity of **1** in displacing BRD4 from nuclear chromatin and inducing squamous differentiation and growth arrest in BRD4-dependant carcinomas such as NMC. This activity against BRD4-dependent cancer was extended in vivo with activity against multiple patient-derived xenograft models [55–58]. **1** was made available to researchers through the Structural Genomics Consortium (SGC) and was featured in a number of additional studies highlighting

the effect of BET inhibition against a range of c-MYC driven cancer types including Merkel cell carcinoma (MCC) [55] and leukemia.

BET tool compound PFI-1 (**2**), described in 2013, was the result of a collaboration between Pfizer and the SGC [59, 60]. The compound was identified by alpha assay displacement of histone H4 peptide acetylated at lysine residues K5, K8, K12, and K16 with an $IC_{50} = 220$ nM and $IC_{50} = 98$ nM, for BRD4(1) and BRD2(2), respectively. ITC was performed producing K_D determinations in good alignment with the IC_{50} values, confirmed similar affinities for other members of the BET family, and showed selectivity over a number of other bromodomains. **2** binds to the conserved NAc interacting residue Asp140 through the carbonyl and nitrogen of the dihydroquinazoline-2-one ring system and also forms a water-mediated hydrogen bond with Tyr98. On-target cellular effects of this inhibitor were demonstrated by the observation of diffusion of GFP-BRD4 from chromatin using a FRAP binding assay in BRD4-dependent NMC cell line. Furthermore, **2** inhibits proliferation in a subset of leukemic cells which contained known oncogenic rearrangements in the MLL locus. Concurrent with **2** treatment, the authors observe a significant downregulation of Aurora kinase B. Aurora B activity is linked with c-MYC function [61], and the authors observed that **2** was strongly synergistic with the potent pan-Aurora kinase inhibitor VX-680.

2 has a good selectivity profile against a range of GPCRs, ion channels, and kinases. Rat PK showed the compound to have moderate clearance in good agreement with values predicted by rat liver microsomes and moderate oral bioavailability (38%) believed to be driven at least in part by limited solubility in the gut.

I-BET151 (**3**) represents a second distinct chemotype discussed here which are potent inhibitors of BET bromodomain proteins BRD2, BRD3, and BRD4 [62–64]. The other chemotype is represented by the clinical compound **3**, discussed later in this chapter. **3** is a potent inhibitor of BRD2, BRD3, and BRD4 with reported $pIC_{50} = 6.3 \pm 0.39$, 6.6 ± 0.26, and 6.1 ± 0.22, respectively. From a cancer context, the compound was shown to have efficacy in models of murine MLL-AF9 and human MLL-AF4 leukemia. The GSK team has also proposed the mode of action of this compound to act, at least in part, by inhibition of transcription at some key genes including *BCL2*, *c-MYC*, and *CDK6* via displacement of BRD3/BRD4, PAFc, and SEC components from chromatin.

BET Inhibitor Clinical Compounds

Clinical investigation of bromodomain compounds in cancer indications has focused primarily with BET inhibitor space. Development of clinical candidates has been rapidly pursued by a number of companies with a total of seven compounds in early stages of clinical development by late 2015 (Table 2). Many of the chemotypes are related to the original diazepine ring system. Listed below are a few examples of these clinical candidate compounds.

Table 2 BET bromodomain inhibitors in the clinic

Drug name	Status	Indication
MK-8628/OTX015	Phase I/II	Glioblastoma
INCB054329	Phase I/II	Advanced malignancies
ABBV-075	Phase I	Advanced cancers
BAY-1238097	Phase I	Neoplasms
BMS-986158	Phase I	Solid tumors
CPI-0610	Phase I	Lymphoma
TEN-010	Phase I	AML and solid tumors

GlaxoSmithKline disclosed iBET-762 (**4**) contemporaneously with **1** in 2010 as an equipotent inhibitor of BRD2/BRD3/BRD4 (32–42 nM, FRET assay), binding in both of the tandem bromodomains of BET [65]. Compound **4** was identified by a combination of diversity and targeted screening for activators of an ApoA1-luciferase reporter in HepG2 cells, highlighting molecules which were able to upregulate reporter gene activity [66]. This was also the primary cellular assay employed in the lead optimization toward **4**. The compound was shown to have a favorable selectivity profile against a range of bromodomains including BAZ20B, SP140, ATAD2, CREBBP, and PCAF [67]. Beyond bromodomains, iBET-762 displayed a favorable profile against a CEREP type panel of other targets (<30% when screen at 10 μM) and was not mutagenic in the Ames test. This chemical series shares the benzodiazepine scaffold with GABA$_A$ allosteric modulators such as alprazolam, and selectivity against GABA receptor activity was achieved through meta- or para-substitution on the pendant phenyl ring. **4** has a free fraction of approximately 20% and shows moderately low levels of clearance coupled with oral bioavailability (%F) around 50% in primates and dogs. Higher levels of clearance were observed in rodents. The compound is currently in clinical trials against NUT midline carcinoma [68] and relapsed and refractory hematological malignancies [69]. The GSK team has also proposed prostate cancer as a potential indication for **4** [42]. To date, there have been no disclosures on tolerability of the compounds in these early clinical studies. GSK has also shown potential for use of BET inhibitors in non-oncology indications such as rheumatoid arthritis [65].

An additional GSK-derived BET inhibitor (GSK2820151) was disclosed in late 2015 as the company initiated a phase I dose escalation study of subjects with advanced or recurrent solid tumors [70]; however, no additional information is currently available.

OncoEthix SA, a small Swiss biotechnology company, in-licensed OTX-015 (**5**) in 2012 from Mitsubishi Tanabe. Following initiation of clinical development, OncoEthix was purchased by Merck in 2014. In the process Merck captured the potential first-in-class oral BET inhibitor. The compound (subsequently named MK-8628-001) is a potent binder to BRD2/BRD23/BRD24 with EC50s ranging from 10 to 19 nM and competitive inhibition against acetylated histone 4 [71]. This

binding activity translated to a compelling in vitro response with a range of <500 nM gIC_{50} values in a range of leukemia, lymphoma, and multiple myeloma cell lines [72]. **5** initially induced cell cycle arrest with G_1 accumulation and a decrease in S-phase and was predominantly cytostatic but induced apoptosis after longer periods of treatment. The compound was shown to reduce the levels of BRD2 and BRD4 but induced little reduction of BRD3 levels during compound treatment of AML and ALL cells. Observed reductions in *c-MYC* expression and protein levels are a broad class effect and attributed to the BRD4 reduction [73, 74]. The BRD2 reduction is also believed to contribute to the antiproliferative effect by inhibition of the Stat5 activity. Indeed, **5** negatively regulated transcripts encoding members of the NF-kB, TLR, and JAK/STAT signaling pathways. In an additional recent study in B-cell lymphoid tumors, **5** has shown antiproliferative activity in multiple in vitro and in vivo experiments. Several synergies were also observed in combination with many known anticancer drugs covering a range of mechanisms of activity (Table 3).

A phase Ib dose-escalation study of **5** in patients with hematological malignancies was recently discussed in which samples from a total of 81 patients were collected [75]. The data derived from this study suggested the compound has an absorption rate constant $(k_a) = 0.73$ h^{-1}, volume of distribution $= 71$ L, and clearance $= 8.5$ L h^{-1}. When coupled with the relative half-life of around 5.7 h, the group suggested that steady state is reached after only 2 days with dosing at 80 mg QD. Thrombocytopenia was considered to be the principal dose-limiting toxicity in this study.

Constellation Pharmaceuticals first disclosed their clinical candidate BET inhibitor CPI-0610 (**6**) in 2015 [76, 77] with early details on tolerability from a phase I study. In this early study, CPI-0610 was reportedly dosed QD for 14 days of a 21-day cycle, and the compound has an apparent oral clearance rate of 15.1 ± 7.0 L h^{-1} with a pharmacokinetic half-life of 10.7 ± 3.5 h. During the early part of the study, expression of the BET target gene CCR1 was suppressed at

Table 3 Combination effects observed with MK-8628/OTX015 and oncology therapies with a range of targets

Drug	Combination drug MOA	Activity
Everolimus	mTOR	Strong synergy
Ibrutinib	BTK inhibitor	Strong synergy
Idelalisib	PI3K-delta inhibitor	Synergy
Vorinostat	Class I and II HDAC inhibitor	Synergy
Rituximab	Anti-CD20 mAb	Synergy
Decitabine	DNMT inhibitor	Synergy
Lenalidomide	Immunomodulant	Synergy
Romidepsin	Class I HDAC inhibitor	Moderately additive
Bendamustine	DNA modifying	Moderately additive
Doxorubicin	DNA intercalation	Moderately additive

multiple doses suggestive of a pharmacodynamic effect in patients. The principal finding from dosing this compound appeared to be a reversible dose-dependent thrombocytopenia. Despite the early stages of the trial, some anti-lymphoma activity was observed with compound **6** treatment.

2.2.2 Other Bromodomain Tool Compounds
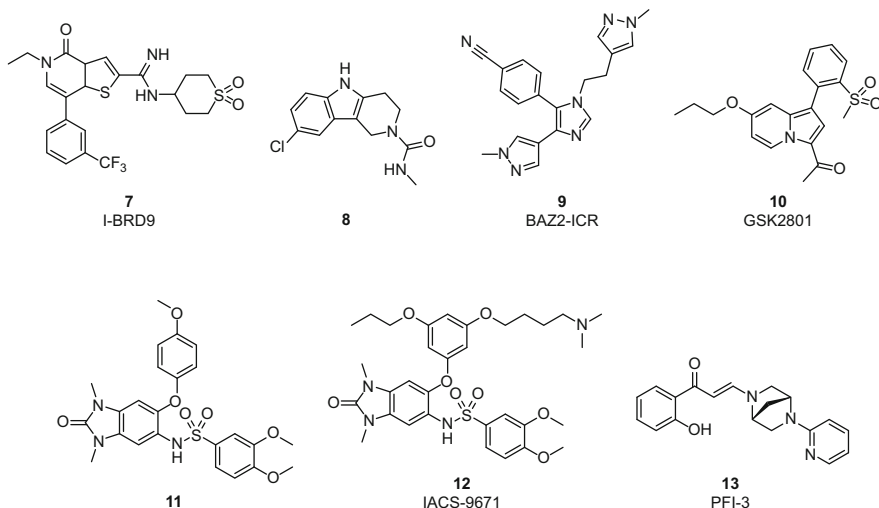
A broad collaborative group from GSK and the Universities of Cambridge and Strathclyde published the first example of a series of compounds exemplified by tool compound I-BRD9 (**7**) [78]. Compound **7** was developed from an initial screen against a GSK internal library. The compound has potent inhibitory activity against BRD9 ($pIC_{50} = 7.3$) and displays >700-fold selectivity over the remaining BET family. Furthermore, **7** is >70-fold selective over a panel of 34 additional human bromodomains and exhibited no activity <5 μM on a range of additional biological targets including receptors, transporters, ion channels, and kinases when compared to BRD4. Endogenous protein binding in cells was confirmed using a NanoBRET assay. A comparative treatment of **7** and pan BET inhibitor **4** was performed in Kasumi-1 cells which highlighted a number of genes downregulated by the selective **7** inhibitor not seen in the **4**. Many of these genes have roles in cancer and immunology pathways. No data has been provided on the ADME/PK performance of **7**.

BAZ Inhibitors

The bromodomain adjacent to zinc domain (BAZ) family of proteins was assessed by Vidler et al. to be one of the most difficult bromodomain members to drug. The reason for this low druggability scoring derived from a lack of a deep, enclosed hydrophobic pocket seen in other higher scoring bromodomains such as the BET family, despite having an open active site. The BAZ family members are ubiquitously expressed proteins with conserved domain structure including PHD and bromodomain main tail reader motifs [79]. A frequent target of hit-finding efforts, BAZ2A is a component of the nucleolar remodeling complex (NoRC) and a member of the "imitation switch chromatin remodeling complexes" or ISWI [80], which plays a role in regulating the expression of noncoding RNAs and in the formation and repressive heterochromatin. High expression of BAZ2A has been reported in prostate cancer and has been suggested to be a prognostic marker of metastatic potential. Little is known in contrast, about the biological role of BAZ2B; however, high expression levels are associated with poor outcome of pediatric B-cell lymphoblastic leukemia (B-ALL) [81].

Members of the Structural Genomics Consortium (SGC) based at the University of Oxford recently published details of a number of small-molecule fragments which can inhibit BAZ2B [82]. The compounds were identified after an AlphaScreen assay with BAZ2B and a histone H3 peptide acetylated at lysine 14. Compound **8** inhibits BAZ2B with an $IC_{50} = 9 \pm 4$ μM, thus suggesting the BAZ family may indeed be druggable. Additional screening and assessment of binding via differential scanning fluorimetry (DSF) on BRD2-BD1 and CREBBP suggested that **8** may have some degree of selectivity for BAZ2B.

Following this initial study, the SGC in collaboration with researchers at the Institute of Cancer Research (ICR) published data on BAZ2-ICR (**9**), a nanomolar BAZ2A/B inhibitor [83]. After identification of a low micromolar hit, again by AlphaScreen assay, the hit was found to occupy the bromodomain binding site with a phenyl ring positioned in the site normally occupied by the acetylated lysine. After installation of a pyrazole group to act as an acetyl-lysine mimetic and a second (tethered to a flexible alkyl chain) to retain an intramolecular π-stacking interaction, tool compound **9** was identified. The molecule is an inhibitor of BAZ2A and BAZ2B (130 and 180 nM, respectively) in the biochemical readout and was shown to displace BAZ2 proteins from chromatin in living cells in a fluorescence recovery after photobleaching (FRAP) assay. Compound **9** also has potential as an in vivo tool compound having moderate clearance and good oral bioavailability ($F = 70\%$).

An additional BAZ2A/B inhibitor chemotype was contemporaneously discovered by a different group of SGC members at Oxford University, this time in collaboration with GSK [84]. The fruit of this research was probe compound GSK2801 (10), which inhibits BAZ2A and BAZ2B with an $IC_{50} = 400$ nM and $IC_{50} = 420$ nM, respectively. Compound 10 was selected as a tool compound as it represented the best selectivity SAR profile against BRD4(1) and BRD9 (>50-fold). Like 9, 10 effectively demonstrated the expected cellular mode of action using a FRAP-based assay and has a pharmacokinetic profile suitable for use as an in vivo tool compound.

TRIM24 Inhibitors

Two independent studies from the SGC/University of Oxford (compound 11) [85] and the MD Anderson Cancer Center IACS-9671 (12) [86] published tool compounds with similar chemotypes as dual inhibitors of bromodomains TRIM24 and bromodomain-PHD finger protein (BRPF). Identification of precursors for both of these compounds was enabled by an AlphaScreen of TRIM24 using a histone H3K23Ac peptide. In both studies, the compounds were shown to interact with TRIM24 and BPRF 1 and BPRF2 in a cellular context but do not discuss the ADME or PK properties of these chemotypes.

SWI/SNF Inhibitor

The switch/sucrose non-fermentable (SWI/SNF) is a multi-subunit chromatin remodeling complex which has gathered considerable attention as a potential target in cancer research as various subunits are mutated or lost at high frequency in human tumors. The complex contains one of two mutually exclusive helicase/ATPase catalytic subunits, SMARCA2 and SMARCA4. Together with core and regulatory subunits, SMARCA2/SMARCA4 couples ATP hydrolysis to the perturbation of histone-DNA contacts. In recent studies using genetic loss-of-function (LOF) approaches, three groups have independently identified SMARCA2 as an essential gene in SMARCA4-deficient lung cancer [87–89] proposing a synthetic lethality therapeutic approach. However, it was unclear whether small-molecule inhibitors of the SMARCA2 bromodomain or ATPase domain would be the most pharmacologically relevant target [90].

A group of researchers from MD Cancer Center and Pfizer published results on a potent inhibitor of both SMARCA2 and SMARCA4 PFI-3 (13) [28]. Despite producing a potent and cell-permeable probe molecule capable of displacing ectopically expressed, GFP-tagged SMARCA2-bromodomain from chromatin, the compounds do not display antiproliferative phenotypes. The authors further confirmed via inducible RNAi and cDNA complementation (with bromodomain and ATPase-dead constructs) that the antiproliferative phenotype is driven by the ATPase region and not the bromodomain.

3 Writers: Methyltransferases

3.1 Introduction and Structural Biology

Collectively known as protein methyltransferases (PMTs), some 96 proteins have been suggested to perform methylation on histones and other proteins. These PMTs catalyze the transfer of a methyl group from the cofactor S-5′-adenosyl-L-methionine (SAM) to arginine (R) or lysine (K) residues and are further classified based upon this function as RMT or KMTs (Fig. 5a, b). Based upon their protein sequences, phylogenic trees of the KMT and RMT families were created and are shown in Fig. 5c.

3.2 Arginine Methyltransferases

3.2.1 Tool Compounds
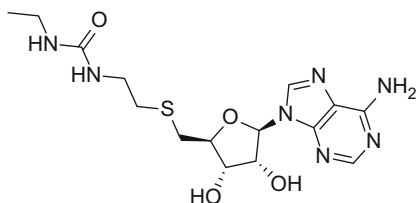
14
DS-437
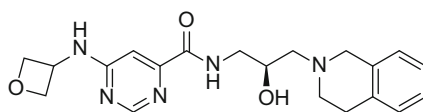
15
EPZ015666
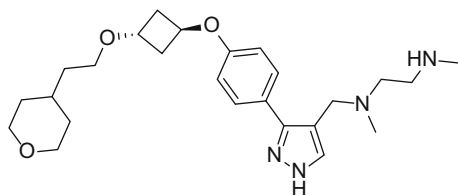
16
EPZ020411
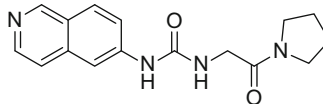
17
SGC707
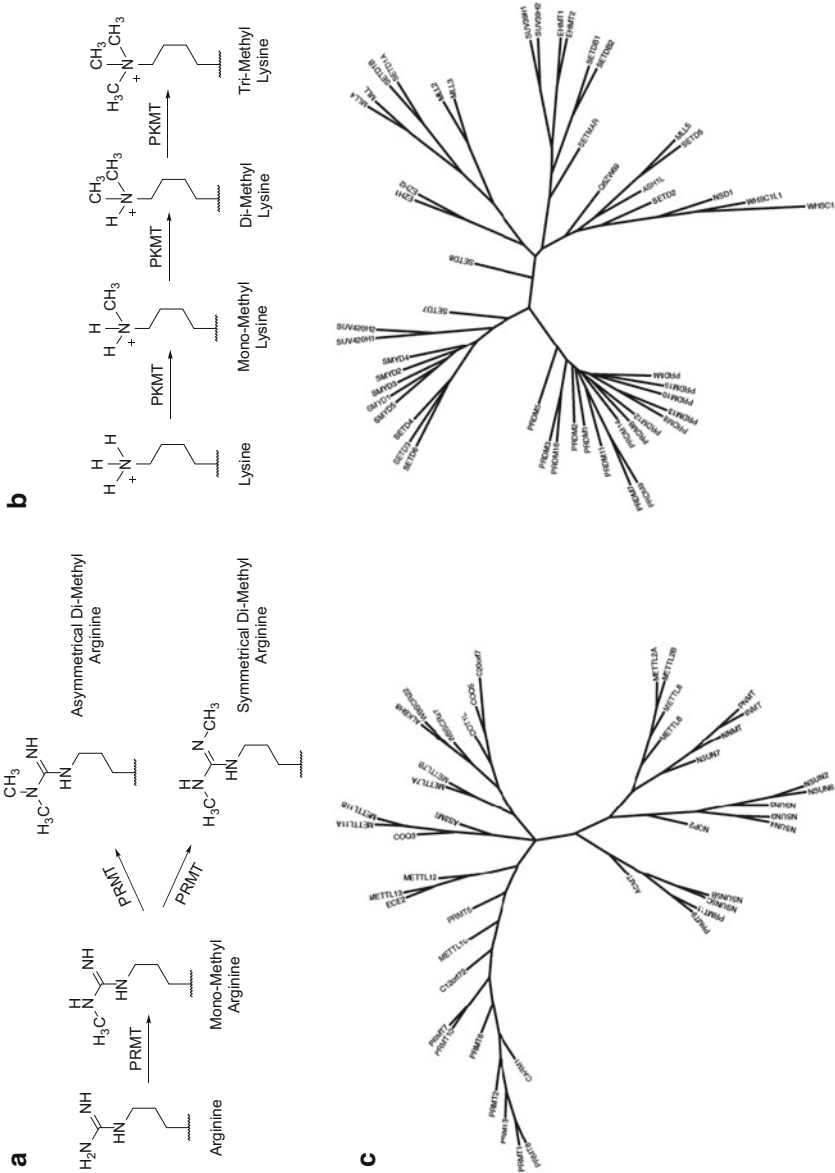
Fig. 5 The 96-member protein methyltransferase class. (**a**) The mechanism of methylation for RMTs; (**b**) Mechanism of methylation for KMTs; (**c**) Phylogenic trees for the RMT and KMT enzymes

PRMT5

PRMT5 is a type II arginine methyltransferase capable of performing mono- and symmetric dimethylation of arginine residues on a range of nuclear and cytoplasmic protein substrates and is currently believed to be the predominant enzyme for symmetric dimethylation. PRMT5 may play an important role in tumorigenesis and is upregulated in several human malignancies [91–97]. The mechanism behind the cell-transforming capabilities of PRMT5 has been postulated to have roles in cell death, cell cycle progression, and cell growth and proliferation but is still under investigation [98]. Whether PRMT5 drives tumorigenesis by direct signal transduction, regulation of gene expression or by some other mechanism is generally unknown; however, recent studies highlight a dependency on PRMT5 as part of the spliceosomal machinery with Sm proteins, particularly for MYC-driven tumors [99].

In almost every biological role hypothesized for PRMT5, the enzyme functions as part of a binary complex with the protein MEP50 (methylsome protein 50). MEP50 was initially identified as a WD40 repeat protein, a family of proteins known to play roles in scaffolding, recognition, and activation by mediating interactions between binding partners and substrates. The roles of MEP50 and PRMT5 are inextricably linked as improvements in stability and activation with the complex have been reported by multiple groups. The PRMT5/MEP50 complex was crystallized in 2012 by researchers at Eli Lilly [100], highlighting the tight binding between the two proteins and further confirming the functional role of the complex.

In 2015, the SGC published a nucleoside-derived inhibitor DS-437 (**14**) with biochemical inhibitory activity against both PRMT5 and PRMT7 ($IC_{50} = 5.9$ and 6.0 µM, respectively) [101]. The compound is a SAM competitive inhibitor of PRMT5 and displayed inhibition of known PRMT5 spliceosomal protein substrates (SmB, SmD1, 3) between 10 and 30 µM. This study was followed a month later by a publication from researchers at Ohio State University who described that PRMT5 is overexpressed following EBV infection and drives B-lymphocyte transformation [102]. In this paper, the group described a small molecule identified from a virtual screen on a PRMT5 homology model. This compound was capable of blocking EBV-driven transformation; however, no biochemical IC_{50} against PRMT5 was reported. At the same time, Epizyme described the first small-molecule inhibitor of PRMT5 to demonstrate in vitro and in vivo activity in mantel cell lymphoma [103]. Identified from an HTS screen of PRMT5/MEP50, this group identified a hit compound which inhibits PRMT5 enzymatic activity with an $IC_{50} = 325$ nM.

This compound was optimized with a blend of structure- and property-guided design [104] leading to tool compound EPZ015666 (**15**), an orally bioavailable compound which demonstrated robust tumor growth inhibition and a corresponding inhibition of SmD3 in multiple MCL xenografts. Having observed a reduction of cytoplasmic PRMT5 substrates, the group was unable to observe levels of any histone target, H2AR3, H3R8, or H3R4, after tool compound treatment. Whether or not this observation is a limitation of available antibody reagents to visualize subtle histone methyl mark changes or that the observed antitumor effects are driven by other PRMT5-mediated mechanism remains to be determined. In addition to the tool compound, GSK announced in 2016 initiation of the first in human clinical study with an RMT inhibitor with compound GSK3326595 (EPZ015938), a product from their alliance with Epizyme [105].

PRMT6

PRMT6 is reported to play a role in a variety of processes including DNA repair [106] and regulation of cell cycle [107]. Its overexpression in several cancer types has linked the enzyme to bladder, lung [108], and prostate cancers [109] and melanoma [110]. EPZ020411 (**16**) is a PRMT6 inhibitor from Epizyme described in 2015, which demonstrates selectivity of ≥tenfold for PRMT6 over other RMT enzymes such as PRMT8 and PRMT1 [111]. The tool compound displays an IC_{50} = 10 nM against PRMT6 and elicits a concomitant reduction in PRMT6-induced H3R2 methylation in A375 cells (IC_{50} = 0.637 ± 0.241 μM). PK evaluation of the tool compound showed it to have modest CL (19.7 ± 1.0 mL/min/kg) and good bioavailability (F = 65.6 ± 4.3%) after subcutaneous administration.

PRMT3

PRMT3 plays a role in ribosomal biosynthesis and has been implicated in inactivation of certain tumor suppression pathways. The first PRMT3 inhibitor, resulting from a high-throughput screen of 16,000 chemical compounds and confirmed by SPR, was reported by the Jin Lab in 2012. The resultant 2.5 μM inhibitor was found to have an allosteric binding mode, noncompetitive with peptide and cofactor, and was successfully co-crystalized in conjunction with the SGC to afford a 2 Å crystal structure bound to PRMT3 (3SMQ). Compound 1 was determined to be a selective inhibitor of PRMT3 over KMTs and the more closely related RMTs PRMT1, PRMT4, and PRMT8; this selectivity is hypothesized to result from the novel binding mode of the inhibitor. The initial compound was deemed not appropriate for cellular assays, but further SAR led to a related piperidine-containing compound SGC707 (**17**) with 31 nM inhibitory activity and improved drug properties [112, 113].

3.3 Lysine Methyltransferases

3.3.1 DOT1

Target Introduction

Disrupter of telomeric silencing-1-like (DOT1L), the human homolog of the yeast protein DOT1, is a lysine methyltransferase responsible for catalyzing the methylation of H3K79 [114–117]. The enzyme can catalyze the mono-, di-, and trimethylation in a distributive (i.e., non-processive) manner [118, 119]. Since its discovery, this PMT has been implicated in transcriptional regulation, cell cycle regulation, and DNA damage response. Knockout studies in mice have shown that mouse DOT1L plays an essential role in embryonic development, hematopoiesis, cardiac function, and the development of leukemia [120]. It is the involvement of DOT1L enzymatic activity in leukemogenesis driven by a subset of MLL (mixed-lineage leukemia) fusion proteins which has engendered interest in the possibility of targeting DOT1L as a potentially viable target in oncology.

MLL is a genetically distinct form of acute leukemia that constitutes over 70% of infant and around 10% of adult acute myeloid leukemias (AMLs). In every case, MLL represents an aggressive form of leukemia and is generally associated with a poor prognosis and with poor response rates from existing therapies. MLL is characterized by a translocation of the MLL gene on chromosome 11q23 [121, 122]. Patients harboring these translocations typically have an overall 5-year survival rate of just 10–20%.

Under normal conditions, the MLL gene encodes for a SET domain PMT which catalyzes the methylation of H3K4 at specific gene loci [123, 124], with gene localization determined by specific interactions with recognition elements outside the SET domains. However, under the disease-linked translocations, the H3K4-directed SET domain is lost, and the remaining MLL protein is fused to a range of protein partners, including members of the AF and ENL family of proteins. With these alternate fusion partners, the MLL protein is capable of recruiting DOT1L, promoting methylation of H3K79 in place of H3K4, leading to enhancement expression of leukemogenic genes including HOXa and MEIS1 [125, 126].

Structural Biology

Full-length human DOT1L consists of some 1,537 amino acids, but less than 400 of these are shared with its yeast homolog DOT [114]. The crystal structure of DOT1L containing its methylating co-factor SAM was published in 2003 by Min et al. [118]. DOT1L is unique within the KMT family as it contains no SET domain and the conformation of SAM within the active site is closer to that of RMT members [127]. Despite this similarity in SAM-binding conformation, no data has emerged that suggests DOT1L is capable of methylation of arginine substrates.

Tool Compound Studies
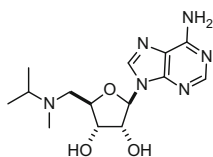
18
EPZ002446
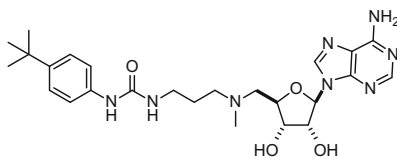
19
EPZ003696
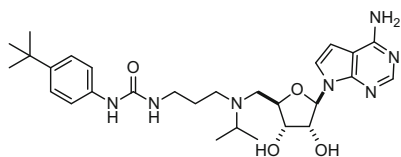
20
EPZ004777
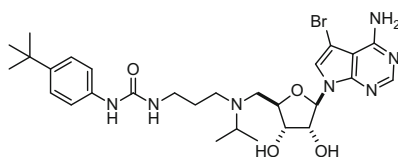
21
SGC0946
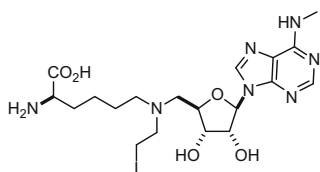
22
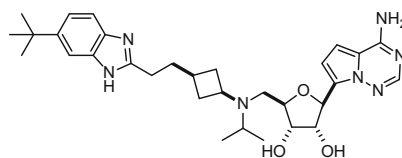
23
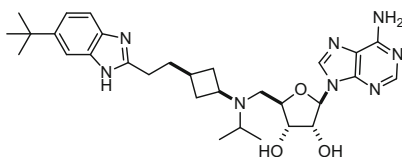
24
Pinometastat
EPZ-5676

Epizyme initiated a DOT1L drug discovery program based upon analogs of the co-factor, SAM. This effort produced the small-molecule probe compound EPZ004777 (**20**) in 2011 [128]. Starting from amino nucleoside compound **18** (K_i = 12,000 nM), a series of alkyl chain extensions delivered increasing potency which provided **19** (K_i = 13 nM). Further modifications of the nucleoside lead to tool compound **20** which inhibits DOT1L with a K_i = 0.3 nM [129] [Basavapathruni, 2012]. Throughout the evolution of SAR, the binding mode of the nucleoside portion of the molecule remained consistent with SAM. However, the increasing amino alkyl chain region of the analogs promotes a distal conformational change not present in the apo form of the enzyme. This conformational alteration creates a hydrophobic pocket to accommodate the substituted phenyl ring of **19** and

20. The new inhibitor-induced conformation also led to an increase in inhibitor residence time [129].

Compound **20** has selectivity against a number of additional PMT enzymes, (1,280-fold against PRMT5, >100,000 fold against other tested PMTs). H3K79 mono- and dimethyl levels were reduced in multiple cell lines including MLL fusion-expressing MV4-11 cells. Methyl mark depletion was observed after 24 h but required up to 4 days to reach maximum levels. In addition, **20** blocks expression of leukemogenic genes and results in selective killing of cells bearing the MLL gene translocation. MV4-11 cells transduced with pMMP-LucNeo retrovirus [130] were used to establish a genetically engineered disseminated leukemia model. **20** was dosed to this model via subcutaneous infusion over a period of 14 days resulting in a dose-dependent increase in median survival.

The Structural Genomics Consortium followed the publication of **20** with a report highlighting data on analog SGC0946 (**21**) with similar biochemical potency against DOT1L and selectivity profile. **21** did, however, report an approximate tenfold improvement in cellular potency as demonstrated by reduction of H3K79m2 levels in MCF10A cells. This increased cellular activity was attributed to an improvement in cellular membrane permeability coupled with the extended residence time observed with this chemical series.

Additional chemotypes have been described in the patent applications as inhibitors of DOT1L. Epizyme has also created non-ribose-related analog of **20** [131]. Baylor University has also published on related nucleoside-containing compounds with significant biochemical activity by extending substitution of the iPr group in **20** with the design tenant of gaining access to the lysine binding channel, compound **22** a key component of this design [132, 133]. Finally, Kainos Medicine Inc. also published a set of adenosine mimic compounds similar to compound **23** [134].

Clinical Development

Only one DOT1L-targeted compound has progressed to clinical trials. Described in 2013 by Epizyme Inc. [135], pinometostat (EPZ-5676) (**24**) entered phase I clinical evaluation in 2012 in advanced hematologic malignancies, including acute leukemia with rearrangement of the MLL gene [136]. An additional pediatric trial commenced in 2014 as a large number of pediatric leukemias carry the MLL rearrangement. **24** inhibits DOT1L with a $K_i = 0.08$ nM, displays a residence time of over 24 h, and is over 37,000-fold selective over other PMTs tested. In a cellular context, the compound inhibits H3K79me2 and proliferation of MV4-11 cells with an IC_{50} around 3 nM. In non-MLL rearranged cells, methyl mark inhibition was also observed but with minimal effect on proliferation. PK parameters for **24** were consistent with earlier tool compounds, and continuous IV infusion was required for dosing in the clinical setting. From a multispecies study, the excretory and metabolic pathways for EPZ-5676 were determined to be similar with low renal excretion of both parent **24** and related metabolites

[137]. Fecal excretion of the parent **24** and a major metabolic mono-hydroxylation of the tertiary butyl group accounted for the majority of drug-related elimination. The group has explored alternative forms for dosing with at least one report investigating subcutaneous, extended-release formulations.

As of the end of 2015 [138], dose-proportional PK was observed with rapid attainment of steady-state plasma concentrations (Css) on day 1 of treatment. Css correlated with inhibition of global H3K79me2 in PBMCs. H3K79me2 ChIP-Seq demonstrated **24** induced reductions in methylation at MLL-r target genes HOXA9 and MEIS1 (median inhibition = 61%; range = 13–91%) and was consistent with DOT1L inhibition. Fifteen of 51 patients had either marrow response or resolution of leukemia cutis or leukocytosis/differentiation. Two complete responses and one partial response were observed in patients shown to have rearrangement of the MLL gene. The compound was deemed to have good tolerability with only nine patients displaying grade ≥ 3 non-hematologic-related toxicities including hypophosphatemia ($n = 1$), decreased ejection fraction ($n = 3$), or elevated transaminases ($n = 1$). Overall adverse events were limited to >15% of patients.

24 has shown synergistic antiproliferative activity in MLL-r cell lines when in combination with a number of AML standard of care therapies, hypomethylating agents, and other epigenetic targeted therapies currently in early stages of clinical development including LSD-1 and bromodomain inhibitors [139].

3.3.2   EZH2

Target Introduction

The extensive protein machinery involved in chromatin remodeling works in concert to modify nucleosome-DNA contacts resulting in the selective gene transcription required for myriad biological processes from maintenance of pluripotency to DNA damage repair and tumor suppression. Vulnerabilities can emerge with change-of-function mutations of EZH2 in the context of the larger PRC2 complex. Additionally, in EZH2 antagonizing, chromatin remodeling systems, such as SWI/SNF and BAP1, loss-of-function mutations can lead to H3K27 hypermethylation – by relieving the antagonistic activity of the systems with regard to PRC2 function – and alternate disease states. The known genetic alterations and their resulting cancer indications are listed in Table 4 [140].

There is a growing support in the literature that EZH2 is central to tumor biology, but the oncogenic role of EZH2 may be dependent on the cellular context. For example, EZH2 loss of function in bone marrow cells has been attributed to oncogenesis of T-cell leukemia [145, 146]. Additionally, evidence of tumor suppressor functions has emerged in myeloid malignancies where EZH2 inactivation is correlated with poor prognosis [147]. Recent publications have also highlighted EZH2 inactivation as a promoter of drug resistance in multiple myeloma [148]. Interestingly, EZH2 has been implicated in methylation of STAT3 which

Table 4 Genetic alteration or disease associations of the EZH2-containing PCR2 complex

Target	Genetic alteration or disease association	Indication	References
PRC2 (EZH2)	Heterozygous activating mutations occurring at Y641, A677, and A687 that result in hypertrimethylation of H3K27	Lymphoma	[141–144]
	Deletion of miR-101 leads to EZH2 overexpression	Prostate cancer	
	Deletion of INI1 leads to EZH2 dependency	Malignant rhabdoid tumors	
	Deletion of SMARCA4 leads to EZH2 dependency	Malignant rhabdoid tumor of the ovary	
	Heterozygous mutations at Y153, H694Y, and P132S	Weaver syndrome	
	Deletion of BAP1 leads to EZH2 dependency	Mesothelioma	

contributes to tumor progression in glioblastoma [149], but other studies have shown that prolonged EZH2 knockdown may lead to an increased level of proliferation and tumor progression [150]. It is clear that H3K27me3 is a mark that plays a significant role in cell fate determination during development. For example, in the mammalian B-cell life cycle, an unnatural trimethylated state of H3K27 arrests the germinal center in the dark zone, preventing differentiation and resulting in aberrant proliferation as opposed to transition to the light zone and either further B-cell maturation, if needed, or alternative apoptosis in a healthy immune system [151]. Preclinically, it has been observed that treatment with EZH2 inhibitors leads to enrichment of B-cell maturation gene sets, suggesting that EZH2 inhibition could result in a cancer cell differentiation event that would lead, in time, to selective apoptosis [152]. One of the advantages of a selective EZH2 inhibitor is that only cells with a genetic addiction to EZH2 activity should be affected by global reduction in H3K27me3 which could enable dosing of therapeutics up to efficacious exposures without deleterious side effects from general cellular toxicity. As compounds move into more advanced clinical trials and additional preclinical experiments are enabled with active tool compounds, we expect our collective understanding of the role of EZH2 in cancer to continue to expand in the near future.

The EZH2 Mutant Hypothesis

Point mutations at or near the catalytic domain of EZH2 have been found in approximately 20–30% of germinal center diffuse large B-cell lymphoma and follicular lymphoma populations of non-Hodgkin lymphoma patients. All identified mutated residues, such as Y641, A677, and A687 (nomenclature referring to *EZH2* variant NM_001203247), are change in function mutations that present in patients heterozygously and function to alter substrate specificity. WT EZH2 is effective at increasing methylation from H3K27 to H3K27me and from H3K27 to H3K27me2, but catalytic efficiency wanes progressively with each successive methylation

event. The result is low concentrations of H3K27me3 in most WT cell populations. In the case of heterozygous Y646X mutants (X = F, N, S, C, or H), however, the mutant enzyme is complementarily more efficient at catalyzing the final methylation step, leading to high levels of H3K27me3 at the expense of H3K27me2 when combined with the WT enzyme activity (Fig. 6). The A677G and A687V mutants, by contrast, lead to hypertrimethylation irrespective of the presence of WT EZH2 and as a result have been referred to as "super-EZH2" enzymes [153].

EZH2 became an attractive target in the personalized medicine era, in part due to the fact that the mutational status of the patient population could be used as a biomarker to potentially predict successful outcome upon treatment with small-molecule inhibitors. Based upon preclinical data in human-derived xenograft models, patients bearing specific EZH2 mutations may benefit greatly from treatment with EZH2 inhibitors. To date, only a small number of mutant-bearing NHL patients have been dosed with EZH2 inhibitors; hence, this hypothesis remains to be tested fully. It is worth noting, however, that NHL patients without EZH2 mutation have also benefitted from treatment with EZH2 inhibitors suggesting that mutational status is not a requirement for treatment efficacy.

SWI/SNF Complex Machinery Impacts PRC2 Gene Expression

DNA transcription and repair is also governed by ATP-dependent chromatin remodelers. One such remodeler is the switch/sucrose non-fermentable factor, or SWI/SNF complex, a 14-protein megastructure that regulates transcription by mobilizing nucleosomes. As part of the network of interconnected gene expression machinery, SWI/SNF acts as a tumor suppressor in part by antagonizing the activity of the PRC2 complex in normal cells [154]. However, inactivating subunit mutations of SWI/SNF are found in ~20% of human cancers and cancer cells [155]. When biallelic mutations of the SWI/SNF complex lead to inactivation by
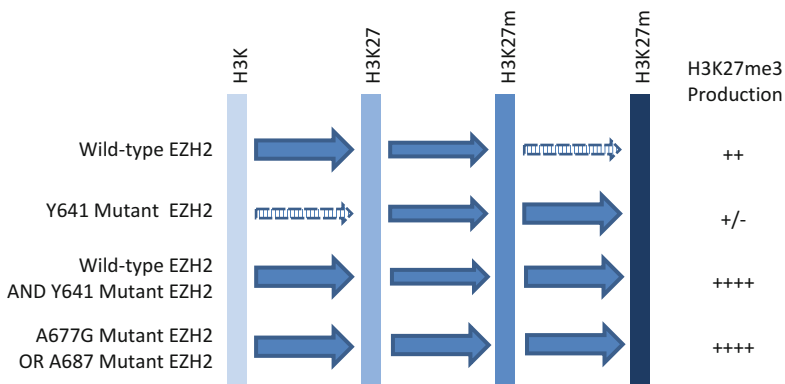
Fig. 6 Predicted effect of mutational status on H3K27 methylation. Wild-type EZH2 produces little H3K27me3 on its own but, in conjunction with a heterozygous mutation, leads to a hypermethylated state

loss of certain specific subunits like INI1 or SMARCA4 or SMARCA2, there can be resultant activation of the PRC2 complex and increased EZH2 activity. This, in turn, leads to the potentiation of stem cell programs through repression of target genes that drive to a subset of solid cancers such as malignant rhabdoid tumors (MRT) [156]. MRT is particularly devastating, being characterized by an approximate 12-month median post-relapse survival rate, and although it can occur in adults, it most often affects young children. A related disease, known as malignant rhabdoid tumor of the ovary (MRTO), occurs in young women and constitutes a particular form of ovarian cancer (it is also referred to as small cell carcinoma of the ovary, hypercalcemic type or SCCOHT) [157]. MRTs have no current standard of care treatment and respond poorly to conventional chemotherapies, but are hypothesized to be treatable with EZH2 inhibitors, which would block the associated activation of the PRC2 complex that attends SWI/SNF loss of function mutations.

Loss of BAP1 Leads to EZH2-Dependent Transformation

BAP1 is a tumor suppressor that exists in a multi-protein complex with ASXL1 (another tumor suppressor). The two proteins act in concert to remove posttranslational, monoubiquitination marks from histone H2A lysine 119 (H2AK119Ub). BAP1 loss-of-function mutations are found in almost half of all mesothelioma. Significantly, like the SWI/SNF relationship, loss of BAP1 is associated with increased H3K27me3 levels and increased expression of EZH2 protein. Recently, Levine's group described the interplay between BAP1 and EZH2, where the myeloid cell-stimulating effects induced by loss of BAP1 function are ameliorated by concomitant loss of EZH2. They also showed that mesothelioma cells resulting from BAP1 loss-of-function mutants are sensitive to treatment with EZH2 inhibitor **EPZ011989** (see Sect. 3.2.2.1) [144]. BAP1 represents a second example of how a loss-of-function mutation in one complex is pathobiologically equivalent to a gain of function of EZH2, thus leading to the potential for targeted intervention with an enzyme inhibitor. This discovery was revealed through careful analysis of The Cancer Genome Atlas (TCGA) which shows that EZH2 mRNA expression was increased in mesothelioma tumors compared to healthy tissue. Continued preclinical studies are ongoing to reveal additional potential indications that share this common phenotype.

The Glucocorticoid Receptor Antagonist Synergy Hypothesis

A great majority of relapsed or refractory NHL patients have previously been treated with a standard of care cocktail of drugs known as R-CHOP (rituximab, cyclophosphamide, hydroxydaunorubicin, Oncovin, and prednisone). This treatment can result in a 60–70% complete response rate, but approximately one third of

responding patients relapse, and the recurrent lymphoma can exhibit resistance to a wide array of cancer drugs. The efficacy of EZH2 inhibitors in heavily pretreated patients or as combination therapy in frontline treatment is a subject that has attracted significant attention from companies pursuing EZH2 inhibitors for the market.

Preclinical assessment of EZH2 inhibitors with each of the active ingredients in CHOP individually revealed an intriguing synergy between EZH2 inhibition and glucocorticoid receptor antagonists like prednisolone, the active metabolite of prednisone [158]. Moreover, although mutant cell lines are known to be sensitive to EZH2 inhibition in vitro, EZH2 wild-type GCB lymphoma cell lines (e.g., DOHH2 and OCI-LY19) have demonstrated limited response to these compounds. However, when prednisone is co-administered with EZH2 inhibitors, a marked antiproliferative effect is seen, even in the insensitive DOHH2 WT line with a tenfold improvement over prednisone alone. The potential for this combination to render refractory GCB lines more sensitive to EZH2 inhibitors is intriguing and could lead to new frontline therapy combinations including EZH2 inhibitors.

Structure and Function

EZH2 is the primary catalytic center of the multiprotein polycomb repressive complex 2 (PRC2), the only known complex responsible for distributive methylation of lysine 27 on the histone H3 subunit (H3K27). PRC2 catalyzes transformation from the native lysine to the mono-, di-, and trimethylated forms, using S-adenosyl methionine (SAM) at each step as the methyl-donating co-factor. EZH2 acts as an epigenetic regulator because the trimethylated form of H3K27 (H3K27me3) induces a heterochromatic state that is transcriptionally repressive, blocking programmed gene expression [159].

The closely related EZH1 has a lower catalytic activity as a component of PRC2 but is highly related to EZH2 with 96% homology in the active SET domain. Unlike EZH1, however, EZH2 is found primarily in rapidly dividing cells like stem cells and is found to be overexpressed in a broad range of cancer types.

Until recently, structural information on the SET domain active site of EZH2 has been limited. The primary reason for this is that the SET domain is at the junction of three proteins, EZH2, EED, and SUZ12, which comprise the active form of the PRC2. Inactive forms of EZH2 have been successfully crystallized, but all three proteins need to be crystallized together with an H3K27me3 peptide truncate and the cofactor SAH to obtain meaningful insight into the catalytic domain of the complex. This was accomplished only recently by a group at UT Southwestern with protein from a heat-tolerant eukaryotic fungus strain *Chaetomium thermophilum* at 2.3 Å resolution [160]. Through this work, Liu et al. have elucidated the intimate relationship between protein subunits, in particular EED and EZH2, and the autocatalytic nature of H3K27me3 in transcriptional repression.

In Vitro Tool Compound Development

25
EPZ005687

26
GSK-126

27
GSK-343

28
EI-1

29
UNC-1999

30
Tazemetostat
EPZ-6438

31
EPZ011989

32
CPI-1205

33
CPI-169

34
Pfizer-253

35

36
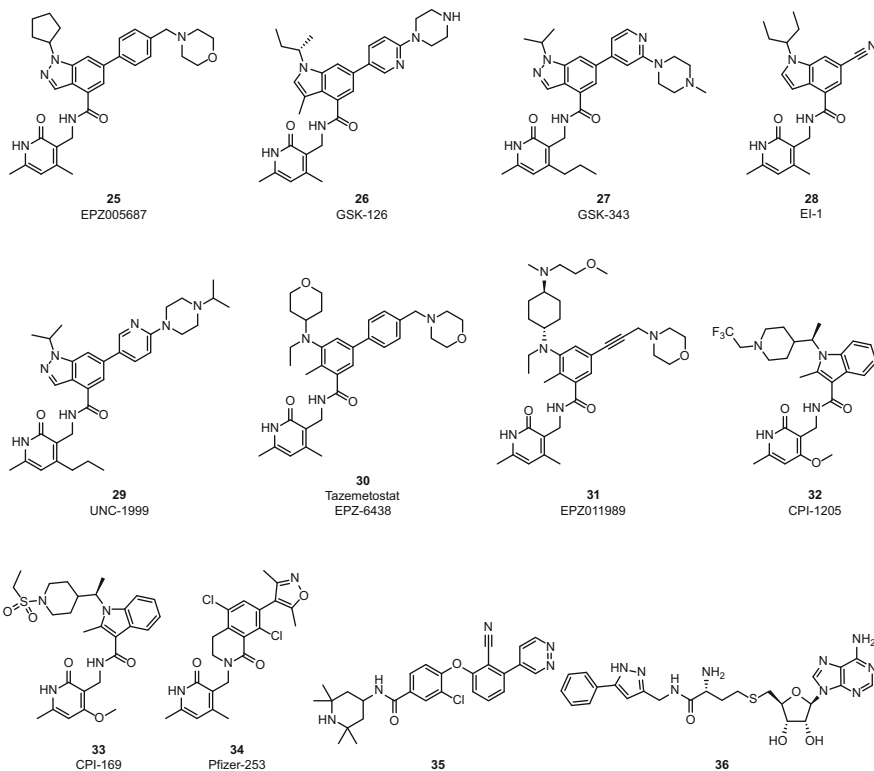
The first series of in vitro tool compounds, developed to establish proof-of-concept antiproliferative effects in cell lines bearing mutant EZH2 isoforms, began to emerge as a group at the end of September 2012 with the publication of Epizyme's selective EZH2 inhibitor, EPZ005687 (**25**) (54 nM EZH2 IC_{50}) [161]. Soon after, GSK followed with the publication of the compound that would later become their clinical candidate GSK-126 (**26**) (10 nM EZH2 IC_{50}; see clinical section for further discussion) [162]. This report was closely followed by a second publication from GSK demonstrating the synthesis and EZH2 inhibitory activity of two closely related compounds, GSK-343 (**27**) (9 nM EZH2 IC_{50}) and GSK-946 [163]. Later, in November of 2012, Novartis reported their preclinical efforts with the disclosure of EI-1 (**28**) (4 nM EZH2 IC_{50}) [164], and in April 2013, UNC reported on what they claimed was the first orally bioavailable EZH2 inhibitor, UNC-1999 (**29**) (<10 nM EZH2 IC_{50}) [165]. No clearance values were reported for the UNC compound so it is unclear whether the compound has the ability to reach efficacious levels of target occupancy upon oral dosing. The most conspicuous conclusion to be drawn from the structures of the first disclosed EZH2 inhibitors is that they all bear a common feature in the 4,6-disubstituted pyridone. With the exception of the UNC

compound (which is structurally related to compound **27** in the GSK publication from June of the previous year), all of the lead compounds emerged from unique high-throughput screening efforts of commercial or internal diversity chemical libraries.

The cellular activity of each of the in vitro tool compounds has been described in their corresponding papers with a dose-dependent cell killing for each compound in cell lines bearing various EZH2 mutations. The collective data represents an in vitro target engagement proof of concept milestone for these EZH2 inhibitors. Pfeiffer cells which contain the A677G mutation are particularly sensitive to **26**. In contrast, other Y646X mutant cell lines appear to require dosing at higher concentrations over longer periods of time to achieve a similar response levels.

Although modifications at the 4,6-dimethylpyridone have been made and attempts to replace the pyridone have also been reported, it is accurate to state that the pyridone is an important feature driving potency of EZH2 inhibitors. Without specific structural information of a compound bound in the active domain, we can only speculate that the pyridone amide is acting as both a hydrogen bond acceptor as well as hydrogen bond donor in a network that is optimally oriented by the 4,6-disubstitution pattern.

In a recent medicinal chemistry optimization paper describing clinical candidate EPZ-6438 (**30**) [166], SAR generated during lead optimization depicts the importance of the orienting methyl substitution on various parts of the EZHZ scaffolds (Fig. 7). The sequential additional of methyl groups on the pyridone ring in compounds **37–42** results in a concomitant increase in inhibitory activity against EZH2. In addition, blocking of the pyridone amide carbonyl was identified to have a more significant effect on biochemical potency than blocking the amide NH hydrogen bond donor group. This suggests that it is the amido (**41**) and not the imido (**42**) tautomer which confers activity and that the carbonyl oxygen makes a highly favorable interaction with the enzyme. GSK and Constellation teams have reported improved in vitro activity with the 4-N-propyl substitution and 4-methoxy substitution, respectively, but to date, they have not published orally bioavailable analogs bearing these modifications.

A second notable similarity between the in vitro tool compounds presented by each of the major groups in the field is that each contains a bicyclic core with an amide at the 4-position and a highly lipophilic group at the N1-indole or indazole position, an example of which is compound **42** (Fig. 8). In the bicyclic series, very little is tolerated at the N1-position suggesting a highly lipophilic pocket is accessed
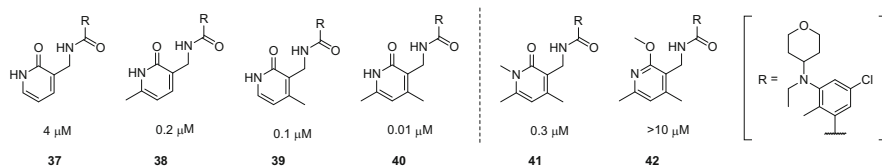
Fig. 7 Impact of pyridone methyl substitution is additive and prefers the free amide carbonyl
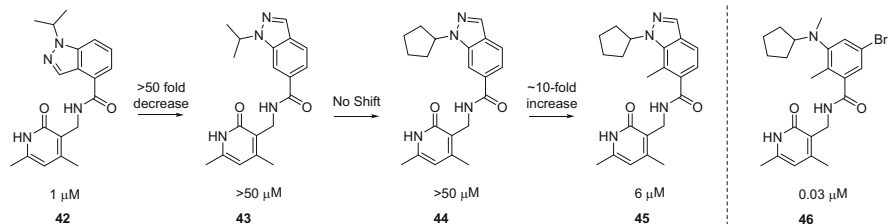
Fig. 8 Identification EZH2 inhibitors with an aryl core scaffold

along this vector. The significance of the orientation of the bicycle with respect to the pyridone-bearing amide was not fully understood until a more thorough investigation of the core revealed that the orientation of the bicycle was not as critical to identifying potency against EZH2, but instead a steric blocking group that forced the amide out of plane is a significant driver of potency (**45**). Retaining this "magic methyl" and replacing the indole ring for an aryl ring delivered a path to increased potency as shown with compound **46**.

Next-Generation Tool Compounds

Since the initial disclosure of in vitro tool compounds, continued compound development has led to a series of more advanced compounds available for preclinical evaluation. EPZ011989 (**31**) (EZH2 IC_{50} = <3 nM), reported in early 2015, has good oral bioavailability and demonstrated robust tumor regression in an in vivo xenograft model using the KARPAS-422 cell line implanted into SCID mice, when dosed at 250 mg/kg twice daily (BID) for 21 days [167]. Low unbound clearance and strong potency against EZH2 make **31** an ideal in vivo tool compound for probing additional cancer indications that may be susceptible to EZH2 inhibition. Constellation also reported a new indole core chemotype that, although not orally bioavailable, demonstrated a >10 h half-life when dosed subcutaneously (SC). In vivo efficacy for compound CPI-22 (**32**) (EZH2 IC_{50} = 2 nM) was reported in a similar xenograft model using KARPAS-422 cells at 200 mg/kg BID with complete tumor regression observed by day 28. Additionally, Pfizer reported a ring closed scaffold analog PFI-253 (**33**) that locks the freely rotating pyridine to the core ring with a two- or three-atom tether (EZH2 IC_{50} = <4 nM). No biological data was reported in the patent that discloses this new chemotype, but the reduction of H-bond donors in this scaffold suggests the high potential for this new class to deliver oral drug-like molecules.

Alternative Scaffolds

One of the most successful attempts to broaden the scope of selective EZH2 inhibitors came from the optimization of another high-throughput screening hit by Constellation Pharmaceuticals [168]. The medicinal chemistry team identified a weakly potent (51 μM) EZH2 inhibitor bearing an unusual 2,2′,6,6′-tetramethylpiperine component that, like the pyridine class, demonstrated a SAM competitive phenotype. After an unsuccessful attempt at replacing the diphenyl ether linkage, the terminal phenyl moiety was optimized effectively to deliver a 32 nM inhibitor with potent activity in vitro (**34**). The cellular antiproliferative activity reached 9.5 μM in the KARPAS-422 EZH2 Y646N mutant cell line with a concomitant reduction in H3K27me3, but the team appeared unable to deliver a bioavailable compound from this class; hence, no in vivo studies have been reported to date.

Using a strategy similar to that employed in the development of DOT1L inhibitors (Sect. 3.3.1.3), a team at Pfizer, La Jolla, has reported a subset of EZH2 inhibitors designed directly from the reaction product SAH [169]. These nucleoside-based inhibitors, exemplified by compound **35**, demonstrated selective WT and Y646N mutant EZH2 inhibition of 270 and 70 nM, respectively. However, no cellular activity was achieved due to perceived permeability limitations.

Clinical Progress with EZH2 Inhibitors

One of the advantages of EZH2 as a therapeutic target is that incoming patients can be screened to determine their mutational status. This can be used to stratify the treatment population into groups that have or do not have the EZH2 mutation to determine if there is any advantage one way or the other. A second advantage of EZH2 as a drug target is the specificity of the enzymatic action on this epigenetic mark. This specificity allows for the measurement of EZH2 inhibitors in vivo activity of by monitoring the amount of methylated H3K27 present in tumor or surrogate tissue. This signal loss can be used as a pharmacodynamic (PD) readout of inhibitor activity that can then be correlated with tumor growth inhibition as a less invasive means for measuring in situ target occupancy.

Three compounds had entered phase I human trials for NHL by the end of 2014 and one compound, **30**, initiated phase II studies in Europe and the USA in 2015 for NHL and solid tumors, respectively, at the time of writing (Table 5). Significant preclinical evidence supports EZH2 inhibitor activity in specific NHL patient populations for which there exists a significant population that is refractory to current treatment modalities and with a relapse rate suggestive of a clear need for novel therapies.

Table 5 Clinical studies with inhibitors of EZH2

Drug name	Target class/enzyme	Status	Indication
Tazemetostat	HMT/EZH2	Phase I/II	Lymphoma, INI-deficient tumors, synovial sarcoma, SMARCA4-negative tumors
CPI-1205	HMT/EZH2	Phase I	B-cell lymphoma
GSK2816126	HMT/EZH2	Phase I	B-cell lymphoma, follicular lymphoma

The Epizyme clinical tazemetostat **30** was realized through reduction of the bicyclic core of **25** to a substituted phenyl core as shown earlier. This allowed for property optimization to afford a compound with improved potency and PK properties. **30** was granted the generic name tazemetostat by the WHO in 2015.

The phase I clinical trial with **30** was designed as a 3 + 3 dose escalation study starting at 100 mg BID, dosed orally and targeting a maximum dose of 1,600 mg BID. The trial was open to NHL and solid tumor patients with the primary endpoint and was identified as establishment of the maximum tolerated dose and measurement of the objective response rate. Secondary endpoints were assessment of PK, duration of response, and progression-free survival, to be measured at 8-week intervals.

A phase II was initiated in June 2015 in patients with DLBCL or FL for determination of efficacy and safety in five independent cohorts determined by histology, cell of origin, and EZH2 mutational status. This NHL clinical trial is being conducted in Europe, Australia, Canada, and the USA. In addition, separate phase II trials in patients with advanced solid tumors characterized by INI1 or SMARCA4 negativity or synovial sarcoma were initiated in adults and in pediatric subjects in the USA, Australia, Europe, Canada, and Asia in December 2015.

In January 2014, **26** was progressed to the clinic as a twice weekly intravenous (IV) infusion. The phase I trial was conducted in adult patients with relapsed/refractory diffuse large B-cell and transformed follicular lymphoma malignancies. The starting dose was 50 mg in water solution, infused over a 2 h period twice weekly, initially with 3 weeks on and 1 week off in each 28 day cycle, with a maximum tolerated dose cutoff of 3,000 mg twice weekly. The primary endpoint was to explore the recommended phase II dose in relapsed/refractory germinal center B cell-like diffuse large B-cell lymphoma (GCB-DLBCL) subjects with EZH2 wild-type and EZH2 mutant-positive lymphoma prior to the initiation of an expansion phase. Phase I data are not currently available, but if merited, the expansion phase was projected to have minimally two cohorts based on EZH2 mutation status.

The first example of a pyridone-containing EZH2 inhibitors to be published from Constellation Pharmaceuticals was an advanced compound containing a 4-methoxy-6-methylpyridone and a methyl-bearing indole core (CPI-169, **33**) appearing in a

Chemistry & Biology paper published in 2014 [170]. The compound reported was dosed subcutaneously (SC) in the preclinical models of antitumor activity, but an orally bioavailable analog of **33** was discovered and has advanced through IND-enabling studies and into the clinic, CPI-1205 (**32**) [171].

The Constellation phase I human trial was initiated with CPI-1205 (**32**) in patients with a confirmed diagnosis of a B-cell lymphoma that has progressed in spite of prior treatment [172]. The reported primary outcome measures are frequency of dose-limiting toxicities to be assessed in the first 28 days on study (Cycle 1). Expected enrollment is 41 patients, and the study is predicted to collect all the necessary data by the end of December 2016.

EZH2 Resistance Mechanisms

A large body of preclinical data exists that describes the robust effects of EZH2 inhibitors on in vivo xenograft implanted tumor cells bearing EZH2 mutations. However, cancer is highly adaptable, and using an artificial in vitro system, several specific mutations that give certain cell lines the power of resistance to EZH2 inhibitors have been produced [173]. The resistant mutations were identified by a team at Ariad Pharmaceuticals by using forward genetics in the Pfeiffer B-cell lymphoma line bearing an A677G super-EZH2 mutation. After the cells were mutagenized, drug-resistant outgrowths were observed to increase cell viability scores by 1,000-fold posttreatment with EZH2 inhibitors (**25**, **27**). Sequencing of the resistant lines leads to the discovery that the new mutation was not found in the SET domain, but instead a high-frequency EZH2 Y111D missense mutation, along with several additional low-frequency missense mutations, was identified in the N-terminal allosteric D1 domain. It is notable that at higher doses of inhibitor, no new outgrowth was observed, and Y646F mutant EZH2 lines were shown to be less susceptible to the same mutational resistance.

Importantly, no patients bearing a Y111D mutation have been identified in a clinical setting, and if they do exist, the mutation can be identified by conventional screening and can be treated with alternative therapeutics or higher doses of a EZH2 inhibitor. The authors also suggest that next-generation EZH2 inhibitors could focus on this allosteric site at the EZH2/EED nexus to mitigate acquired resistance mechanisms. Interestingly, targeting this protein-protein interaction was the subject of a recent publication where a cell-permeable stapled peptide with a K_D of 264 nM ($SN_LFSSNRQKILERTXILNXEWKQRRIQPV$) was shown to reduce H3K27me3 in a MLL-AF9 leukemia cell line [174].

As with many of these types of early mutation studies, there is currently no data confirming that these in vitro selection experiments can or will be recapitulated in a clinical setting. Additionally, as suggested in the paper, higher doses of EZH2 inhibitor may mitigate any specific Y111D mutation.

3.3.3 Additional KMT Tool Compounds

47 BIX-01294

48 UNC-0638

49 A-366

50 AZ-505

51 LLY-507

52 A-893

53 BAY-598

54

55 EPZ030456

56 EPZ031686

57 BCI-121

58 (*R*)-PFI-2
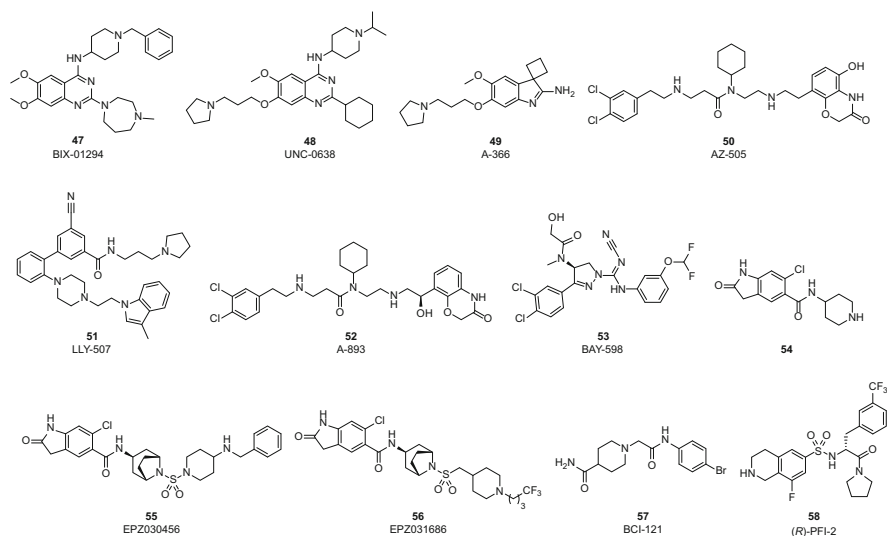
EHMT2

EHMT2, or euchromatin histone methyltransferase 2, is the gene name for a lysine methyltransferase, also commonly referred to as G9a. As the gene name suggests, the enzyme is associated with the installation of a transcriptional repressive methyl mark. EHMT2 and its close relative EHMT1 (GLP) are known to methylate H3K9 to the mono- and dimethyl state but have also been reported to be able to methylate H3K27 to a lesser degree. EHMT2 belongs to the SET domain-containing family of proteins that include SUV39, SETDB1, and DIM-5 [175]. A number of substrate competitive small-molecule inhibitors have been disclosed by Boehringer Ingelheim (BIX-01294, **47**) [176], the University of North Carolina (UNC-038, **48**) [177], and Abbvie (A-366, **49**) [178].

A number of potential cancer indications have been postulated for EHMT2 including leukemia [179], head and neck cancer [180], esophageal cancer [181], and glioma [182]. Additionally, it was shown recently that EHMT2 appears to also play a role in activation of the β-globin gene and potentially the induction and of fetal hemoglobin [183–185].

SMYD2

SMYD2 stands for SET and MYND domain-containing protein 2 and is histone methyltransferase that is responsible for monomethylation of H3K4 and the addition of a second methyl group to H3K36me, using SAM as cofactor. Despite some localization to the nucleus, active SMYD2 is largely cytoplasmic (~80%) and also responsible for methylation of a number of non-histone substrates including p53, HSP90, ERα [186], and PARP1 [187]. Early reports on the cellular function of SMYD2 suggested a possible role in restricting cellular proliferation [188], and SMYD2 has been also implicated as a possible oncogene due to its inactivating methylation of Lys370 of p53, a known tumor suppressor [189]. However, later publications have linked SMYD2 overexpression to poor outcomes in esophageal squamous cell carcinoma [190], gastric cancer [191], and pediatric ALL [192] suggesting the tumor suppression potential of inhibition of this target. Despite the connection to cancer therapy, to date, SMYD2 knockout or inhibition has failed to demonstrate global effects on H3K4 or H3K36 methylation states. Whether this unique lack of effect is due to the cytosolic localization of the enzyme or another, yet unknown factor is the subject of current research with newly developed tool compounds designed to probe the SMYD2 mechanism. Crystal structures of SMYD2 constructs have been reported with SAM bound (3TG4, 3S7J), SAH and p53 bound (3TG5), as well as with methyltransferase inhibitors sinefungin (3QWW), LLY-507 (**51**) (4WUY), and A-893 (**52**) (4YND).

To gain a better understanding of the biology in play when SMYD2 is inhibited in a cellular context, a number of tool compounds have emerged from industry and institutional research programs. The first reported inhibitor, AZ-505 (**50**), was from AstraZeneca [193]. This compound was developed from a 1.23 million compound HTS campaign using AlphaScreen technology. Compound **50** is a potent and selective inhibitor of SMYD2 with a biochemical IC_{50} of 120 nM and >70-fold selectivity over SMYD3, the nearest homolog. **50** was also found to bind in the SET domain of SMYD2 in a peptide competitive and SAM noncompetitive inhibition mode, identified through crystallography efforts. Although no cellular data has been provided for **50**, a structurally related compound was recently reported by AbbVie in conjunction with the SGC, **52,** that has an additional chiral alcohol that confers a significant increase in biochemical potency ($IC_{50} = 3$ nM). This increased potency, along with the removal of the 5-hydroxy component of the benzoxazinone, is projected to allow for functional activity to be observed via suppression of p53K370 methyl mark in relevant lung carcinoma cell lines [194].

Two additional cell active tool compounds for SMYD2 were also released in 2015. The first compound, produced by a team at Lily Pharmaceuticals, **51,** is a potent (<15 nM) inhibitor of SMYD2 with a >100-fold selectivity over other tested HMTs [195]. Importantly, however, **51** demonstrated p53K370 methyl mark inhibition with an IC_{50} of 0.6 μM in U2OS cells. Compound **51** further inhibited the proliferation of KYSE-150 (esophageal) and MDA MB-231 (breast cancer) cell lines in an apparent dose-dependent manner. Despite the increased cellular activity of **51** and **52**, neither of these dibasic compounds allow for oral dosing to enable

in vivo experiments. **53**, a compound developed by Bayer and made available to the scientific community by the SGC, is reported to inhibit SMYD2 at 27 nM with good selectivity and cell activity (<1 μM) [196].

SMYD3

SMYD3 plays an important role in the regulation of gene transcription through complexation with the RNA polymerase complex, and overexpression of this histone modifier is linked to enhancement of cell growth. SMYD3 is responsible for H3K4 and H4K5 di- and trimethylation in the nucleus. It also plays a significant role in the cytoplasmic methylation of MAPK3 (MEKK2) at lysine 260, which may result in an activated MAPK state required for KRAS-driven oncogenesis. Although a full understanding of the mechanism in cancer is still unknown, whether by modification of nuclear or cytoplasmic proteins, SMYD3 activity has been linked to the development and cell survival of breast [197], prostate [198], pancreatic, lung [199], and gastric [200] cancer types. Until recently, validated chemical probes for understanding the biology around SMYD3 and cell viability have been limited. In 2015, however, two new inhibitor chemotypes were introduced. Crystal structures of SMYD3 have been solved with SAM (3MEK), sinefungin (3RUO), small-molecule inhibitor **54** (5CCL), and EPZ030456 (**55**) bound (5CCM).

The first reported tool compounds to selectively target SMYD3 were developed by Epizyme and reported in 2015 [111]. In vitro tool compounds **55** and **56** were developed through optimization of a proprietary library hit, compound **54**, by modifying the aminopiperidine into a rigidified sulfonamide with a 4-aminopiperidine or a substituted 4-methylpiperidine tail. The resulting compounds bind in a noncompetitive mode with respect to MEKK2 substrate and mixed-competitive mode versus SAM; however, the compounds do not make many significant interactions with the SMYD3 protein outside of the 6-chloro-2-oxoindoline-5-carboxamide head group. Despite this, both compounds have single-digit nM IC_{50} values against SMYD3, and this translates to 48 and 36 nM cellular activity in a MEKK2 In-Cell Western (ICW) Assay for **55** and **56**, respectively. Additionally, **56** was identified as a good candidate for in vivo studies with in vitro ADME (mouse liver microsomes, 24 mL/min/kg and mouse plasma protein binding, 0.53 unbound fraction) and PK studies that demonstrated high oral bioavailability (>48 ± 5%F) suitable for further efficacy assessment in mouse xenograft models of disease.

A second chemotype identified as a SMYD3 inhibitor was also recently published by an academic group in Bari, Italy [201]. Although proliferation data was provided for BCI-121 (**57**) in a number of relevant cancer cell lines, the reported data are insufficient to exclude a general cytotoxic effect producing the observed antiproliferative effects. However, the chemotype of **57** is drug-like and may warrant further examination.

SETD7

SETD7 is another SET domain-containing lysine methyltransferase, responsible for monomethylation of H3K4 and the resultant transcriptional activation. SETD7 expression is known to be active in skeletal muscle differentiation [202], but the exact role of SETD7 in cellular signaling pathways and the progression of disease is still poorly understood. (R)-PFI-2 (58) is a selective small-molecule inhibitor first reported by the SGC in conjunction with Pfizer that has a peptide competitive and SAM uncompetitive binding modality [203]. A 1.9 Å structure of 58 has been solved in the SETD7 SET domain showing binding in the substrate pocket and hydrophobic interaction of the amide pyrrolidine with the mobile charged methyl group of SAM. Importantly, the R-enantiomer has a K_I^{app} of 0.33 nM (500 times more potent than the corresponding S-enantiomer) and has demonstrated cellular activity in NHLF cells [204]. Using this newly available tool compound, He et al. have reported that SETD7 is implicated in cellular response to oxidative stress through regulation of mitochondrial function. More studies are currently underway with this tool compound to further elucidate the role of SETD7 in disease.

4 Erasers: Lysine Demethylases

4.1 Introduction

Histone demethylases (HDMs) are a large class of chromatin-modifying enzymes commonly referred to as "erasers" that include peptidyl arginine deiminases (PADI) [205] and the lysine-specific demethylase (KDM) family members 1–8 and their closely related subtypes. Table 6 provides a complete list of the KDMs and their commonly used synonyms [206]. Lysine demethylases can be further stratified into two main groups. The first group contain a Jumonji domain (JmjC) and demethylate through hydroxylation and decomposition of the resulting aminal to formaldehyde employing the cofactors Fe(II) and α-ketoglutarate in the active site (KDMs 2-8). The second group, KDM1 (LSD1), are amino oxygenases that harness molecular oxygen to oxidatively remove methyl marks relying on flavin adenine dinucleotide (FAD) as cofactor and producing formaldehyde and hydrogen peroxide as by-products. While JmjC-containing demethylases are capable of demethylation of trimethylated lysine residues and indeed may prefer Kme3 as substrates [207], they are complementary to the amino oxygenase demethylases which can mechanistically only remove di- and monomethylated marks.

Lysine demethylases have emerged as a critical part to the chromatin remodeling family, linked to the growth and differentiation of embryonic stem cells, ectopic expression, spermatogenesis, and many other biological functions. Additionally, HDMs and the KDM subtypes have been implicated in a number of diseases including leukemia, prostate cancer, squamous cell carcinoma, and X-linked mental retardation.

Table 6 Lysine demethylases with associated names and synonyms

Approved symbol	Previous symbols	Synonyms
KDM1A	AOF2, KDM1	KIAA0601, BHC110, LSD1
KDM1B	C6orf193, AOF1	FLJ34109, FLJ33898, dJ298J15.2, bA204B7.3, FLJ43328, LSD2
KDM2A	FBXL11	KIAA1004, FBL11, LILINA, DKFZP434M1735, FBL7, FLJ00115, CXXC8, JHDM1A
KDM2B	FBXL10	PCCX2, CXXC2, Fbl10, JHDM1B
KDM3A	*JMJD1*, *JMJD1A*	TSGA, KIAA0742, JHMD2A
KDM3B	C5orf7, *JMJD1B*	KIAA1082, NET22
KDM4A	*JMJD2*, *JMJD2A*	KIAA0677, JHDM3A, TDRD14A
KDM4B	*JMJD2B*	KIAA0876, TDRD14B
KDM4C	*JMJD2C*	GASC1, KIAA0780, TDRD14C
KDM4D	*JMJD2D*	FLJ10251
KDM4E	KDM4DL	*JMJD2E*
KDM5A	RBBP2, JARID1A	
KDM5B	JARID1B	RBBP2H1A, PLU-1, CT31
KDM5C	SMCX, JARID1C	DXS1272E, XE169
KDM5D	HYA, HY, SMCY, JARID1D	KIAA0234
KDM6A	UTX	
KDM6B	JMJD3	KIAA0346
KDM8	JMJD5	FLJ13798

4.1.1 LSD1 (KDM1A)

Target Introduction

LSD1 expression is reportedly elevated in a number of human cancers including lung, breast, prostate, and common blood cancers such as AML. Preclinical studies report LSD1 inhibitors having antiproliferative effects in numerous solid and hematological human cancer cell lines in vitro [208]. Moreover, small cell lung cancer (SCLC) LX48 cell line xenograft experiments have demonstrated significant tumor growth inhibition when treated with an oral small-molecule LSD1 inhibitor (vide infra). However, whether LSD1 upregulation or downregulation is beneficial, like histone methyltransferase activity, may be cancer-type specific. It has been observed that LSD1 is downregulated in breast carcinomas which activates the TGFβ1 signaling pathways and increases the potential for metastasis [209]. Alternatively, high levels of LSD1 are associated, in part, with the likelihood of relapse in prostate cancers post radical prostatectomy [210]. In blood cancer, specific effects of LSD1 inhibitors have been reported on a treatment resistant subset of acute myeloid leukemia (AML) known as acute promyelocytic leukemia (APL) when dosed in conjunction with retinoid standard of care therapy [211]. Others have shown that LSD1 is an essential regulator of leukemia stem cell (LSC) effectors via

in vivo xenograft models in which cells bearing MLL translocations were targeted over normal hematopoietic stem and progenitor cells (HSPCs) [212]. Recently, Wada et al. have reported LSD1 overexpression appears to correspond with increased incidence of T-cell lymphoblastic leukemia (T-LBL) via upregulation of HoxA family members and increased cellular self-renewal properties [213]. Although the emerging role of LSD1 in cancer appears complex, in order to probe LSD1 biology further, selective cell active inhibitors have been developed to test the above cancer hypotheses.

LSD1 Structural Biology

Prior to 2004, histone methylation was thought to be unidirectional and therefore a static histone modification installed by histone methyltransferases. LSD1 (KDM1A) was the first histone demethylase to be identified and is unique to the family because it also belongs to the FAD-dependent amine oxidase family that also includes MAO-A and MAO-B. LSD1 is responsible for catalyzing the dynamic demethylation of mono- and dimethylated lysines K4 and K9 on the histone H3 subunit. Cellularly, LSD1 is commonly localized in CoREST repressor complexes that also include HDAC family members, and it is believed that CoREST may be responsible for targeting LSD1 to DNA [214]. Additionally, LSD1 is known to be present in the Mi-2/nucleosome remodeling complex (NuRD) where it can interact with metastasis tumor antigens 1–3 that restrict transcription through interactions of promoter regions [209]. Alternatively, LSD1 can also function as an activator required for expression of androgen receptor (AR) and estrogen receptor (ER) target genes by removing the H3K9me2 repressive methyl mark [215]. Other activator complexes that employ LSD1 include the elongation factor RNA polymerase II (ELL) [216] and the MLL epigenetic modifying supercomplex. LSD1, like many related epigenetic enzymes, may perform multiple roles in the maintenance of balanced gene expression, but it has emerged as an important transcriptional factor that is highly expressed in certain forms of cancer, and this makes it an appealing target for drug discovery.

The structure of a truncated LSD1 peptide was solved in 2008 by Chen et al. at the University of Michigan Medical School [217]. The initial structure identified an amine oxidase-like (AOL) catalytic center lined with highly negative electrostatic regions and an N-terminal SWIRM domain responsible for stability and binding interactions with chromatin remodeling machinery. Since that time, crystal structures of covalent inhibitors of LSD1 have also been published [218]. LSD1 is differentiated from the close homolog LSD2, in part, by the presence of a Tower domain which consists of two α-helices arranged in a typical antiparallel coiled coil. This substructure emerges from the center of the AOL, contains a repeating pattern of seven amino acid residues, and plays a critical role in mediating the interaction with the CoREST complex.

Tool Compound Development

The design and development of LSD1 inhibitors has expanded greatly as research into LSD1 overexpression and role as a potential oncogenic driver in certain cancers has developed. To date, inhibitors can be classified into two different groups, covalent inhibitors modeled after their MAO inhibitor forebears and reversible inhibitors that do not interact directly with FAD upon binding. The benefits and safety of selective, covalent modifiers have been showcased in a number of recent high-profile drug approvals [219]. Irreversible inhibitors commonly lead to enzyme degradation and therefore can lead to a robust time dependent inhibition response at lower concentrations. However, there still remains active interest in developing reversible inhibitors that can differentiate from the irreversible inhibitors in measures of selectivity and safety.

Covalent Inhibitors

Because MAO inhibitors have long been studied for treatment of depression, a host of compounds known to be active against the FAD-dependent enzymes were used as starting points for LSD1 inhibitor programs. Tranylcypromine [220], an early MAO inhibitor that entered the market for depression in 1960 itself, has inhibitory activity against LSD1 (214 μM) although it is 50-fold more potent against MAO-A. Tranylcypromine reacts with FAD via a radical transfer mechanism, leading to an atropaldehyde adduct in MAOs, but due to the nature of the binding pocket of LSD1, the cinnamaldehyde adduct is favored which can further modify FAD to the five-membered intramolecular cycle adduct (Fig. 9) [221, 222].
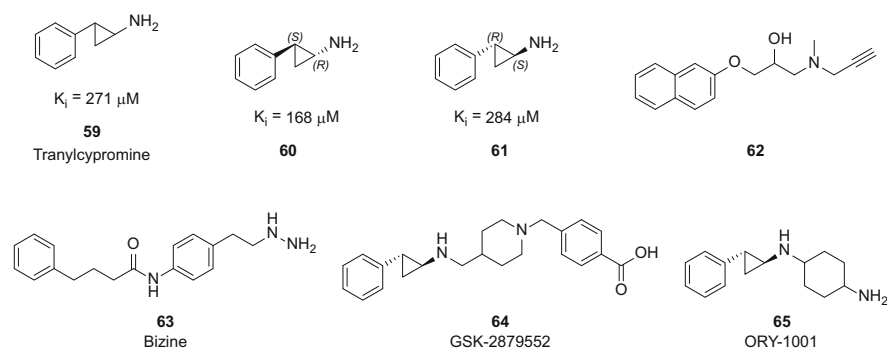
Tranylcypromine-based tool compounds **59–61** are the most commonly reported LSD1 inhibitors in the literature. Early SAR concentrated on the aromatic component of the molecule, and it was found that increased activity correlated with increased lipophilicity on the phenyl ring of the molecule. Additionally, a thorough investigation of the stereochemistry of the cyclopropane showed marked preference for the trans isomer, and furthermore the specific 1S,2R-enantiomer has the strongest
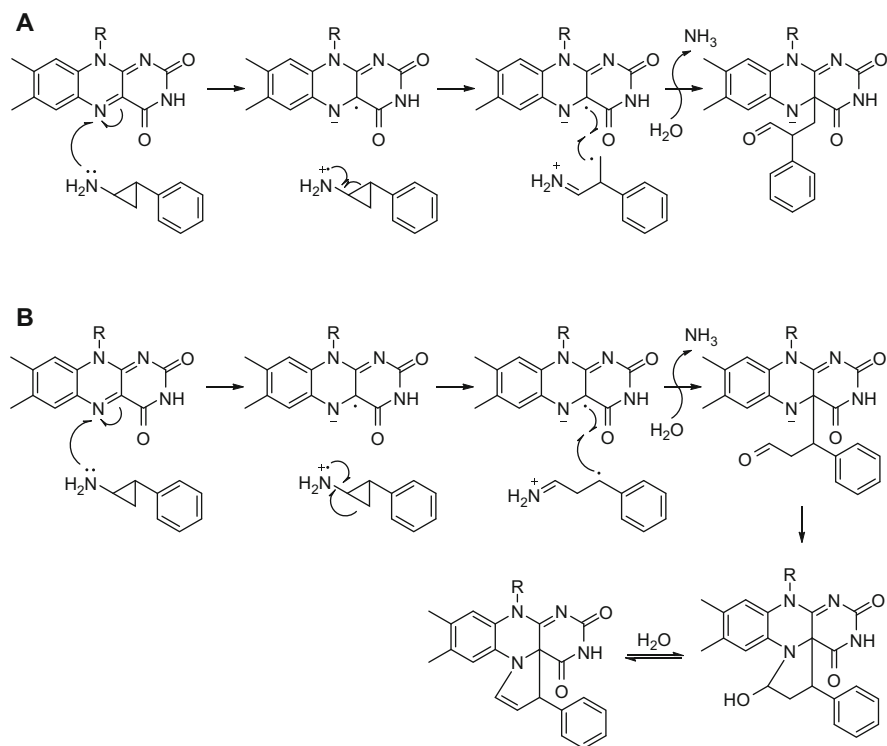
Fig. 9 Proposed FAD modification by tranylcypromine to form (**a**) atropaldehyde [221] or (**b**) cinnamaldehyde [222] adducts

binding potential [221]. Subsequently, a new class of compounds with defined stereochemistry and aliphatic substitution on the amine moiety emerged, leading to highly active and more selective inhibitors available for preclinical proof-of-concept experiments, and have been reviewed [223]. Other MAO inhibitor phenotypes have also been explored as irreversible LSD1 antagonists. For example, Schmitt et al. have reported a pargyline analog, containing a FAD reactive propargyl amine moiety (compound **62**), as a 52 μM inhibitor of LSD1 with modest selectivity over MAO-A and MAO-B [224]. Additionally, the mechanism-based hydrazine-based derivative Bizine (**63**), presented by Prusevich et al., has demonstrated LSD1 activity and selectivity over MAO-A (23-fold), MAO-B (63-fold), and LSD2 (>100-fold) [225].

While irreversible MAO inhibitors have demonstrated clinical efficacy for depression, they are not widely used today because of their potential for off-target activity and adverse effects. Additionally, certain dietary restrictions limit their utility as a lifetime daily dosing regimen. While the newly designed LSD1 inhibitors

based on the tranylcypromine scaffold are far more selective than the early FAD-modifying antidepressants, there exists the possibility of a negative side-effect profile. As a result, an active effort to discover more traditional modes of inhibition, including reversible inhibitors, has been initiated by a number of research groups.

Reversible Inhibitors
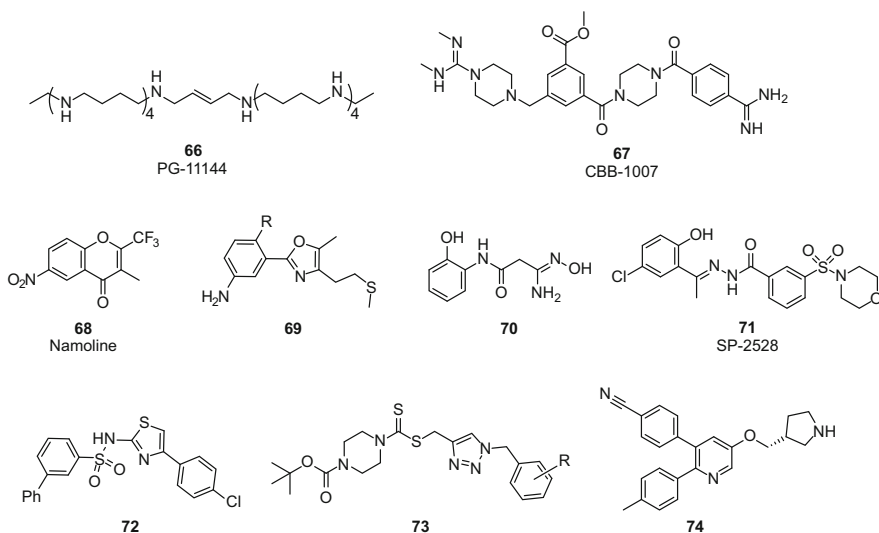
Reversible inhibitors of LSD1 are a much more diverse class of compounds that are currently in various stages of preclinical advancement. An excellent, in-depth review published by Mould et al. highlights some of the strengths and weaknesses of the many proposed reversible inhibitors for LSD1 [226]. Some of the earliest purported LSD1 inhibitors reported were polyamine compounds like Progen's PG-11144 (**66**) which has demonstrated in vitro increases in H3K4me2 in human colorectal cancer cell lines (HCT116) [227]. While related compounds are progressing through the clinic for various tumor types, the cytotoxic effects of this class are difficult to attribute directly to one particular mode of action. **66** was divested from Progen's portfolio in 2010, and no information on any further development of this compound has been reported. Wang et al. report an analogous diguanidyl compound (CBB-1007, **67**) with a rigidified backbone that reached a 2.1 μM IC$_{50}$ with a comparable cellular EC$_{50}$ of 1–5 μM. Although the compound has low potency, unlike the flexible polyamines **67**, it appears to have direct effects on LSD1.

In more recent reports, a host of compounds have been discovered through high-throughput screening efforts and virtual screens but lack the data to correlate

biochemical activity with cellular antiproliferative effect required for validation of their identity as specific LSD1 inhibitors. For example, chromenone derivative Namoline (**68**) has weak LSD1 activity (51 μM) and is generally cytotoxic in vitro at low concentrations [215]. A second series of phenyl oxazoles as represented by compound **69**, based on earlier MAO inhibitors, produced only 10 μM biochemical inhibition; however, the reported IC_{50} curves have high Hill slopes potentially indicative of non-specific inhibition. The amidoxime series presented by Hazeldine et al. (e.g., compound **70**) demonstrated 17 μM biochemical IC_{50} against LSD1 but failed to demonstrate consistent cellular increases in H3K4me2 [228]. Lastly, a set of hydrazide inhibitors were discovered by Sorna et al. through virtual modeling of the FAD pocket [229]. Salarius Pharmaceuticals was created to advance the optimized hydrazide compound SP-2509 (**71**) (13 nM) through IND-enabling studies, but although activity has been reported in a wide number of cancer cell lines, including Ewing's Sarcoma [230], the correlation between biochemical effect and cell activity suggested **71** activity is a non-specific cytotoxic effect. It is possible that the 2-hydroxybenzylidene)hydrazide moiety is a pan-assay interference structure (PAINS) [231] or cleavage of the hydrazide results in the in situ formation of acyl hydrazines, which are known irreversible and non-specific FAD-dependent enzyme inhibitors.

Despite the high number of unsubstantiated claims, there have also emerged a set of compounds with reliable data that warrant further investigation. These include a series of aminothiazoles (**72**) generated by fragment library screening at the Institute of Cancer Research in London [232]. Optimized to a top IC_{50} of 0.4 μM, this series demonstrated consistent SAR and was found to be reversible with enzyme, selective against MAO-A and translated to expected antiproliferative effects in the expected low-micromolar range. Additionally, a series of dithiocarbamates (e.g., compound **73**) was reported by Zheng et al. that show reliable correlation between biochemical and cellular activity but contain a potential cytotoxic chemotype that may limit use of this series as in vivo tool candidates [233]. Lastly, GSK-354 (**74**), reported in 2013, has the combined features of high biochemical potency with a drug-like core that translates to 1.4 μM cellular activity resulting in a FAD noncompetitive reversible compound suitable for in vitro and in vivo testing [234].

Clinical Progress

As was the case with MAO inhibitors, the first LSD1 inhibitors to enter the clinic possess an irreversible mechanism of action. To date there have been three clinical efforts to treat human cancer in a clinical setting (Table 7). The first trial to initiate was in December 2013 with GSK's tranylcypromine prodrug GSK2879552 targeting AML and SCLC solid tumors in two separate phase I trials [235, 236]. This was followed closely by Oryzon who entered the clinic at the

Table 7 Inhibitor of LSD1 in oncology clinical trials

Drug name	Target class/enzyme	Status	Indication
ORY-1001	KDM/KDM1A	Phase I/II	AML
Tranylcypromine	KDM/KDM1A	Phase I/II	AML
GSK2879552	KDM/KDM1A	Phase I	AML

very end of 2013 to treat refractory acute leukemia. Late in September of 2014, as proposed by Schenk et al. in 2012 [211], racemic tranylcypromine itself is being tested in combination with the all trans-retinoic acid (ATRA) drug tretinoin for relapsed/refractory AML in a small group of patients in Germany and the USA in parallel. The two stand-alone treatments will be discussed in detail below.

GSK-2879552 (**64**) is an irreversible inhibitor of LSD1 activity that, as a prodrug, is converted to their earlier reported tool compound, with an LSD1 activity of 5 nM, through metabolic cleavage of the benzyl benzoic acid component. The compound is reported to be selective for LSD1 inhibition, requiring FAD for activation, and tested negative against a panel of FAD utilizing enzymes, such as MAO-B.

64 entered human testing at the end of 2013 in a phase I trial designed to treat patients with relapsed or refractory small cell lung cancer (SCLC). Additionally, patients were requested to avoid citrus fruits, suggesting a CYP3A4 route of clearance that if blocked could lead to higher than expected drug exposures. The primary objective of the escalation phase is to establish recommended phase II dose (RP2D) and understand any dose-limiting toxicity as guided by the Neuenschwander-continuous reassessment method (N-CRM). The planned expansion cohorts are expected to enroll patients with relapsed or refractory SCLC to understand efficacy in a larger patient population.

GSK has also initiated a phase I trial with **64** in patients with acute myeloid leukemia (AML) as of June 2014. Enrollment requirements include classification as relapsed or refractory AML patients with no available standard therapies remaining available for treatment of the disease state. Response rate, maximum tolerated dose, and establishment of a recommended phase II dose were identified as the primary objective outcomes from this study to be evaluated as per the SCLC trial above.

ORY-1001 (**65**) was originally developed by Oryzon Genomics, in Spain, for the treatment of adult patients with relapsed or refractory acute leukemia [237]. In April 2014, the Oryzon Genomics LSD1 program was licensed by Roche pharmaceuticals before the end of phase I. In August 2015, Oryzon received the first milestone from Roche upon finalization of the multiple ascending dose (MAD) stage of its phase I clinical trial to evaluate the safety, tolerability, and pharmacokinetics of ORY-1001. In November of that same year, Oryzon announced initiation of the expansion of the phase I study to additional sites in Spain, the UK, and France.

4.1.2 Additional Tool Compounds

75   **76**   **77**
GSK-J1
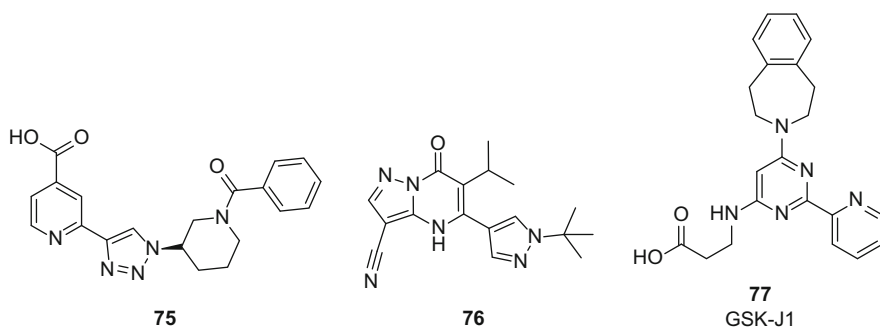
Although small-molecule inhibitors of Jumonji domain-containing (JmjC) lysine demethylase targets have, until recently, largely been the purview of academic researchers, there has been a significant increase in publications and patents emerging from industry in 2015 [238]. This increase in activity parallels growing evidence that supports the hypothesis that aberrant KDM activity is linked to eukaryotic transcription, treatment resistance mechanisms [239], and the development of physiological disease states. In the subsequent subsections, we describe the four families for which selective small-molecule inhibitors have been described in the current literature.

KDM2 Family

KDM2A and KDM2B are Fe-dependent lysine demethylases that act upon H3K36 with a preference for the dimethylated substrate H3K36me2. KDM2A activity has been implicated in maintaining centromeric integrity and genomic stability [240, 241] and regulation of NF-kB [242] and has been shown to be overexpressed in certain lung, ovarian, bladder, and esophageal cancer patient samples. Recently, KDM2A has also been reported as a potential tumor suppressor in breast cancer [243]. Structures of human KDM2A are known with the 2-OG co-factor bound (4QWN, 4QX7), with NOG surrogate co-factor (4QXC, 4QXH), and with a small-molecule inhibitor contributed by the SGC (4URA). This inhibitor was modified using medicinal chemistry approaches into a selective KDM2A inhibitor, **75**, with a >30-fold separation from its nearest measured homolog KDM5C. Unfortunately, compound **75** has poor cellular permeability, however, and in vitro experiments with the methyl ester prodrug are planned to be reported in due course [244].

KDM5 Family

KDM5 lysine demethylases were first reported by Klose et al. in 2007 with the discovery of retinoblastoma-binding protein 2 (RBBP2), later renamed JARID1A and KDM5A, as a demethylase of H3K4me3 and H3Kme2 [245, 246]. KDM5B and KDM5C family members would follow, but KDM5A alone has been identified as a prognostic marker for colorectal [247] and lung cancer [248], implicated in cell fate determination and tumorigenesis [249], drug resistance [250], and AML leukemia [251]. To date crystallographic structures of KDM5 family members remain limited with one linked JmjN and JmjC domain construct of KDM5A crystallized with 2-OG (5E6H) and two small-molecule bound structures of KDM5B with pyridine 2,6-dicarboxylate (5A3W) and a 2-amidomethyl substituted pyridine 4-carboxylate (5A3T). Additional chemotypes have emerged in the patent and literature recently, including potent and cell-active inhibitors from Constellation Pharmaceuticals [252–254]. Compound **76** has shown <100 nanomolar IC_{50} potency and significant selectivity over KDM2B, KDM3B, KDM4C, KDM6A, and KDM7B homologs in biochemical assays. Compound **76** also specifically affected H3K4me3 and H3K4me2 methylation levels in melanoma (M14), breast (SKBR3), and NSCLC (PC9) cells and demonstrated a reduction in the number of drug-tolerant persister cancer cells (DTPs), making it an appealing in vitro tool compound for further exploration of KDM5 family target validation efforts.

KDM6 Family

KDM6A and KDM6B were identified by Hong et al. in 2007 to be specific lysine demethylases for H3K27 preferring trimethylated and dimethylated H3K27 as substrate [255]. Early reports on KDM6 family members suggested a potential role in proliferation and transcriptional changes [256], but KDM6 family members have also been implicated as tumor suppressors [257]. More recently a male-specific homolog KDM6C (UTY) has been reported to be completely inactive in cells [258]. KDM6B structures are known in the apo form (4EZ4), 2-OG bound (2XUE), peptide and NOG-bound (4EZH), and with 2-OG competitive small-molecule inhibitors 8-hydroxyquinolone (2XXZ) and GSK-J1 (**77**) (4ASK).

Compound **77** was one of the first reported small-molecule inhibitors reported by industrial researchers [259]. **77** was reported to exploit the 2-OG-binding site, making a bidentate interaction with the catalytic iron center and was shown to be selective over the KDM4 family homologs. This early tool compound was poorly cell permeable as well, but the ethyl ester was used to demonstrate specific cellular activity of KDM6B on pro-inflammatory gene activation in macrophages. This hypothesis was later challenged by a group at EpiTherapeutics who showed in an expanded battery of cellular assay equal potency for the ethyl ester against KDM4C, KDM5B, and KDM6B suggesting that observed gene effects could not specifically be attributed to KDM6 alone [260].

5 Future of Epigenetic Drug Discovery

The field of epigenetic drug discovery has grown tremendously over the past decade. After the initial HDAC inhibitor approval in 2006, academia and industrial groups have forged countless discoveries in the understanding of the roles of epigenetic mechanisms in oncology. These discoveries effectively initiated the processes which led not only to new drug discovery targets but validated discovery efforts across three entire classes of potential targets focusing on methyl mark addition (writing), elimination (erasing), and acetyl mark recognition (reading). The clinical targets leading the charge in these spaces are arguably the most biologically validated, which undoubtedly promoted them to the top of the list for many groups as they prioritized efforts to identify druggable chemical matter.

With the kinases, novel chemical matter starting points with little or no selectivity across a range of family members eventually morphed into the ability to design selective inhibitors and thus provide extremely powerful tool compounds to further validate biological hypotheses. In contrast, there does not seem to be a promiscuous PMT inhibitor. In fact, many selective chemotypes have been identified for individual targets or highly structurally related members of a particular branch of a phylogenic tree. This feature has brought with it the advantage of rapid evolution of high-quality chemical biology tools to pharmacologically validate targets which appear interesting from siRNA knockdown or genetic knockout studies. As discussed in this chapter, tool compounds effectively cast doubt on the role of a particular epigenetic target in both methyltransferase (SMYD2) and bromodomain (SMARCA2) areas. Going forward, tool compounds will remain a crucial component in enablement of additional epigenetic-focused drug targets, and perhaps newer techniques such as CRISPR can elucidate protein domains to prioritize drug discovery effort [261].

Over the next 10 years, we will see exactly which of the current clinical programs can actually deliver upon the promise of targeted therapies for hard-to-treat cancers such as INI1-negative malignant rhabdoid tumors (EZH2 inhibitors) or NUT midline carcinoma (BRD inhibitors). New epigenetic drugs could also potentially add synergistic benefits to existing standard-of-care oncology treatments and perhaps new transformative immunotherapy regimes as they emerge. Whatever happens, it promises to be an interesting time for medicinal chemists.

References

1. Maurer-Stroh S et al (2003) The tudor domain "Royal Family": tudor, plant agenet, chromo, PWWP and MBT domains. Trends Biochem Sci 28(2):69–74
2. Camerino MA et al (2013) The structure-activity relationships of L3MBTL3 inhibitors: flexibility of the dimer interface. Med Chem Commun 4(11):1501–1507
3. James LI et al (2013) Discovery of a chemical probe for the L3MBTL3 methyl-lysine reader domain. Nat Chem Biol 9(3):184–191

4. James LI et al (2013) Small-molecule ligands of methyl-lysine binding proteins: optimization of selectivity for L3MBTL3. J Med Chem 56(18). https://doi.org/10.1021/jm400919p
5. Biel M et al (2004) Design, synthesis, and biological evaluation of a small-molecule inhibitor of the histone acetyltransferase Gcn5. Angew Chem Int Ed 43(30):3974–3976
6. Bowers EM et al (2010) Virtual ligand screening of the p300/CBP histone acetyltransferase: identification of a selective small molecule inhibitor. Chem Biol 17(5):471–482
7. Chimenti F et al (2009) A novel histone acetyltransferase inhibitor modulating Gcn5 network: cyclopentylidene-[4-(4′-chlorophenyl)thiazol-2-yl)hydrazone. J Med Chem 52 (2):530–536
8. Tsukada Y-I et al (2006) Histone demethylation by a family of JmjC domain-containing proteins. Nature 439(7078):811–816
9. Klose RJ, Kallin EM, Zhang Y (2006) JmjC-domain-containing proteins and histone demethylation. Nat Rev Genet 7(9):715–727
10. Chang B et al (2007) JMJD6 is a histone arginine demethylase. Science 318(5849):444–447
11. Han G et al (2012) The hydroxylation activity of Jmjd6 is required for its homo-oligomerization. J Cell Biochem 113(5):1663–1670
12. Bicker KL, Thompson PR (2013) The protein arginine deiminases (PADs): structure, function, inhibition, and disease. Biopolymers 99(2):155–163
13. Grant S, Easley C, Kirkpatrick P (2007) Vorinostat. Nat Rev Drug Discov 6(1):21–22
14. Bradbury RH (2007) Cancer. Topics in medicinal chemistry1st edn. Springer, Heidelberg, Berlin, p 452. XIV
15. Tamkun JW et al (1992) Brahma: a regulator of Drosophila homeotic genes structurally related to the yeast transcriptional activator SNF2SWI2. Cell 68(3):561–572
16. Filippakopoulos P, Knapp S (2014) Targeting bromodomains: epigenetic readers of lysine acetylation. Nat Rev Drug Discov 13(5):337–356
17. Yang X-J et al (1996) A p300/CBP-associated factor that competes with the adenoviral oncoprotein E1A. Nature 382(6589):319–324
18. Dhalluin C et al (1999) Structure and ligand of a histone acetyltransferase bromodomain. Nature 399(6735):491–496
19. Gregory GD et al (2007) Mammalian ASH1L is a histone methyltransferase that occupies the transcribed region of active genes. Mol Cell Biol 27(24):8466–8479
20. Malik S, Bhaumik SR (2010) Mixed lineage leukemia: histone H3 lysine 4 methyltransferases from yeast to human. FEBS J 277(8):1805–1821
21. Rahman S et al (2011) The Brd4 extraterminal domain confers transcription activation independent of pTEFb by recruiting multiple proteins, including NSD3. Mol Cell Biol 31 (13):2641–2652
22. Trotter KW, Archer TK (2008) The BRG1 transcriptional coregulator. Nucl Recept Signal 6: e004
23. Barbieri I, Cannizzaro E, Dawson MA (2013) Bromodomains as therapeutic targets in cancer. Brief Funct Genomics 12(3):219–230
24. Muller S, Filippakopoulos P, Knapp S (2011) Bromodomains as therapeutic targets. Expert Rev Mol Med 13
25. Delvecchio M et al (2013) Structure of the p300 catalytic core and implications for chromatin targeting and HAT regulation. Nat Struct Mol Biol 20(9):1040–1046
26. Kasper LH et al (1999) CREB binding protein interacts with nucleoporin-specific FG repeats that activate transcription and mediate NUP98-HOXA9 oncogenicity. Mol Cell Biol 19 (1):764–776
27. Deguchi K et al (2003) MOZ-TIF2-induced acute myeloid leukemia requires the MOZ nucleosome binding motif and TIF2-mediated recruitment of CBP. Cancer Cell 3(3):259–271
28. Picaud S et al (2015) Generation of a selective small molecule inhibitor of the CBP/p300 bromodomain for leukemia therapy. Cancer Res 75(23):5106–5119
29. Hay DA et al (2014) Discovery and optimization of small-molecule ligands for the CBP/p300 bromodomains. J Am Chem Soc 136(26):9308–9319

30. Ciró M et al (2009) ATAD2 is a novel cofactor for MYC, overexpressed and amplified in aggressive tumors. Cancer Res 69(21):8491–8498
31. Revenko AS et al (2010) Chromatin loading of E2F-MLL complex by cancer-associated coregulator ANCCA via reading a specific histone mark. Mol Cell Biol 30(22):5260–5272
32. Leachman NT et al (2010) ATAD2B is a phylogenetically conserved nuclear protein expressed during neuronal differentiation and tumorigenesis. Dev Growth Differ 52 (9):747–755
33. Tsai W-W et al (2010) TRIM24 links a noncanonical histone signature to breast cancer. Nature 468(7326):927–932
34. Cui Z et al (2013) TRIM24 overexpression is common in locally advanced head and neck squamous cell carcinoma and correlates with aggressive malignant phenotypes. PLoS One 8 (5):e63887
35. Li H et al (2012) Overexpression of TRIM24 correlates with tumor progression in non-small cell lung cancer. PLoS One 7(5):e37657
36. Liu X et al (2014) Overexpression of TRIM24 is associated with the onset and progress of human hepatocellular carcinoma. PLoS One 9(1):e85462
37. Miao Z-F et al (2015) TRIM24 is upregulated in human gastric cancer and promotes gastric cancer cell growth and chemoresistance. Virchows Arch 466(5):525–532
38. Zhang LH et al (2015) TRIM24 promotes glioma progression and enhances chemoresistance through activation of the PI3K/Akt signaling pathway. Oncogene 34(5):600–610
39. Wang J et al (2014) Knockdown of tripartite motif containing 24 by lentivirus suppresses cell growth and induces apoptosis in human colorectal cancer cells. Oncol Res 22(1):39–45
40. Mujtaba S, Zeng L, Zhou MM (2007) Structure and acetyl-lysine recognition of the bromodomain. Oncogene 26(37):5521–5527
41. Vidler LR et al (2012) Druggability analysis and structural classification of bromodomain acetyl-lysine binding sites. J Med Chem 55(17):7346–7359
42. Wyce A et al (2013) Inhibition of BET bromodomain proteins as a therapeutic approach in prostate cancer. Oncotarget 4(12):2419–2429
43. Fu L-l et al (2015) Inhibition of BET bromodomains as a therapeutic strategy for cancer drug discovery. Oncotarget 6(8):5501–5516
44. Wu S, Chiang C (2007) The double bromodomain-containing chromatin adaptor Brd4 and transcriptional regulation. J Biol Chem 282:13141–13145
45. Vollmuth F, Blankenfeldt W, Geyer M (2009) Structures of the dual bromodomains of the P-TEFb-activating protein Brd4 at atomic resolution. J Biol Chem 284(52):36547–36556
46. Gamsjaeger R et al (2011) Structural basis and specificity of acetylated transcription factor GATA1 recognition by BET family bromodomain protein Brd3. Mol Cell Biol 31 (13):2632–2640
47. Sengupta S et al (2015) Inhibition of BET proteins impairs estrogen-mediated growth and transcription in breast cancers by pausing RNA polymerase advancement. Breast Cancer Res Treat 150(2):265–278
48. Shang E et al (2007) The first bromodomain of Brdt, a testis-specific member of the BET sub-family of double-bromodomain-containing proteins, is essential for male germ cell differentiation. Development 134(19):3507–3515
49. Fromont G et al (2013) 8q24 amplification is associated with Myc expression and prostate cancer progression and is an independent predictor of recurrence after radical prostatectomy. Hum Pathol 44(8):1617–1623
50. French CA (2010) NUT midline carcinoma. Cancer Genet Cytogenet 203(1):16–20
51. Mele DA et al (2013) BET bromodomain inhibition suppresses T(H)17-mediated pathology. J Exp Med 210(11):2181–2190
52. Khan YM et al (2014) Brd4 is essential for IL-1β-induced inflammation in human airway epithelial cells. PLoS One 9(4):e95051
53. Miyoshi S et al (2009) Antitumor agent. Patent WO2009084693

54. Filippakopoulos P et al (2010) Selective inhibition of BET bromodomains. Nature 468 (7327):1067–1073
55. Shao Q et al (2014) BET protein inhibitor JQ1 attenuates Myc-amplified MCC tumor growth in vivo. Cancer Res 74(23):7090–7102
56. Xu C et al (2015) NSCLC driven by DDR2 mutation is sensitive to dasatinib and JQ1 combination therapy. Mol Cancer Ther 14(10):2382–2389
57. Trabucco SE et al (2015) Inhibition of bromodomain proteins for the treatment of human diffuse large B-cell lymphoma. Clin Cancer Res 21(1):113–122
58. Asangani IA et al (2014) Therapeutic targeting of BET bromodomain proteins in castration-resistant prostate cancer. Nature 510(7504):278–282
59. Picaud S et al (2013) PFI-1 – a highly selective protein interaction inhibitor targeting BET bromodomains. Cancer Res 73(11):3336–3346
60. Fish PV et al (2012) Identification of a chemical probe for bromo and extra C-terminal bromodomain inhibition through optimization of a fragment-derived hit. J Med Chem 55 (22):9831–9837
61. Yang D et al (2010) Therapeutic potential of a synthetic lethal interaction between the MYC proto-oncogene and inhibition of aurora-B kinase. Proc Natl Acad Sci U S A 107 (31):13836–13841
62. Dawson MA et al (2011) Inhibition of BET recruitment to chromatin as an effective treatment for MLL-fusion leukaemia. Nature 478(7370):529–533
63. Seal J et al (2012) Identification of a novel series of BET family bromodomain inhibitors: binding mode and profile of I-BET151 (GSK1210151A). Bioorg Med Chem Lett 22 (8):2968–2972
64. Mirguet O et al (2012) From ApoA1 upregulation to BET family bromodomain inhibition: discovery of I-BET151. Bioorg Med Chem Lett 22(8):2963–2967
65. Nicodeme E et al (2010) Suppression of inflammation by a synthetic histone mimic. Nature 468(7327):1119–1123
66. Mirguet O et al (2013) Discovery of epigenetic regulator I-BET762: lead optimization to afford a clinical candidate inhibitor of the BET bromodomains. J Med Chem 56 (19):7501–7515
67. French CA (2012) Pathogenesis of NUT midline carcinoma. Annu Rev Pathol 7(1):247–265
68. A study to investigate the safety, pharmacokinetics, pharmacodynamics, and clinical activity of GSK525762 in subjects with NUT midline carcinoma (NMC) and other cancers. https://clinicaltrials.gov/ct2/show/NCT01587703?term=GSK525762&rank=2
69. A dose escalation study to investigate the safety, pharmacokinetics (PK), pharmacodynamics (PD) and clinical activity of GSK525762 in subjects with relapsed, refractory hematologic malignancies. https://clinicaltrials.gov/ct2/show/NCT01943851?term=GSK525762&rank=1
70. Dose escalation study of GSK2820151 in subjects with advanced or recurrent solid tumors. https://clinicaltrials.gov/ct2/show/NCT02630251
71. Boi M et al (2015) The BET bromodomain inhibitor OTX015 affects pathogenetic pathways in preclinical B-cell tumor models and synergizes with targeted drugs. Clin Cancer Res 21 (7):1628–1638
72. Coudé M-M et al (2015) BET inhibitor OTX015 targets BRD2 and BRD4 and decreases c-MYC in acute leukemia cells. Oncotarget 6(19):17698–17712
73. Gaudio E et al (2015) The BET bromodomain inhibitor OTX015 (MK-8628) in mantle cell lymphoma (MCL): in vivo activity and identification of novel combinations to overcome adaptive resistance. In: Molecular targets and cancer therapeutics. AACR-NCI-EORTC, Boston, MA
74. Henssen AG et al (2016) Targeting MYCN-driven transcription by BET-bromodomain inhibition. Clin Cancer Res 22(10):2470–2481

75. Odore E et al (2015) Phase I population pharmacokinetic assessment of the oral bromodomain inhibitor OTX015 in patients with haematologic malignancies. Clin Pharmacokinet 1–9

76. Sims R (2015) Discovery of CPI-0610: a novel BET protein bromodomain inhibitor for hematologic malignancies in annual meeting of the American Association for Cancer Research. AACR, Philadelphia, PA

77. Abramson JS et al (2015) BET inhibitor CPI-0610 is well tolerated and induces responses in diffuse large B-cell lymphoma and follicular lymphoma: preliminary analysis of an ongoing phase 1 study. In: 57th annual meeting & exposition of the American Hematological Society. ASH, Orlando, FL

78. Theodoulou NH et al (2016) Discovery of I-BRD9, a selective cell active chemical probe for bromodomain containing protein 9 inhibition. J Med Chem 59(4):1425–1439

79. Jones MH et al (2000) A novel family of bromodomain genes. Genomics 63(1):40–45

80. Strohner R et al (2001) NoRC – a novel member of mammalian ISWI-containing chromatin remodeling machines. EMBO J 20(17):4892–4900

81. Arking DE et al (2011) Identification of a sudden cardiac death susceptibility locus at 2q24.2 through genome-wide association in European ancestry individuals. PLoS Genetics 7(6): e1002158

82. Ferguson FM et al (2013) Targeting low-druggability bromodomains: fragment based screening and inhibitor design against the BAZ2B bromodomain. J Med Chem 56(24):10183–10187

83. Drouin L et al (2015) Structure enabled design of BAZ2-ICR, a chemical probe targeting the bromodomains of BAZ2A and BAZ2B. J Med Chem 58(5):2553–2559

84. Chen P et al (2016) Discovery and characterization of GSK2801, a selective chemical probe for the bromodomains BAZ2A and BAZ2B. J Med Chem 59(4):1410–1424

85. Bennett J et al (2016) Discovery of a chemical tool inhibitor targeting the bromodomains of TRIM24 and BRPF. J Med Chem 59(4):1642–1647

86. Palmer WS et al (2016) Structure-guided design of IACS-9571, a selective high-affinity dual TRIM24-BRPF1 bromodomain inhibitor. J Med Chem 59(4):1440–1454

87. Oike T et al (2013) A synthetic lethality-based strategy to treat cancers harboring a genetic deficiency in the chromatin remodeling factor BRG1. Cancer Res 73(17):5508–5518

88. Hoffman GR et al (2014) Functional epigenetics approach identifies BRM/SMARCA2 as a critical synthetic lethal target in BRG1-deficient cancers. Proc Natl Acad Sci U S A 111 (8):3128–3133

89. Wilson BG et al (2014) Residual complexes containing SMARCA2 (BRM) underlie the oncogenic drive of SMARCA4 (BRG1) mutation. Mol Cell Biol 34(6):1136–1144

90. Vangamudi B et al (2015) The SMARCA2/4 ATPase domain surpasses the bromodomain as a drug target in SWI/SNF mutant cancers: insights from cDNA rescue and PFI-3 inhibitor studies. Cancer Res 75(18):3865–3878

91. Cho EC et al (2012) Arginine methylation controls growth regulation by E2F-1. EMBO J 31:1785–1797

92. Chung J et al (2013) Protein arginine methyltransferase 5 (PRMT5) inhibition induces lymphoma cell death through reactivation of the retinoblastoma tumor suppressor pathway and polycomb repressor complex 2 (PRC2) silencing. J Biol Chem 288(49):35534–35547

93. Pal S et al (2007) Low levels of miR-92b/96 induce PRMT5 translation and H3R8/H4R3 methylation in mantle cell lymphoma. 26 3558–3569

94. Pal S et al (2004) Human SWI/SNF-associated PRMT5 methylates histone H3 arginine 8 and negatively regulates expression of ST7 and NM23 tumor suppressor genes. Mol Cell Biol 24 (21):9630–9645

95. Powers MA et al (2011) Protein arginine methyltransferase 5 accelerates tumor growth by arginine methylation of the tumor suppressor programmed cell death 4. Cancer Res 71 (16):5579–5587

96. Wang L, Pal S, Sif S (2008) Protein arginine methyltransferase 5 suppresses the transcription of the RB family of tumor suppressors in leukemia and lymphoma cells. Mol Cell Biol 28 (20):6262–6277

97. Wei T-YW et al (2012) Protein arginine methyltransferase 5 is a potential oncoprotein that upregulates G1 cyclins/cyclin-dependent kinases and the phosphoinositide 3-kinase/AKT signaling cascade. Cancer Sci 103(9):1640–1650

98. Karkhanis V et al (2011) Versatility of PRMT5-induced methylation in growth control and development. Trends Biochem Sci 36(12):633–641

99. Koh CM et al (2015) MYC regulates the core pre-mRNA splicing machinery as an essential step in lymphomagenesis. Nature 523(7558):96–100

100. Antonysamy S et al (2012) Crystal structure of the human PRMT5:MEP50 complex. Proc Natl Acad Sci 109(44):17960–17965

101. Smil D et al (2015) Discovery of a dual PRMT5–PRMT7 inhibitor. ACS Med Chem Lett 6 (4):408–412

102. Alinari L et al (2015) Selective inhibition of protein arginine methyltransferase 5 blocks initiation and maintenance of B-cell transformation. Blood 125(16):2530–2543

103. Chan-Penebre E et al (2015) A selective inhibitor of PRMT5 with in vivo and in vitro potency in MCL models. Nat Chem Biol 11(6):432–437

104. Duncan KW et al (2015) Structure and property guided design in the identification of PRMT5 tool compound EPZ015666. ACS Med Chem Lett 7(2):162–166

105. Dose escalation study of GSK3326595 in subjects with solid tumors and non-Hodgkin's lymphoma. https://clinicaltrials.gov/ct2/show/NCT02783300?term=NCT02783300&rank=1

106. El-Andaloussi N et al (2006) Arginine methylation regulates DNA polymerase beta. Mol Cell 22(1):51

107. Kleinschmidt MA et al (2012) Cell cycle regulation by the PRMT6 arginine methyltransferase through repression of cyclin-dependent kinase inhibitors. PLoS One 7(8): e41446

108. Yoshimatsu M et al (2011) Dysregulation of PRMT1 and PRMT6, type I arginine methyltransferases, is involved in various types of human cancers. Int J Cancer 128(3):562

109. Vieira FQ et al (2014) Deregulated expression of selected histone methylases and demethylases in prostate carcinoma. Endocr Relat Cancer 21(1):51

110. Limm K et al (2013) Deregulation of protein methylation in melanoma. Eur J Cancer 49 (6):1305

111. Mitchell LH et al (2015) Aryl pyrazoles as potent inhibitors of arginine methyltransferases: identification of the first PRMT6 tool compound. ACS Med Chem Lett 6(6):655–659

112. Kaniskan HÜ et al (2015) A potent, selective and cell-active allosteric inhibitor of protein arginine methyltransferase 3 (PRMT3). Angew Chem Int Edit 54(17):5166–5170

113. Liu F et al (2013) Exploiting an allosteric binding site of PRMT3 yields potent and selective inhibitors. J Med Chem 56(5):2110–2124

114. Feng Q et al (2002) Methylation of H3-lysine 79 is mediated by a new family of HMTases without a SET domain. Curr Biol 12(12):1052–1058

115. Lacoste N et al (2002) Disruptor of telomeric silencing-1 is a chromatin-specific histone H3 methyltransferase. J Biol Chem 277(34):30421–30424

116. Ng HH et al (2002) Lysine methylation within the globular domain of histone H3 by Dot1 is important for telomeric silencing and Sir protein association. Genes Dev 16(12):1518–1527

117. van Leeuwen F, Gafken PR, Gottschling DE (2002) Dot1p modulates silencing in yeast by methylation of the nucleosome core. Cell 109(6):745–756

118. Min J et al (2003) Structure of the catalytic domain of human DOT1L, a non-SET domain nucleosomal histone methyltransferase. Cell 112(5):711–723

119. Frederiks F et al (2008) Nonprocessive methylation by Dot1 leads to functional redundancy of histone H3K79 methylation states. Nat Struct Mol Biol 15(6):550–557

120. Nguyen AT, Zhang Y (2011) The diverse functions of Dot1 and H3K79 methylation. Genes Dev 25(13):1345–1358
121. Hess JL (2004) MLL: a histone methyltransferase disrupted in leukemia. Trends Mol Med 10 (10):500–507
122. Krivtsov AV, Armstrong SA (2007) MLL translocations, histone modifications and leukaemia stem-cell development. Nat Rev Cancer 7(11):823–833
123. Milne TA et al (2002) MLL targets SET domain methyltransferase activity to Hox gene promoters. Mol Cell 10(5):1107–1117
124. Nakamura T et al (2002) ALL-1 is a histone methyltransferase that assembles a supercomplex of proteins involved in transcriptional regulation. Mol Cell 10(5):1119–1128
125. Guenther MG et al (2008) Aberrant chromatin at genes encoding stem cell regulators in human mixed-lineage leukemia. Genes Dev 22(24):3403–3408
126. Krivtsov AV et al (2008) H3K79 methylation profiles define murine and human MLL-AF4 leukemias. Cancer Cell 14(5):355–368
127. Richon VM et al (2011) Chemogenetic analysis of human protein methyltransferases. Chem Biol Drug Des 78(2):199–210
128. Daigle SR et al (2011) Selective killing of mixed lineage leukemia cells by a potent small-molecule DOT1L inhibitor. Cancer Cell 20(1):53–65
129. Basavapathruni A et al (2012) Conformational adaptation drives potent, selective and durable inhibition of the human protein methyltransferase DOT1L. Chem Biol Drug Des 80 (6):971–980
130. Armstrong SA et al (2003) Inhibition of FLT3 in MLL: validation of a therapeutic target identified by gene expression based classification. Cancer Cell 3(2):173–183
131. Chesworth R et al (2011) 7-Deazapurine modulators of histone methyltransferase, and methods of use thereof in. Patent WO2012075500
132. Yao Y et al (2011) Selective inhibitors of histone methyltransferase DOT1L: design, synthesis and crystallographic studies. J Am Chem Soc 133(42):16746–16749
133. Song Y et al (2014) Selective inhibitors of histone methyltransferase dot1l. Patent US20140100184
134. Lee JM, Choi M (2014) Compounds and compositions for modulating histone methyltransferase activity. Patent WO2014035140
135. Daigle SR et al (2013) Potent inhibition of DOT1L as treatment of MLL-fusion leukemia. Blood 122(6):1017–1025
136. Epizyme I. A phase 1 dose escalation and expanded cohort study of EPZ-5676 in the treatment of pediatric patients with relapsed/refractory leukemias bearing a rearrangement of the MLL gene. https://clinicaltrials.gov/ct2/show/NCT02141828?term=5676&rank=1
137. Waters NJ et al (2015) Metabolism and disposition of the DOT1L inhibitor, pinometostat (EPZ-5676), in rat, dog and human. Cancer Chemother Pharmacol 77(1):43–62
138. Stein EM et al (2015) A phase 1 study of the DOT1L inhibitor, pinometostat (EPZ-5676), in adults with relapsed or refractory leukemia: safety, clinical activity, exposure and target inhibition, in 57th annual meeting & exposition. American Association of Hematologists, Orlando, FL
139. Raimondi A et al (2015) Abstract B82: pinometostat (EPZ-5676) enhances the antiproliferative activity of MAP kinase pathway inhibitors in MLL-rearranged leukemia cell lines. Mol Cancer Therapeut 14(12 Suppl 2):B82
140. Finley A, Copeland RA (2014) Small molecule control of chromatin remodeling. Chem Biol 21(9):1196–1210
141. Morin RD et al (2010) Somatic mutation of EZH2 (Y641) in follicular and diffuse large B-cell lymphomas of germinal center origin. Nat Genet 42(2):181–185
142. Wilson BG et al (2010) Epigenetic antagonism between polycomb and SWI/SNF complexes during oncogenic transformation. Cancer Cell 18(4):316–328
143. Gibson WT et al (2012) Mutations in EZH2 cause weaver syndrome. Am J Hum Genet 90 (1):110–118

144. LaFave LM et al (2015) Loss of BAP1 function leads to EZH2-dependent transformation. Nat Med 21(11):1344–1349

145. Ntziachristos P et al (2012) Genetic inactivation of the PRC2 complex in T-cell acute lymphoblastic leukemia. Nat Med 18(2):298–301

146. Simon C et al (2012) A key role for EZH2 and associated genes in mouse and human adult T-cell acute leukemia. Genes Dev 26(7):651–656

147. Shih AH et al (2012) The role of mutations in epigenetic regulators in myeloid malignancies. Nat Rev Cancer 12(9):599–612

148. Brown R et al (2014) Poised epigenetic states and acquired drug resistance in cancer. Nat Rev Cancer 14(11):747–753

149. Kim E et al (2013) Phosphorylation of EZH2 activates STAT3 signaling via STAT3 methylation and promotes tumorigenicity of glioblastoma stem-like cells. Cancer Cell 23 (6):839–852

150. de Vries NA et al (2015) Prolonged Ezh2 depletion in glioblastoma causes a robust switch in cell fate resulting in tumor progression. Cell Rep 10(3):383–397

151. Basso K, Dalla-Favera R (2015) Germinal centres and B cell lymphomagenesis. Nat Rev Immunol 15(3):172–184

152. Johnston D et al (2015) EZH2 plays a critical role in B cell maturation and in non-Hodgkin's lymphoma: interplay between EZH2 function and B-cell activation. In: 57th annual meeting and exposition. American Society of Hematologists, Orlando, FL

153. Swalm BM et al (2014) Reaction coupling between wild-type and disease-associated mutant EZH2. ACS Chem Biol 9(11):2459–2464

154. Shain AH et al (2012) Convergent structural alterations define SWItch/sucrose nonfermentable (SWI/SNF) chromatin remodeler as a central tumor suppressive complex in pancreatic cancer. Proc Natl Acad Sci U S A 109(5):E252–E259

155. Shain AH, Pollack JR (2013) The spectrum of SWI/SNF mutations, ubiquitous in human cancers. PLoS One 8(1):e55119

156. Knutson SK et al (2013) Durable tumor regression in genetically altered malignant rhabdoid tumors by inhibition of methyltransferase EZH2. Proc Natl Acad Sci U S A 110 (19):7922–7927

157. Errico A (2014) Genetics: SMARCA4 mutated in SCCOHT. Nat Rev Clin Oncol 11 (6):302–302

158. Knutson SK et al (2014) Synergistic anti-tumor activity of EZH2 inhibitors and glucocorticoid receptor agonists in models of germinal center non-Hodgkin lymphomas. PLoS One 9 (12):e111840

159. Cao R et al (2002) Role of histone H3 lysine 27 methylation in polycomb-group silencing. Science 298(5595):1039–1043

160. Jiao L, Liu X (2015) Structural basis of histone H3K27 trimethylation by an active polycomb repressive complex 2. Science 350(6258)

161. Knutson SK et al (2012) A selective inhibitor of EZH2 blocks H3K27 methylation and kills mutant lymphoma cells. Nat Chem Biol 8(11):890–896

162. McCabe MT et al (2012) EZH2 inhibition as a therapeutic strategy for lymphoma with EZH2-activating mutations. Nature 492(7427):108–112

163. Verma SK et al (2012) Identification of potent, selective, cell-active inhibitors of the histone lysine methyltransferase EZH2. ACS Med Chem Lett 3(12):1091–1096

164. Qi W et al (2012) Selective inhibition of Ezh2 by a small molecule inhibitor blocks tumor cells proliferation. Proc Natl Acad Sci U S A 109(52):21360–21365

165. Konze KD et al (2013) An orally bioavailable chemical probe of the lysine methyltransferases EZH2 and EZH1. ACS Chem Biol 8(6):1324–1334

166. Kuntz KW et al (2016) The importance of being me: magic methyls, methyltransferase inhibitors, and the discovery of tazemetostat. J Med Chem 59(4):1556–1564

167. Campbell JE et al (2015) EPZ011989, a potent, orally-available EZH2 inhibitor with robust in vivo activity. ACS Med Chem Lett 6(5):491–495

168. Nasveschuk CG et al (2014) Discovery and optimization of tetramethylpiperidinyl benzamides as inhibitors of EZH2. ACS Med Chem Lett 5(4):378–383
169. Kung P-P et al (2015) SAH derived potent and selective EZH2 inhibitors. Bioorg Med Chem Lett 25(7):1532–1537
170. Bradley WD et al (2014) EZH2 inhibitor efficacy in non-Hodgkin's lymphoma does not require suppression of H3K27 monomethylation. Chem Biol 21(11):1463–1475
171. Vaswani RG et al (2016) Identification of (R)-N-((4-methoxy-6-methyl-2-oxo-1,2-dihydropyridin-3-yl)methyl)-2-methyl-1-(1-(1-(2,2,2-trifluoroethyl)piperidin-4-yl)ethyl)-1H-indole-3-carboxamide (CPI-1205), a potent and selective inhibitor of histone methyltransferase EZH2, suitable for phase I clinical trials for B-cell lymphomas. J Med Chem 59(21):9928–9941
172. A study evaluating CPI-1205 in patients with B-cell lymphomas. https://clinicaltrials.gov/ct2/show/NCT02395601
173. Baker T et al (2015) Acquisition of a single EZH2 D1 domain mutation confers acquired resistance to EZH2-targeted inhibitors. Oncotarget 6(32)
174. Kim W et al (2013) Targeted disruption of the EZH2/EED complex inhibits EZH2-dependent cancer. Nat Chem Biol 9(10):643–650
175. Shankar SR et al (2013) G9a, a multipotent regulator of gene expression. Epigenetics 8 (1):16–22
176. Chang Y et al (2010) Adding a lysine mimic in the design of potent inhibitors of histone lysine methyltransferases. J Mol Biol 400(1):1–7
177. Vedadi M et al (2011) A chemical probe selectively inhibits G9a and GLP methyltransferase activity in cells. Nat Chem Biol 7(8):566–574
178. Sweis RF et al (2014) Discovery and development of potent and selective inhibitors of histone methyltransferase G9a. ACS Med Chem Lett 5(2):205–209
179. Pappano WN et al (2015) The histone methyltransferase inhibitor A-366 uncovers a role for G9a/GLP in the epigenetics of leukemia. PLoS One 10(7):e0131716
180. Liu S et al (2015) G9a is essential for EMT-mediated metastasis and maintenance of cancer stem cell-like characters in head and neck squamous cell carcinoma. Oncotarget 6 (9):6887–6901
181. Zhong X et al (2015) Overexpression of G9a and MCM7 in oesophageal squamous cell carcinoma is associated with poor prognosis. Histopathology 66(2):192–200
182. Tao H et al (2014) Histone methyltransferase G9a and H3K9 dimethylation inhibit the self-renewal of glioma cancer stem cells. Mol Cell Biochem 394(1):23–30
183. Chaturvedi C-P et al (2009) Dual role for the methyltransferase G9a in the maintenance of β-globin gene transcription in adult erythroid cells. Proc Natl Acad Sci U S A 106 (43):18303–18308
184. Renneville A et al (2015) EHMT1 and EHMT2 inhibition induces fetal hemoglobin expression. Blood 126(16):1930–1939
185. Krivega I et al (2015) Inhibition of G9a methyltransferase stimulates fetal hemoglobin production by facilitating LCR/γ-globin looping. Blood 126(5):665–672
186. Zhang X et al (2013) Regulation of estrogen receptor α by histone methyltransferase SMYD2-mediated protein methylation. Proc Natl Acad Sci U S A 110(43):17284–17289
187. Piao L et al (2014) The histone methyltransferase SMYD2 methylates PARP1 and promotes poly(ADP-ribosyl)ation activity in cancer cells. Neoplasia 16(3):257–264.e2
188. Brown MA et al (2006) Identification and characterization of Smyd2: a split SET/MYND domain-containing histone H3 lysine 36-specific methyltransferase that interacts with the Sin3 histone deacetylase complex. Mol Cancer 5:26–26
189. Huang J et al (2006) Repression of p53 activity by Smyd2-mediated methylation. Nature 444 (7119):629–632
190. Komatsu S et al (2009) Overexpression of SMYD2 relates to tumor cell proliferation and malignant outcome of esophageal squamous cell carcinoma. Carcinogenesis 30(7):1139–1146

191. Komatsu S et al (2015) Overexpression of SMYD2 contributes to malignant outcome in gastric cancer. Br J Cancer 112(2):357–364
192. Sakamoto LHT et al (2014) SMYD2 is highly expressed in pediatric acute lymphoblastic leukemia and constitutes a bad prognostic factor. Leuk Res 38(4):496–502
193. Ferguson AD et al (2011) Structural basis of substrate methylation and inhibition of SMYD2. Structure 19(9):1262–1273
194. Sweis RF et al (2015) Discovery of A-893, a new cell-active benzoxazinone inhibitor of lysine methyltransferase SMYD2. ACS Med Chem Lett 6(6):695–700
195. Nguyen H et al (2015) LLY-507, a cell-active, potent, and selective inhibitor of protein-lysine methyltransferase SMYD2. J Biol Chem 290(22):13641–13653
196. Stresemann C et al (2015) Abstract 2829: discovery and in vitro and in vivo characterization of aminopyrazoline-based SMYD2 inhibitors. Cancer Res 75(Suppl 15):2829
197. Hamamoto R et al (2006) Enhanced SMYD3 expression is essential for the growth of breast cancer cells. Cancer Sci 97(2):113–118
198. Vieira FQ et al (2015) SMYD3 contributes to a more aggressive phenotype of prostate cancer and targets Cyclin D2 through H4K20me3. Oncotarget 6(15):13644–13657
199. Mazur PK et al (2014) SMYD3 links lysine methylation of MAP3K2 to Ras-driven cancer. Nature 510(7504):283–287
200. Liu Y et al (2015) Overexpression of SMYD3 and matrix metalloproteinase-9 are associated with poor prognosis of patients with gastric cancer. Tumor Biol 36(6):4377–4386
201. Peserico A et al (2015) A SMYD3 small-molecule inhibitor impairing cancer cell growth. J Cell Physiol 230(10):2447–2460
202. Keating ST et al (2014) Deep sequencing reveals novel Set7 networks. Cell Mol Life Sci 71 (22):4471–4486
203. Barsyte-Lovejoy D et al (2014) (R)-PFI-2 is a potent and selective inhibitor of SETD7 methyltransferase activity in cells. Proc Natl Acad Sci U S A 111(35):12853–12858
204. He S et al (2015) Lysine methyltransferase SETD7 (SET7/9) regulates ROS signaling through mitochondria and NFE2L2/ARE pathway. Sci Rep 5:14368
205. Bannister AJ, Schneider R, Kouzarides T (2002) Histone methylation: dynamic or static? Cell 109(7):801–806
206. Cloos PAC et al (2008) Erasing the methyl mark: histone demethylases at the center of cellular differentiation and disease. Genes Dev 22(9):1115–1140
207. Culhane JC, Cole PA (2007) LSD1 and the chemistry of histone demethylation. Curr Opin Chem Biol 11(5):561–568
208. Mohammad HP et al (2015) A DNA hypomethylation signature predicts antitumor activity of LSD1 inhibitors in SCLC. Cancer Cell 28(1):57–69
209. Wang Y et al (2009) LSD1 is a subunit of the NuRD complex and targets the metastasis programs in breast cancer. Cell 138(4):660–672
210. Kahl P et al (2006) Androgen receptor coactivators lysine-specific histone demethylase 1 and four and a half LIM domain protein 2 predict risk of prostate cancer recurrence. Cancer Res 66(23):11341–11347
211. Schenk T et al (2012) Inhibition of the LSD1 (KDM1A) demethylase reactivates the all-trans-retinoic acid differentiation pathway in acute myeloid leukemia. Nat Med 18(4):605–611
212. Harris WJ et al (2012) The histone demethylase KDM1A sustains the oncogenic potential of MLL-AF9 leukemia stem cells. Cancer Cell 21(4):473–487
213. Wada T et al (2015) Overexpression of the shortest isoform of histone demethylase LSD1 primes hematopoietic stem cells for malignant transformation. Blood 125(24):3731–3746
214. Lee MG et al (2005) An essential role for CoREST in nucleosomal histone 3 lysine 4 demethylation. Nature 437(7057):432–435
215. Metzger E et al (2005) LSD1 demethylates repressive histone marks to promote androgen-receptor-dependent transcription. Nature 437(7057):436–439

216. Biswas D et al (2011) Function of leukemogenic mixed lineage leukemia 1 (MLL) fusion proteins through distinct partner protein complexes. Proc Natl Acad Sci U S A 108 (38):15751–15756
217. Chen Y et al (2006) Crystal structure of human histone lysine-specific demethylase 1 (LSD1). Proc Natl Acad Sci U S A 103(38):13956–13961
218. Mimasu S et al (2008) Crystal structure of histone demethylase LSD1 and tranylcypromine at 2.25 Å. Biochem Biophys Res Commun 366(1):15–22
219. Singh J et al (2011) The resurgence of covalent drugs. Nat Rev Drug Discov 10(4):307–317
220. Fiedorowicz JG, Swartz KL (2004) The role of monoamine oxidase inhibitors in current psychiatric practice. J Psychiatr Pract 10(4):239–248
221. Schmidt DMZ, McCafferty DG (2007) Trans-2-phenylcyclopropylamine is a mechanism-based inactivator of the histone demethylase LSD1. Biochemistry 46(14):4408–4416
222. Yang M et al (2007) Structural basis for the inhibition of the LSD1 histone demethylase by the antidepressant trans-2-phenylcyclopropylamine. Biochemistry 46(27):8058–8065
223. Yi CZ et al (2016) Irreversible LSD1 inhibitors: application of tranylcypromine and its derivatives in cancer treatment. Curr Top Med Chem 16:1–1
224. Schmitt ML et al (2013) Non-peptidic propargylamines as inhibitors of lysine specific demethylase 1 (LSD1) with cellular activity. J Med Chem 56(18):7334–7342
225. Prusevich P et al (2014) A selective phenelzine analogue inhibitor of histone demethylase LSD1. ACS Chem Biol 9(6):1284–1293
226. Mould DP et al (2015) Reversible inhibitors of LSD1 as therapeutic agents in acute myeloid leukemia: clinical significance and progress to date. Med Res Rev 35(3):586–618
227. Huang Y et al (2009) Novel oligoamine analogues inhibit lysine-specific demethylase 1 (LSD1) and induce re-expression of epigenetically silenced genes. Clin Cancer Res 15 (23):7217–7228
228. Hazeldine S et al (2012) Low molecular weight amidoximes that act as potent inhibitors of lysine-specific demethylase 1. J Med Chem 55(17):7378–7391
229. Sorna V et al (2013) High-throughput virtual screening identifies novel N′-(1-phenylethylidene)-benzohydrazides as potent, specific, and reversible LSD1 inhibitors. J Med Chem 56(23):9496–9508
230. Sankar S et al (2014) Reversible LSD1 inhibition interferes with global EWS/ETS transcriptional activity and impedes Ewing sarcoma tumor growth. Clin Cancer Res 20 (17):4584–4597
231. Baell JB, Holloway GA (2010) New substructure filters for removal of pan assay interference compounds (PAINS) from screening libraries and for their exclusion in bioassays. J Med Chem 53(7):2719–2740
232. Hitchin JR et al (2013) Development and evaluation of selective, reversible LSD1 inhibitors derived from fragments. Med Chem Commun 4(11):1513–1522
233. Zheng Y-C et al (2013) Triazole-dithiocarbamate based, selective LSD1 inactivators inhibit gastric cancer cell growth, invasion and migration. J Med Chem 56(21). https://doi.org/10.1021/jm401002r
234. Dhanak D (2013) Proceedings of the 104th annual meeting of the American Association for Cancer Research
235. Investigation of GSK2879552 in subjects with relapsed/refractory small cell lung carcinoma. https://clinicaltrials.gov/ct2/show/NCT02034123?term=GSK2879552&rank=1
236. A phase I dose escalation study of GSK2879552 in subjects with acute myeloid leukemia (AML). https://clinicaltrials.gov/ct2/show/NCT02177812?term=GSK2879552&rank=2
237. A phase I study of human pharmacokinetics and safety of ORY-1001, and LSD1 inhibitor, in relapsed or refractory acute leukaemia (AL). https://www.clinicaltrialsregister.eu/ctr-search/trial/2013-002447-29/ES
238. McAllister TE et al (2015) Recent progress in histone demethylase inhibitors. J Med Chem
239. Hoffmann I et al (2012) The role of histone demethylases in cancer therapy. Mol Oncol 6 (6):683–703

240. Cheng Z et al (2014) A molecular threading mechanism underlies Jumonji lysine demethylase KDM2A regulation of methylated H3K36. Genes Dev 28(16):1758–1771
241. Frescas D et al (2008) KDM2A represses transcription of centromeric satellite repeats and maintains the heterochromatic state. Cell Cycle 7(22):3539–3547
242. Lu T et al (2009) Validation-based insertional mutagenesis identifies lysine demethylase FBXL11 as a negative regulator of NFκB. Proc Natl Acad Sci U S A 106(38):16339–16344
243. Rizwani W et al (2014) Mammalian lysine histone demethylase KDM2A regulates E2F1-mediated gene transcription in breast cancer cells. PLoS One 9(7):e100888
244. England KS et al (2014) Optimisation of a triazolopyridine based histone demethylase inhibitor yields a potent and selective KDM2A (FBXL11) inhibitor. Med Chem Commun 5 (12):1879–1886
245. Klose RJ et al (2007) The retinoblastoma binding protein RBP2 is an H3K4 demethylase. Cell 128(5):889–900
246. Christensen J et al (2007) RBP2 belongs to a family of demethylases, specific for tri- and dimethylated lysine 4 on histone 3. Cell 128(6):1063–1076
247. Uemura M et al (2010) Jumonji domain containing 1A is a novel prognostic marker for colorectal cancer: in vivo identification from hypoxic tumor cells. Clin Cancer Res 16 (18):4636–4646
248. Teng Y-C et al (2013) Histone demethylase RBP2 promotes lung tumorigenesis and cancer metastasis. Cancer Res 73(15):4711–4721
249. Lin W et al (2011) Loss of the retinoblastoma binding protein 2 (RBP2) histone demethylase suppresses tumorigenesis in mice lacking Rb1 or Men1. Proc Natl Acad Sci U S A 108 (33):13379–13386
250. Hou J et al (2012) Genomic amplification and a role in drug-resistance for the KDM5A histone demethylase in breast cancer. Am J Transl Res 4(3):247–256
251. de Rooij JDE et al (2013) NUP98/JARID1A is a novel recurrent abnormality in pediatric acute megakaryoblastic leukemia with a distinct HOX gene expression pattern. Leukemia 27 (12):2280–2288
252. Albrecht BK et al (2015) Therapeutic compounds and uses thereof. Patent WO2015135094
253. Vinogradova M et al (2016) An inhibitor of KDM5 demethylases reduces survival of drug-tolerant cancer cells. Nat Chem Biol 12(7):531–538
254. Gehling VS et al (2016) Identification of potent, selective KDM5 inhibitors. Bioorg Med Chem Lett 26(17):4350–4354
255. Hong S et al (2007) Identification of JmjC domain-containing UTX and JMJD3 as histone H3 lysine 27 demethylases. Proc Natl Acad Sci 104(47):18439–18444
256. van Haaften G et al (2009) Somatic mutations of the histone H3K27 demethylase, UTX, in human cancer. Nat Genet 41(5):521–523
257. Lederer D et al (2012) Deletion of KDM6A, a histone demethylase interacting with MLL2, in three patients with kabuki syndrome. Am J Hum Genet 90(1):119–124
258. Walport LJ et al (2014) Human UTY(KDM6C) is a male-specific N(ε)-methyl lysyl demethylase. J Biol Chem 289(26):18302–18313
259. Kruidenier L et al (2012) A selective jumonji H3K27 demethylase inhibitor modulates the proinflammatory macrophage response. Nature 488(7411):404–408
260. Heinemann B et al (2014) Inhibition of demethylases by GSK-J1/J4. Nature 514(7520):E1–E2
261. Shi J et al (2015) Discovery of cancer drug targets by CRISPR-Cas9 screening of protein domains. Nat Biotechnol 33(6):661–667

Antibody–Drug Conjugates

Dorin Toader

Abstract Antibody-drug conjugates (ADCs) are a therapeutic modality that enables the targeted delivery of highly potent cytotoxic payloads to tumors. This chapter describes the components of the ADCs and discusses the medicinal chemistry principles that guide the design of this class of therapeutics. A description of main classes of drugs and the linkers used to attach to monoclonal antibodies with an emphasis on the design, historical development, and linking strategies is presented. Clinical use of the approved ADCs for the treatment of cancer is briefly described.

Keywords ADCs, Cancer, Cytotoxic payloads, Design, Linker, Medicinal chemistry, Monoclonal antibodies

Contents

D. Toader (✉)
Mersana Therapeutics Inc., Cambridge, MA, USA
e-mail: DToader@mersana.com

1   Introduction

Antibody–drug conjugates (ADCs) can be described as a sum of components that are subject to several processes that lead to the desired outcome of selective delivery of a drug to an entity targeted by the specificity of the antibody. While the concept upon which ADCs are built appears deceptively simple, the elements involved in putting this concept into practice and the interdependencies between these components underscore the complexity of this family of drugs. The components of an ADC are monoclonal antibody, a set of linking sites targeted with bioorthogonal conjugation chemistry, a tether that bridges the linking site to the "prodrug," the drug releasing moiety (sometimes called a "trigger") that acts as both a tether and a means for selective release of the active "drug" to the desired tissue compartment and the drug. A set of processes are required for achieving efficacy with an ADC: plasma stability is a desired characteristic for ADCs as all ADCs known to date are administered IV, binding to the antigen situated on the surface of the cell is followed by internalization of the ADC-antigen complex that carries the ADC through the endosomal-lysosomal pathway leading to protein degradation by the action of hydrolases and release of the active drug followed by cytoplasmic and nuclear delivery of the active drug that interacts with the intracellular target. In case of anti-cancer drugs the cell dies and releases the drug into the tumor environment and, depending on the cell membrane permeability of the drug, can affect neighboring cells that do not express the antigen at the levels needed for a pharmacological effect, a process called "bystander effect." The aim of this account is to describe the design principles of the components of ADCs and capture how those design principles translate into therapeutic outcomes. So far most of the applications of this therapeutic modality have been in Oncology where a highly cytotoxic drug is delivered to tumor cells. In an oncology setting minimizing the innate toxicity of the drug to healthy tissues becomes a critical design criterion.

2   Components of the ADCs

2.1   *The Monoclonal Antibody*

Antibodies, also called immunoglobulins or Ig, are ~150 kDa proteins that are produced by the immune system in response to the presence of foreign proteins

called antigens. In human blood, IgG is the major type of antibody present. The use of antibodies as therapeutics was made possible by the work of Köhler and Millstein [1] who described methods to produce murine hybridomas that led to development of monoclonal antibody (mAb) technology. It took over 20 years to develop cancer targeting monoclonal antibodies with clinical applications. These cancer therapeutics bind to tumor antigens, protein expressed on the surface of the cancer cells, to induce tumor cell death [2]. The efficiency of cancer cell killing by immunotherapies can be enhanced by attachment of cytotoxic drugs to antibodies [3]. As opposed to chemotherapy where the cytotoxic drugs are administered systemically, the concept of ADCs introduced the possibility of targeted cytotoxic killing by virtue of mAb binding to antigens selectively expressed on cancer cells. mAbs are proteins with a defined chemical structure represented by a sequence of amino acids. The chemical structure of antibodies is determinant for the function of these molecules. The key function of the antibody is to preferentially bind to antigens on target cells. These Y-shaped molecules (Fig. 1) present a C2 symmetry with two identical arms held together by disulfide bonds and non-covalent interactions. Each
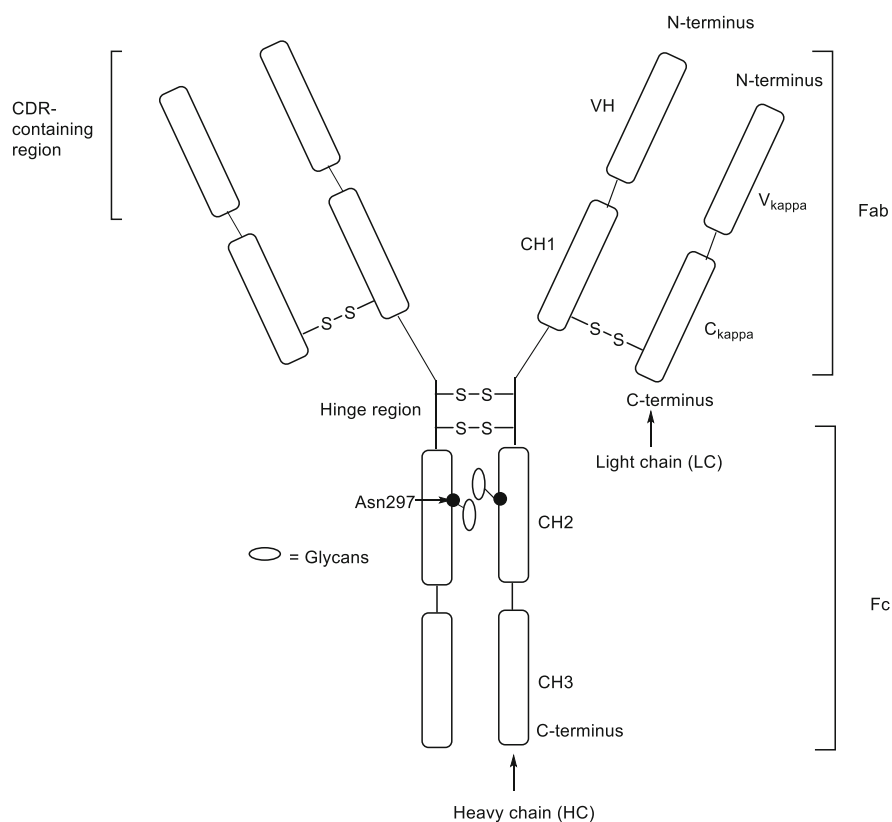
Fig. 1 Components of immunoglobulin G antibody (IgG$_1$ is shown for illustrative purposes)

half is made of a large subunit (~50 kDa) called heavy chain (HC) and a smaller subunit (~23 kDa) called light chain (LC). The assembly of two subunits of HCs and entire two LCs forms two variable units are called Fabs (fragments of antigen binding) while the constant unit made of HC is called Fc (fragment crystallizable). In terms of primary protein structure each chain contains a large constant region (C) and a variable (V) region. Within the heavy chain (also named gamma chain) there are 3 constant regions CH1, CH2, and CH3 encompassing positions ~120–446 at the C-terminus and one variable region at the N-terminus of about 120 amino acid residues. The light chain also named (kappa chain) consists of 214 amino acid sequence of which the N-terminus 108 amino acids are variable and the remaining amino acid sequence is constant. Within the variable regions, there are complementarity-determining regions (CDR) that are essential for antigen binding. The tertiary structure of these regions derived from the unique sequence of amino acids leads to large diversity of structure and accounts for the antibody specificity. CH2 region of the IgG contains an amino acid Asp 297 that is the anchor for N-glycans that contain a defined sequence of monosaccharides with various degrees of heterogeneity. The Fc is responsible for the effector function of the mAb by interacting with receptors present on cells of the immune system. The carbohydrate chains are important for Fc receptor recognition. The Fab and the Fc regions are connected by a sequence of amino acids, called the hinge, that allow for ample movement of the distinct regions that is essential for the function of the mAb. The number of amino acids of the hinge region varies between different subclasses of mAbs with the most commonly used IgG1 subclass having 15 amino acids while IgG4 subclass has just two amino acids. IgG1 is most commonly used as a therapeutic agent and it has a total of 32 cysteine residues forming disulfide bridges within the macromolecule. Twenty-four of these form intrachain disulfide bonds. They are in general considered to be less solvent accessible and hence less reactive than the eight cysteines that form interchain disulfides, including two that are located at the hinge region of the antibody. A crystal structure of an IgG was reported at high resolution (PDB: 1hzh) [4].

Early clinical experience with mAbs used murine monoclonal antibodies. It was quickly recognized that murine molecules led to development of immune responses (were immunogenic) that resulted in rapid clearance of the drug and impaired efficacy. The continuous improvements in antibody engineering technologies led to gradual elimination of murine elements in therapeutic mAbs as follows: chimeric format where variable regions of both HC and LC were murine, humanized format that used mouse CDR regions and finally, the currently preferred format for ADCs, fully human antibodies. The half-lives of human mAbs are up to 3 weeks, significantly longer than the murine mAb that could only be detected in the blood for a few days.

2.2 Biorthogonal Conjugation Chemistry

Two factors have shaped the process of attachment a drug to an antibody and those were the requirement that conjugation be performed under aqueous conditions within a narrow range of pH and the constraints imposed by the reactivity of the natural amino acid residues. The amino group in lysine residues and the thiol group in cysteines are functional groups that were widely used for conjugation to a drug by reaction with electrophiles.

A human antibody contains 80–90 lysine residues of which a small number will react selectively without causing changes to the stability of or antigen binding ability of the antibody. Acylation of lysine residue leads to a stable amide bond. The reaction is performed with heterobifunctional N-hydroxysuccinimide-activated ester (NHS esters). Most common reagents for antibody lysine functionalization are N-succinimidyl-4-(2-pyridyldithio)butanoate (SPDB), N-succinimidyl-4-(2-pyridyldithio)pentanoate (SPP), N-succinimidyl 4-methyl-4-(2-pyridyldithio) pentanoate (SMPP), and succinimidyl-4-(N-maleimidomethyl)cyclohexane-1-car-boxylate (SMCC) (Fig. 2). The resulting labelled antibody displays disulfide or maleimide groups, which can react with thiols. While lysine conjugation is a chemically straightforward process, controlling the number and location of modi-fied lysine residue remains a great challenge. The extent of modification of solvent accessible lysine residue will be dependent on the molar equivalents of added heterobifunctional reagent and various other parameters of the conjugation proto-col. The product of this process will have a stochastic distribution of reactive residues ranging between 0–10 modified residues with most conjugates having an average number of 3.5–4 molecules per antibody.

Cysteine conjugation to an antibody requires partial reduction of native interchain disulfides by a mild reducing agent such as 1,4-Dithiothreitol (DTT) or tris(2-carboxyethyl)phosphine (TCEP) followed by modification of the sulfhydryl group by nucleophilic addition to a Michael acceptor or nucleophilic displacement with the thiolate group as a nucleophile. Conjugation to maleimide leads to a stochastic distribution of several species with 0, 2, 4, 6 and 8 functionalized residues with the species bearing 2 and 4 conjugated molecules being predominant.
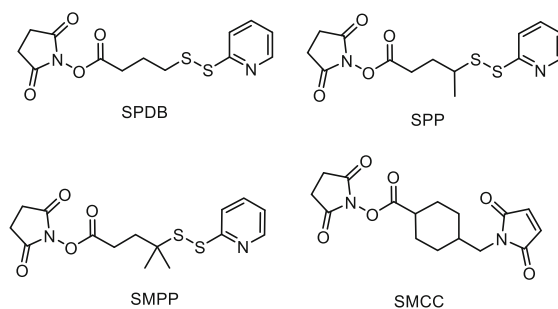
Fig. 2 Reagents used for functionalization of mAbs
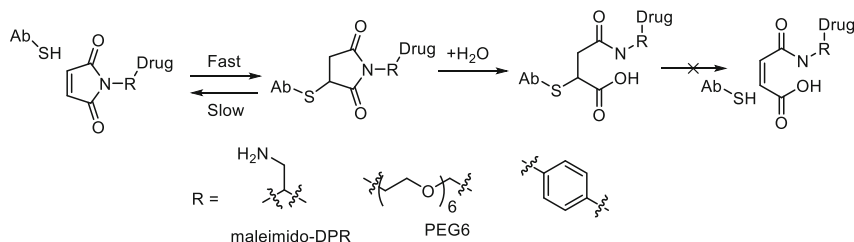
Fig. 3 The chemistry of maleimide-cysteine conjugation

The most common reagent for cysteine conjugation is maleimide and the resulting thiosuccinimide product (Fig. 3) was shown to undergo retro-Michael addition reactions in the presence of thiols [5]. Loss of drug due to retro-Michael deconjugation was recognized as a potential safety liability and several groups have provided evidence that rapid hydrolysis of the resulting thiosuccinimide leads to lower propensity to loss of drug by deconjugation [6].Several approaches were shown to achieve hydrolysis of the succinimide: the use of a proximal basic amine was shown to improve stability of the cysteine conjugates by promoting hydrolysis of the succinimide "maleimido-DPR" [7], promoting hydrolysis by introduction of N-PEG tethers and higher pH [8] or use of phenylmaleimides that have a propensity for hydrolysis once conjugated [9]. Reduced interchain disulfides were targeted with bisalkylating reagents that replace the disulfide bridge with a propylidene-disulfide by an addition-elimination-second addition reaction sequence [10]. This approach allows for generation of ADCs with 1–4 drugs per antibody that are stable in presence of thiol-bearing plasma proteins [11]. A similar approach used dibromomaleimide [12] or dibromopyridazinedione [13] to cross-link the reduced disulfide bonds based on a concept introduced by Smith [14]. This approach presents the potential drawback of incorrectly re-bridged IgG1 mAb where the hinge cysteines form an intra-heavy-chain cross-linked product as opposed to inter-heavy-chain cross-linked product. This drawback was addressed by using a reagent that contains a TCEP-like structural moiety and a re-bridging moiety within the same molecule that allows for reduction and functional re-bridging. Reagent **1** was shown to lead to homogenous ADCs with no observable scrambling of the di-sulfide staple (Fig. 4) [15].

In addition to lysine and cysteine one additional native amino acid – glutamine – was used for conjugation. Conjugation to glutamine uses the enzymatic recognition of a specific amino-acid sequence that contains the amino acid in the primary structure of the antibody. This approach leads to conjugates at a specified site of the antibody thus allowing for modulation of properties of the resulting conjugate. Glutamine conjugation to antibodies utilizes a bacterial transglutaminase (TG) isolated from *Streptoverticillium mobaraense* [16]. Unlike common transgluta-minases that can catalyze the formation of amide bonds between the primary amine of a lysine and the amide group of any glutamine, the bacterial TG can catalyze the formation of an amine bond between any primary amine and the amide
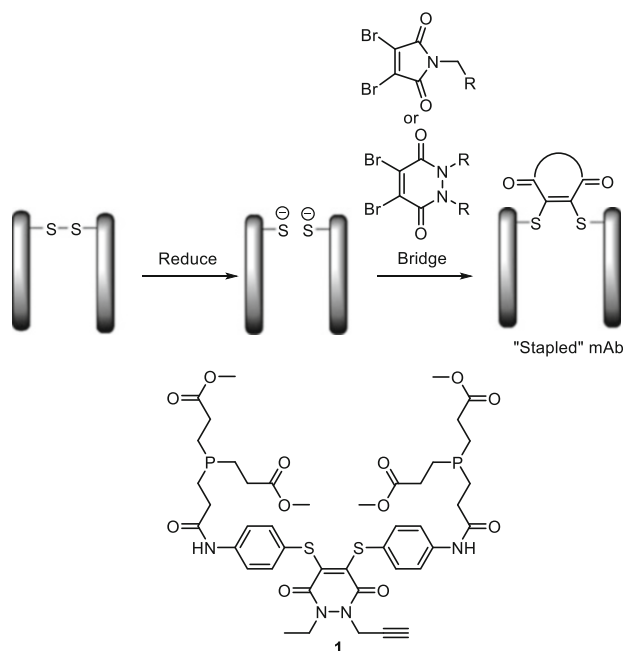
Fig. 4 Rebridging reagent that contains disulfide bridge reducing moiety

group of sequence specific glutamines [17]. A positional scan of antibody constant domains was performed by engineering a glutamine tag (LLQG) into surface accessible regions of an IgG$_1$ antibody and several sites were identified that showed good biophysical properties and a high degree of conjugation [18].

A chemoenzymatic bioconjugation approach to cysteine conjugation used formyl glycine generating enzyme (FGE). FGE recognizes a pentapeptide consensus sequence, CxPxR, and it specifically oxidizes the cysteine in this sequence to an unusual aldehyde-bearing formyl glycine (fGly) [19]. This "tagged" construct is produced recombinantly in cells that coexpress the FGE, which co-translationally converts the cysteine within the tag into an fGly residue, generating an antibody expressed with two aldehyde tags per molecule. The aldehyde functional group serves as a chemical handle for bioorthogonal conjugation. A hydrazino-iso-Pictet-Spengler (HIPS) ligation was used to connect the payload to fGly, resulting in the formation of a stable, covalent C–C bond between the cytotoxin payload and the antibody [20]. This approach was used to generate ADCs that showed the desired activity [21]. Conjugation chemistry with faster kinetics that uses formyl glycine was described recently. The new technology is described as trapped-Knoevenagel ligation using a thiopyrazolone nucleophile (Fig. 5) [22]. One drawback of the formyl glycine approach is the observed formation of the aldehyde hydrate species that can impact the efficiency of conjugation under suboptimal conditions [19].
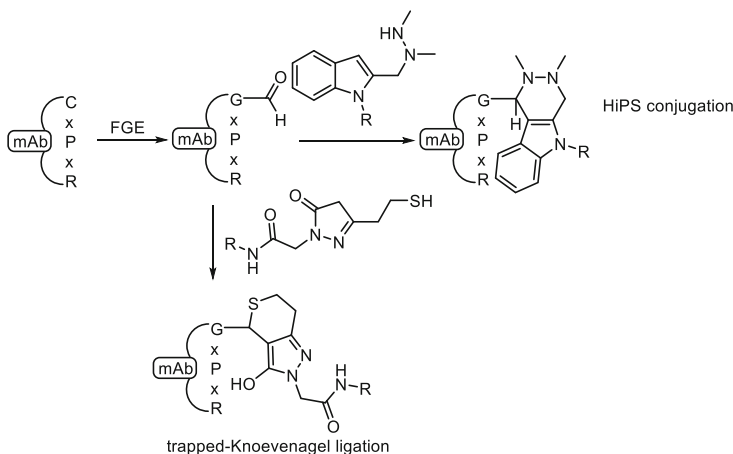
Fig. 5 HIPS conjugation and Trapped-Knoevenagel ligation

Glycoengineering was used for generation of site specific conjugates by either metabolic engineering or post-translational remodeling of native glycan located at Asn-297 conserved position in the Fc domain of the antibody. The objective of glycoengineering is modification of the glycan in a manner that a functional group becomes available for biorthogonal conjugation. Metabolic engineering was achieved by substituting the fucose residue with a functionalized fucose residue that had a reactive handle for conjugation. A thiofucose residue was incorporated in the mAb during expression in CHO cells in medium that contained the modified fucose. The resulting antibody was used to generate conjugates where maleimide-bearing payloads were conjugated at the thiofucose site. The efficiency of the process did not exceed 70% thus limiting the utility of this particular conjugation technique [23]. Early efforts around post translational remodeling of native glycans have used a chemical oxidation step of the carbohydrate [24] or enzymatic introduction of sialic acid [25] to generate aldehyde functional group for oxime ligation. Engineering the active site of glycosyltransferases has provided tools for introducing chemically modified sugar substrates [26]. Native IgGs were converted to a homogenous G0f glycoform population by using β-1,4-galactosidase from *Streptococcus pneumoniae*. The resulting antibody was modified with a synthetic galactose bearing a chemical handle at the C2 position by using mutant β4Gal-T1-Y289L [27]. A keto- or an azido-group can be introduced in a site specific manner to generate an antibody with four functional groups. Further refinement of this technique was presented recently where an endoglycosidase was used to trim the antibody glycan to the fucosylated Acetylglucosamine (GlcNAc). Transfer of N-azidoacetylgalactosamine (GalNaz) in presence of β4Gal-T1-Y289L led to efficient installation of two azide groups onto the antibody [28].

Recent advances in development of methodologies for the genetic incorporation of unnatural amino acids into proteins [29] opened the possibility of site-selective modification of antibodies [30]. The side chains of unnatural amino acids provide

novel functional groups for biorthogonal chemistry thus enabling generation of stable conjugates. The two main functional groups introduced using genetic incorporation of non-natural amino acids are the keto- and azido- that showed utility for conjugation by oxime ligation and the Huisgen alkyne-azide cycloaddition ("click") reaction, respectively. The incorporation of p-acetylphenylalanine into trastuzumab generated an antibody with ~2 acetyl groups that were used for conjugation with alkoxyamine to generate the oxime at pH 4.5 with >95% efficiency [31]. N^6-((2-azidoethoxy)carbonyl)-L-lysine was efficiently incorporated into trastuzumab and generated antibodies with ~2 azide groups that were efficiently conjugated by both strain promoted alkyl azide cycloaddition (SPAAC) and Cu(I) alkyl azide cycloaddition (CuAAC) to generate homogenous ADCs [32].

2.3   The Linking Sites

Conjugation to antibodies is governed by two parameters: the position of the amino acid in the protein sequence that carries the conjugated moiety and the number of amino acid residues that are functionalized during the conjugation process known as the drug-to-antibody ratio (DAR). Both these parameters impact the in vivo behavior of ADCs. Stochastic conjugation to Lys or native cysteines generates a heterogeneous mixture of molecular species where the sites of conjugation are random and the drug-to-antibody ratio is defined as an average [33, 34]. Each of the molecular species of such a mixture would display a distinct behavior in vivo as a consequence of different pharmacokinetics [35]. Discovery of solvent exposed engineered Cys IgGs was driven by the need to introduce a thiol-labelling site that did not adversely affect the structure or function of the antibody [36]. Following expression in mammalian cells mutant cysteines were capped with either a Cys or glutathione. Efforts to find an uncapping reagent that did not affect the native disulfide bonds were partially successful when alkylation with iodoacetate of a serine to cysteine mutant at the position 442 in the Fc domain was attempted [37]. These early discoveries set the stage for the development of antibodies containing engineered reactive cysteine residues at specific sites in antibodies that allow for drugs to be conjugated with defined stoichiometry without disruption of interchain disulfide bonds (termed THIOMABS) [38, 39]. These ADCs were produced by global reduction of blocked cysteine residues and interchain disulfides, subsequent oxidation in the presence of $CuSO_4$ or dehydroascorbic acid to regenerate the interchain disulfide bonds, and then conjugation of the reactive cysteine thiol to maleimide reagents. This method generated site specifically modified ADCs with a homogenous distribution consisting of 92.1% species with two drugs/antibody. Importantly, the THIOMAB conjugate displayed a larger therapeutic index, as it was tolerated at much higher doses in animals and displayed better in vivo activity. The higher therapeutic index correlated with a higher in vivo stability of the THIOMAB when compared to equivalent stochastic ADCs. The authors hypothesized that engineered cysteines may be in relatively "protected" sites that

resist proteolytic attack in circulation and they observed that the accessibility of a cysteine residue varies depending on the position of the mutated amino acid in the antibody protein sequence [39]. In a subsequent study the THIOMAB team explored whether the conjugation site could modulate the stability of a cysteine-maleimide adducts. The Genentech team prepared three THIOMABs of trastuzumab in which the mutant cysteine residues were positioned at sites that differed by their local structural environment. One site was chosen based on high solvent accessibility, while the other two were relatively buried sites but one was located in a positively charged environment while the other was in a relatively neutral environment. The in vitro potency of the three ADCs was comparable for all sites but the serum stability showed significant differences in the stability of the ADCs: the solvent-accessible conjugate underwent rapid thiol exchange with serum albumin, the conjugate at the positively charged site showed succinimide hydrolysis, resulting in improved stability, and the conjugate at the neutral site exhibited intermediate behavior between the other two ADCs. Serum stability results correlated well with in vivo efficacy, pharmacokinetic properties, and toxicity. That study demonstrated for the first time that the structural and chemical dynamics of the conjugation site can be exploited to design optimal protein conjugates for therapeutic applications [6]. A team at Seattle Genetics that were exploring conjugation of a highly hydrophobic drug pyrrolobenzodiazepine (PBD, see below) was faced with the challenge of finding a solution to the issues associated with stochastic conjugation of the maleimide-bearing PBD that led to formation of high percentage of aggregate. Scanning various conjugation sites with solvent accessible Cys mutants led to the discovery of position S239C on the HC where they conjugated the hydrophobic payload with only 1.6% aggregate. Thus they concluded that the recombinant construct provided superior ADCs compared to hinge disulfide conjugates in terms of ADC uniformity and aggregation levels [40].

2.4   The Drug

The choice of effective cytotoxic drugs for ADCs is governed by the relatively small number of antigen molecules on the cancer cell surface to which the antigen can bind ($\sim 10^4$–10^6 receptors/cell) and by the efficiency of the internalization of cell-surface bound antigen–antibody complex and intracellular processing to release the active drug. Provided the intracellular delivery and release are efficient, the number of cytotoxic drug delivered to the individual cell by the ADC needs to be well above the number of cytotoxic agent molecules required to kill a cell. Thus cytotoxic drugs with potency in the pM range are needed. The early ADCs used drugs that were cancer chemotherapeutics as is the case with vinblastine analogs or doxorubicin. Following conjugation to an antibody both these drugs showed diminished potency as ADCs. This observation was attributed to the different modes of cellular uptake of the conjugated vs. non-conjugated drug. For cell membrane permeable drugs, the free diffusion can lead to high concentration of the drug

inside the cell dependent on the dose of the administered drug. In addition to normal tissue target-mediated uptake that can be minimized by judicious choice of tumor-specific target, non-specific uptake by pinocytosis and plasma degradation of the ADC in circulation means that only ~1% of the administered ADC reaches the desired tumor tissue [41]. From a medicinal chemistry perspective, the hydrophobicity of the drug and its impact upon aqueous solubility could present a significant challenge. Also medicinal chemists need to develop structure activity relationships that reveal sites on the cytotoxic drug that tolerate a linker and possess the required reactivity for attachment to an antibody as well as enable the release of the drug inside the cancer cell. All cytotoxic drugs that have been reported as ADC therapeutics are derived from naturally occurring molecules and have very large molecular surfaces that appear to be a common feature for all highly potent cytotoxic molecules. Consequently, the structural complexity of the cytotoxic drugs for ADCs presents a major challenge for development of such molecules. The intracellular targets of cytotoxic drugs are quite limited and two main mechanisms have been targeted successfully with ADCs, i.e. tubulin and DNA.

2.4.1 Antimitotic Drugs

Disruption of microtubule dynamics impairs the ability of mitotic spindles to assemble and alter the architecture of the cytoskeleton, causing cell death [42]. Due to their mechanism of action, antimitotic agents are particularly cytotoxic to cancer cells that divide faster than non-cancerous cells. However, normal tissues that contain rapidly dividing cells such as cells lining the digestive tract, hair follicles, and bone marrow can also be killed, causing undesired toxicity.

Maytansines

Maytansine **2** (Fig. 6) is a benzoansamacrolide that was first isolated from the bark of the Ethiopian shrub *Maytenus ovatus* [43]. Maytansine binds to tubulin and causes disruption of microtubule dynamics resulting in cell death by apoptosis. While being widely cytotoxic, maytansine was shown to be particularly highly toxic against breast cancer cell lines, i.e. SK-BR3 and MCF-7 with an IC_{50} in the 30–40 pM range [44]. Structure–activity relationship studies on maytansine showed that several pharmacophores were required to maintain in vitro cytotoxicity. The carbinolamide at C9 and the ester side chain at C3 were required for biological activity, but the structure of this side chain could be varied without loss of potency (Fig. 5) [45]. Since the C3 position was amenable to modification, it was chosen for the incorporation of new ester side chains bearing a functional group to enable linkage to antibodies. Maytansine can be synthesized from ansamitocins that are obtained as a mixture of esters by fermentation of the microorganism *Actinosynnema pretiosum*. Ester hydrolysis in ansamitocins was shown to be challenging due to propensity for elimination of the C3 ester under basic conditions
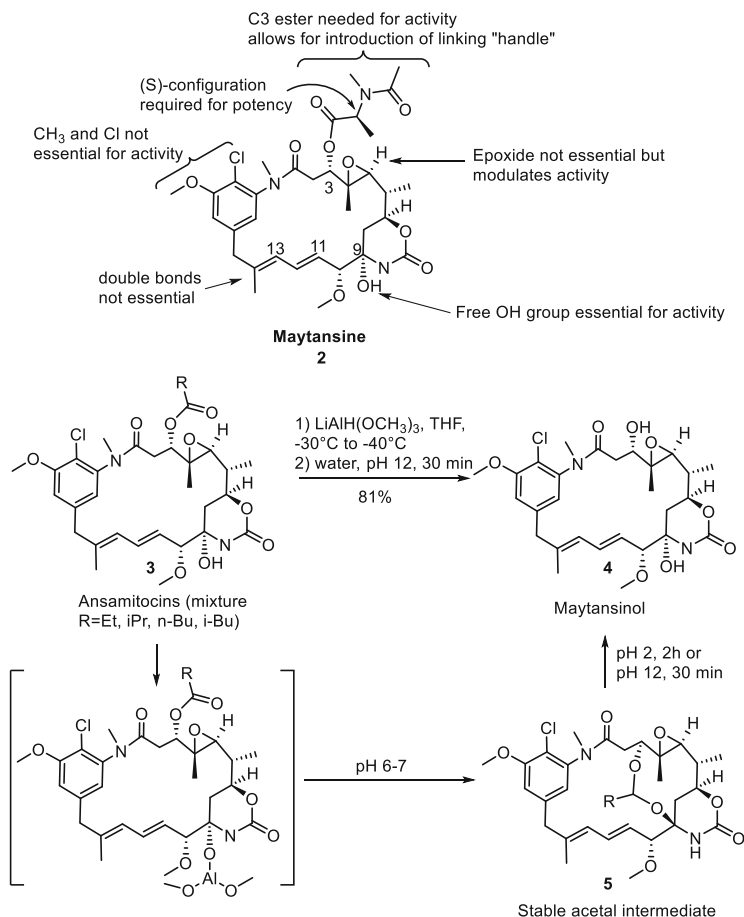
Fig. 6 Maytansinoids SAR and semisynthetic approach to Maytansinol

[46]. The ester group in the ansamitocins **3** (Fig. 6) was efficiently cleaved using the mild reducing agent lithium trimethoxyaluminum hydride, under controlled temperature (−30 to −40°C), to give maytansinol **4** in good yields [44]. A stable acetal intermediate **5** that can be stored was synthesized when the pH was adjusted to neutral following the reaction. The stable intermediate generated the desired maytansinol under specific conditions (Fig. 6). With maytansinol in hand, a thiol-based linking was pursued for linking to mAbs functionalized with thiol-reactive groups (SPBD, SPP or SMPP) resulting in disulfide linkages or thiosuccinimide (maleimide). The disulfide linkage in the ADC was hypothesized to be stable in circulation due to low concentration of thiol-bearing species in the blood while still able to release the drug in the reducing environment of the cytoplasm (where concentration of glutathione is 1–10 mM). A series of drug-maytansinoids DM1, DM3, and DM4 that were capped with a thiomethyl were made by coupling a series of disulfide-bearing acids (Fig. 7) to maytansinol in presence of a coupling agent
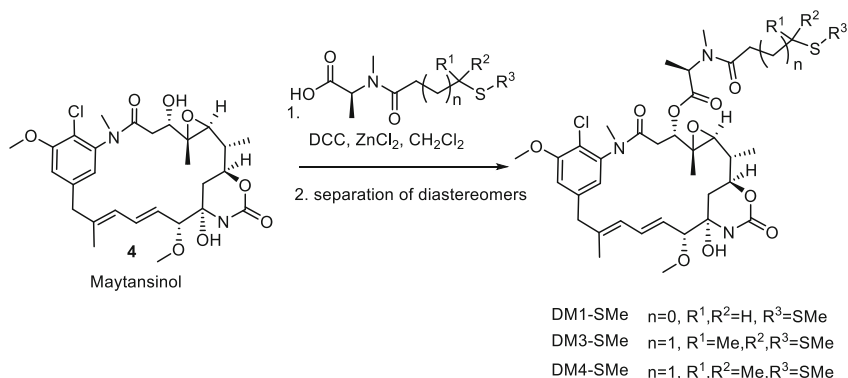
Fig. 7 Synthesis of maytansinoid DM family of drugs

(DCC, EDC, etc.) and a Lewis acid (ZnCl$_2$). All resulting maytansinoid disulfides showed cytotoxicity as least as potent as maytansine [44]. These compounds were reduced with a mild agent, as is the case with dithiothreitol (DTT) prior to conjugation to functionalized mAbs.

Auristatins

Following 15 years of work isolating and characterizing a series of cytotoxic peptides extracted from the sea hare *Dolabella auricularia*, Pettit discovered Dolastatin 10 (Fig. 8) that was at the time the most potent cytotoxic molecule ever known [47] with a potency of 50–300 pM against most cancer cell lines tested. The discovery and characterization of the molecule was an extraordinary achievement as it required extensive fractionation and purification followed by characterization by mass spectrometry and NMR. The definitive structure of Dolastatin 10 was established following the publication of the absolute configuration and the total synthesis of the molecule [48]. Dolastatin 10 and its derivatives have been shown to inhibit tubulin-dependent GTP binding, cause noncompetitive inhibition of vincristine binding to tubulin, and inhibit microtubule dynamics resulting in cell cycle arrest and apoptosis [49] that was confirmed by an X-ray crystal structure of a synthetic analog – soblidotin – bound to tubulin [50]. Following the discovery of Dolastatin 10, a significant effort was dedicated to making analogs in a quest for compounds with chemotherapeutic utility. The analogs of Dolastatin 10 were named "auristatins" and Pettit described Auristatin Phe and Auristatin E (Fig. 8) both with slightly attenuated cytotoxicity (200–400 pM) by replacing the C-terminal Dolaphenine with a Phe methyl ester and norephedrine moiety, respectively [51]. While several of the auristatin analogs were tested in the clinic, none of them progressed due to unacceptable side effects at doses that did not achieve efficacy. An important discovery was made that the N-terminal end of the molecule tolerates a secondary amine resulting in monomethyl auristatin D (MMAD)
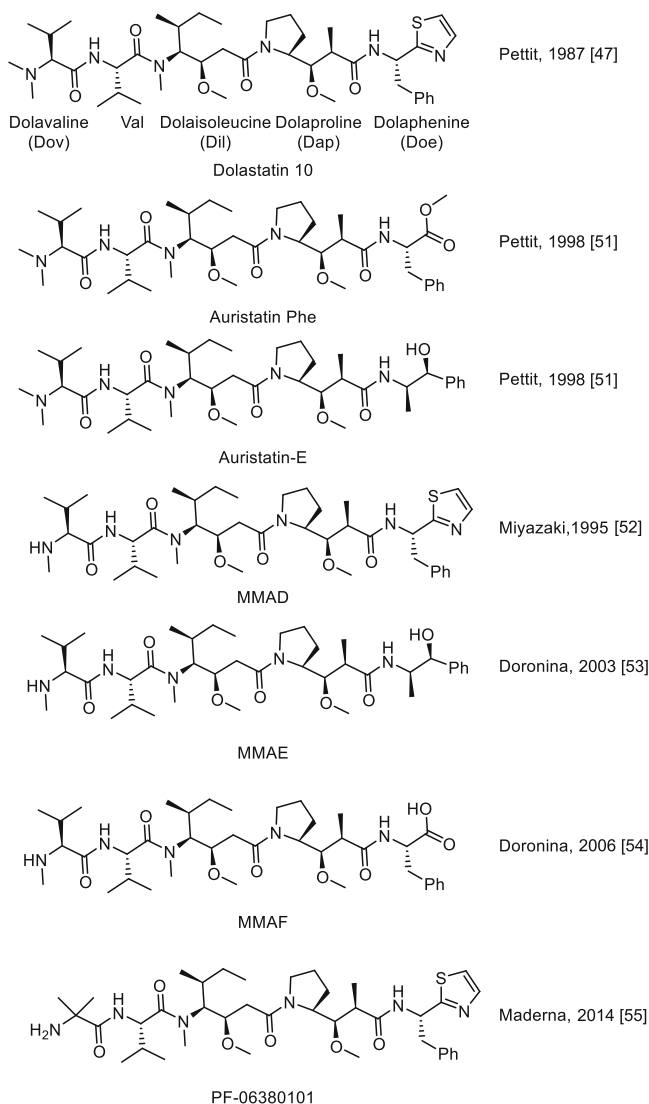
Fig. 8 Development of synthetic drugs derived from natural product Dolastatin 10

(Fig. 8), which opened the door to attaching a linker to these molecules [52]. The significance of this discovery was recognized in 2003 when scientists at Seattle Genetics developed monomethyl auristatin E (MMAE) (Fig. 8) as a hybrid of Pettit's Auristatin E and MMAD [53]. This allowed, for the first time, the linking of an auristatin to a monoclonal antibody. The Seattle Genetics team later developed monomethyl auristatin F (MMAF) (Fig. 8). MMAF showed weak cytotoxic activity and was initially overlooked as a potential drug for ADCs. Working on the

hypothesis that the lack of activity was due to poor cell membrane permeability (that was supported by the observation that an Auristatin Phe analog of MMAF showed activity) they envisaged that delivering MMAF intracellularly could overcome this drawback. This work led to discovery of the first auristatin non-cleavable payload mcMMAF [54]. Recently a team at Pfizer used crystallography data for auristatin analogs bound at the α,β-tubulin interface to design analogs where the dolavaline in Dolastatin 10 was replaced with a variety of amino acids. This work led to the discovery of PF-06380101 (Fig. 8) that is being progressed into the clinic as a drug for ADCs [55]. Research targeting new auristatins for ADCs is very active and is expected to continue in the future [56].

Tubulysins

Tubulysins were isolated from myxobacteria and were described as a family of tetrapeptides that displayed antimitotic activity in a series of cancer cell lines including multidrug resistant cell lines [57]. Tubulysin D was reported to display 10–500 times higher cytotoxicity than paclitaxel and vinblastine [58] while the family of natural tubulysins A–I (Fig. 9) showed IC_{50} values in the range of

Fig. 9 Tubulysin natural product family and synthetic analogs used as drugs
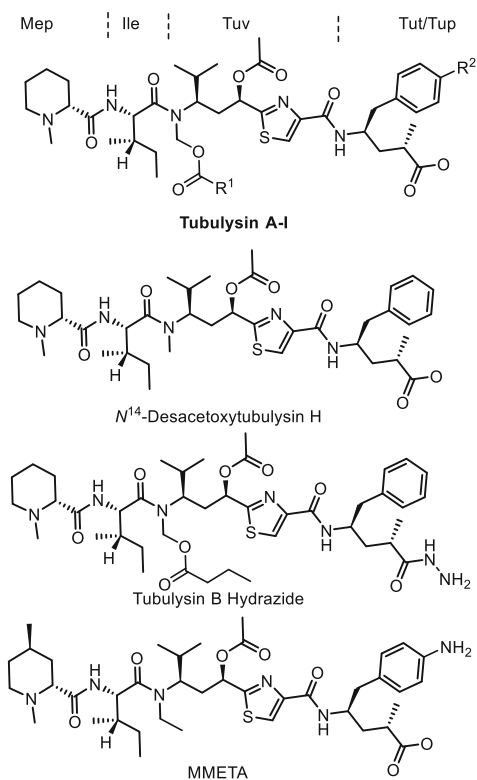
0.3–8.4 nM in human cervix carcinoma, multidrug-resistant cell line KB-V1 [59]. Structurally, the tubulysins (Fig. 9) consist of an (R)-N-methylpipecolic acid (Mep), a natural amino acid L-Ile, a tubuvaline (Tuv) containing a thiazole and two potentially labile acyloxymethyl and acetate ester groups and two defined chiral centers and a tubuphenylalanine (Tup) (R_2 = H) or tubuphenyltyrosine (Tut) (R_2 = OH) each displaying two defined chiral centers (Fig. 9). Simplified synthetic analogs of natural tubulysins were described where the acyloxymethyl group was replaced with a methyl group [60–62]. The cellular potency of the resulting derivative N^{14}-desacetoxytubulysin H (Fig. 9) was shown to be little affected by this structural alteration (L929 IC_{50} = 0.34 nM; SW-480 IC_{50} = 0.02 nM, KB-3-1 IC_{50} = 0.19 nM) [61]. Linking tubulysin requires introduction of a reactive group that comes at a cost for potency. Endocyte developed a folate conjugate that contained a derivative of Tubulysin B (R_1 = butyrate, R_2 = OH), i.e. Tubulysin B hydrazide that was shown to be ~3-fold less potent than the corresponding acid [63]. Introducing an aniline in the molecule of Tubulysin (R_2 = NH_2) leads to substantial drop-off in potency, however the potency is regained by modification of the N-substituent of tubuvaline (Tuv) as illustrated by MMETA that was developed by MedImmune/Astrazeneca. MMETA [64] (Fig. 9) showed consistent sub-nM potency in a wide range of tumor cell lines (DU 145 IC_{50} = 0.2 nM; MDA-MB-361 IC_{50} = 0.05 nM, NCI-N87 IC_{50} = 0.04 nM)) [65]. The aniline was used to generate payloads that were successfully conjugated to antibodies.

2.4.2 DNA Targeting Drugs

Calicheamicin

The calicheamicins are a family of antibiotics isolated as fermentation products of the bacterium *Micromonospora echinospora* ssp. *calichensis* [66]. At the time of their discovery they were considered the most potent tumor agent ever known with a potency 1,000 times higher than adriamycin [67]. Calicheamicin γ_1^I, the most well-known member of this family (Fig. 10), contains two functional regions: a complex bicyclic enediyne unit with a methyl trisulfide moiety that can induce DNA double-strand scission and an extended sugar residue, which possesses a fully substituted benzene ring that has the ability to bind in a sequence-specific manner to DNA minor grove [67]. The reactive functional region of calicheamicins displays a fascinating mechanism of action (Fig. 10). The enediyne warhead positioned within DNA double helix can be attacked by a nucleophile (e.g., glutathione) at the methyl trisulfide thus releasing a free thiol. The free thiol triggers a cascade of events starting with attack of the α,β-unsaturated ketone followed by a Bergman cyclo-aromatization reaction leading to a 1,4-benzene diradical. The diradical thus formed abstracts hydrogen atoms from both strands of the duplex DNA which in the presence of oxygen leads to cleavage of DNA double strands and subsequent cell death. The high potency makes Calicheamicin γ_1^I an ideal candidate for an ADC drug and finding a linking modality was pursued soon after its discovery.
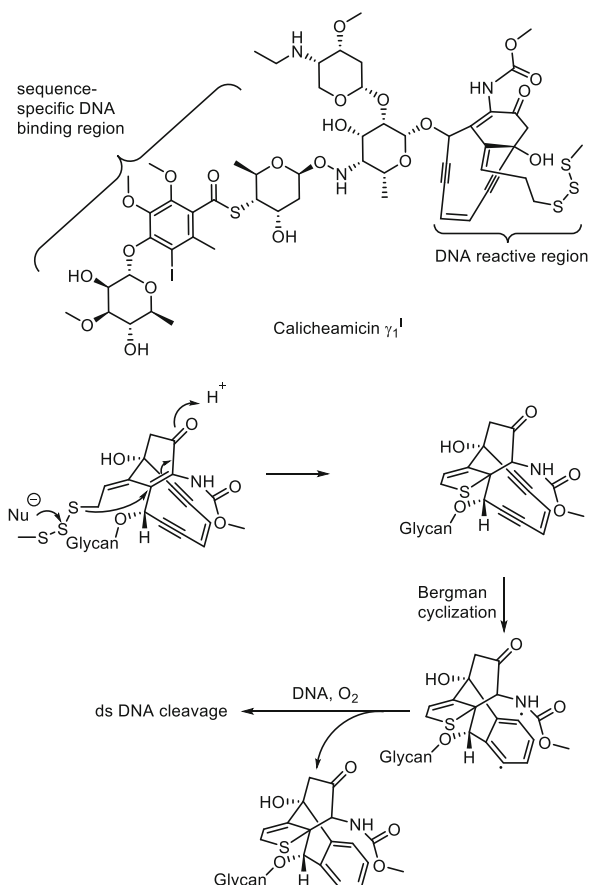
Acetylation of secondary amine in Calicheamicin γ_1^I led to a less toxic 5.6 nM in MX-1 breast carcinoma cells pM derivative N-Acetyl-calicheamicin γ_1^I **6** that was further functionalized to a dimethylhydrazide (DMH) **7** that was used to generate conjugates (Fig. 11) [68].

Duocarmycins

The duocarmycin natural product (+)-CC-1065 was isolated from *Streptomyces zelensis* as a potent antitumor antibiotic with a potency of $IC_{90} = 56$ pM [69]. The cytotoxic activity of this natural product was explained by its ability to alkylate adenine in DNA in a sequence specific manner. In case of (+)-CC-1065, the non-covalent DNA binding region (Fig. 12) positions the DNA alkylating region of the molecule into the minor groove where it alkylates the N3 of adenine via the cyclopropane moiety in spirocyclic cyclopropapyrrolo-indole (CPI) unit [70]. (+)-CC-1065 was not progressed into the clinic due to observed delayed
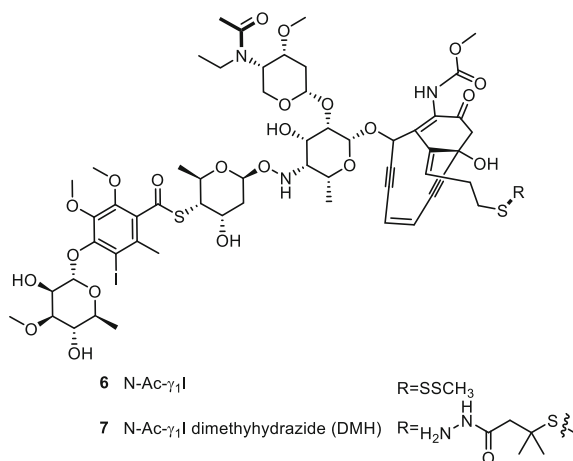
Fig. 11 Calicheamicin drugs used in ADCs
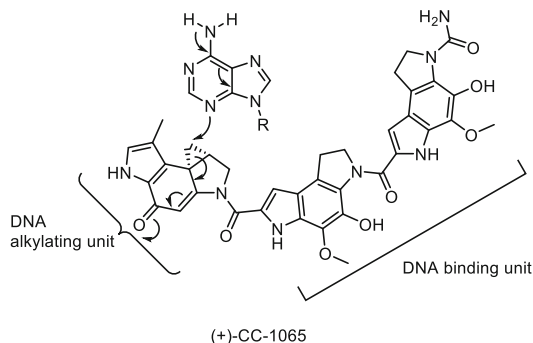
Fig. 12 Structure of CC-1065 and mechanism of DNA alkylation

hepatotoxicity in preclinical animal studies [71]. A series of analogs were made in an attempt to find molecules with properties suitable for clinical development. The discovery of cyclopropabenzindole (CBI) unit and the corresponding chloromethyl substituent as a precursor to the cyclopropyl ring constituted a breakthrough. This discovery addressed the relatively poor stability of the CPI unit in serum and opened the door for pro-drugging this highly reactive structural feature [72]. The chloromethyl substituent in *O*-pro-drugged-(*S*)-1-(chloromethyl)-2,3-dihydro-1H-benzo[e]indol-5-ol generates CBI following the enzymatic removal of the phenol-capping group and a Winstein cyclization (Fig. 13). This approach presented an opportunity for linking this potent warhead to an antibody and also for introduction of much needed water solubilizing groups for this chemotype.

Two duocarmycin containing ADCs have been progressed into the clinic. MED-A used the pro-drugging site to introduce a solubilizing moiety and an aniline in the DNA-binding region for linking to the antibody [73] and *seco*-DUBA where the DNA-binding region was modified to introduce hydrophilic residue that could

Fig. 13 CBI mechanism of formation following enzymatic cleavage

Fig. 14 CBI-based duocarmycin drugs progression to the clinic

promote solubility while the linking was done through the DNA-alkylating unit phenol (Fig. 14). Seco-DUBA showed IC_{50} = 90–430 pM potency in a range of cancer cell lines [74]. An interesting detoxification mechanism was described for DUBA, the active species following removing of the phenol capping group, where the cleavage of the amide bond between the alkylating region and the binding region in plasma leads to weakly cytotoxic molecules. This degradation was shown to be species dependent with only 2.6% of the DUBA left in rat plasma after 180 min and 68% remaining in human plasma [74].

Pyrrolobenzodiazepine Dimers

Anthramycin, the first member of this family of antibiotics, was isolated as the active constituent from the fermentation broth of *Streptomyces refuineus* var. *thermotolerans* [75]. Many analogs have been discovered or synthesized since then (Fig. 15). The key analogs that led to warheads currently used in ADCs are

Fig. 15 Naturally occurring pyrrolobenzodiazepines
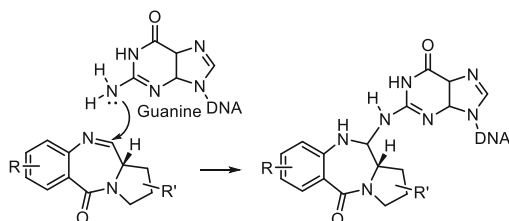
Fig. 16 Mechanism of DNA alkylation with PBDs

Tomaymycin [76] and Sibiromycin [77]. The key features of pyrrolobenzodiazepines (PBDs) are the presence of a substituted phenyl ring A, the diazepine ring B, a nitrogen containing five-membered heterocycle C containing various levels of unsaturation and a specific (*S*)-configuration at the B-C ring junction, which is essential for the interaction with the DNA minor groove (Fig. 15). PBDs are believed to owe their biological activity to their ability to react at the electrophilic N10–C11 imine with the amino group in C2 position of a guanine residue within the minor groove (Fig. 16) [78]. PBD monomers have shown nM toxicity against cancer cell lines and have limited applications for ADCs. A seminal discovery was made when a 1,3-propane-diether-linked dimer was shown to have much improved cytotoxicity due to its ability to bind to minor groove DNA over a span of six base pairs. The dimer **8** (DSB-120) showed up to 600 times improved activity over the monomer [79]. Further improvements in potency were made by introduction of unsaturation at C2 that led to the discovery of **9** (SJG-136 and SG2000), which was progressed into the clinic for hematological malignancies [80, 81]. Low pM in vitro potency was achieved by making the tether between the two PBD monomers longer, i.e.1,5-pentane-diether as illustrated by the discovery of **10** (SG2057) that showed 212 pM potencies in cancer cell lines [82]. In addition, highly potent analogs of PBD dimers were obtained when an aryl group was introduced at the C2-position; compounds **11** (SG2202) and its water soluble analog **13** (SG2285) showed 1.3–53.5 pM activity in a panel of cancer cell lines [83]. Compound **11** presented the opportunity to introduce a functional group for linking to an antibody when it was shown that an aniline at C-2 as in **12** (SG1882) showed 0.1–1 nM activity in a panel of lymphoma and renal cell carcinoma cell line panel [40].

An interesting linking strategy was used for the warhead in compound **14** (D6.5) where the N-10 position was used to introduce the linker [84] (Fig. 17).
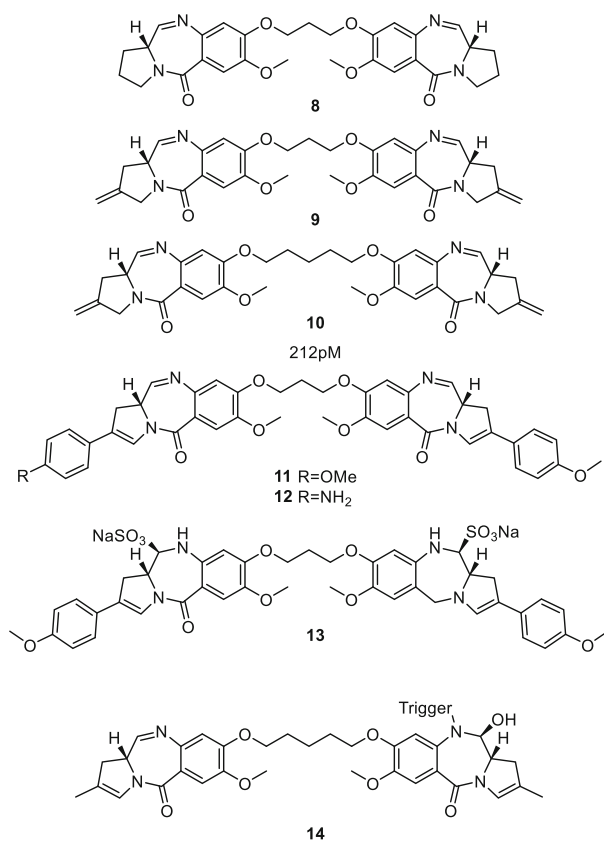
Fig. 17 Pyrrolobenzodiazepine dimers that were progressed into the clinic

2.4.3 Anthracyclines

Doxorubicin was used in early ADCs in which the molecule was linked to the antibody via a hydrazone formed with the ketone functional group (Fig. 18). In a randomized trial, chimeric BR96 antibody was conjugated to doxorubicin and the resulting ADC BR96-doxorubicin was advanced to a Phase II human clinical trial in metastatic breast cancer. The trial failed to show meaningful therapeutic benefit [85]. Clinical use of doxorubicin analogs is limited by their dose-related cardiotoxicity. Compound **15** (Nemorubicin, MMDX) (Fig. 18) was a synthetic analog of doxorubicin that showed reduced toxicity of 400–800 nM against doxorubicin resistant cancer cell lines [86]. During preclinical studies involving incubation of the drug with NADPH-supplemented rat liver microsomes a highly toxic metabolite was identified compound **16** (PNU-159682) (Fig. 18). This metabolite was shown to be 3,000-fold more cytotoxic than the parent **15**. The cytotoxicity against cultured human cancer cell lines was 0.07–0.58 nM/L [87]. The mechanism of action of **16** is intercalation
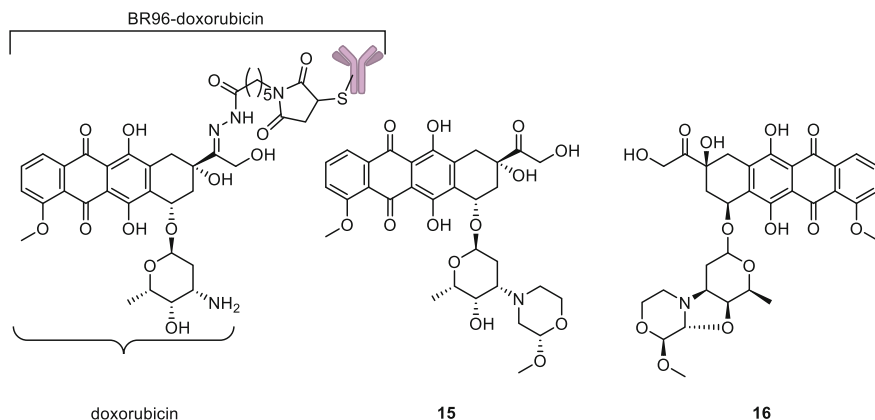
Fig. 18 Anthracycline drugs for antibody drug conjugates

between CG base pairs with a much higher binding affinity than **15** [88]. Compound **16** was linked to antibodies via the hydroxyl group (Fig. 18).

2.4.4 RNA Polymerase Inhibitors

α-Amanitin

α-Amanitin **17** is a bicyclic octapeptide isolated from Amanita mushrooms and responsible for their extreme toxicity (Fig. 19). Amanitin binds with high specificity and low nM affinity near the catalytic active site of RNA polymerase II, as shown by its high resolution structure bound to the enzyme [89]. α-Amanitin "freezes" the enzyme in a conformation that prevents nucleotide incorporation and stops translocation of the transcript [90, 91]. Despite its low cell membrane permeability, α-amanitin is hepatotoxic by a mechanism that involves the organic anion-transporting polypeptide (OATP3), which acts as an uptake transporter in human hepatic cells [92]. α-Amanitin was conjugated to proteins in the 1980s by using the phenol as the linking functional group or a diazo-linker with uncertain structure [93]. It was shown that once conjugated to antibodies via the 4-hydroxy-L-allothreonine **18** (Fig. 19), the anti-epithelial cell adhesion molecule (EpCAM) targeting amanitin ADCs showed 10^5 enhancement of cytotoxicity as an ADC targeting an antigen expressed on the Colo205 cancer cell lines [94]. This observation was later attributed to the fact that suppression of RNA polymerase IIA with amanitin led to selective inhibition of proliferation, survival and tumorigenic potential of colorectal cancer cells with hemizygous TP53 loss in a p53-independent manner [95]. Introducing a linking reactive group or a phenyl-ether **19** (Fig. 19) led to potent anti-PSMA targeting ADCs that showed 17–620 pM potency in PSMA expressing cells in vitro. The corresponding cleavable
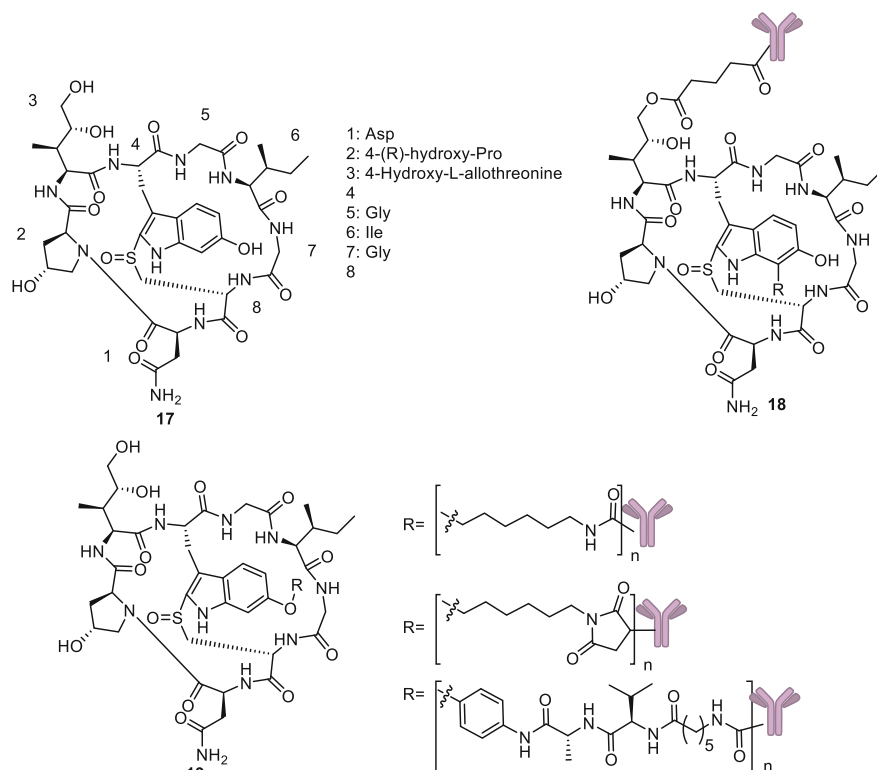
Fig. 19 Structure of natural α-amanitin and derivatives for linked drugs

and non-cleavable conjugates showed tumor stasis in CWR-22rv1 mouse model at an iv dose of 150 μg/kg with respect to toxin [96].

SN-38 and the Camptothecins

Camptothecin (CPT) was first isolated from the *Camptotheca acuminata* tree in 1966 (Fig. 20) [97]. Preclinical studies revealed that CPT had remarkable activity against leukemia cell lines. The low aqueous solubility of CPT led to its use as a sodium salt of the open cycle lactone end of the molecule, which leads to loss of activity. In efforts to improve the aqueous solubility of analogs, the derivatives Topotecan and Irinotecan were developed. The potent antitumor activity of CPT was attributed to selective inhibition of DNA topoisomerase I, thus impairing DNA replication and resulting in the apoptotic cell death of tumor cells [98]. The X-ray crystal structure of a ternary complex formed between DNA, topoisomerase I and Topotecan showed the only H-bond interaction between the drug and the enzyme was with the 20-hydroxy-group of Topotecan and an important water interaction was observed with the phenol [99]. This discovery provided an explanation
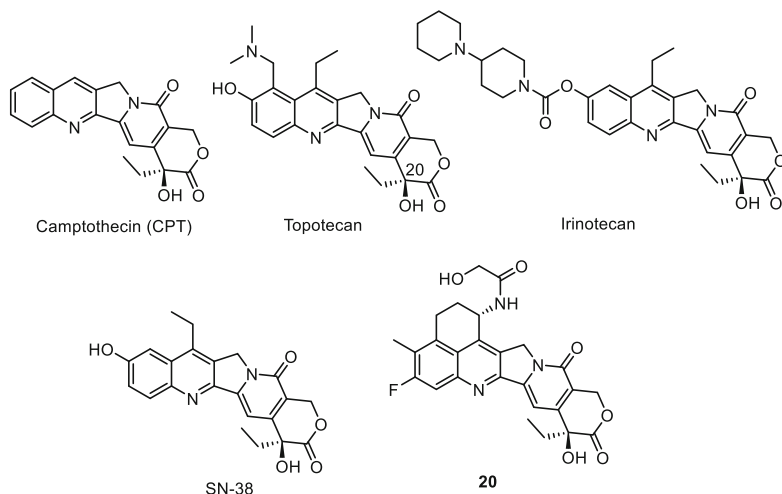
Fig. 20 Structure of camptothecin and derivatives used as cytotoxic drugs and as linked drugs

for much lower potency for Irinotecan, a result of inefficient carboxylesterase-catalyzed hydrolysis of the prodrug to its active metabolite in patients. The active metabolite of Irinotecan (SN38) was plagued by low aqueous solubility despite higher activity than CPT. However, SN-38 was successfully conjugated to an antibody via its hydroxy group at C20 [100]. Compound **20** (Dxd, DX-8951) was described as an inhibitor of Topoisomerase I with higher potency than SN-38. The warhead was incorporated into an ADC by linking with the hydroxyacetate via an aminomethylene moiety [101]. A trastuzumab conjugate with compound **20** showed activity in breast cancer patients [102].

2.5 The Tether

The tether is defined as the region of the linker that connects the drug to a reactive group that accomplishes the conjugation to the antibody as described in Sect. 2.2. The tether must be stable in plasma for the period between the IV administration and cellular internalization and processing thus addressing the primary drug loss mechanism from the ADC (Fig. 21). The secondary source of drug loss is the stability of the whole conjugate in plasma. The attachment of the linked drug negatively impacts the pharmacokinetics of the ADC, thus leading to release of drug by virtue of antibody plasma metabolism (Fig. 21) and the tether can minimize the negative impact of drug conjugation on pharmacokinetics by counterbalancing the hydrophobicity of the drug. In addition to modulation of the overall stability of the ADC, the tether can provide at least one intracellular specific mechanism of release of the active species. Based on these considerations the tether plays a critical

Fig. 21 Representative pharmacokinetic profiles of molecular components of ADCs
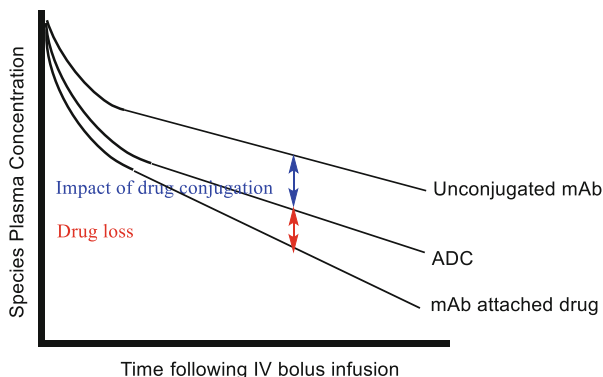
role in achieving true targeted delivery of the drug by harnessing the long half-lives of mAbs and utilizing tumor and cancer cell specific cytotoxic drug release. Two classes of tethers have been utilized in generation of ADCs: non-cleavable and cleavable tethers.

2.5.1 Non-cleavable Tethers

A non-cleavable tether does not contain a tumor or cancer cell-specific release unit, called a "trigger." For a medicinal chemist, the use of a non-cleavable tether poses the challenge of finding a linking site on the cytotoxic drug where attachment of the tether will not impact cytotoxicity. Additionally, following cellular catabolism, the non-cleavable tether ADCs generates a species that contains a residual charged amino acid residue. In vitro assessment of the cytotoxicity of such species is not always trivial due to the potential low cell membrane permeability thus making the evaluation of linked drugs with non-cleavable tethers challenging. The particular nature of non-cleavable tethers has two apparently conflicting consequences: on one hand the stable linkage translates to higher plasma stability and reduced toxicity as shown by higher Maximum Tolerated Dose (MTD) in vivo. On the other hand, in tumors with heterogeneous expression of the antigen, the efficacy can be negatively affected by the reduced cell membrane permeability of the active species, leading to reduced ability of the resulting drug to kill neighboring cells.

Two prominent examples of non-cleavable tether linked warheads are MCC-DM-1 and mc-MMAF (maleimidocaproyl-MMAF). The lysosomal catabolites of ADCs containing these linked drugs are DM1-MCC-Lys **21** and MMAF-mc-Cys **22**, respectively (Fig. 22). As the catabolism of ADCs was shown to be lysosomal [103] and the target of these drugs is located in the cytoplasm, the exact mechanism of lysosomal escape was unknown. Recent data suggest that protein transporters imbedded in the lysosomal membrane could be responsible for the exit of these highly charged molecules from the lysosomal compartment into the cytoplasm. Moreover, the study showed that transporters have the ability to
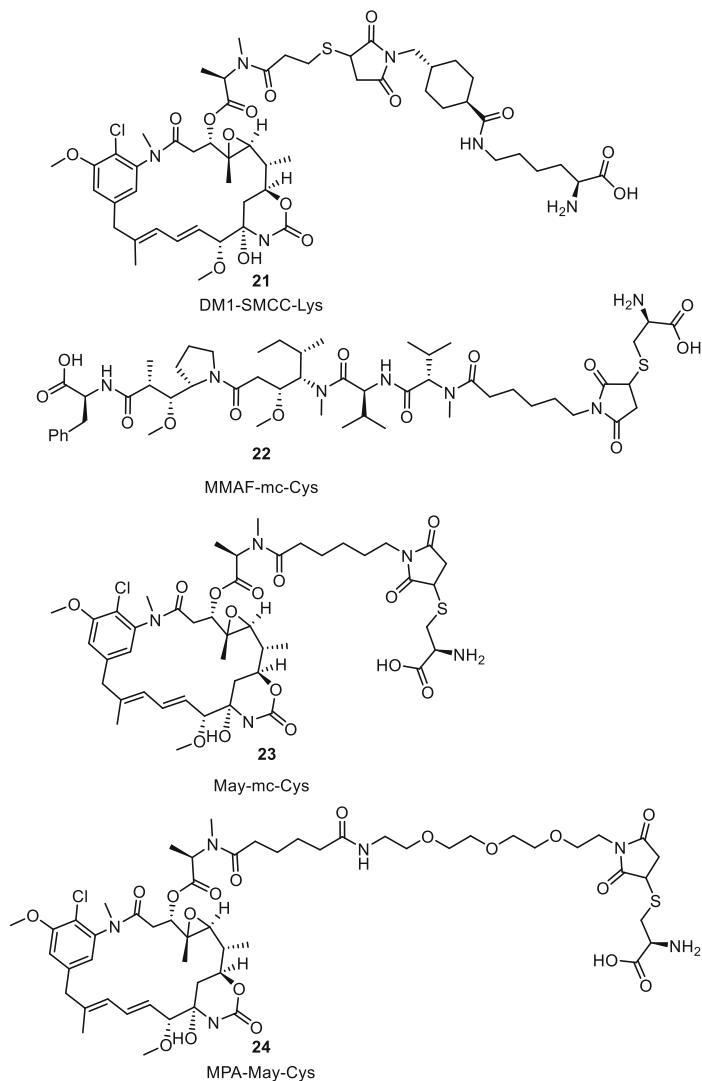
Fig. 22 Linked drugs with non-cleavable tethers

selectively transport species with certain linked drug structure thus providing evidence that development of non-cleavable tethers could face higher hurdles than is the case for cleavable analogs [104].

MCC-DM-1 contains the thiosuccinimide moiety, which was shown to lead to drug loss following exchange with thiol-containing plasma protein, i.e. albumin. Two truly non-cleavable linkers that lacked the reversible thioether succinimide connection between the drug and antibody were shown to possess superior efficacy and stability relative to MCC-DM1. These two linkers are May-mc **23** and

May-MPA **24** and the corresponding lysosomal released drugs are shown in Fig. 22 [105].

2.5.2 Cleavable Tethers

Cleavable tethers contain a spacer and a structural feature designed to release the drug inside the cell called a "trigger." The spacer is usually a short carbon chain for most ADCs but for some is a series of polyethylene glycol units, which are designed to reduce the logP of the linked drug during the conjugation process and minimize the impact of drug lipophilicity upon the pharmacokinetics of the ADC. The trigger is a tool that exploits changes that occur in vesicles along the endosomal, lysosomal and cytoplasmic pathway following receptor-mediated endocytosis [106]. The changes that have been exploited by trigger designs are: (1) gradual drop in pH from physiological range at the cell surface of 7.2–7.4 to 5.5–6 within the endosome and to ~5.0 in lysosome; (2) the activation of protein digesting enzymes at the lower pH of the lysosome; and (3) the increase in concentrations of reducing co-factors such as glutathione and cysteine and activation of enzymes that can reduce disulfide bonds [107].

Early examples of pH sensitive triggers are shown in Fig. 23. The linker in gemtuzumab ozogamicin (Mylotarg) showed good stability at pH 7.4 (94%) and complete hydrolysis at pH 4.5 (97%) following an investigation of a range of structural analogs. This linker, called AcBut, showed the best stability at pH resembling plasma yet can be efficiently cleaved in the acidic environment of the lysosome. AcBut led to ADC that showed potency 100,000-fold higher toward antigen-positive HL-60 cells than when conjugated to a non-targeted antibody [108]. One additional example of an acid sensitive trigger is AEVB (Fig. 23), which contains Auristatin E linked at the alcohol moiety as an ester to a ketone
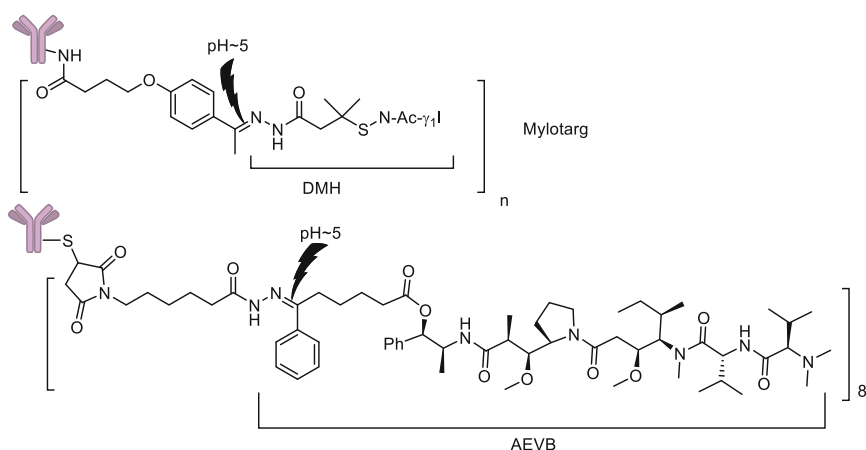
Fig. 23 Low pH cleavable hydrazone-linked drugs

containing acid. The ketone is linked to the antibody via a pH sensitive hydrazone. The linkage was relatively stable at pH 7.2 ($t_{1/2}$ >60 h) but labile at pH 5.0 ($t_{1/2}$ 3 h). Once conjugated, AEVB was released non-enzymatically at pH 5 ($t_{1/2}$ 4.4 h) more rapidly than at pH 7.2 ($t_{1/2}$ 183 h). A human plasma stability study showed that after 4 days ~30% hydrazine was hydrolyzed. In mouse plasma ~40% of drug was cleaved at the ester site after 4 days incubation [53].

The most successful trigger has been the peptidase-cleavable peptide pioneered following discoveries made at Bristol Myers Squibb in the late 1990s. Dubowchik and his colleagues hypothesized that replacing the hydrazone trigger with a cathepsin B cleavable peptide should lead to tethers that are stable in circulation, due to absence of the protease in extracellular space, yet labile in the lysosomal compartment, thus releasing the drug intracellularly [109]. The study showed that cathepsin B–mediated release of doxorubicin from constructs containing various dipeptide triggers was observed only when a spacer was introduced between the bulky doxorubicin and the dipeptide. The spacer chosen was para-amino-benzyl (PAB) that presented the unique feature of self-immolation at pH ~5. An illustration of the dipeptide linker design (Fig. 24) uses mc-VC-MMAE. The dipeptide used in this tether is Valine-Citrulline flanked by a maleimidocaproyl spacer at the N-terminus and by the PAB spacer at the C-terminus. Upon cleavage of the PAB-Cit amide bond, a MMAE-PAB carbamate is released. This species can be identified transiently but it decomposes by a 1,6-elimination with the release of unstable MMAE carbamic acid, which spontaneously eliminates carbon dioxide to generate the active drug. In a detailed comparison of peptide and hydrazone cleavable tethers, scientists brought strong evidence that peptide tethers were superior in almost all aspects when linking auristatins to antibodies [53]. In addition to the Val-Cit
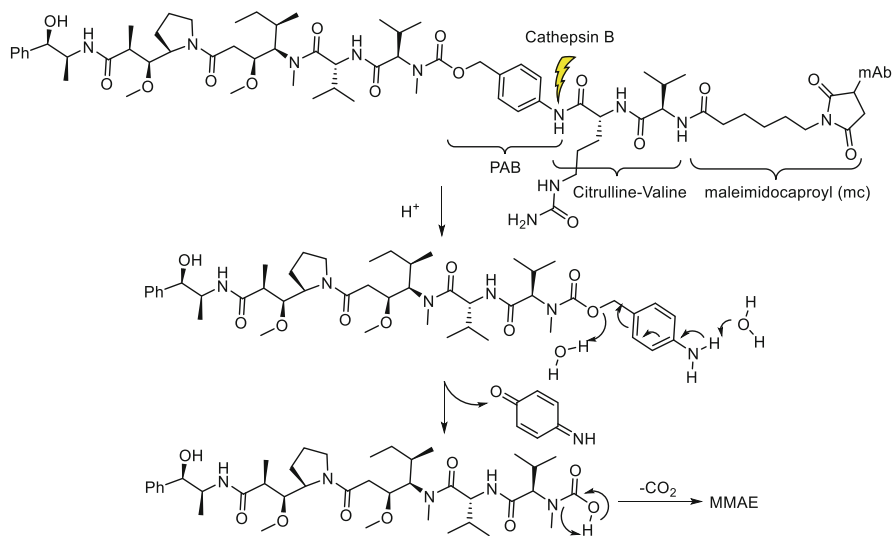
Fig. 24 Dipeptide trigger design for linked MMAE
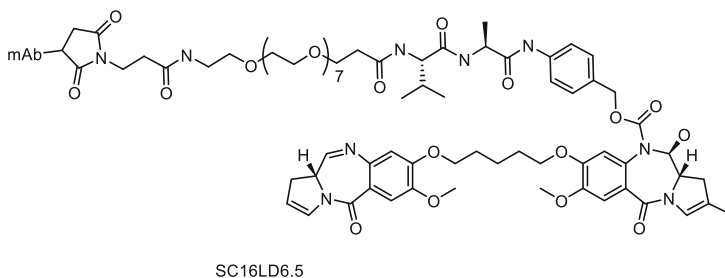
SC16LD6.5

Fig. 25 Val-Ala dipeptide trigger in a PBD dimer linked drug

peptide trigger, several groups have employed a Val-Ala linker as the one described in SC16LD6.5, in which the tether for pyrolobenzodiazepine dimer D6.5 contains a Val-Ala-PAB trigger and a PEG8, which lowers the hydrophobicity of the whole payload (Fig. 25) [84].

A highly complex linker design was reported for duocarmycin in SYD985 [74]. The main challenge with duocarmycin derived ADCs is linking via a phenol group. Design criteria employed for linking seco-DUBA were: introducing a tether that lowers lipophilicity, as is the case with PEGs and alcohols, use of a self-immolative 1,5-cyclization moiety and use of a valine-citrulline-PAB cathepsin B-sensitive trigger. Unlike the Val-Cit-PAB alone, for which a mildly acidic environment is needed to facilitate enzymatic cleavage, the tether in SYD985 requires a pH of greater than 6 for efficient release of the DUBA active species. This requirement is met by the transport of the prodrug carbamate from the lysosomal compartment to the cytoplasm where the higher pH triggers the release of DUBA (Fig. 26) [74]. This additional step could present challenges as it was shown that transporter proteins could play a critical role [103] and structural characteristics of the tether may impact the efficiency of crossing intracellular membranes. The tether in NMS249 utilizes a similar self-immolative 1,5-cyclization unit that connects the protease cleavable trigger to a primary alcohol. This tether is more hydrophobic and contains no PEG to attach the maleimide. This design was driven by the hydrophilic nature of the PNU-159682 parent drug and the presence of a primary alcohol as the linking handle (Fig. 27) [110]. The Val-Cit-PAB motif adds considerable hydrophobicity to tethers and ultimately to ADCs.

Unlike small molecule drugs mAb-based drugs owe their long half lives in circulation, among other factors, to their peptidic structures and optimal lipophilicity. Structural modifications of mAb that add hydrophobicity to the molecule have been shown to reduce the half-life of these constructs in circulation. Hydrophobic interaction chromatography (HIC) is an analytical tool that allows for evaluation of "hydrophobic penalty" paid by ADCs following linking drugs to antibodies. This penalty is evidenced by a longer retention time in HIC when compared to unconjugated mAb and has a significant impact upon pharmacokinetics of the conjugate in vivo [35, 111]. To illustrate the impact of hydrophobicity on pharmacokinetics, a tether that contained a hydrophilic moiety (AT-glu-Dpr-(mDpr)) in which the phenylalanine
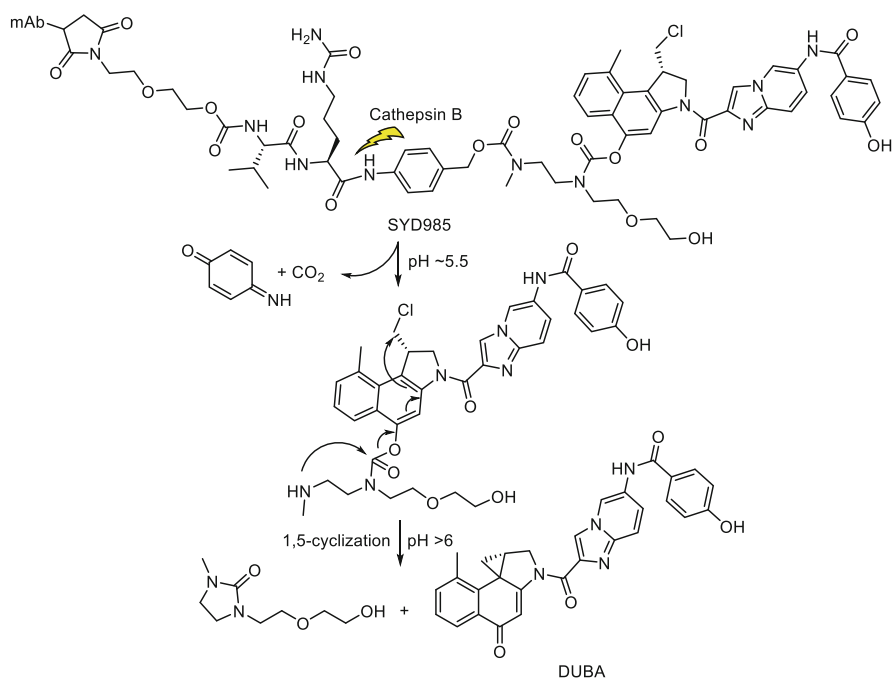
Fig. 26 Design of phenol-linked dipeptide-trigger duocarmycin in SYD985
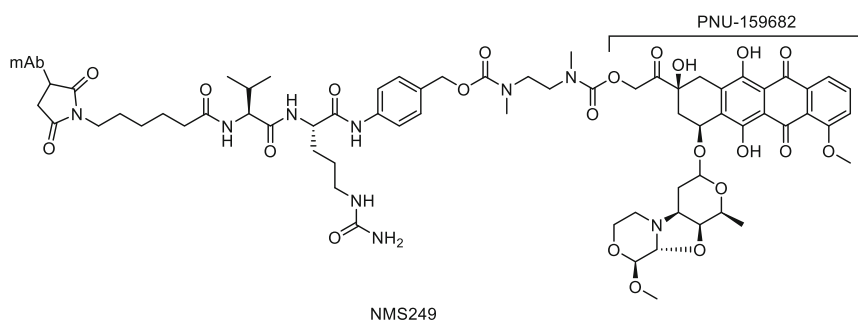
Fig. 27 Design for linking a primary alcohol with a dipeptide trigger anthracycline linked drug in NMS249

of MMAF was replaced with threonine and linked directly to a hydrophilic cleavable peptide via a hydrolysable maleimide tether (see earlier) was designed. The resulting ADC was compared to the mc-MMAF and mc-VC-PAB-MMAF in the HIC assay (Fig. 28). As mentioned previously, for a given ADC, the number of drugs loaded to a mAb is defined as drug to antibody ratio (DAR). In the context of hydrophobic penalty, the DAR refers to the number of molecular entities attached to the mAb
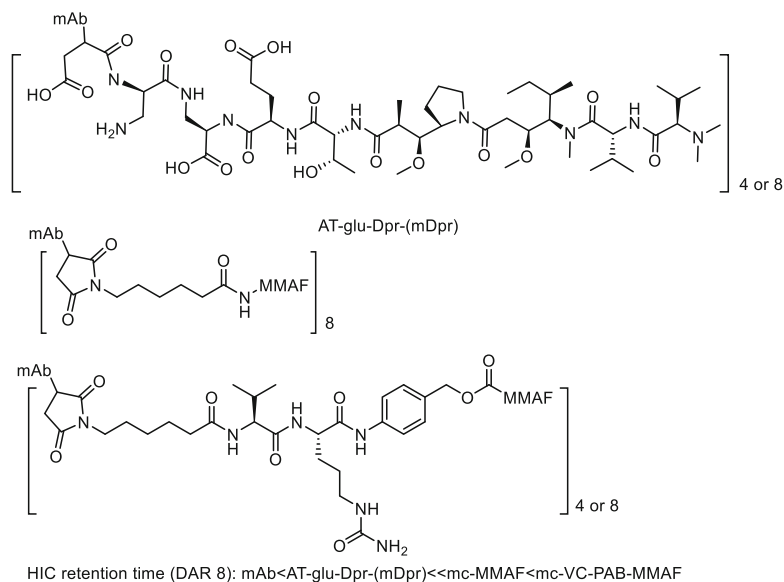
Fig. 28 Structure of linked drugs used to evaluate the hydrophilic linked auristatins

that contain the active drug that contributes to added hydrophobicity to the ADC. In the study above, the hydrophilic tether ADC showed a retention time similar to unconjugated antibody even at a high DAR 8. The observed plasma pharmacokinetics with DAR 8 mirrored the HIC hydrophobicity profiles. Moreover, the in vivo efficacy for an ADC with a DAR of 4 with mc-VC-PAB tether was significantly higher than an analogous ADC with a DAR of 8. By contrast, the efficacy of a DAR 8 hydrophilic AT-glu-Dpr-(mDpr) tether ADC was much higher than DAR 8 with mc-VC-PAB tether at one quarter of the dose [111].

The PAB spacer in peptide triggers was omitted in cases where a phenyl group is part of the warhead. The peptide trigger was attached directly to the warhead via an aniline. The PBD dimer **12** (SG1882) (Fig. 17) was linked to an antibody via a tether that contained the Val-Ala-mc. Compound **25** (Fig. 29) was conjugated at position HC S239C to yield the ADC (see Sect. 3 for discussion) [40]. Another example of a minimalistic linker is mc-Lys-MMETA **26** where a Lys was linked directly to the warhead to yield highly potent ADCs following conjugation (Fig. 29).

β-Glucuronidase is an enzyme that was shown to be highly abundant in breast tumor tissue and peritumoral space [112]. β-Glucuronidase can cleave the glycosidic bond between glucuronic acid and a hydroxyl-bearing substrate. In the context of ADCs a β-glucuronide trigger was coupled to a tri-substituted self-immolative tether that acts a linking point for antibody attachment and as a drug release device analogous to the previously described PAB. This type of linker was used to link MMAF to CD30 and CD70 targeting antibodies where the resulting ADCs showed pM potency in antigen positive cancer cell lines (Fig. 30) [113]. The ability of

SG1882   **25**

mc-Lys-MMETA   **26**
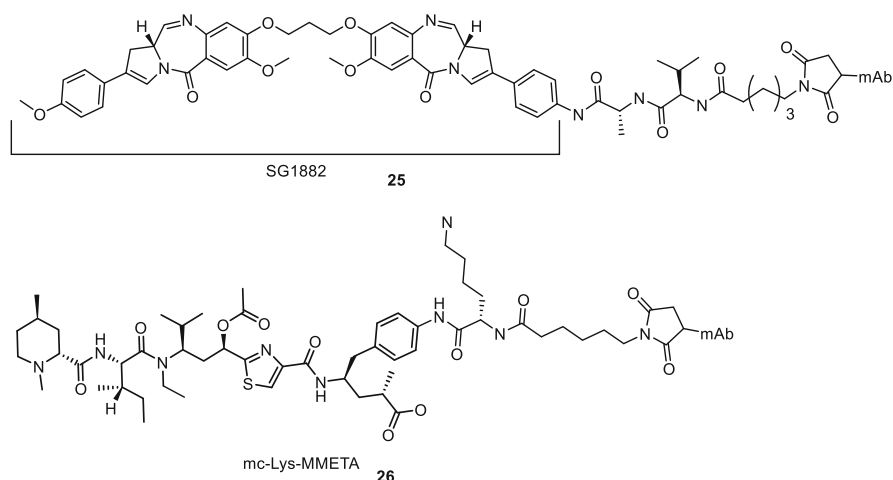
Fig. 29 Linked drugs that do not use a spacer for dipeptide trigger

β–glucuronidase

1,6-elimination
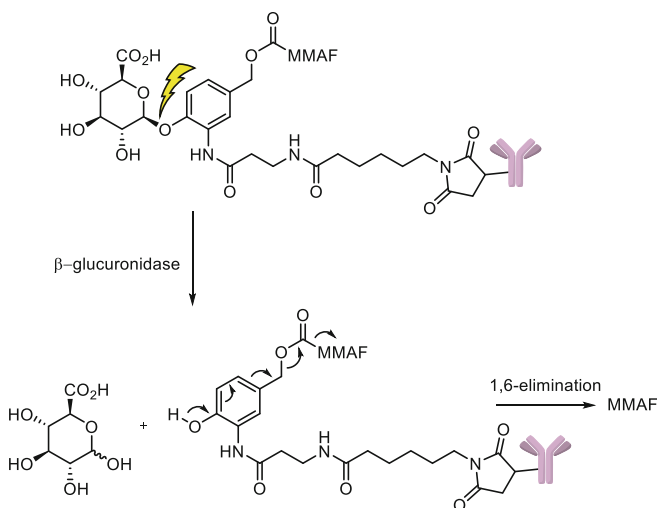
MMAF

Fig. 30 Glucuronide as a trigger for linked MMAF

this tether to generate increase hydrophilicity was exploited when hydrophobic Duocarmycin analogs were successfully conjugated to anti-CD30 and anti-CD70 antibodies to yield potent ADCs [114]. A recent extension of the glucuronide linking technology used a quaternary ammonium linker (Fig. 31) instead of a carbamate to link the self-immolative moiety to the drug. This approach introduces one additional hydrophilic element to the tether thus leading to highly hydrophilic ADCs, which have improved pharmacokinetics. This new technology was used to link Auristatin E, the drug in GlucQ-AE, and N^{14}-desacetoxy-tubulysin H, the drug
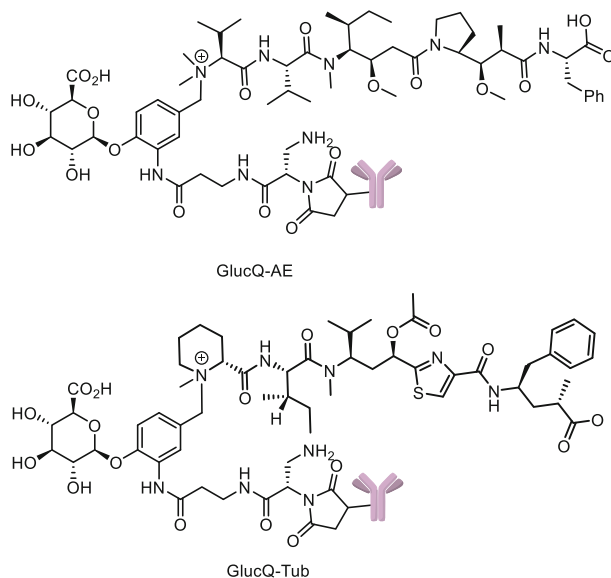
Fig. 31 Quaternary ammonium linker combined with glucuronide trigger

DTT stability a<c<<e~b<d<<f
in vivo PK $t_{1/2}$ 27a=15h, 27b=47h, 27c=87, 27d=218h
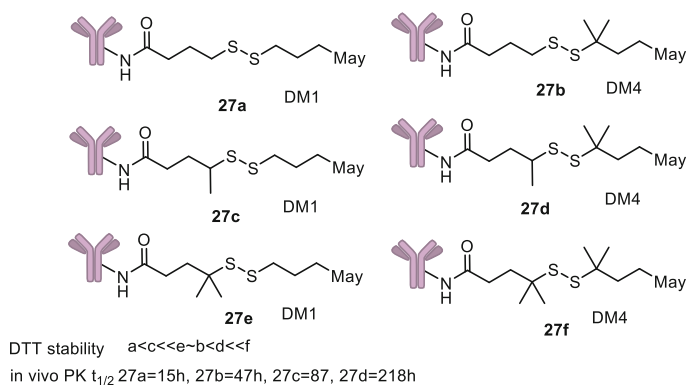
Fig. 32 Maytansine disulfide linkers stability studies

in GlucQTub, to anti-CD30 and anti-CD70 antibodies with a DAR of 4 that showed potent cytotoxicity in an antigen specific cytotoxicity assay (Fig. 31) [115].

The higher concentration of glutathione (0.5–10 mmol/L) and relatively low extracellular concentration (2–10 μm/L in plasma) [116] was exploited by tether design for ADCs. In addition to hydrolysis of the hydrazine, the calicheamicin conjugates require the reduction of a disulfide bond for activity (see above). The development of a plasma stable disulfide tether that could efficiently release the drug in the intracellular compartment was critical for the development of the maytansinoid drugs DM1 and DM4 with cleavable linkers (Fig. 32). A series of

huC242 ADCs **27a–f** were prepared with the intent to explore the effect of steric hindrance adjacent to the disulfide bond upon the ADC characteristics. All ADCs were highly active (low pM potency) and the activity was antigen expression status specific [117]. The conjugates were incubated with DTT at pH 6.5 to determine the relative loss of drug and it was shown that higher hindrance leads to much slower drug release. The higher stability of the disulfide translated to improved pharma-cokinetics as defined by the half-life but the tolerability in vivo was not affected by hindrance (Fig. 32). In comparison to non-cleavable linker DM1-SMCC-tether, the cleavable disulfide ADCs were less well tolerated in mice. The disulfide tethers however showed increased bystander activity (as defined above). A bystander kill assay, in which the ADCs were incubated with antigen negative cells and increasing number of antigen positive cells, was carried out for ADCs **27c** and **27b** in Fig. 33 along with the non-cleavable DM1-SMCC. As long as enough antigen positive cells were present, the cleavable linker containing ADC was able to kill antigen negative cells, with ADC **27b** showing much higher efficiency than **27c** while the non-cleavable tether was ineffective. An understanding of this behavior was achieved using a radiolabeled maytansinoid conjugated to huC242 by using SPP (**27c** in Fig. 33) and SPDB (**27b** in Fig. 33) tethers for DM1 and DM4, along with the non-cleavable DM1-SMCC. The study analyzed the products of cell catabolism for all ADCs. All ADCs yielded Lys-bearing catabolites, indicating full degradation of the antibody in the lysosome. The non-cleavable tether was not further degraded but the cleavable tethers yielded the reduced drugs DM1 and DM4 following disulfide reduction. Interestingly the *S*-methylated analogs of the two drugs were observed as well with that being the major species for DM4 while for DM1only small amounts of methylated analog were observed. This indicated that DM4 was efficiently methylated by endogenous *S*-methyl transferases. This finding, associated with the enhanced cell membrane permeating ability of the *S*-Me analogs, explained the observed differential activity against non-antigen expressing cells (Fig. 29) [118].
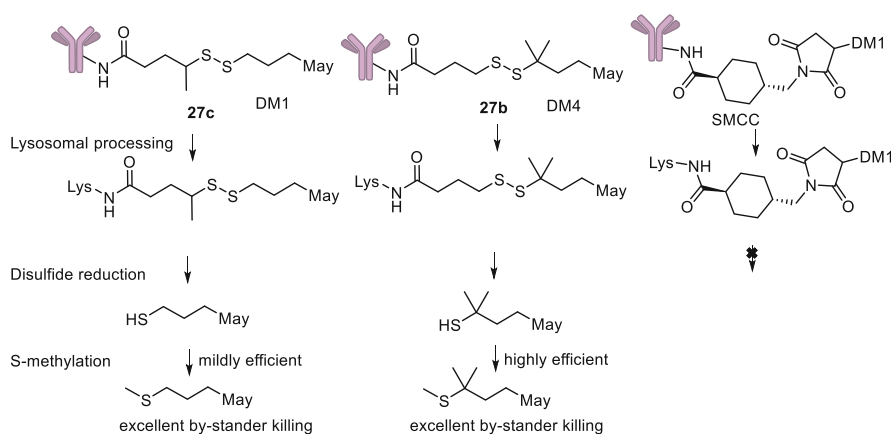
Fig. 33 Disulfide trigger intracellular processing cleavables vs. non-cleavable

3 Processes

3.1 Antigen Binding and Internalization

At a cellular level, multiple factors contribute to efficient targeting of the cancer cells and subsequent tumor destruction: the antigen copy number expressed on the surface of the cancer cell (as mentioned above), the affinity of ADC for the antigen, the rate and efficiency of internalization of the ADC-antigen complex, the rate of recycling of the complex back to the cell surface and the efficiency of trafficking to the appropriate compartment for drug release and ultimately achieving the interaction with the intracellular target leading to cell death all play critical roles in the success of targeted cancer therapy. Most of these characteristics are antibody target dependent and judicious target selection will have a significant impact on the clinical success of the ADC [119]. However, the efficiency of internalization of the ADC could be induced by conjugation of the drug to the non-internalizing mAbs. Several reports showed that upon binding of unconjugated mAb to the antigen, the antibody/antigen complex remains on the surface while conjugation to drugs such as auristatins L49 mAb [120] or anti-CD-20 [121] led to molecules that efficiently internalize once bound to cell surface antigen. Whether this applies to any drug conjugated to non-internalizing mAbs still remains to be demonstrated.

3.2 ADC Intracellular Processing

Trafficking and intracellular fate of ADCs following internalization has been the object of several detailed studies [118, 122, 123]. Anti-CD30 conjugates bearing the protease cleavable tether mc-VC-MMAE and the non-cleavable mc-MMAF were generated and were shown to display comparable binding and internalization rates with both ADCs showing efficient and antigen-dependent cancer cell killing. Immunofluorescence microscopy showed that the ADC localized to lysosomes following 16 h incubation in L540cy cells. When inhibitors of trafficking (ammonium chloride) were used prior to addition of ADCs to the cells the total intracellular level of ADC was significantly diminished while flow cytometry and fluorescence microscopy showed accumulation of ADC at the surface of the cell. Inhibitors of cathepsin B-mediate proteolysis significantly enhanced the intracellular levels of ADCs. The lysosomal metabolism of the ADC caused the released of the drug was probed by using inhibitors of cysteine proteases that showed subdued cytotoxicity when incubated with the cancer cell pretreated with inhibitor. Interestingly, when the inhibitors were added to the cells hours after the ADC treatment there was minimal effect upon cytotoxicity [123].

4 Clinical Experience

4.1 Hematological Cancers

4.1.1 Gemtuzumab Ozogamicin

Gemtuzumab ozogamicin (Mylotarg) was approved by the FDA in 2000 and was the first ADC to reach the market. It is a humanized IgG_4 mAb directed against CD33, a surface antigen present in 85–90% of acute myeloid leukemia (AML), conjugated by random Lys conjugation to N-Ac-γ_1^I dimethyhydrazide (DMH) (Fig. 11) with an average of DAR4. It was prescribed as a monotherapy in patients over the age of 60 with AML who were not candidates for cytotoxic chemotherapy. Mylotarg was withdrawn in 2010 after a phase III study showed no clinical benefit and a higher risk of fatal adverse events [124].

4.1.2 Brentuximab Vedotin

Brentuximab vedotin (Adcetris) is composed of a mouse IgG_1 anti-CD30 mAb conjugated to mc-VC-MMAE via maleimides to native cysteine residues with an average DAR of 4. Adcetris binds to the cell surface CD30 with high affinity (3 nM) and has high potency against CD30+ Hodgkin lymphoma and ALCL tumor cells in vitro (IC_{50} values of 3–50 pM) [125]. The clinical MTD of Adcetris was 1.8 mg/kg every 3 weeks. At this dose objective responses were obtained, including complete responses (4 of 12 patients) and partial responses (2 of 12 patients) in relapsed CD30-positive lymphomas [126] in a first Phase I study. In a second Phase I trial of brentuximab vedotin carried out to test its effects, when administered weekly the dosing range was 0.4–1.4 mg/kg, the MTD was 1.2 mg/kg and the overall response rate (ORR) was 59%, with 34% complete responses [127]. Adcetris was approved for the treatment of patients with relapsed or refractory CD30+ Hodgkin lymphoma following autologous stem cell transplant (ASCT) or patients not eligible for ASCT who have failed at least two other chemotherapy treatments. Adcetris has also been approved for patients with anaplastic large cell lymphoma (ALCL) as a second line following a phase II study where 86% of patients showed an overall response rate and 54% complete responses [128]. The most common adverse reactions were peripheral sensory neuropathy, neutropenia, fatigue, nausea, and thrombocytopenia.

4.2 Solid Tumors

4.2.1 Ado-Trastuzumab Emtansine

Ado-trastuzumab Emtansine (T-DM1, Kadcyla) [129] is composed of trastuzumab, an anti-Her2 humanized IgG_1 antibody random conjugated via Lys to non-cleavable

SMCC-DM1 with an average DAR of 3.5. In vitro potency of trastuzumab-MCC-DM1 in a panel of human breast cancer cell lines expressing Her2 was IC_{50} 4–15 ng/mL [129]. The clinical MTD was 3.6 mg/kg every 3 weeks with a $t_{1/2}$ of 3.5 days [130]. In early 2013, T-DM1 was approved as a new therapy for patients with HER2-positive, late-stage (metastatic) breast cancer. Currently, T-DM1 is the only ADC approved for treating metastatic breast cancer that overexpresses the HER2 antigen [131, 132].

5 Future Directions and Perspective

Therapeutic ADCs for cancer treatment are experiencing encouraging success with the approval of Adcetris and Kadcyla and promising results with several clinical candidates in advanced clinical trials [133, 134]. The recent advances in linker development led to a breakthrough in the ability to achieve good clinical efficacy with limited toxicity. The two parameters that define the therapeutic index of ADCs are Minimum Effective dose (MED) and MTD and while ADCs present certain advantages over chemotherapy with regard to systemic toxicity still most current ADCs are dosed at or close to the maximum tolerated dose. The most encouraging aspect of ADC development is that targeted therapy, with very few examples, has delivered on its promise of showing efficacy against tumors defined by a particular target. The main challenge for next generation of ADCs is to improve their tolerability. While on-target toxicity can be addressed by a careful choice of target antigen, the off-target toxicity can be addressed with medicinal chemistry. Highly potent drugs have contributed to the success of the current generation of ADCs but all have shown significant dose-limiting toxicities [135]. Generation of homogenous ADCs is a reality with the establishment of site-specific conjugation technology used by ADCs currently in the clinic. This technology, along with the advances in control of the hydrophobicity of linked drugs should lead to significant improvement in pharmacokinetics to a point where the half-lives of the ADCs should closely resemble the ones for the parent mAbs. The small fraction of current ADCs reaching the tumor [41] presents an excellent opportunity for improving the therapeutic index as just a small improvement in efficient targeting could have a great impact on both the MED and MTD. The non-specific uptake of ADC via target-independent internalization, i.e. pinocytosis, was recognized as an area of intervention [136]. Exploiting the genetic differences between tumor and normal cells is in its infancy and medicinal chemists and cell biologists are faced with a great opportunity to harness these yet unknown devices that will enhance the ability to kill cancer cells with future ADCs. Uncovering tumor-specific mechanisms of release will require development of new triggers or combination of triggers within the same tether or linked drug. The suggested dependence of lysosomal escape upon the structure of the linked drug gave us a glimpse into the types of opportunities available to ADC medicinal chemists [104]. From a structural perspective, the interaction of the linked drugs with the antibody is far from being understood.

Developing an understanding of these interactions could provide design principles for medicinal chemists when building linked drugs for mAbs. Such an advance could be achieved by making use of molecular modelling or, ideally, by obtaining crystal structures of ADCs.

The efficacy of ADCs is dependent on whether the intracellularly released active species is a substrate of multidrug resistance (MDR) proteins. Most of the ADCs in clinical trials use a small set of cytotoxic warheads: auristatin and maytansinoids. Resistance, innate or acquired, to these drugs could lead to loss of clinical efficacy [137]. It was shown that the chemical structure of the tether can enable the active species to evade efflux mechanisms. Medicinal chemists will always be challenged to discover new chemical warheads that are not efflux substrates, while still displaying the required potency for ADCs. The interaction of medicinal chemists with protein engineers, oncologists, cell biologists, and clinicians will result in better ADCs. These interactions present excellent opportunities to demonstrate that medicinal chemistry is a central science that can provide innovative solutions to the problems currently faced by this fascinating field of scientific endeavor.

References

1. Köhler G, Milstein C (1975) Continuous cultures of fused cells secreting antibody of predefined specificity. Nature 256:495–497
2. Scott AM, Wolchok JD, Old L (2012) Antibody therapy of cancer. Nat Rev Cancer 12:278–287
3. Schrama D, Reiseld RA, Becker JC (2006) Antibody targeted drugs as cancer therapeutics. Nat Rev Drug Discov 5:147–159
4. Saphire EO, Parren PW, Pantophlet R, et al. (2001) Crystal structure of a neutralizing human IGG against HIV-1: a template for vaccine design. Science 293:1155–1159
5. Alley SC, Benjamin DR, Jeffrey SC, et al. (2008) Contribution of linker stability to the activities of anticancer immunoconjugates. Bioconjug Chem 19(3):759–765
6. Shen BQ, Xu K, Liu L, Raab H, et al. (2012) Conjugation site modulates the in vivo stability and therapeutic activity of antibody-drug conjugates. Nat Biotechnol 30(2):184–189
7. Lyon RP, Setter JR, Bovee TD, et al. (2014) Self-hydrolyzing maleimides improve the stability and pharmacological properties of antibody-drug conjugates. Nat Biotechnol 32 (10):1059–1063
8. Tumey LN, Charati M, He T, et al. (2014) Mild method for succinimide hydrolysis on ADCs: impact on ADC potency, stability, exposure, and efficacy. Bioconjug Chem 25:1871–1880
9. Christie RJ, Fleming R, Bezabeh B, et al. (2019) Stabilization of cysteine-linked antibody drug conjugates with N-aryl maleimides. J Control Release 220(Pt B):660–670
10. Badescu G, Bryant P, Bird M, et al. (2014) Bridging disulfides for stable and defined antibody drug conjugates. Bioconjug Chem 25(6):1124–1136
11. Bryant P, Pabst M, Badescu G, et al. (2015) In vitro and in vivo evaluation of cysteine rebridged trastuzumab–MMAE antibody drug conjugates with defined drug-to-antibody ratios. Mol Pharm 12(6):1872–1879
12. Behrens CR, Ha EH, Chinn LL, et al. (2015) Antibody–Drug Conjugates (ADCs) derived from interchain cysteine cross-linking demonstrate improved homogeneity and other pharmacological properties over conventional heterogeneous ADCs. Mol Pharm 12(11):3986–3998

13. Maruani A, Smith ME, Miranda E, et al. (2015) A plug-and-play approach to antibody-based therapeutics via a chemoselective dual click strategy. Nat Commun 6:6645
14. Smith ME, Schumacher FF, Ryan CP, et al. (2010) Protein modification, bioconjugation, and disulfide bridging using bromomaleimides. J Am Chem Soc 132(6):1960–1965
15. Lee MTW, Maruani A, Baker JR, et al. (2016) Enabling the controlled assembly of antibody conjugates with a loading of two modules without antibody engineering. Chem Sci 7:799–802
16. Kashiwagi T, Yokoyama K, Ishikawa K, et al. (2002) Crystal structure of microbial transglutaminase from Streptoverticillium mobaraense. J Biol Chem 277(46):44252–44260
17. Jeger S, Zimmermann K, Blanc A, et al. (2010) Site-specific and stoichiometric modification of antibodies by bacterial transglutaminase. Angew Chem Int Ed Engl 49(51):9995–9997
18. Strop P, Liu SH, Dorywalska M, et al. (2013) Location matters: site of conjugation modulates stability and pharmacokinetics of antibody drug conjugates. Chem Biol 20(2):161–167
19. Rabuka D, Rush JS, deHart GW, et al. (2012) Site-specific chemical protein conjugation using genetically encoded aldehyde tags. Nat Protoc 7(6):1052–1067
20. Agarwal P, Kudirka R, Albers AE, et al. (2013) Hydrazino-Pictet-Spengler ligation as a biocompatible method for the generation of stable protein conjugates. Bioconjug Chem 24:846–851
21. Drake PM, Albers AE, Baker J, et al. (2014) Aldehyde tag coupled with HIPS chemistry enables the production of ADCs conjugated site-specifically to different antibody regions with distinct in vivo efficacy and PK outcomes. Bioconjug Chem 25:1331–1341
22. Kudirka R, Barfield RM, McFarland J, et al. (2015) Generating site-specifically modified proteins via a versatile and stable nucleophilic carbon ligation. Chem Biol 22(2):293–298
23. Okeley NM, Toki BE, Zhang X, et al. (2013) Metabolic engineering of monoclonal antibody carbohydrates for antibody−drug conjugation. Bioconjug Chem 24(10):1650–1655
24. Hamann PR, Hinman LM, Beyer CF, et al. (2005) An anti-MUC1 antibody-calicheamicin conjugate for treatment of solid tumors. Choice of linker and overcoming drug resistance. Bioconjug Chem 16:346–353
25. Zhou Q, Stefano JE, Manning C, et al. (2014) Site-specific antibody-drug conjugation through glycoengineering. Bioconjug Chem 25:510–520
26. Ramakrishnan B, Qasba PK (2002) Structure-based design of β1,4-galactosyltransferase I (β4Gal-T1) with equally efficient N-acetylgalactosaminyltransferase activity: point mutation broadens β4Gal-T1 donor specificity. J Biol Chem 277(23):20833–20839
27. Ramakrishnan B, Boeggeman E, Pasek M, Qasba PK (2011) Bioconjugation using mutant glycosyltransferases for the site-specific labeling of biomolecules with sugars carrying chemical handles. Methods Mol Biol 751:281–296
28. van Geel R, Wijdeven MA, Heesbeen R, et al. (2015) Chemoenzymatic conjugation of toxic payloads to the globally conserved N-glycan of native mAbs provides homogeneous and highly efficacious antibody−drug conjugates. Bioconjug Chem 26(11):2233–2242
29. Dumas A, Lukas L, Christopher D, et al. (2015) Designing logical codon reassignment – expanding the chemistry in biology. Chem Sci 6:50–69
30. Hallam TJ, Wold E, Wahl A, Smider VV (2015) Antibody conjugates with unnatural amino acids. Mol Pharm 12(6):1848–1862
31. Axup JY, Bajjuri KM, Ritland M, et al. (2012) Synthesis of site-specific antibody-drug conjugates using unnatural amino acids. Proc Natl Acad Sci U S A 109(40):16101–16106
32. VanBrunt MP, Shanebeck K, Caldwell Z, et al. (2015) Genetically encoded azide containing amino acid in mammalian cells enables site-specific antibody−drug conjugates using click cycloaddition chemistry. Bioconjug Chem 26(11):2249–2260
33. Wang L, Amphlett G, Blättler WA, et al. (2005) Structural characterization of the maytansinoid−monoclonal antibody immunoconjugate, huN901−DM1, by mass spectrometry. Protein Sci 14:2436–2446
34. Sun MM, Beam KS, Cerveny CG, et al. (2005) Reduction−alkylation strategies for the modification of specific monoclonal antibody disulfides. Bioconjug Chem 16:1282–1290

35. Hamblett KJ, Senter PD, Chace DF, et al. (2004) Effects of drug loading on the antitumor activity of a monoclonal antibody drug conjugate. Clin Cancer Res 10(20):7063–7070
36. Lyons A, King DJ, Owens RJ, et al. (1990) Site-specific attachment to recombinant antibodies via introduced surface cysteine residues. Protein Eng 3(8):703–708
37. Stimmel JB, Merrill BM, Kuyper LF, et al. (2000) Site-specific Conjugation on Serine→Cysteine Variant Monoclonal Antibodies. J Biol Chem 275(39):30445–30450
38. Junutula JR, Raab H, Clark S, et al. (2008) Site-specific conjugation of a cytotoxic drug to an antibody improves the therapeutic index. Nat Biotechnol 26(8):925–932
39. Junutula JR, Bhakta S, Raab H, et al. (2008) Rapid identification of reactive cysteine residues for site-specific labeling of antibody-Fabs. J Immunol Methods 332(1–2):41–52
40. Jeffrey SC, Burke PJ, Lyon RP, et al. (2013) A potent anti-CD70 antibody-drug conjugate combining a dimeric pyrrolobenzodiazepine drug with site-specific conjugation technology. Bioconjug Chem 24:1256–1263
41. Teicher BA, Chari RV (2011) Antibody conjugate therapeutics: challenges and potential. Clin Cancer Res 17(20):6389–6397
42. Dumontet C, Jordan MA (2010) Microtubule-binding agents: a dynamic field of cancer therapeutics. Nat Rev Drug Discov 9(10):790–803
43. Kupchan SM, Komoda Y, Court WA, et al. (1972) Maytansine, a novel antileukemic ansa macrolide from Maytenus ovatus. J Am Chem Soc 94(4):1354–1356
44. Widdison WC, Wilhelm SD, Cavanagh EE, et al. (2006) Semisynthetic maytansine analogues for the targeted treatment of cancer. J Med Chem 49(14):4392–4408
45. Cassady JM, Chan KK, Floss HG, Leistner E (2004) Recent developments in the maytansinoid antitumor agents. Chem Pharm Bull (Tokyo) 52(1):1–26
46. Kupchan SM, Sneden AT, Branfman AR, et al. (1978) Structural requirements for antileukemic activity among the naturally occurring and semisynthetic maytansinoids. J Med Chem 21(1):31–37
47. Pettit GR, Kamano Y, Herald CL, et al. (1987) The isolation and structure of a remarkable marine animal antineoplastic constituent: dolastatin 10. J Am Chem Soc 109(22):6883–6885
48. Pettit GR, Singh SB, Hogan F, et al. (1989) Antineoplastic agents. Part 189. The absolute configuration and synthesis of natural (−)-dolastatin 10. J Am Chem Soc 111(14):5463–5465
49. Bai R, Pettit GR, Hamel E, et al. (1990) Dolastatin 10, a powerful cytostatic peptide derived from a marine animal. Inhibition of tubulin polymerization mediated through the vinca alkaloid binding domain. Biochem Pharmacol 39(12):1941–1949
50. Cormier A, Marchand M, Ravelli RB, et al. (2008) Structural insight into the inhibition of tubulin by vinca domain peptide ligands. EMBO Rep 9(11):1101–1106
51. Pettit GR, Srirangam JK, Barkoczy J, et al. (1998) Antineoplastic agents 365. Dolastatin 10 SAR probes. Anticancer Drug Des 13(4):243–277
52. Miyazaki K, Kobayashi M, Natsume T, et al. (1995) Synthesis and antitumor activity of novel dolastatin 10 analogs. Chem Pharm Bull (Tokyo) 43(10):1706–1718
53. Doronina SO, Toki BE, Torgov MY, et al. (2003) Development of potent monoclonal antibody auristatin conjugates for cancer therapy. Nat Biotechnol 21(7):778–784
54. Doronina SO, Mendelsohn BA, Bovee TD, et al. (2006) Enhanced activity of monomethylauristatin F through monoclonal antibody delivery: effects of linker technology on efficacy and toxicity. Bioconjug Chem 17(1):114–124
55. Maderna A, Doroski M, Subramanyam C, et al. (2014) Discovery of cytotoxic dolastatin-10 analogs with N terminal modifications. J Med Chem 57:10527–10543
56. Maderna A, Leverett CA (2015) Recent advances in the development of new auristatins: structural modifications and application in antibody drug conjugates. Mol Pharm 12 (6):1798–1812
57. Sasse F, Steinmetz H, Heil J, et al. (2000) Tubulysins, new cytostatic peptides from myxobacteria acting on microtubuli. Production, isolation, physico-chemical and biological properties. J Antibiot (Tokyo) 53(9):879–885

58. Höfle G, Glaser N, Leibold T, et al. (2003) Semisynthesis and degradation of the tubulin inhibitors epothilone and tubulysin. Pure Appl Chem 75(2–3):167–178

59. Steinmetz H, Glaser N, Herdtweck E, et al. (2004) Isolation, crystal and solution structure determination, and biosynthesis of tubulysins – powerful inhibitors of tubulin polymerization from myxobacteria. Angew Chem Int Ed Engl 43(37):4888–4892

60. Wipf P, Wang Z (2007) Total synthesis of N^{14}-desacetoxytubulysin H. Org Lett 9(8):1605–1607

61. Patterson AW, Peltier HM, Sasse F, Ellman JA (2007) Design, synthesis, and biological properties of highly potent tubulysin D analogs. Chemistry 13(34):9534–9541

62. Patterson AW, Peltier HM, Ellman JA (2008) Expedient synthesis of N-methyl tubulysin analogues with high cytotoxicity. J Org Chem 73(12):4362–4369

63. Leamon CP, Reddy JA, Vetzel M, et al. (2008) Folate targeting enables durable and specific antitumor responses from a therapeutically null tubulysin B analogue. Cancer Res 68 (23):9839–9844

64. Li J, Perry SR, Muniz-Medina V, et al. (2016) A biparatopic HER2-targeting antibody-drug conjugate induces tumor regression in primary models refractory to or ineligible for HER2-targeted therapy. Cancer Cell 29(1):117–129

65. Toader D, Harper J et al (2015) Discovery of tubulysin payloads for antibody drug conjugates with potent in vitro activity and in vivo efficacy in solid tumor models. Presented at molecular targets and cancer therapeutics, Boston, MA, 5–9 Nov 2015. Mol Cancer Ther 14(12 Suppl 2):Abstract nr B170

66. Lee MD, Ellestad GA, Borders DB (1991) Calicheamicins: discovery, structure, chemistry, and interaction with DNA. Acc Chem Res 24:235–243

67. Zein N, Sinha AM, McGahren WJ, Ellestad GA (1988) Calicheamicin γ_1^I: an antitumor antibiotic that cleaves double-stranded DNA site specifically. Science 240(4856):1198–1201

68. Hinman LM, Hamann PR, Wallace R, et al. (1993) Preparation and characterization of monoclonal antibody conjugates of the calicheamicins: a novel and potent family of antitumor antibiotics. Cancer Res 53(14):3336–3342

69. Hanka LJ, Dietz A, Gerpheide SA, et al. (1978) CC-1065 (NSC-298223), a new antitumor antibiotic. Production, in vitro biological activity, microbiological assays and taxonomy of the producing microorganism. J Antibiot (Tokyo) 31(12):1211–1217

70. Boger DL, Johnson DS (1995) CC-1065 and the duocarmycins: unraveling the keys to a new class of naturally derived DNA alkylating agents. Proc Natl Acad Sci U S A 92(9):3642–3649

71. McGovren JP, Clarke GL, Pratt EA, DeKoning TF (1984) Preliminary toxicity studies with the DNA-binding antibiotic, CC-1065. J Antibiot (Tokyo) 37(1):63–70

72. Boger DL, Ishizaki T, Kitos PA, Suntornwat O (1990) Synthesis of N-(tert-butyloxycarbonyl)-CBI, CBI, CBI-CDPI1, and CBI-CDPI2: enhanced functional analogs of CC-1065 incorporating the 1,2,9,9a-tetrahydrocyclopropa[c]benz[e]indol-4-one (CBI) left-hand subunit. J Org Chem 55(23):5823–5832

73. Wang H, Rangan VS, Sung MC, et al. (2016) Pharmacokinetic characterization of BMS-936561, an anti-CD70 antibody-drug conjugate, in preclinical animal species and prediction of its pharmacokinetics in humans. Biopharm Drug Dispos 37(2):93–106

74. Elgersma RC, Coumans RGE, Huijbregts T, et al. (2015) Design, synthesis, and evaluation of linker-duocarmycin payloads: toward selection of HER2-targeting antibody-drug conjugate SYD985. Mol Pharm 12(6):1813–1835

75. Leimgruber W, Batcho AD, Schenker F (1965) The structure of anthramycin. J Am Chem Soc 87:5793–5795

76. Tozuka Z, Yazawa H, Murata M, Takaya T (1983) Studies on tomaymycin. III. Syntheses and antitumor activity of tomaymycin analogs. J Antibiot (Tokyo) 36(12):1699–1708

77. Brazhnikova MG, Konstantinova NV, Mesentsev AS (1972) Sibiromycin. Isolation and characterization. J Antibiot (Tokyo) 25(11):668–673

78. Hurley LH, Thurston DE (1984) Pyrrolo(l,4)benzodiazepine antitumor antibiotics: chemistry, interaction with DNA, and biological implications. Pharm Res 1(2):52–59

79. Subhas Bose D, Thompson AS, Ching J, et al. (1992) Rational design of a highly efficient irreversible DNA interstrand cross-linking agent based on the pyrrolobenzodiazepine ring system. J Am Chem Soc 114:4939–4941

80. Hartley JA, Spanswick VJ, Brooks N, et al. (2004) SJG-136 (NSC 694501), a novel rationally designed DNA minor groove interstrand cross-linking agent with potent and broad spectrum antitumor activity: Part 1: Cellular pharmacology, in vitro and initial in vivo antitumor activity. Cancer Res 64(18):6693–6699

81. Hartley JA, Hamaguchi A, Coffils M, et al. (2010) SG2285, a novel C2-aryl-substituted pyrrolobenzodiazepine dimer prodrug that cross-links DNA and exerts highly potent antitumor activity. Cancer Res 70(17):6849–6858

82. Hartley JA, Hamaguchi A, Suggitt M, et al. (2010) DNA interstrand cross-linking and in vivo antitumor activity of the extended pyrrolo[2,1-c][1,4]benzodiazepine dimer SG2057. Investig New Drugs 30(3):950–958

83. Howard PW, Chen Z, Gregson SJ, et al. (2009) Synthesis of a novel C2/C2′-aryl-substituted pyrrolo[2,1-c][1,4]benzodiazepine dimer prodrug with improved water solubility and reduced DNA reaction rate. Bioorg Med Chem Lett 19(22):6463–6466

84. Saunders LR, Bankovich AJ, Anderson WC, et al. (2015) A DLL3-targeted antibody-drug conjugate eradicates high-grade pulmonary neuroendocrine tumor-initiating cells in vivo. Sci Transl Med 7(302):302ra136

85. Tolcher AW, Sugarman S, Gelmon KA, et al. (1999) Randomized phase II study of BR96-doxorubicin conjugate in patients with metastatic breast cancer. J Clin Oncol 17(2):478–484

86. Bakker M, Renes J, Groenhuijzen A, et al. (1997) Mechanisms for high methoxymorpholino doxorubicin cytotoxicity in doxorubicin-resistant tumor cell lines. Int J Cancer 73(3):362–366

87. Quintieri L, Geroni C, Fantin M, et al. (2005) Formation and antitumor activity of PNU-159682, a major metabolite of nemorubicin in human liver microsomes. Clin Cancer Res 11(4):1608–1617

88. Mazzini S, Scaglioni L, Mondelli R, et al. (2012) The interaction of nemorubicin metabolite PNU-159682 with DNA fragments d(CGTACG)(2), d(CGATCG)(2) and d(CGCGCG)(2) shows a strong but reversible binding to G:C base pairs. Bioorg Med Chem 20(24):6979–6988

89. Bushnell DA, Cramer P, Kornberg RD (2002) RNA polymerase II cocrystal at 2.8 A resolution. Proc Natl Acad Sci U S A 99:1218–1222

90. Kaplan CD, Larsson KM, Kornberg RD (2008) The RNA polymerase II trigger loop functions in substrate selection and is directly targeted by alpha-amanitin. Mol Cell 30:547–556

91. Brueckner F, Cramer P (2008) Structural basis of transcription inhibition by alpha-amanitin and implications for RNA polymerase II translocation. Nat Struct Mol Biol 15:811–818

92. Letschert K, Faulstich H, Keller D, Keppler D (2006) Molecular characterization and inhibition of amanitin uptake into human hepatocytes. Toxicol Sci 91:140–149

93. Faulstich H, Fiume L (1985) Protein conjugates of fungal toxins. Methods Enzymol 112:225–237

94. Moldenhauer G, Salnikov AV, Lüttgau S, et al. (2012) Therapeutic potential of amanitin-conjugated anti-epithelial cell adhesion molecule monoclonal antibody against pancreatic carcinoma. J Natl Cancer Inst 104(8):622–634

95. Liu Y, Zhang X, Han C, et al. (2015) TP53 loss creates therapeutic vulnerability in colorectal cancer. Nature 520(7549):697–701

96. Hechler T, Kulke M, Mueller C et al (2014) Amanitin-based antibody-drug conjugates targeting the prostate-specific membrane antigen. Poster presented at annual meeting of the American Association for Cancer Research, San Diego, CA, 5–9 Apr 2014. Cancer Res 74(19 Suppl):Abstract nr 664

97. Wall ME, Wani MC, Cook CE, et al. (1966) Plant antitumor agents. I. The isolation and structure of camptothecin, a novel alkaloidal leukemia and tumor inhibitor from Camptotheca acuminate. J Am Chem Soc 88:3888–3890

98. Hsiang YH, Hertzberg R, Hecht S, Liu LF (1985) Camptothecin induces protein-linked DNA breaks via mammalian DNA topoisomerase I. J Biol Chem 260:14873–14878

99. Staker BL, Hjerrild K, Feese MD, et al. (2002) The mechanism of topoisomerase I poisoning by a camptothecin analog. Proc Natl Acad Sci U S A 99(24):15387–15392

100. Moon SJ, Govindan SV, Cardillo TM, et al. (2008) Antibody conjugates of 7-ethyl-10-hydroxycamptothecin (SN-38) for targeted cancer chemotherapy. J Med Chem 51:6916–6926

101. Ogitani Y, Yamaguchi J, Ishii C et al (2015) DS-8201a, a novel HER2-targeting ADC with a novel DNA topoisomerase I inhibitor, demonstrates a potent anti-tumor efficacy with differentiation from T-DM1 in preclinical studies. Poster presented at international conference: molecular targets and cancer therapeutics, Boston, MA, 5–9 Nov 2015. Mol Cancer Ther 14 (12 Suppl 2):Abstract nr A145

102. Tamura K, Shitara K, Naito Y, et al. (2016) Single agent activity of DS-8201a, a HER2-targeting antibody-drug conjugate, in breast cancer patients previously treated with T-DM1: phase 1 dose escalation. Ann Oncol 27(suppl 6):LBA17

103. Rock BM, Tometsko ME, Patel SK, et al. (2015) Intracellular catabolism of an antibody drug conjugates with a noncleavable linker. Drug Metab Dispos 43:1341–1344

104. Hamblett KJ, Jacob AP, Gurgel JL, et al. (2015) SLC46A3 is required to transport catabolites of noncleavable antibody maytansine conjugates from the lysosome to the cytoplasm. Cancer Res 75(24):5329–5340

105. Pillow TH, Tien J, Parsons-Reponte KL, et al. (2014) Site-specific trastuzumab maytansinoid antibody-drug conjugates with improved therapeutic activity through linker and antibody engineering. J Med Chem 57:7890–7899

106. Dubowchik GM, Walker MA (1999) Receptor-mediated and enzyme-dependent targeting of cytotoxic anticancer drugs. Pharmacol Ther 83:67–123

107. Saito G, Swanson JA, Lee KD (2003) Drug delivery strategy utilizing conjugation via reversible disulfide linkages: role and site of cellular reducing activities. Adv Drug Deliv Rev 55:199–215

108. Hamann PR, Hinman LM, Hollander I, et al. (2002) Gemtuzumab ozogamicin, a potent and selective anti-CD33 antibody-calicheamicin conjugate for treatment of acute myeloid leukemia. Bioconjug Chem 13(1):47–58

109. Dubowchik GM, Firestone RA, Padilla L, et al. (2002). Bioconjug Chem 13(4):855–869

110. Yu SF, Zheng B, Go M, et al. (2015) A novel anti-CD22 anthracycline-based antibody-drug conjugate (ADC) that overcomes resistance to auristatin-based ADCs. Clin Cancer Res 21 (14):3298–3306

111. Lyon RP, Bovee TD, Doronina SO, et al. (2015) Reducing hydrophobicity of homogeneous antibody-drug conjugates improves pharmacokinetics and therapeutic index. Nat Biotechnol 33(7):733–735

112. Albin N, Massaad L, Toussaint C, et al. (1993) Main drug metabolizing enzyme systems in human breast tumors and peritumoral tissues. Cancer Res 53:3541–3546

113. Jeffrey SC, Andreyka JB, Bernhardt SX, et al. (2006) Development and properties of beta-glucuronide linkers for monoclonal antibody-drug conjugates. Bioconjug Chem 17:831–840

114. Jeffrey SC, Nguyen MT, Moser RF, et al. (2007) Minor groove binder antibody conjugates employing a water soluble beta-glucuronide linker. Bioorg Med Chem Lett 17:2278–2280

115. Burke PJ, Hamilton JZ, Pires TA, et al. (2016) Development of novel quaternary ammonium linkers for antibody-drug conjugates. Mol Cancer Ther 15(5):938–945

116. Wu G, Fang YZ, Yang S, et al. (2004) Glutathione metabolism and its implications for health. J Nutr 134(3):489–492

117. Kellogg BA, Garrett L, Kovtun Y, et al. (2011) Disulfide-linked antibody-maytansinoid conjugates: optimization of in vivo activity by varying the steric hindrance at carbon atoms adjacent to the disulfide linkage. Bioconjug Chem 22(4):717–727

118. Erickson HK, Park PU, Widdison WC, et al. (2006) Antibody-maytansinoid conjugates are activated in targeted cancer cells by lysosomal degradation and linker-dependent intracellular processing. Cancer Res 66:4426–4433

119. Sadekar S, Figueroa I, Tabrizi M (2015) Antibody drug conjugates: application of quantitative pharmacology in modality design and target selection. AAPS J 17(4):828–836
120. Smith LM, Nesterova A, Alley SC, et al. (2006) Potent cytotoxicity of an auristatin-containing antibody-drug conjugate targeting melanoma cells expressing melanotransferrin/p97. Mol Cancer Ther 5(6):1474–1482
121. Law CL, Cerveny CG, Gordon KA, et al. (2004) Efficient elimination of B-lineage lymphomas by anti-CD20-auristatin conjugates. Clin Cancer Res 10:7842–7851
122. Okeley NM, Miyamoto JB, Zhang X, et al. (2010) Intracellular activation of SGN-35, a potent anti-CD30 antibody-drug conjugate. Clin Cancer Res 16(3):888–897
123. Sutherland MS, Sanderson RJ, Gordon KA, et al. (2006) Lysosomal trafficking and cysteine protease metabolism confer target-specific cytotoxicity by peptide-linked anti-CD30-auristatin conjugates. J Biol Chem 281(15):10540–10547
124. Petersdorf SH, Kopecky KJ, Slovak M, et al. (2013) A phase 3 study of gemtuzumab ozogamicin during induction and postconsolidation therapy in younger patients with acute myeloid leukemia. Blood 121(24):4854–4860
125. Senter PD, Sievers EL (2012) The discovery and development of brentuximab vedotin for use in relapsed Hodgkin lymphoma and systemic anaplastic large cell lymphoma. Nat Biotechnol 30(7):631–637
126. Younes A, Bartlett NL, Leonard JP, et al. (2010) Brentuximab vedotin (SGN-35) for relapsed CD30-positive lymphomas. N Engl J Med 363:1812–1821
127. Fanale MA, Forero-Torres A, Rosenblatt JD, et al. (2012) A phase I weekly dosing study of brentuximab vedotin in patients with relapsed/refractory CD30-positive hematologic malignancies. Clin Cancer Res 18:248–255
128. Pro B, Advani R, Brice P, et al. (2012) Brentuximab vedotin (SGN-35) in patients with relapsed or refractory systemic anaplastic large-cell lymphoma: results of a phase II study. J Clin Oncol 30(18):2190–2196
129. Lambert JM, Chari RV (2014) Ado-trastuzumab Emtansine (T-DM1): an antibody-drug conjugate (ADC) for HER2-positive breast cancer. J Med Chem 57:6949–6964
130. Krop IE, Beeram M, Modi S, et al. (2010) Phase I study of trastuzumab−DM1, an HER2 antibody−drug conjugate, given every 3 weeks to patients with HER2-positive metastatic breast cancer. J Clin Oncol 28:2698–2704
131. LoRusso PM, Weiss D, Guardino E, Girish S, Sliwkowski MX (2011) Trastuzumab emtansine: a unique antibody-drug conjugate in development for human epidermal growth factor receptor 2-positive cancer. Clin Cancer Res 17(20):6437–6447
132. Verma S, Miles D, Gianni L, et al. (2012) Trastuzumab emtansine for HER2-positive advanced breast cancer. N Engl J Med 367(19):1783–1791
133. Diamantis N, Banerji U (2016) Antibody-drug conjugates – an emerging class of cancer treatment. Br J Cancer 114(4):362–367
134. Smaglo BG, Aldeghaither D, Weiner LM (2014) The development of immunoconjugates for targeted cancer therapy. Nat Rev Clin Oncol 11(11):637–648
135. Hinrichs MJ, Dixit R (2015) Antibody drug conjugates: nonclinical safety considerations. AAPS J 17(5):1055–1064
136. Polakis P (2016) Antibody drug conjugates for cancer therapy. Pharmacol Rev 68(1):3–19
137. Shefet-Carasso L, Benhar I (2015) Antibody-targeted drugs and drug resistance-challenges and solutions. Drug Resist Updat 18:36–46

Isoform Selective PI3K Inhibitors for Treating Cancer

Steven T. Staben

Abstract The PI3K/AKT pathway is one of the most frequently altered in cancer and several promising small-molecule inhibitors of this pathway have entered advanced stages of clinical research. This chapter intends to highlight substantial medicinal chemistry lead identification and optimization efforts that led to the discovery of key isoform- and PIK family-selective PI3K inhibitors. Coverage is given for those disclosed PI3K isoform-selective inhibitors that have entered clinical trials in oncology, regardless of their current status. Where possible based on existing information, a focus is placed on discussion of potential structural rationale for isoform selectivity.

Keywords Isoform selectivity, Kinase inhibitors, PI3K, Structure based design

Contents

S.T. Staben (✉)
Discovery Chemistry, Genentech Inc., 1 DNA Way, South San Francisco, CA 94080, USA
e-mail: staben.steven@gene.com

Abbreviations

AE   Adverse event
AI   Aromatase inhibitor
AKT   Protein kinase B
AUC   Area under the curve
CaCo   Heterogeneous human epithelial colorectal adenocarcinoma cells
CI   Confidence interval
Cl_{hep} Predicted hepatic clearance
Cl_{int} Intrinsic clearance
CLL   Chronic lymphocytic leukemia
Cl_p Plasma clearance
DNA-PK   DNA-dependent protein kinase
ER   Estrogen receptor
FDG-PET   Fluorodeoxyglucose positron emission tomography
FL   Follicular lymphoma
HEP   Hepatocytes
HER2   Receptor tyrosine protein kinase ErbB2
HR   Hazard ratio
HR+   Hormone receptor positive
HTS   High throughput screen
LLE   Lipophilic ligand efficiency
LM   Liver microsomes (H, human; R, rat; M, mouse)
MDCK   Madin-Darby canine kidney cells
mPFS   Median progression free survival
MTD   Maximum tolerated dose
mTOR   Mechanistic target of rapamycin
ORR   Overall response rate
pAKT   Phosphorylated protein kinase B
P_{app} Apparent passive permeability
PI3K   Phosphatidylinositide-3-kinase
PIK   Phosphoinositide kinases
PIP2   Phosphatidylinositol-4,5-bisphosphonate
PIP3   Phosphatidylinositol (3,4,5)-triphosphate
p-loop   Phosphate-binding loop (glycine-rich loop)
PR   Partial response
pRTK   Phosphorylated receptor tyrosine protein kinase
PTEN   Phosphatase and tensin homologue
Ras   Rat sarcoma
RTK   Receptor tyrosine protein kinase
SH2   Src homology domain
SLL   Small lymphocytic lymphoma
TPSA   Topological polar surface area
UDP   Uridine diphosphate

UDGPA   Uridine 5′-diphosphoglucuronic acid
VPS34   Vacuolar sorting protein-34

1 Introduction

There are four isoforms of phosphatidylinositide-3-kinase (PI3K) referred to as PI3Kα, -β, -δ, and -γ. These Class-I PI3Ks exist as heterodimers between catalytic p110 isoforms (α, β, δ, γ) and regulatory subunits (i.e., p85α, p50α, p85β, p55γ). The Class-I PI3Ks have proven to play a crucial role in signaling networks that promote cell growth and survival [1, 2]. All PI3K isoforms propagate a signaling cascade by phosphorylation of PIP2 (phosphatidylinositol-4,5-bisphosphonate) to PIP3 (phosphatidylinositol (3,4,5)-triphosphate). The lipid messenger PIP3 mediates activation of several downstream protein kinases, including promoting phosphorylation and activation of AKT.

The summation of over 20 years of preclinical and clinical investigation supports the importance of phosphoinositol-3-kinases in oncology. As may be expected based on their cellular function, activation of the PI3K/AKT pathway is a frequent event in human tumors. This activation can be achieved by several mechanisms. Somatic loss of PTEN, upregulation of upstream RTKs, and genetic modification of PI3K itself can lead to pathway dysregulation [3]. PIK3CA (the gene that encodes for p110α) itself is found to be mutated in a high percentage of a number of cancers [3, 4]. For example, in a study of 452 patients with unilateral invasive primary breast cancer, PIK3CA mutations were identified in 151 tumors (33.4%) [5].

Most early PI3K inhibitors that entered clinical investigation for oncology indications were pan-isoform PI3K inhibitors, many of which also inhibited other PIK-family members (PIK: phosphatidylinositol kinases, e.g. mTOR, DNA-PK, see the chapter "Modulation of the DNA Damage-Response by Inhibitors of the Phosphatidylinositol 3-Kinase Related Kinase (PIKK) Family"). The clinical efficacy of these pan-isoform PI3K inhibitors has been described as "modest at best" [6]. Pivotal Ph-II and -III results from pictilisib (GDC-0941) and buparlisib (BKM-120) in mBC are informative as these are perhaps the most advanced pan-isoform PI3K inhibitors in patients.

pictilisib
GDC-0941

buparlisib
BKM-120
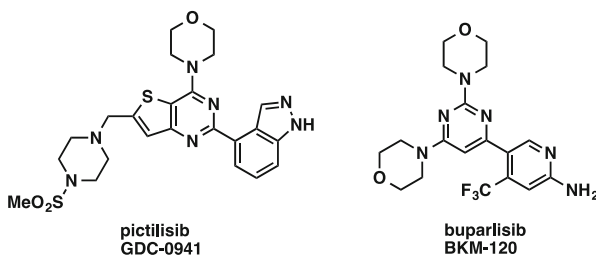
Both studies are promising and provide proof-of-concept for PI3K inhibition in breast cancer, however, the changes in median progression free survival (mPFS) and overall response rate (ORR) were not as substantial as hoped. In late 2014, the

results of pictilisib in combination with fulvestrant vs. fulvestrant plus placebo in patients with AI-resistant ER+ advanced or metastatic breast cancer were reported (168 total patients, "FERGI" trial [7]). In analysis of the full population, addition of pictilisib to fulvestrant was associated with an mPFS improvement from 3.8 to 6.2 mo (HR, 0.77; 95% CI, 0.50–1.19). In 2015, the results of a phase III investigation of buparlisib in combination with fulvestrant vs. fulvestrant plus placebo in patients with HR+/HER- AI-resistant advanced breast cancer were reported (1,147 patients, "BELLE-2" trial [8]). In analysis of the full population, addition of buparlisib to fulvestrant was associated with an mPFS (median progression free survival) improvement from 5.0 to 6.9 mo (HR, 0.78; $P < 0.001$). The overall response rate (ORR) for the treated vs. control group in the total population was 11.8% vs 7.7%.

One hypothesis for the modest mPFS and ORR for these agents (and others) is the exposure, and thus efficacy, of pan-PI3K inhibitors is limited by toxicity associated with the simultaneous inhibition of multiple PI3K isoforms. Common human adverse events resulting from pan-PI3K inhibition are hyperglycemia, maculopapular rash, gastrointestinal intolerance (anorexia, nausea, vomiting, dyspepsia, severe diarrhea/colitis), and stomatitis [9]. Although not transformative for many patients, clinical efficacy for these pan-inhibitors has been observed and has supported further investigation of clinical PI3K inhibitors.

Despite similar structure and catalytic function, preclinical observations of different mechanisms of activation, tissue localization, and phenotypes resultant from genetic alteration suggest distinct native physiological roles of each PI3K isoform [3]. Thus, a diverse pharmacology/toxicity is likely associated with inhibition of specific isoforms. p110α and p110β are ubiquitously expressed in normal tissues. Correspondingly, homozygous genetic loss of p110α or β in mice results in embryonic lethality [10, 11]. Even heterozygous mice expressing one copy each of kinase dead and wild-type p110α show metabolic defects including reduced body weight, insulin resistance, and increased adiposity [12]. p110δ and p110γ are primarily restricted to leukocytes. Deletion of p110δ and p110γ leads to viable mice, but they have immune deficiencies. For example, p110δ was shown to play a critical role in B cell homeostasis and function [13] and p110γ was shown important in thymocyte development, T-cell activation, and neutrophil migration [14]. p110δ kinase-dead knock-in mice show impaired immune responses and develop inflammatory bowel disease [15].

Whilst predicted to have efficacy in broad tumor types, the above-mentioned preclinical and clinical toxicities associated with pan-PI3K inhibition may limit the therapeutic index of pan-PI3K inhibitors. The development of isoform-selective PI3K inhibitors may thus improve therapeutic outcomes as single agents or in combination. There is great interest in the clinical study of selective PI3Kα inhibitors in cancers with PIK3CA mutations, PI3Kβ inhibitors in tumors with PTEN loss and PI3Kδ in hematological malignancies. Several of these "next generation" isoform-selective PI3K inhibitors are expanding the understanding and re-invigorating the enthusiasm of therapeutic intervention within this pathway. This chapter intends to highlight the significant medicinal chemistry efforts leading to isoform- and PIK family- selective PI3K inhibitors that entered clinical trials in oncology.

2 Structural Biology

Drug discovery programs directed at PI3-kinases have been highly enabled through analysis of ligand-bound and apo X-ray structures of catalytic p110 subunits alone. It is apparent that most drug discovery programs, regardless of targeted isoform selectivity profile, initially relied on the well precedented p110γ co-crystallization system of Walker et al. [16, 17]. Homology models for other isoforms derived from these p110γ structures were also utilized. Reports of X-ray structures for the p110 subunits of the α [18–20], β [21], and δ [22] isoforms have been of more recent value for designing and/or rationalizing isoform selective inhibitors.

2.1 Domains of p110 and Interaction with Regulatory Domains

Class IA (PI3Kα, β, δ) and class IB (PI3Kγ) PI3Ks possess multi-domain catalytic p110 subunits. For reference, an X-ray structure and the domain sequence architecture of p110α (PDB-id 4JPS) are displayed in Fig. 1 [23]. Class 1A p110s include an adapter binding domain (ABD), a Ras binding domain (RBD), a C2 domain, a helical domain, and a kinase domain. The class 1B p110γ shares similar structural features, however lacks an ABD at the N-terminus. The kinase domain (magenta Fig. 1) is mechanistically responsible for the primary function of the PI3Ks: ATP-mediated phosphorylation of membrane localized phosphatidylinositol-4,5-bisphosphonate (PIP2) to phosphatidylinositol (3,4,5)-triphosphate (PIP3). The
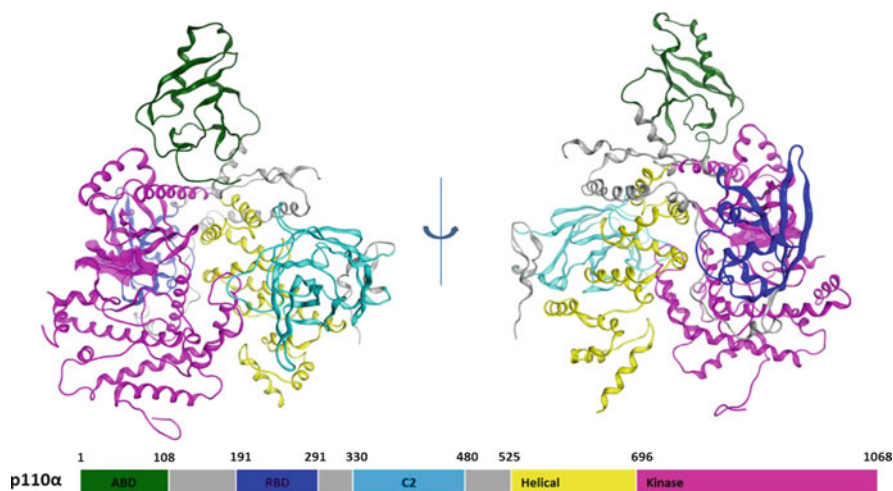
Fig. 1 Ribbon diagram of the p110α structure (2.2 Å resolution, PDB-id 4JPS) highlighting the different domains of this catalytic subunit [23]. The ATP-binding site of the kinase domain (magenta) occupied by BYL-719 is shown as the magenta solvent-accessible surface. Domain boundaries adapted from Huang et al. [18]

kinase domain is the site of action of all clinical PI3K inhibitors which act ATP-competitive.

As noted above, PI3Ks exist as heterodimers between catalytic subunits (p110) and regulatory subunits (p85 and splice variants p55, p50). There are multiple mechanisms hypothesized for activating and localizing PI3Ks at the membrane where PIP2 is located. Binding to pRTKs, RAS superfamily members, GPCRs, Gβγ subunits, and plasma membrane have all been proposed as important depending on stimulus and PI3K isoform invoked [24]. The specific manners of activation and localization are structurally dependent on the different domains of p110 isoforms as well as regulatory subunits that are associated as part of the heterodimeric PI3K complex. The regulatory subunits contain SH2 (Src homology 2) domains thought to interact with RTKs in response to RTK auto-phosphorylation generated by ligand stimulus. It is hypothesized that these pRTK (and/or membrane) interactions are a major mechanism to achieve active and localized p110 subunits. In all reported structures of p110 isoforms, the DFG and αC-helix are "in" suggesting a persistent catalytically active state of p110. This may be consistent with the hypothesis that PI3K activity is controlled primarily by co-peptide binding (i.e., pRTKs, Ras) and co-localization at the membrane with PIP2.

Although a complete structure of a heterodimer has not been disclosed, a model for p110/p85 interaction can be built based on aligned overlays of partial structures. Shown in Fig. 2 is an overlay of structures containing full p110α and p110β with partial p85 fragments [19, 21]. From this model, positioning of the inter-, n-terminal, and c-terminal SH2 domains can be approximated. The regulatory p85 makes extensive contacts with different domains of p110; in particular, a significant contact along the spine of the i-SH2. Contacts between the n- and c-SH2 domains are predicted to be mediated by only a few residues. It is believed that the n-terminal and/or c-terminal SH2 domains are substantially displaced upon pRTK binding. It is interesting to note that two hotspot mutations of p110α (H1047R and E545K, shown in red), as well as many others reported in the literature, occur at or near the interface of the n- and c-SH2 domains of p85 [4].

2.2 Structural Features of the ATP Site and Inhibitors

A number of different chemotypes have been discovered to selectively inhibit PI3-kinases. There are some general features of the ATP-binding site that are typically exploited for potency and/or selectivity. A representation of the key features of the ATP binding site is shown schematically in Fig. 3. The N- and C-lobes of p110 subunits for the ATP pocket and solvent access occurs between the lower hinge and p-loop/kβ3 strand (kβ3 = kinase beta 3, nomenclature adapted from Walker [16]). Three key isoform-conserved residues border the adenine pocket: a hinge valine, a gatekeeper isoleucine, and a tyrosine residue. PI3K inhibitors necessitate a hydrogen bond from this valine hinge residue. Interestingly, as opposed to many other kinase inhibitors, single- rather than dual- interaction with this valine residue is common for PI3K inhibitors. The phosphate binding pocket ("affinity pocket"; Berndt [22]) is lined, as typical across the kinome, with a

Fig. 2 Aligned overlay of X-ray structures of niSH2-p85α/p110α (PDB-id: 4L23) and ciSH2-p85β/p110β (2Y3A) [19, 21]. The p110α and p110β subunits are represented by *dark gray* and *light gray ribbon* diagram, respectively. The niSH2-p85α is represented by *dark blue ribbon*; the ciSH2-p85β is colored *magenta*. Key residues H1047 and E545 of p110α (highlighted *red*) likely influence contact with the cSH2 and nSH2 domains of p85α
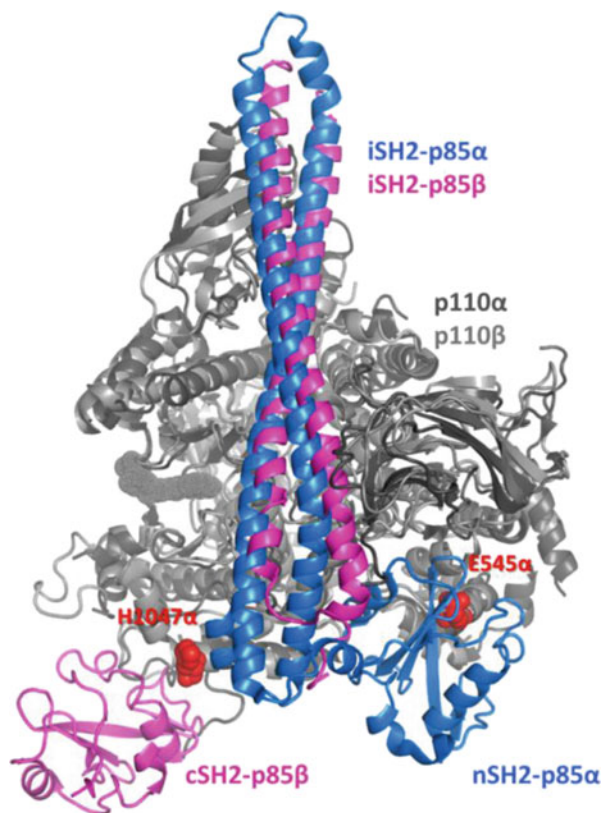
catalytic lysine and an acidic residue projecting from the αC-helix (aspartate in the case of p110s). Many PI3K inhibitors fill this pocket directly or indirectly (through water) interacting with the tyrosine, lysine, and/or aspartate residues. Many inhibitors also occupy a hydrophobic pocket on the N-lobe side of the ribose pocket. Lipophilic substitution of the ligand here is enclosed by isoform-conserved hydrophobic amino acid side-chains (catalytic lysine Cα-Cγ methylenes, proline, and methionine from the kβ4 strand and an isoleucine from the kβ5 strand; residues not shown). With little exception [25], isoform selective or specific inhibitors primarily take advantage of structural differences in the lower hinge (C-lobe) or kβ3/kβ4 strands (N-lobe, discussed below). Representative in Fig. 3 is a schematic representation of clinical PI3K-inhibitor BYL719 is mapped onto the above description of key binding features. The aminothiazole contacts the hinge, polar and hydrophobic interactions are achieved from the 4-pyridyl and substituents. Isoform selectivity is achieved through interaction with the lower hinge (discussed later).

Representative of all p110 isoforms, the ATP-binding site of p110γ (PDB-id 3DBS) in complex with pan-PI3K inhibitor GDC-0941 (pictilisib) is shown in Fig. 4. The key isoform-conserved residues within the binding site, mentioned above, are highlighted (hinge Val882γ, catalytic Lys833γ, αC-helix Asp841γ, and the DFG motif). A series of β-strands (kβ3–kβ7) forms the N-lobe of the ATP-binding site, as typical for protein kinases. The formal gatekeeper residue in
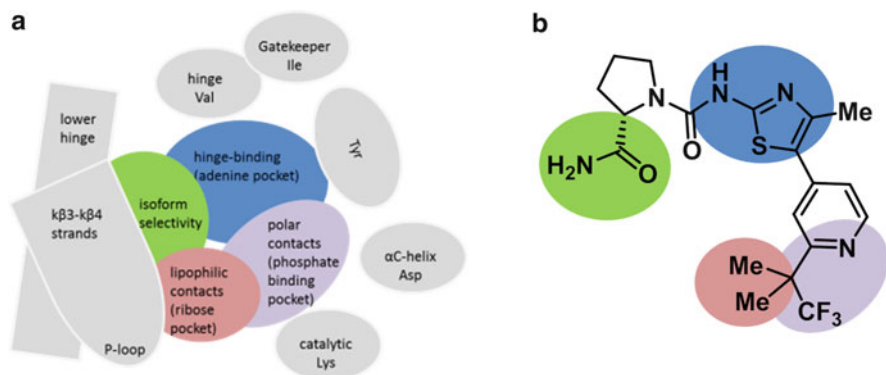
Fig. 3 (**a**) Schematic representation of key residues and features of the ATP binding site of catalytic p110 subunits (*gray*) and typical features of ligands (*multicolored*). (**b**) Ligand features mapped on to PI3Kα-selective inhibitor BYL719
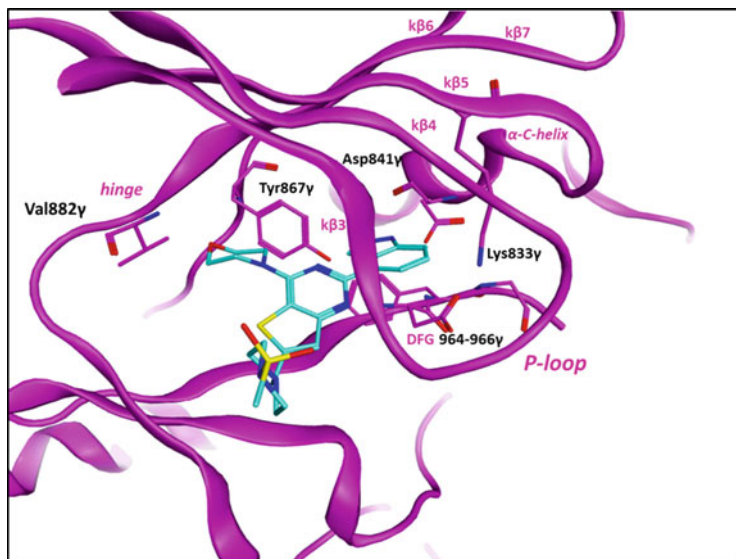
Fig. 4 X-ray structure of GDC-0941 (*blue*) bound to p110γ (*magenta*) [PDB-id: 3DBS] [26]. Key conserved residues across p110 isoforms are labelled with *black text*; key motifs are highlighted in *magenta text*.

all p110 isoforms is an isoleucine (Ile879γ, not shown). However, due to a change in orientation of the kβ7 strand (kinase beta strand 7) leading to the hinge, Tyr876γ (on the kβ6 strand, conserved across isoforms) acts as a functional gatekeeper. We hypothesize that this change in strand orientation accommodates ligands with non-aromatic, sterically encumbering hinge-binding motifs (i.e., the morpholine of GDC-0941). This may lead to a greater volume for ligand binding and may
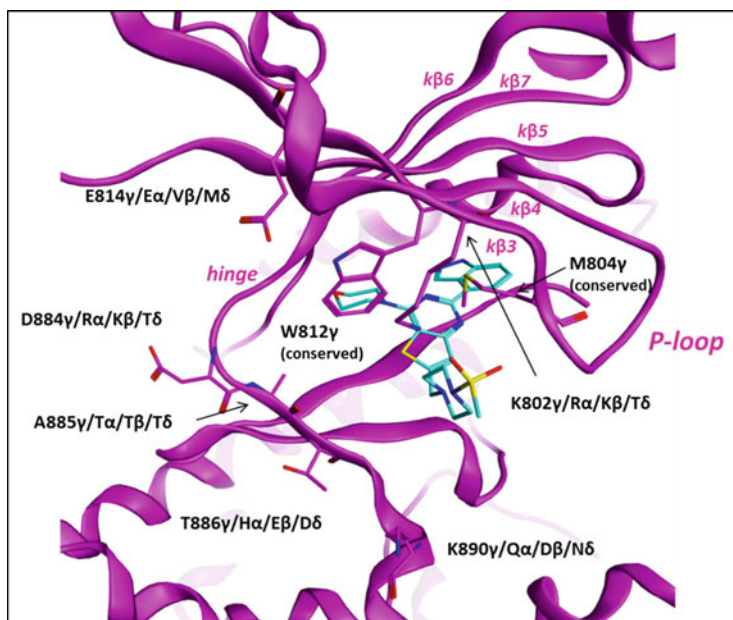
Fig. 5 X-ray structure of GDC-0941 (*blue*) bound to p110γ (*magenta*) [PDB-id: 3DBS] [26]. Residues on the kβ3/kβ4 strands and lower hinge that have been hypothesized to aid in isoform selective inhibition are labelled in *black text*

explain the relative ease of attaining selectivity for PIK family members over the broad kinome by PI3K inhibitors.

Despite a high degree of homology among the isoforms, there are notable differences in primary structure and amino acid sidechain mobility within the lower hinge and kβ3/kβ4 strands. Most isoform selective inhibitors reported were designed for (or later rationalized by) exploitation of these particular differences. Key differences in primary structure on the kβ3/kβ4 strands and lower hinge are labelled in Fig. 5 (GDC-0941 in p110γ). For example, a difference in residue Lys809γ (Gln859α, Asp856β, Asn836δ) is believed to key in a mechanism of selectivity for NVP-BYL-719 (selective interaction with Gln859α; Furet [23]). It has been hypothesized that mobility/flexibility of conserved Met804γ and Trp812γ contribute to the selectivity of inhibitors. These differences have been used to rationalize PI3Kβ [27] and PI3Kδ [22] selective inhibitors, as well as those that spare inhibition of PI3Kβ [28].

3 Tabulated Selectivity Data for Isoform Selective PI3K Inhibitors

Inhibitors discussed in this chapter are presented in Table 1. Activity against the different PI3K isoforms is reported as disclosed by the various discovery teams.

Table 1 Biochemical activity against Class-I PI3K isoforms for inhibitors detailed in this chapter

Clinical compound	Primary PI3K isoform target (IC$_{50}$ or K$_i$)	Normalized selectivity relative to primary target				Reference
		PI3Kα	PI3Kβ	PI3Kδ	PI3Kγ	
Cal-101	PI3Kδ (19 nM)	453x	211x	1x	111x	[29]
IPI-145	PI3Kδ (2.5 nM)	641x	34x	1x	11x	[30]
SAR260301	PI3Kβ (23 nM)	67x	1x	20x	>435x	[31]
GSK2636771	PI3Kβ (5 nM)	>1,160x	1x	12x	>2,520x	[32]
AZD8186	PI3Kβ (4 nM)	9x	1x	3x	169x	[33]
GDC0032	PI3Kα (0.29 nM)	1x	31x	0.4x	3.3x	[34]
CH5132799	PI3Kα (14 nM)	1x	9x	36x	3x	[35]
AZD8835	PI3Kα (6.2 nM)	1x	72x	0.9x	15x	[36]
BYL719	PI3Kα (5 nM)	1x	240x	58x	50x	[23]
INK1117	PI3Kα (15 nM)	1x	300x	927x	127x	[37]

4 Medicinal Chemistry: Discoveries Leading to Isoform Selective PI3K Inhibitors

4.1 PI3Kδ Inhibitors

The most efficacious single-agent PI3K inhibitors to date are those of that selectively target PI3Kδ in hematological malignancies, including US FDA approved Zydelig®. Notably, dramatic responses are observed even though genetic alteration of the PI3K pathway in these patients is not present. The compounds block signaling downstream of the B-cell receptor [13], thus targeting dysfunctional leukemic B-cells.

4.1.1 Cal-101 (GS-1101, Idelalisib, Zydelig®), PI3Kδ Inhibitor

Idelalisib (Cal-101, GS-1101, compound **1**, Scheme 1), originally discovered by Icos Corporation, entered clinical trials in 2008 and was approved under the trade name Zydelig® by the FDA in 2014 for relapsed CLL, FL, and SLL. Idelalisib is reported to have high isoform selectivity for PI3Kδ over the other Class-1 isoforms [29]. Despite being the most advanced and only approved PI3K inhibitor, very little has been published related to the medicinal chemistry effort that led to this groundbreaking compound.

The structure of idelalisib is exemplified in a 2005 patent application from Icos Corporation where they disclose a series of quinazolinone inhibitors of PI3Kδ

1
Cal-101, GS-1101
idelalisib, Zydelig™
PI3Kα IC$_{50}$ = 2600 nM
PI3Kβ IC$_{50}$ = 4000 nM
PI3Kδ IC$_{50}$ = 19 nM
PI3Kγ IC$_{50}$ = 2100 nM

δ isoform selectivity:
α/δ = 453x, β/δ = 211x, γ/δ = 111x
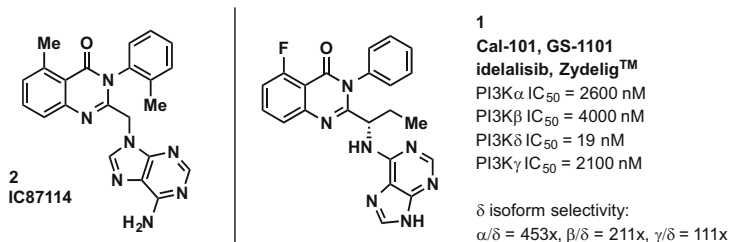
Scheme 1 Chemical structures of IC87114 and idelalisib. Biochemical data from Somoza et al. [29]
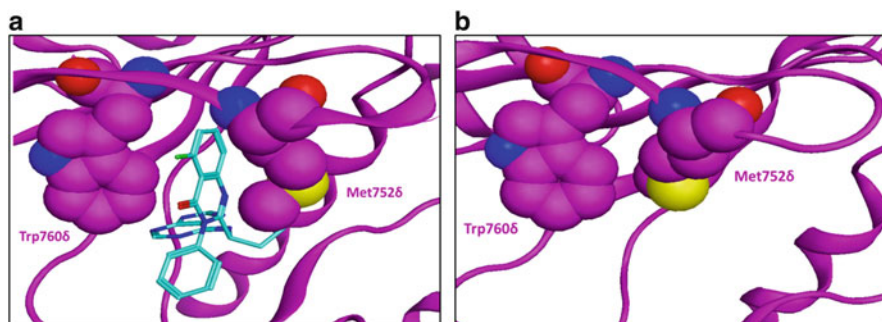
Fig. 6 Induced fit binding of "T-shaped" PI3Kδ inhibitors exemplified by idelalisib (**1**). (**a**) p110δ in complex with idelalisib (4XE0). (**b**) p110δ apo structure (pdb id 2WXR). A reorganization of residues on the kβ3 and kβ4 strands (p-loop) is required for binding to idelalisib

[38]. An earlier structurally related compound, compound **2**, was reported by Icos to be a "close analog" of a compound identified from a screen of their diverse chemical matter. It is presumed that this was a lead that resulted in the discovery of idelalisib (**1**).

The crystal structure of idelalisib in p110δ was recently disclosed [29] confirming the hypothesized binding mode [22]. Most PI3Kδ selective inhibitors possess a unique three dimensional architecture compared to pan-PI3K inhibitors, commonly referred to as "propeller" or "T-shaped." In a seminal publication containing the first crystal structures of p110δ, Berndt et al. [22] proposed that selectivity for PI3Kδ was achieved for this class of inhibitors through exploitation of a differential conformational flexibility and sequence identity of active-site residues that aren't important for ATP binding. This conformational mobility can be visualized in Fig. 6 through examination of the induced fit binding of compound **1** to p110δ (pdb id: 4XE0, Somoza et al. [29]) compared to the p110δ apo structure (pdb id: 2WXR, Berdnt et al. [22]). The adenine of compound **1** exists in the expected plane bisecting the N- and C-lobes of p110δ. Consistent with many

other PI3Kδ selective inhibitors, this inhibitor appears to interact with the hinge-valine and does not appear to directly make any contacts to conserved residues in the phosphate binding pocket. The quinazolinone is oriented orthogonal to this plane and occupies a region between a tryptophan and methionine residues that are conserved among the isoforms. This occupied pocket doesn't exist in the apo form of p110δ (or other isoforms) and Berdnt et al. hypothesize this conformational flexibility is more facile in p110δ compared to the other isoforms.

This inhibitor is an exciting treatment for patients with relapsed refractory CLL. For example, in a phase III study of idelalisib in combination with rituximab vs. rituximab alone, patients receiving idelalisib had improved overall response rates (81% vs. 13%) and overall survival at 12 months (92% vs. 80%, Furman et al. [39]).

4.1.2   INK-1197 (IPI-145, Duvelisib), PI3Kδ/γ Inhibitor

In 2011, INK-1197 (**3**) entered a phase I dose escalation in patients with advanced hematological malignancies. The structure of INK-1197 is exemplified in a 2009 application from Intellikine [40] and acknowledged first as the clinical candidate in a 2013 research publication [30]. INK-1197 was renamed as IPI-145 when licensed to Infinity in 2011. Infinity has subsequently partnered with Abbvie to co-develop this inhibitor which recently entered phase III clinical trials in patients with hematological malignancies.

There hasn't been any information disclosed about the optimization of this compound. The quinazolone of idelalisib (**1**) is replaced with an isoquinolone (Scheme 2).

The compound **3** has been claimed to be differentiated from idelalisib (**1**) on the basis of improved activity against the PI3Kγ isoform. Although structurally similar, **3** possesses greater dual activity against PI3Kδ and PI3Kγ. A structure based rationale for this feature has not been reported. However, based on structural similarity, compound **3** very likely adopts an induced fit binding to PI3Kδ akin to compound idelalisib (**1**).

Given there are distinct roles and expression of PI3Kδ and PI3Kγ isoforms in lymphocyte subset function, it has been hypothesized that activity associated with

Scheme 2 Chemical structure and biochemical isoform inhibition data for INK-1197 (**3**) [30]

3
INK-1197
IPI-145

PI3Kα IC$_{50}$ = 1602 nM
PI3Kβ IC$_{50}$ = 85 nM
PI3Kδ IC$_{50}$ = 2.5 nM
PI3Kγ IC$_{50}$ = 27 nM

δ isoform selectivity:
α/δ = 641x, β/δ = 34x, γ/δ = 11x
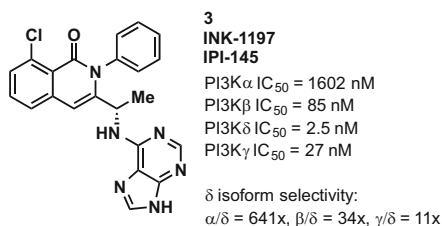
dual inhibition may differ from that of inhibition of PI3Kδ alone [30, 41, 42]. Clinical results for INK-1197 in hematological malignancies have been compelling but it remains to be seen whether differentiation from idelalisib is possible with this unique selectivity profile.

4.2 PI3Kβ Inhibitors

PI3Kβ inhibitors, such as TGX-221 and AZD6482, appear to have been originally developed with the promise of preventing platelet aggregation and blood clots. More recently, reports of the importance of the PI3Kβ isoform in PTEN-deficient or null cancers [43, 44] has moved some interest into treating this specific population of cancer patients. PTEN (phosphatase and tensin homolog) is a negative regulator of PI3K signaling and catalyzes the dephosphorylation of PIP3 to PIP2 [45]. Indeed, one of the most common observed mechanisms leading to activated PI3K signaling in patients is somatic loss of PTEN through epigenetic or genetic alteration [46].
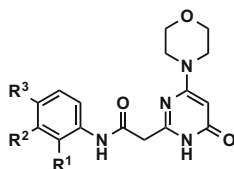
4.2.1 SAR260301, PI3Kβ

In 2012, SAR260301 (**4**, Scheme 3) entered phase I dose escalation to determine MTD in patients with advanced solid tumors. SAR260301 is reported to be a selective inhibitor of PI3Kβ, with >20-fold selectivity over the other PI3K isoforms. The Sanofi oncology drug discovery group published a series of manuscripts from 2012 to 2014 detailing a successful optimization campaign [31, 47, 48].
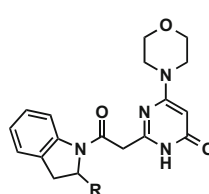
Lead compound **5** was identified following up a high throughput screen of 550 K compounds. Compound **5** is reported to be active against PI3Kβ ($IC_{50} = 42$ nM) and to possess variant selectivity over the PI3Kα, δ and γ isoforms (IC_{50} = 2,138, 118 and >10,000 nM, respectively). Optimization of potency and selectivity for PI3Kβ was achieved through monitoring a biochemical assay as well as pAKT inhibition in a PC3 line (PTEN-deficient prostate cancer cell line). Initial efforts were directed at positional scan of substitution on the pendant aniline, and representative data is shown in Table 2. Small para (fluoro, **6**) and meta-substitution (methoxy, **7**) gave analogs that were slightly more potent against the PI3Kβ
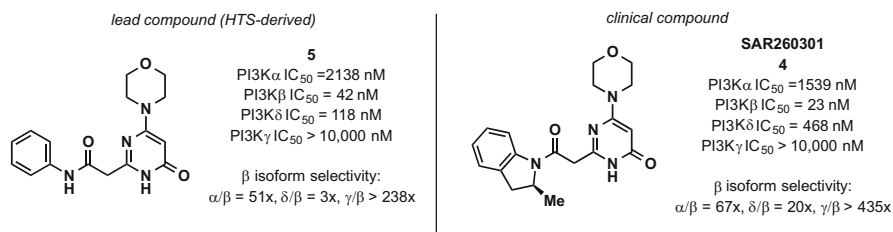
Scheme 3 Lead compound **5** and SAR260301 (**4**)

Table 2 Influence of aniline substitution on PI3Kβ potency and isoform selectivity profile

Compound	R_1, R_2, R_3	PI3Kβ IC$_{50}$ (nM)	α/β, δ/β, γ/β
6	H, H, F	13	221x, 7x, >769x
7	H, OMe, H	15	158x, 41x, >667x
8	H, OMe, F	3	1,153x, 49x, >3,333x
9	Me, H, H	236	>42x, 18x, >42x

10
PI3Kα IC$_{50}$ >10,000 nM
PI3Kβ IC$_{50}$ = 82 nM
PI3Kδ IC$_{50}$ = 779 nM
PI3Kγ IC$_{50}$ > 10,000 nM

β isoform selectivity:
α/β > 122x, δ/β = 10x, γ/β > 122x
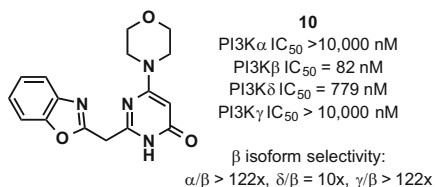
compound	R	PI3Kβ IC$_{50}$	α/β, δ/β, γ/β	pH 7.4 solubility
11	H	4	115x, 7x, >2500x	12 μM
4	(S)-Me	23 nM	67x, 20x, >435x	928 μM
12	(R)-Me	6 nM	95x, 1x, 552x	2497 μM

Fig. 7 Aniline modification through cyclization including benzoxazole **10** and indolines **4**, **11** and **12**

isoform. Ortho substitution (methyl, **9**) was detrimental to PI3Kβ potency. Most interestingly, meta and ortho substitution, in general, improved selectivity over PI3Kδ.

Two strategies were reported that called for more drastic changes to the potentially labile aniline amide. Isosteric replacement via a benzimidazole and benzoxazole was well tolerated (Fig. 7; Certal et al. [47]). Representative is benzoxazole **10**, which has similar levels of activity and isoform selectivity compared to starting anilide **5**. Cyclization of the aniline amide to indoline **11** gave a very potent and isoform selective PI3Kβ inhibitor [31]. The low aqueous solubility of **11** was hypothesized to be a result of strong crystal packing, confirmed by a high melting point of the crystalline solid (285°C). An analysis of the small molecule X-ray structure indicated intermolecular hydrogen bonding interactions between pyridone monomers as well as π-stacking of the indoline moieties. Blocking the intermolecular hydrogen bonds by introduction of an N-methyl within the pyridone

resulted in a loss of activity without strong improvement of aqueous solubility. Indoline methyl substitution, however, in analogs **12** and **4** gave a dramatic improvement in solubility. The (S)-methyl enantiomer possessing the greater level of selectivity over the PI3Kδ isoform. Compound **4** was advanced based on its overall combination of activity, selectivity, solubility, permeability (Caco2 $P_{app} = 48 \times 10^{-6}$ cm/s), and microsomal stability (57% remaining after 20 min incubation with HLM).

Compound **4** was shown to inhibit pAKT-S473 formation in vitro in a PC3 cell line with an $IC_{50} = 49$ nM. Pathway suppression and tumor growth inhibition were demonstrated in two PTEN-deficient xenograft models, PC3 and UACC-62.

Notably, this group also was able to solve a crystal structure of murine p110β in complex with **4** (Fig. 8) [31]. The binding mode of **4** was in good agreement with that hypothesized throughout the optimization process. The morpholine contacts the hinge-valine (residue 848). The pyrimidone carbonyl engages in a likely water-mediated interaction with Tyr833, whereas the "propeller" shape of the inhibitor directs the indoline under the p-loop in between Trp781 and Met773. Notably, the orientation of the Trp781 and Met773 residues differ substantially compared to the structure of p110β with pan-inhibitor GDC-0941 (pdb id: 2Y3A). The authors propose this flexibility in PI3Kβ and PI3Kδ allows for selectivity over the PI3Kα and PI3Kγ isoforms. They also hypothesize that the differences they observe in PI3Kβ over PI3Kδ activity can be attributed to a difference in primary structure on the kβ3 strand in this area: Lys771β vs. Thr750δ. Indeed, some of the divergent SAR against the PI3Kβ and PI3Kδ isoforms based on changes in the 4-position of the indoline [31] and aniline substitution of compound **5** above may be explainable by this difference in primary structure.

The results of the phase I dose escalation of **4** were disclosed at the 2015 ASCO annual meeting. A maximum tolerated dose was not reached and no objective responses were observed (3 of 21 patients were PTEN null, Bedard et al. [49]). The authors concluded that the rapid clearance observed for **4** was responsible for a lack of sustained pathway inhibition that was necessary to see anti-tumor activity in preclinical models.
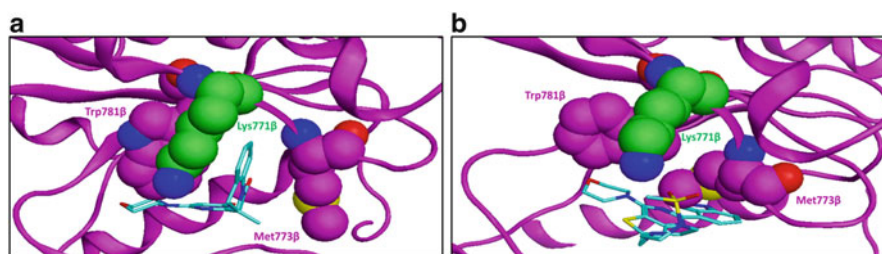
Fig. 8 (**a**) Structure of SAR260301 (**4**) in p110β (pdb id: 4BFR). (**b**) Structure of pan-inhibitor GDC-0941 in p110β (pdb id: 2Y3A). Compound **4** occupies a hydrophobic cleft created by reorientation of the Trp781 and Met773 residues relative to the GDC-0941 structure

4.2.2 GSK2636771, PI3Kβ

In 2011, GSK2636771 (**13**) entered a phase I dose escalation in patients with advanced solid tumors with PTEN-deficiencies. The structure and initial clinical data for **13** was disclosed in 2012 [50]; the structure is disclosed in a 2012 patent application (Qu et al. [32], Example 31) and subsequent combination method of use applications (Scheme 4).

Medicinal chemistry was directed at ligand-based modification of TGX-221 (**14**). A series of publications from GSK detailed a number of different scaffolds possessing similar binding motifs (Scheme 5). Representative chemotypes included imidazopyrimidones (i.e., **15**, Lin et al. [27]), triazolopyrimidinones (i.e., **16**, Sanchez et al. [51]), pyrazolopyrimidines (i.e., **17**, Yu et al. [52]), and thiazolopyrimidinones (i.e., **18**, Lin et al. [53]).

Representative of all of these scaffolds, optimization to **15** was accomplished through a combination of SAR at the 1- and 2-positions of the imidazopyrimidinone core (Table 3). Dual ortho and meta substitution (R_1 = Me, R_2 = CF$_3$) was preferred to achieve maximum inhibition of PI3Kβ (compare **19**, **20** and **21**). Notably, these modifications did not strongly influence the selectivity for PI3Kβ over PI3Kδ (five to eightfold selectivity). Imidazopyrimidinone 2-methyl substitution resulted in a modest improvement in potency against PI3Kβ and larger substitution such as ethyl was tolerated (compound **22**).
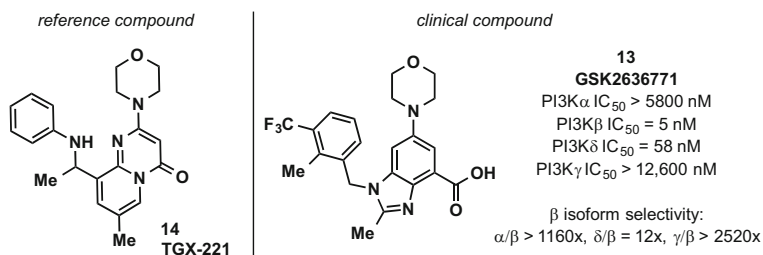
Scheme 4 TGX-221 (**14**) and GSK2636771 (**13**)
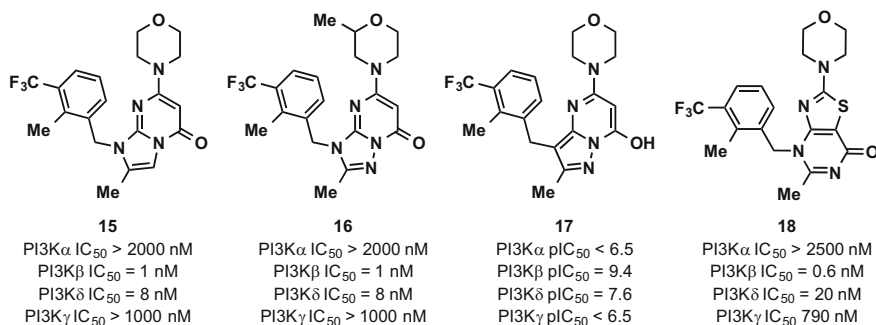
Scheme 5 Chemotypes published by GSK related to GSK2636771

Table 3 SAR within an imidazopyrimidinone series of PI3Kβ inhibitors from GSK
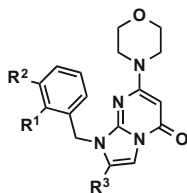
Compound	R_1, R_2, R_3	PI3Kβ IC_{50} (nM)	α/β, δ/β, γ/β
19	Me, H, H	40	>100x, 5x, 125x
20	H, CF_3, H	100	63x, 8x, >63x
21	Me, CF_3, H	3	333x, 7x, 1,067x
15	Me, CF_3, Me	1	>2,000x, 8x, >1,000x
22	Me, CF_3, Et	2	>800x, 8x, >800x

Scientists at GSK used p110β homology models for structure based design and there aren't any published crystal structures from within these chemical series. However, binding modes can be assumed based on those observed for TGX-221 and SAR260301 (Fig. 8). All 5,6-bicyclic heteroaromatic scaffolds possess morpholino substitution which presumably interact with the conserved hinge valine. The ring carbonyls likely make a water mediated interaction with the tyrosine in the back pocket. The arene substitution of these "propeller-shaped" inhibitors likely relies on the induced fit movement of the conserved methionine and tryptophan residues (akin to SAR260301).

GSK2636771 itself diverges from what is published in these manuscripts as it has a carboxylate substituent in replacement of the carbonyl present in TGX-221, **15**, **16**, **17**, and **18**. The patent application that exemplifies GSK2636771 has many examples where substitution at this position is changed including carboxylic acid derivatives and small aromatic heterocycles. It is likely that the carboxylate substitution results in displacement of a back pocket water molecule and results in direct interaction with the tyrosine and catalytic lysine residues.

Within this patent application, GSK2636771 (**13**) is reported to inhibit soft-agar growth of PC3 cells (PTEN-null) with an $IC_{50} = 27$ nM and promote tumor growth stasis in a PC3-xenograft model at doses ≥10 mg/kg.

Results from the phase I dose escalation were reported at ASCO in 2014 [54]. In this disclosure, **13** was reported to be a potent inhibitor of PI3Kβ ($IC_{50} = 0.89$ nM) with >900-fold selectivity over PI3Kα/γ and >10-fold selectivity over PI3Kδ. MTD was determined to be 500 mg and substantial pAKT suppression in surrogate tissue was noted. One patient had a RECIST PR and 13 patients had stable disease (53 patients reported to be treated).

4.2.3 AZD8186, PI3Kβ/δ

In 2013, AZD8186 (**23**) entered phase I dose escalation including patients with PTEN-deficient/mutated or PIK3CB mutated/amplified advanced solid malignancies tumors classified as PTEN-null or low. AZD8186 is reported to have good biochemical potency against the PI3K-β and -δ isoforms, reduced activity against the PI3K-α isoform and minimal activity against the PI3K-γ isoform. It is commonly referred to as a β/δ inhibitor as it is approximately 200-fold more potent in PTEN-null MDA-MB-468 cells compared to a PIK3CA-mt line, B7H4. Several sites at Astra Zeneca collaborated on a series of publications in 2014 describing medicinal chemistry leading to this unique selectivity profile [33, 55, 56].

AZD8186 (**23**) was generated by a combination of properties and structure guided-design that started from TGX-221 (**14**, Scheme 6). A related early compound, AZD6482, originally disclosed by some of the academic researchers that discovered TGX-221 [57], was progressed into clinical trials in healthy volunteers to assess influence on platelet activation. Although well tolerated, this compound was apparently discontinued as a result of significant concentration-dependent increase in plasma insulin as well as relatively short plasma half-life. Subsequently this compound was optimized to oral inhibitor AZD8186.

A crystal structure of compound **24** in PI3Kγ (pdb id: 4URK) indicates a predictable binding mode wherein the morpholine makes a single point interaction with the hinge valine and the 4-carbonyl interacts with the catalytic lysine. This compound adopts a "T-shape" with orthogonal orientation of the anthranilic acid. Compounds of this type likely derive isoform selectivity through the induced fit model discussed above (Fig. 8). Optimization from **24** is reported to have focused on improving the pharmacokinetic profile to allow once a day dosing as well as alterations in the overall isoform selectivity profile. Elimination of the carboxylate improved passive permeability, however, didn't improve metabolic stability even though addressing an observation of UDP-mediated acyl glucuronide formation in human hepatocytes (compound **25**, Scheme 7). The ADME properties of this series were improved through a series of LogD reductions. Amido substitution at the 7-position of the pyridopyrimidinone (i.e., compound **26**) gave some improvement in human hepatocyte stability. Although poorly soluble, compound **26** was able to
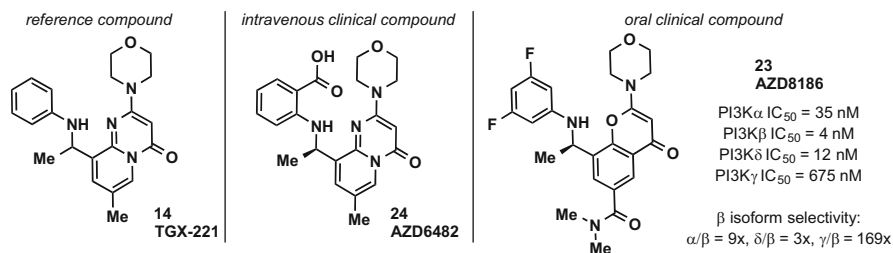
Scheme 6 Chemical structures of TGX-221 (**14**), AZD6482 (**24**), and AZD8186 (**23**)

24
R = CO_2H
$LogD_{7.4}$ = 0.75
PI3Kβ IC_{50} = 10 nM
P_{app} = 18 x 10^{-6}cm/s
hHEP Cl_{int} = 17.5 μL/min/10^6 cells

25
R = H
$LogD_{7.4}$ = 3.6
PI3Kβ IC_{50} = 49 nM
P_{app} = 66 x 10^{-6}cm/s
hHEP Cl_{int} = 20 μL/min/10^6 cells

26
$LogD_{7.4}$ = 2.7
PI3Kα IC_{50} = 340 nM
PI3Kβ IC_{50} = 7 nM
PI3Kδ IC_{50} = 45 nM
PI3Kγ IC_{50} = 3000 nM
P_{app} = 44 x 10^{-6}cm/s
hHEP Cl_{int} = 9 μL/min/10^6 cells
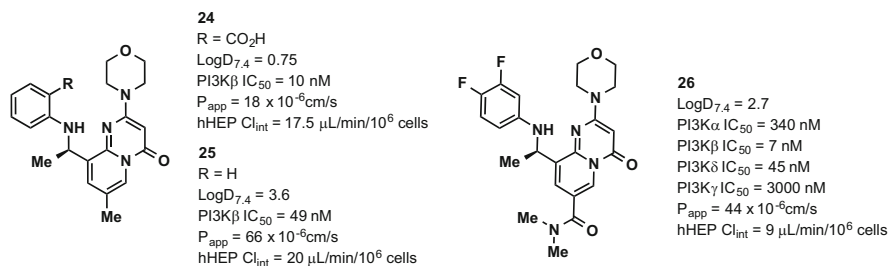
Scheme 7 Replacement of the anthranilic acid and re-distribution of polarity led to analog **26** (P_{app} measured in a Caco-2 cell line)

show some efficacy at high doses in nude mice implanted with a PC3 prostate tumor xenograft.

Replacement of the pyridopyrimidinone core by a more polar variant was targeted to further reduce lipophilicity in order to improve solubility and metabolic stability with hopes of maintaining high potency. Although calculated to be more lipophilic, chromenone replacement of the pyridopyrimidinone resulted in a consistent decrease in Log D. A matched-pair analysis over 54 pairs showed an average Log $D_{7.4}$ decrease of 0.69. Chromenone **23** (AZD8186) has improved metabolic stability in human hepatocytes (Cl_{int} < 4 μL/min/10^{-6} cells) and acceptable permeability (P_{app} = 8 × 10^{-6} cm/s). Compound **23** has moderate/high clearance and moderate/low bioavailability in mice and dogs. It was active in PTEN-null breast adenocarcinoma MDA-MB-463 cells (pAKT IC_{50} = 3 nM) and a cell-line sensitive to PI3Kδ inhibition (Jeco B cell pAKT IC_{50} = 17 nM). It was not active in a cell line sensitive to PI3Kα inhibition, B7H4 (PIK3CA mutant breast ductal carcinoma, pAKT IC_{50} = 752 nM). Pathway modulation and tumor growth inhibition was demonstrated in a PC3-xenograft model where ABT co-administration was necessary to achieve tumor stasis at 60 mg/kg of compound **23**.

Clinical results for this inhibitor have not been disclosed.

4.3 PI3Kα Inhibitors

Selective inhibition of PI3Kα is anticipated to be desirable in patient populations with solid tumors that have activating PIK3CA (or PIK3R1) mutations. In this patient population, off-target inhibition of PI3Kβ, PI3Kδ, and PI3Kγ may cause unnecessary adverse events related to metabolic function, immune suppression, or activation. Avoiding adverse events related to inhibition of isoforms that do not contribute to efficacy is hypothesized to lead to greater efficacy compared to pan-inhibitors like pictilisib and buparlisib within this PIK3CA mutant population.

4.3.1 GDC0032 (Taselisib), PI3Kα/δ/γ

At the AACR in 2013, researchers at Genentech reported the structure and preclinical activity of GDC0032 (Olivero et al. [58], later given the generic name taselisib). GDC0032 (**27**) is a pan PI3K inhibitor with the exception that it substantially spares the PI3Kβ isoform. The desired profile at this stage of Genentech's PI3K effort was to eliminate PI3Kβ activity with the hypothesis that resultant compounds would have decreased metabolic effects in patients. GDC0032 was discovered through a combination of structure and property guided optimization from high-throughput screening hit thienobenzopyran **28** [59]. Throughout optimization, starting from lipophilic lead compound **28**, polarity was progressively increased and LLE improved (Scheme 8).

A positional scan of arene substituents of compound **28** identified a modest potency improvement with 2-chloroarene **29** substitution. Thienobenzopyran compounds such as **28** and **29** possess a doubly activated methylene believed likely susceptible to metabolism. In addition, many compounds made were found to be unstable presumably via hydrolytic ring opening at this position. Simple ring expansion to thienobenzoxepin **30** resulted in a ~5-fold increase in biochemical potency and solved chemical stability issues [59]. Metabolic stability determined through in vitro and in vivo experimentation was still poor for this chemical series (i.e., **30**, HLM $Cl_{hep} > 18$ mL/min/kg, rat $Cl_p = 60$ mL/min/kg). Researchers hypothesized that cleavage of the aniline amide could be leading to instability and the concomitant production of potentially reactive/toxic metabolites. The hypothesis was supported by substantial turnover of most compounds from this series was observed in HLM in the absence of NADPH. The investigators sought to modify amide substitution, as in analogs **31** and **32**, but potency was decreased substantially. Presumably this is a result of the unique *cis*-amide preferred small molecule conformation of *N*-methyl aniline amides (Scheme 9).

Isosteric replacement of the *N*-methyl amide with 5- and 6-membered heterocycles that would enforce the observed binding conformation was successful (Fig. 9; Staben et al. [60]). This replacement, in turn, allowed replacement of the arene with smaller alkyl substituents. A class effect was noted in this effort: greater aqueous solubility, passive permeability, and HLM stability for alkyl-substituted heterocyles compared to compounds possessing the *N*-methyl amide. For alkyl triazole
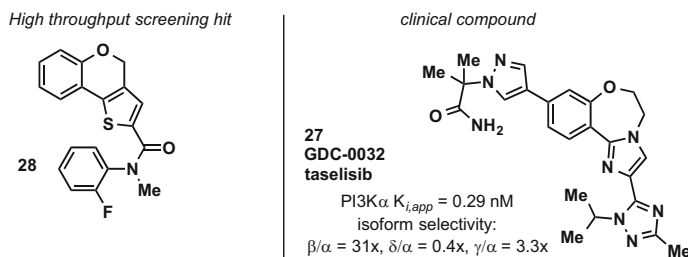
Scheme 8 Chemical structures of thienobenzopyran HTS hit **28** and benzoxazepin GDC-0032 (**27**)

28 (R = F, n = 1)
PI3Kα IC$_{50}$ = 0.254 μM

29 (R = Cl, n = 1)
PI3Kα IC$_{50}$ = 0.108 μM

30 (R = Cl, n = 2)
PI3Kα IC$_{50}$ = 0.024μM
improved chemical stability

30 (2-Cl-C$_6$H$_4$)
PI3Kα IC$_{50}$ = 0.024μM

31 (R = ^{i}Pr)
PI3Kα IC$_{50}$ > 2.0 μM

32 (R = cyclohexyl)
PI3Kα IC$_{50}$ = 0.885 μM
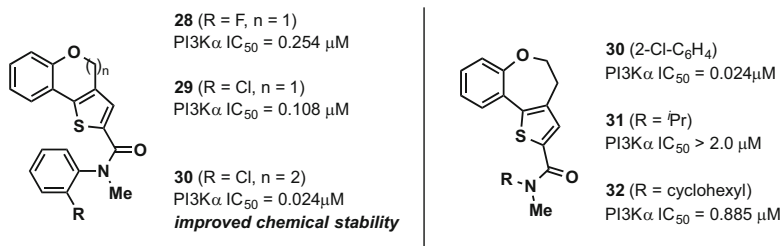
Scheme 9 Ring expansion to thienobenzoxepin **30** and attempted aniline amide replacement

compound	**33**	**34**
cLogD/TPSA/MW	3.5/72/413	3.6/83/354
PI3kα IC$_{50}$	1.5 nM	4 nM
LM stability (H/R/M)- mL/min/kg	18/43/79	10/29/63
Rat Cl$_p$ (Cl$_{p,u}$) mL/min/kg	88 (2100)	13 (230)
MDCK P$_{app}$ A-B (cm 10^{-6}/s)	2.1	20
thermodynamic solubility	ND	53 μg/mL
AUC$_u$ @ 100 mg/kg MCT suspension, nude mouse	ND	17.8 μM
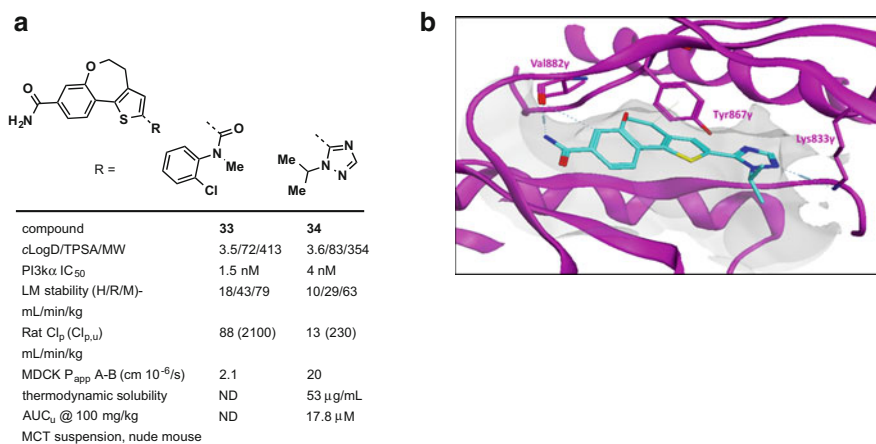
Fig. 9 (**a**) Alkyl triazole **34** had improved ADME properties with maintained potency. (**b**) Crystal structure of compound **34** in p110γ (pdb id: 4HLE) [60]. The triazole makes polar contacts within the phosphate binding region including accepting an H-bond from catalytic Lys833

34, higher solubility and permeability improved bioavailability. A large improvement in rodent free clearance and free exposure on oral dosing was observed. A crystal structure of compound **34** in p110γ confirmed polar back pocket interactions of the triazole.

Additional efforts focused on improving selectivity over PI3Kβ and structural replacement of the thiophene (Scheme 10). Compound **34** had ~7-fold selectivity for PI3Kα over PI3Kβ and this could be improved through larger substitution at the 8-position of the tricyclic core [59, 61]. For example, compound **35** and **27** possess 8-(4-pyrazolyl) substitution and had 56- and 31-fold selectivity over PI3Kβ, respectively. Five-membered heteroarenes were designed to maintain appropriate bi-aryl dihedral with the 1-isopropyl-1,2,4-triazole. The replacement of the core thiophene with an imidazole gave inhibitors with the highest LLE and superior ADME properties; most notable was an improvement in free clearance that allowed for higher free exposure. This trend is observed across a series of matched pairs looking
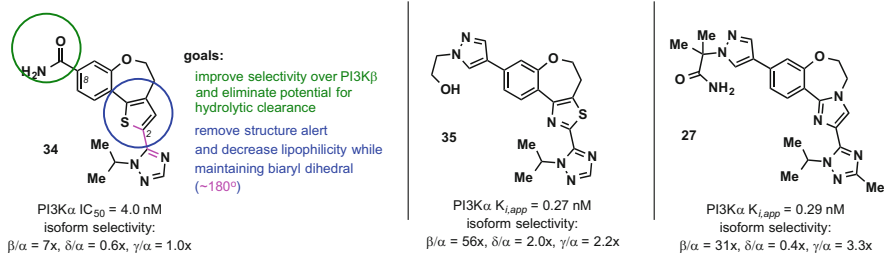
Scheme 10 Modifications from compound **34** targeted at improving selectivity over PI3Kβ and isosteric replacement of the thiophene

at direct replacement of the 5-membered ring [34]. This imidazole is a key feature in GDC0032 (compound **27**).

Selectivity over PI3Kβ was followed empirically throughout the optimization process as there was only access to crystal structures of compounds bound to PI3Kγ. Publication of crystal structures of all PI3K isoforms has allowed subsequent evolution of a model for observed selectivity for compounds like **27** and **35** [28]. A conserved tryptophan among the PI3K isoforms is predicted to be in close proximity to the 1-alkylpyrazole substituent. This tryptophan adopts a unique orientation in PI3Kβ which is hypothesized to be driven by steric insult of nearby residues. This conformer would result in greater steric clash with the 1-alkylpyrazole substituent.

Compound **27** inhibits pAKT and proliferation in an MCF7-neo/HER2 cell line at IC_{50} values equal to 4 and 25 nM, respectively. Maximal suppression of pAKT and tumor growth stasis is observed in an MCF7-neo/HER2-xenograft model at doses ≥ 5.8 mg/kg.

A notable feature of GDC0032 is its reported mutant selectivity [58, 62, 63]. While most PI3K inhibitors have increased anti-proliferative activity in PIK3CA-mutant cell lines due to the cell lines oncogene addition, GDC0032 uniquely is able to selectively inhibit the PI3K pathway and proliferation in PIK3CA-mutant lines compared to those that are pathway wild-type. In an isogenic matched set containing stable knock-in of wt-PI3Kα, H1047R-PI3Kα and E545K-PI3Kα (SW48 cells), GDC0032 selectively inhibits signaling and growth in the mutant lines. It is anticipated that this feature could improve the ability to provide efficacy in PIK3CA-mutant patients while minimizing wt-PI3Kα driven pharmacological effects.

In a phase I dose escalation that enrolled 34 patients, clinical partial responses were observed in 5 patients treated with doses of GDC-0032 ranging from 3 to 12 mg. GDC-0032 has a notable oral half-life of 40 h. Metabolic partial responses were observed via FDG-PET in 7 of 13 patients assessed [64]. A number of clinical trial are ongoing including "SANDPIPER," a phase III study to examine the efficacy of taselisib in combination with fulvestrant in patients with ER-positive, HER2-negative mBC enriched for patients that have PIK3CA mutant tumors [65].

4.3.2 CH5132799, PI3Kα/β/γ

In 2011, researchers at Chugai disclosed the structure, in vitro activity, and pre-clinical pharmacology of clinical PI3Kα/γ selective inhibitor CH5132799 (**36**, Tanaka et al. [66]). CH5132799 (**36**) bears a 2-morpholino-dihydropyrrolopyrimidine skeleton that was designed by a ligand based approach combining attributes of PI103 (**37**) and an early Chiron/Novartis PI3K inhibitor (**38**) (Scheme 11; Tanaka et al. [66]; Owada et al. [35]). Compound **36** is reported to have a unique profile with 9-fold and 36-fold selectivity for PI3Kα over the PI3Kβ and PI3Kδ isoforms, respectively.

An early ligand based combination of PI103 and compound **37** was 2-morpholino-dihydropyrrolopyridine **39**. Compound **39** is reported to have a PI3Kα $IC_{50} = 8.6$ nM (activity against other isoforms is not reported, Scheme 12). In vitro testing of phenolic compound **39** identified glucuronidation as a potential mechanism for clearance. Incubation of compound **39** with alamethicin-treated human or mouse liver microsomes with added UDPGA resulted in rapid turnover of compound **39** ($T_{1/2} = 11$ min, 6.1 min for human and mouse, respectively). The medicinal chemistry team triaged designs of phenolic isosteres using virtual docking in PI3Kγ and compounds were subsequently tested for activity in the PI3Kα biochemical assay. Many common isosteric replacements for phenols such as the indazole in compound **40** (PI3Kα $IC_{50} > 50$ μM) were not tolerated. A 5-(2-amino)-pyrimidine replacement of the phenol gave compound **41** with only moderate loss in potency. Notably, this compound was more resistant to glucuronidation and had greater overall metabolic stability when tested in human liver microsomes (HLM).
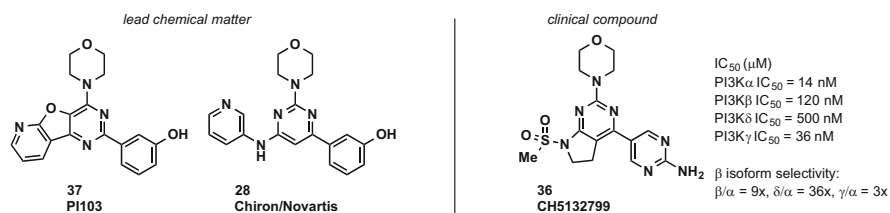
Scheme 11 Lead structures used in ligand-based design leading to CH5132799 (**36**)
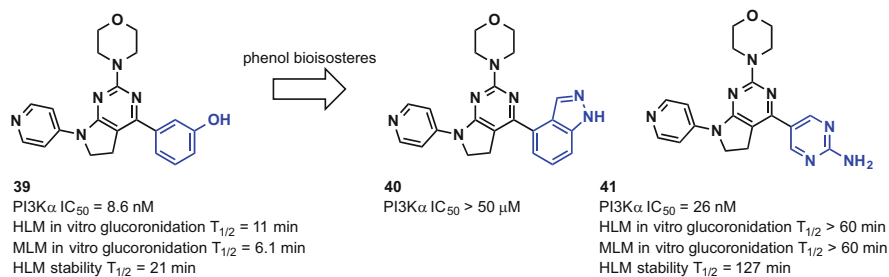
Scheme 12 Isosteric replacement of the phenol of compound **39** to reduce glucuronidation

Further optimization was focused on dihydropyrrolopyrimidinyl 7-substitution to improve ADME properties. Notably, replacing typical heteroaryl substitution as in pyridine **41** with a methanesulfonyl (**36**, CH5132799, Kawada et al. [67]) reduced HLM clearance and improved bioavailability in mouse. CH5132799 (**36**) possesses very high selectivity over other PIK-family kinases, such as PI3K C2 α/β, VPS34 and mTOR. This compound has strong anti-proliferative activity in a range of PIK3CA-mutant cancer cells (KPL4 IC_{50} = 32 nM; T-47D IC_{50} = 56 nM; ME-180 IC_{50} = 140 nM). A combination of good PK properties and strong cellular potency in PIK3CA mutant cell lines led to strong efficacy at relatively low dose in a number of reported efficacy studies with xenograft-implanted mice [66]. For example, tumor regression was observed in mice containing a KPL-4 xenograft at doses greater than 1.6 mg/kg.

A crystal structure of CH5132799 has been reported in p110γ (PDB ID: 3APC, Fig. 10). The morpholine is in position to accept a hydrogen-bond from hinge Val882, whilst the aminopyrimidine is in proximity to both donate hydrogen bonds to α-C-helix Asp841 and Asp836 and accept a hydrogen-bond from the catalytic Lys833. Although not observed, there is likely a water molecule that bridges interaction between the remaining pyrimidine nitrogen and functional-gatekeeper Tyr867. This same key pentad of interactions has also been described for other classes of morpholine containing pan-PI3K inhibitors such as GDC-0980 and BKM-120. Given the lack of disclosed isoform selectivity SAR, as well as absence of a p110α crystal structure of CH5132799, hypotheses surrounding the structural basis of isoform selectivity over the PI3Kδ and PI3Kβ isoforms cannot be supported. However, the sulfonamide interestingly is directed toward the vicinity of differences in primary sequence among the isoforms (underneath the kβ3/4 strands and adjacent to the lower hinge).
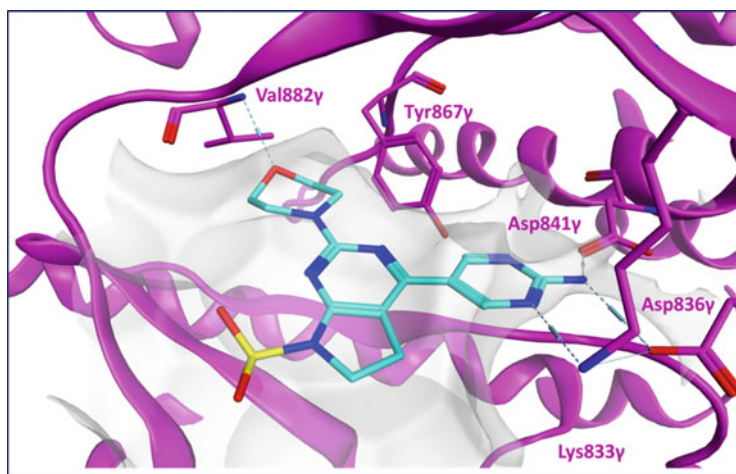
Fig. 10 X-ray structure of **36** in p110γ. The pyrimidine makes polar contacts with residues in the phosphate binding region. The sulfonamide is directed toward the solvent front

Data from a first-in-human study of CH5132799 was disclosed in 2014 [68]. Thirty-eight patients were treated in the dose escalation and an MTD of 48 mg BID was determined. A metabolic partial response was observed in five of seven patients assessed at MTD. Preliminary clinical activity was observed but no RECIST partial or complete responses were recorded.

4.3.3   AZD8835, PI3Kα/δ

In 2015 and 2016, researchers at Astra Zeneca disclosed the structure, in vitro activity and preclinical pharmacology of the clinical PI3K-α/δ inhibitor AZD8835 (compound **42**, Barlaam et al. [69]; Hudson et al. [36]). AZD8835 (**42**, Scheme 13) is reported to be a single digit nM inhibitor of PI3Kα and δ while substantially sparing the β and γ isoforms.

Early lead compound **43** identified by Astra Zeneca researchers possessed good potency against PI3Kα and good levels of selectivity over PI3Kβ. However, containing a common hinge-binding aminopyrazine, these compounds were not particularly selective over the broad kinome [70].

Crystal structures of these ligands in PI3K isoforms have not been published, but the authors report docking studies in PI3Kα and a hypothesized binding mode. The aminopyrazine making a donor–acceptor interaction with the hinge (Val851 and Glu849), the pyrazine 3-substitutent directed toward the phosphate-binding region and the 5-substituent directed toward the solvent front in between the lower hinge and β3/4 strands. The authors hypothesize the 5-membered heteroarene is within proximity to make a single-point interaction with Gln859 (PI3Kα) which they believe provides their observed selectivity over PI3Kβ for the entire series.

The team pursued two strategies to improve selectivity over non-lipid kinases while maintaining a level of isoform selectivity over the PI3Kβ isoform: modification of the 5-membered heteroarene (pyrazole) and replacement of the benzotriazole. The former proved effective (Scheme 14). While early lead compound **43** inhibits 13 of 76 tested kinases at >80% when tested at 1 μM concentration, compound **44** (pyrazole replaced with a 1,2,4-triazole) is significantly more selective, inhibiting only 3 of 76 kinases at >60%. The authors provide a number of potential explanations for the improved kinase selectivity resultant from this 5-membered heterocycle
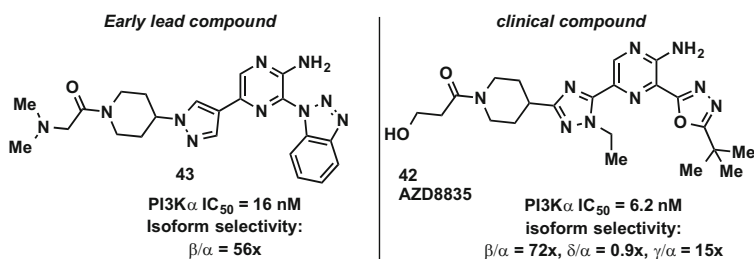
Scheme 13 Early lead compound **43** and clinical PI3K α/δ inhibitor AZD8835
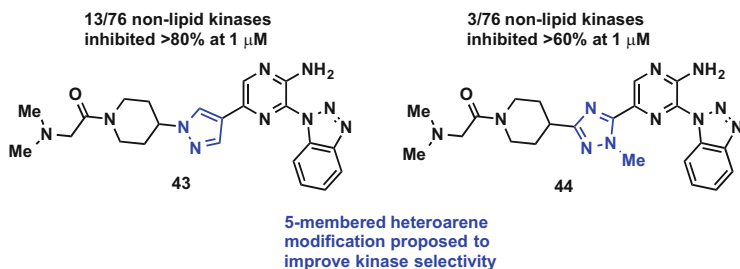
Scheme 14 Kinase selectivity of compounds **43** and **44**

Table 4 Structure activity and property relationships for aminopyrazine PI3K inhibitors

Compound	R^1, R^2, R^3	IC$_{50}$ (μM)		HLM CI$_{int}$[a]	Log D$_{7.4}$
		PI3Kα	PI3Kβ		
45	Me, Me, ^{t}Bu	0.068	9.6	9.4	2.1
46	Me, Et, ^{t}Bu	0.008	0.95	25	2.5
42	–CH$_2$CH$_2$OH, Et, ^{t}Bu	0.0062	0.431	8.1	1.9

[a]Human liver microsome clearance: μL/min/mg

modification. While designed to electronically repel with the hinge carbonyl residues in off-target kinases, the authors hypothesize insult of residues on the p-loop of off-target kinases and selective π-stacking with the PI3K-conserved tryptophan (Trp780, PI3Kα) may also contribute to this desirable property.

AZD8835 (compound **42**) was subsequently identified through simultaneous optimization potency and HLM stability within a related subseries of aminopyrazines containing a 1,3,4-oxadiazole at the 3-position (Table 4). Piperidine amide (R1), Triazole 1-subsitution (R2), and oxadiazole 5-substitution were explored. The authors noted larger triazole substituents, such as ethyl (**46**), improved potency (compare **45** to **46**, Table 4). Amongst disclosed examples, human liver microsome stability seemed to roughly correlate with measured Log D$_{7.4}$. Piperidine amide substitution was modified to decrease Log D and resulted in stable compound **42**.

The reported biochemical isoform selectivity for AZD8835 has been supported by additional pharmacological assessment in cell based assays [36, 69]. This molecule is very active in cells sensitive to PI3Kα inhibition (i.e., BT7H4 pAKT IC$_{50}$ = 57 nM) and PI3Kδ (i.e., Jeko-1 pAKT IC$_{50}$ = 49 nM), but less active in PI3Kβ-sensitive PTEN null lines (i.e., MDA-MB-468) or PI3Kγ-sensitive lines (i.e. RAW264 cells). AZD8835 was shown to have good activity in PIK3CA-mutant xenograft models, such as BT474 where 93% TGI was observed dosing

AZD8835 at 25 mg/kg BID. The authors also explored intermittent dose scheduling as a single agent or in combination [36].

AZD8835 entered a phase I clinical trial in patients with advanced solid tumors in 2014. Results from clinical studies have not been presented to date.

4.3.4 BYL-719 (NVP-BYL-719, Alpelisib), PI3Kα

In 2013, researchers at Novartis disclosed the structure and first-in-human clinical data PI3Kα-specific inhibitor BYL-719 (**47**, Gonzalez-Angulo et al. [71]). BYL-719 was generated from a medicinal chemistry campaign that spanned multiple Novartis sites starting from screening compound acylaminothiazole **48** (Scheme 15). The Novartis aminothiazoles, such as **42**, were the first selective PI3Kα inhibitors reported and they were the first to publish a structure-based hypothesis for achieving PI3Kα selectivity (for a similar hypothesis, see also Heffron et al. [72]).

In a 2012 publication [73], Bruce et al. disclose a parallel chemistry optimization to make isoform selective tool compounds starting with non-selective screening hit **48**. A reduction in TPSA and donor count was realized by replacement of the primary sulfonamide with a methyl sulfone, *N*-pyrazole, or methyl ketone resulting in analogs with improved cell potency as exemplified by compound **49** (Scheme 16). This analog has moderate potency against PI3Kα, but little selectivity over the δ or γ
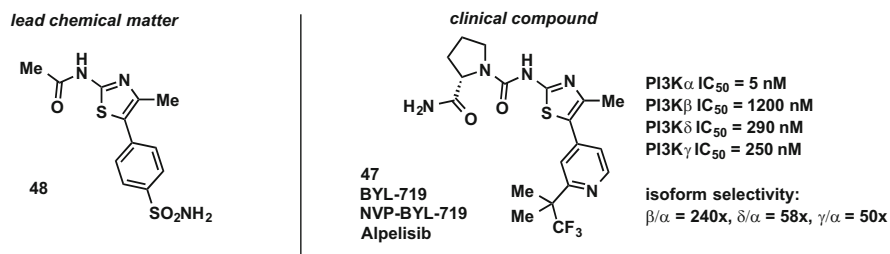
Scheme 15 Optimization of aminothiazole **43** led to BYL-719 (**42**)
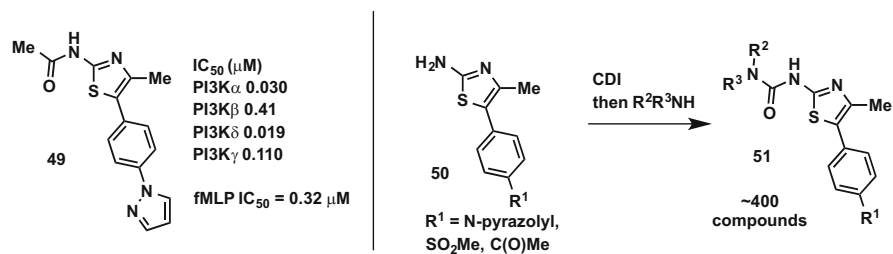
Scheme 16 Representative early inhibitor compound **44** and focused combinatorial library strategy

isoforms. Compound **49** had an IC_{50} of 0.32 μM in a neutrophil/B-cell respiratory burst assay (fMLP = f-Met-Leu-Phe).

Novartis researchers hypothesized that modification near the solvent front of ligands such as **49** (binding mode discussed later) would alter isoform selectivity as this was a region of sequence diversity among the isoforms. They took a combinatorial approach to test this hypothesis. A library of 80 amines was reacted with aminothiazoles **50** to generate ureas **51** (Scheme 16). Trends in isoform selectivity were realized and the process repeated with more focused amine sets. An outcome of this effort was PI3Kα selective compound **52** (Scheme 17). Compound **52** is a single-digit nanomolar inhibitor of PI3Kα with >44-fold selectivity over the other isoforms. Also, it isn't active against other PIK-family kinases like mTOR, DNA-PK, or Vps34. Quite notably this diversity approach resulted in selective inhibitors of not only PI3Kα but also the δ and γ isoforms [73].

An improvement in physical properties of compound **52** was made by removing of the 4-N-pyrazolobenzene and replacing with substituted pyridine and pyrimidine derivatives. The pyridyl 2-substitution occupies the hydrophobic side of the ribose pocket of p110α and these analogs maintained strong inhibition of PI3Kα and high selectivity (Scheme 17 [23]). Metabolite ID of compound **53** leant evidence to potential hydroxylation of one of the tert-butyl methyl groups. Replacement of one of the methyls with a trifluoromethyl gave BYL-719 (**47**). Compared to **53**, **47** had lower turnover in rat liver microsomes and somewhat lower rat clearance in vivo. Compound **47** was tested in cell assays to confirm isoform selectivity. Compound **47** inhibited pAKT with IC_{50} values of 0.074 uM, 2.2 uM and 1.2 uM in Rat1 cells containing transfected Myr-p110α, β and δ, respectively (Myr = myristoylated).

The aminothiazole core both accepts and donates a hydrogen bond to hinge-residue Val851 (Fig. 11). Notably, there aren't the typical significant polar interactions with back-pocket residues Asp810 or Lys802 observed for most PI3-kinase inhibitors. The trifluoromethyl substituent resides in a hydrophobic region of the ribose pocket and potentially interacts with Lys802 via nonclassical hydrogen bonds. Novartis researchers nicely rationalize that selective PI3Kα inhibition is accomplished through an isoform-specific interaction between the primary amide and Gln859. This residue deviates from glutamine in PI3Kβ (aspartate), in PI3Kδ (asparagine), and in PI3Kg (lysine). At the time of this review, this is the only reported structure-based hypothesis that rationalizes PI3Kα selectivity (similar to
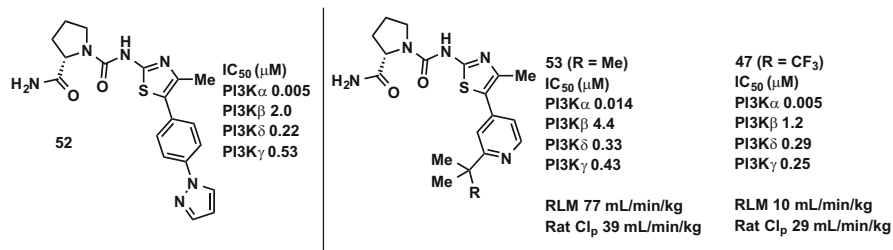
Scheme 17 Optimization of back pocket substitution leading to compound **47**
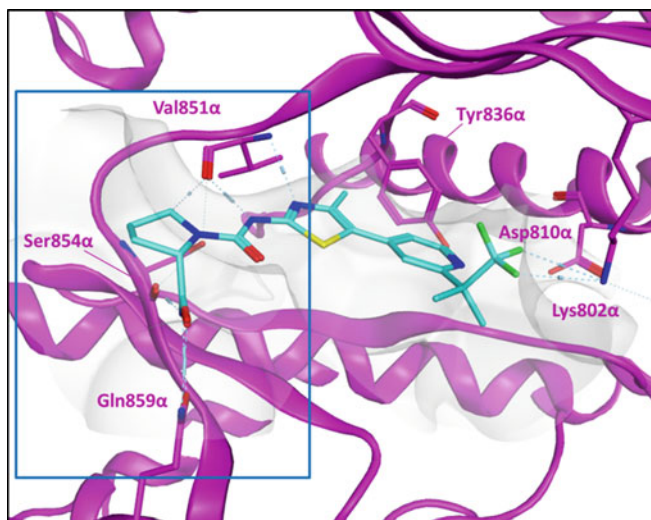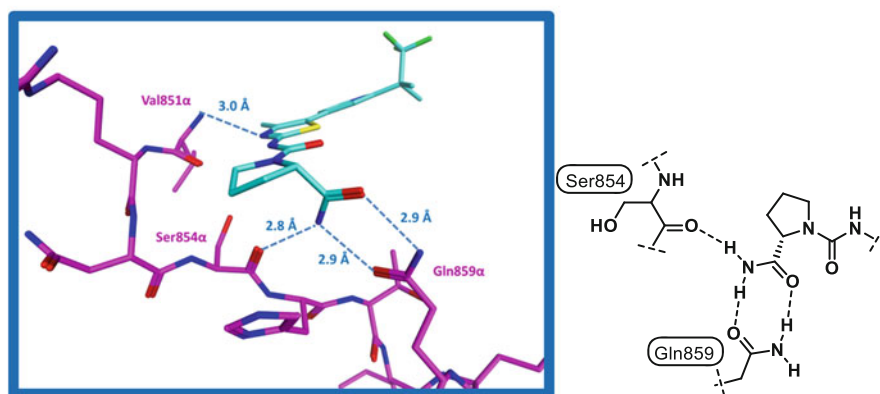
Fig. 11 (**a**) X-ray structure of **47** in p110α (pdb id: 4JPS) [23]. (**b**) Expansion and schematic highlighting interactions of the primary amide with Gln859α

Heffron et al. [72]). In support of this hypothesis, a crystal structure of BYL-719 in PI3Kα details the proximity of the key primary amide to Gln859 (Fig. 11). A series of three hydrogen bonds are noted: the primary amide of BYL-719 accepts and donates a hydrogen bond to Gln859 as well as accepts a hydrogen bond from a backbone N-H from Ser854 of the lower hinge.

This structure-based rationale is backed-up by data for closely related analogs from these optimization disclosures (Table 5). Compound **54** containing the (S)-pyrrolidine carboxamide moiety present in BYL-719 shows good inhibition of the PI3Kα isoform and corresponding selectivity over PI3Kβ, δ and γ. When the

Table 5 SAR probing the specific interaction with Gln859α contribution to isoform selectivity
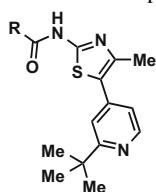
Compound	R =	IC$_{50}$ (μM)			
		PI3Kα	PI3Kβ	PI3Kδ	PI3Kγ
54	(S)-pyrrolidine carboxamide	0.014	4.4	0.33	0.43
55	pyrrolidine	0.62	4.9	0.59	0.93
56	(S)-pyrrolidine N-methyl-carboxamide	2.7	>9.1	4.2	4.6
57	(R)-pyrrolidine carboxamide	>9.1	8.2	3.3	>10

carboxamide is completely absent as in pyrrolidine **55** a large drop in activity and isoform selectivity is observed. Similarly, secondary amide (S)-pyrrolidine N-methyl-carboxamide **56** is quite inactive and non-selective. Even inversion of the stereochemistry eliminated PI3Kα inhibition resulting in non-selective high micro-molar inhibitor **57**. It is indeed striking that this single residue at the solvent front of PI3Kα can be harnessed to achieve such high selectivity.

Thirty-six patients with advanced solid tumors carrying a somatic mutation of PIK3CA were dosed in the first-in-human study up to 450 mg/day [71]. The MTD for once daily dosing was determined to be 400 mg/day. Four confirmed partial responses were reported. At the time of writing, Alpelisib continues on in late stage clinical trials, recently initiating a pivotal PhIII trial in ER+ metastatic breast cancer in combination with letrozole. The PI3K community urgently awaits the results of this trial of the most advanced pure PI3Kα inhibitor.

4.3.5 INK1117 (MLN1117), PI3Kα

In 2011, researchers at Intellikine announced the discovery of INK1117 and entry in to phase I clinical trials. INK1117 was later renamed MLN1117 after Intellikine was acquired by Millenium (Takeda) in 2011. The structure of INK1117 has not been directly announced and there has not been a report of medicinal chemistry optimization leading to its discovery.

To the author's knowledge, the reported PI3Kα isoform selectivity for INK1117 is the highest for any disclosed PI3K inhibitor. It is believed that INK1117 is exemplified in a 2011 patent application primarily disclosing a series of 5,6 and 6,5 heterobicyclic PI3K inhibitors [74]. "Compound 54" (**58**) from this patent application (Scheme 18) was latter the sole exemplification in a latter Intellikine patent application claiming a method for polymorph synthesis (**58** referred to as Formula 1, Martin et al. [75]). It was also the sole exemplification in a latter Millenium patent application focused on pharmaceutical combinations comprising

Reported data for
INK1117 (MLN1117):

PI3Kα IC$_{50}$ = 15 nM
PI3Kβ IC$_{50}$ = 4500 nM
PI3Kδ IC$_{50}$ = 13900 nM
PI3Kγ IC$_{50}$ = 1900 nM

α isoform selectivity:
β/α = 300x, δ/α = 927x, γ/α = 127x
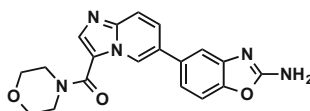
58

"Compound 54" (WO 2011022439)
"Formula 1 compound" (WO 2013071272)
"Compound A" (WO 2015051193)

Scheme 18 Reported data and hypothesized structure (compound **58**) of INK1117

inhibitors of PI3Ks (**58** referred to as "compound A," Zoren et al. [76]). Within this application, clinical AE data for 35 patients treated with **58** was reported. Thus, **58** is a hypothesized but unconfirmed structure of INK1117 (MLN1117).

Although details have not been reported, INK1117 is reported to have high isoform selectivity as a result of structure based design. Similar imidazopyridines, such as compound **59**, are known to bind to PI3K in a fashion where they accept (and in some cases donate) a hydrogen bond from the hinge valine whilst projecting 6-substitution to the polar back pocket that contains the catalytic lysine and αC-helix aspartate (pdb ID: 4KZC, Fig. 12). It is likely that compound **52** also binds through in a similar orientation, accepting a hydrogen bond from Val882α and projecting the aminobenzoxazole substituent to achieve hydrogen-bonding interactions with Lys802α and Asp810α. These hypothesized interactions are with residues conserved among the PI3K isoforms. The 3-amido-substitution of the imidazopyridine core is hypothesized to extend toward the solvent front between the lower hinge and β3/β4 strands. Although this is a region that has differences among the isoforms, it is difficult to propose a rationale for the striking isoform selectivity reported. Modelling into the active site suggests a potential single point interaction between the morpholine oxygen and α-specific Gln859.

It is interesting that inhibitors from the 2011 patent application that are unlikely to encroach regions of differences in primary structure possess qualitative differences in isoform selectivity. For example, structurally related quinolone **60** (example 205, Ren et al. [74]) is reported to also have very high selectivity for PI3Kα.
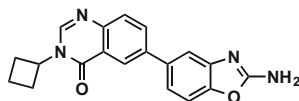
60
IC$_{50}$ (μM)
PI3Kα < 0.100
PI3Kβ > 10.0
PI3Kδ > 10.0
PI3Kγ > 10.0

MLN1117 is currently in phase I clinical trials and the results from the first-in-human dose escalation and regimen frequency study in patients with advanced solid
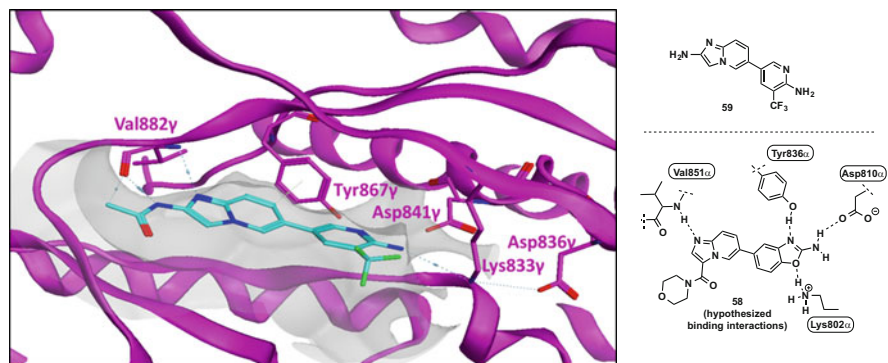
Fig. 12 X-ray structure of **59** in p110γ and schematic representation of the hypothesized binding mode of compound **58**

malignancies were reported in 2015 [37]. At the time of report, 76 patients had enrolled and 4 confirmed partial responses (RECIST) were observed.

5 Conclusion and Perspective

The past 15+ years of research directed at the discovery of small-molecule inhibitors of PI3Ks and 9 years of clinical research has resulted in great advancements in our understanding of the therapeutic potential of these targets. Early on, a majority of pharmaceutical companies focused on the discovery and development of pan-PI3K or multi-PIK family inhibitors for solid tumors. Although some would argue the modest clinical success of these pan-inhibitors has not justified the enormous resource investment, clinical results have supported proof-of-efficacy and provided hypotheses for maximizing therapeutic benefits of PI3K inhibition. Pan-PI3K inhibitors may not provide sufficient efficacy/safety in all situations and there is a theoretical advantage to isoform-selective inhibition of PI3K. Inhibition of PI3K isoforms that don't contribute strongly to efficacy within a given population can lead to undesirable pharmacology/toxicity. Indeed, the extent and duration of the oncogenic driver, and subsequent clinical efficacy, could be limited by toxicity driven by a lack of selectivity. Optimism remains in the form of isoform selective inhibitors. Clinical success in treating solid tumors with PI3K inhibitors will likely be a result of maximizing therapeutic index through this selectivity for oncogenic drivers in diagnostically driven patient populations and appropriate combination therapies.

Pharmaceutical research teams have now provided the tools to test these hypotheses. The outstanding, transformative clinical efficacy of PI3Kδ-specific inhibitors such as Idelalisib against hematological malignancies has proven the validity of isoform-specific inhibition. Early clinical efficacy of PI3Kβ and PI3Kα isoform

selective inhibitors observed in first-in-human dose escalation studies has been promising. Ongoing, pivotal, clinical trials in combination with SOC agents will determine if there is advantage to PI3Kα-selective or PI3Kβ-selective inhibitors in patients with solid tumors over their pan-PI3K predecessors.

References

1. Katso R, Okkenhaug K, Ahmadi K, White S, Timms J, Waterfield MD (2001) Cellular function of phosphoinositide 3-kinases: implications for development, homeostasis and cancer. Annu Rev Cell Dev Biol 17:615–675
2. Engleman JA, Luo J, Cantley LC (2006) The evolution of phosphatidylinositol 3-kinases as regulators of growth and metabolism. Nat Rev Genet 7:606–619
3. Thorpe LM, Yuzugullu H, Zhao JJ (2015) PI3K in cancer: divergent roles of isoforms, modes of activation and therapeutic targeting. Nat Rev Cancer 15:7–24
4. Samuels Y, Wang Z, Bardelli A (2004) High frequency of mutations of the PIK3CA gene in human cancer. Science:304–554
5. Cizkova M, Susini A, Vacher S, Cizeron-Clairac G, Andrieu C, Driouch K, Fourme E, Lidereau R, Bieche I (2012) PIK3CA mutation impact on survival in breast cancer patients and in ERα, PR and ERBB2-based subgroups. Breast Cancer Res 14:R28
6. Rodon J, Dienstmann R, Serra V, Tabernero J (2013) Development of PI3K inhibitors: lessons learned from early clinical trials. Nat Rev Clin Oncol 10:143–153
7. Krop I, Johnston S, Mayer IA, Dickler M, Ganju V, Forero-Torres A, Melichar B, Morales S, de Boer R, Gendreau S, Dernck M, Lackner M, Spoerke J, Yeh R, Levy G, Ng V, O'Brien C, Savage H, Xiao Y, Wilson T, Lee SC, Petrakova K, Vallentin S, Yardley D, Ellis M, Piccart M, Perez EA, Winer E, Schmid P (2014) The FERGI phase II study of the PI3K inhibitor pictilisib (GDC-0941) plus fulvestrant vs fulvestrant plus placebo in patients with ER+, aromatase inhibitor (AI)-resistant advanced or metastatic breast cancer – Part 1. Results. In: San Antonio Breast Cancer Society annual meeting 2014, Abstract S2-02
8. Baselga J, Im S, Iwata H, Clemons M, Ito Y, Awada A, Chia S, Jagiello-Gruszfeld A, Pistilli B, Tseng L, Hurvits S, Masuda N, Cortés J, De Laurentiis M, Arteaga CL, Jiang Z, Jonat W, Hachemi S, Le Maouhaer S, Di Tomaso E, Urban P, Massacesi C, Campone M (2015) PIK3CA status in circulating tumor DNA (ctDNA) predicts efficacy of buparlisib (BUP) plus fulvestrant (FULV) in postmenopausal women with endocrine-resistant HR+/HER2− advanced breast cancer (BC): first results from the randomized, phase III BELLE-2 trial. In: San Antonia Breast Cancer Society annual meeting 2015, Abstract S6-01
9. Chia S, Gandhi S, Joy AA, Edwards S, Gorr M, Hopkins S, Kondejewski J, Ayoub JP, Califaretti N, Rayson D, Dent SF (2015) Novel agents and associated toxicities of inhibitors of the PI3K/AKT/mTOR pathway for the treatment of breast cancer. Curr Oncol 22:33–48
10. Bi L, Okabe I, Bernard DJ, Wynshaw-Boris A, Nussbaum RL (1999) Proliferative defect and embryonic lethality in mice homozygous for a deletion in the p110α subunit of PI3K-kinase. J Biol Chem 274:10963–10968
11. Bi L, Okabe I, Bernard DJ, Nussbaum RL (2002) Early embryonic lethality in mice deficient in the p110β catalytic subunit of PI3-kinase. Mamm Genome 13:169–172
12. Foukas LC, Claret M, Pearce W, Okkenhaug K, Meek S, Peskett E, Sancho S, Smith AJH, Withers DJ, Vanhaesebroeck B (2006) Critical role for the p110α phosphoinositide-3-OH kinase in growth and metabolic regulation. Nature 441:366–370
13. Clayton E, Bardi G, Bell SE, Chantry D, Downes CP, Gray A, Humphries LA, Rawlings D, Reynolds H, Vigorito E, Turner M (2002) A crucial role for the p110δ subunit of phosphatidylinositol 3-kinase in B cell development and activation. J Exp Med 196:753–763

14. Sasaki T, Irie-Sasaki J, Jones RG, Oliveira-dos-Santos AJ, Stanford WL, Bolon B, Wakeham A, Itie A, Bouchard D, Kozieradzki I, Joza N, Mak TW, Ohashi PS, Suzuki A, Penninger JM (2000) Function of PI3Kgamma in thymocyte development, T cell activation, and neutrophil migration. Science 287:1040–1046

15. Okkenhaug K, Bilancio A, Farjot G, Priddle H, Sancho S, Peskett E, Pearce W, Meek SE, Salpekar A, Waterfield MD, Smith AJH, Vanhaesebroeck B (2002) Impaired B and T cell antigen receptor signaling in p110δ PI 3-kinase mutant mice. Science 297:1031–1034

16. Walker EH, Perisic O, Ried C, Stephens L, Williams RL (1999) Structural insights into phosphoinositide 3-kinase catalysis and signaling. Nature 402:313–320

17. Walker EH, Pacold ME, Perisic O, Stephans L, Hawkins PT, Wymann MP, Williams RL (2000) Structural determinants of phosphoinositide 3-kinase inhibition by wortmannin, LY294002, quercetin, myricetin, and staurosporine. Mol Cell 6:909–919

18. Huang C-H, Mandelker D, Schmidt-Kittler O, Samules Y, Velculescu VE, Kinzler KW, Vogelstein B, Gabeli SB, Amzel LM (2007) The structure of human p110α/p85α complex elucidates the effects of oncogenic PI3Kα mutations. Science 318:1744–1748

19. Zhao Y, Zhang X, Lu S, Peng Y, Wang X, Guo C, Zhang J, Luo Y, Shen Q, Ding J, Meng L, Zhang J (2014) Crystal structures of PI3Kα complexed with PI103 and its derivatives: new directions for inhibitors design. ACS Med Chem Lett 5:138–142

20. Mandelker D, Gabelli SB, Schmidt-Kittler O, Zhu J, Cheong I, Huang CH, Kinzler KW, Vogelstein B, Amzel LM (2009) A frequent kinase domain mutation that changes the inter-action between PI3Kalpha and the membrane. Proc Natl Acad Sci U S A 106:16996–17001

21. Zhang X, Vadas O, Perisic O, Anderson KE, Clark J, Hawkins PT, Stephens LR, Williams RL (2011) Structure of lipid kinase p110β/p85β elucidates and unusual SH2-domain-mediated inhibitory mechanism. Mol Cell 41:567–578

22. Berndt A, Miller S, Williams O, Lee DD, Housman BT, Pacold JI, Gorrec F, Hon W-C, Liu Y, Rommel C, Gaillard P, Ruckle T, Schwarz MK, Shokat KM, Shaw JP, Williams RL (2010) The p110 delta structure: mechanisms for selectivity and potency of new PI(3)K inhibitors. Nat Chem Biol 6:117–124

23. Furet P, Guagnano V, Fairhurst RA, Imbach-Weese P, Bruce I, Knapp M, Fritsch C, Blasco F, Blanz J, Aichholz R, Hamon J, Fabbro D, Caravatti G (2013) Discovery of NVP-BYL719 a potent and selective phosphatidylinositol-3 kinase alpha inhibitor selected for clinical evalu-ation. Bioorg Med Chem Lett 23:3741–3748. PDB-id 4JPS. The p85 iSH2 domain and small isothiocyanate fragment present in this structure have been removed for presentation clarity

24. Cully M, You H, Levine AJ, Mak TW (2006) Beyond PTEN mutations: the PI3K pathway as an integrator of multiple inputs during tumorigenesis. Nat Rev Cancer 6:184–192

25. Safina BS et al. (2012) Discovery of novel PI3-kinase-delta specific inhibitors for the treatment of rheumatoid arthritis: taming CYP3A4 time-dependent inhibition. J Med Chem 55:5887–5900

26. Folkes AJ, Ahmadi K, Alderton WK, Alix S, Baker SJ, Box G, Chuckowree IS, Clarke PA, Depledge P, Eccles SA, Friedman LS, Hayes A, Hancox TC, Kugendradas A, Lensun L, Moore P, Olivero AG, Pang J, Patel S, Pergl-Wilson GH, Raynaud FI, Robson A, Saghir N, Salphati L, Sohal S, Ultsch MH, Valenti M, Wallweber HJA, Wan NC, Wiesmann C, Workman P, Zhyvoloup A, Zvelebil MJ, Shuttleworth SJ (2008) The identification of 2-(1H-indazol-4-yl)-6-(4-methanesulfonyl-piperazin-1-ylmethyl)-4-morpholin-4-yl-thieno [3,2-d]pyrimidine (GDC-0941) as a potent, selective, orally bioavailable inhibitor of class I PI3 kinase for the treatment of cancer. J Med Chem 51:5522–5532

27. Lin H, Shulz MJ, Xie R, Zeng J, Luengo JI, Squire MD, Tedesco R, Qu J, Erhard K, Mack JF, Raha K, Plant R, Rominger CM, Ariazi JL, Sherk CS, Schaber MD, McSurdy-Freed J, Spengler MD, Davis CB, Hardwicke MA, Rivero RA (2012) Rational design, synthesis and SAR of a novel thiazolopyrimidinone series of selective PI3K-beta inhibitors. ACS Med Chem Lett 3:524–529

28. Staben ST, Ndubaku C, Blaquiere N, Belvin M, Bull RJ, Dudley D, Edgar K, Gray D, Heald R, Heffron TP, Jones GE, Jones M, Kolesnikov A, Lee L, Lesnick J, Lewis C, Murray J, McLean

NJ, Nonomiya J, Olivero AG, Ord R, Pang J, Price S, Prior W, Rouge L, Salphati L, Sampath D, Wallin J, Wang L, Wei B, Wiesmann C, Wu P (2013) Discovery of thiazolo-benzoxepin PI3-kinase inhibitors that spare the PI3-kinase B isoform. Bioorg Med Chem Lett 23:2606–2613

29. Somoza JR, Koditek D, Villasenor AG, Novikov N, Wong MH, Liclican A, Xing W, Lagpacan L, Wang R, Schultz BE, Papalia GA, Samuel D, Lad L, McGrath ME (2015) Structural, biochemical, and biophysical characterization of idelalisib binding to phospho-inositide 3-kinase δ. J Biol Chem 290:8439–8446

30. Winkler DG, Faia KL, DiNitto JP, Ali JA, White KF, Brophy EE, Pink MM, Proctor JL, Lussier J, Martin CM, Hoyt JG, Tillotson B, Murphy EL, Lim AR, Thomas BD, MacDougall JR, Ren P, Liu Y, Li L, Jenssen KA, Fritz CC, Dunbar JL, Porter JR, Rommel C, Palombella VJ, Changelian PS, Kutok JL (2013) PI3K-δ and PI3K-γ inhibition by IPI-145 abrogates immune responses and suppresses activity in autoimmune and inflammatory disease models. Chem Biol 20:1364–1374

31. Certal V, Carry J, Halley F, Virone-Oddos A, Thompson F, Filoche-Rommé B, El-Ahmad Y, Karlsson A, Charrier V, Delorme C, Rak A, Abecassis P, Amara C, Vincent L, Bonnevaux H, Nicolas J, Mathieu M, Bertrand T, Marguette J, Michot N, Benard T, Perrin M, Lemaitre O, Guerif S, Perron S, Monget S, Gruss-Leleu F, Doerflinger G, Guizani H, Brollo M, Delbarre L, Bertin L, Richepin P, Loyau V, Garcia-Echeverria C, Lengauer C, Schio L (2014) Discovery and optimization of pyrimidone indoline amide PI3Kβ inhibitors for the treatment of Phosphatase and Tensin Homologue (PTEN)-deficient cancers. J Med Chem 57:903–920

32. Qu J, Rivero R, Sanchez R, Tedesco R. Benzimidazole derivatives as PI3 kinase inhibitors. WO2012047538

33. Barlaam B, Cosulich S, Degorce S, Fitzek M, Green S, Hancox U, Labert-van der Brempt C, Lohmann J, Maudet M, Morgantin R, Pasquet M, Péru A, Plé P, Saleh T, Vautier M, Walker M, Ward L, Warin N (2015) Discovery of (R)-8-(1-(3,5-difluorophenylamino)ethyl)-N,N-dimethyl-2-morpholinio-4-oxo-4H-chromen-6-carboxamide (AZD8186): a potent and selective inhibitor of PI3Kβ and PI3Kδ for the treatment of PTEN-deficient cancers. J Med Chem 58:943–962

34. Ndubaku C, Heffron TP, Staben ST, Baumgardner M, Blaquiere N, Bradley E, Bull R, Do S, Dotson J, Dudley D, Edgar KA, Friedman LS, Goldsmith R, Heald RA, Kolesnikov A, Lee L, Lewis C, Nannini M, Nonomiya J, Pang J, Price S, Prior W, Salphati L, Sideris S, Wallin JJ, Wang L, Wei B, Sampath D, Olivero AG (2013) Discovery of 2-{3-[2-(1-isopropyl-3-methyl-1H-1,2–4-triazol-5-yl)-5,6-dihydrobenzo[f]imidazo[1,2-d][1,4]oxazepin-9-yl]-1H-pyrazol-1-yl}-2-methylpropanamide (GDC-0032): a β-sparing phosphoinositide 3-kinase inhibitor with high unbound exposure and robust in vivo antitumor. J Med Chem 56:4597–4610

35. Ohwada J, Ebiike H, Kawada H, Tsukazaki M, Nakamura M, Miyazaki T, Morikami K, Yoshinari K, Yoshida M, Kondoh O, Kuramoto S, Ogawa K, Aoki Y, Shimma N (2011) Discovery and biological activity of a novel class I PI3K inhibitor, CH5132799. Bioorg Med Chem Lett 21:1767–1772

36. Hudson K, Hancox UJ, Trigwell C, McEwen R, Polanska UM, Nikolaou M, Gutierrez PM, Avivar-Valderas A, Delpuech O, Dudley P, Hanson L, Ellston R, Jones A, Cuberbatch M, Cosulich SC, Ward L, Cruzalegui F, Green S (2016) Intermittent high-dose scheduling of AZD8835, a novel selective inhibitor of PI3Kα and PI3Kδ, demonstrates treatment strategies for PIK3CA-dependent breast cancers. Mol Cancer Ther. doi:10.1158/1535-7163.MCT-15-0687

37. Juric D, De Bono JS, LoRusso P, Nemunaitis JJ, Heath EI, Kwak EL, Macarulla T, Geuna E, Luken MJM, Patel C, Kuida K, Sankoh S, Zohren F, Shou Y, Tabernero J (2015) First-in-human, phase I, dose-escalation study of selective PI3Kα isoform inhibitor MLN1117 in patients (pts) with advanced solid malignancies. In: ASCO annual meeting 2015, Abstract 2501

38. Fowler KW, Huang D, Kesicki EA, Ooi HC, Oliver AR, Ruan F, Treiberg J, Puri KD. Quinazolinones as inhibitors of human phosphatidylinositol 3-kinase delta. WO2005113556

39. Furman RR, Sharman JP, Coutre SE, Cheson BD, Pagel JM, Hillmen P, Barrientos JC, Zelenetz AD, Kipps TJ, Flinn I, Ghia P, Eradat H, Ervin T, Lamanna N, Coiffier B, Pettitt

AR, Path FRC, Ma S, Stilgenbauer S, Cramer P, Aiello M, Johnson DM, Miller LL, Li D, Jahn (2014) Idelalisib and rituximab in relapsed chronic lymphocytic leukemia. N Engl J Med 370: 997–1007

40. Ren P, Liu Y, Wilson TE, Li L, Chan K, Rommel C. Substituted isoquinolin-1(2H)-ones, and methods of use thereof. US20090312319

41. Okkenhaug K (2013) Two birds with one stone: dual p110δ and p110γ inhibition. Chem Biol 20:1309–1310

42. Balakrishnan K, Peluso M, Fu M, Rosin NY, Burger JA, Wierda WG, Keating MJ, Faia K, O'Brien S, Kutok JL, Gandhi V (2015) The phosphoinositide-3-kinase (PI3K)-delta and gamma inhibitor, IPI-145 (Duvelisib), overcomes signals from the PI3K/AKT/S6 pathway and promotes apoptosis in CLL. Leukemia 29:1811–1822

43. Edgar KA, Wallin JJ, Berry M, Lee LB, Prior WW, Sampath D, Friedman LS, Belvin M (2010) Isoform-specific phosphoinositide 3-kinase inhibitors exert distinct effects in solid tumors. Cancer Res 70:1164–1172

44. Wee S, Wiederschain D, Maira S-M, Loo A, Miller C, de Beaumont R, Stegmeir F, Yao Y-M, Lengauer C (2008) PTEN-deficient cancers depend on PIK3CB. Proc Natl Acad Sci U S A 105:13057–13062

45. Song MS, Salamena L, Pandolfi PP (2012) The functions and regulation of the PTEN tumour suppressor. Nat Rev Mol Cell Biol 13:283–296

46. Parsons R (2004) Human cancer, PTEN and the PI-3 kinase pathway. Semin Cell Dev Biol 15:171–176

47. Certal V, Halley F, Virone-Oddos A, Thompson F, Filoche-Rommé B, El-Ahmad Y, Carry J, Delorme C, Karlsson A, Abecassis P, Vincent L, Bonnevaux H, Nicolas J, Morales R, Michot N, Vade I, Louboutin A, Perron S, Doerlinger G, Tric B, Monget S, Lengauer C, Schio L (2012) Preparation and optimization of new 4-(morpholin-4-yl)-(6-oxo-1-6-dihydropyrimidin-2-yl)amide derivatives as PI3Kβ inhibitors. Bioorg Med Chem Lett 23: 6381–6384

48. Certal V, Halley F, Virone-Oddos A, Delorme C, Karlsson A, Rak A, Thompson F, Filoche-Rommé B, El-Ahmad Y, Carry J, Abecassis P, Lejeune P, Vincent L, Bonnevaux H, Nicolas J, Bertrand T, Marquette J, Michot N, Benard T, Below P, Vade T, Chatreaux F, Lebourg G, Pilorge F, Angouillant-Boniface O, Louboutin A, Langauer C, Schio L (2012) Discovery and optimization of new benzimidazole- and benzoxazole-pyrimidone selective PI3Kβ inhibitors for the treatment of phosphatase and TENsin homology (PTEN)-deficient cancers. J Med Chem 55:4788–4805

49. Bedard PL, Davies MA, Kopetz S, Flaherty KT, Shapiro G, Luke JJ, Spreafico A, Wu B, Gomex C, Cartot-Cotton S, Mazuir F, Micallef S, Demers B, Juric D, Margaret P (2015) First-in-human phase I trial of the PI3Kb-selective inhibitor SAR260301 in patients with advanced solid tumors. In: ASCO annual meeting 2015, Abstract 2564

50. Blackman SC, Gainer SD, Suttle BB, Skordos KW, Greshock JD, Motwani M, Roadcap LT, Hardwicke MA, Wooster RF (2012) Abstract 1752: a phase I/IIa, first time in human, open-label dose-escalation study of GSK2636771 in subjects with advanced solid tumors with PTEN deficiency. In: AACR 103rd annual meeting 2012

51. Sanchez RM, Erhard K, Hardwicke MA, Lin H, McSurdy-Freed J, Plant R, Raha K, Rominger CM, Schaber MD, Spengler MD, Moore ML, Yu H, Luengo JI, Tedesco R, Rivero RA (2012) Synthesis and structure-activity relationships of 1,2,4-triazolo[1,5-a]pyrimidin-7(3H)-ones as novel series of potent β isoform selective phosphatidylinositol 3-kinase inhibitors. Bioorg Med Chem Lett 22:3198–3202

52. Yu H, Moore ML, Erhard K, Hardwicke MA, Lin H, Luengo JI, McSurdy-Freed J, Plant R, Qu J, Raha K, Rominger CM, Schaber MD, Spengler MD, Rivero RA (2013) [3a,4]-dihydropyrazolo[1,5a]pyrimidines: novel, potent, and selective phophatidylinositol-3-kinase β inhibitors. ACS Med Chem Lett 4:230–234

53. Lin H, Erhard K, Hardwicke AA, Luengo JI, Mack JF, McSurdy-Freed J, Plant R, Raha K, Rominger CM, Sanchez RM, Schaber MD, Shulz MJ, Spengler MD, Tedesco R, Xsie R, Zeng

JJ, Rivero RA (2012) Synthesis and structure-activity relationships of imidazo[1,2-a]pyrimidin-5-(1H)-ones as a novel series of beta isoform selective phosphatidylinositol 3-kinase inhibitors. Bioorg Med Chem Lett 22:2230–2234

54. Arkenau H-T, Mateo J, Lemech CR, Infante JR, Burris HA, Bang Y-J, Eder JP, Herbst RS, Sharma S, Chung HC, Decordova S, Swales KE, Garrett MD, Loftiss JI, Durante M, Russo MW, Suttle BB, Motwani M, Kumar R, De Bono JS (2014) A phase I/II, first-in-human dose-escalation study of GSK2636771 in patients (pts) with PTEN-deficient advanced tumors. In: 2014 ASCO annual meeting, Abstract 2514

55. Barlaam B, Cosulich S, Degorce S, Fitzek M, Giordanetto F, Green S, Inghardt T, Hennequin L, Hancox U, Lambert-van der Brempt C, Morgentin R, Pass S, Plé P, Saleh T, Ward L (2014) Discovery of 9-(1-anilinoethyl)-2-morpholino-4-oxo-pyrido[1,2-a]pyrimidine-7-carboxamides as PI3Kβ/δ inhibitors for the treatment of PTEN-deficient tumours. Bioorg Med Chem Lett 24:3928–3935

56. Giordanetto F, Barlaam B, Berglund S, Edman K, Karlsson O, Lindberg J, Nylander S, Inghardt T (2014) Discovery of 9-(1-phenoxyethyl)-2-morpholino-4-oxo-pyrido[1,1-a]pyrimidine-7-carboxamides as oral PI3Kβ inhibitors, useful as antiplatelet agents. Bioorg Med Chem Lett 24:2936–2943

57. Kim S, Mangin P, Dangelmaier C, Lillian R, Jackson SP, Daniel JL, Kunapuli SP (2009) Role of phosphoinositide 3-kinase β in glycoprotein VI-mediated Akt activation in platelets. J Biol Chem 284:33763–33772

58. Olivero A et al (2013) Discovery of GDC-0032: a beta-sparing PI3K inhibitor active against PIK3CA mutant tumors. In: AACR 2013, Washington, 6–10 Apr 2013, Abstract DDT02-01

59. Staben ST, Siu M, Goldsmith R, Olivero AG, Do S, Burdick DJ, Heffron TP, Dotson J, Sutherlin DP, Zhu B-Y, Tsui V, Le H, Lee L, Lesnick J, Lewis C, Murray JM, Nonomiya J, Pang J, Prior WW, Salphati L, Rouge L, Sampath D, Sideris S, Wiesmann C, Wu P (2011) Structure-based design of thienobenzoxepin inhibitors of PI3K. Bioorg Med Chem Lett 21:4054–4058

60. Staben ST, Blaquiere N, Tsui V, Kolesnikov A, Do S, Bradley EK, Dotson J, Goldsmith R, Heffron TP, Lesnick J, Lewis C, Murray J, Nonomiya J, Olivero AG, Pang J, Rouge L, Salphati L, Wei B, Wiesmann C, Wu P (2013) Cis-amide isosteric replacement in thienobenzoxepin inhibitors of PI3-kinase. Bioorg Med Chem Lett 23:897–901

61. Heffron TP, Wei B, Olivero A, Staben ST, Tsui V, Do S, Dotson J, Folkes A, Goldsmith P, Goldsmith P, Gunzner J, Lesnick J, Lewis C, Mathieu S, Nonomiya J, Shuttleworth S, Sutherlin DP, Wan NC, Wang S, Wiesmann C, Zhu B-Y (2011) Rational design of phosphoinositide 3-kinase alpha inhibitors that exhibit selectivity over the phosphoinositide 3-kinase beta isoform. J Med Chem 54:7815–7833

62. Belvin M, Friedman L, Sampath D, Wallin J. Mutant selectivity and combinations of a phosphoinositide 3 kinase inhibitor compound and chemotherapeutic agents for the treatment of cancer. WO2013182668

63. Edgar KA, Nannini M, Hong R, Eigenbrot C, Schmidt S, Young A, Sampath D, Wallin JJ, Friedman LS (2015) Characterization of the enhanced potency of PI3K inhibitor taselisib (GDC0032) in PI3K mutant cell lines and models. In: AACR 106th annual meeting 2015, Abstract 2672

64. Juric D, Krop I, Ramanathan RK, Xiao J, Sanabria S, Wilson TR, Choi Y, Parmar H, Hsu J, Baselga J, Von Hoff DD (2013) Abstract LB-64: GDC-0032, a beta isoform-sparing PI3K inhibitor: results of a first-in-human phase Ia dose escalation study. In: AACR annual meeting 2013

65. Baselga J, Cortes J, De Laurenitis M, Diéras V, Harbeck N, Im Y, Jacot W, Krop IE, Verma S, Wilson TR, Lin R, Schimmoller F, Hsu JY (2015) SANDPIPER: phase III study of the PI3-kinase (PI3K) inhibitor taselisib (GDC-0032) plus fulvestrant in patients (pts) with estrogen receptor (ER)-positive, HER2-negative locally advanced or metastatic breast cancer (BC) enriched for pts with PIK3CA mutant tumors. In: ASCO annual meeting 2015, Abstract TPS629

66. Tanaka H, Yoshida M, Tanimura H, Fujii T, Sakata K, Tachibana Y, Ohwada J, Ebiike H, Kuramoto S, Morita K, Yoshimura Y, Yamazaki T, Ishii N, Kondoh O, Aoki Y (2011) The selective class I PI3K inhibitor CH5132799 targets human cancers harboring oncogenic PIK3CA mutations. Clin Cancer Res 17:3272–3281

67. Kawada H, Ebiike H, Tsukazaki M, Nakamura M, Morikami K, Yoshinari K, Yoshida M, Ogawa K, Shimma N, Tsukuda T, Ohwada J (2013) Lead optimization of a dihydro-pyrrolopyrimidine inhibitor against phosphoinositide 3-kinase (PI3K) to improve the phenol glucuronic acid conjugation. Bioorg Med Chem Lett 23:673–678

68. Blagden S, Omlin A, Josephs D, Stavraka C, Zivi A, Pinato DJ, Anthoney A, Decordova S, Swales K, Riisnaes R, Pope L, Noguchi K, Shiokawa R, Inatani M, Prince J, Jones K, Twelves C, Spicer J, Banerji U (2014) First-in-human study of CH5132799, an oral class I PI3K inhibitor, studying toxicity, pharmacokinetics and pharmacodynamics in patients with metastatic cancer. Clin Cancer Res 20:5908–5917

69. Barlaam B, Cosulich S, Delouvrié B, Ellston R, Fitzek M, Germain H, Green S, Hancox U, Harris CS, Hudson K, Labert-van der Brempt C, Lebraud H, Magnien F, Lamorlette M, Le Griffon A, Morgentin R, Ouvry G, Page K, Pasquet G, Polanska U, Ruston L, Saleh T, Vautier M, Ward L (2015) Discovery of 1-(4-(5-(5-amino-6-(5-tert-butyl-1,3,4-oxadiazol-2-yl) pyrazin-2-yl)-1-ethyl-1,2,4-triazol-3-yl)piperidin-1-yl)-3- hydroxypropan-1-one (AZD8835): a potent and selective inhibitor of PI3Kα and PI3Kδ for the treatment of cancers. Bioorg Med Chem Lett 25:5155–5162

70. Barlaam B, Cosulich S, Fitzek M, Green S, Harris CS, Hudson K, Lambert-van der Brempt C, Ouvry G, Page K, Ruston L, Ward L, Delouvrié B (2015) Design of selective PI3Kα inhibitors starting from a promiscuous pan kinase scaffold. Bioorg Med Chem Lett 25:2679–2685

71. Gonzalez-Angulo AM, Juric D, Argilés G, Schellens JHM, Burris HA, Berlin J, Middleton MR, Shuler MH, Van Geel R, Helgason T, Bootle D, Boehm M, Goggin TK, Demanse D, Quadt C, Baselga J (2013) Safety, pharmacokinetics, and preliminary activity of the α-specific PI3K inhibitor BYL719: results from the first-in-human study. In: ASCO annual meeting 2013, Abstract 2531

72. Heffron TP, Heald RA, Ndubaku C, Wei B, Augistin M, Do S, Edgar K, Eigenrot C, Friedman L, Gancia E, Jackson PS, Jones G, Kolesnikov A, Lee LB, Lesnick JD, Lewis C, McLean N, Mörtl M, Nonomiya J, Pang J, Price S, Prior WW, Salphati L, Sideris S, Staben ST, Steinbacher S, Tsui V, Wallin J, Sampath D, Olivero AG (2016) The rational design of selective benzoxazepin inhibitors of the α-isoform of phosphoinositide 3-kinase culminating in the identification of (S)-2-((2-(1-isopropyl-1H-1,2,4-triazol-5-yl)-5,6-dihydrobenzo[f] imidazo[1,2-d][1,4]oxepin-9-yl)oxy)propanamide (GDC-0326). J Med Chem 59:985–1002

73. Bruce I, Akhlaq M, Bloomfield GC, Budd E, Cox B, Cuenoud B, Finan P, Gedeck P, Hatto J, Hayler JF, Head D, Keller T, Kirman L, Leblanc C, Le Grand D, McCarthy C, O'Connor D, Owen C, Oza MS, Pilgrim G, Press NE, Sviridenko L, Whitehead L (2012) Development of isoform selective PI3-kinase inhibitors as pharmacological tools for elucidating the PI3K path-way. Bioorg Med Chem Lett 22:5445–5550

74. Ren P, Liu Y, Li L, Chan K, Wilson TE, Cambell SF. Heterocyclic compounds and uses thereof. WO 2011022439. Only qualitative PI3K isoform inhibition data is reported in this patent application for select compounds

75. Martin M, Worrall CP, Gancedo SD, Ren P. Kinase inhibitor polymorphs. WO2013071272

76. Zohren F, Patel C. Enhanced treatment regimens using PI3Kα inhibitors. WO2015051193

Inhibitors of the Kynurenine Pathway

Check for updates

Ute F. Röhrig, Vincent Zoete, and Olivier Michielin

Abstract A central role in the immune escape of tumors has been attributed to the kynurenine pathway of tryptophan metabolism, leading to the depletion of tryptophan and the production of different bioactive metabolites. The first and rate-limiting step in this pathway is catalyzed by the phylogenetically unrelated enzymes indoleamine 2,3-dioxygenase 1 (IDO1) and tryptophan 2,3-dioxygenase (TDO), which have both been shown to be expressed in different cancers. Intense efforts in academia and in pharmaceutical companies to develop novel inhibitor scaffolds yielded a few compounds currently undergoing clinical trials. Here, we review the most significant compounds in the field and discuss potential issues in the development of kynurenine pathway inhibitors for cancer therapy.

Keywords Immuno-oncology, Indoleamine 2,3-dioxygenase, Kynurenine pathway, Tryptophan 2,3-dioxygenase, Tryptophan metabolism

Contents

U.F. Röhrig (✉) and V. Zoete (✉)
SIB Swiss Institute of Bioinformatics, Lausanne, Switzerland
e-mail: ute.roehrig@sib.swiss; vincent.zoete@sib.swiss

O. Michielin (✉)
SIB Swiss Institute of Bioinformatics, Lausanne, Switzerland

Ludwig Center for Cancer Research of the University of Lausanne, Dep. of Oncology, Univ. of Lausanne and Centre Hospitalier Universitaire Vaudois (CHUV), Lausanne, Switzerland
e-mail: olivier.michielin@sib.swiss

1 Introduction

Cancer immunotherapy is a rapidly evolving field [1], which has generated much excitement among scientists and cancer patients over the last years because of the efficacy of immune checkpoint inhibitors [2], chimeric antigen receptor T-cell therapy [3], and adoptive cell therapy with tumor infiltrating lymphocytes [4]. These promising new therapies, as well as more traditional approaches such as vaccination, chemotherapy, or radiotherapy could benefit from the combination with a strategy to overcome tumor-induced immunosuppression [5–7]. A central role in immune escape is played by the kynurenine pathway of L-tryptophan (L-Trp) metabolism (Fig. 1) [8–11]. This pathway, which has been estimated to be responsible for more than 99% of L-Trp degradation in humans [12, 13], leads to the depletion of L-Trp and to the production of kynurenine metabolites and causes local immunosuppression [14–17]. The pathway is not only involved in the immune system, for example, in establishing immune tolerance versus the fetus during pregnancy [18] and in the response to infections [19], but it also influences the nervous system and plays a major role in neurological and mental disorders [20, 21]. The first and rate-limiting step in the kynurenine pathway is the oxidation of L-Trp to N-formylkynurenine (NFK, Fig. 1). This reaction is catalyzed by two evolutionarily unrelated heme enzymes, tryptophan 2,3-dioxygenase (TDO, EC 1.13.11.11) and indoleamine 2,3-dioxygenase 1 (IDO1, EC 1.13.11.52). TDO is a homotetrameric enzyme, upregulated by glucocorticoid hormones and the availability of L-Trp, constitutively expressed in the liver, and responsible for regulating systemic L-Trp levels [16]. IDO1 on the other hand is a monomeric enzyme induced by interferon gamma and expressed in different cell types and tissues [16, 22]. IDO1 has first been implicated in tumoral immune resistance in 2003 [23], a discovery that initiated a very active field of drug
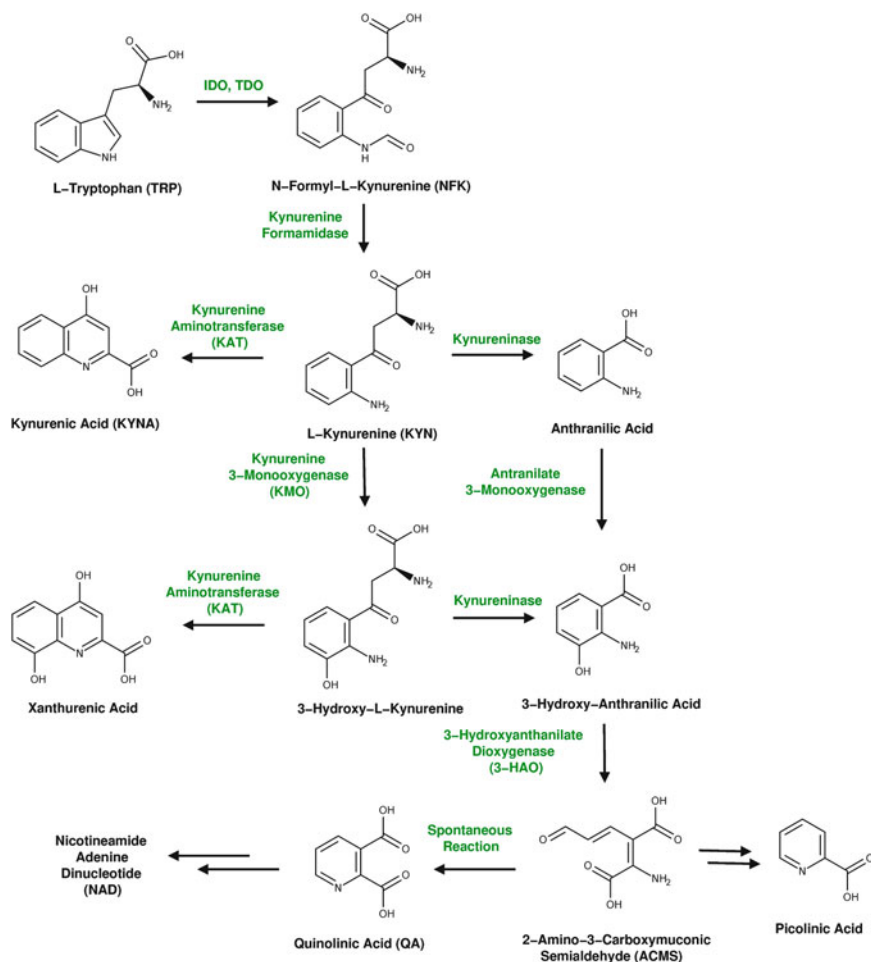
Fig. 1 Kynurenine pathway

development. The implication of TDO in similar mechanisms has been described more recently [24, 25]. The role of the IDO1 paralogue indoleamine 2,3-dioxygenase 2 (IDO2) [26–28] remains less clear due to ambiguous experimental findings. IDO2 shows a very low affinity for L-Trp and a low turnover rate [29]. Different issues have hampered biological studies of L-Trp metabolism, such as: (1) difficulties in obtaining gene knockout mice lacking both IDO1 and IDO2 [30], (2) antibody reagents against murine IDO1 lacking specificity [31, 32], and (3) the widespread use of high concentrations of the very unspecific IDO1 inhibitor 1-methyl-tryptophan (1MT), which has been shown to additionally induce IDO1 [24] and to be contaminated with L-Trp [33].

Here, we concentrate on the description of small molecule inhibitors of the first step of L-Trp metabolism, namely of IDO1, TDO, and IDO2, as these are the main targets for cancer therapy.

2 Indoleamine 2,3-Dioxygenase 1 Inhibitors

IDO1 (EC 1.13.11.52) is the most well-established target in the kynurenine pathway for cancer immunotherapy [22]. It has been shown to be expressed by tumor cells in order to escape a potentially effective immune response [14, 23, 34, 35], and high IDO1 expression is associated with poor prognosis in different cancer types [36]. In vitro and in vivo studies demonstrate that administration of an IDO1 inhibitor improves the efficacy of therapeutic vaccination, chemotherapy, or radiation therapy [23, 37–40].

IDO1 is a heme enzyme that catalyzes the oxidation of L-Trp to NFK by the incorporation of molecular oxygen and the cleavage of the pyrrole ring of the substrate. The crystal structures of human IDO1 [41–43] show one binding pocket in the distal heme site (Pocket A, Fig. 2a), connected to a second pocket towards the entrance of the active site (Pocket B, Fig. 2a) [44]. The "height" of the A pocket varies among different X-ray structures, as evident from Fig. 2a–d.

Intense efforts in academia and in the pharmaceutical industry to develop IDO1 inhibitors led to at least three compounds in clinical trials so far. The most advanced compound, at the time of writing, was the hydroxyamidine **18** (INCB024360, epacadostat) [38, 45–47] developed by Incyte Corporation, which had been tested in combination with different other cancer therapies and partners in clinical trials up to phase III. A second compound in phase I clinical studies at the time of writing is the imidazole GDC-0919 (formerly known as NLG919 or RG6078, structure not disclosed) [48, 49] discovered by NewLink Genetics and developed together with Genentech. iTeos Therapeutics [50–53] in partnership with Pfizer initiated a phase I study with compound PF-06840003 (undisclosed structure) for patients with malignant gliomas (NCT02764151).

In addition to academic groups, the pharma companies Amgen [54], Bristol-Myers Squibb [55–58], Curadev [59–61] (partnering with Roche), Dainippon Sumitomo Pharma Corporation [42], Flexus Biosciences [62–65] (acquired by Bristol-Myers Squibb in 2015), IOmet Pharma [66–70] (acquired by Merck & Co. in 2016), Merck Group [71], Redx Pharma [72, 73], and Vertex Pharmaceuticals [74] have all reported work on the development of IDO1 inhibitors.

IDO1 inhibitory properties have been attributed to thousands of compounds, but many of them may act through unspecific mechanisms [75]. Here, we limit ourselves to discuss the most relevant and novel scaffolds. A complete review of IDO1 inhibitors described before February 2015 can be found in a recent review [75]. In the following figures, ligands are shown in their putative binding conformation to IDO1 according to Fig. 2 whenever possible, with the heme-iron facing group in the lower
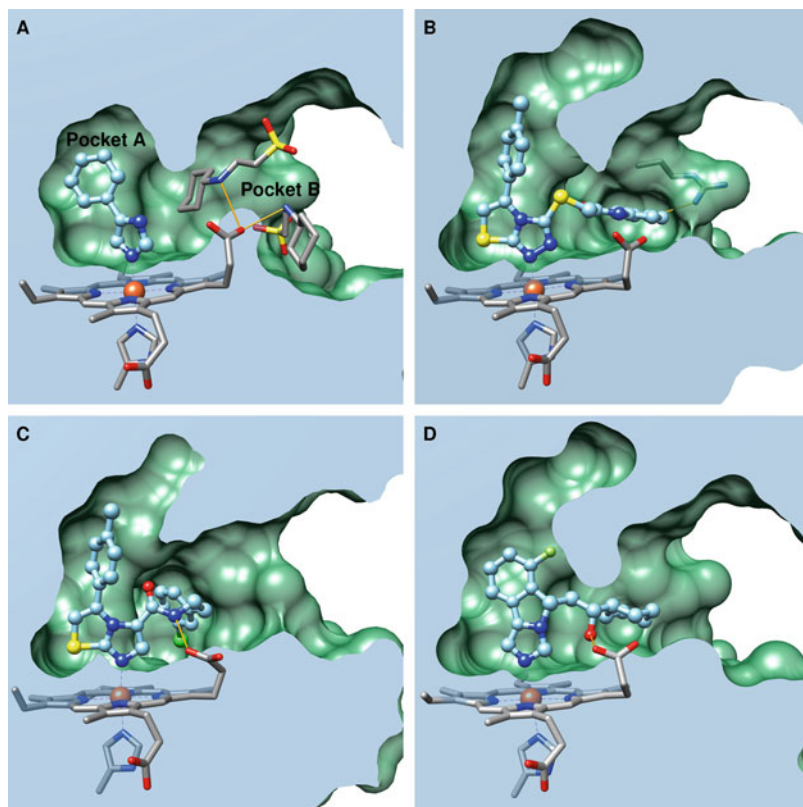
Fig. 2 X-ray structures of indoleamine 2,3-dioxygenase 1 (IDO1) [41–43]. Only the active site is shown, displaying the protein in surface representation, heme and His346 in stick representation, and the ligand in ball and stick representation. Heteroatoms are colored as follows: *blue* (nitrogen), *red* (oxygen), *yellow* (sulfur), *green* (chloride), and *orange* (iron). Hydrogen bonds are shown as *thin orange lines*. (**a**) Structure 2D0T bound to 4PI (**7**) and two molecules of CHES buffer (displayed in stick representation) [41]. The A pocket above the heme distal site and the B pocket towards the entrance of the active site [44] are highlighted. (**b**) Structure 4PK5 bound to compound **38** [42]. (**c**) Low resolution (3.45 Å) structure 4PK6 bound to an imidazothiazole derivative [42]. (**d**) Structure 5EK4 bound to compound **15**, an analog of GDC-0919 [43]

left, the A-pocket binding group in the upper left, and the B-pocket binding group extending to the right.

2.1 1-Methyl-Tryptophan

The most widely used IDO1 inhibitor in biological studies up to date is 1MT [76] despite its moderate activity ($K_i = 19$–53 µM) [39, 76–80]. 1MT, like tryptophan, is a chiral compound, and it has been shown that only the L enantiomer (**1**, Fig. 3)

Fig. 3 IDO1 inhibitors based on the indole scaffold. L-1MT (**1**), D-1MT (**2**), keto-indole (**3**) [81], oxindole (**4**) [66], indole-2-carboxamide (**5**) [67], and 6-fluoro indole (**6**) [53]
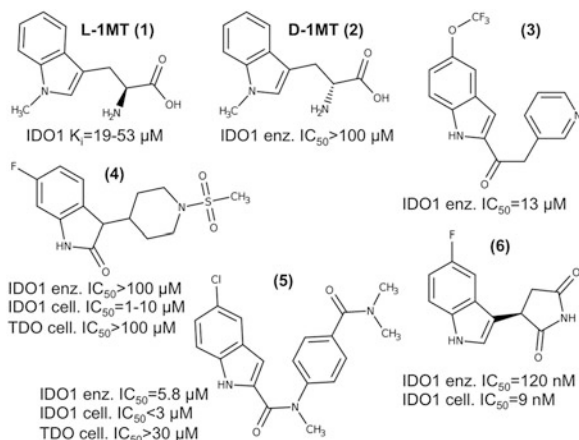
inhibits the enzymatic activity of IDO1 in vitro [77, 78] However, based on the findings that the D enantiomer (**2**, Fig. 3) was more efficacious as an anticancer agent in vivo [78], NewLink Genetics initiated clinical trials with D-1MT (indoximod) as anticancer agent. As a possible explanation of the better in vivo activity of D-1MT it was later suggested that D-1MT preferentially inhibits the IDO1 paralogue IDO2 [27], but this finding was rejected by subsequent studies [82–85]. Therefore, the mechanism of action of D-1MT as a kynurenine pathway inhibitor is still under debate [24, 34, 86–89]. Additional complications in interpreting experimental data generated with the tool compound 1MT may arise from the facts that D-1MT has been shown to induce IDO1 expression [24] and that L-1MT can be substantially contaminated with L-Trp [33].

At present, it is clear that D-1MT is not a human IDO1 inhibitor. The use of L-1MT as a tool compound for IDO1 inhibition should be avoided due to its low activity and specificity, and due to the availability of more active and selective inhibitors.

2.2 Indoles

IDO1 inhibitors known before the implication of this enzyme in tumoral immune resistance were of moderate micromolar activity [90]. Many of these were analogs of the substrate L-Trp or its indole scaffold [76, 77, 91–94]. However, as L-Trp itself shows only a moderate affinity for IDO1 ($K_d = 290$–320 μM) [41, 95], also most of its analogs were only moderately active towards IDO1. Double-digit micromolar activities were reached by some keto indoles discovered by virtual screening (**3**, Fig. 3) [81, 96].

IOmet Pharma (now Merck & Co.) tested 3-substituted indoles and oxindoles for IDO1 and TDO inhibition (Fig. 3) [66]. Although none of the compounds displayed an enzymatic IC_{50} value below 100 μM on IDO1, some were low micromolar IDO1 inhibitors in a cellular context with at least tenfold selectivity over TDO (**4**), while other compounds were selective for TDO (Sect. 3.1). The observation that compounds display better cellular IC_{50} values than enzymatic IC_{50} values has been frequently observed for IDO1 and could be due to off-target effects or the artificial reducing cofactors routinely used in the enzymatic assay [75].

In the following, IOmet Pharma described a large series of indole-2-carboxamides [67]. Many compounds displayed cellular IC_{50} values below 3 μM on hIDO1 and more than tenfold selectivity with respect to TDO. For a few compounds, an enzymatic IC_{50} value below 10 μM was cited (**5**). Interestingly, the indole-2-carboxamide scaffold has also been shown to possess high antitubercular activity in an animal model of tuberculosis [97, 98], and IDO1 has been implicated in tuberculosis infection [99].

More recently, iTeos Therapeutics described a series of 3-indol-3-yl-pyrrolidine-2,5-diones (succinimides) with potent IDO1 inhibitory properties [53]. The most potent compound (**6**) in its enantiopure *R* form displayed an enzymatic IC_{50} value of 120 nM, nanomolar cellular activities, an IC_{50} value of 3 μM in a human whole blood assay, an EC_{50} value of 74 nM in an IDO1-dependent cellular T-cell proliferation assay, in vivo reduction of kynurenine levels in the blood of healthy mice of up to 68% (100 mg/kg), as well as in vivo inhibition of tumor growth in different cancer models.

In summary, it seems to be challenging to develop potent selective IDO1 inhibitors based on the indole scaffold. At the time of writing, only iTeos Therapeutics succeeded in developing a nanomolar indole IDO1 inhibitor.

2.3 Imidazoles

The known heme-binder 4-phenylimidazole (4PI, **7**, Fig. 4) was described as an IDO1 inhibitor in 1989 [100] and gained attention due to its co-crystallization with IDO1 in 2006 (Fig. 2a) [41]. A structure-based approach led to 4PI derivatives that were up to tenfold more potent than the parent compound **8** [101]. Fungistatic drugs of the 1-substituted imidazole type, such as miconazole and econazole (**9**), were discovered in two independent screens to be active against IDO1, while similar 1,2,4-triazole drugs such as fluconazole were completely inactive [102, 103]. Structure-based modifications of the 1-substituted imidazole antifungal scaffold led to more soluble but less potent compounds (**10**) [103].

Fallarini and coworkers created a virtual library of 1,5- and 4,5-disubstituted imidazoles and selected 25 compounds for synthesis and evaluation [104]. While the 1,5-disubstituted imidazoles were inactive with one exception (**11**), the best 4,5-disubstituted imidazoles displayed low micromolar enzymatic and cellular IC_{50} values (**12**). However, the presence of bulky substituents next to the heme-iron
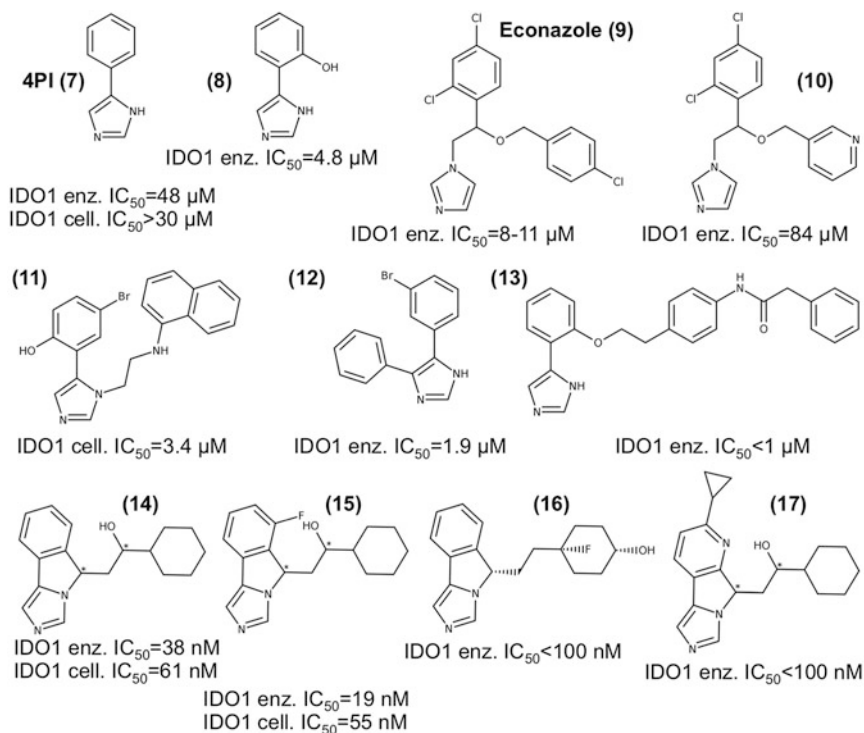
Fig. 4 IDO1 inhibitors with imidazole scaffold. 4-phenylimidazole (4PI, **7**) [100, 101], 4PI derivative (**8**) [101], econazole (**9**) [102, 103], derivative of fungistatic imidazoles (**10**) [103], disubstituted imidazoles (**11**, **12**) [104], 4PI derivative (**13**) [105], and fused imidazole-isoindoles (**14**, **15**, **16**, **17**) [71, 106]. Stereocenters discussed in the main text are marked by an *asterisk*

binding imidazole nitrogen should sterically hinder their direct heme binding, so it is not clear how they bind to IDO1.

NewLink Genetics developed further 4-substituted phenylimidazoles with nanomolar potency but a low ligand efficiency, because they featured a long extension into the B pocket (**13**) [105]. Fusion of the two aromatic rings of 4PI by an aliphatic carbon atom to yield imidazo-isoindoles (**14**), however, strongly enhanced potency with less impact on efficiency [106]. Two compounds of this series (**14**, **15**) were tested in vivo for antitumor activity in mouse models of colorectal, bladder, mammary, and lung cancer as single agents or in combination with other chemotherapies. These tests showed that both compounds had a significant antitumor activity either as single agent or in combination therapy, leading to a significantly reduced rate of tumor growth and improved survival time [106]. Based on these results, it is likely that the clinical candidate GDC-0919 has a structure similar to compounds **14**, **15**. These compounds contain two asymmetric carbon atoms, marked by asterisks in Fig. 4, leading to four stereoisomers. For compound **14**, it was found that

the *S*-isomers of the carbon atom in the tricyclic scaffold were responsible for the nanomolar potency of the mixture of stereoisomers [106].

The pioneering work of NewLink Genetics stimulated other groups to work on the imidazole scaffold. Peng and coworkers evaluated some of the NewLink Genetics compounds and new analogs and provided IDO1-bound X-ray structures for three imidazole-isoindole derivatives and one pyridine analog (Fig. 2d) [43]. The most potent compound described in this work, which corresponds to compound **15** (Fig. 4) [106], was shown to display an enzymatic IC_{50} value of 19 nM and a cellular IC_{50} value of 55 nM. Its X-ray structure (PDB ID: 5EK4, Fig. 2d) revealed a hydrogen bond from its hydroxy group to the heme propionate, and the placement of the cyclohexyl group in the B pocket [43]. Here, the A pocket is much higher than in the 4PI-bound structure (Fig. 2a), but this additional volume is apparently neither filled by the ligand nor by solvent molecules. The parent compound without fluoro substituent (**14**), which displayed an enzymatic IC_{50} value of 38 nM and a cellular IC_{50} value of 61 nM, was investigated in more detail regarding the activity of its stereoisomers, and it was found that the individual enzymatic IC_{50} values of the four stereoisomers were 20 nM, 29 nM, 2.4 μM, and >10 μM [43]. Again, the *S*-isomers of the carbon atom in the tricyclic scaffold were found to be responsible for the nanomolar potency of the mixtures of stereoisomers.

Merck Group patented a series of related enantiopure tricyclic imidazo-isoindole compounds of high enzymatic potency (**16**, **17**, Fig. 4, IC_{50} values < 100 nM) [71], finding the same preference for the *S*-isomers.

In summary, the phenylimidazole scaffold provides a popular and promising starting point for the development of IDO1 inhibitors. Its binding mode to the active site is known through X-ray crystallography [41, 43], it does not show promiscuous enzyme inhibition, rational modifications have been shown to be feasible, and interpretable structure–activity relationships are observed. The fact that 4PI and the fungistatic imidazoles inhibit various heme enzymes suggests that specificity for IDO1 needs to be achieved through optimized interactions with IDO1, for example, through molecular recognition by the B pocket. Selective TDO (Sect. 3.2) and dual IDO1/TDO inhibitors (Sect. 4.1) based on this scaffold have also been described.

2.4 *N-Hydroxyamidines and Structurally Related Compounds*

In 2009, Incyte Corporation reported N-hydroxyamidines as potent, reversible, competitive IDO1 inhibitors (Fig. 5) [45]. The most potent compound of this series, compound **19**, displayed enzymatic and cellular IC_{50} values of 67 and 19 nM, suppressed kynurenine generation in vivo, and inhibited melanoma growth in a mouse model [45]. Modeling of the binding of **19** to IDO1 predicted that the oxygen of the hydroxyamidine binds to the heme iron, and that the amidine adopts a cis conformation. The phenyl ring was placed inside the A pocket, producing a tight fit, while the
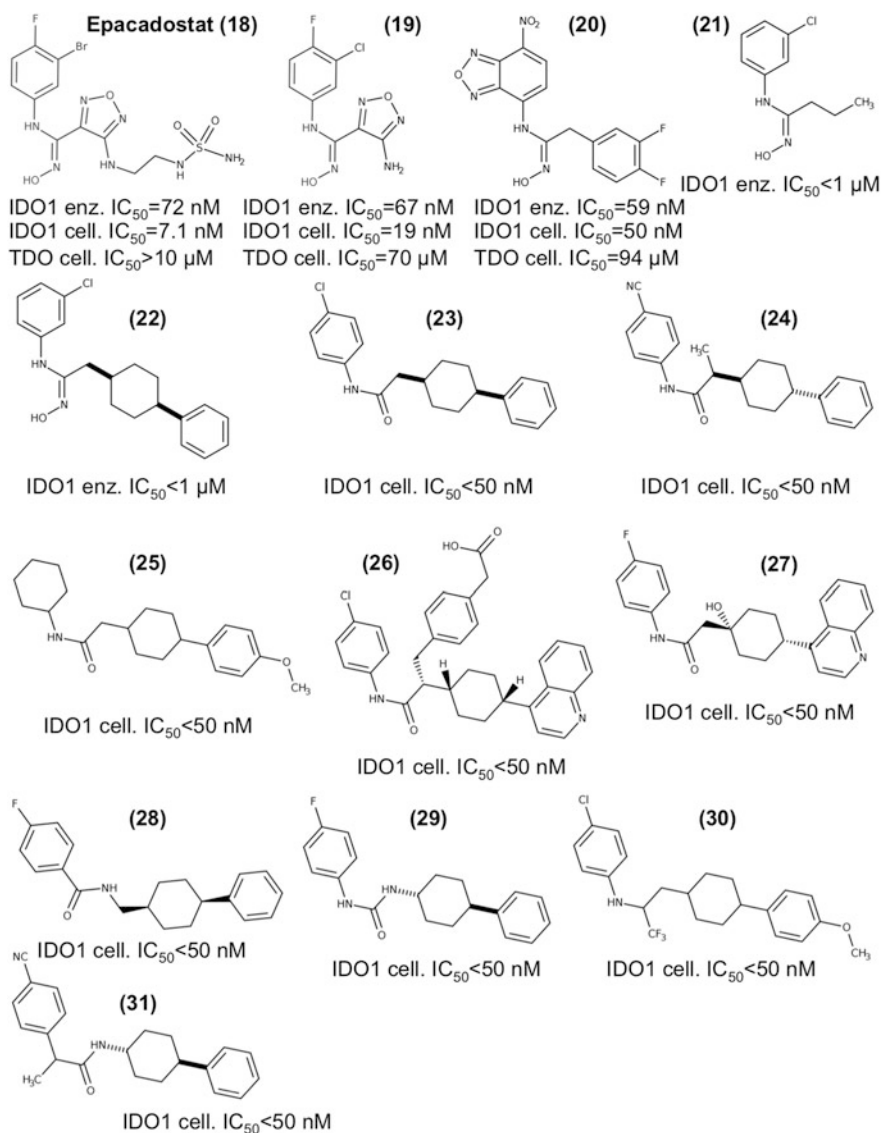
Fig. 5 IDO1 inhibitors based on the N-hydroxyamidine and related scaffolds. Epacadostat (**18**) [107], N-hydroxyamidine (**19**) [45], nitrobenzofurazan N-hydroxyamidine (**20**) [108], N-hydroxyamidines (**21**, **22**) [62], N-phenylamides (**23**, **24**) [65], N-cyclohexylamide (**25**) [65], further modified N-phenylamides (**26**, **27**) [63], benzamide (**28**) [64], phenylurea (**29**) [64], aniline (**30**) [64], and 2-phenyl-propanamide (**31**) [64]

amino substituent on the furazan ring could form a hydrogen bond to the propanoic acid group on the heme ring [45]. The clinical candidate (**18**, epacadostat, CAS# 1204669-58-8) belongs to a further optimized series of N-hydroxyamidines with extension to the B pocket [107, 109]. Epacadostat was shown to inhibit IDO1 in

enzymatic ($IC_{50} = 72$ nM) and in cellular tests ($IC_{50} = 7.1$ nM), to suppress Trp catabolism in vivo, to impede tumor growth, and not to inhibit IDO2, TDO, tryptophan transport, or a panel of 50 other proteins [38, 46].

Nitrobenzofurazan derivatives of the N-hydroxyamidine scaffold (**20**) [108] showed very good activities in enzymatic and cellular tests but a lower ligand efficiency than the Incyte compound **19**. The described compounds were strongly selective for IDO1 over TDO by factors of 200–1,700.

Flexus Biosciences successfully modified Incyte's N-hydroxyamidine scaffold first by simplifying the presumed B-pocket extension of the N-hydroxyamidines without the furazan ring and preserving nanomolar potencies (**21**, **22**) [62]. Later, they replaced the N-hydroxyamidine group by a simple amide function and to obtain a large number of analogs with cellular IC_{50} values below 50 nM (**23, 24, 25**, Fig. 5) [65]. Most modifications again affected the B-pocket extensions, with many potent compounds showing a cyclohexyl-phenyl motif. However, the A pocket also seems to tolerate many changes, for example, the replacement of the phenyl ring by a cyclohexyl ring (**25**).

In two concurrent patent applications, Flexus described further modifications of the scaffold. In one, modifications to the B-pocket extension were mainly based on a cyclohexyl-quinoline motif, potentially with another substituent next to the amide (**26**, **27**) [63]. In the other [64], modifications to the presumed heme-binding moieties are described, such as N-phenylamide to N-benzylamide, N-phenylsulfonamide, benzamide (**28**), phenylurea (**29**), aniline (**30**), and phenylacetamide (**31**, Fig. 5). The nanomolar activities of these compounds with electronically very different heme-facing moieties are quite astonishing and might suggest that the optimal filling of the B pocket plays a crucial role here.

In summary, the N-hydroxyamidine scaffold and related compounds have proven to provide a very promising route to the development of selective IDO1 inhibitors.

2.5 1,2,3-Triazoles

4-Aryl-1,2,3-triazoles were discovered in 2010, with the parent compound (**32**, Fig. 6) displaying an enzymatic IC_{50} value of 60 μM [44]. The rationally designed triazole **33** (MMG-0358) [110] showed nanomolar activities both in enzymatic and cellular assays, no cellular toxicity, and a high selectivity for IDO1 over TDO [110]. Nanomolar cellular IC_{50} values were also reported for the N-phenyl-1,2,3-triazol-4-amine compounds from Vertex (**34**) [74]. However, bioisosteric replacement of imidazole by 1,2,3-triazole in the NewLink Genetic fused compounds led to only moderately active compounds (**35**) [112].

The 1,2,3-triazole scaffold provides an interesting alternative to the imidazole scaffold, as it could exhibit better specificity with respect to other heme proteins. However, no potent compounds with a B-pocket extension have been reported so far.
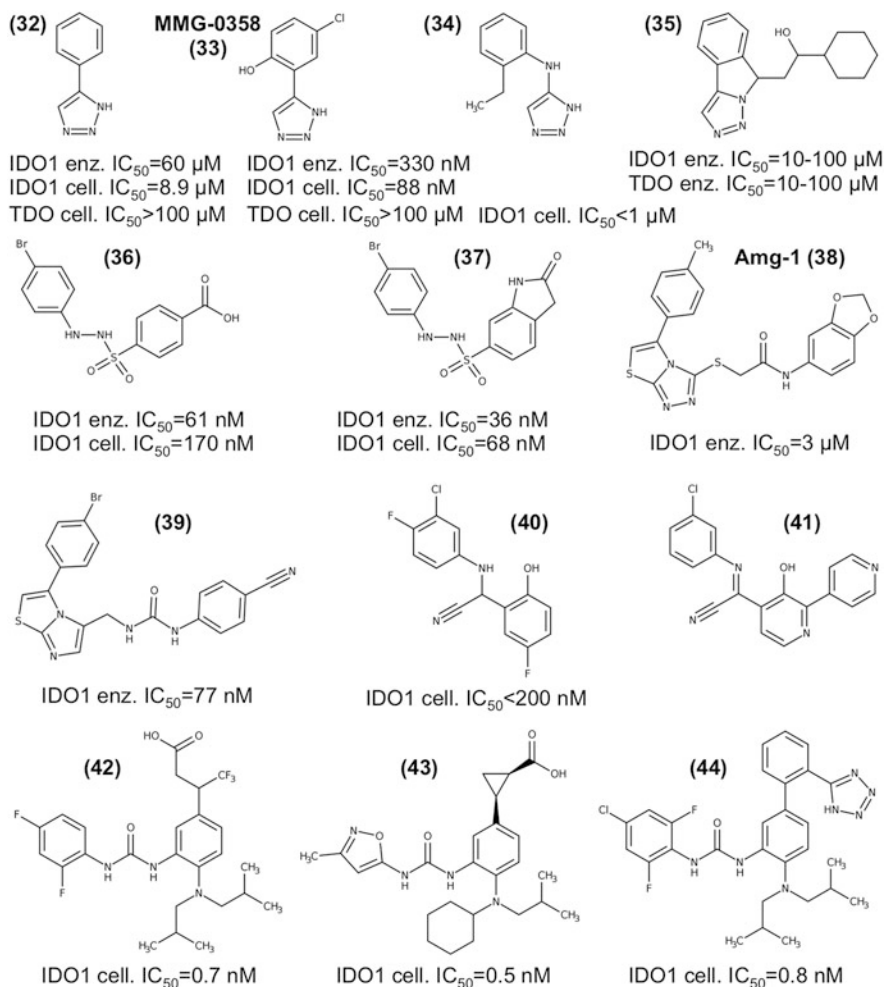
Fig. 6 Other IDO1 inhibitors with published activity data. 4-phenyl-1,2,3-triazole (**32**) [44, 110, 111], 1,2,3-triazoles (**33**, **34**) [74, 110], fused 1,2-3-triazole (**35**) [112], benzenesulfonyl hydrazides (**36**, **37**) [113, 114], triazolothiazole Amg-1 (**38**) [54], imidazothiazole (**39**) [42], aminonitrile (**40**) [59], iminonitrile (**41**) [61], and 2-amino-phenylureas (**42**, **43**, **44**) [55, 56, 115]

2.6 Phenyl Benzenesulfonylhydrazides

A series of phenyl benzenesulfonyl hydrazides (**36**, Fig. 6) displayed nanomolar IC_{50} values in both enzymatic and cellular assays [113]. In a further development of this scaffold, an optimized lead compound (**37**) with an enzymatic IC_{50} value of 36 nM, a cellular IC_{50} value of 68 nM, selectivity for IDO1 over 68 other protein targets, good oral bioavailability in rats, significant reduction of the Kyn/Trp ratio in the murine CT26 syngeneic colorectal cancer model, and significant tumor volume reduction in the same model was described [114].

2.7 Fused Thiazoles

The triazolo thiazole (Amg-1, **38**, Fig. 6) was reported by Amgen to inhibit IDO1 with an enxymatic IC_{50} value of 3 μM, and its selectivity for IDO1 over IDO2 and TDO was demonstrated [54]. Amg-1 was later co-crystallized with IDO1 (Fig. 2b) and used for rational compound optimization. This led to the discovery of imidazothiazole derivatives occupying both pocket A and pocket B [42]. Nanomolar enzymatic inhibition activities were obtained with a urea linker, with the best compound in the series showing an enzymatic IC_{50} value of 77 nM (**39**).

2.8 Aminonitriles and Iminonitriles

Curadev reported aminonitriles as IDO1 inhibitors with enzymatic IC_{50} values below 200 nM [59]. One compound (**40**, Fig. 6) was shown to reduce plasma KYN levels by 40% in mice after inflammatory lipopolysaccharide (LPS) injection used to induce IDO1 expression. Later, the scaffold was modified to feature unsaturated iminonitriles and pyridines (**41**) [61]. For these compounds, only in vivo KYN level reduction values were given, which reached up to 87% after 2 h. Apparently, the predicted promiscuity of this scaffold due to their chemical reactivity as phenolic Mannich bases [75, 116, 117] does not hamper its in vivo use for IDO1 inhibition.

2.9 2-Amino-Phenylureas

In several patent applications, Bristol-Myers Squibb described a 2-amino-phenylurea scaffold and related compounds for IDO1 inhibition yielding low nanomolar to picomolar cellular IC_{50} values (**42**, **43**, **44**, Fig. 6) [55–58, 115]. These are the most potent compounds reported to date, but no data is available about their specificity and mode of action. The three-dimensional structures of the compounds do not seem to be able to fill the IDO1 active site without clashing with surrounding protein residues, suggesting that they could display a novel alternative binding mode.

3 Tryptophan 2,3-Dioxygenase Inhibitors

TDO (EC 1.13.11.11), a functionally related but evolutionarily distant enzyme to IDO1, is constitutively expressed in the liver and regulates systemic L-Trp levels [16]. TDO is a tetrameric enzyme with a higher substrate specificity for L-Trp than IDO1. Recently, it was shown to play a complementary role in different types of cancer [25, 118]. There are nine X-ray structures of TDO available from the RCSB

Fig. 7 X-ray structure of tryptophan 2,3-dioxygenase (TDO) (PDB ID 2NW8) from xanthomonas campestris in complex with ferrous heme and tryptophan [120]. Only the active site is shown, displaying the protein in surface representation, heme, selected protein side chains, and resolved solvent molecules in stick representation, and the ligand in ball and stick representation. Heteroatoms are colored as follows: *blue* (nitrogen), *red* (oxygen), and *orange* (iron). Hydrogen bonds are displayed as *thin orange lines*
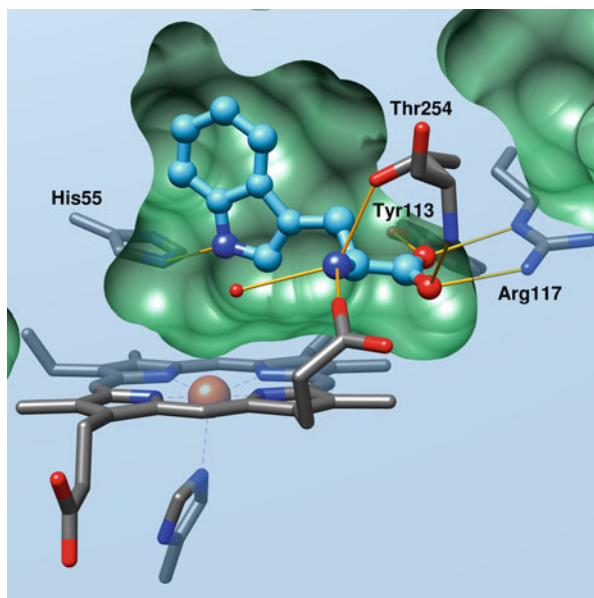
protein data bank, including a heme-free apo structure of human TDO [119] and a structure from xanthomonas campestris in complex with ferrous heme and trypto-phan (Fig. 7) [120]. Xanthomonas campestris shares a 34% sequence identity with human TDO, and nine out of 11 L-Trp binding residues are conserved [120].

3.1 6-Fluoro Indoles

L-Trp and its analogues 6-F-Trp and 5-F-Trp show a much higher affinity for TDO [120, 121] than IDO1, which facilitated the development of selective TDO inhib-itors based on the indole scaffold (Fig. 8).

The oldest and most used TDO inibitor is the 6-fluoroindole 680C91 (**45**) [122, 123], which displayed a K_i of 30 nM for rat TDO and was shown to be selective for TDO over IDO1 [122, 123]. Its regioisomer 709W92 (**46**) displayed the same K_i for rat TDO, but as it also inhibits serotonin uptake, it has been less used [123, 124]. Re-cently the K_i of **45** for human TDO was determined to be 880 nM (IC_{50} 280 nM), but it was shown to suffer from limited solubility and bioavailability [25].

Based on these compounds and motivated by the discovery that TDO is impli-cated in tumoral immune escape, Frédérick and coworkers described a series of more than 70 derivatives of **45**, systematically analyzing and varying all parts of the compound separately [125]. Cellular IC_{50} values on murine TDO were determined and used to develop a structure–activity relationship. Surprisingly, they did not find any compound more potent than **45**, but replacing the pyridine ring by a negatively
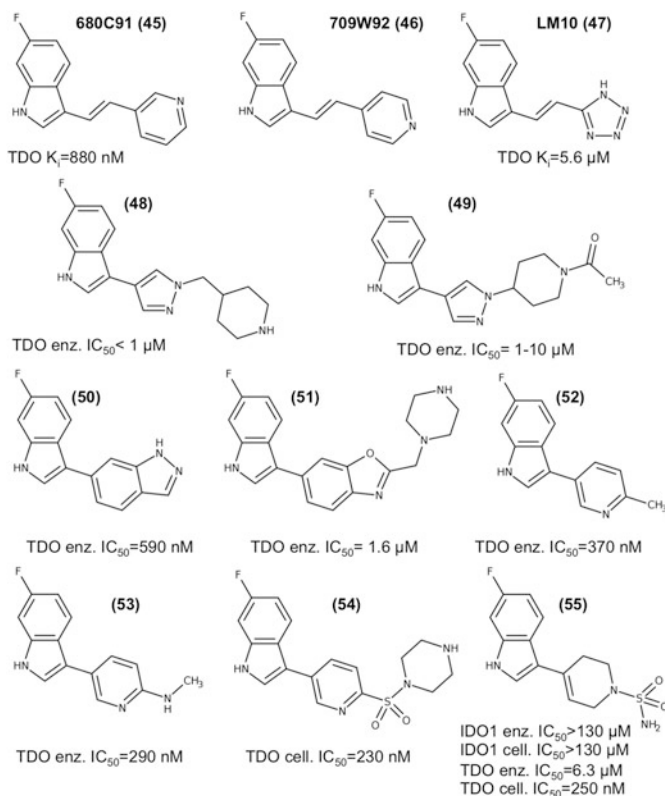
Fig. 8 TDO inhibitors based on 6-fluoro indole scaffold. 680C91 (**45**) [122, 123], 709W92 (**46**) [123, 124], LM10 (**47**) [25, 125], pyrazole derivatives (**48, 49**) [50], indazole derivative (**50**) [52], benzoxazole derivative (**51**) [52], pyridine derivatives (**52, 53, 54**) [51], and tetrahydropyridine derivative (**55**) [66]

charged group such as a carboxylate or a tetrazole preserved the favorable interactions of L-Trp with Thr254 (Thr342 in hTDO) and Arg117 (Arg144 in hTDO, Fig. 7) and led to more soluble and stable compounds. In the selected lead compound (**47**), the pyridine ring was replaced by a tetrazole. This compound showed a K_i of 5.6 μM on a crude extract of human TDO as well as selectivity over hIDO1, type A and B monoamine oxidase, 15 receptors, and three transporters. Unlike the parent compound **45**, it demonstrated a very good solubility and high oral bioavailability in mice [125]. Under the label LM10, **47** was used to show that TDO inhibition could reduce the growth of TDO-expressing P815 mastocytoma cells in mice without producing signs of liver toxicity [25].

Further work of iTeos Therapeutics on the indole scaffold led to the discovery of potent 3-substituted indole compounds with low micromolar or nanomolar enzymatic and cellular activities on hTDO (**48, 49, 50, 51, 52, 53, 54**). In three patents, they describe indoles with different heterocyclic substitutents. Besides citing

nanomolar enzymatic and cellular activities, a few compounds were shown to increase circulating L-Trp in mice when administered orally by gavage at 100 mg/kg [50–52]. While pyrazole derivatives were less efficient in this respect (**49**, +40% L-Trp) [50], benzoxazole (**51**, +80% L-Trp) [52] and especially pyridines (**54**, +140% L-Trp) [51] were more efficient.

IOmet Pharma also developed 3-substituted indoles and oxindoles for IDO1 (Sect. 2.2) and TDO inhibition. Three compounds demonstrated nanomolar enzymatic IC_{50} values on TDO and selectivity over IDO1 [66]. The representative compound **55** was selective for TDO, with an anzymatic IC_{50} value of 6.3 μM (IDO1: >130 μM), and a cellular IC_{50} value of 250 nM (IDO1: >100 μM) [66, 126].

Most but not all of these indole-based TDO inhibitors contain a 6-fluoro substituent on the indole ring. For xanthomonas campestris TDO, it has been shown that 6-F-L-Trp has a high affinity for TDO and that it is an efficient TDO substrate [120].

3.2 Imidazoles

While selective IDO1-inhibiting imidazoles are described in Sect. 2.3, and dual IDO1/TDO compounds in Sect. 4.1, TDO-selective imidazole inhibitors have also been discovered (Fig. 9). In the very active imidazo-indole inhibitors developed by Redx Pharma (**56, 57, 58, 59**) [72], the hydroxylated alkyl chain of the imidazo-indole from NewLink Genetics (**62**, Fig. 10) was replaced by an ether or an amino linker. These compounds displayed at least about 20-fold selectivity for TDO over IDO1.
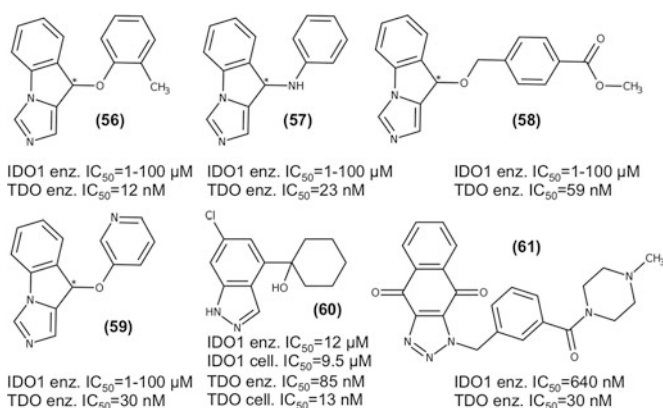
Fig. 9 Other TDO inhibitors. Fused imidazo-indoles (**56**, **57**, **58**, **59**) [72], 4-substituted indazole (**60**) [70], and naphthotriazoledione (**61**) [127]. Stereocenters discussed in the main text are marked by an *asterisk*
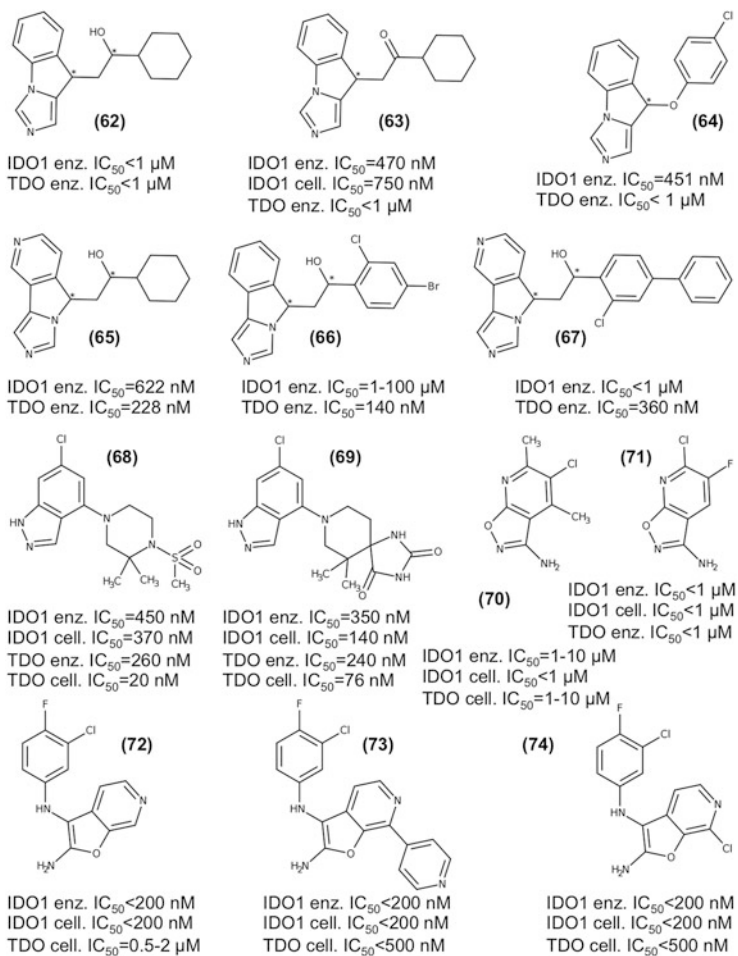
Fig. 10 Dual IDO1/TDO inhibitors. Fused imidazole-indoles (**62**, **63**, **64**) [72, 112], fused imidazole-isoindoles (**65**, **66**, **67**) [73], 4-substituted indazoles (**68**, **69**) [70], 3-aminoisoxazolopyridines (**70**, **71**) [128], and furopyridines (**72**, **73**, **74**) [60]. Stereocenters discussed in the main text are marked by an asterisk

3.3 Indazoles

Replacing the indole scaffold by an indazole, IOmet Pharma developed selective TDO and dual IDO1/TDO inhibitors based on the indazol-4-amine scaffold [70]. Many compounds displayed at least 1.5 log units better enzymatic and cellular activities towards TDO than IDO1. Compound **60** is selective for TDO, with an enzymatic IC_{50} value of 85 nM vs. 12 μM.

3.4 Quinones

As early as 1961, it was shown that the quinones or hydroquinones catechol, quinol, p-quinone, L-dihydroxyphenylalanine, and L-epinephrine were able to inhibit TDO [129]. In 2014, a screening of 2,800 compounds from the library of the National Cancer Institute (USA) identified seven compounds inhibiting TDO, among them six quinones such as β-lapachone, taxifolin, nanaomycin A, and mitomycin C [130]. Later, the same group described derivatives of the naturally ocurring quinone isatin for TDO and IDO1 inhibition [131]. In these works, only enzymatic assay results were reported, and no additional tests were carried out.

Naphthotriazolediones were discovered as TDO inhibitors based on a structure-based virtual screening [127]. The best compound (**61**, Fig. 9) displayed an IC_{50} value of 30 nM on hTDO and 20-fold selectivity over IDO. Further investigations of this compound suggested that it does not act through redox cycling and that it is selective for TDO over several other unrelated targets.

4 Dual Indoleamine 2,3-Dioxygenase 1/Tryptophan 2,3-Dioxygenase Inhibitors

As both IDO1 and TDO seem to play complementary roles in cancers, and as their active sites share many similarities, development of dual IDO1/TDO inhibitors is particularly attractive (Fig. 10).

4.1 Imidazoles

After describing fused imidazo-isoindole derivatives for IDO1 inhibition (**14**, **15**, Fig. 4), NewLink Genetics also described imidazo-indole derivatives to be dual potent inhibitors of IDO1 and TDO (**62**, **63**, Fig. 10) [112].

Redx Pharma built upon the work of NewLink Genetics, describing nanomolar enzymatic IDO1 and TDO inhibitors based on both the imidazo-indole [72] and the imidazo-isoindole [73] scaffolds. They determined the enzymatic IC_{50} value of one of the four stereoisomers the imidazo-indole compound **62** to be 94 nM [72]. Some new imidazo-indoles, such as, for example, the ether (**64**), seemed to be nearly equipotent towards IDO1 and TDO. The imidazo-isoindoles described by Redx (**65**, **66**, **67**) [73] were somewhat more active towards TDO. Incorporation of a pyridine ring into the tricyclic scaffold was found to be beneficial (**65**, **67**), and the placement of a second aromatic ring in the B pocket (**67**) was tolerated.

4.2 Indazoles

The indazol-4-amine scaffold developed by IOmet Pharma yielded selective TDO inhibitors (Sect. 3.3) and dual IDO1/TDI inhibitors [70]. Compounds **68**, **69** displayed enzymatic IC_{50} values below 500 nM towards both IDO1 and TDO.

4.3 3-Aminoisoxazolopyridines

Researchers from the University of Auckland developed very small dual IDO1/TDO inhibitors based on the 3-aminoisoxazolopyridine scaffold (**70**, **71**, Fig. 10) [128]. Compound **70** displayed an enzymatic IC_{50} value of 1–10 μM and a cellular IC_{50} value below 1 μM on IDO1, as well as a cellular IC_{50} value of 1–10 μM on TDO. It reduced the KYN/Trp ratio in plasma and tumors of a glioma mouse model, reduced tumor growth, and led to increased survival when administered in combination with an anti-PD1 antibody [128]. Compound **71** displayed even more potent enzymatic and cellular inhibition of IDO1 and TDO.

Bulky substituents on the pyridine ring as well as substituents of the amino group led to much less active compounds.

4.4 Furopyridines

Curadev reported di-amino substituted furopyridines as dual IDO1/TDO inhibitors (**72**, **73**, **74**, Fig. 10) [60]. Here, many compounds displayed enzymatic and cellular IC_{50} values below 200 nM on hIDO1 and enzymatic IC_{50} values below 500 nM on TDO. Two compounds, including compound **72**, also inhibited IDO2 with nanomolar IC_{50} values. Reduction of LPS-induced plasma KYN levels in mice above 50% were reported for a number of compounds. Compounds **72** and **73** were shown to reduce tumor volumes in vivo in the murine CT26 syngeneic colorectal cancer model, to reduce KYN levels in tumor tissue, and to be capable of penetrating the blood–brain barrier [60].

5 Indoleamine 2,3-Dioxygenase 2 Inhibitors

According to recent work [16], human IDO2 is weakly expressed in the liver, testes, and thyroid, but in contrast to previous reports [86, 132] not in human tumors. Two commonly occurring single nucleotide polymorphisms in the coding region of human IDO2 lead to more than 25% of humans having enzymatically inactive IDO2 [27].

Only a few IDO2 inhibitors have been reported (Fig. 11), probably due to the difficulties in expressing and purifying active human IDO2 [133]. L-1MT (**1**, Fig. 3) has been reported to inhibit human IDO2 with K_i values in the range of 300 [85] to 425 μM [134]. In 2010, Incyte reported preliminary results of potent mouse IDO2 inhibitors with more than 100-fold selectivity over mIDO1 but did not disclose their structures [135].

Two years later, a library of 640 FDA-approved drugs were screened in cellular assays on mIDO1 and on mIDO2, and 12 compounds were reported to inhibit mIDO2 at low micromolar concentrations and with selectivity over mIDO1 [102]. For example, the proton pump inhibitor tenatoprazole (**75**) displayed cellular IC_{50} values of 1.8 and >100 μM for mIDO2 and mIDO1, respectively. However, these proton pump inhibitors are known to be prodrugs whose active sulfenamide moiety covalently binds with selected cysteine residues of hydrogen potassium ATPase [136]. Inhibition of IDO1 by cysteine-binding compounds such as ebselen has been demonstrated earlier [137]. Apparent lower inhibition of IDO1 could be due to the fact that the same incubation time was used for both enzymes, but as IDO1 degrades L-Trp much faster than IDO2 [133], this assay was not in its linear phase anymore.

Curadev reported two compounds (**72**, Fig. 10 and **76**, Fig. 11) to inhibit both human IDO1 and human IDO2 in enzymatic assays with IC_{50} values below 1 μM [60].

4-phenyl-1,2,3-triazoles were tested for mIDO2 inhibition in cellular assays, and it was noted that compounds filling only the A pocket were highly selective for IDO1, while compounds filling both A and B pockets displayed similar cellular IC_{50} values for hIDO1 and mIDO2 in the micromolar range (**77**) [133].

Tryptanthrins were also reported as potent hIDO2 inhibitors, but they show much better inhibition of hIDO1 than of hIDO2 (**78**) [134].

In summary, it seems to be challenging to develop selective IDO2 inhibitors, and their practical value has not been unequivocally established.

Fig. 11 Indoleamine 2,3-dioxygenase 2 (IDO2) inhibitors. Tenatoprazole (**75**) [102], furopyridine (**76**) [60], 4-phenyl-1,2,3-triazole (**77**) [133], and tryptanthrine (**78**) [134]
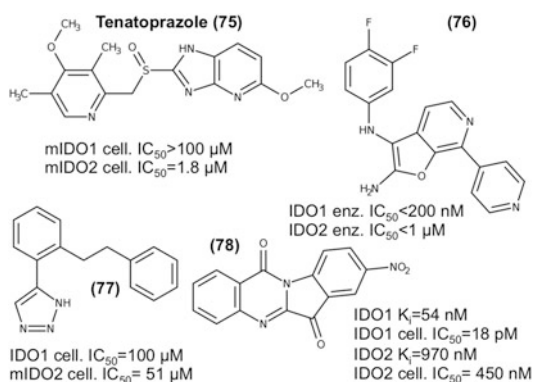
6 Conclusions

Thus far, IDO1 and TDO inhibition has been the main approach to address L-Trp metabolism as therapeutic target. The regulation of their expression might have different effects, as IDO1 has been shown to act also as a signaling protein independently from its enzymatic function [138]. Therapeutic vaccination against IDO1 has demonstrated disease stabilization without toxicity in patients with non-small cell lung cancer (NSCLC) [139]. If tryptophan depletion is the main cause of immune suppression (tryptophan depletion hypothesis), interference with the sensing of low L-Trp levels by the stress kinase GCN2 and the mTOR signaling pathway may provide different access points. Therapeutic regulation of L-Trp levels by modulation of transcellular L-Trp transport might be an alternative [15]. On the other hand, if bioactive L-Trp metabolites such as L-kynurenine (KYN), 3-hydroxy-L-kynurenine (3-HK), kynurenic acid (KA), or quinolinic acid (QUIN) are mainly responsible for immune suppression (tryptophan utilization hypothesis) [8], the inhibition of downstream enzymes along the kynurenine pathway (Fig. 1) such as kynurenine monooxygenase (KMO) or kynurenine aminotransferase II (KAT II) [21] or the suppression of the signaling pathways of the kynurenines, for example, through the aryl hydrocarbon receptor (AhR) [118, 140, 141], could be additional viable targets. Here, knowledge gained from many years of research into neurological disorders may be of value [142].

References

1. Khalil DN, Smith EL, Brentjens RJ, Wolchok JD (2016) Nat Rev Clin Oncol 13:273. doi:10.1038/nrclinonc.2016.25
2. Postow MA, Callahan MK, Wolchok JD (2015) J Clin Oncol 33:1974. doi:10.1200/JCO.2014.59.4358
3. Jackson HJ, Rafiq S, Brentjens RJ (2016) Nat Rev Clin Oncol 13:370. doi:10.1038/nrclinonc.2016.36
4. Yang JC, Rosenberg SA (2016) In: Tumor immunology, vol 130, 1st edn. Elsevier Inc., pp 279–294. doi: 10.1016/bs.ai.2015.12.006
5. Holmgaard RB, Zamarin D, Munn DH, Wolchok JD, Allison JP (2013) J Exp Med 210:1389. doi:10.1084/jem.20130066
6. Spranger S, Koblish HK, Horton B, Scherle PA, Newton R, Gajewski TF, Immunother J (2014) Cancer 2:3. doi:10.1186/2051-1426-2-3
7. Crunkhorn S (2014) Nat Rev Drug Discov 13:879. doi:10.1038/nrd4502
8. Stone TW, Stoy N, Darlington LG (2013) Trends Pharmacol Sci 34:136. doi:10.1016/j.tips.2012.09.006

9. Hayaishi O (1993) Protein Sci 2:472. doi:10.1002/pro.5560020320
10. Munn DH, Mellor AL (2013) Trends Immunol 34:137. doi:10.1016/j.it.2012.10.001
11. Barth H, Raghuraman S (2014) Crit Rev Microbiol 40:360. doi:10.3109/1040841X.2012.742037
12. Wolf H (1974) Scand J Clin Lab Invest 33(suppl 136):1. doi:10.3109/00365517409104201
13. Peters JC (1991) Adv Exp Med Biol 294:345. doi:10.1007/978-1-4684-5952-4_32
14. Platten M, Wick W, Van den Eynde BJ (2012) Cancer Res 72:5435. doi:10.1158/0008-5472.CAN-12-0569
15. Platten M, von Knebel Doeberitz N, Oezen I, Wick W, Ochs K (2015) Front Immunol 5:673. doi:10.3389/fimmu.2014.00673
16. van Baren N, Van den Eynde BJ (2015) Front Immunol 6:34. doi:10.3389/fimmu.2015.00034
17. Badawy AAB, Namboodiri AMA, Moffett JR (2016) Clin Sci 130:1327. doi:10.1042/CS20160153
18. Munn DH, Zhou M, Attwood JT, Bondarev I, Conway SJ, Marshall B, Brown C, Mellor AL (1998) Science 281:1191
19. Murakami Y, Ito H, Saito K (2015) In: Engin A, Engin BA (eds) Tryptophan metabolism: implications for biological processes, health and disease. Springer International Publishing, Cham, pp. 95–120
20. Vécsei L, Szalárdy L, Fülöp F, Toldi J (2013) Nat Rev Drug Discov 12:64. doi:10.1038/nrd3793
21. Dounay AB, Tuttle JB, Verhoest PR (2015) J Med Chem 58:8762. doi:10.1021/acs.jmedchem.5b00461
22. Yeung AW, Terentis AC, King NJ, Thomas SR (2015) Clin Sci 129:601. doi:10.1042/CS20140392
23. Uyttenhove C, Pilotte L, Théate I, Stroobant V, Colau D, Parmentier N, Boon T, Van den Eynde BJ (2003) Nat Med 9:1269. doi:10.1038/nm934
24. Opitz CA, Litzenburger UM, Opitz U, Sahm F, Ochs K, Lutz C, Wick W, Platten M (2011) PLoS One 6:e19823. doi:10.1371/journal.pone.0019823
25. Pilotte L, Larrieu P, Stroobant V, Colau D, Dolušić E, Frédérick R, Plaen ED, Uyttenhove C, Wouters J, Masereel B, Van den Eynde BJ (2012) Proc Natl Acad Sci U S A 109:2497. doi:10.1073/pnas.1113873109
26. Ball HJ, Sanchez-Perez A, Weiser S, Austin CJD, Astelbauer F, Miu J, McQuillan JA, Stocker R, Jermiin LS, Hunt NH (2007) Gene 396:203. doi:10.1016/j.gene.2007.04.010
27. Metz R, DuHadaway JB, Kamasani U, Laury-Kleintop L, Muller AJ, Prendergast GC (2007) Cancer Res 67:7082. doi:10.1158/0008-5472.CAN-07-1872
28. Yuasa HJ, Hasegawa T, Nakamura T, Suzuki T (2007) Comp Biochem Physiol B Biochem Mol Biol 146:461. doi:10.1016/j.cbpb.2006.11.028
29. van Baren N, Van den Eynde BJ (2015) Cancer Immunol Res 3:978. doi:10.1158/2326-6066.CIR-15-0095
30. Murray PJ (2016) Nat Immunol 17:132. doi:10.1038/ni.3323
31. Thomas S, DuHadaway J, Prendergast GC, Laury-Kleintop L (2014) J Cell Biochem 115:391. doi:10.1002/jcb.24674
32. Van de Velde LA, Gingras S, Pelletier S, Murray PJ (2016) Cell Metab 23:389. doi:10.1016/j.cmet.2016.02.004
33. Schmidt SK, Siepmann S, Kuhlmann K, Meyer HE, Metzger S, Pudelko S, Leineweber M, Däubener W (2012) PLoS One 7:e44797. doi:10.1371/journal.pone.0044797
34. Prendergast GC, Smith C, Thomas S, Mandik-Nayak L, Laury-Kleintop L, Metz R, Muller AJ (2014) Cancer Immunol Immunother 63:721. doi:10.1007/s00262-014-1549-4
35. Théate I, van Baren N, Pilotte L, Moulin P, Larrieu P, Renauld JC, Hervé C, Gutierrez-Roelens I, Marbaix E, Sempoux C, Van den Eynde BJ (2015) Cancer Immunol Res 3:161. doi:10.1158/2326-6066.CIR-14-0137
36. Godin-Ethier J, Hanafi LA, Piccirillo CA, Lapointe R (2011) Clin Cancer Res 17:6985. doi:10.1158/1078-0432.CCR-11-1331

37. Muller AJ, DuHadaway JB, Donover PS, Sutanto-Ward E, Prendergast GC (2005) Nat Med 11:312. doi:10.1038/nm1196
38. Liu X, Shin N, Koblish HK, Yang G, Wang Q, Wang K, Leffet L, Hansbury MJ, Thomas B, Rupar M, Waeltz P, Bowman KJ, Polam P, Sparks RB, Yue EW, Li Y, Wynn R, Fridman JS, Burn TC, Combs AP, Newton RC, Scherle PA (2010) Blood 115:3520. doi:10.1182/blood-2009-09-246124
39. Yang S, Li X, Hu F, Li Y, Yang Y, Yan J, Kuang C, Yang Q (2013) J Med Chem 56:8321. doi:10.1021/jm401195n
40. Li M, Bolduc AR, Hoda MN, Gamble DN, Dolisca SB, Bolduc AK, Hoang K, Ashley C, McCall D, Rojiani AM, Maria BL, Rixe O, MacDonald TJ, Heeger PS, Mellor AL, Munn DH, Johnson TS (2014) J Immunother Cancer 2:21. doi:10.1186/2051-1426-2-21
41. Sugimoto H, Oda S, Otsuki T, Hino T, Yoshida T, Shiro Y (2006) Proc Natl Acad Sci U S A 103:2611. doi:10.1073/pnas.0508996103
42. Tojo S, Kohno T, Tanaka T, Kamioka S, Ota Y, Ishii T, Kamimoto K, Asano S, Isobe Y (2014) ACS Med Chem Lett 5:1119. doi:10.1021/ml500247w
43. Peng YH, Ueng SH, Tseng CT, Hung MS, Song JS, Wu JS, Liao FY, Fan YS, Wu MH, Hsiao WC, Hsueh CC, Lin SY, Cheng CY, Tu CH, Lee LC, Cheng MF, Shia KS, Shih C, Wu S (2016) J Med Chem 59:282. doi:10.1021/acs.jmedchem.5b01390
44. Röhrig UF, Awad L, Grosdidier A, Larrieu P, Stroobant V, Colau D, Cerundolo V, Simpson AJG, Vogel P, Van den Eynde BJ, Zoete V, Michielin O (2010) J Med Chem 53:1172. doi:10.1021/jm9014718
45. Yue EW, Douty B, Wayland B, Bower M, Liu X, Leffet L, Wang Q, Bowman KJ, Hansbury MJ, Liu C, Wei M, Li Y, Wynn R, Burn TC, Koblish HK, Fridman JS, Metcalf B, Scherle PA, Combs AP (2009) J Med Chem 52:7364. doi:10.1021/jm900518f
46. Koblish HK, Hansbury MJ, Bowman KJ, Yang G, Neilan CL, Haley PJ, Burn TC, Waeltz P, Sparks RB, Yue EW, Combs AP, Scherle PA, Vaddi K, Fridman JS (2010) Mol Cancer Ther 9:489. doi:10.1158/1535-7163.MCT-09-0628
47. Tao M, Frietze W, Meloni DJ, Weng L, Zhou J, Pan Y (2015) Process for the synthesis of an indoleamine 2,3-dioxygenase inhibitor. Patent WO 2015/070007
48. Mautino MR, Jaipuri FA, Waldo J, Kumar S, Adams J, Van Allen C, Marcinowicz-Flick A, Munn D, Vahanian NN, Link CJ (2013) Proceedings of the 104th annual meeting of the American Association for Cancer Research. In: Cancer research, vol 73, Washington, DC, Philadelphia (PA)
49. Nayak A, Hao Z, Sadek R, Vahanian N, Ramsey W, Kennedy E, Mautino M, Link C, Bourbo P, Dobbins R, Adams K, Diamond A, Marshall L, Munn DH, Janik J, Khleif SN (2014) J Immunother Cancer 2:P250. doi:10.1186/2051-1426-2-S3-P250
50. Crosignani S, Cauwenberghs S, Deroose F, Driessens G (2015) 4-(indol-3-yl)-pyrazole derivatives, pharmaceutical compositions and methods for use. Patent WO 2015/067782
51. Crosignani S, Cauwenberghs S, Driessens G, Deroose F (2015) Novel 3-(indol-3-yl)-pyridine derivatives, pharmaceutical compositions and methods for use. Patent WO 2015/121812
52. Cauwenberghs S, Crosignani S, Driessens G, Deroose F (2015) Novel 3-indol substituted derivatives, pharmaceutical compositions and methods for use. Patent WO 2015/140717
53. Crosignani S, Cauwenberghs S, Driessens G, Deroose F (2015) Pyrrolidine-2,5-dione derivatives, pharmaceutical compositions and methods for use as IDO1 inhibitors. Patent WO 2015/173764
54. Meininger D, Zalameda L, Liu Y, Stepan LP, Borges L, McCarter JD, Sutherland CL (2011) Biochim Biophys Acta 1814:1947. doi:10.1016/j.bbapap.2011.07.023
55. Balog J, Huang A, Chen B, Chen L, Shan W (2014) IDO inhibitors. Patent WO 2014/150646
56. Balog J, Huang A, Chen B, Chen L, Seitz S, Hart A, Markwalder J (2014) Inhibitors of indoleamine 2,3-dioxygenase (IDO). Patent WO 2014/150677
57. Markwalder J, Seitz S, Balog J, Huang A, Mandal S, Williams D, Hart A, Inghrim J (2015) IDO inhibitors. Patent WO 2015/002918
58. Markwalder J, Balog J, Huang A, Seitz S (2015) IDO inhibitors. Patent WO 2015/006520

59. Banerjee M, Middya S, Shrivastava R, Raina S, Surya A, Yadav VK, Kapoor KK (2014) Aminonitriles as kynurenine pathway inhibitors. Patent WO 2014/141110

60. Banerjee M, Middya S, Shrivastava R, Raina S, Surya A, Yadav DB, Yadav VK, Kapoor KK, Venkatesan A, Smith RA, Thompson SK (2014) Inhibitors of the kynurenine pathway. Patent WO 2014/186035

61. Middya S, Yadav DB, Shrivastava R, Raina S, Banerjee M, Surya A (2016) Novel iminonitrile derivatives. Patent WO 2016/027241

62. Jaen JC, Osipov M, Powers JP, Shunatona HP, Walker JR, Zibinsky M (2015) Immunoregulatory agents. Patent WO 2015/188085

63. Beck HP, Jaen JC, Osipov M, Powers JP, Reilly MK, Shunatona HP, Walker JR, Zibinsky M, Balog JA, Williams DK, Markwalder JA, Cherney EC, Shan W (2016) Immunoregulatory agents. Patent WO 2016/073770

64. Beck HP, Jaen JC, Osipov M, Powers JP, Reilly MK, Shunatona HP, Walker JR, Zibinsky M, Balog JA, Williams DK, Markwalder JA, Seitz SP, Cherney L, Zhang EC, Shan W (2016) Immunoregulatory agents. Patent WO 2016/073774

65. Beck HP, Jaen JC, Osipov M, Powers JP, Reilly MK, Shunatona HP, Walker JR, Zibinsky M, Balog JA, Williams DK, Guo W (2016) Immunoregulatory agents. Patent WO 2016/073738

66. Cowley P, Wise A (2015) Tryptophan-2,3-dioxygenase (TDO) and/or indolamine-2,3-dioxygenase (IDO) inhibitors and their use. Patent WO 2015/082499

67. Cowley P, Wise A (2015) Indole derivatives for use in medicine. Patent WO 2015/150097

68. Cowley P, Wise A (2016) Pharmaceutical compound. Patent WO 2016/026772

69. Cowley P, Wise A (2016) Inhibitors of tryptophan 2,3-dioxygenase or indoleamine 2,3-dioxygenase. Patent WO 2016/071283

70. Cowley P, Wise A (2016) Pharmaceutical compound. Patent WO 2016/071293

71. Sherer BA (2016) Cyclohexyl-ethyl substituted diaza- and triaza-tricyclic compounds as indole-amine-2,3-dioxygenase (IDO) antagonists for the treatment of cancer. Patent WO 2016/037026

72. Armer R, Bingham M, Pesnot T, Gignoux C (2016) 4h-imidazo[1,5-a]indole derivatives and their use as indoleamine 2,3-dioxygenase (IDO) and/or tryptophan 2,3-dioxygenase (TD02) modulators. Patent WO 2016/051181

73. Armer R, Bingham M, Pesnot T, Gignoux C (2016) 6,7-heterocyclic fused 5h-pyrrolo[1,2-c] imidazole derivatives and their use as indoleamine 2,3-dioxygenase (IDO) and/or tryptophan 2,3-dioxygenase (TD02) modulators. Patent WO 2016/059412

74. Boyall D, Davis C, Dodd J, Everitt S, Miller A, Weber P, Westcott J, Young S (2014) Compounds useful as inhibitors of indoleamine 2,3-dioxygenase. Patent WO 2014/081689

75. Röhrig UF, Majjigapu SR, Vogel P, Zoete V, Michielin O (2015) J Med Chem 58:9421. doi:10.1021/acs.jmedchem.5b00326

76. Cady SG, Sono M (1991) Arch Biochem Biophys 291:326

77. Peterson AC, Migawa MT, Martin MJ, Hamaker LK, Czerwinski KM, Zhang W, Arend RA, Fisette PL, Okazi Y, Will JA, Brown RR, Cook JM (1994) Med Chem Res 3:531

78. Hou DY, Muller AJ, Sharma MD, DuHadaway J, Banerjee T, Johnson M, Mellor AL, Prendergast GC, Munn DH (2007) Cancer Res 67:792. doi:10.1158/0008-5472.CAN-06-2925

79. Nakashima H, Uto Y, Nakata E, Nagasawa H, Ikkyu K, Hiraoka N, Nakashima K, Sasaki Y, Sugimoto H, Shiro Y, Hashimoto T, Okamoto Y, Asakawa Y, Hori H (2008) Bioorg Med Chem 16:8661. doi:10.1016/j.bmc.2008.07.087

80. Yu CJ, Zheng MF, Kuang CX, Huang WD, Yang Q (2010) J Alzheimers Dis 22:257. doi:10.3233/JAD-2010-100684

81. Dolušić E, Larrieu P, Blanc S, Sapunaric F, Norberg B, Moineaux L, Colette D, Stroobant V, Pilotte L, Colau D, Ferain T, Fraser G, Galleni M, Frère JM, Masereel B, Van den Eynde B, Wouters J, Frédérick R (2011) Bioorg Med Chem 19:1550. doi:10.1016/j.bmc.2010.12.032

82. Yuasa HJ, Ball HJ, Austin CJD, Hunt NH (2010) Comp Biochem Physiol B Biochem Mol Biol 157:10. doi:10.1016/j.cbpb.2010.04.006

83. Austin CJD, Mailu BM, Maghzal GJ, Sanchez-Perez A, Rahlfs S, Zocher K, Yuasa HJ, Arthur JW, Becker K, Stocker R, Hunt NH, Ball HJ (2010) Amino Acids 39:565. doi:10.1007/s00726-010-0475-9

84. Qian F, Liao J, Villella J, Edwards R, Kalinski P, Lele S, Shrikant P, Odunsi K (2012) Cancer Immunol Immunother 61:2013. doi:10.1007/s00262-012-1265-x

85. Pantouris G, Serys M, Yuasa HJ, Ball HJ, Mowat CG (2014) Amino Acids 46:2155. doi:10.1007/s00726-014-1766-3

86. Löb S, Königsrainer A, Zieker D, Brücher BLDM, Rammensee HG, Opelz G, Terness P (2009) Cancer Immunol Immunother 58:153. doi:10.1007/s00262-008-0513-6

87. Löb S, Königsrainer A, Rammensee HG, Opelz G, Terness P (2009) Nat Rev Cancer 9:445. doi:10.1038/nrc2639

88. Qian F, Villella J, Wallace PK, Mhawech-Fauceglia P, Tario JD, Andrews C, Matsuzaki J, Valmori D, Ayyoub M, Frederick PJ, Beck A, Liao J, Cheney R, Moysich K, Lele S, Shrikant P, Old LJ, Odunsi K (2009) Chem Rev 69:5498. doi:10.1158/0008-5472.CAN-08-2106

89. Metz R, Rust S, DuHadaway JB, Mautino MR, Munn DH, Vahanian NN, Link CJ, Prendergast GC (2012) Oncoimmunology 1:1460. doi:10.4161/onci.21716

90. Muller AJ, Malachowski WP, Prendergast GC (2005) Expert Opin Ther Targets 9:831. doi:10.1517/14728222.9.4.831

91. Watanabe Y, Fujiwara M, Hayaishi O (1978) Biochem Biophys Res Commun 85:273. doi:10.1016/S0006-291X(78)80039-4

92. Saito K, Chen CY, Masana M, Crowley JS, Markey SP, Heyes MP (1993) Biochem J 291:11. doi:10.1042/bj2910011

93. Sono M, Roach M, Coulter E, Dawson J (1996) Chem Rev 96:2841. doi:10.1021/cr9500500

94. Southan M, Truscott R, Jamie J, Pelosi L, Walker M, Maeda H, Iwamoto Y, Toné S (1996) Med Chem Res 6:343

95. Chauhan N, Basran J, Rafice SA, Efimov I, Millett ES, Mowat CG, Moody PCE, Handa S, Raven EL (2012) FEBS J 279:4501. doi:10.1111/febs.12036

96. Dolušić E, Larrieu P, Blanc S, Sapunaric F, Pouyez J, Moineaux L, Colette D, Stroobant V, Pilotte L, Colau D, Ferain T, Fraser G, Galleni M, Frère JM, Masereel B, Van den Eynde B, Wouters J, Frédérick R (2011) Eur J Med Chem 46:3058. doi:10.1016/j.ejmech.2011.02.049

97. Kondreddi RR, Jiricek J, Rao SPS, Lakshminarayana SB, Camacho LR, Rao R, Herve M, Bifani P, Ma NL, Kuhen K, Goh A, Chatterjee AK, Dick T, Diagana TT, Manjunatha UH, Smith PW (2013) J Med Chem 56:8849. doi:10.1021/jm4012774

98. Stec J, Onajole OK, Lun S, Guo H, Merenbloom B, Vistoli G, Bishai WR, Kozikowski AP (2016) J Med Chem 59:6232–6247. doi:10.1021/acs.jmedchem.6b00415

99. Schmidt SV, Schultze JL (2014) Front Immunol 5:384. doi:10.3389/fimmu.2014.00384

100. Sono M, Cady SG (1989) Biochemistry 28:5392

101. Kumar S, Jaller D, Patel B, LaLonde JM, DuHadaway JB, Malachowski WP, Prendergast GC, Muller AJ (2008) J Med Chem 51:4968. doi:10.1021/jm800512z

102. Bakmiwewa SM, Fatokun A, Tran A, Payne RJ, Hunt NH, Ball HJ (2012) Bioorg Med Chem Lett 22:7641. doi:10.1016/j.bmcl.2012.10.010

103. Röhrig UF, Majjigapu SR, Chambon M, Bron S, Pilotte L, Colau D, Van den Eynde BJ, Turcatti G, Vogel P, Zoete V, Michielin O (2014) Eur J Med Chem 84:284. doi:10.1016/j.ejmech.2014.06.078

104. Fallarini S, Massarotti A, Gesù A, Giovarruscio S, Coda Zabetta G, Bergo R, Giannelli B, Brunco A, Lombardi G, Sorba G, Pirali T (2016) Med Chem Commun 7:409. doi:10.1039/C5MD00317B

105. Mautino M, Kumar S, Jaipuri F, Waldo J, Kesharwani T, Zhang X (2011) Imidazole derivatives as IDO inhibitors. Patent WO 2011/056652

106. Mautino M, Kumar S, Waldo J, Jaipuri F, Kesharwani T (2012) Fused imidazole derivatives useful as IDO inhibitors. Patent WO 2012/142237

107. Combs A, Yue E, Sparks R, Zhu W, Zhou J, Lin Q, Weng L, Yue T, Liu P (2010) 1,2,5-oxadiazoles as inhibitors of indoleamine 2,3-dioxygenase. Patent WO 2010/005958

108. Paul S, Roy A, Deka SJ, Panda S, Trivedi V, Manna D (2016) Eur J Med Chem 121:364. doi:10.1016/j.ejmech.2016.05.061

109. Combs A, Zhu W, Sparks RB (2008) N-hydroxyamidinoheterocycles as modulators of indoleamine 2,3-dioxygenase. Patent WO 2008/058178

110. Röhrig UF, Majjigapu SR, Grosdidier A, Bron S, Stroobant V, Pilotte L, Colau D, Vogel P, Van den Eynde BJ, Zoete V, Michielin O (2012) J Med Chem 55:5270. doi:10.1021/jm300260v

111. Huang Q, Zheng M, Yang S, Kuang C, Yu C, Yang Q (2011) Eur J Med Chem 46:5680. doi:10.1016/j.ejmech.2011.08.044

112. Kumar S, Waldo J, Jaipuri F, Mautino M (2014) Tricyclic compounds as inhibitors of immunosuppression mediated by tryptophan metabolization. Patent WO 2014/159248

113. Cheng MF, Hung MS, Song JS, Lin SY, Liao FY, Wu MH, Hsiao W, Hsieh CL, Wu JS, Chao YS, Shih C, Wu SY, Ueng SH (2014) Bioorg Med Chem Lett 24:3403. doi:10.1016/j.bmcl.2014.05.084

114. Lin SY, Yeh TK, Kuo CC, Song JS, Cheng MF, Liao FY, Chao MW, Huang HL, Chen YL, Yang CY, Wu MH, Hsieh CL, Hsiao W, Peng YH, Wu JS, Lin LM, Sun M, Chao YS, Shih C, Wu SY, Pan SL, Hung MS, Ueng SH (2016) J Med Chem 59:419. doi:10.1021/acs.jmedchem.5b01640

115. Markwalder J, Seitz S, Balog J, Huang A, Williams DK, Chen L, Mandal SK (2015) IDO inhibitors. Patent WO 2015/031295

116. Baell JB, Holloway G (2010) J Med Chem 53:2719. doi:10.1021/jm901137j

117. Bruns RF, Watson I (2012) J Med Chem 55:9763. doi:10.1021/jm301008n

118. Opitz CA, Litzenburger UM, Sahm F, Ott M, Tritschler I, Trump S, Schumacher T, Jestaedt L, Schrenk D, Weller M, Jugold M, Guillemin GJ, Miller CL, Lutz C, Radlwimmer B, Lehmann I, von Deimling A, Wick W, Platten M (2011) Nature 478:197. doi:10.1038/nature10491

119. Meng B, Wu D, Gu J, Ouyang S, Ding W, Liu ZJ (2014) Proteins 82:3210. doi:10.1002/prot.24653

120. Forouhar F, Anderson JLR, Mowat CG, Vorobiev SM, Hussain A, Abashidze M, Bruckmann C, Thackray SJ, Seetharaman J, Tucker T, Xiao R, Ma LC, Zhao L, Acton TB, Montelione GT, Chapman SK, Tong L (2007) Proc Natl Acad Sci U S A 104:473. doi:10.1073/pnas.0610007104

121. Thackray SJ, Bruckmann C, Anderson JLR, Campbell LP, Xiao R, Zhao L, Mowat CG, Forouhar F, Tong L, Chapman SK (2008) Biochemistry 47:10677. doi:10.1021/bi801202a

122. Salter M, Hazelwood R, Pogson CI, Iyer R, Madge DJ (1995) Biochem Pharmacol 49:1435

123. Madge D, Hazelwood R, Iyer R, Jones H, Salter M (1996) Bioorg Med Chem Lett 6:857. doi:10.1016/0960-894X(96)00124-2

124. Salter M, Hazelwood R, Pogson CI, Iyer R, Madge DJ, Jones HT, Cooper BR, Cox RF, Wang CM, Wiard RP (1995) Neuropharmacology 34:217

125. Dolušić E, Larrieu P, Moineaux L, Stroobant V, Pilotte L, Colau D, Pochet L, Van den Eynde B, Masereel B, Wouters J, Frédérick R (2011) J Med Chem 54:5320. doi:10.1021/jm2006782

126. Hunter B, McElroy S, Wise A (2015) Screening method. Patent WO 2015/091862

127. Wu JS, Lin SY, Liao FY, Hsiao WC, Lee LC, Peng YH, Hsieh CL, Wu MH, Song JS, Yueh A, Chen CH, Yeh SH, Liu CY, Lin SY, Yeh TK, Hsu JTA, Shih C, Ueng SH, Hung MS, Wu SY (2015) J Med Chem 58:7807. doi:10.1021/acs.jmedchem.5b00921

128. Palmer BD, Ching LM, Gamage SA (2015) Inhibitors of tryptophan dioxygenases (IDO1 and TDO) and their use in therapy. Patent WO 2015/024233

129. Frieden E, Westmark GW, Schor JM (1961) Arch Biochem Biophys 92:176

130. Pantouris G, Mowat CG (2014) Biochem Biophys Res Commun 443:28. doi:10.1016/j.bbrc.2013.11.037

131. Pantouris G, Loudon-Griffiths J, Mowat CG (2016) J Enzyme Inhib Med Chem 6366:1. doi:10.3109/14756366.2016.1170013

132. Witkiewicz AK, Costantino CL, Metz R, Muller AJ, Prendergast GC, Yeo CJ, Brody JR (2009) J Am Coll Surg 208:781. doi:10.1016/j.jamcollsurg.2008.12.018

133. Röhrig UF, Majjigapu SR, Caldelari D, Dilek N, Reichenbach P, Ascencao K, Irving M, Coukos G, Vogel P, Zoete V, Michielin O (2016) Bioorg Med Chem Lett 26:4330. doi:10.1016/j.bmcl.2016.07.031

134. Li J, Li Y, Yang D, Hu N, Guo Z, Kuang C, Yang Q (2016) Eur J Med Chem 123:171. doi:10.1016/j.ejmech.2016.07.013

135. Liu X, Yang G, Wang Q, Leffet L, Katiyar K, Waeltz P, Burns T, Combs A, Newton R, Scherle P (2010) EJC Suppl 8:206. doi:10.1016/S1359-6349(10)72367-3

136. Welage LS (2003) Pharmacotherapy 23:74S. doi:10.1592/phco.23.13.74S.31929

137. Terentis AC, Freewan M, Sempértegui Plaza TS, Raftery MJ, Stocker R, Thomas SR (2010) Biochemistry 49:591. doi:10.1021/bi901546e

138. Pallotta MT, Orabona C, Volpi C, Vacca C, Belladonna ML, Bianchi R, Servillo G, Brunacci C, Calvitti M, Bicciato S, Mazza EMC, Boon L, Grassi F, Fioretti MC, Fallarino F, Puccetti P, Grohmann U (2011) Nat Immunol 12:870. doi:10.1038/ni.2077

139. Andersen MH, Svane IM (2015) Oncoimmunology 4:e983770. doi:10.4161/2162402X.2014.983770

140. Mezrich JD, Fechner JH, Zhang X, Johnson BP, Burlingham WJ, Bradfield CA (2010) J Immunol 185:3190. doi:10.4049/jimmunol.0903670

141. Bessede A, Gargaro M, Pallotta MT, Matino D, Servillo G, Brunacci C, Bicciato S, Mazza EMC, Macchiarulo A, Vacca C, Iannitti R, Tissi L, Volpi C, Belladonna ML, Orabona C, Bianchi R, Lanz TV, Platten M, Della Fazia MA, Piobbico D, Zelante T, Funakoshi H, Nakamura T, Gilot D, Denison MS, Guillemin GJ, DuHadaway JB, Prendergast GC, Metz R, Geffard M, Boon L, Pirro M, Iorio A, Veyret B, Romani L, Grohmann U, Fallarino F, Puccetti P (2014) Nature 511:184. doi:10.1038/nature13323

142. Maddison DC, Giorgini F (2015) Semin Cell Dev Biol 40:134. doi:10.1016/j.semcdb.2015.03.002

143. Pettersen EF, Goddard T, Huang C, Couch G, Greenblatt D, Meng E, Ferrin TE (2004) J Comput Chem 25:1605

Protein–Protein Interaction Inhibitors

Check for
updates

Ian Robert Hardcastle

Abstract The study of cellular mechanisms of cancer growth and survival has revealed a complex web of signalling pathways that produce the 'hallmarks of cancer'. A number of critical cellular signalling nodes have been characterised from which many new drug targets have been proposed. A number of these nodes are regulated by protein–protein interactions, and so present attractive, if challenging, targets for drug discovery. Drug discovery efforts towards three PPI families have resulted in clinically investigated drugs: i.e. Bcl-2 family inhibitors, MDM2-p53 inhibitors and IAP inhibitors. The discovery and optimisation of these drug classes are detailed in this chapter.

Keywords Bcl-2, IAP, Inhibitors, MDM2-p53, Protein–protein interactions

Contents

I.R. Hardcastle (✉)
Newcastle Cancer Centre at the Northern Institute for Cancer Research, School of Chemistry,
Newcastle University, Bedson Building, Newcastle upon Tyne NE1 7RU, UK
e-mail: Ian.Hardcastle@ncl.ac.uk

Abbreviations

ALL	Acute lymphoblastic leukaemia
Bad	Bcl-2-associated death promoter
Bak	Bcl-2-homologous antagonist killer
Bax	Bcl-2-associated protein
Bcl-2	B-cell lymphoma 2
Bcl-B	B-cell lymphoma/leukaemia 11B protein
Bcl-w	Bcl-2-like protein 2
Bcl-xL	B-cell lymphoma-extra large
Bid	BH3 interacting-domain death agonist
CLL	Chronic lymphocytic leukaemia
Mcl-1	Induced myeloid leukaemia cell differentiation protein
MDM2	Mouse double minute 2
mTOR	Mammalian target of rapamycin protein
NF-κB	Nuclear factor-kappa-B
NIK	NF-kappa-B-inducing kinase
PUMA	p53 upregulated modulator of apoptosis
RIPK1	Receptor-interacting serine/threonine-protein kinase 1
SCLC	Small cell lung cancer
SLL	Small lymphocytic leukaemia
Smac	Second mitochondria-derived activator of caspases
t-Bid	Truncated BH3 interacting-domain death agonist
TRAIL	TNF-related apoptosis-inducing ligand
XIAP	X-linked inhibitor of apoptosis protein

1   PPI Targets in Cancer

The modern understanding of cancer biology is that tumour cells have acquired the characteristic 'hallmarks of cancer' through gain-of-function mutations to oncogenes and loss-of-function of tumour suppressor genes [1]. Detailed examination of signalling pathways associated with hallmark traits has allowed the identification of numerous potential targets for intervention by therapeutic agents, in many cases with small-molecule drugs. A number of pathways investigated thus far rely on

signalling *via* nodes regulated by protein–protein interactions (PPIs). In particular, PPIs regulating the apoptotic response of a cell have been characterised, providing promising areas for drug discovery, for example, between members of the B-cell lymphoma 2 (Bcl-2) family, the mouse double minute 2 (MDM2)–p53 interaction, and the interaction of second mitochondria-derived activator of caspases protein with X-linked inhibitor of apoptosis protein (Smac-XIAP). This chapter will describe each of these PPI targets and the discovery of small-molecule PPI inhibitor drugs that have entered clinical trials.

1.1   PPI Chemotherapy Drugs

Historically, extensive screening of natural products was used to identify compounds with cytotoxic activity for use in chemotherapy regimens. For a number of compounds investigated, the molecular mechanism of action was identified to be the disruption of a PPI (Table 1).
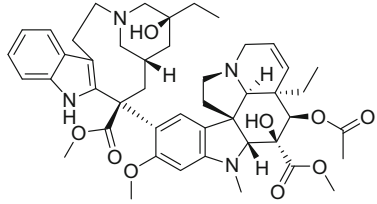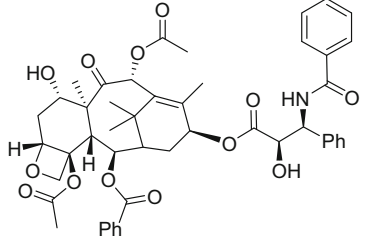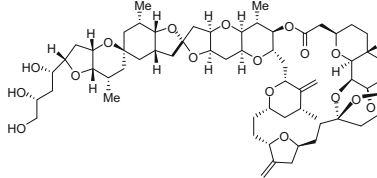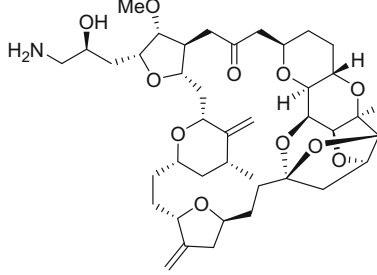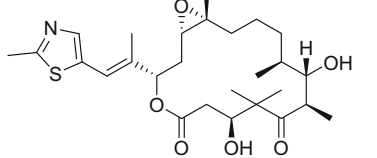
The regulation of microtubule cycling by the polymerisation and depolymerisation of α,β-tubulin is essential for the organisation of DNA during the M-phase of the cell cycle, and is targeted by a number of natural products from diverse sources. Isolated from plant sources, the vinca alkaloids e.g. vinblastine (**1**), and the taxoids e.g. taxol (**2**) were initially thought to share the same mechanism of action. However, detailed studies indicated that vinblastine (**1**) acts by binding into a hydrophobic groove at the interface of the α- and β-tubulin subunits at the ends of microtubules, and stabilises the microtubule at low concentrations, but induces depolymerisation at higher concentrations [2]. In contrast, taxol (**2**) binds to the β-tubulin subunit close to the GTP-binding site [3–5]. A conformational change is induced by drug binding that results in an unusually strong interaction between subunits and consequently microtubules grow in an uncontrolled manner. Isolated from marine sponges, the natural product Halichondrin B (**3**) and the simplified synthetic derivative Erubilin (**4**) also bind to microtubules close to the vinca binding site, and overlapping with the GTP-binding site, suppressing the growth of microtubules [6, 7]. Isolated from the myxobacteria *Sorangium cellulosum*, Epothilones e.g. **5** have a similar mechanism of action as the taxoids, and promote microtubule growth.

The semi-synthetic derivative of rapamycin, temsirolimus (**6**) inhibits the kinase activity of the mammalian target of rapamycin protein (mTOR) by forming a protein–protein complex with the FK506 binding protein 12 (FKBP12) [8].

1.2   Druggability of PPIs
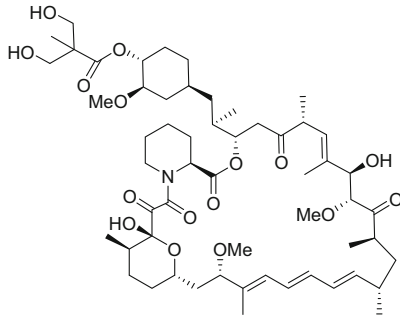
Despite the serendipitous discovery of PPIs as cancer therapies, until recently the established view from medicinal chemists has been that PPI targets are significantly less 'druggable' than enzyme or receptor targets. The reasoning for this is based on

Table 1 Natural product derived PPI drugs

Name	Compound	Structure
Vinblastine	1	
Taxol	2	
Halichondrin B	3	
Eribulin	4	
Epothilone B	5	

(continued)

Table 1 (continued)

Name	Compound	Structure
Temsirolimus	**6**	

the high surface area for PPI targets (1,500–4,660 Å^2) compared with other drug–protein interfaces (1,200–2,000 Å^2), and their relatively high binding affinities ($\Delta G = -7.0$ to -17.2 kcal/mol) [9]. Other analyses suggested that PPIs are more circular, flatter, less polar, and present fewer opportunities for H-bonding than enzyme or receptor drug targets [10]. The negative outlook from these global analyses of PPIs has been contradicted by detailed investigations of PPI binding sites, including alanine-scanning mutagenesis, that have revealed that many PPIs include small regions of high binding affinity called 'hot-spots' that can have attractive features for small molecule binding [11, 12]. Hot-spots may include the binding sites for large amino acid side chains on one protein that bind to small pockets on the partner protein, and may be circled by polar residues [13]. 'Hot segments' are larger continuous epitopes that contribute the majority of the binding energy of a PPI [14]. The most tractable of these for drug discovery are the interactions between a continuous peptide sequence of one peptide that interacts with a defined domain of the partner protein. The interfaces between protein and α-helical epitopes have demonstrated good tractability as drug targets, as exemplified by the development of Bcl-2 family and MDM2-p53 PPI inhibitors (*vide infra*).

Targeting PPIs with small-molecules may have some advantages as they represent an under exploited class within the 'druggable genome' and may present opportunities to inhibit cellular pathways that would be difficult to approach through other target classes [15]. PPIs may offer better opportunities for selectivity in comparison to competitive inhibition of enzymes at their substrate of co-factor binding sites due to the size and structural diversity of the interactions targeted. Unfortunately, the proposal that PPI inhibitors will offer a lower likelihood of developing resistance has not been borne out in clinical experience, especially in the case of MDM2-p53 inhibitors [16, 17].

2   Bcl Family Inhibitors

2.1   *Biology*

The response of cells to a variety of signals resulting in programmed cell death or apoptosis is controlled by the PPIs of a family of proteins related to Bcl-2 [18, 19]. Within the family, proteins can be grouped according to their role (Fig. 1). The BH3-only proteins [e.g. Bcl-2-associated death promoter (Bad) and p53 upregulated modulator of apoptosis (PUMA)] act as initiators of apoptosis in response to cytokine deprivation, intracellular damage or oncogenic signalling, whereas truncated BH3 interacting-domain death agonist (t-Bid) is activated by the death receptor and signalling via caspase 8. Activation of BH3 proteins induces both the negative regulation of the pro-survival Bcl-2 proteins, and the activation of the pro-apoptotic effector proteins: either Bcl-2-associated protein (Bax) or Bcl-2-homologous antagonist killer (Bak), which disrupt the outer membrane of mito-chondria and initiate the apoptotic cascade.

Given the pivotal role of the Bcl-2 proteins in regulating cell death, it is not surprising that dysregulation of the pathway is strongly linked to the development of cancer. Overexpression of pro-survival proteins is linked to tumours, e.g. Bcl-2 overexpression is found in 90% of follicular centre B cell lymphomas [20], and *MCL-1* or *BCL2L1* is amplified in a variety of tumours [21]. Similarly, deletion or downregulation of BH3 initiator genes, *BIM* and *PUMA* has been observed in tumours [22–24]. Abnormalities in the Bcl-2 pathway are also associated with resistance to chemotherapy and radiotherapy [25].

The prospect of activating apoptosis in tumour cells where the Bcl-2 pathway is defective provides an attractive approach to new cancer therapies. Compounds have been sought that mimic the action of pro-apoptotic BH3 proteins by binding to Bcl-2 family members to block their pro-survival action and so induce apoptosis directly.
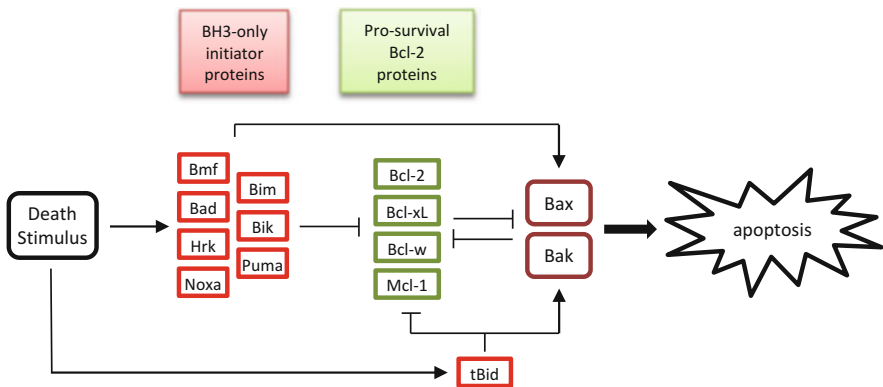
Fig. 1   Apoptotic signalling via the Bcl-family proteins

2.2 Structural Biology and Peptides

NMR and X-ray studies with the B-cell lymphoma-extra large (Bcl-xL) protein provided a structural understanding of the domains involved in the anti- and pro-apoptotic activity of the protein [26]. The tBH1, BH2 and BH3 domains of Bcl-xL form a hydrophobic cleft, which is the site for interactions with the pro-death proteins, Bax and Bak. The NMR solution structure of Bcl-xL bound to a Bak BH3 domain peptide shows the Bak peptide forms an amphipathic α-helix, which binds via the hydrophobic side chains of the Val74, Leu78, Ile81 and Ile85 residues into a hydrophobic groove on the surface of Bcl-xL (Fig. 2) [27]. Investigations with mutant Bak peptides showed that the peptide binds as an amphipathic α-helix. Hydrophobic interactions between the side-chains of Val574, Leu578, Ile581 and Ile585 of Bak and a hydrophobic groove formed by Tyr101, Leu108, Val126 and Phe146 on the surface of Bcl-xL contribute the majority of the interaction affinity. In addition, Asp583 of the Bak peptide and Arg139 of Bcl-xL form an important electrostatic interaction. The identification of key interactions across a short peptide epitope encouraged the development of small molecule inhibitors of the interaction.
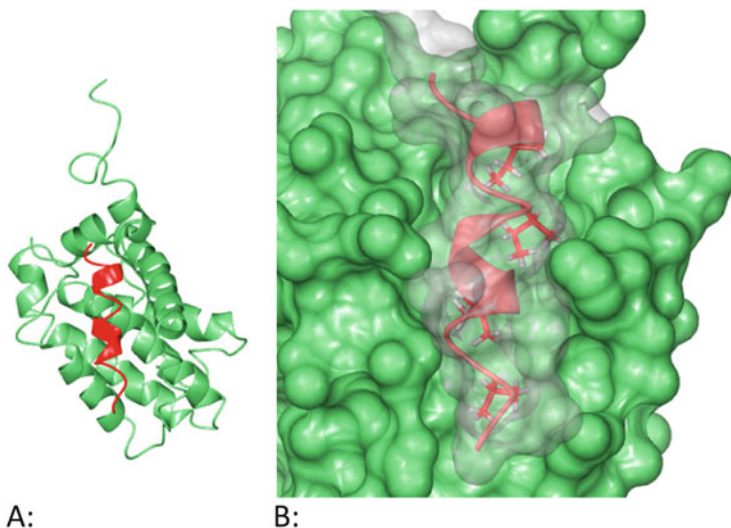
Fig. 2 NMR solution structure of Bcl-xL (*green*) bound to a peptide of residues 572–587 of Bak (*red*) (pdb 1BXL) [27]. (**a**) Ribbons; (**b**) Bcl-xL surface (*green*) and Bak (*red* with *grey surface*) showing the key sidechain interactions

2.3 Small Molecule Bcl Family Inhibitors

α-Helix mimics based on a terephthalamide scaffold have been designed to mimic the side chain interactions of the Bak peptide as Bcl-xL inhibitors. Compound **7** inhibits the BH3 domain of Bak binding to Bcl-xL with a similar affinity to the peptide ($K_i = 0.78$ μM) (Fig. 3) [28]. Such compounds offer additional validation of the tractability of the Bcl-xL PPI as a target for small molecule inhibitors. However, the poor physicochemical properties of the compound (e.g. cLogP 7.4) prevent their optimisation as drugs.

Screening of a library of natural products using NMR and fluorescence polarisation (FP) assays identified Gossypol (**8**) and Purpurogallin (**9**) as competitive inhibitors of the binding of a labelled BH3 peptide to Bcl-xL ($K_i = 0.3$ and 2.2 μM, respectively) (Fig. 4). Binding to Bcl-xL BH3 binding pocket was confirmed by NMR. Gossypol induces multiple cellular effects, some of which can be attributed to it acting as a BH3 mimetic [29]. Despite known liabilities of undesirable redox chemistry and protein reactivity for polyphenolic compounds [30], Gossypol and (R)-gossypol (AT-101) have been evaluated in clinical trials, but with limited efficacy observed in breast and prostate cancer [31–33].

A structure based approach was used to design a series of Bcl-2 inhibitors based on the docked structure of Gossypol (**8**) bound to Bcl-2 [34]. The most potent compound TW-37 (**10**) retains the extensive hydrogen-bonding of one triphenolic moiety combined with a larger hydrophobic group. The second half of **8** is replaced with a hydrophobic amide that allows more extensive contacts with the BH3 binding pocket resulting in improved potency. **10** inhibits Bcl-2, Bcl-xL, and induced myeloid leukaemia cell differentiation protein (Mcl-1) interactions
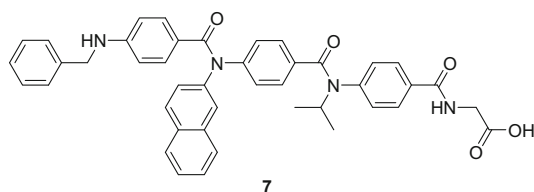
Fig. 3 Terephthalamide α-helix mimic (**7**)
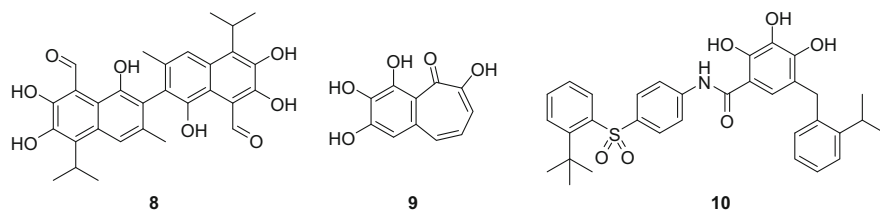
Fig. 4 Bcl-2 inhibitors Gossypol (**8**), Purpurogallin (**9**), and TW-37 (**10**)

(K_i = 0.29, 1.1, and 0.26 μM, respectively) and induces apoptosis in the PC3 prostate cancer cell line (GI$_{50}$ = 200 nM).

Fragment based screening offers an alternative to the optimisation of relatively high molecular weight hits from screening library compounds or natural products. Bcl-2 family inhibitors have been discovered and optimised using "SAR by NMR". This is a two-step method, in which the first step identifies low molecular weight fragments by observing chemical shift changes in the ^{15}N- or ^{1}H–HSQC NMR spectrum of the protein on binding of the ligand. In the second step, additional fragments occupying different binding sites close to the first fragment hits are identified. NMR or X-ray crystallography is used to determine binding site and orientation of both fragments prior to the design of a suitable linking group. The linked fragments should result in a higher affinity ligand that accesses both binding sites [35].

Fragments binding to two subpockets of the BH3 interacting-domain death agonist (Bid) BH3 domain were identified in an NMR screen [36]. The interaction sites of the fragments were mapped to specific amino acids on the Bid surface using additional NMR experiments and docking used to determine the likely binding modes. A small library of sulfonamides was prepared to evaluate linking of the fragments together, giving rise to sulfonamide **11** (Fig. 5). Binding of **11** to the Bid BH3 domain was confirmed by NMR. Compound **11** was able to inhibit t-Bid induced Smac release in a mitochondrial assay and t-Bid induced apoptosis in transformed HeLa cells. Although further developments to this series have not been reported, this study confirmed the tractability of BH3 domains for NMR based fragment screening and the utility of the fragment linking approach.

Another application of the SAR by NMR method gave rise to fragment hits for Bcl-xL that bound with millimolar potency. Modification of the fragment bound to Site 1 to an acylsulfonamide allowed linking to the second fragment site and maintained the acidic hydrogen (Fig. 6). Parallel synthesis identified compound **12** (K_i = 36 nM), incorporating the 3-nitro-4-(2-phenylthioethyl)amino phenol group that both acts as a linker and occupies the second fragment site. Structure-guided optimisation of **12** allowed the identification of modifications to reduce binding to human serum albumin (HSA) whilst maintaining affinity for Bcl-xL. The
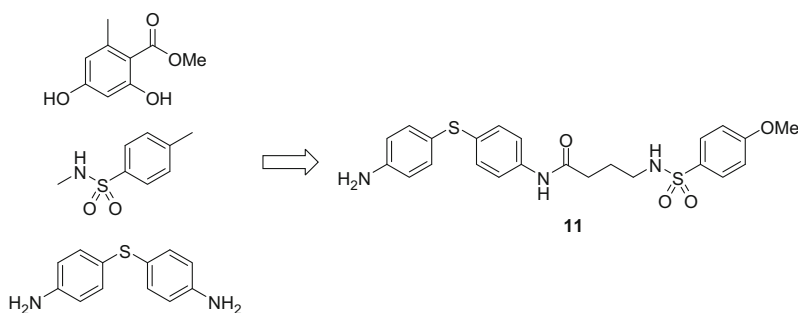
Fig. 5 Linking of Bid BH3 fragment hits
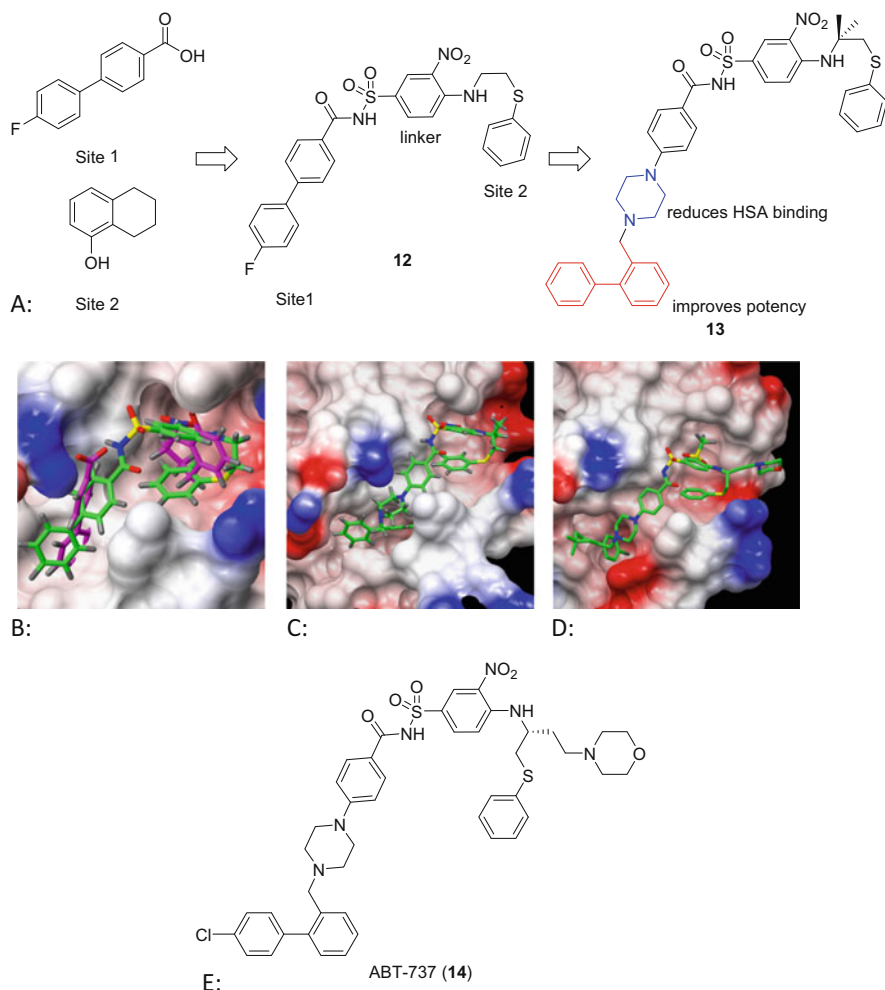
Fig. 6 (**a**) Linking of Bcl-xL bound fragments and optimisation by linking and structure-based design; (**b**) solvent accessible surface of the NMR structure of Bcl-xL with **12** (*green*) bound (1YSI), overlaid with fragments (*magenta*) from 1YSG; (**c**) solvent accessible surface of the NMR structure of Bcl-xL with **13** (*green*) bound (2O2N); (**d**) solvent accessible surface of the X-ray structure of Bcl-xL with **14** (*green*) bound (4LVT); (**e**) chemical structure of ABT-737 (**10**)

replacement of one phenyl ring with a piperazine ring reduced binding to HSA and allowed the introduction of a biphenyl group, as seen in compound **13**, binding deep into a hydrophobic cleft on Bcl-xL that is not seen in the peptide bound structure. The addition of a basic group to the thioethylaminoethyl group further reduced HSA binding giving ABT-737 (**13**) [37, 38].

ABT-737 (**14**) binds potently ($K_i \leq 1$ nM) to Bcl-xL, Bcl-2, and Bcl-2-like protein 2 (Bcl-w) proteins, but less well to family members with lower homology,

e.g. B-cell lymphoma/leukaemia 11B protein (Bcl-B), Mcl-1 and Bcl-2-related protein A1 (K_i = 460 nM and >1,000 nM, respectively). In cells, **14** acts in a similar manner to an apoptosis sensitising Bad-BH3 peptide by binding to and inhibiting anti-apoptotic Bcl-2 proteins thus removing their protection from apoptosis. **14** does not directly cause cytochrome c release or directly activate the pro-apoptotic proteins Bak and Bax. **14** showed synergism in combination with chemotherapeutics (2–20-fold) and radiation (2–4-fold). **14** induced tumour regression in Bcl-2 overexpressing small cell lung cancer (SCLC) xenografts (100 mg/kg/d ip) and showed improved activity in combination with etoposide [39].

Promising results with ABT-737 prompted further rounds of structure-guided optimisation resulting in Navitoclax (ABT-263, **15**) [40]. In this case modifications were designed that did not disrupt the core binding motif and aimed to optimise aqueous solubility, cellular activity, and ultimately oral bioavailability. Modulation of the acidity of the sulfonamide group by variation of the 3-nitro group enhanced oral bioavailability, and switching the basic dimethylamino group to a morpholine reduced metabolism and improved oral exposure. A 3-trifluoromethylsulfone group proved to be the optimal replacement for the nitro group. Modifications to the 4-chlorobiphenyl moiety gave improved metabolic stability and cellular activity when the internal phenyl ring was replaced with a cyclohexenyl or *gem*-dimethylcyclohexenyl group. ABT-263 (**15**) has a high molecular weight (974 Da) and falls outside of other commonly used drug-like parameters, indicating the difficulty of addressing relatively long lipophilic binding sites. However, **15** shows cellular activity including mechanism-based cytotoxicity in Bcl-2 or Bcl-xL dependent models, and has acceptable oral bioavailability and PK properties [41]. In vivo efficacy with complete regressions was observed in SCLC and acute lymphoblastic leukaemia (ALL) based xenografts (100 mg/kg qd p.o.). Reversible thrombocytopenia was noted as a mechanism related toxicity.

A selective Bcl-2 inhibitor was designed with the aim of avoiding the thrombocytopenia observed with **15**, attributed to the inhibition of Bcl-xL, and so improving the therapeutic window [42]. In order to separate Bcl-2 binding from Bcl-xL, a series of compounds was prepared starting from **15** with the removal or replacement of key binding moieties. Removal of the thiophenyl group of **15** (e.g. **16**) allowed the key hydrophobic interaction to be achieved from a different vector with an azaindole group, and optimisation of the *gem*-dimethylcyclohexenyl group resulted in the discovery of venetoclax (ABT-191, **17**) (Fig. 7). Venetoclax (**17**) is a potent Bcl-2 inhibitor (K_i < 0.01 nM) with good selectivity over Bcl-xL and Bcl-w (K_i = 48 and 245 nM, respectively). Selective cellular activity was seen for **17** in Bcl-2 dependent lines but not in Bcl-xL lines. In vivo antitumour activity was demonstrated for **17** in a selection of haematological tumour xenografts on a single oral dose. Ex vivo studies with human platelets showed that **17** was significantly less toxic than **15**.

Obatoclax (**18**) was identified in an FP assay measuring the displacement of a BH3 peptide from Bcl-2 family proteins as an inhibitor Bcl-2, Bcl-xL, Mcl-1, Bcl-w, A1, and Bcl-B ($K_i \approx$ 1–7 μM) (Fig. 8) [43]. Docking to the Bcl-2 NMR structure predicted that **18** binds to the BH3 binding groove in a hydrophobic pocket. The
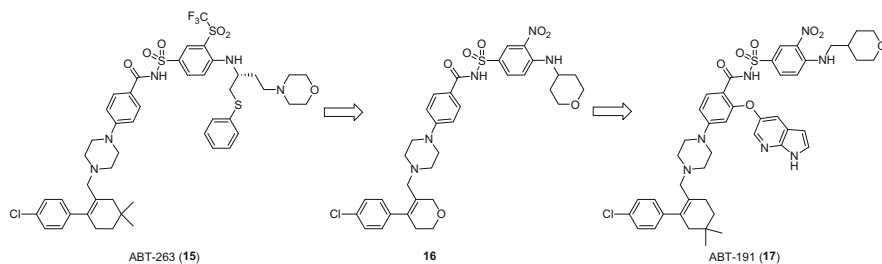
Fig. 7 Design evolution of ABT-191 (**17**) from ABT-263 (**15**)
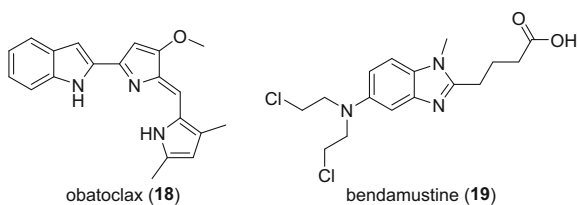
Fig. 8 Obatoclax (**18**) and bendamustine (**19**)

hydrophobicity of **18** (cLogP >4) was expected to favour membrane localisation, so studies with isolated mitochondria were used to demonstrate disruption of Mcl-1-Bak interactions. In whole cells, treatment with **18** initiates apoptosis, and is able to overcome Mcl-1 overexpression induced resistance to the Bcl-2 inhibitor ABT-737 (**14**) and bortezomib. Single agent antitumour activity was demonstrated in SCID mice bearing human C33A cervical carcinoma tumors with IV dosing at 0.25 and 0.5 mg/kg. A Phase I dose finding study with obatoclax in various tumour types by IV infusion established the tolerability and pharmacokinetics of the drug with some indication of clinical activity [44].

2.4 Clinical Development of Bcl-2 Inhibitors

Three Bcl-2 family inhibitors have progressed to clinical trials. Given the central role Bcl-2 family proteins play in the development of many lymphomas, this has been a key focus of clinical studies. A Phase I study with the pan Bcl-family inhibitor Navitoclax (**15**) in relapsed or refractory lymphoid malignancies established the optimum dosing regimen, pharmacokinetics, pharmacodynamics and tolerability of the drug and demonstrated some efficacy [45]. Chronic lymphocytic leukaemia (CLL) is characterised by over-expression of Bcl-2, and a Phase I study in CLL with **15** demonstrated substantial efficacy [46]. In SCLC and other solid tumours, a Phase I clinical trial with **15**, under intermittent or continuous oral dosing schedules, established a maximum tolerated dose and demonstrated the safety of the drug and antitumour activity was observed [47]. A Phase IIa single-agent trial of **15** in SCLC

also demonstrated safety and biomarker modulation, however, efficacy was limited [48]. Clinical studies with **15** in solid tumours are ongoing as a single agent and in combination with other therapies.

Despite promising results with **15**, the Bcl-xL induced thrombocytopenia observed was dose limiting and so attention switched to the Bcl-2 selective inhibitor venetoclax (**17**) [49]. A single agent Phase I study of **17** in CLL and small lymphocytic leukaemia (SLL) showed an 84% response rate in CLL patients without significant reports of thrombocytopenia [50]. A Phase II study of **17** in ALL demonstrated activity in this indication, particularly in patents with a poor prognosis [51]. A combination of **17** with the anti-CD20 antibody rituximab was evaluated to determine the maximum tolerated dose and safety profile, producing an overall response rate of 88% with good tolerability [52]. A Phase 1b combination study of **17** with bendamustine (**19**) in relapsed non-Hodgkin lymphoma established the safety of the combination, and showed good evidence of efficacy [53]. A Phase 2 study of **17** in relapsed or refractory CLL patients with a chromosome 17p deletion showed an 80% response rate, demonstrating the effectiveness single agent **17** in a patient group that responds poorly to immunotherapy [54]. On the basis of these results venetoclax (**17**) received accelerated clinical approval in the US and Europe.

In a phase I trial with obatoclax (**18**) in advanced CLL acceptable safety, and phamacodynamic responses (Bax and Bak elevation) were observed. Modest single agent activity was seen with 1/26 patients achieving a partial response [55].

3 MDM2-p53

3.1 *Biology*

The p53 tumour suppressor acts as a central node in the cellular response to stress and DNA-damage [56]. Activation of p53 produces an active tetramer that can transcribe around 150 genes, giving rise to a number of cellular effects including initiating apoptosis, cell-cycle arrest, DNA-repair, senescence or altered metabolism [57]. MDM2, itself a product of p53 mediated transcription, acts as a negative repressor of p53 by binding to and occluding the p53 transactivation domain and by acting as an E3-ubiquitin ligase, targeting the complex for proteasomal degradation [58, 59]. The MDM2–p53 interaction forms an autoregulatory feedback loop, ensuring that cellular activation of p53 is transient.

Amplification of the *MDM2* gene and overexpression of MDM2 protein occurs in around 10% of common cancers. The highest incidence is found in hepatocellular carcinoma (44%), lung (15%), sarcomas and osteosarcomas (28%), and Hodgkin disease (67%) [60]. MDM2 overexpression overrides p53 activation and inactivates its tumour suppressor function, thus rendering the cells effectively p53 null.

Inhibitors of the MDM2-p53 PPI have been sought as they should act to reactivate p53-mediated cell death by removing MDM2 mediated repression of

transcription. Tumour selectivity is predicted to result from the removal of an MDM2 block on pre-existing DNA-damage or oncogenic activation signals, thus allowing p53-mediated activation of apoptosis.

3.2   Structural Biology and Peptides

The NMR structure of MDM2 reveals that the protein adopts multiple conformations [61], with residues 16–24 of the N-terminal region forming a flexible lid that closes over the p53 binding site [62]. p53 easily displaces the lid to form a more stable complex [63]. The X-ray structure of a p53 peptide and MDM2 interaction shows the surface MDM2 forms a hydrophobic cleft into which the p53 peptide binds as an amphipathic α-helix (Fig. 5a) [64]. Epitope scanning determined that three p53 residues, Phe19, Trp23 and Leu26, form the principal interactions with MDM2, secured by two intermolecular hydrogen-bonds, between the backbone of Phe19 of p53 and the Gln72 side chain of MDM2, and between the p53 Trp23 indole NH and the backbone carbonyl of Leu54 from MDM2 (Fig. 9a). Potent inhibitors of the MDM2–p53 interaction were discovered from synthetic peptide libraries, including the AP peptide ($IC_{50} = 5$ nM) that incorporates 6-chlorotryptophan, and phosphonomethylphenylalanine residues [65]. The X-ray structure of the AP peptide bound to MDM2 (Fig. 9b) shows the 6-chlorotryptophan group occupies additional space below the Trp23 site, and makes additional van der Waals contacts with Phe86 and Ile99 of MDM2.

Hydrocarbon stapled α-helical peptides e.g. SAH-p53-8, Ac-QSQQTF*NLWRLL*QN-NH$_2$ (* indicates the position of the hydrocarbon staple), have shown excellent potency as MDM2-p53 inhibitors [66, 67]. The X-ray crystal structure of SAH-p53-8 bound to MDM2 shows that the key binding residues Phe19, Trp23 and Leu26 form part of a short α-helix that binds to MDM2 (Fig. 9c) [68]. SAH-p53-8 induces p53 mediated cytotoxicity in MDM2 overexpressing cells. Similarly, the stapled peptide ATSP-7041, Ac-LTP*EYWAQAba*SAA-NH$_2$, is a potent dual inhibitor of both MDM2-p53 ($K_i = 0.9$ nM) and MDMX-p53
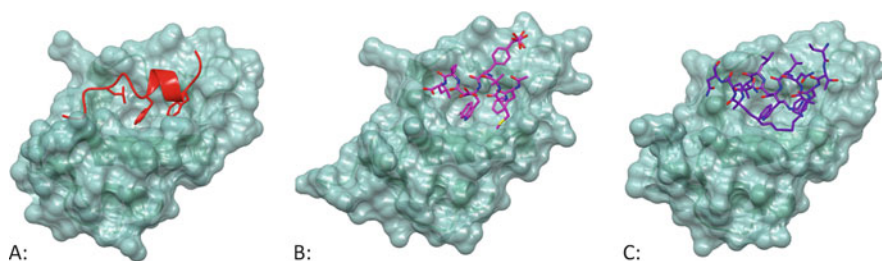
Fig. 9 X-ray structure of MDM2 (ribbon – *green*, surface – *light green*) bound to (**a**) residues 15–29 of p53 showing the key hydrophobic sidechains (*red*) (pdb 1YCR), (**b**) AP peptide (*magenta*) (pdb: 2GV2) (**c**) SAH-p53-8 (*purple*) (pdb: 3V3B)

($K_i = 6.8$ nM), which has been optimised for solubility, and cellular potency [69]. The X-ray structure of ATSP-7041 bound to MDMX shows that the hydrocarbon staple makes significant interactions with the protein and so contributes to binding affinity. ATSP-7041 showed activity in vivo in MDM2 and MDMX overexpressing human tumour xenografts. Other peptide derived MDM2-p53 inhibitors using alternative backbones have been investigated with varying success including retero-inverso D-peptides [70, 71], β-peptides [72–74], di-proline β-hairpins [75, 76] and peptoids [77].

3.3 Hit Discovery and Optimisation

A variety of peptide mimetic approaches have been employed, using differing structures to array side chains in the appropriate orientation to recapitulate the peptide interaction with the MDM2 binding cleft (Fig. 10) [78]. Terphenyls e.g. **20** demonstrated the validity of this approach [79]. α-Helix mimics based on an oligoamide scaffold (**21** and **22**) were weak MDM2-p53 inhibitors [80, 81]. The
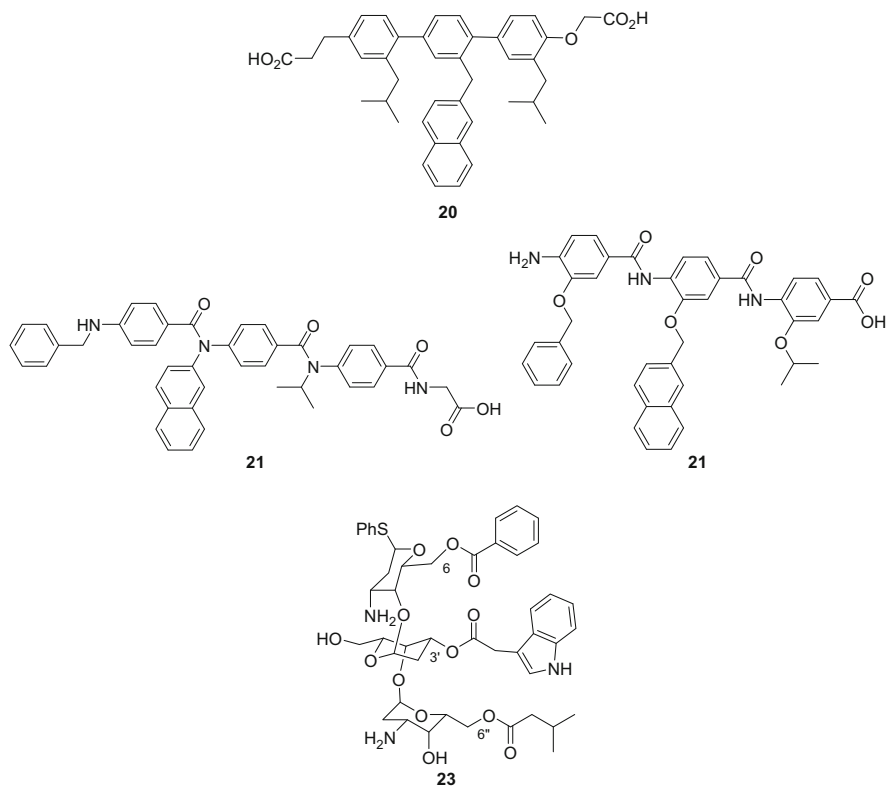
Fig. 10 α-Helix mimetic MDM2-p53 inhibitors

α-1,4 linked oligogalactose **23**, bearing groups corresponding to the important p53 side chains from alternate C-6 and C-3 hydroxyl groups, showed weak MDM3-p53 inhibitory activity [82]. Although these approaches offer interesting insights into the binding requirements for MDM2, the compounds' high molecular weights and poor drug-like properties prevent their development.

The Nutlins are *cis*-imidazoline containing compounds, which were identified by HTS as inhibitors of MDM2-p53 with IC$_{50}$ values in the 100–300 nM range (e.g. **24**, IC$_{50}$ = 90 nM) [83]. The series yielded the first reported X-ray and NMR structures of small molecules in complex with MDM2, showing that the heterocyclic scaffold arrays its substituents to mimic the side-chains of an α-helical peptide (Fig. 11a, pdb 4J3E) [84]. Structure-guided optimisation enabled improvements to stability at the imidazoline heterocycle by the introduction of two *cis*-methyl groups and by modification of the metabolically labile 4-methoxy group to a *tert*-butyl group. Additional potency and favourable PK properties were gained by the addition of a hydrophilic sulfone chain to the piperazine moiety, giving rise to the clinical candidate RG-7112 (**25**, IC$_{50}$ = 18 nM). The X-ray co-crystal structure of MDM2 with **25** (Fig. 11b) shows it has a similar binding mode to Nutlin-3a, with the methylsulfone side chain extending into solvent.

Modification of the Nutlin scaffold to a dihydroimidazothiazole resulted in the identification of a series of potent MDM2 inhibitors, such as **26** (IC$_{50}$ = 90 nM). Addition of the 6-methyl group is sufficient to stabilise the imidazoline ring to oxidation. The bicyclic scaffold orientates the 3-isopropyl group into the MDM2 Phe19 pocket, and addition of an amide at the 4-position gave additional potency [85, 86]. The X-ray structure of **26** bound to MDM2 shows the imidazole ring and

Fig. 11 X-ray structure of MDM2 (electrostatic surface) bound to (**a**) Nutlin 3a 24 (*green*) (pdb 4J3E), (**b**) RG7112 25 (*pink*) (pdb: 4IPF)
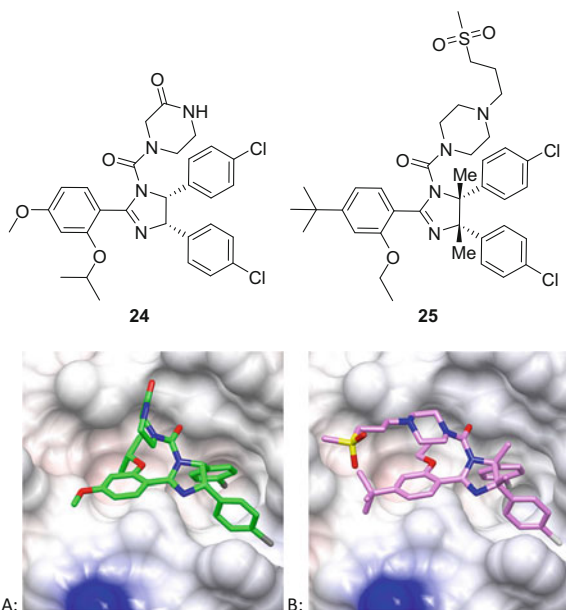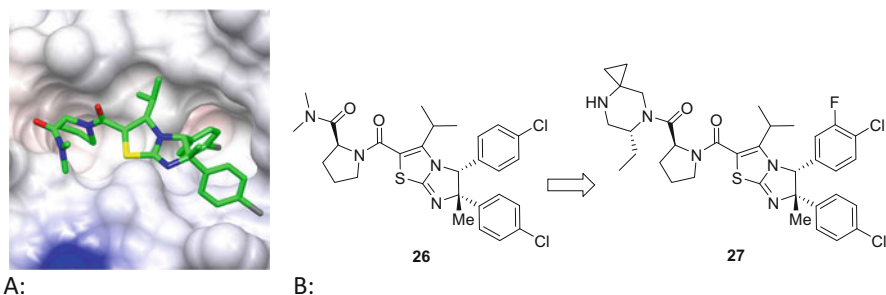
Fig. 12 (**a**) X-ray structure of MDM2 (electrostatic surface) bound to dihydroimidazothiazole **26** (*green*) (pdb 3VZV), (**b**) Design evolution of DS-5272 (**27**) from **26**

chlorophenyl groups occupying similar space to the Nutlin series (Fig. 12a). The thiazole and isopropyl groups fill space occupied by the alkoxyphenyl group of **24**, and the amide side-chain occupies a surface groove formed by the movement of a flexible loop. Interactions in the Trp23 binding pocket were optimised by the addition of a 3-fluoro-4-chlorophenyl group, and the amide moiety was elaboration with a 4,7-diazaspiro[2,5]octane group giving DS-5272 (**27**, IC_{50} = 24 nM, Fig. 12b) [87]. DS-5272 showed good cellular activity, solubility, microsomal stability and acceptable in vivo PK properties. Anti-tumour efficacy was demonstrated in an MDM2-amplified mouse xenograft model (50 mg/kg/qdx4 p.o.). The authors suggest that DS-5272 is a possible candidate for clinical development, but the structure of the clinical candidate DS-3032b has not been disclosed.

A series of spirooxindoles, e.g. **28** (K_i = 86 nM), were identified initially by substructure searching for oxindole containing natural products designed to mimic the tryptophan of p53 (Fig. 7) [88]. Structure-based elaboration of the amide group and addition of a 5-fluoro group resulted in improved potency, e.g. **29** (IC_{50} = 28 nM) (Fig. 13) [89, 90]. The X-ray co-crystal structure of **29** bound to MDM2 shows the oxindole ring occupying the Trp pocket, with hydrogen bonds between the oxindole NH and the backbone carbonyl of Val54, and His96 NH and the amide side-chain carbonyl group, the 3-chloro-2-fluorophenyl group fills the Leu pocket, and the *t*-butyl group is in the Phe pocket (Fig. 14). The diol MI-147 (**31**, IC_{50} = 16 nM) showed cellular activation of p53 and in vivo activity in an MDM2 amplified tumour xenograft. Importantly, spirooxindoles e.g. **30** were found to epimerise under oxidative conditions to diastereomeric mixtures and the most stable diastereoisomer proved to have improved potency and in vivo activity [91, 92].

SAR405838 (**32**, K_i = 0.88 nM) was selected from a series of amides as it showed improved chemical and metabolic stability, in addition to potent MDM2 binding affinity, selectivity, and growth inhibitory activity [93] (Fig. 13). Spirooxindole **32** induced complete tumour regression in SJSA-1 mouse xenografts with a single oral dose (100 mg/kg) and on repeat dosing. The in vivo efficacy of **32** was also demonstrated in a multiple tumour types without *MDM2* amplification. Consequently, **32** was selected as a clinical candidate from the spirooxindole series.
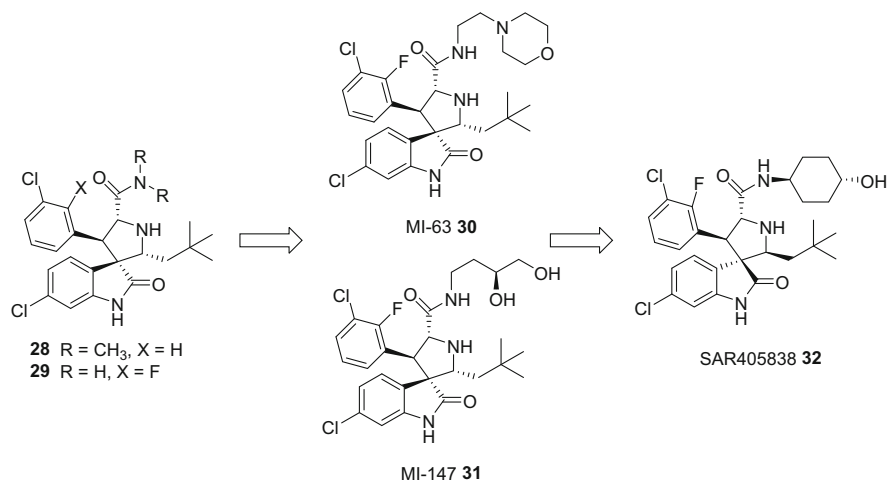
Fig. 13 Design evolution of SAR405838 (**32**) from **28**
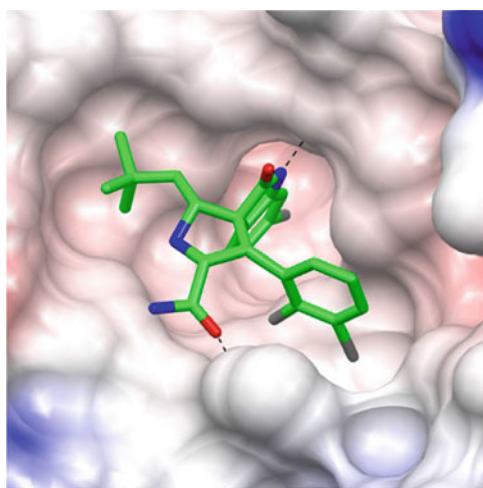
Fig. 14 X-ray structure of MDM2 (electrostatic surface) bound to oxindole **29** (*green*) (pdb 3LBL)

Further structure-guided optimisation of the spirooxindole series aimed to remove instability due to epimerisation [94]. Replacement of the 2′-neopentyl group of **32** with a cyclohexyl ring removed one chiral centre and maintained interactions in the Phe19 pocket of MDM2. Introduction of a carboxylic acid to the amide side-chain improved cell-free potency with the bicyclo[2.2.2]octane moiety as a phenyl ring replacement conferring improved PK characteristics. The alkylation of the pyrrolidine nitrogen was necessary to improve the cellular PD response of the compound. The resulting compound APG115 (**33**) showed anti-

tumour efficacy in a SJSA-1 mouse xenograft model (100 mg/kg/qd p.o.) and has entered phase I clinical trials (Fig. 15).

The spirocyclic amide scaffold of spirooxindole **32** was simplified to a cyano-pyrrolidine core allowing a "*cis*" configuration of aromatic groups e.g. **34** (IC$_{50}$ = 196 nM) [95]. The X-ray co-crystal structure of **34** bound to MDM2 shows the 4-chlorophenyl ring occupying the Trp pocket, with a hydrogen bond between His96 NH and the amide side-chain carbonyl group, the 3-chlorophenyl group fills the Leu pocket, with the cyano group projecting into solvent and the *t*-butyl group occupies the Phe pocket (Fig. 16). The addition of fluoro substituents to both aromatic rings was found to improve MDM2 inhibitory potency. Optimisation of the PK profile was achieved at the amide side chain substituent, that was also found to modulate cellular potency. A 4-benzenecarboxylic group gave the desired properties, and SAR studies around the ring revealed that the *ortho*-methoxy group, **35** (RG7388), had the ideal combination of MDM2 binding affinity, cellular potency and selectivity. RG7388 (**35**) gave complete tumour regression in vivo in an SJSA-1 xenograft model (25 mg/kg p.o.), and a favourable PK profile. RG7388 (**35**) was selected as the second generation MDM2-p53 clinical trial candidate owing to its improved potency, cellular selectivity and PK properties over RG7112 (**25**).

Substituted piperidines, e.g. **36** (IC$_{50}$ = 600 nM), were identified as hits from an FP-based HTS (Fig. 17a) [96]. Introduction of a 2-methoxyethoxyphenyl
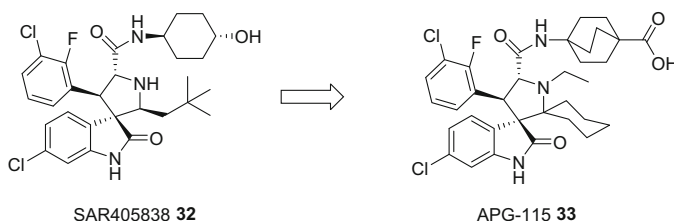
Fig. 15 Design of APG115 (**33**) from **32**
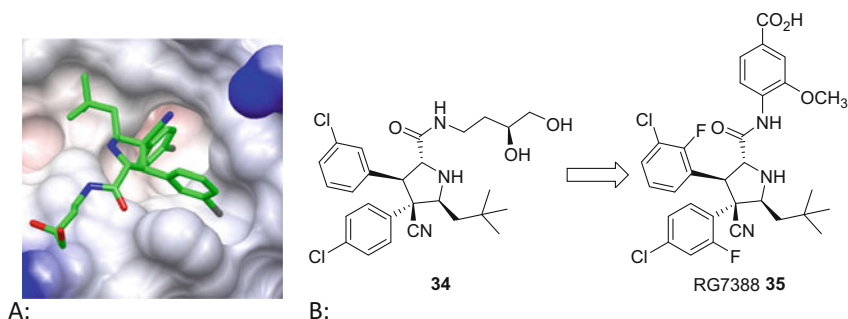
Fig. 16 (**a**) X-ray structure of MDM2 (electrostatic surface) bound to cyanopyrrole **34** (*green*) (pdb 4JRG); (**b**) Design evolution of RG7388 (**35**) from **34**
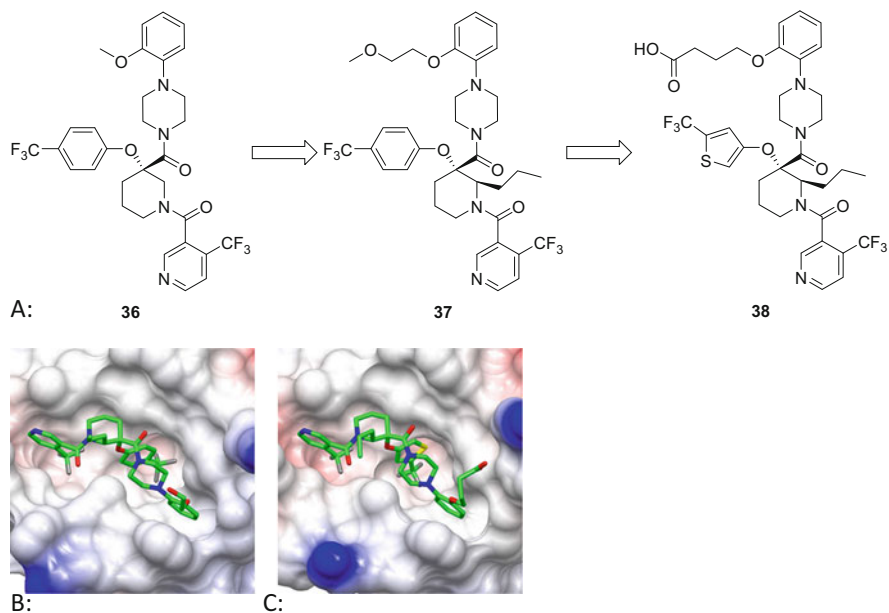
substituent gave improved potency and the alkyl substituent on the piperidine ring was found to be essential to promote the optimum conformation of the ring e.g. **37** (IC$_{50}$ = 40 nM) [97, 98]. The MDM2 bound X-ray structure of **36** identified the main interactions as the trifluoromethylpyridine occupying the Phe19 pocket, the trifluoromethylphenyl residue projecting into the Trp23 pocket and the Leu26 pocket filled by the alkoxyphenyl group (Fig. 17b). Structure-guided optimisation resulted in **38** (Fig. 17c) [99]. A combination of a 2-trifluoromethylthiophene replacement for the trifluoromethylphenyl residue and a butanoic acid substituent to the alkoxyphenyl group gave a fivefold improvement in potency and cellular activity (**38**, IC$_{50}$ = 7 nM). Compound **38** showed single agent activity in an A549 tumour xenograft at 200 mg/kg qd and in combination with taxoids.

A structure-based design approach identified the piperidone series of inhibitors (e.g. AM-8553, **39**, IC$_{50}$ = 1.1 nM) [100]. An X-ray structure of **39** bound to MDM2 showed that the (3R)-carboxyl group at C3 forms a key interaction with His96, the 4-chlorophenyl group occupies the Typ pocket, the 3-chlorophenyl group fills the Leu pocket and the N-alkyl chain projects into the Phe pocket (Fig. 18a). Modifications to the N-substituent aimed to optimise interactions with the 'glycine shelf' region, a hydrophobic region on the surface of MDM2 formed by Gly58 (Fig. 18b) [101, 102]. Sulfone **40** (AMG 232, IC$_{50}$ = 0.6 nM) showed excellent cell-free potency and cell growth inhibitory activity. Complete tumour regression in SJSA-1 xenografts observed (60 mg/kg/qd p.o.), and so AMG 232 was
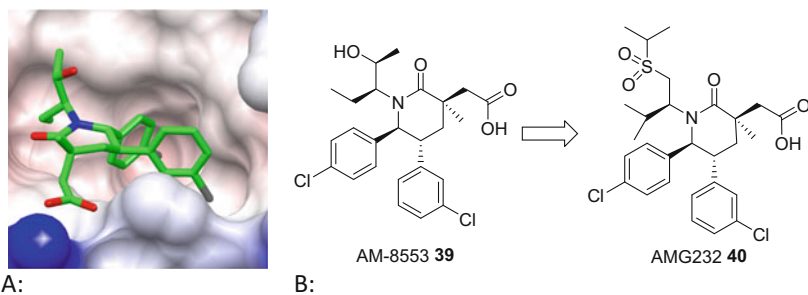
Fig. 18 X-ray structure of MDM2 (electrostatic surface) bound to (**a**) AM-8553 **39** (*green*) (pdb 4ERF) (**b**) Design of AMG232 **40**
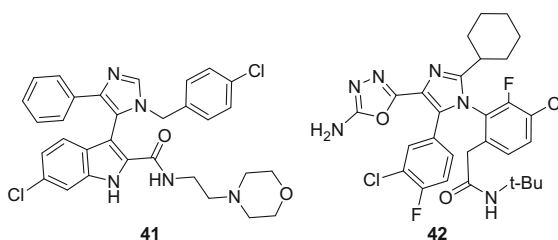
Fig. 19 Substituted imidazole MDM2-p53 inhibitors (**41** and **42**)

selected for clinical trials [103]. Additional SAR studies around the carboxylic acid moiety resulted in compounds with equivalent potency [104, 105].

Rational design based on the X-ray structure of the AP peptide bound to MDM2 (Fig. 5b) gave rise to the 'central valine' concept, resulting in the identification of substituted imidazole (**41**, $IC_{50} = 30$ nM) (Fig. 19) [106]. Structure-guided modifications to optimise potency and solubility gave rise to compound **42** ($IC_{50} = 2$ nM), however, the cellular activity in this series is poor compared with other series displaying similar MDM2-p53 potency [107].

Virtual screening identified dihydroisoquinolinone **43** as a hit MDM2-p53 inhibitor ($IC_{50} = 540$ nM) (Fig. 20a) [108]. An X-ray structure of **44** bound to MDM2 showed an unexpected binding mode, significantly different to most MDM2 inhibitors, whereby the Leu26 sub-pocket is occupied by the C7 ethyl ether and not a substituted phenyl ring as seen in the majority of other inhibitor series (Fig. 20b). X-ray structure guided optimisation gave rise to **45** ($IC_{50} = 8$ nM) with excellent cellular activity (Fig. 20c). An X-ray structure of **45** showed that chlorophenyl group requires to be in the (*S*)-configuration at C1 and showed opportunities for optimisation around in the Phe pocket occupied by the 4-pyridinyl group (Fig. 20c). Replacement of the pyridyl group with a *trans*-cyclohexyl amine gave NVP-CGM097 (**46**, $IC_{50} = 1.7$ nM) with good cellular and ADME properties [109]. The X-ray structure of **46** bound to MDM2 shows the

A:

43: X = MeO, Y = H
44: X = Me, Y = [tetrazole structure]
45
46

B: C: D:
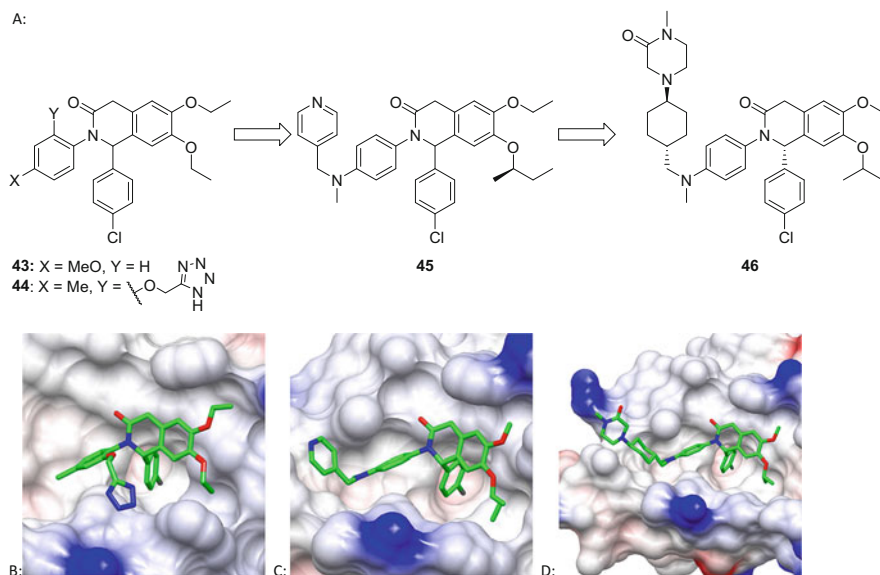
Fig. 20 (**a**) Design evolution of NVP-CGM097 (**46**); X-ray structure of MDM2 (electrostatic surface) bound to (**b**) dihydroisoquinolinone **43** (*green*) (pdb 4ZYC); (**c**) dihydroisoquinolinone **45** (*green*) (pdb 4ZYI); (**d**) NVP-CGM097 (**46**) (*green*) (pdb 4ZYF)

41   47   48
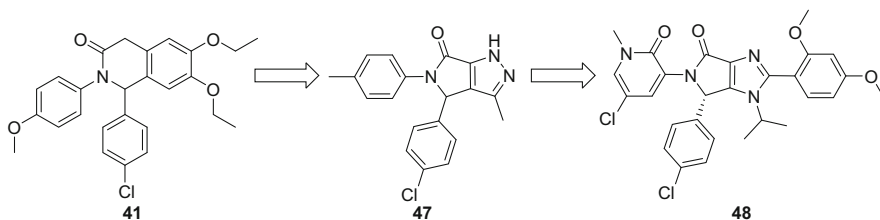
Fig. 21 Design of HDM-201 (**48**)

Trp23 pocket is filled by the C1 4-chlorophenyl group, the Leu26 pocket filled by the C7 isopropyl ether, and the Phe19 sub-pocket is occupied and extended by movement of the protein to accommodate the large amine side-chain (Fig. 20d). NVP-CGM097 showed good PK properties in a number of mammalian species and induced tumour regression in SJSA-1 xenografts (30 mg/kg/qd p.o.). NVP-CGM097 (**46**) has been selected for clinical trials.

In an alternative approach, based on hit compound **41** structural considerations gave rise to a new scaffold comprising a substituted delta-lactam fused to a five-membered ring. Substructure searching identified lactam **47** as a novel hit with modest potency (IC$_{50}$ = 1.5 μM) (Fig. 21) [110]. Elaboration of hit **47** identified structural requirements for potency including, introduction of a 5-chloropyridin-2-one moiety to occupy the Leu23 pocket and stack efficiently with His96. The

clinical trial candidate from this series HDM-201 (**48**) was reported recently as a potent inhibitor with favourable PK and PD profiles in animal studies [111].

3.4 Clinical Development Summary

A number of MDM2-p53 inhibitors have entered clinical trials in solid and haematological malignancies (Table 2). A Phase I clinical trial of RG7112 **25** in liposarcoma patients showed responses to therapy in 16 from 20 patients as partial response or stable disease [112]. A poor PK profile was observed, PD markers for apoptosis and p53 activation showed a linear relationship with drug exposure and a food effect was noted [113]. Some toxicity was observed including neutropenia and thrombocytopenia. A Phase I trial of **25** in various leukaemias showed activity in patients with AML [114]. The second generation inhibitor RG7388 (**35**) is under clinical investigation in a Phase III trial in AML [115, 116]. SAR405838 (**32**) was selected as the clinical candidate from the spirooxindole series and entered Phase I clinical trials as a single agent and in combination with the MEK1/2 inhibitor pimasertib. APG-115 (**33**) has entered Phase I clinical trials in advanced solid tumours and lymphomas as a single agent.

A Phase I/II trial of AMG232 (**40**) is ongoing in metastatic melanoma, in combination with the MEK1/2 inhibitor trametinib and the B-Raf inhibitor

Table 2 MDM2 inhibitors in clinical trials

Compound	Structure	Company	Clinical trial	Indications	ID	Reference
RG7112	**25**	Roche	Phase I	Liposarcoma	NCT00623870	[112–114]
Idasanutlin RG7388	**35**	Roche	Phase III	Acute myeloid leukaemia	NCT02545283	[115, 116]
SAR405838	**32**	Sanofi	Phase I	Liposarcoma	NCT01636479	
APG-115	**33**	Ascentage	Phase I	Solid tumors, lymphomas	NCT02935907	
AMG232	**40**	Amgen	Phase I/II	Metastatic melanoma	NCT02110355	
DS-3032b	nd	Daiich-Sankyo	Phase 1 (x3)	Solid tumours, lymphomas, haematological, refractory multiple myeloma	NCT01877382	[117]
MK-8242	nd	Merck Sharp & Dohme	Phase I	Solid tumours, AML	NCT01463696	[118, 119]
CGM097	**46**	Novartis	Phase I	Solid tumours	NCT01760525	
HDM201	**48**	Novartis	Phase I/II combination with LEE011	Liposarcoma	NCT02343172	

dabrafinib. DS-3032b has been evaluated in a Phase I trial with some evidence of efficacy, and on target toxicity [117]. Phase I trials of MK-8242 demonstrated some activity in liposarcoma and in AML [118, 119]. Results of trials of CGM097 (**46**) and HDM201 (**48**) have not been reported to date.

Overall, a number of agents have shown efficacy in both MDM2 amplified tumours e.g. liposarcomas and AML. Dose limiting p53 mediated on target toxicity, including thrombocytopenia, has been reported. To date, no MDM2-p53 inhibitor has been approved, and the second generation inhibitor RG7388 has advanced the furthest.

4 SMAC-XIAP

4.1 Biology

The inhibitor of apoptosis (IAP) family of proteins inhibits entry into apoptosis at the point of caspase activation [120]. XIAP binds to the N-terminal amino acids of caspases 3, 7 and 9 via its BIR domains and directly inhibits their activity. The activating Smac promotes apoptosis by binding to XIAP [121]. The ML-IAP proteins bind to Smac, preventing its association with XIAP and so inhibiting apoptosis (Fig. 22). The c-IAPs have a different mechanism, acting as negative regulators of the alternative NF-κB pathway by inhibiting NF-kappa-B-inducing kinase (NIK), and as activators of the classical NF-κB pathway by acting on Receptor-interacting serine/threonine-protein kinase 1 (RIPK1). Amplification or overexpression of XIAP has been observed in haematological and solid tumours, and is linked to poor prognosis and poor response to therapy. Similarly, amplification or over-expression of c-IAPs has been identified in a large variety of tumour types. The role of XIAP at the convergence of multiple apoptotic signaling pathways has made it an attractive target for therapeutic intervention.
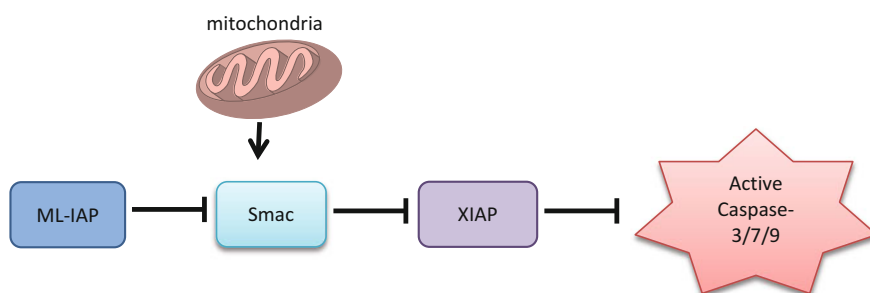
Fig. 22 The role of IAP proteins in caspase activation

4.2 Peptides and Structural Biology

The X-ray structure of Smac bound to XIAP shows the N-terminal four residues of Smac bound to a groove on the surface of XIAP (Fig. 23a, b) [122]. Validation of targeting the Smac-IAP interaction as a therapeutic strategy was demonstrated using cell-penetrant synthetic peptides including seven N-terminal residues of Smac and a cell penetrating TAT domain were found to sensitise TNF-related apoptosis-inducing ligand (TRAIL)-induced apoptosis and cytotoxic drug treatment in cells, but did not initiate apoptosis as single agents [123]. N-Terminal Smac mimetic tetrapeptide libraries established the pharmacophore for the binding to BIR3 (Fig. 23c) [124]. Modifications of the alanine residue at position 1 are limited to small L-amino acids, e.g. Abu, and retention of the NH is essential. Substitution at position 2 (Val) is tolerated, consistent with this residue projecting into solution, but D-amino acids are not tolerated. The proline ring at position 3 was required for activity, only the four-membered azetidine substitution was tolerated. Replacement of the isoleucine at position 4, with aromatic rings e.g. Phe or Nal, was favoured. Non-amino acid substituents at position 4 reduced the peptidic nature of the compounds and improved activity e.g. **49** ($K_D = 12$ nM). Substitution onto the proline ring added potency, e.g. **50** ($K_D = 5$ nM). Structure based design of peptide inhibitors gave **51** [125, 126].
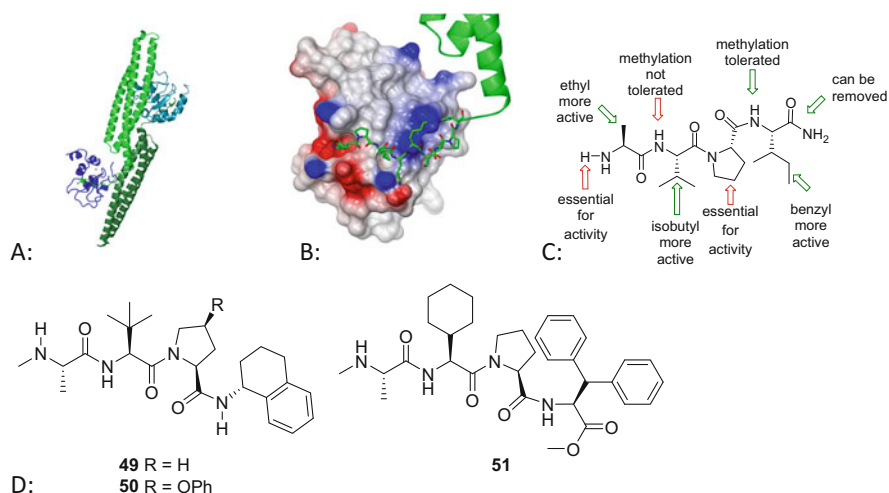
Fig. 23 X-ray structure of the BIR3 domain of XIAP complexed to Smac (**a**) dimeric structure of XIAP (*blue*) and Smac (*green*); (**b**) X-ray structure of the BIR3 domain of XIAP (electrostatic surface) complexed to Smac (*green*) (pdb 1G73); (**c**) pharmacophore for tetrapeptide Smac-mimetic IAP inhibitors; (**d**) structures of peptide IAP inhibitors **49–51**

4.3 Hit Discovery and Optimisation

A number of structurally diverse of peptidomimetic scaffolds have been used to develop potent mono-valent Smac mimetics that show a range of selectivity between cIAP-1 and -2 and XIAP. Structure-based design of cIAP selective inhibitors revealed that variations at the P4 amino acid gave good selectivity, 2-pyrimidinyl compound (**52**) was a selective inhibitor of cIAP-1 and -2, but >2,000-fold less potent vs XIAP [127]. The selectivity was explained by modelling that showed an adverse lone–pair interaction in the P4 binding pocket between the pyrimidine nitrogens and the hydroxyl of Thr308 in XIAP, that is not seen for Arg313 in IAP-1. Structure-based design established the [7,5]-bicycle as a suitable dipeptide replacement for the second and third amino acid positions (Fig. 24) [128]. Compound **53** showed potent inhibition of BIR3-IAP interactions and was cytotoxic as a single agent and in combination with doxorubicin.

Smac mimetic AT-406 (Fig. 25, **54**) incorporates a [5,8]-fused bicyclic replacement for residues 2 and 3 and is predicted to make additional hydrophobic contacts from the amide sidechain to Trp323 in the XIAP BIR3 domain [129]. AT-406 (**54**) is a pan-selective IAP inhibitor (BIR3 K_d = 4.4, 0.7, 1.9 nM XIAP, cIAP1, cIAP2, respectively), and is cytotoxic in a number of cell lines. AT-406 (**54**) shows good oral PK in a number of mammalian species.

In order to rapidly determine the optimal substitutions of tetrapeptide Smac mimetics, solid-phase peptide libraries were employed [130]. A scan of the P1-P3
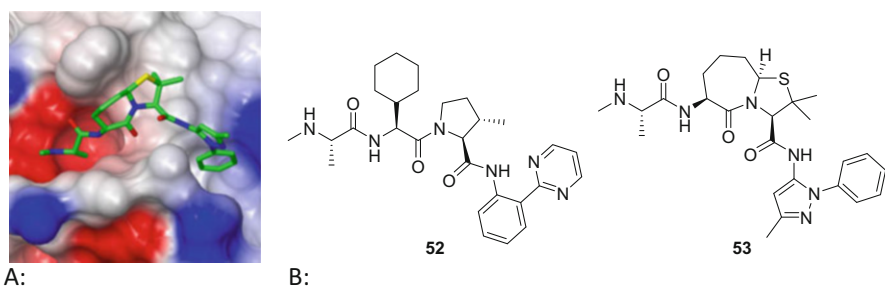
Fig. 24 (**a**) X-ray structure of the BIR3 domain of XIAP complexed to **49** (*green*) (pdb 2I3I); (**b**) XIAP inhibitors **52** and **53**
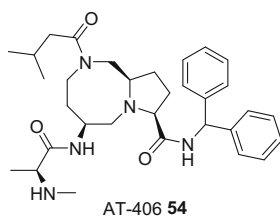
Fig. 25 XIAP inhibitor AT-406 (**54**)

positions identified MeAla, ChGly and Pro, for each position, respectively. Similarly, a systematic scan of the P4 position showed a diphenylethylamine moiety conferred potency. Additional SAR studies at the P4 position were restricted to amines connected to an aromatic ring by one or two carbons. The thiadiazole compound GDC-0152 (**55**) showed improved potency (BIR3 K_i = 28, 17, 43 nM XIAP, cIAP1, cIAP2, respectively). The X-ray structure of **55** bound to chimeric BIR3 domains (Fig. 26) shows the thiadiazole ring positions the phenyl residue into the P4 pocket. **55** showed efficacy in an MDA-MD-231 breast cancer xenograft, and a reasonable PK profile. On the basis of these results **55** was selected for clinical trials. GDC-0917 (**56**) is a second generation IAP inhibitor which is orally active and has improved PK [131].

NMR and X-ray based fragment screening with XIAP-BIR3 domain identified weakly binding fragment **57**, which bound with the piperazine ring in the P1 pocket (Fig. 27a) and the piperidine ring in the P3 pocket [132]. Elaboration of the fragment by the addition of a methyl group to access the alanine pocket and switching to a pyrrolidine amide gave **58** (XIAP-BIR3 IC_{50} = 52% at 1 mM) (Fig. 27b). Amide **55** (XIAP-BIR3 IC_{50} = 5.5 μM) was identified from a virtual screening library of amides and the *gem*-dimethyl group added to improve potency and the metabolic stability of the azaindoline. Introduction of a methoxymethyl group on the piperazine ring improved potency (**60**), and the addition of a 6-benzyl group improved interactions with the P4 pocket (**61**, XIAP-BIR3 IC_{50} = 0.16 μM). Elaboration of the piperazine substituent to an *iso*-indolinone resulted in ASTX660 (**62**), a potent inhibitor of XIAP and c-IAP1 that was selected for clinical trials.

Birinapant (Fig. 28, TL32711, **63**) is a bivalent Smac-mimetic that shows potent XIAP and cIAP antagonism, and induces the downregulation of specific pools of cIAPs in cells [133, 134]. **63** induced apoptosis in cell lines either as a single agent by inducing the formation of a RIPK1-caspase 8 protein complex. **63** has been shown to potentiate some chemotherapy drugs in a p53-independent manner.
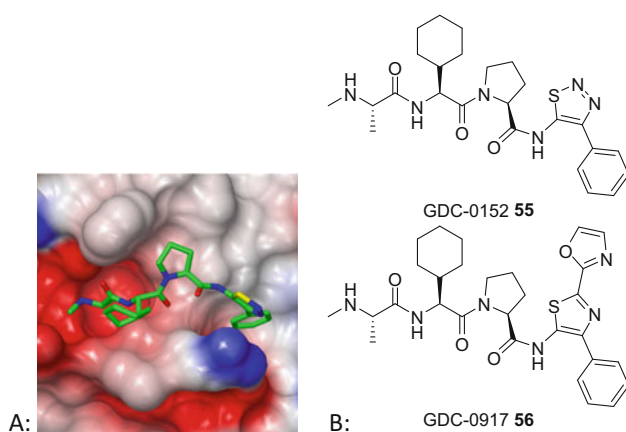
Fig. 26 (**a**) X-ray structure of cIAP1/XIAP chimeric BIR3 domain with **51**; (**b**) GDC-0152 (**55**) and GDC-0917 (**56**)
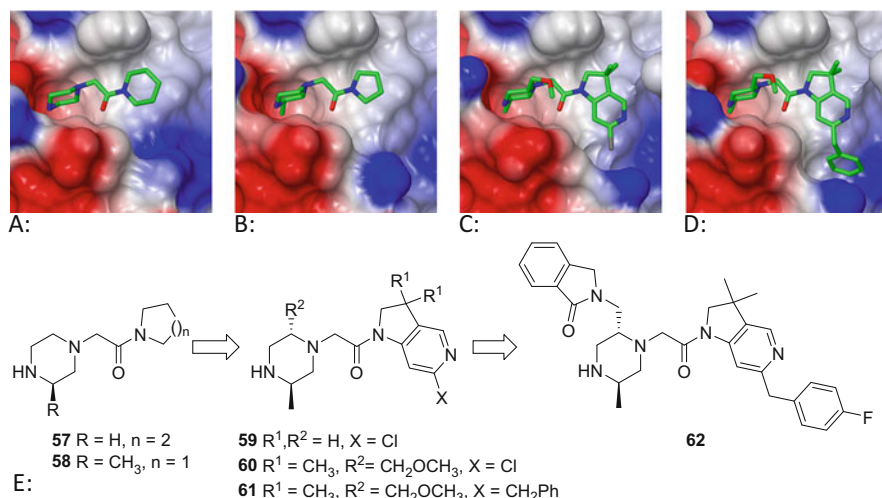
Fig. 27 Evolution of ASTX-660 (**58**). X-ray structure of XIAP-BIR3 (electrostatic surface, *ligand green*) with (**a**) **57** (pdb 5C3H); (**b**) **58** (pdb 5C7B); (**c**) **60** (pdb 5C84); (**d**) **61** (pdb 5C83); (**e**) Evolution of ASTX660 (**62**) from **57**
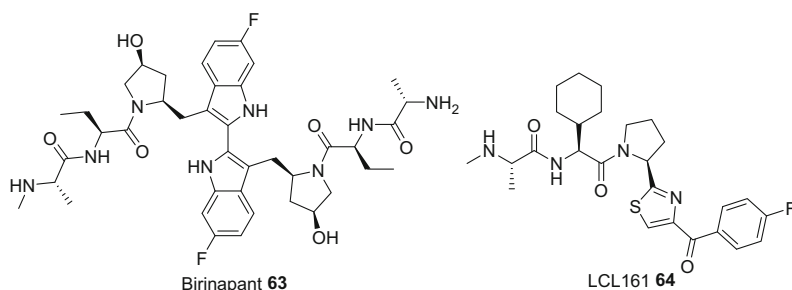
Fig. 28 Clinical trial candidates Birinipant (**63**) and LCL161 (**64**)

Single-agent anti-tumour activity was demonstrated in patient derived xenograft models of ovarian cancer, colorectal cancer and melanoma. Birinapant **63** is currently undergoing clinical trials in solid and haemaotological malignancies.

4.4 Clinical Development Summary

A number of XIAP and c-IAP inhibitors are in clinical trials currently in solid and haematological malignancies, as single agents and in combination with chemotherapy or anti-PD1 antibody therapies (Table 3) [138]. In Phase I trial GDC-0917 (**52**) was well tolerated and showed good PK and PD properties, 2/42 patients showed a complete response (one ovarian cancer and one MALT lymphoma), four patients

Table 3 IAP inhibitors in clinical trials

Compound	Structure	Company	Clinical trial	Indications	ID	Reference
AT-406	**54**	Ascenta/ Debiopharm	Phase I/II	Head and neck squamous cell carcinoma – combination with chemo-radiation	NCT02022098	[129]
GDC-0152 (RG-7419)	**55**	Roche (Genentech)	Phase I	Solid cancers	NCT00977067	[130]
GDC-0917 (CUDC-427)	**56**	Curis (Genentech)	Phase I	Lymphoma and solid tumours	NCT01908413	[131, 135]
ASTX660	**62**	Astex Therapeutics	Phase I/II	Lymphoma and solid tumours	NCT02503423	[132]
Birinapant (TL32711)	**63**	Tetralogic Pharma	Phase I/II	Soild tumours – combination with pembrolizumab	NCT02587962	[133, 134]
AEG40826 (HGS1029)	nd	Aegera and Human Genome Sciences	Phase I	Solid tumours	NCT00708006	[136]
LCL161	**64**	Novartis	Phase II	Multiple myeloma – combination with cyclophosphamide	NCT01955434	[137]

had stable disease [131, 135]. A Phase I trial of LCL161 (Fig. 28, **64**) showed the drug was well tolerated and significant degradation of cIAP1 indicated a PD effect [137]. Although clinical evaluation of IAP inhibitors is in the early stages, initial results are encouraging.

5 Outlook and Conclusions

PPIs are a challenging class of molecular targets to address with small-molecule inhibitors. The importance of PPIs in the biology of cancer, and particularly the regulation of apoptosis, has stimulated considerable drug discovery effort. The application of modern technologies such as screening of virtual, fragment, and lead-like libraries, coupled with structure-based design has enabled the discovery of potent and selective PPI inhibitors. The inhibitors profiled in some cases stray outside the confines of the 'rule-of-five' emphasising the challenge of targeting large, lipophilic sites [139].

The first PPI inhibitor has been licenced for clinical use in CLL, demonstrating the efficacy of selective Bcl-2 inhibition. Clinical trials of MDM2-p53 and IAP inhibitors are at an earlier stage. Preliminary results with MDM2-p53 inhibitors show promise, but with the limitations of on-target toxicity. The IAP inhibitors show less toxicity and some efficacy.

References

1. Hanahan D, Weinberg RA (2000) The hallmarks of cancer. Cell 100:57–70
2. Gigant B et al (2005) Structural basis for the regulation of tubulin by vinblastine. Nature 435:519–522
3. Manfredi JJ, Horwitz SB (1984) Taxol: an antimitotic agent with a new mechanism of action. Pharmacol Ther 25:83–125
4. Cragg GM (1998) Paclitaxel (Taxol): a success story with valuable lessons for natural product drug discovery and development. Med Res Rev 18:315–331
5. Amos LA, Löwe J (1999) How Taxol® stabilises microtubule structure. Chem Biol 6:R65–R69
6. Towle MJ et al (2001) In vitro and in vivo anticancer activities of synthetic macrocyclic ketone analogues of halichondrin B. Cancer Res 61:1013–1021
7. Smith JA et al (2010) Eribulin binds at microtubule ends to a single site on tubulin to suppress dynamic instability. Biochemistry 49:1331–1337
8. Rini B, Kar S, Kirkpatrick P (2007) Temsirolimus. Nat Rev Drug Discov 6:599–600
9. Wells JA, McClendon CL (2007) Reaching for high-hanging fruit in drug discovery at protein-protein interfaces. Nature 450:1001–1009
10. Young L, Jernigan RL, Covell DG (1994) A role for surface hydrophobicity in protein-protein recognition. Protein Sci 3:717–729
11. Clackson T, Wells JA (1995) A hot spot of binding energy in a hormone-receptor interface. *Science* 267:383–386
12. Bogan AA, Thorn KS (1998) Anatomy of hot spots in protein interfaces. J Mol Biol 280:1–9
13. DeLano WL (2002) Unraveling hot spots in binding interfaces: progress and challenges. Curr Opin Struct Biol 12:14–20
14. London N, Raveh B, Schueler-Furman O (2013) Druggable protein-protein interactions – from hot spots to hot segments. Curr Opin Chem Biol 17:952–959
15. Overington JP, Al-Lazikani B, Hopkins AL (2006) How many drug targets are there? Nat Rev Drug Discov 5:993–996
16. Laraia L, McKenzie G, Spring DR, Venkitaraman AR, Huggins DJ (2015) Overcoming chemical, biological, and computational challenges in the development of inhibitors targeting protein-protein interactions. Chem Biol 22:689–703
17. Cinatl J, Speidel D, Hardcastle I, Michaelis M (2014) Resistance acquisition to MDM2 inhibitors. Biochem Soc Trans 42:752–757
18. Gross A, McDonnell JM, Korsmeyer SJ (1999) BCL-2 family members and the mitochondria in apoptosis. Genes Dev 13:1899–1911
19. Czabotar PE, Lessene G, Strasser A, Adams JM (2014) Control of apoptosis by the BCL-2 protein family: implications for physiology and therapy. Nat Rev Mol Cell Biol 15:49–63
20. Tsujimoto Y, Cossman J, Jaffe E, Croce CM (1985) Involvement of the bcl-2 gene in human follicular lymphoma. Science 228:1440–1443
21. Beroukhim R et al (2010) The landscape of somatic copy-number alteration across human cancers. Nature 463:899–905
22. Garrison SP et al (2008) Selection against PUMA gene expression in Myc-Driven B-Cell lymphomagenesis. Mol Cell Biol 28:5391–5402
23. Piazza R et al (2013) Epigenetic silencing of the proapoptotic gene BIM in anaplastic large cell lymphoma through an MeCP2/SIN3a deacetylating complex. Neoplasia 15:511–IN17
24. Tagawa H et al (2005) Genome-wide array-based CGH for mantle cell lymphoma: identification of homozygous deletions of the proapoptotic gene BIM. Oncogene 24:1348–1358
25. Happo L et al (2010) Maximal killing of lymphoma cells by DNA damage-inducing therapy requires not only the p53 targets Puma and Noxa, but also Bim. Blood 116:5256–5267
26. Muchmore SW et al (1996) X-ray and NMR structure of human Bcl-xL, an inhibitor of programmed cell death. Nature 381:335–341
27. Sattler M et al (1997) Structure of Bcl-xL-Bak peptide complex: recognition between regulators of apoptosis. Science 275:983–986

28. Yin H, Hamilton AD (2004) Terephthalamide derivatives as mimetics of the helical region of Bak peptide target Bcl-xL protein. Bioorg Med Chem Lett 14:1375–1379

29. Gao P et al (2010) The Bcl-2 homology domain 3 mimetic gossypol induces both Beclin 1-dependent and Beclin 1-independent cytoprotective autophagy in cancer cells. J Biol Chem 285:25570–25581

30. Baell JB, Holloway GA (2010) New substructure filters for removal of pan assay interference compounds (PAINS) from screening libraries and for their exclusion in bioassays. J Med Chem 53:2719–2740

31. Van Poznak C et al (2001) Oral gossypol in the treatment of patients with refractory metastatic breast cancer: a phase I/II clinical trial. Breast Cancer Res Treat 66:239–248

32. Stein RC et al (1992) A preliminary clinical study of gossypol in advanced human cancer. Cancer Chemother Pharmacol 30:480–482

33. Liu G et al (2009) An open-label, multicenter, phase I/II study of single-agent AT-101 in men with castrate-resistant prostate cancer. Clin Cancer Res 15:3172–3176

34. Wang G et al (2006) Structure-based design of potent small-molecule inhibitors of anti-apoptotic Bcl-2 proteins. J Med Chem 49:6139–6142

35. Shuker SB, Hajduk PJ, Meadows RP, Fesik SW (1996) Discovering high-affinity ligands for proteins: SAR by NMR. Science 274:1531–1534

36. Becattini B et al (2004) Targeting apoptosis via chemical design: inhibition of bid-induced cell death by small organic molecules. Chem Biol 11:1107–1117

37. Oltersdorf T et al (2005) An inhibitor of Bcl-2 family proteins induces regression of solid tumours. Nature 435:677–681

38. Bruncko M et al (2007) Studies leading to potent, dual inhibitors of Bcl-2 and Bcl-xL. J Med Chem 50:641–662

39. Hann CL et al (2008) Therapeutic efficacy of ABT-737, a selective inhibitor of BCL-2, in small cell lung cancer. Cancer Res 68:2321–2328

40. Park C-M et al (2008) Discovery of an orally bioavailable small molecule inhibitor of prosurvival B-cell lymphoma 2 proteins. J Med Chem 51:6902–6915

41. Tse C et al (2008) ABT-263: a potent and orally bioavailable Bcl-2 family inhibitor. Cancer Res 68:3421–3428

42. Souers AJ et al (2013) ABT-199, a potent and selective BCL-2 inhibitor, achieves antitumor activity while sparing platelets. Nat Med 19:202–208

43. Nguyen M et al (2007) Small molecule obatoclax (GX15-070) antagonizes MCL-1 and overcomes MCL-1-mediated resistance to apoptosis. Proc Natl Acad Sci 104:19512–19517

44. Hwang JJ et al (2010) Phase I dose finding studies of obatoclax (GX15-070), a small molecule Pan-BCL-2 family antagonist, in patients with advanced solid tumors or lymphoma. Clin Cancer Res 16:4038–4045

45. Wilson WH et al (2010) Navitoclax, a targeted high-affinity inhibitor of BCL-2, in lymphoid malignancies: a phase 1 dose-escalation study of safety, pharmacokinetics, pharmacodynamics, and antitumour activity. Lancet Oncol 11:1149–1159

46. Roberts AW et al (2012) Substantial susceptibility of chronic lymphocytic leukemia to BCL2 inhibition: results of a phase I study of navitoclax in patients with relapsed or refractory disease. J Clin Oncol 30:488–496

47. Gandhi L et al (2011) Phase I study of navitoclax (ABT-263), a novel Bcl-2 family inhibitor, in patients with small-cell lung cancer and other solid tumors. J Clin Oncol 29:909–916

48. Rudin CM et al (2012) Phase II study of single-agent navitoclax (ABT-263) and biomarker correlates in patients with relapsed small cell lung cancer. Clin Cancer Res 18:3163–3169

49. Cang S, Iragavarapu C, Savooji J, Song Y, Liu D (2015) ABT-199 (venetoclax) and BCL-2 inhibitors in clinical development. J Hematol Oncol 8:129

50. Davids MS et al (2013) Bcl-2 inhibitor ABT-199 (GDC-0199) monotherapy shows anti-tumor activity including complete remissions in high-risk relapsed/refractory (R/R) chronic lymphocytic leukemia (CLL) and small lymphocytic lymphoma (SLL). Blood 122:872–872

51. Konopleva M et al (2014) A phase 2 study of ABT-199 (GDC-0199) in patients with acute myelogenous leukemia (AML). Blood 124:118–118

52. Roberts AW et al (2014) Determination of recommended phase 2 dose of ABT-199 (GDC-0199) combined with rituximab (R) in patients with relapsed/refractory (R/R) chronic lymphocytic leukemia (CLL). Blood 124:325–325

53. de Vos S et al (2014) The BCL-2 inhibitor ABT-199 (GDC-0199) in combination with bendamustine and rituximab in patients with relapsed or refractory non-Hodgkin's lymphoma. Blood 124:1722

54. Stilgenbauer S et al (2016) Venetoclax in relapsed or refractory chronic lymphocytic leukaemia with 17p deletion: a multicentre, open-label, phase 2 study. Lancet Oncol 17:768–778

55. O'Brien SM et al (2009) Phase I study of obatoclax mesylate (GX15-070), a small molecule pan-Bcl-2 family antagonist, in patients with advanced chronic lymphocytic leukemia. Blood 113:299–305

56. Lane DPC (1992) p53, guardian of the genome. Nature 358:15–16

57. Bode AM, Dong Z (2004) Post-translational modification of p53 in tumorigenesis. Nat Rev Cancer 4:793–805

58. Momand J, Wu H-H, Dasgupta G (2000) MDM2 – master regulator of the p53 tumor suppressor protein. Gene 242:15–29

59. Momand J, Zambetti GP, Olson DC, George D, Levine A (1992) The mdm-2 oncogene product forms a complex with p53 protein and inhibits p53-mediated transactivation. Cell 69:1237–1245

60. Toledo F, Wahl GM (2006) Regulating the p53 pathway: in vitro hypotheses, in vivo veritas. Nat Rev Cancer 6:909–923

61. Uhrinova S et al (2005) Structure of free MDM2 N-terminal domain reveals conformational adjustments that accompany p53-binding. J Mol Biol 350:587–598

62. McCoy MA, Gesell JJ, Senior MM, Wyss DF (2003) Flexible lid to the p53-binding domain of human Mdm2: implications for p53 regulation. PNAS 100:1645–1648

63. Schon O, Friedler A, Bycroft M, Freund SMV, Fersht AR (2002) Molecular mechanism of the interaction between MDM2 and p53. J Mol Biol 323:491–501

64. Kussie PH et al (1996) Structure of the MDM2 oncoprotein bound to the p53 tumor suppressor transactivation domain. *Science* 274:948–953

65. Garcia-Echeverria C, Chene P, Blommers MJJ, Furet P (2000) Discovery of potent antagonists of the interaction between human double minute 2 and tumor suppressor p53. J Med Chem 43:3205–3208

66. Bernal F et al (2010) A stapled p53 helix overcomes HDMX-mediated suppression of p53. Cancer Cell 18:411–422

67. Bernal F, Tyler AF, Korsmeyer SJ, Walensky LD, Verdine GL (2007) Reactivation of the p53 tumor suppressor pathway by a stapled p53 peptide. J Am Chem Soc 129:2456–2457

68. Baek S et al (2012) Structure of the stapled p53 peptide bound to Mdm2. J Am Chem Soc 134:103–106

69. Chang YS et al (2013) Stapled α-helical peptide drug development: a potent dual inhibitor of MDM2 and MDMX for p53-dependent cancer therapy. Proc Natl Acad Sci U S A 110: E3445–E3454

70. Sakurai K, Chung HS, Kahne D (2004) Use of a retroinverso p53 peptide as an inhibitor of MDM2. J Am Chem Soc 126:16288–16289

71. Liu M et al (2010) D-peptide inhibitors of the p53–MDM2 interaction for targeted molecular therapy of malignant neoplasms. Proc Natl Acad Sci 107:14321–14326. doi:10.1073/pnas. 1008930107

72. Kritzer J a, Stephens OM, Guarracino D a, Reznik SK, Schepartz A (2005) β-peptides as inhibitors of protein–protein interactions. Bioorg Med Chem 13:11–16

73. Kritzer JA et al (2006) Miniature protein inhibitors of the p53-hDM2 interaction. Chembiochem 7:29–31

74. Michel J, Harker EA, Tirado-Rives J, Jorgensen WL, Schepartz A (2009) In silico improvement of β3-peptide inhibitors of p53•hDM2 and p53•hDMX. J Am Chem Soc 131:6356–6357
75. Fasan R et al (2004) Using a β-hairpin to mimic an α-helix: cyclic peptidomimetic inhibitors of the p53–HDM2 protein–protein interaction. Angew Chem Int Ed 43:2109–2112
76. Fasan R et al (2006) Structure-activity studies in a family of β-hairpin protein epitope mimetic inhibitors of the p53-HDM2 protein-protein interaction. Chembiochem 7:515–526
77. Hara T, Durell SR, Myers MC, Appella DH (2006) Probing the structural requirements of peptoids that inhibit HDM2-p53 interactions. J Am Chem Soc 128:1995–2004
78. Whitby LR, Boger DL (2012) Comprehensive peptidomimetic libraries targeting protein-protein interactions. Acc Chem Res 45:1698–1709
79. Yin H et al (2005) Terphenyl-based helical mimetics that disrupt the p53/HDM2 interaction. Angew Chem Int Ed 44:2704–2707
80. Campbell F, Plante JP, Edwards TA, Warriner SL, Wilson AJ (2010) N-alkylated oligoamide α-helical proteomimetics. Org Biomol Chem 8:2344
81. Plante JP et al (2009) Oligobenzamide proteomimetic inhibitors of the p53-hDM2 protein-protein interaction. Chem Commun 34:5091–5093. doi:10.1039/b908207g
82. Sakurai K, Kahne D (2010) Design and synthesis of functionalized trisaccharides as p53-peptide mimics. Tetrahedron Lett 51:3724–3727
83. Vassilev LT (2004) In vivo activation of the p53 pathway by small-molecule antagonists of MDM2. Science 303:844–848
84. Vu B et al (2013) Discovery of RG7112: a small-molecule MDM2 inhibitor in clinical development. ACS Med Chem Lett 4:466–469
85. Miyazaki M et al (2012) Discovery of novel dihydroimidazothiazole derivatives as p53-MDM2 protein-protein interaction inhibitors: synthesis, biological evaluation and structure-activity relationships. Bioorg Med Chem Lett 22:6338–6342
86. Miyazaki M et al (2013) Lead optimization of novel p53-MDM2 interaction inhibitors possessing dihydroimidazothiazole scaffold. Bioorg Med Chem Lett 23:728–732
87. Miyazaki M et al (2015) Discovery of DS-5272 as a promising candidate: a potent and orally active p53-MDM2 interaction inhibitor. Bioorg Med Chem 23:2360–2367
88. Ding K et al (2005) Structure-based design of potent non-peptide MDM2 inhibitors. J Am Chem Soc 127:10130–10131
89. Ding K et al (2006) Structure-based design of spiro-oxindoles as potent, specific small-molecule inhibitors of the MDM2-p53 interaction. J Med Chem 49:3432–3435
90. Yu S et al (2009) Potent and orally active small-molecule inhibitors of the MDM2−p53 interaction. J Med Chem 52:7970–7973
91. Zhao Y et al (2013) Diastereomeric spirooxindoles as highly potent and efficacious MDM2 inhibitors. J Am Chem Soc 135:7223–7234
92. Zhao Y et al (2013) A potent small-molecule inhibitor of the MDM2–p53 interaction (MI-888) achieved complete and durable tumor regression in mice. J Med Chem 56:5553–5561
93. Wang S et al (2014) SAR405838: an optimized inhibitor of MDM2-p53 interaction that induces complete and durable tumor regression. Cancer Res 74:5855–5865. doi:10.1158/0008-5472.CAN-14-0799
94. Aguilar A et al (2017) Discovery of 4-((3′ R, 4′ S, 5′ R)-6″-Chloro-4′-(3-chloro-2-fluorophenyl)-1′-ethyl-2″-oxodispiro[cyclohexane-1,2′-pyrrolidine-3′,3″-indoline]-5′-carboxamido)bicyclo[2.2.2]octane-1-carboxylic Acid (AA-115/APG-115): a potent and orally. J Med Chem 60:2819–2839. doi:10.1021/acs.jmedchem.6b01665
95. Ding Q et al (2013) Discovery of RG7388, a potent and selective p53–MDM2 inhibitor in clinical development. J Med Chem 56:5979–5983
96. Ma Y et al (2014) Substituted piperidines as HDM2 inhibitors. Bioorg Med Chem Lett 24:1026–1030
97. Pan W et al (2014) Core modification of substituted piperidines as novel inhibitors of HDM2–p53 protein–protein interaction. Bioorg Med Chem Lett 24:1983–1986

98. Ma Y et al (2014) Pivotal role of an aliphatic side chain in the development of an HDM2 inhibitor. ACS Med Chem Lett 5:572–575

99. Bogen SL et al (2016) Discovery of novel 3,3-disubstituted piperidines as orally bioavailable, potent, and efficacious HDM2-p53 inhibitors. ACS Med Chem Lett 7:324–329. doi:10.1021/acsmedchemlett.5b00472

100. Rew Y et al (2012) Structure-based design of novel inhibitors of the MDM2–p53 interaction. J Med Chem 55:4936–4954

101. Sun D et al (2014) Discovery of AMG 232, a potent, selective, and orally bioavailable MDM2–p53 inhibitor in clinical development. J Med Chem 57:1454–1472

102. Yu M et al (2014) Discovery of potent and simplified piperidinone-based inhibitors of the MDM2–p53 interaction. ACS Med Chem Lett 5:894–899

103. Ye Q et al (2015) Pharmacokinetics and metabolism of AMG 232, a novel orally bioavailable inhibitor of the MDM2–p53 interaction, in rats, dogs and monkeys: in vitro–in vivo correlation. Xenobiotica 45:681–692

104. Gonzalez AZ et al (2014) Novel inhibitors of the MDM2-p53 interaction featuring hydrogen bond acceptors as carboxylic acid isosteres. J Med Chem 57:2963–2988

105. Rew Y et al (2014) Discovery of AM-7209, a potent and selective 4-amidobenzoic acid inhibitor of the MDM2–p53 interaction. J Med Chem 57:10499–10511

106. Furet P et al (2012) The central valine concept provides an entry in a new class of non peptide inhibitors of the p53-MDM2 interaction. Bioorg Med Chem Lett 22:3498–3502

107. Vaupel A et al (2014) Tetra-substituted imidazoles as a new class of inhibitors of the p53-MDM2 interaction. Bioorg Med Chem Lett 24:2110–2114

108. Gessier F et al (2015) Discovery of dihydroisoquinolinone derivatives as novel inhibitors of the p53–MDM2 interaction with a distinct binding mode. Bioorg Med Chem Lett 25:3621–3625

109. Holzer P et al (2015) Discovery of a dihydroisoquinolinone derivative (NVP-CGM097): a highly potent and selective MDM2 inhibitor undergoing phase 1 clinical trials in p53wt tumors. J Med Chem 58:6348–6358

110. Furet P et al (2016) Discovery of a novel class of highly potent inhibitors of the p53–MDM2 interaction by structure-based design starting from a conformational argument. Bioorg Med Chem Lett 26:4837–4841

111. Holzer P et al (2016) Discovery of NVP-HDM201 – first disclosure of a next-generation Mdm2 inhibitor with superior characteristics. Cancer Res 76., Abstract 4855

112. Ray-Coquard I et al (2012) Effect of the MDM2 antagonist RG7112 on the P53 pathway in patients with MDM2-amplified, well-differentiated or dedifferentiated liposarcoma: an exploratory proof-of-mechanism study. Lancet Oncol 13:1133–1140

113. Patnaik A et al (2013) Clinical pharmacology characterization of RG7112, an MDM2 antagonist, in patients with advanced solid tumors. Aacr 76:587–595

114. Andreeff M et al (2015) Results of the phase 1 trial of RG7112, a small-molecule MDM2 antagonist in leukemia. Clin Cancer Res 22:1–10

115. Yee K et al (2014) Phase 1/1b study of RG7388, a potent MDM2 antagonist, in acute myelogenous leukemia (AML) patients (Pts). Blood 124:116

116. Siu LL (2014) DT: CP and ET: poster: phase 1 dose escalation, food effect, and biomarker study of RG7388, a more potent second-generation MDM2 antagonist, in patients (pts) with solid tumors. J Clin Oncol 32., Abstract #2535

117. Bauer T et al (2015) Abstract B27: a phase I dose escalation study of the MDM2 inhibitor DS-3032b in patients with advanced solid tumors and lymphomas. Mol Cancer Ther 14:B27–B27

118. Wagner AJ et al (2015) A phase I trial of the human double minute 2 (HDM2) inhibitor MK-8242 in patients (pts) with advanced solid tumors. J Clin Oncol 33:10564

119. Ravandi F et al (2015) A phase I trial of the human double minute 2 inhibitor (MK-8242) in patients with refractory/recurrent acute myelogenous leukemia (AML). J Clin Oncol 33:7070

120. LaCasse EC et al (2008) IAP-targeted therapies for cancer. Oncogene 27:6252–6275

121. Fulda S, Vucic D (2012) Targeting IAP proteins for therapeutic intervention in cancer. Nat Rev Drug Discov 11:109–124
122. Shi Y et al (2000) Structural basis of IAP recognition by Smac/DIABLO. Nature 408:1008–1012
123. Fulda S, Wick W, Weller M, Debatin K-M (2002) Smac agonists sensitize for Apo2L/TRAIL- or anticancer drug-induced apoptosis and induce regression of malignant glioma in vivo. Nat Med 8:808–815
124. Oost TK et al (2004) Discovery of potent antagonists of the antiapoptotic protein XIAP for the treatment of cancer. J Med Chem 47:4417–4426
125. Sharma SK, Straub C, Zawel L (2006) Development of peptidomimetics targeting IAPs. Int J Pept Res Ther 12:21–32
126. González-Lpez M et al (2011) Design, synthesis and evaluation of monovalent Smac mimetics that bind to the BIR2 domain of the anti-apoptotic protein XIAP. Bioorg Med Chem Lett 21:4332–4336
127. Ndubaku C et al (2009) Antagonism of c-IAP and XIAP proteins is required for efficient induction of cell death by small-molecule IAP antagonists. ACS Chem Biol 4:557–566
128. Zobel K et al (2006) Design, synthesis, and biological activity of a potent Smac mimetic that sensitizes cancer cells to apoptosis by antagonizing IAPs. ACS Chem Biol 1:525–533
129. Cai Q et al (2011) A potent and orally active antagonist (SM-406/AT-406) of multiple inhibitor of apoptosis proteins (IAPs) in clinical development for cancer treatment. J Med Chem 54:2714–2726
130. Flygare JA et al (2012) Discovery of a potent small-molecule antagonist of inhibitor of apoptosis (IAP) proteins and clinical candidate for the treatment of cancer (GDC-0152). J Med Chem 55:4101–4113
131. Wong H et al (2013) Learning and confirming with preclinical studies: modeling and simulation in the discovery of GDC-0917, an inhibitor of apoptosis proteins antagonist. Drug Metab Dispos 41:2104–2113
132. Chessari G et al (2015) Fragment-based drug discovery targeting inhibitor of apoptosis proteins: discovery of a non-alanine lead series with dual activity against cIAP1 and XIAP. J Med Chem 58:6574–6588
133. Allensworth JL, Sauer SJ, Lyerly HK, Morse MA, Devi GR (2013) Smac mimetic Birinapant induces apoptosis and enhances TRAIL potency in inflammatory breast cancer cells in an IAP-dependent and TNF-α-independent mechanism. Breast Cancer Res Treat 137:359–371
134. Benetatos CA et al (2014) Birinapant (TL32711), a bivalent SMAC mimetic, targets TRAF2-associated cIAPs, abrogates TNF-induced NF-κB activation, and is active in patient-derived xenograft models. Mol Cancer Ther 13:867–879
135. Tolcher AW et al (2013) Phase I study of safety and pharmacokinetics (PK) of GDC-0917, an antagonist of inhibitor of apoptosis (IAP) proteins in patients (Pts) with refractory solid tumors or lymphoma. | 2013 ASCO Annual Meeting | Abstracts | Meeting Library. J Clin Oncol 31:2503
136. Sikic BI et al (2011) Safety, pharmacokinetics (PK), and pharmacodynamics (PD) of HGS1029, an inhibitor of apoptosis protein (IAP) inhibitor, in patients (Pts) with advanced solid tumors: results of a phase I study. J Clin Oncol 29:3008
137. Weisberg E et al (2010) Smac mimetics: implications for enhancement of targeted therapies in leukemia. Leukemia 24:2100–2109
138. Hird AW, Aquila BM, Hennessy EJ, Vasbinder MM, Yang B (2015) Small molecule inhibitor of apoptosis proteins antagonists: a patent review. Expert Opin Ther Pat 1:1–20
139. Lipinski CA, Lombardo F, Dominy BW, Feeney PJ (2001) Experimental and computational approaches to estimate solubility and permeability in drug discovery and development settings. Adv Drug Deliv Rev 46:3–26

Small Molecule Inhibitors of ALK

John M. Hatcher and Nathanael S. Gray

Abstract Anaplastic lymphoma kinase (ALK) is a receptor tyrosine kinase that has attracted a great deal of attention due to its oncogenic potential and essential role in the pathogenesis of a wide variety of human cancers, such as anaplastic large cell lymphomas (ALCLs), non-small cell lung cancer (NSCLC), breast cancer, colorectal cancer, neuroblastoma, and ovarian cancer. Despite the remarkable clinical success of crizotinib (Xalkori), the first ALK inhibitor approved in 2011 for the treatment of NSCLC, the emergence of resistance mutations frequently causes relapse in patients. As a result, a variety of second and third generation ALK inhibitors have been developed to overcome these mutations. This chapter presents an overview of the hit-to-drug evolution strategies as well as the biological activities of several second and third generation ALK inhibitors.

Keywords ALK inhibitor, Anaplastic large cell lymphomas (ALCLs), Anaplastic lymphoma kinase (ALK), Non-small cell lung cancer (NSCLC)

Contents

J.M. Hatcher and N.S. Gray (✉)
Longwood Center, Dana Farber Cancer Institute, Room 2209, 360 Longwood Avenue, Boston, MA 02215, USA
e-mail: Nathanael_Gray@DFCI.HARVARD.EDU

Anaplastic lymphoma kinase (ALK) is a member of the insulin receptor tyrosine kinase family (RTK). Members of this family include α and β type PDGF receptors, EGF receptor, HER2/neu, insulin, and IGF-1 receptors, which regulate cellular growth and may trigger neoplastic transformation when mutated, translocated, or expressed aberrantly [1–3]. Multiple mutations involving the ALK gene have been implicated in the pathogenesis of anaplastic large cell lymphoma (ALCL), rhabdomyosarcoma [4], inflammatory myofibroblastic pseudo tumor [5], neuroblastoma [6], and non-small cell lung cancer [7] (NSCLC).

Deregulation of ALK was first identified in ALCL, a subtype of non-Hodgkins lymphoma, in which the t(2;5)(p23;q35) chromosomal translocation involving the ALK gene was first described [8]. This translocation results in the fusion of nucleophosmin (NPM) to a truncated form of the ALK gene, which encodes a chimeric receptor tyrosine kinase (RTK) that is de-regulated and constitutively activated leading to an "oncogene-addicted" state. The NPM-ALK fusion leads to activation of phospholipase C-γ (PLC-γ), which leads to growth factor independent proliferation of lymphocytes [7]. In addition, fusion of ALK with NPM leads to hyperphosphorylation and activation of p80. This constitutively active p80 is localized to the cytoplasm and catalyzes the phosphorylation of SH2 domain-containing transforming protein (SHC), an adaptor protein, and insulin receptor substrate 1 (IRS-1) with downstream effects on RAS and epidermal growth factor receptor (EGFR) pathways [9]. NPM-ALK has also been shown to act through the signal transducer and activator of transcription (STAT), primarily STAT3 and STAT5 [10–12]. STAT3 is activated by NPM-ALK phosphorylation and is actively involved in the malignant transformation of NPM-ALK expressing lymphocytes [11]. Activated STAT3 enhances the positive autocrine loop involving IL-6 and the IL-6 receptor (IL6R), which in turn up-regulates the expression of anti-apoptotic factors Bcl-xL and Survivin [12]. STAT5 activation is also thought to protect cells from apoptosis, likely from activation of anti-apoptotic factors such as A1 (or its human homologue, Bfl-1), Bcl-xL, PIM-1, and oncostatin M [10].

The EML4-ALK fusion gene was initially identified in 2007 in non-small cell lung cancer (NSCLC) [13]. This mutation arises from inv(2)(p21p23) and leads to the fusion of echinoderm microtubule-associated protein like-4 (EML4) gene with ALK gene resulting in EML4-ALK fusion protein with aberrant kinase activity. The fusion protein plays a pivotal role in the malignant transformation of susceptible lung parenchyma [14]. EML4 is a member of the EMAP-like (EML) protein family and plays an important role in the correct formation of microtubules [15]. The EML4-ALK fusion kinase has an ALK fragment identical to the ALK fragment in NPM-ALK. It contains the amino-terminal half of EML4 and the intracellular catalytic domain of ALK, which results in constitutive dimerization of the kinase domain of ALK leading to aberrant activation of downstream signaling such as Akt, STAT3, and extracellular signal regulated kinase 1 and 2 (ERK1/2) [16, 17]. Lung cancers with ALK rearrangements are highly sensitive to ALK tyrosine kinase inhibition, further underscoring the notion that such cancers are addicted to ALK kinase activity. This chapter outlines the discovery and optimization of first, second, and third generation ALK inhibitors.

Crizotinib (PF-02341066, Xalkori) was the first ALK inhibitor approved for ALK-positive NSCLC. Crizotinib was originally developed as an inhibitor of the mesenchymal epithelial transition factor (c-MET) and was later repurposed for anaplastic lymphoma kinase (ALK) following the discovery of the EML4-ALK translocation in NSCLC. Crizotinib was developed by scientists at Sugen (later acquired by Pfizer) during a campaign to optimize the known c-MET inhibitor **1** [18]. The indoline-2-one **1** demonstrated potent and selective inhibition of c-MET autophosphorylation and related biological functions in both in vitro and in vivo studies, but suffered from poor pharmaceutical properties including low solubility, high metabolic clearance, and poor permeability [19], which limited further development for human clinical studies. To improve the drug-like properties of compound **1**, lipophilic efficiency (LipE) was used to guide further optimization in conjunction with a structure-based drug design strategy [20, 21]. LipE = [pK_i (or pIC_{50}) − clogD] is an important parameter, which is used to evaluate the effect of structural modifications on both potency and lipophilicity. The co-crystal structure of **1** with c-MET was analyzed looking for opportunities to improve LipE. A significant portion of the indolinone ring along with the sulfone linker was deemed inefficient scaffolding for the 2,6-dichlorophenyl group, which led to the introduction of the 2-aminopyridine scaffold shown in Fig. 1. The 2-amino pyridine NH and ring nitrogen were expected to make hydrogen bonds to the hinge residues P1158 and M1160 similar to the oxindole ring of **1**. The design concept was tested with a small set of compounds, exemplified by compound **2** with the same amide group as **1**, showed an improvement in potency and LipE with a K_i of 0.46 μM and LipE of 3.11 (cell)). The co-crystal structure also revealed a small lipophilic pocket adjacent to the benzyloxy linker. Adding small hydrophobic group such as an α-methyl substituent led to enhanced potency and efficiency. Further optimization of the 2,6-dichlorophenyl group led to the incorporation of a fluorine at the 3-position. Combining the α-methyl group and 3-fluorine modifications imparted a dramatic
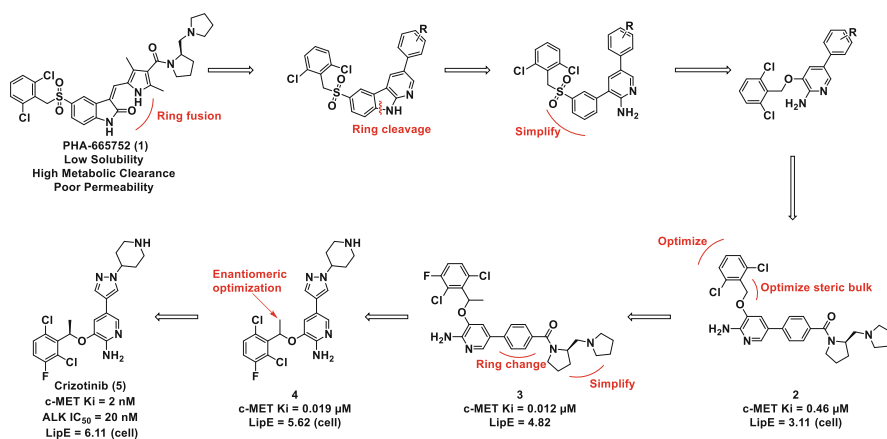
Fig. 1 Discovery of crizotinib (**5**)

improvement in potency ($K_i = 0.012$ μM) and lipophilic efficiency (LipE = 4.60) exemplified by compound **3**. In order to maximize the chances of good ADME properties and improved potencies, a series of smaller, less lipophilic 5-heteroaryl analogues bearing a solubilizing group were prepared to replace the large aryl amide, which led to compound **4**. This modification improved enzymatic and cell potency by 10- to 20-fold and improved the LipE as seen in Fig. 1. Examination of the co-crystal structure of **4** showed that only the R configuration of the α-methyl group provides the right fit into the small hydrophobic pocket. Both enantiomers were prepared and as predicted, the R configuration of the α-methyl group was much more potent than the S configuration (Fig. 1), which led to the discovery of Crizotinib (**5**) with a K_i of 0.002 μM against c-MET and a LipE of 6.11 [19].

Crizotinib (**5**) was tested against a panel of 120 human kinases and found to display ALK (20 nM) and ROS1 (80 nM) activity whilst showing >100-fold selectivity for c-Met against all other kinases [22]. Although ROS1 shares only 49% amino acid homology with the kinase domains of ALK and 77% homology of the ATP-binding site, several ALK inhibitors show inhibitory activity against ROS1. In different ALK-related cellular assays, crizotinib inhibited the tyrosine phosphorylation of NPM–ALK in KARPAS-299 and SU-DHL-1 (ALCL) cells with IC_{50} values of 32 nM and 43 nM, respectively. An in vivo study following oral administration of crizotinib in a mouse model bearing the KARPAS-299 tumor xenograft at 10 mg/kg/day for 15 days resulted in complete tumor regression [23]. These promising results suggested that crizotinib is a potent ALK inhibitor suitable for the treatment of ALK-related cancers.

Further profiling using Ambit Kinomescan at a concentration 10 μM showed inhibition of 143 of 442 kinases >90% of control as shown in Fig. 2. Human plasma pharmacokinetics for crizotinib following single administration of an intravenous single dose of crizotinib were calculated and are shown in Table 1 [24].

The impact of crizotinib on the clinical course of patients with ALK-positive NSCLC was quickly realized after the results of the PROFILE 1001 study were published in 2010 [25]. In this open-label, Phase I study, 82 patients who had ALK-positive NSCLC were treated with crizotinib. An objective response rate (ORR) of 57% was observed, and stable disease was seen in an additional 33% of patients. Crizotinib was well tolerated with mild gastrointestinal symptoms as the most common reported adverse event (AE) [25]. The overall survival (OS) in this cohort of 82 patients at 1 and 2 years was 74% and 54% respectively [26]. Crizotinib was compared with single agent chemotherapy (pemetrexed or docetaxel) in an open-label, Phase III trial PROFILE 1007 study involving 347 patients with ALK-positive NSCLC [27]. These patients were randomly assigned to receive either 250 mg twice daily of oral crizotinib vs intravenous pemetrexed or docetaxel. The median progression-free survival (PFS) was 7.7 months (95% CI 6.0–8.8) in crizotinib group compared with 3.0 (95% CI 2.6–4.3) months in the chemotherapy group. The ORR was 65% (95% CI 58–72) in crizotinib compared to 20% (95% CI 14–26) in the chemotherapy group ($P < 0.001$). The adverse events reported were mostly grades 1 or 2. Grade 3 or 4 events were elevated aminotransferase levels and neutropenia, which occurred in 16 and 13% of patients respectively [27]. The
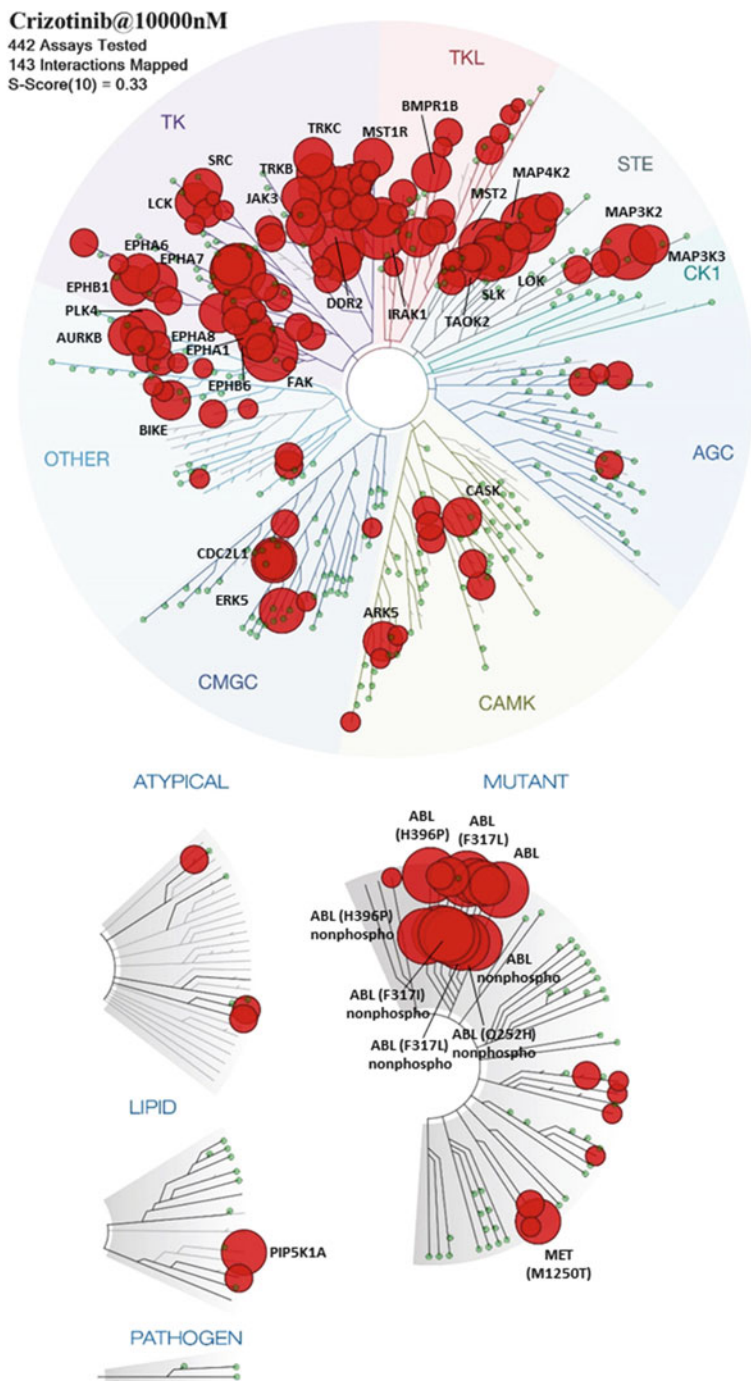
Fig. 2 Kinomescan analysis of crizotinib (**5**) at a concentration of 10 μM

Table 1 Plasma crizotinib pharmacokinetic parameters

Parameter (units)	Crizotinib 50 mg iv	Crizotinib 250 mg oral
Crizotinib	$n = 14$	$n = 14$
AUC_{INF} (ng h mL^{-1})	1,067	2,321
AUC_{last} (ng h mL^{-1})	1,007	2,250
C_{max} (ng mL^{-1})	155	99.6
T_{max} (h)	1.92	5.00
$T_{1/2}$ (h)	38.9	29
CL/F (L h^{-1})	–	108
Vz/F (L)	–	4,478
CL (L h^{-1})	46.8	–
V_{ss} (L)	1,772	–
AUC_{INF} (dn) (ng h mL^{-1} mg^{-1})	21.4	9.28
AUC_{Last} (dn) (ng h mL^{-1} mg^{-1})	20.1	9.00
C_{max} (dn) (ng mL^{-1})	3.10	3.98

AUC_{inf} area under the plasma concentration–time profile from time zero extrapolated to infinite time, AUC_{last} area under the plasma concentration–time profile from time zero to the time of the last quantifiable concentration (C_{last}), CL systemic clearance, CL/F apparent oral clearance after oral dose, C_{max} maximum observed concentration, CV coefficient of variation, dn dose-normalized, iv intravenous, $T_{1/2}$ terminal half-life, T_{max} time for C_{max}, V_{ss} volume of distribution, Vz/F apparent volume of distribution

PROFILE 1014 study compared crizotinib to chemotherapy in 343 patients who had no previous treatment for advanced NSCLC [28]. They were randomized to either receive crizotinib or pemetrexed plus platinum (cisplatin or carboplatin). Progression-free survival for crizotinib group ($n = 172$) was 10.9 months and for chemotherapy group ($n = 171$) was 7.0 months. The ORR was 74% (95% CI 67–81) for crizotinib group vs 45% (95% CI 37–53) for chemotherapy ($P < 0.001$). Median OS was not reached in either group at the time of report (hazard ratio for death with crizotinib, 0.82; 95% CI, 0.54–1.26; $P = 0.36$); the 1 year estimated survival rate was 84% with crizotinib versus 79% with chemotherapy. Crizotinib-associated AEs were vision disorders, diarrhea, nausea, and edema. It was concluded from the PROFILE 1014 study that crizotinib was superior to standard first-line pemetrexed-plus-platinum chemotherapy in patients with previously untreated advanced ALK-positive NSCLC [28]. Hence, crizotinib is currently approved for first line in ALK + NSCLC.

However, despite a high response rate in ALK rearranged NSCLC, most patients develop resistance to crizotinib after 1 year of treatment [27, 29]. In particular, the central nervous system (CNS) is one of the most common sites of relapse in patients with ALK-positive NSCLC [30, 31]. Studies of lung cancers harboring ALK rearrangements with acquired resistance to crizotinib have identified ALK fusion gene amplification and secondary ALK kinase domain mutations in approximately one-third of cases [32–34]. The most frequently identified secondary mutations are L1196M (gatekeeper mutation), G1269A, 1151T-ins, L1152R, C1156Y, G1202R, F1174L, and S1206Y [32, 35–38].

1   NVP-TAE684 and Ceritinib

Ceritinib is an orally available second-generation ALK inhibitor developed by Novartis, which received accelerated approval by the FDA in April 2014 as a treatment for patients with ALK-positive metastatic NSCLC, who were previously treated with crizotinib. Ceritinib was developed based on TAE684 (**6**), which was identified during a cellular screening campaign designed to discover compounds with activity against NPM-ALK transduced Ba/F3 cells [39]. TAE684 showed strong inhibitory activity against Ba/F3 NPM–ALK with an IC_{50} value of 3 nM and displayed higher potency against the two EML4–ALK positive NSCLC cell lines, NCI-H2228 and NCI-H3122 (IC_{50} values of 16 and 44 nM) compared to crizotinib (871 nM and 1,551 nM, respectively) [39]. Although TAE684 showed potent in vivo efficacy, clinical development was not pursued due to the potential for toxicity associated with formation of a 1,4-diiminoquinone metabolite that is produce as a result of oxidative metabolism. Formation of the 1,4-diiminoquinone intermediate metabolite was confirmed by incubating TAE684 with liver micro-somes, and trapping the formed 1,4-diiminoquinone by glutathione. Approximately 20% conversion to the metabolite was detected by LC-MS [40]. This led researchers at Novartis to develop a new compound to overcome the metabolic liability by adding a methyl group to the aryl ring para to the alkoxy group and introducing a carbon linkage to the piperidine substituent to avoid the formation of 1,4-diiminoquinone. After synthesizing several analogues using the design strategy shown in Fig. 3, ceritinib (**7**) was found to be the most effective against NPM–ALK transduced Ba/F3 and KARPAS-299 cells with IC_{50} values of 26 nM and 22.8 nM, respectively. In Ba/F3 cells engineered to express 18 kinases, ceritinib displayed strong inhibitory activity against Ba/F3–ALK and Ba/F3–EML4–ALK with IC_{50} values of 40.7 nM and 2.2 nM, respectively [40].
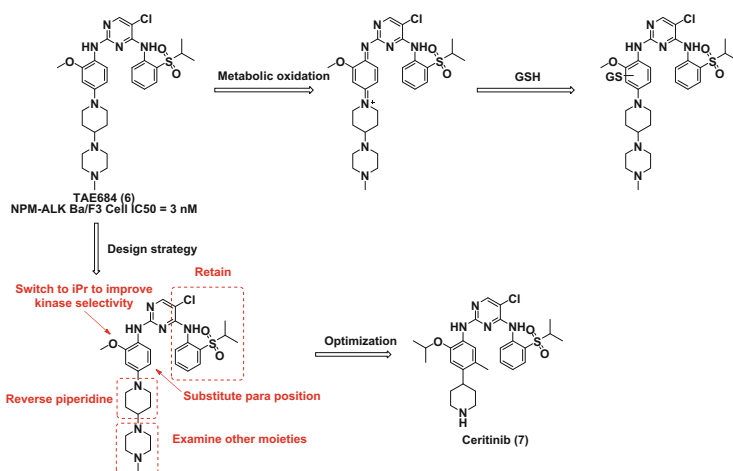
Fig. 3   The evolution of ceritinib (**7**) from initial hit TAE684 (**6**)

TAE684 was screened against a panel of 353 kinases at a concentration of 1 μM using Ambit KINOMEscan, which showed inhibition of 231 kinases at >90% of control. Ceritinib demonstrated much improved selectivity, inhibiting only 25 of 468 kinases at >90% of control in the same screen (Fig. 4).

The PK profile of ceritinib was determined in mouse, rat, dog, and monkey and exhibited low plasma clearance in all animals compared to liver blood flow. The volume of distribution at steady state (V_{ss}) was high and approximately tenfold greater than total body water. Half-life ($T_{1/2}$) ranged from moderate to long (6.2–26 h). Following a single oral administration of ceritinib as a solution or suspension, the oral bioavailability was good (~55%) in mouse, rat, dog, and monkey. Time of maximal concentration (T_{max}) occurred consistently late in animal species tested, indicating slow oral absorption as seen in Table 2 [40].

Ceritinib induced dose-dependent growth inhibition and tumor regression in both KARPAS-299 (25 or 50 mg kg^{-1}, po, qd) and NCI-H2228 (25 mg kg^{-1}, po, qd) mouse xenograft models for 2 weeks with excellent tolerability. More importantly, ceritinib exhibited potent inhibitory activity against Ba/F3 cells expressing
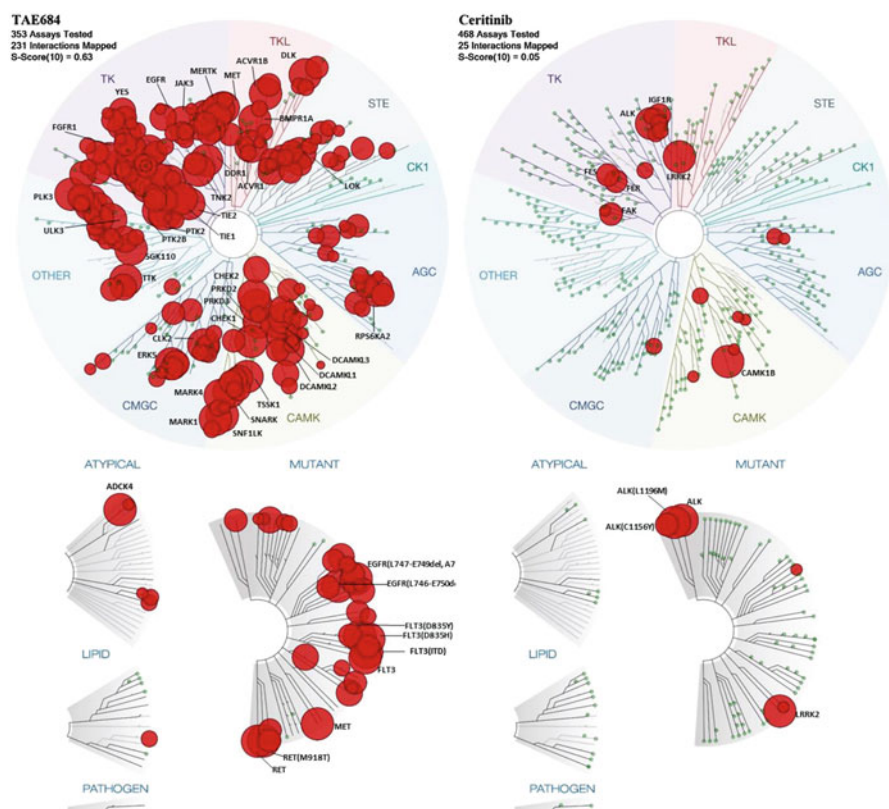
Fig. 4 Comparison of kinase selectivity of TAE684 (**6**) and Ceritinib (**7**)

Table 2 Pharmacokinetic parameters of ceritinib (**7**)

Parameter	Mouse		Rat		Dog		Monkey	
	iv	po	iv	po	iv	po	iv	po
Dose (mg kg^{-1})	5	20	3	10	5	20	5	60
AUC (h nM)	5,634	12,296	2,779	6,092	18,096	67,904	11,305	76,325
CL (mL min^{-1} kg^{-1})	26.6	–	36.8	–	9.2	–	12.8	–
V_{ss} (L kg^{-1})	9.7	–	21.2	–	13.5	–	15	–
C_{max} (nM)	1,756	696	770	259	2,329	1,899	2,526	1,697
T_{max} (h)	0.03	7.0	0.03	7.0	0.03	8.0	–	13
$T_{1/2}$ (h)	6.2	–	9.1	–	21	–	26	–
F (%)	–	55	–	66	–	119	–	56

four crizotinib-resistant ALK mutations: L1196M, G1269M, I1171T, and S1206Y [40]. However, ceritinib is not able to overcome the C1156Y, G1202R, 1151Tins, L1152R, or F1174C mutations [41].

2 Alectinib and JH-VIII-157-02

Alectinib (**12**) is an orally active, second-generation ALK inhibitor developed by Chugai/Roche bearing a unique tetracyclic core. Importantly, alectinib shows potent antitumor activity and is capable of inhibiting crizotinib-resistant L1196M and C1156Y mutants, as well as inhibiting EML4–ALK$_{L1196M}$ driven cell growth. Alectinib was developed from "hit" compound **8**, which was identified following a high-throughput screen of an in house library for biochemical ALK inhibitors (HTS) [42]. Compound **8** exhibited modest potency of IC$_{50}$ = 1.3 μM against ALK and an IC$_{50}$ of >50 μM against c-MET. Replacement of the benzofuran scaffold with an indole ring in order to increase the H-bonding interaction between the carbonyl group at the 11-position and the hinge region Met-1199 of ALK led to an increase in potency. Replacement of the ethoxy group at the 3-position with a cyano group led to compound **9**, which exhibited a 100-fold increase in ALK activity compared to compound **8** and also possessed good cell growth inhibition against NPM–ALK driven cell line KARPAS-299, with an IC$_{50}$ value of 60 nM [42]. Unfortunately, compound **9** was found to have high in vitro clearance in both mouse (CL = 51 mL min^{-1} mg^{-1}) and human (CL = 55 mL min^{-1} mg^{-1}) liver microsomes, likely due to dealkylation of the diethylamino group. The next step was to modify the 8-position substituent of the 3-cyanobenzo[b]carbazole scaffold in order to block or slow down the metabolism and clearance. It was found that substituents with a cationic nitrogen atom at the 8-position would interact with the solvent-accessible region of the ALK protein, as seen in the N-oxetan-3-yl-piperidin-4-yl derivative **10**, which led to improved metabolic stability (CL = 10 mL min^{-1} mg^{-1} in human liver microsomes). Compound **10** showed inhibitory activity against enzymatic ALK and cellular KARPAS-299 with IC$_{50}$

values of 1.5 nM and 21 nM, respectively. Compound **10** also showed significant tumor regression in both KARPAS-299 (20 mg kg^{-1}, po, qd) and NCI-H2228 (6 mg kg^{-1}, po, qd) mouse xenograft models for 11 days without any significant weight loss [42]. Compound **10** was found to have weak inhibitory activity against c-Met (IC$_{50}$ = 7.2 μM). However, it was much more active against kinase insert domain receptor (KDR) (IC$_{50}$ = 100 nM), which is associated with the potential to induce hypertensive side effects. Therefore, further optimization focused on improving the selectivity to remove KDR activity. Docking studies of compound **10** to an ALK homology model revealed a hydrophobic pocket adjacent to carbon 9 of the tetracyclic core, which could be used to improve kinase selectivity [43]. Several analogs were prepared with various alkyl and alkynyl groups at the 9-position and an N-(oxetan-3-yl)piperazine moiety at the 8-position. Compound **11** with an ethyl substituent in the 9-position showed excellent potency against enzymatic ALK (IC$_{50}$ = 2.9 nM) with no KDR inhibition (IC$_{50}$ > 5,000 nM). The greatly improved selectivity of compound **11** compared to that of compound **10**, along with strong antiproliferative activity against KARPAS-299 cells (IC$_{50}$ = 12.8 nM), suggested further testing of this compound would be worthwhile. In vivo studies of compound **11** revealed significant tumor regression at a 20 mg kg^{-1} oral dose without significant body weight loss in NPM–ALK positive ALCL mouse xenograft models [43]. The final design focused on varying the substituents at the 8-position to achieve better ADME properties, since compound **11** only had 28.2% oral bioavailability. Various analogues were prepared, which led to Compound **12** (alectinib) bearing the 4-morpholinopiperidine group [43].

Alectinib (**12**) displayed superior bioavailability (F = 50% in monkey) compared to compound **11**, and showed potent activity against enzymatic ALK$_{WT}$ (1.9 nM) as well as ALK$_{L1196M}$ (IC$_{50}$ = 1.6 nM), ALK$_{F1174L}$ (IC$_{50}$ = 1.0 nM), and ALK$_{R1275Q}$ (IC$_{50}$ = 3.5 nM) (Fig. 5). Alectinib displayed strong antiproliferative activity in different ALK-driven cell lines including NCI-H2228 (IC$_{50}$ = 53 nM), KARPAS-299 (IC$_{50}$ = 3.0 nM), SR-786 (IC$_{50}$ = 6.9 nM), NB-1 (IC$_{50}$ = 4.5 nM), and KELLY (IC$_{50}$ = 62 nM), as well as cell growth inhibition
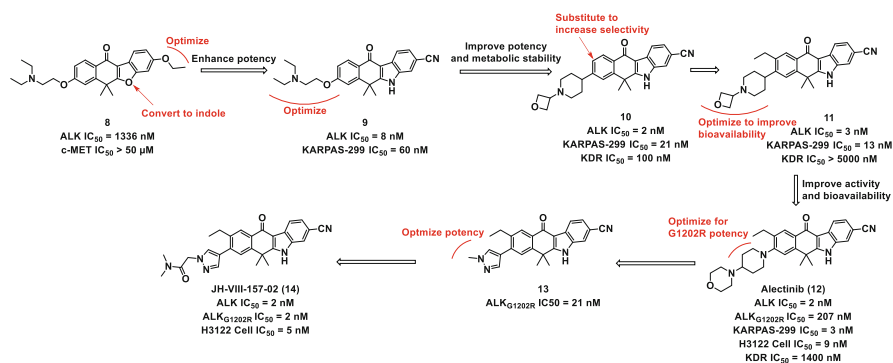
Fig. 5 Optimization strategy of hit **8** leading to the development of alectinib (**12**) and JH-VIII-157-02 (**14**)

against Ba/F3–EML4–ALK cell lines harboring L1196M and C1156Y mutation that are resistant to crizotinib. Once daily oral administration of alectinib induced dose-dependent growth inhibition and tumor regression ($ED_{50} = 0.46$ mg kg^{-1}) in NCI-H2228 mouse xenograft models. Treatment of 20 mg kg^{-1} alectinib showed rapid tumor regression (168% tumor growth inhibition; $P < 0.001$), and the tumor volume in any mouse was <30 mm^3 after 11 days of treatment. A potent antitumor effect was maintained, and tumor regrowth did not occur throughout the 4-week drug-free period. Alectinib was found to have a half-life of 8.6 h and an oral bioavailability of 70.8% in mice. At a repeated dose of 6 mg kg^{-1}, the mean plasma levels reached 1,707, 1,455, and 317 nM at 2, 7, and 24 h post-dose, respectively. In addition, oral administration of alectinib resulted in significant tumor regression at 60 mg kg^{-1} qd for 8 days in mice bearing Ba/F3–EML4–ALK$_{L1196M}$ and in other mouse xenograft models, including two ALK-related ALCL cell lines (KARPAS-299 and SR-786) and ALK-amplified neuroblastoma cells (NB-1) [44, 45]. Based on these results, alectinib was chosen as a promising second-generation ALK inhibitor.

In a multicenter, single-arm, open-label Phase I–II study conducted in Japan (AF-001JP), ALK inhibitor naïve patients who had ALK-positive NSCLC were treated with alectinib [46]. In the dose escalation phase, which included 24 such patients, increasing doses in the 20–300 mg range were used. No dose-limiting toxicities (DLT) were noted. Hence, 300 mg twice daily was established as the recommended dose for phase II. The phase II portion enrolled 46 patients. Forty-one of these patients had a partial response (PR) and two had complete responses (CR). Hence, ORR was around 94% (95% CI: 82–98). Grade 3 adverse events were reported in 26% ($n = 12$) of patients and included elevated creatinine phosphokinase and neutropenia [46]. In another phase I–II single-arm open-label study, 47 patients with ALK-positive NSCLC who had resistance to crizotinib or were intolerant were treated with alectinib. In the dose escalation phase, doses were escalated from 300 to 900 mg in seven different cohorts of patients [47]. DLTs were seen in the 900 mg cohort, including a grade 3 headache in one patient and grade 3 neutropenia in another patient. Three patients dropped out of the study due to adverse events, including grade 3 dyspnea, grade 4 CNS metastasis, and grade 3 abdominal pain. Out of the 47 patients, 44 were assessed for response and the ORR was found to be 55% (24 PR, one CR). ORR for the 21 patients who had baseline CNS metastasis was 52% (5 CR and another 6 having partial CNS response). This study showed that alectinib not only was effective in patients pretreated with first-generation ALK inhibitor but also was active for CNS metastasis [47]. Alectinib is now FDA-approved for the treatment of metastatic ALK + NSCLC in patients who have progressed on or are intolerant to crizotinib.

3   JH-VIII-157-02

Acquired secondary mutations in the anaplastic lymphoma kinase (ALK) gene have been identified in ALK positive non–small-cell lung cancer (NSCLC) patients treated with crizotinib (**5**) and ceritinib (**7**). While alectinib (**12**) is able to overcome many of these mutations, it, along with all but one clinical ALK inhibitor (Lorlatinib, **32**), is unable to overcome the G1202R mutation [41]. One study found that 20% of ceritinib resistant patients harbored only the G1202R mutation, 10% harbored only the F1174C/V mutation, 10% of patients harbored both G1202R and F1174C mutations, and 60% presented with a wild-type ALK kinase domain [29]. Hence, G1202R is one of the leading ALK secondary mutations causing resistance to ceritinib, accounting for 75% of all identified ALK secondary mutations in ceritinib resistant patients. A similar profile to that of ceritinib resistance has been reported for alectinib, identifying the G1202R and F1174V mutations in patients [48]. Based on these findings, researchers at Dana-Farber Cancer Institute set out to modify alectinib in order to increase its potency against the G1202R mutation, while maintaining potency against the commonly found mutations including L1196M (gatekeeper mutation), G1269A, 1151T-ins, L1152R, C1156Y, G1202R, F1174L, and S1206Y. A molecular modeling study using the co-crystal structure of alectinib and EML4-ALK (PDB: 3AOX) (Fig. 6a) incorporating the 1202R mutation was conducted and found that the morpholino piperidine ring of alectinib was predicted to be in very close proximity to the G1202 residue, and therefore likely responsible for the loss of activity in the G1202R mutant due to steric clash with the 1202R residue (Fig. 6b) [41].

A variety of analogues were prepared replacing the morpholino piperidine ring with small aromatic heterocycles with a basic nitrogen in order to gain an additional hydrogen bonding interaction with the arginine residue of the G1202R mutant,
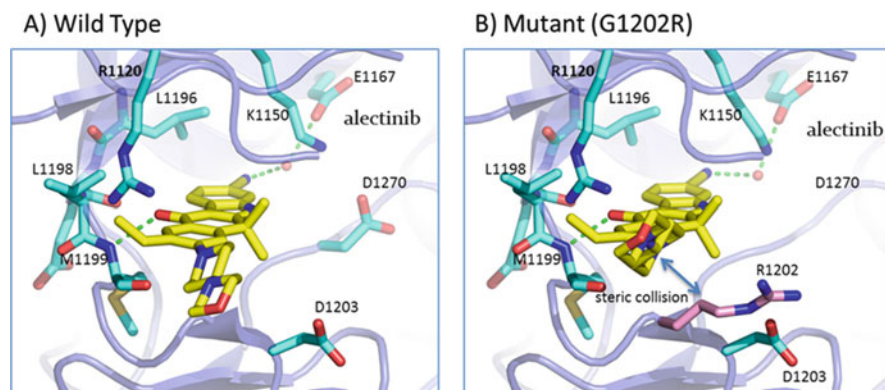
Fig. 6 Co-crystal structure of **12** in complex with wild-type ALK and docked pose of **12** with a molecular model of ALK-G1202R. (**a**) Binding conformation of **12** (*yellow stick*) in the ATP binding site of ALK-wt (PDB 3AOX). Hydrogen bonds are indicated by *dashed lines*. (**b**) Binding conformation of **12** in the ATP binding site of ALK with a model of the G1202R mutation. Hydrogen bonds are indicated by *dashed lines*

which led to compound **13**. Compound **13** showed a tenfold increase in potency against EML4-ALK$_{G1202R}$ Ba/F3 cells compared to alectinib with an IC$_{50}$ of 21 nM compared to 207 nM for alectinib. However, compound **13** showed a loss of between 4- and 20-fold potency against other clinically relevant mutants. Smaller alkyl rings including a dimethylamino piperidine and methyl piperazine were tested, but results in a two- to threefold loss of potency against the G1202R mutant likely due to the close proximity of the 1202R residue, which is better accommodated by flat aromatic heterocycles. Substituted pyrazoles were then tested, leading to JH-VIII-157-02 (**14**), which showed a 100-fold increase in potency against EML4-ALK$_{G1202R}$ Ba/F3 cells compared to alectinib with an IC$_{50}$ of 2 nM compared to 207 nM for alectinib. To better understand the enhanced potency of JH-VIII-157-02, a molecular modeling study based upon the co-crystal structure of ALK with alectinib (PDB: 3AOX) was performed. This study suggested that JH-VIII-157-02 makes the same backbone hinge contact as alectinib; however, JH-VIII-157-02 forms two additional hydrogen bond interactions between the guanidine moiety of R1120 and the carbonyl group of the dimethyl acetamide group (Fig. 7a). Furthermore, in the G1202R mutant, JH-VIII-157-02 forms an additional hydrogen bond interaction between the guanidine moiety of R1202 and the nitrogen of the pyrazole ring (Fig. 7b). The modeling study predicted that the methylene spacer between the pyrazole ring and the dimethylacetamide moiety is required for the carbonyl amide of JH-VIII-157-02 to interact with the guanidine moiety of R1120 [41].

To evaluate the inhibitory activity of JH-VIII-157-02 against different ALK fusion and mutant ALK kinases, it was tested alongside the clinical stage ALK inhibitors alectinib (**12**), ceritinib (**7**), Brigatinib (**18**), and crizotinib (**5**) against a panel of cell lines derived from NSCLC (H3122, DFCI76, and DFCI114) and
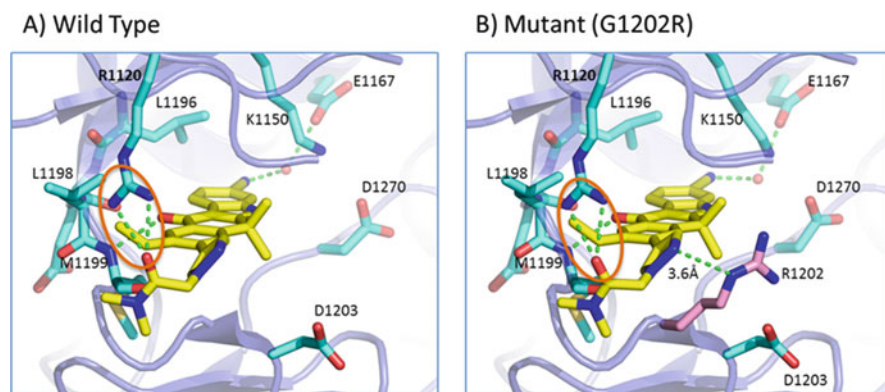
Fig. 7 Molecular docking study of JH-VIII-157-02 with wild-type ALK and a model of G1202R ALK. (**a**) Binding conformation of JH-VIII-157-02 (*yellow sticks*) in the ATP binding site of ALK-wt (*blue ribbon*). Hydrogen bonds are indicated by *dashed lines*. (**b**) Predicted binding conformation of JH-VIII-157-02 (*yellow sticks*) in the ATP binding site of ALK-G1202R. Hydrogen bonds are indicated by *dashed lines*

neuroblastoma (Kelly, LAN-1, SH-SY5Y (F1174L), SK-N-SH (F1174L), LAN-5 (R1275Q), SMS-KCNR (R1275Q), CHLA-20 (R1275Q), SK-N-BE2 (wt), SK-N-FI (wt), and SK-N-AS (wt) Table 3. JH-VIII-157-02 possessed submicromolar EC50 values across the entire panel of cell lines and showed a marked increase in potency against all of the neuroblastoma cell lines and the ALK TKI sensitive H3122 cells with comparable potency to alectinib against the L1152R EML4-ALK mutant DFCI76 cell line [41].

The mouse pharmacokinetic profile of JH-VIII-157-02 demonstrated good oral bioavailability (87%F), a half-life of 1.69 h, and a plasma exposure of 64,635 (min ng/mL, AUC_{last}) following an oral dose of 10 mg/kg (Table 4). Additionally, 2 h after an oral dose of 10 mg/kg, JH-VIII-157-02 showed a plasma exposure of 0.34 μM, and a brain exposure of 0.03 μM which equates to a low total brain/plasma concentration ratio of 0.1 [41].

JH-VIII-157-02 was screened against a panel of 456 kinases using KINOME*scan*™ methodology at a concentration of 1 μM and was found to be less selective than the parent compound alectinib as shown in Fig. 8.

4 AP26113 (Brigatinib)

In a campaign to develop next-generation ALK inhibitors with enhanced potency towards secondary mutants and to also explore the use of stable phosphorus functionality in drug design, researchers at Ariad Pharmaceuticals developed brigatinib starting from the diamino pyrimidine scaffold used in TAE684 (**6**) and ceritinib (**7**) [49]. In a previous medicinal chemistry effort from Ariad to develop SRC inhibitors, incorporation of a dimethylphosphine oxide (DMPO) moiety led to a 70-fold increase in potency as well as enhanced pharmaceutical properties [49]. These findings provided motivation to incorporate a DMPO moiety in an ALK inhibitor. Based on the prevalence of the substituted 2-aminopyrimidine scaffold in clinical and preclinical kinase inhibitors, a library of substituted 2-aminopyrimidines was constructed and tested for ALK activity with the hope that introduction of diversified functional groups such as DMPO at C2, C4, and C5 on the pyrimidine core might favorably alter kinase selectivity of 2-anilinopyrimidine-based ALK inhibitors. In particular, the activity of new inhibitors against insulin receptor kinase (InsR) and insulin like growth factor receptor (IGF1R) was monitored because both kinases bear high sequence homology with ALK and are important for maintaining glucose homeostasis. As a result of their screening effort, compound **15** was identified as a starting point, with an ALK enzyme IC_{50} of 2.1 nM and an IC_{50} of 349 nM in KARPAS-299 cells [49]. Incorporation of DMPO at the 4′ position of the aniline led to compound **16**, which showed enhanced potency against ALK with an IC_{50} of 0.31 nM; however, it was also potent against IGF1R and InsR with IC_{50}'s of 1.9 nM and 9.9 nM, respectively. A homology-based molecular modeling study revealed that ortho-substituents on the C4 anilines can potentially form an intramolecular hydrogen bond to the aniline

Table 3 Antiproliferative EC_{50}'s of compounds tested against a panel of NSCLC and neuroblastoma cell lines

Cell line	MYCN	Histology	EC50 (nM)				
			Crizotinib (5)	Ceritinib (7)	Alectinib (12)	JH-VIII-157-02 (14)	Brigatinib (18)
H3122		NSCLC	32	15	9	5	5
DFCI76 (L1152R)		NSCLC	233	72	511	19	30
DFCI114 (G1269A)		NSCLC	1,615	18	207	419	9
Kelly (F1174L)	Amplified	Neuroblastoma	211	142	434	147	127
LAN-1 (F1174L)	Amplified	Neuroblastoma	1,346	549	2,004	571	2,853
SH-SY5Y (F1174L)	Non-amplified	Neuroblastoma	523	186	1,150	413	986
SK-N-SH (F1174L)	Non-amplified	Neuroblastoma	370	303	872	245	1,988
LAN-5 (R1275Q)	Amplified	Neuroblastoma	232	122	617	192	790
SMS-KCNR (R1275Q)	Amplified	Neuroblastoma	179	92	765	133	535
CHLA-20 (R1275Q)	Non-amplified	Neuroblastoma	439	363	430	218	8,667
SK-N-BE2 (wt)	Amplified	Neuroblastoma	710	593	1,554	623	2,928
SK-N-FI (wt)	Non-amplified	Neuroblastoma	1,469	349	2,401	973	2,645
SK-N-AS (wt)	Non-amplified	Neuroblastoma	1,473	1,045	2,139	775	776

Table 4 Pharmacokinetic properties of JH-VIII-157-02 (**14**)

Compd	Matrix	Route	Dose (mg/kg)	$T_{1/2}$	T_{max} (h)	C_{max} (ng/mL)	C_{max} (μM)	AUC_{last} (min * ng/mL)	AUC_{last} (μM h)	AUC_{INF_obs} (min * ng/mL)	AUC (% Extrap)	CL_obs (mL/min/kg)	Vss_obs (L/kg)	% F
JH-VIII-157-02	Plasma	iv	2	1.64	0.08	35,250	75.71	150,478	27.56	780,621	1.74	3.55	0.38	–
		po	10	1.69	0.83	373	0.8	655,320	2.31	67,036	3.66	154.83	–	87
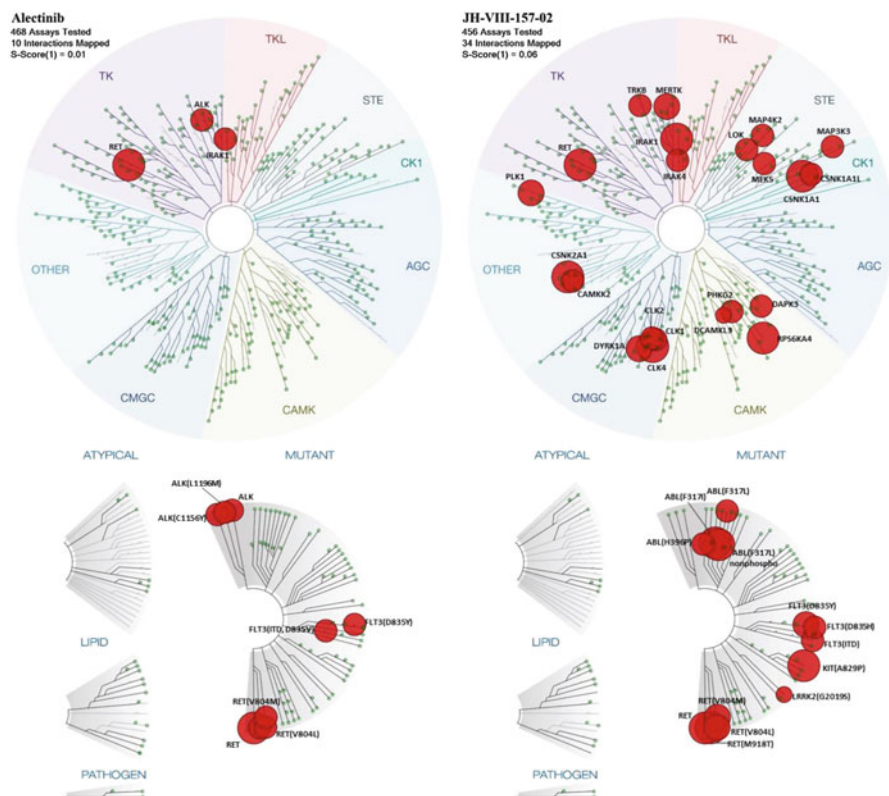
Fig. 8 Kinase selectivity of JH-VIII-157-02 compared to alectinib

NH or hydrogen bond with Lys-NH (K1150). This led to the exploration of the H-bonding potential of the DMPO functionality near the hinge region. The double-phosphorylated compound **17** was synthesized and tested. Although compound **17** did not exhibit increased ALK activity relative to compound **16**, it showed improved selectivity over both IGF1R and InsR. Based on this finding, the ortho DMPO-substituted aniline at C4 was used for the duration of the study while optimizing C2 and C5 substitutions to improve both potency and the overall drug metabolism and pharmacokinetics (DMPK) profile. Given the hydrophilic nature of the bis-DMPO inhibitor **17** (cLogP = 0.4), a large focused library of diverse basic amine-containing solubilizing groups was designed and synthesized to decrease the hydrophilicity, resulting in brigatinib (**18**) with an ALK enzyme IC_{50} of 0.37 nM and an IC_{50} of 24.9 nM in KARPAS-299 cells. Compound **18** also showed selectivity for ALK compared to InsR (IC_{50} = 285 nM) and IGF1R (IC_{50} = 43 nM). Further optimization was conducted at the C5 position of the pyrimidine by substitution with different halogens, small alkyl groups and a methoxy group, all of which maintained potent ALK enzyme activity, but showed a considerable loss in cellular potency. Therefore, the chlorine substitution at C5 was maintained and

the methoxy group on the aniline ring was replaced with an ethoxy and isopropoxy group; however, both showed a decrease in ALK activity. Based on these results, brigatinib (**18**) was selected for further testing [49] (Fig. 9).

Brigatinib was screened against a panel of 289 kinases, mutants, and isoforms and was found to inhibit 4% (11 out of 289) of the kinases with an IC_{50} of <10 nM, indicating a relatively high degree of selectivity. Among them, brigatinib potently inhibited FLT3 and ROS1 with IC_{50} values of 2.1 and 1.9 nM, respectively. Unlike crizotinib, which is characterized as a dual c-Met/ALK inhibitor that also potently inhibits Ron, brigatinib did not show significant activity toward c-Met or Ron up to 1 μM. The pharmacokinetic profile of brigatinib in rats was determined as shown in Table 5 [49].

The activity of brigatinib was tested in a mouse model of NSCLC (H3122 cells expressing the EML4-ALK fusion). In this model, once-daily oral administration for 19 days of brigatinib resulted in dose-dependent antitumor activity, with tumor regressions observed at all doses tested (including the lowest 10 mg/kg dose). In addition, no signs of toxicity or body weight loss were observed at any dose level tested [49]. An initial dose-finding study was initiated and evaluated 18 patients with ALK-positive NSCLC. Of these patients, 3 had no prior treatment with ALK TKI, and 12 had prior treatment with crizotinib; of these, 67% responded, including two complete responses [50]. Radiographic improvement was seen in four of five patients with untreated or progressing CNS lesions. There were 16 patients enrolled with EGFRm history (15 NSCLC, 1 SCLC); 14 patients had received prior treatment of an EGFR TKI. Of 12 EGFRm patients with a follow-up scan, 1 patient who had previously received treatment with erlotinib responded at 120 mg, 6 patients had stable disease [50].
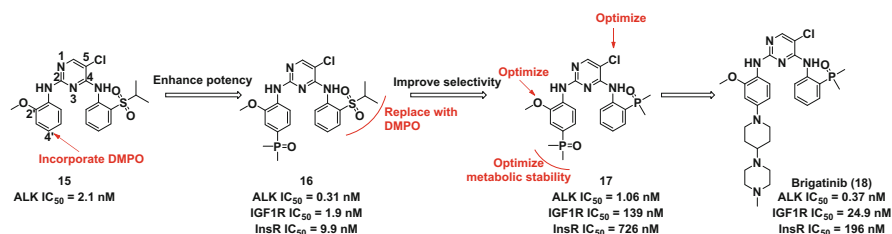
Fig. 9 Design strategy used to develop brigatinib (**18**)

Table 5 Pharmacokinetic properties of brigatinib in CD rats

Compd	Matrix	Route	Dose (mg kg^{-1})	$T_{1/2}$	T_{max} (h)	C_{max} (ng mL)	CI_obs (mL h^{-1} kg^{-1})	Vss_obs (L kg^{-1})	% F
Brigatinib	Plasma	iv	3	4.8	–	–	0.46	7.8	–
		po	10	3.4	4.0	305	–	–	52

In a phase I/II single-arm, open label, multicenter study in patients with advanced malignancies (NCT01449461), patients received brigatinib as the following: phase I: 30–300 mg/day total daily dose; phase II: 90, 180, or 90 mg/day for 7 days followed by 180 mg/day. In crizotinib-naïve patients, an ORR of 7/7 (100%) was observed with a PFS of 56 weeks. In crizotinib-failure patients, an ORR of 45/65 (69%) was observed with a PFS of 47 weeks. In patients with CNS metastases, an ORR of 14/38 (37%) was seen along with a PFS of 97 weeks. Most common adverse events included nausea, diarrhea, fatigue, cough, and headache. Early-onset pulmonary events were observed less frequently with the 90 mg starting dose compared with higher doses. Therefore, brigatinib was active in crizotinib-resistant NSCLC and showed activity in CNS lesions. A randomized phase II trial of brigatinib in crizotinib-resistant ALK-positive NSCLC (ALTA) is underway.

5 CEP-28122 and CEP-37440

As part of a program to develop novel ALK inhibitors with the dianilino pyrimidine scaffold, researchers at Cephalon identified the 7-amino-1,3,4,5-tetrahydrobenzo-[b]azepin-2-one derivative **19** that displayed potent activity against ALK (IC$_{50}$ = 15 nM) with only a 1.5-fold margin against InsR [51]. Inhibition of NPM-ALK autophosphorylation in KARPAS-299 cells was quite robust (IC$_{50}$ = 30 nM). Early SAR identified benzamide or sulfonamide functionality as a key potency determinant for ALK. The aryl ring was replaced with cis-3-amino-bicyclo[2.2.1]hept-5-ene-2-carboxamide, which resulted in a slight drop-off in ALK activity. However, it resulted in a promising fivefold InsR selectivity. Based on these findings, further optimization was conducted by changing the substituents on the 7-amino-1,3,4,5-tetrahydrobenzo [b]aze-pin-2-one moiety. As a result, an ethyl substituent on the azepinone nitrogen was found to improve PK parameters. In addition, an ortho methoxy group at position 6 was found to enhance selectivity leading to compound **20** with an ALK enzyme IC$_{50}$ of 14 nM, an IC$_{50}$ of 45 nM in KARPAS-299 cells and an InsR enzyme IC$_{50}$ of 597 nM. While compound **20** provided a balanced profile consisting of ALK potency and global kinase selectivity, the modest InsR/ALK selectivity led the team to optimize the diaminopyrimidine series further in an effort to improve selectivity toward InsR (enzymatic InsR/ALK IC$_{50}$ ratio of >100). In addition, compound **20** lacked the ability to be dose escalated in preclinical toxicological species, precluding its further development [52]. The 2,3,4,5-tetrahydro-1H-benzo[d]azepine A-ring motif was identified as a replacement of the 7-amino-1,3,4,5-tetrahydrobenzo[b] aze-pin-2-one moiety due to the azepine nitrogen, which provided a site for additional functional group modification to balance potency with favorable physicochemical properties. A variety of substituents incorporated on the azepine nitrogen, however, only showed modest selectivity towards InsR (InsR/ALK = 43). The basic nitrogen was then moved outside of the 7-membered ring. Compounds with a variety of substituents on the exocyclic nitrogen were prepared, which led to the discovery of CEP-28122 (**21**) with an ALK enzyme IC$_{50}$ of 2 nM, an IC$_{50}$ of 20 nM in KARPAS-

299 cells and >600-fold selectivity with respect to the insulin receptor [52]. It also inhibited the growth of neuroblastoma cell lines NB-1643 and SHSY5Y, harboring ALK activating mutants F1174L and R1275Q. Moreover, CEP-28112 led to tumor regression in two ALK-positive ALCL mouse tumor xenografts, KARPAS-299 (30 mg kg^{-1}, po, bid) and Sup-M2 (55 or 100 mg kg^{-1}, po, bid for 4 weeks) [52]. In EML4–ALK-positive NSCLC mouse xenograft models (NCI-H2228, NCI-H3122, and NB-1), CEP-28112 demonstrated good antitumor activities at 50 mg kg^{-1}, po, bid for 12 days [52]. However, the development of CEP-28122 was terminated due to the occurrence of severe lung toxicity in 4- and 13-week monkey studies [53]. Identification of metabolic hotspots from liver microsome incubation provided a clear path forward to remove the toxicity associated with compound **21** [53]. As shown in Fig. 10, the two major locations for oxidative metabolism proved to be the morpholine ring, which was oxidized and degraded, and the olefin of the bicyclo[2.2.1] system which was epoxidized [53]. The degree and location of metabolism in rat and human liver microsomes were quite similar; therefore, in vitro and in vivo screening in rats was used to predict improvements in metabolic stability. The morpholine ring was moved to the α-position resulting in a loss in potency against ALK; however, when it was moved to the α′ position as in compound **22**, similar potency against ALK was maintained although the $t_{1/2}$ was still short in liver microsomes (5 min). The morpholine ring was changed to an N-methyl piperazine ring, which showed an increase in the microsomal $t_{1/2}$ (5–39 min) while still maintaining potency against ALK (enzyme IC$_{50}$ = 14 nM). Unfortunately, when the pharmacokinetic parameters were determined in rats, a low oral bioavailability (F = 11%) was observed. The N-methyl group was changed to a hydroxyethyl group, which led to improved potency in cells (cellular IC$_{50}$ = 30 nM compared to 200 nM). However, compound **23** still showed a low bioavailability of 10%. At this point, focus
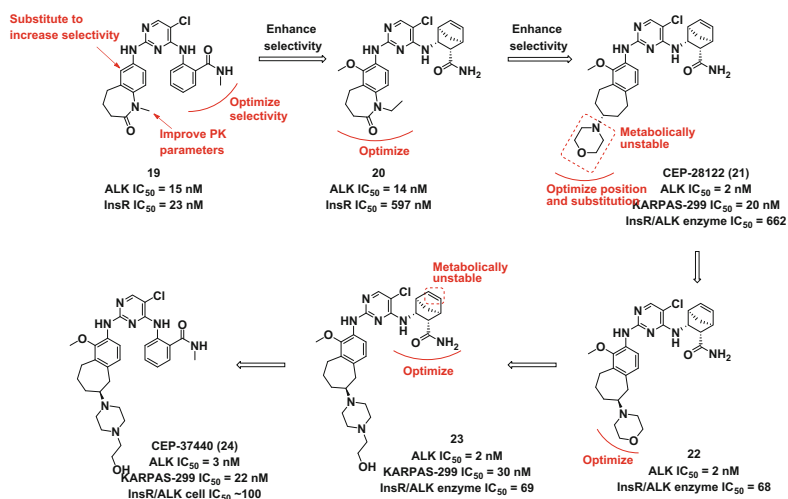
Fig. 10 The development strategy for CEP-28112 (**21**) and CEP-37440 (**24**)

was shifted towards optimizing the olefin of the bicyclo[2.2.1]heptene system since it was also identified as a metabolic hotspot. A series of aryl sulfonamides and aryl amides were prepared including the *N*-methyl aryl amide CEP-37440 (**24**) with an ALK enzyme IC_{50} of 3.1 nM, ~100-fold selectivity with respect to the insulin receptor, a $t_{1/2}$ of 40 min in mice, rat, and human liver microsomes and a bioavailability of 42% in rats [53].

CEP-37440 (**24**) possessed more favorable properties than CEP-28112 (**21**), such as superior solubility and metabolic stability, improved oral bioavailability, as well as lower clearance and toxicity. In vivo pharmacokinetic parameters for CEP-37440 in three different species (CD-1 mouse, Sprague-Dawley rat, and cynomolgus monkey) are shown in Table 6 [53].

In vivo studies of CEP-37440 in both Sup-M2 (30 mg kg^{-1}, po, bid or 50 mg kg^{-1}, po, qd) and KARPAS-299 (30 mg kg^{-1}, po, bid or 50 mg kg^{-1}, po, qd) mouse xenograft models for 12 days displayed complete tumor regression without toxicity and significant body weight loss. Moreover, oral administration of CEP-37440 caused tumor stasis and partial regression in NCI-H3122 (30 mg kg^{-1}, po, bid and 55 mg kg^{-1}, po, bid) mouse xenograft models for 12 days, and exhibited tumor regression in NCI-H2228 (30 mg kg^{-1}, po, qd and bid or 55 mg kg^{-1}, po, bid) mouse xenograft models with no overt toxicity and bodyweight loss [53]. Additionally, from tissue distribution studies in rats at 30 mg kg^{-1} oral dose, total brain exposure relative to plasma was roughly 1.5- to 2-fold [brain C_{max} (3,160 ng g^{-1}) vs plasma C_{max} (2,116 ng g^{-1}; brain AUC_{0-48h} (61,584 ng h mL^{-1}) vs plasma AUC_{0-48h} (31,539 ng h mL^{-1})] which is significant, since one aspect of clinically derived resistance of NSCLC to crizotinib is manifested in the emergence of brain metastases [53]. CEP-37440 is undergoing clinical development in Phase I clinical trials for patients with advanced or metastatic solid tumors.

Table 6 Pharmacokinetic parameters of CEP-37440 in CD-1 mouse, Sprague-Dawley (SD) rats, and cynomolgus monkeys

Route	Parameter	CD-1 mouse	SD rat	Cynomolgus monkey
iv	Dose (mg kg^{-1})	1	1	1
	$t_{1/2}$ (h)	3.0	2.0	5.4
	AUC_{last} (ng h mL^{-1})	1,612	4,005	554
	Vd (L kg^{-1})	2.7	0.8	13.2
	CL (mL min^{-1} kg^{-1})	20	4	30
po	Dose (mg kg^{-1})	10	10	10
	C_{max} (ng mL^{-1})	1,533	1,340	239
	t_{max} (h)	2	3.3	6
	AUC_{last} (ng h mL^{-1})	16,429	8,360	2,757
	F (%)	102	42	50

6 Entrectinib

Entrectinib (**26**) is a potent orally available ALK inhibitor that is active against ALK-dependent cell lines [54], which efficiently crosses the blood–brain barrier (BBB) in different animal species and is highly efficacious in xenograft models. Moreover, entrectinib is highly potent against the closely related tyrosine kinases ROS1 and TRKs, which have been found to be constitutively activated in several tumor types. Entrectinib is currently undergoing Phase I/II clinical trial for the treatment of patients affected by ALK-, ROS1-, and TRK-positive tumors [54].

Researchers at Nerviano Medical Sciences conducted a high throughput screen of their corporate compound collection and the 3-amino-5-substituted indazole **25** emerged as a promising starting point for further optimization with a biochemical IC_{50} of 73 nM against ALK and moderate antiproliferative activity against the ALK-dependent ALCL KARPAS-299 cell line ($IC_{50} = 253$ nM) [54]. A strategy was developed, which focused on the substitution pattern of the fluorinated phenyl ring B, the introduction of substituents on ring A, and the modification of the *N*-methylpiperazinyl solubilizing group at the para position of ring A. A large number of analogues with a variety of primary amines at R3 were prepared. The incorporation of a primary amine at R3 was predicted to stabilize the bioactive conformation of the molecule by forming an intramolecular hydrogen bond with the adjacent amide carbonyl group (Fig. 11). Of these, entrectinib (**26**) emerged as the most potent with a biochemical IC_{50} of 12 nM against ALK, and an IC_{50} of 31 nM in KARPAS-299 cells. In addition, entrectinib showed tenfold selectivity against IGF1R and 20-fold selectivity against InsR. The methylene spacer was left unchanged due to the labile nature of the resulting benzhydryl stereocenter [54].

Exploration of ring B demonstrated the importance of the 3,5-difluoro substitution of the ring. Removal of both fluorines caused a nearly tenfold decrease of biochemical activity on ALK and KARPAS-299 cells. A decrease in potency was observed when replacing one fluorine with a methyl group, likely due to a negative impact on the geometry of the stacking interaction of phenyl B with the phenylalanine 1,127 of the glycine-rich loop. Finally, the importance of the *N*-methyl piperazine group was investigated by preparing several analogues with different solubilizing groups, including the unsubstituted piperazine, which resulted in

Fig. 11 Optimization of hit **25** in the development of entrectinib (**26**)
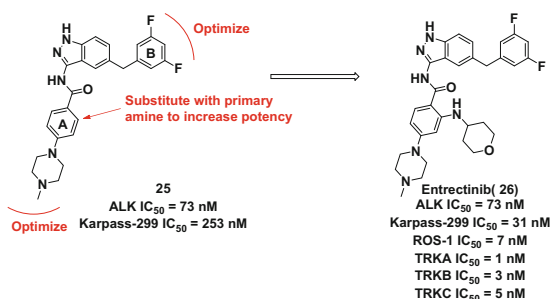
fourfold more potent activity against ALK and KARPAS-299 cells. However, further testing revealed an unsatisfactory pharmacokinetic profile with low permeability and clearance. Based on these findings, entrectinib was selected as the lead compound for further testing. Entrectinib was profiled against a highly diverse panel of 56 biochemical kinase assays and found to have an average IC_{50} of 12 nM and a K_i of 6.2 nM against ALK. Entrectinib was even more potent on the kinases ROS1 (IC_{50} = 7 nM) and on TRKA (IC_{50} = 1 nM). On the basis of the observed activity on TRKA, the biochemical potencies on the related kinases TRKB and TRKC were also evaluated and found to be in the single-digit nanomolar range (TRKB IC_{50} = 2 nM and TRKC IC_{50} = 5 nM), which was promising since both ROS1 and TRKs were found to be constitutively active in several tumor types. Entrectinib showed less than tenfold selectivity against only two additional kinases in the panel (JAK2 and ACK1) [54].

Entrectinib was tested in KARPAS-299 and NCI-H2228 cells for its ability to modulate autophosphorylation of ALK kinase. Following treatment of cells for 2 h with entrectinib, complete inhibition of phosphorylation was observed in both cell lines at very low doses (10 nM for KARPAS-299 cells and 150 nM for NCI-H2228 cells) [54].

To explore the cellular activity on TRKA, the modulation of target phosphorylation was tested in the TRKA-dependent cell line KM12. KM12 cells were treated for 2 h with entrectinib at different concentrations. Complete inhibition of phosphorylation was observed at a concentration of 10 nM of entrectinib, which supported the rationale for considering TRKA-positive patients for clinical development of entrectinib. Entrectinib was tested in a series of Ba/F3 cell lines transfected with different crizotinib or ceritinib-resistant mutated forms of EML4-ALK. Entrectinib demonstrated good antiproliferative activity on EML4-ALK_{wt} (Ba/F3-EML4-ALK_{wt} IC_{50} = 28 nM) and on the gate-keeper mutant EML4-ALK_{L1196M} (Ba/F3-EML4-ALK_{L1196M} IC_{50} = 67 nM), but it was poorly active on the EML4-ALK_{G1202R} mutant (Ba/F3 EML4-ALK_{G1202R} IC_{50} = 897 nM) [54].

In vivo studies of entrectinib in both KARPAS-299 (30 mg kg^{-1}, po, bid or 60 mg kg^{-1}, po, bid) and NCI-H2228 (30 mg kg^{-1}, po, bid or 60 mg kg^{-1}, po, bid) mouse xenograft models for 10 days displayed complete tumor regression without toxicity and significant body weight loss. Furthermore, entrectinib was found to cross the blood–brain barrier with a concentration of nearly 50% of plasma levels following oral administration. The pharmacokinetic parameters of entrectinib were evaluated in rat and dog following doses of 10 mg kg^{-1} for both iv and oral administration. Entrectinib showed good exposure and moderate to good oral bioavailability in both species, with a volume of distribution indicative of tissue distribution and low clearance in both animal species (Table 7) [54].

In ongoing Phase I trials (ALKA-372-001 and STARTRK-1) [55, 56], consisting of a total of 119 patients with a range of solid tumor types, entrectinib (600 mg po once daily) appeared to be well tolerated with the most frequent adverse events consisting of mild to moderate fatigue, altered taste, abnormal sensations in the nerves, nausea, and muscle aches. These phase I clinical trials comprise the largest safety study of any TRK inhibitor in clinical development, with no evidence to date

Table 7 Pharmacokinetic parameters of entrectinib in Sprague-Dawley (SD) rats and beagle dogs

Compd	Species	Route	Dose (mg kg^{-1})	$T_{1/2}$ (h)	T_{max} (h)	AUC$_{last}$ (µM h)	C_{max} (µM)	Cl_obs (mL min^{-1} kg^{-1})	Vss_obs (L kg^{-1})	% F
Entrectinib	Rat	iv	10	3.5	–	15.1	11	20.8	4.0	–
		po	10	3.8	3.08	5.13	0.5	–	–	43
	Dog	iv	10	11.9	–	17.6	8.6	17.5	6.7	–
		po	10	15.2	2.0	5.7	0.6	–	–	32

of cumulative toxicity, or of renal, hepatic or QT$_c$ toxicity. In addition, no patients have discontinued entrectinib due to tolerability issues at the time of publication. In this Phase I trial, there were four patients with *NTRK* fusions, consisting of patients with non-small cell lung cancer (NSCLC), colorectal cancer (CRC), salivary gland cancer, and astrocytoma. All four of these patients demonstrated tumor regression. In addition, there was an 86% confirmed response rate (12 of 14 patients) to entrectinib in patients with ROS1 fusions and a 57% response rate for patients with *ALK* fusions (4 of 7 patients). Many of these responses occurred rapidly, within the first 4 weeks of entrectinib treatment. Eleven of the responders remained on study, with the longest at 27 months. In these phase I studies, entrectinib also demonstrated clinically significant activity in the central nervous system (CNS), achieving both complete and durable responses in patients with CNS disease.

7 Lorlatinib

Lorlatinib (**32**) is a structurally unique macrocyclic inhibitor that is potent against wild-type ALK and clinically reported ALK kinase domain mutations, and also shows CNS availability [57]. Lorlatinib was discovered by Pfizer during a campaign to improve the potency against secondary ALK mutants of their first generation ALK inhibitor crizotinib and to improve CNS ADME for the purposes of targeting the emergence of brain metastases [58]. A structure guided approach was initiated using high resolution crystal structures of apo ALK protein and crizotinib-bound ALK protein. Comparison of the two structures showed that the 2-chloro substituent is in close contact with the backbone carbonyl of G1269 resulting in an unfavorable interaction that causes the carbonyl to rotate ~30° away from the inhibitor to accommodate crizotinib binding [58]. Based on this observation, the 2-des-chloro analogue **27** was designed to relax the G1269 carbonyl and improve the potency. Compound **27** showed increased potency against NIH-3T3 cells stably expressing ALK$_{L1196M}$ mutant with an IC$_{50}$ of 387 nM compared to 843 nM for crizotinib. Further optimization to improve LipE led to the replacement of the 6-chloro substituent with a triazole ring, and removal of the piperidine ring from the pyrazole in favor of the smaller methyl pyrazole leading to compound **28**.

Compound **28** showed further increased potency against both ALK_{L1196M} enzyme and NIH-3T3 cells stably expressing ALK_{L1196M} mutant with IC_{50}s of 2.6 nM and 60 nM, respectively. The co-crystal structure of **28** with ALK showed that the triazole ring forms a 60° torsion angle with the phenyl ring, which puts it in position to make favorable interactions with the backbone residues L1122-G1123. By contrast, the chlorine of crizotinib doesn't extend far enough to make these interactions. While compound **28** exhibited good potency, it was found to be a substrate for glucuronidation at the unsubstituted pyrazole site. Based on these findings, a variety of substituted 5- and 6-membered aromatic groups were used to replace the unsubstituted pyrazole, which led to the thiazole-substituted compound **29**. Compound **29** showed an increase in potency against both ALK_{L1196M} enzyme and NIH-3T3 cells stably expressing ALK_{L1196M} mutant with IC_{50}s of 0.4 nM and 27 nM, respectively. Analysis of the co-crystal structure of **29** with ALK revealed an additional hydrogen bond interaction between the tertiary alcohol and the carbonyl group of D1203. In addition, the co-crystal structure of **29** showed the thiazole aromatic ring was rotated about 30° from the plane of the 2-aminopyridine hinge-binding moiety, which orients the R3 aryl ring in a suitable angle and distance to form a CH donor-pi interaction with G1202. Further analysis of the structure of **29** with the ALK kinase domain showed one methyl group of the 2-propanol moiety to be proximal to the NH of D1203 (4.2 Å). This NH appeared to have no discernible interactions with water, ligand, or protein. Modeling suggested that a hydroxyl group added to this methyl group could act as a hydrogen bond acceptor to the NH and a hydrogen bond donor to either the carboxyl side chain of D1203 or a water molecule stabilized by the carbonyls of G1201 and D1203. This led to the synthesis of compound **30**, which resulted in a fourfold increase in cellular potency. On the basis of improved L1196M mutant potency, lipophilic efficiency, and balanced physicochemical properties, **30** emerged as a candidate for broader profiling in wild-type and mutant ALK driven cell lines and kinase counterscreen assays [58].

As shown in Table 8, compound **30** significantly improved cell potency against ALK WT and ALK clinical mutations compared with crizotinib (**5**). In the engineered WT 3T3-EML4-ALK phosphorylation assay, the potency of **30** was improved 100-fold (from 80 nM for **5** to 0.8 nM for **30**). Across the clinically identified ALK mutants in the engineered cell lines, compound **30** showed a 67- to 825-fold potency increase compared to crizotinib (**5**) (Fig. 12) [58].

Table 8 pALK (IC_{50}) values for 5, 30, and 32 against ALK and clinical mutants of ALK

Compd	ALK phospo in 3T3-EML4-ALK engineered cells IC_{50} (nM)								
	wt	F1174L	C1156Y	G1269A	S1206Y	L1196M	L1152R	G1202R	1151Tins
Crizotinib (5)	80	165	478	605	626	843	1,026	1,148	3,039
30	0.8	0.2	0.6	9.0	4.5	0.8	3.5	–	24
Lorlatinib (32)	1.3	0.2	1.6	15	4.2	21	9.0	77	38
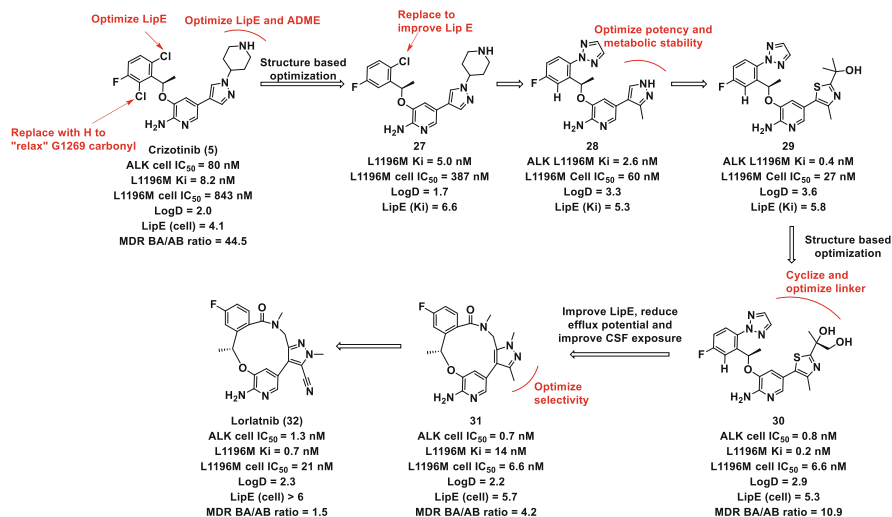
Fig. 12 Optimization of crizotinib (**5**) leading to the discovery of lorlatinib (**32**)

Table 9 Rat pharmacokinetic profile of lorlatinib (32) and 30

Compd	Route	Dose (mg kg^{-1})	AUC$_{inf}$/ AUC$_{(0-24)}$ (ng h mL^{-1})	AUC (nM h)	Free C_{av} (nM)	$T_{1/2}$ (h)	T_{max} (h)	Free C_{max} (nM)	C_{max} (ng mL^{-1})	CI$_p$ (mL min^{-1} kg^{-1})	V_{ss} (L kg^{-1})	%F
Lorlatinib (32)	iv	1	1,150	–	–	2.7	–	–	–	15.5	2.7	
	po	10	14,933	30,700	551	–	1.3	1,530	1,727	–	–	100
30	iv	1	–	667	–	0.9	–	–	–	54	2.0	–
	po	5	–	2,869	–	–	1.3	–	568	–	–	86

The potency gains measured by inhibition of ALK phosphorylation were consistent with the significantly improved antiproliferative potency of **30** relative to crizotinib (**5**) in both wild-type cell lines (H3122, H2228, and KARPAS-299) and engineered mutant lines (H3122-L1196M and H3122-G1269A) [58]. While it was extremely potent against WT and mutant ALK, compound **30** also showed good kinase selectivity. Against a diverse panel of 207 kinases tested at Invitrogen, 33 kinases were reported with >80% inhibition at a concentration of 1 μM [58]. Preclinical pharmacokinetic (PK) data was obtained on **30** to assess rat clearance, volume of distribution, half-life, and bioavailability (Table 9). The compound demonstrated 86% bioavailability in rat. Moderate-to-high in vivo rat plasma clearance with moderate volume of distribution provided about a 1 h half-life in rat [58].

To evaluate the antitumor efficacy of **30**, a mouse tumor xenograft study was performed. Dosing started from day 15 post cell implantation with tumor size

around 250 mm^3. Compound **30** demonstrated dose-responsive tumor growth inhibitory activity in the NCI H3122 cell line expressing the L1196M mutation. It showed tumor stasis (100% TGI) at both the 30 mg kg^{-1} q.d. and 15 mg kg^{-1} b.i.d. doses. The highest dose (50 mg kg^{-1} b.i.d) showed 56% tumor growth regression on day 27 with no significant reduction in body weight observed throughout the course of the study [58]. Unfortunately, the introduction of polar groups to balance out the increase in lipophilicity resulted in high efflux potential and very low rat CSF drug levels [57].

A new strategy was initiated that would lead to higher drug exposure levels in the CNS by improving the lipophilic efficiency while maintaining low efflux potential. Upon examining the co-crystal structure of **30** and its analogues, it was noted that a U-shape confirmation of the inhibitors was maintained with the fluorophenyl head group in close proximity to the heteroaromatic tail [57]. A strategy focused on macrocyclization using a lactam linker was pursued based on the expectation that a macrocyclic analogue would reinforce the binding conformation and provide additional protein ligand interactions in the linker region. Additionally, macrocyclic analogues significantly reduced the number of rotatable bonds and were more compact with increased buried surface area than acyclic analogues, which should improve permeability [57]. Modeling suggested a single carbon atom linking the amide with the proximal pyrazole moiety, leading to a proposed 12-membered lactam (**31**) that would have minimal binding strain. In addition, the *N*-methyl amide group appeared to be in close contact with Leu1122, Gly1123, and Val1130 of the G-loop, and the lactam carbonyl oxygen may act through a structural water to stabilize Lys1150. Importantly, the amide macrocycles also possessed significantly lower lipophilicity, placing them in an optimal log D range (2–3). A set of amide-linked macrocycles was prepared including compound **31**, which improved cellular potency against ALK$_{wt}$ and ALK$_{L1196M}$ by tenfold relative to the acyclic compound and also lowered lipophilicity by 1 unit, without additional molecular weight. As a result, macrocycle **31** had a LipE more than 2 units higher than its acyclic counterpart. A reduction of the in vitro clearance from 56 mL min^{-1} kg^{-1} (high) to the lower limit of detection for the assay demonstrated the inherent metabolic stability of the cyclic structure [57]. Finally, the permeability of **31**, measured by P-glycoprotein efflux potential, was superior to the acyclic analogue. Based on these results, compound **31** was further optimized for overall kinase selectivity by incorporating various groups at the *ortho*-position of the pyrazole, which resulted in a cyano group providing the best balance of potency, low in vitro clearance, selectivity, and low efflux potential. Based on these findings, lorlatinib (**32**) emerged as a candidate for further profiling. As shown in Table 8, lorlatinib significantly improved cell potency against ALK$_{wt}$ and ALK clinical mutations compared with crizotinib (**5**) and maintained similar potency against ALK$_{wt}$ and ALK clinical mutations compared with **30** [57]. Lorlatinib (**32**) was evaluated in biochemical kinase screening assays against a panel of 206 recombinant kinases. In these preliminary biochemical kinase selectivity screens, only 10 off-target kinases were identified that exhibited enzyme-based activity and showed selectivity margins of less than 100-fold compared to the ALK$_{L1196M}$

Table 10 In vivo CNS availability data for lorlatinib

Compd	Matrix	Route	Dose (mg kg^{-1})	AUC (nM h)	Free AUC[a] (nM h)
Lorlatinib (32)	CHSF	po	10	3,475	3,475
	Brain	po	10	19,621	2,355[a]
	Plasma	po	10	30,700	11,052[b]

[a]The free brain AUC was calculated using a brain f_u of 0.12
[b]The free plasma AUC was calculated using a plasma protein binding (PPB) f_u of 0.36

gatekeeper mutant. In rat pharmacokinetic studies, lorlatinib displayed low plasma clearance, a moderate volume of distribution, a reasonable half-life, and a bioavailability of 100% resulting in high free plasma exposures as shown in Table 9 [57].

In addition, CNS penetration of lorlatinib was evaluated in rats. After a single 10 mg kg^{-1} oral dose, samples of CSF, brain, and plasma were collected at 1, 4, 7, 12, and 24 h with the PK parameters shown in Table 10. Area under the curve ratios of CSF to free plasma (0.31) and free brain to free plasma (0.21) suggested CNS penetration of lorlatinib. The rat in vivo data were also supported by in vitro data, which indicated a lack of transporter-mediated efflux in both Pgp- and breast cancer resistance protein (BCRP)-overexpressing cell lines [57].

Data from a Phase I study showed that lorlatinib is active in patients with ALK- or ROS1-positive non–small-cell lung cancer whose tumors have become resistant to other tyrosine kinase inhibitors (TKI), and who have brain metastases. In this study, 41 patients with ALK-positive NSCLC and 12 whose disease was ROS1-positive were treated with lorlatinib across 10 dose levels to establish the recommended daily dose of 100 mg. The majority (87%) had relapsed after at least one prior TKI and 72% also had brain metastases. Among those with *ALK* rearrangements, the confirmed ORR to lorlatinib was 46%, with three complete responses. Median progression-free survival was 11.4 months. Significant tumor shrinkage was also seen in six ROS1-positive patients [59].

Among 18 patients with measurable brain metastases, the confirmed intracranial ORR, assessed through MRI, was 39%, including five complete responses. Lorlatinib was well tolerated overall. The most frequent side effect, hypercholesterolemia, was asymptomatic and readily managed with statin therapy [59].

In summary a number of structurally diverse first and second generation ATP-competitive ALK inhibitors have been successfully developed and have demonstrated significant anti-tumor efficacy. As has been seen with most targeted therapies, resistant tumor cells are selected for and patients eventually relapse with tumors that are resistant to the ALK inhibitor. These findings suggest that more durable responses might be achievable by devising multiple independent pharmacological approaches for restraining ALK-dependent signaling. One strategy might be to identify additional binding sites on ALK, for example in the substrate-binding pocket or in allosteric pockets, that would allow a second mode for inhibition. A second strategy might be to induce proteasome-mediated degradation of ALK using E3-recruiting molecules or by inhibiting the deubiquitinases (DUBs) that target ALK [60]. A third strategy could involve targeting effector pathways of ALK

including the MAPK-pathways, PI3K-Akt, and other transcriptional processes required to maintain the ALK-transformed cellular state [61]. Finally there is the possibility that orthogonal targeting strategies, including a host of recently developed immunological approaches such as relief of check-point blockade (anti-PD1, PD-L1, CTLA-4) or adoptive T-cell therapies [62], might combine well with ALK-targeted therapy. Further preclinical and clinical investigation is likely to lead to more durable therapeutic approaches, which are urgently needed by patients.

References

1. Orscheschek K, Merz H, Hell J, Binder T, Bartels H, Feller AC (1995) Large-cell anaplastic lymphoma-specific translocation (T2-5:P23-Q35) in Hodgkins-disease – indication of a common pathogenesis. Lancet 345(8942):87–90
2. Roskoski R (2013) Anaplastic lymphoma kinase (ALK): structure, oncogenic activation, and pharmacological inhibition. Pharmacol Res 68(1):68–94
3. Ullrich A, Schlessinger J (1990) Signal transduction by receptors with tyrosine kinase-activity. Cell 61(2):203–212
4. Pillay K, Govender D, Chetty R (2002) ALK protein expression in rhabdomyosarcomas. Histopathology 41(5):461–467
5. Cessna MH, Zhou H, Sanger WG, Perkins SL, Tripp S, Pickering D, Daines C, Coffin CM (2002) Expression of ALK1 and p80 in inflammatory myofibroblastic tumor and its mesenchymal mimics: a study of 135 cases. Mod Pathol 15(9):931–938
6. Chen YY, Takita J, Choi YL, Kato M, Ohira M, Sanada M, Wang LL, Soda M, Kikuchi A, Igarashi T, Nakagawara A, Hayashi Y, Mano H, Ogawa S (2008) Oncogenic mutations of ALK kinase in neuroblastoma. Nature 455(7215):971–U56
7. Shinmura K, Kageyama S, Tao H, Bunai T, Suzuki M, Kamo T, Takamochi K, Suzuki K, Tanahashi M, Niwa H, Ogawa H, Sugimura H (2008) EML4-ALK fusion transcripts, but no NPM-, TPM3-, CLTC-, ATIC-, or TFG-ALK fusion transcripts, in non-small cell lung carcinomas. Lung Cancer 61(2):163–169
8. Lebeau MM, Bitter MA, Larson RA, Doane LA, Ellis ED, Franklin WA, Rubin CM, Kadin ME, Vardiman JW (1989) The t(2-5)(p23-q35) – a recurring chromosomal abnormality in ki-1-positive anaplastic large cell lymphoma. Leukemia 3(12):866–870
9. Fujimoto J, Shiota M, Iwahara T, Seki N, Satoh H, Mori S, Yamamoto T (1996) Characterization of the transforming activity of p80, a hyperphosphorylated protein in a Ki-1 lymphoma cell line with chromosomal translocation t(2;5). Proc Natl Acad Sci U S A 93(9):4181–4186
10. Nieborowska-Skorska M, Slupianek A, Xue LQ, Zhang Q, Raghunath PN, Hoser G, Wasik MA, Morris SW, Skorski T (2001) Role of signal transducer and activator of transcription 5 in nucleophosmin/anaplastic lymphoma kinase-mediated malignant transformation of lymphoid cells. Cancer Res 61(17):6517–6523
11. Chiarle R, Simmons WJ, Cai HY, Dhall G, Zamo A, Raz R, Karras JG, Levy DE, Inghirami G (2005) Stat3 is required for ALK-mediated lymphomagenesis and provides a possible therapeutic target. Nat Med 11(6):623–629
12. Zamo A, Chiarle R, Piva R, Howes J, Fan Y, Chilosi M, Levy DE, Inghirami G (2002) Anaplastic lymphoma kinase (ALK) activates Stat3 and protects hematopoietic cells from cell death. Oncogene 21(7):1038–1047

13. Soda M, Choi YL, Enomoto M, Takada S, Yamashita Y, Ishikawa S, Fujiwara SI, Watanabe H, Kurashina K, Hatanaka H, Bando M, Ohno S, Ishikawa Y, Aburatani H, Niki T, Sohara Y, Sugiyama Y, Mano H (2007) Identification of the transforming EML4-ALK fusion gene in non-small-cell lung cancer. Nature 448(7153):561–5U3

14. Mano H (2008) Non-solid oncogenes in solid tumors: EML4-ALK fusion genes in lung cancer. Cancer Sci 99(12):2349–2355

15. Inamura K, Takeuchi K, Togashi Y, Nomura K, Ninomiya H, Okui M, Satoh Y, Okumura S, Nakagawa K, Soda M, Choi YL, Niki T, Mano H, Ishikawa Y (2008) EML4-ALK fusion is linked to histological characteristics in a subset of lung cancers. J Thorac Oncol 3(1):13–17

16. Amin HM, Lai R (2007) Pathobiology of ALK(+) anaplastic large-cell lymphoma. Blood 110(7):2259–2267

17. Chiarle R, Voena C, Ambrogio C, Piva R, Inghirami G (2008) The anaplastic lymphoma kinase in the pathogenesis of cancer. Nat Rev Cancer 8(1):11–23

18. Christensen JG, Burrows J, Salgia R (2005) c-Met as a target for human cancer and characterization of inhibitors for therapeutic intervention. Cancer Lett 225(1):1–26

19. Cui JJ, Tran-Dube M, Shen H, Nambu M, Kung PP, Pairish M, Jia L, Meng J, Funk L, Botrous I, McTigue M, Grodsky N, Ryan K, Padrique E, Alton G, Timofeevski S, Yamazaki S, Li QH, Zou HL, Christensen J, Mroczkowski B, Bender S, Kania RS, Edwards MP (2011) Structure based drug design of crizotinib (PF-02341066), a potent and selective dual inhibitor of mesenchymal-epithelial transition factor (c-MET) kinase and anaplastic lymphoma kinase (ALK). J Med Chem 54(18):6342–6363

20. Leeson PD, Springthorpe B (2007) The influence of drug-like concepts on decision-making in medicinal chemistry. Nat Rev Drug Discov 6(11):881–890

21. Ryckmans T, Edwards MP, Horne VA, Correia AM, Owen DR, Thompson LR, Tran I, Tutt MF, Young T (2009) Rapid assessment of a novel series of selective CB2 agonists using parallel synthesis protocols: a lipophilic efficiency (LipE) analysis. Bioorg Med Chem Lett 19(15):4406–4409

22. Zou HY, Li QH, Lee JH, Arango ME, McDonnell SR, Yamazaki S, Koudriakova TB, Alton G, Cui JJ, Kung PP, Nambu MD, Los G, Bender SL, Mroczkowski B, Christensen JG (2007) An orally available small-molecule inhibitor of c-met, PF-2341066, exhibits cytoreductive antitumor efficacy through antiproliferative and antiangiogenic mechanisms. Cancer Res 67(9):4408–4417

23. Christensen JG, Zou HY, Arango ME, Li Q, Lee JH, McDonnell SR, Yamazaki S, Alton GR, Mroczkowski B, Los G (2007) Cytoreductive antitumor activity of PF-2341066, a novel inhibitor of anaplastic lymphoma kinase and c-Met, in experimental models of anaplastic large-cell lymphoma. Mol Cancer Ther 6(12):3314–3322

24. Xu HP, O'Gorman M, Boutros T, Brega N, Kantaridis C, Tan WW, Bello A (2015) Evaluation of crizotinib absolute bioavailability, the bioequivalence of three oral formulations, and the effect of food on crizotinib pharmacokinetics in healthy subjects. J Clin Pharmacol 55(1):104–113

25. Kwak EL, Bang YJ, Camidge DR, Shaw AT, Solomon B, Maki RG, Ou SHI, Dezube BJ, Janne PA, Costa DB, Varella-Garcia M, Kim WH, Lynch TJ, Fidias P, Stubbs H, Engelman JA, Sequist LV, Tan WW, Gandhi L, Mino-Kenudson M, Wei GC, Shreeve SM, Ratain MJ, Settleman J, Christensen JG, Haber DA, Wilner K, Salgia R, Shapiro GI, Clark JW, Iafrate AJ (2010) Anaplastic lymphoma kinase inhibition in non-small-cell lung cancer. N Engl J Med 363(18):1693–1703

26. Shaw AT, Yeap BY, Solomon BJ, Riely GJ, Gainor J, Engelman JA, Shapiro GI, Costa DB, Ou SHI, Butaney M, Salgia R, Maki RG, Varella-Garcia M, Doebele RC, Bang YJ, Kulig K, Selaru P, Tang YY, Wilner KD, Kwak EL, Clark JW, Iafrate AJ, Camidge DR (2011) Effect of crizotinib on overall survival in patients with advanced non-small-cell lung cancer harbouring ALK gene rearrangement: a retrospective analysis. Lancet Oncol 12(11):1004–1012

27. Shaw AT, Kim DW, Nakagawa K, Seto T, Crino L, Ahn MJ, De Pas T, Besse B, Solomon BJ, Blackhall F, Wu YL, Thomas M, O'Byrne KJ, Moro-Sibilot D, Camidge DR, Mok T, Hirsh V,

Riely GJ, Iyer S, Tassell V, Polli A, Wilner KD, Janne PA (2013) Crizotinib versus chemotherapy in advanced ALK-positive lung cancer. N Engl J Med 368(25):2385–2394

28. Solomon BJ, Mok T, Kim DW, Wu YL, Nakagawa K, Mekhail T, Felip E, Cappuzzo F, Paolini J, Usari T, Iyer S, Reisman A, Wilner KD, Tursi J, Blackhall F, Boyer M, Ganju V, Hughes B, Pavlakis N, Solomon B, Varma S, Berghmans T, Canon JL, Demedts I, Janssens A, Louis R, Pieters T, Schallier D, Surmont V, da Silva CM, Ferreira CGM, Hirsh V, Joy A, Laberge F, Morzycki W, Wierzbicki R, Han B, Liu X, Qin S, Shi Y, Wang Y, Wu G, Wu YL, Zhou C, Ahvonen J, Barlesi F, Cadranel J, Dansin E, Fayette J, Morere JF, Moro-Sibilot D, Pujol JL, Quoix E, Zalcman G, Frickhofen N, Schneider CP, Wehler T, Mok T, So P, Cuffe S, Bearz A, Boni C, Cappuzzo F, Cognetti F, De Braud F, De Pas T, Galetta D, Migliorino M, Rocco D, Scagliotti G, Tagliaferri P, Tiseo M, Aoe K, Hida T, Kato T, Kozuki T, Nakagawa K, Niho S, Nishio M, Nokihara H, Satouchi M, Seto T, Takahashi T, Ahn JS, Kim DW, Kim SW, Berchem G, Rodriguez OA, Biesma B, Dingemans AM, Smit E, Helland A, Barata F, Gorbunova V, Manikhas G, Orlov S, Leong S, Lim HL, Soo R, Tan EH, Nosworthy A, Villena MC, Felip E, Lopez PG, Casado DI, Banaclocha NM, Aix SP, Aransay NR, Abreu DR, Perez JT, Gautschi O, Pless M, Zippelius A, Chang GC, Tsai YH, Shparyk Y, Blackhall F, Steele N, Armenio V, Dragnev K, Dugan M, Gadgeel S, Gerber D, Graziano S, Gurubhagavatula S, Horn L, Jalal S, Lauer R, Mehra R, Mekhail T, Mirshahidi H, Pakkala S, Polikoff J, Raftopoulos H, Saleh M, Salgia R, Waqar S, Investigators P (2014) First-line crizotinib versus chemotherapy in ALK-positive lung cancer. N Engl J Med 371(23):2167–2177

29. Friboulet L, Li NX, Katayama R, Lee CC, Gainor JF, Crystal AS, Michellys PY, Awad MM, Yanagitani N, Kim S, Pferdekamper AC, Li J, Kasibhatla S, Sun F, Sun XY, Hua S, McNamara P, Mahmood S, Lockerman EL, Fujita N, Nishio M, Harris JL, Shaw AT, Engelman JA (2014) The ALK inhibitor ceritinib overcomes crizotinib resistance in non-small cell lung cancer. Cancer Discov 4(6):662–673

30. Awad MM, Shaw AT (2014) ALK inhibitors in non–small cell lung cancer: crizotinib and beyond. Clin Adv Hematol Oncol: H&O 12(7):429–439

31. Costa DB, Shaw AT, Ou SHI, Solomon BJ, Riely GJ, Ahn MJ, Zhou CC, Shreeve M, Selaru P, Polli A, Schnell P, Wilner KD, Wiltshire R, Camidge DR, Crino L (2015) Clinical experience with crizotinib in patients with advanced ALK-rearranged non-small-cell lung cancer and brain metastases. J Clin Oncol 33(17):1881–1U41

32. Doebele RC, Pilling AB, Aisner DL, Kutateladze TG, Le AT, Weickhardt AJ, Kondo KL, Linderman DJ, Heasley LE, Franklin WA, Varella-Garcia M, Camidge DR (2012) Mechanisms of resistance to crizotinib in patients with ALK gene rearranged non-small cell lung cancer. Clin Cancer Res 18(5):1472–1482

33. Gainor JF, Varghese AM, Ou SHI, Kabraji S, Awad MM, Katayama R, Pawlak A, Mino-Kenudson M, Yeap BY, Riely GJ, Iafrate AJ, Arcila ME, Ladanyi M, Engelman JA, Dias-Santagata D, Shaw AT (2013) ALK rearrangements are mutually exclusive with mutations in EGFR or KRAS: an analysis of 1,683 patients with non-small cell lung cancer. Clin Cancer Res 19(15):4273–4281

34. Katayama R, Shaw AT, Khan TM, Mino-Kenudson M, Solomon BJ, Halmos B, Jessop NA, Wain JC, Yeo AT, Benes C, Drew L, Saeh JC, Crosby K, Sequist LV, Iafrate AJ, Engelman JA (2012) Mechanisms of acquired crizotinib resistance in ALK-rearranged lung cancers. Sci Transl Med 4(120):12

35. Choi YL, Soda M, Yamashita Y, Ueno T, Takashima J, Nakajima T, Yatabe Y, Takeuchi K, Hamada T, Haruta H, Ishikawa Y, Kimura H, Mitsudomi T, Tanio Y, Mano H, ALK Lung Cancer Study Group (2010) EML4-ALK mutations in lung cancer that confer resistance to ALK inhibitors. N Engl J Med 363(18):1734–1739

36. Lovly CM, Pao W (2012) Escaping ALK inhibition: mechanisms of and strategies to overcome resistance. Sci Transl Med 4(120):5

37. Sasaki T, Koivunen J, Ogino A, Yanagita M, Nikiforow S, Zheng W, Lathan C, Marcoux JP, Du JY, Okuda K, Capelletti M, Shimamura T, Ercan D, Stumpfova M, Xiao Y, Weremowicz S, Butaney M, Heon S, Wilner K, Christensen JG, Eck MJ, Wong KK,

Lindeman N, Gray NS, Rodig SJ, Janne PA (2011) A novel ALK secondary mutation and EGFR signaling cause resistance to ALK kinase inhibitors. Cancer Res 71(18):6051–6060

38. Sasaki T, Okuda K, Zheng W, Butrynski J, Capelletti M, Wang LP, Gray NS, Wilner K, Christensen JG, Demetri G, Shapiro GI, Rodig SJ, Eck MJ, Janne PA (2010) The neuroblastoma-associated F1174L ALK mutation causes resistance to an ALK kinase inhibitor in ALK-translocated cancers. Cancer Res 70(24):10038–10043

39. Galkin AV, Melnick JS, Kim S, Hood TL, Li NX, Li LT, Xia G, Steensma R, Chopiuk G, Jiang JQ, Wan YQ, Ding P, Liu Y, Sun FX, Schultz PG, Gray NS, Warmuth M (2007) Identification of NVP-TAE684, a potent, selective, and efficacious inhibitor of NPM-ALK. Proc Natl Acad Sci U S A 104(1):270–275

40. Marsilje TH, Pei W, Chen B, Lu WS, Uno T, Jin YH, Jiang T, Kim S, Li NX, Warmuth M, Sarkisova Y, Sun F, Steffy A, Pferdekamper AC, Li AG, Joseph SB, Kim Y, Liu B, Tuntland T, Cui XM, Gray NS, Steensma R, Wan YQ, Jiang JQ, Chopiuk G, Li J, Gordon WP, Richmond W, Johnson K, Chang J, Groessl T, He YQ, Phimister A, Aycinena A, Lee CC, Bursulaya B, Karanewsky DS, Seidel HM, Harris JL, Michellys PY (2013) Synthesis, structure-activity relationships, and in vivo efficacy of the novel potent and selective anaplastic lymphoma kinase (ALK) inhibitor 5-chloro-N2-(2-isopropoxy-5-methyl-4-(piperidin-4-yl) phenyl)-N4-(2-(isop ropylsulfonyl)phenyl)pyrimidine-2,4-diamine (LDK378) currently in phase 1 and phase 2 clinical trials. J Med Chem 56(14):5675–5690

41. Hatcher JM, Bahcall M, Choi HG, Gao Y, Sim T, George R, Janne PA, Gray NS (2015) Discovery of inhibitors that overcome the G1202R anaplastic lymphoma kinase resistance mutation. J Med Chem 58(23):9296–9308

42. Kinoshita K, Ono Y, Emura T, Asoh K, Furuichi N, Ito T, Kawada H, Tanaka S, Morikami K, Tsukaguchi T, Sakamoto H, Tsukuda T, Oikawa N (2011) Discovery of novel tetracyclic compounds as anaplastic lymphoma kinase inhibitors. Bioorg Med Chem Lett 21(12): 3788–3793

43. Kinoshita K, Kobayashi T, Asoh K, Furuichi N, Ito T, Kawada H, Hara S, Ohwada J, Hattori K, Miyagi T, Hong WS, Park MJ, Takanashi K, Tsukaguchi T, Sakamoto H, Tsukuda T, Oikawa N (2011) 9-Substituted 6,6-dimethyl-11-oxo-6,11-dihydro-5H-benzo b carbazoles as highly selective and potent anaplastic lymphoma kinase inhibitors. J Med Chem 54(18):6286–6294

44. Sakamoto H, Tsukaguchi T, Hiroshima S, Kodama T, Kobayashi T, Fukami TA, Oikawa N, Tsukuda T, Ishii N, Aoki Y (2011) CH5424802, a selective ALK inhibitor capable of blocking the resistant gatekeeper mutant. Cancer Cell 19(5):679–690

45. Kinoshita K, Asoh K, Furuichi N, Ito T, Kawada H, Hara S, Ohwada J, Miyagi T, Kobayashi T, Takanashi K, Tsukaguchi T, Sakamoto H, Tsukuda T, Oikawa N (2012) Design and synthesis of a highly selective, orally active and potent anaplastic lymphoma kinase inhibitor (CH5424802). Bioorg Med Chem 20(3):1271–1280

46. Seto T, Kiura K, Nishio M, Nakagawa K, Maemondo M, Inoue A, Hida T, Yamamoto N, Yoshioka H, Harada M, Ohe Y, Nogami N, Takeuchi K, Shimada T, Tanaka T, Tamura T (2013) CH5424802 (RO5424802) for patients with ALK-rearranged advanced non-small-cell lung cancer (AF-001JP study): a single-arm, open-label, phase 1-2 study. Lancet Oncol 14(7): 590–598

47. Gadgeel SM, Gandhi L, Riely GJ, Chiappori AA, West HL, Azada MC, Morcos PN, Lee RM, Garcia L, Yu L, Boisserie F, Di Laurenzio L, Golding S, Sato J, Yokoyama S, Tanaka T, Ou SHI (2014) Safety and activity of alectinib against systemic disease and brain metastases in patients with crizotinib-resistant ALK-rearranged non-small-cell lung cancer (AF-002JG): results from the dose-finding portion of a phase 1/2 study. Lancet Oncol 15(10):1119–1128

48. Ou SHI, Azada M, Hsiang DJ, Herman JM, Kain TS, Siwak-Tapp C, Casey C, He J, Ali SM, Klempner SJ, Miller VA (2014) Next-generation sequencing reveals a novel NSCLC ALK F1174V mutation and confirms ALK G1202R mutation confers high-level resistance to alectinib (CH5424802/RO5424802) in ALK-rearranged NSCLC patients who progressed on crizotinib. J Thorac Oncol 9(4):549–553

49. Huang WS, Liu SY, Zou D, Thomas M, Wang YH, Zhou TJ, Romero J, Kohlmann A, Li F, Qi JW, Cai LS, Dwight TA, Xu YJ, Xu RS, Dodd R, Toms A, Parillon L, Lu XH, Anjum R, Zhang S, Wang F, Keats J, Wardwell SD, Ning YY, Xu QH, Moran LE, Mohemmad QK, Jang HG, Clackson T, Narasimhan NI, Rivera VM, Zhu XT, Dalgarno D, Shakespeare WC (2016) Discovery of brigatinib (AP26113), a phosphine oxide-containing, potent, orally active inhibitor of anaplastic lymphoma kinase. J Med Chem 59(10):4948–4964

50. Huang WS, Li F, Cai LS, Xu YJ, Zhang S, Wardwell SD, Ning YY, Kohlmann A, Zhou TJ, Ye EY, Zhu XT, Narasimhan NI, Clackson T, Rivera VM, Dalgarno D, Shakespeare WC (2015) Discovery of AP26113, a potent, orally active inhibitor of anaplastic lymphoma kinase and clinically relevant mutants. Cancer Res 75:2827

51. Ott GR, Tripathy R, Cheng MG, McHugh R, Anzalone AV, Underiner TL, Curry MA, Quail MR, Lu LH, Wan WH, Angeles TS, Albom MS, Aimone LD, Ator MA, Ruggeri BA, Dorsey BD (2010) Discovery of a potent inhibitor of anaplastic lymphoma kinase with in vivo antitumor activity. ACS Med Chem Lett 1(9):493–498

52. Gingrich DE, Lisko JG, Curry MA, Cheng MG, Quail M, Lu LH, Wan W, Albom MS, Angeles TS, Aimone LD, Haltiwanger RC, Wells-Knecht K, Ott GR, Ghose AK, Ator MA, Ruggeri B, Dorsey BD (2012) Discovery of an orally efficacious inhibitor of anaplastic lymphoma kinase. J Med Chem 55(10):4580–4593

53. Ott GR, Cheng MG, Learn KS, Wagner J, Gingrich DE, Lisko JG, Curry M, Mesaros EF, Ghose AK, Quail MR, Wan WH, Lu LH, Dobrzanski P, Albom MS, Angeles TS, Wells-Knecht K, Huang ZQ, Aimone LD, Bruckheimer E, Anderson N, Friedman J, Fernandez SV, Ator MA, Ruggeri BA, Dorsey BD (2016) Discovery of clinical candidate CEP-37440, a selective inhibitor of focal adhesion kinase (FAK) and anaplastic lymphoma kinase (ALK). J Med Chem 59(16):7478–7496

54. Menichincheri M, Ardini E, Magnaghi P, Avanzi N, Banfi P, Bossi R, Buffa L, Canevari G, Ceriani L, Colombo M, Corti L, Donati D, Fasolini M, Felder E, Fiorelli C, Fiorentini F, Galvani A, Isacchi A, Borgia AL, Marchionni C, Nesi M, Orrenius C, Panzeri A, Pesenti E, Rusconi L, Saccardo MB, Vanotti E, Perrone E, Orsini P (2016) Discovery of entrectinib: a new 3-aminoindazole as a potent anaplastic lymphoma kinase (ALK), c-ros oncogene 1 kinase (ROS1), and pan-tropomyosin receptor kinases (pan-TRKs) inhibitor. J Med Chem 59(7): 3392–3408

55. De Braud FG, Niger M, Damian S, Bardazza B, Martinetti A, Pelosi G, Marrapese G, Palmeri L, Cerea G, Valtorta E, Veronese S, Sartore-Bianchi A, Ardini E, Isachi A, Martignoni M, Galvani A, Luo D, Yeh L, Senderowicz AM, Siena S (2015) Alka-372-001: first-in-human, phase I study of entrectinib – an oral pan-trk, ROS1, and ALK inhibitor – in patients with advanced solid tumors with relevant molecular alterations. J Clin Oncol 33(15):1

56. Patel MR, Bauer TM, Liu SV, Drilon AE, Wheler JJ, Shaw AT, Farago AF, Ou SHI, Luo D, Yeh L, Hornby Z, Senderowicz AM, Lim J (2015) STARTRK-1: Phase 1/2a study of entrectinib, an oral Pan-Trk, ROS1, and ALK inhibitor, in patients with advanced solid tumors with relevant molecular alterations. J Clin Oncol 33(15):1

57. Johnson TW, Richardson PF, Bailey S, Brooun A, Burke BJ, Collins MR, Cui JJ, Deal JG, Deng YL, Dinh D, Engstrom LD, He MY, Hoffman J, Hoffman RL, Huang QH, Kania RS, Kath JC, Lam H, Lam JL, Le PT, Lingardo L, Liu W, McTigue M, Palmer CL, Sach NW, Smeal T, Smith GL, Stewart AE, Timofeevski S, Zhu HC, Zhu JJ, Zou HY, Edwards MP (2014) Discovery of (10R)-7-amino-12-fluoro-2,10,16-trimethyl-15-oxo-10,15,16,17-tetrahydro-2H-8,4-(metheno) pyrazolo 4,3-h 2,5,11-benzoxadiazacyclotetradecine-3-c arbonitrile (PF-06463922), a macrocyclic inhibitor of anaplastic lymphoma kinase (ALK) and c-ros Oncogene 1 (ROS1) with preclinical brain exposure and broad-spectrum potency against ALK-resistant mutations. J Med Chem 57(11):4720–4744

58. Huang QH, Johnson TW, Bailey S, Brooun A, Bunker KD, Burke BJ, Collins MR, Cook AS, Cui JJ, Dack KN, Deal JG, Deng YL, Dinh D, Engstrom LD, He MY, Hoffman J, Hoffman RL, Johnson PS, Kania RS, Lam H, Lam JL, Le PT, Li QH, Lingardo L, Liu W, Lu MW, McTigue M, Palmer CL, Richardson PF, Sach NW, Shen H, Smeal T, Smith GL, Stewart

AE, Timofeevski S, Tsaparikos K, Wang H, Zhu HC, Zhu JJ, Zou HY, Edwards MP (2014) Design of potent and selective inhibitors to overcome clinical anaplastic lymphoma kinase mutations resistant to crizotinib. J Med Chem 57(4):1170–1187

59. Lorlatinib is active in drug-resistant NSCLC (2016) Cancer Discov 6(8):OF1
60. Deshaies RJ (2015) Protein degradation: prime time for PROTACs. Nat Chem Biol 11(9): 634–635
61. Moore NF, Azarova AM, Bhatnagar N, Ross KN, Drake LE, Frumm S, Liu QS, Christie AL, Sanda T, Chesler L, Kung AL, Gray NS, Stegmaier K, George RE (2014) Molecular rationale for the use of PI3K/AKT/mTOR pathway inhibitors in combination with crizotinib in ALK-mutated neuroblastoma. Oncotarget 5(18):8737–8749
62. Blake SJP, Ching ALH, Kenna TJ, Galea R, Large J, Yagita H, Steptoe RJ (2015) Blockade of PD-1/PD-L1 promotes adoptive T-cell immunotherapy in a tolerogenic environment. PLoS One 10(3):e0119483

Index